THE PHYSICS AND CHEMISTRY OF SOLIDS

AN INTERNATIONAL JOURNAL

VOLUME 18 1961

Editor-in-Chief HARVEY BROOKS *Cambridge, Mass.*

Associate Editors H. B. G. CASIMIR *Eindhoven* G. J. DIENES *Brookhaven* JACQUES FRIEDEL *Paris*

E. M. LIFSHITZ *Moscow*

Editorial Advisory Board

U.S.A.

E. N. ADAMS, Pittsburgh
D. ALPERT, Illinois
L. APKER, Schenectady
J. BARDEEN, Illinois
D. S. BILLINGTON, Oak Ridge
R. G. BRECKENRIDGE, Cleveland
LEO BREWER, Berkeley, Calif.
E. BURSTEIN, Penn.
J. A. BURTON, New Jersey
N. CABRERA, Virginia
G. C. DANIELSON, Iowa
I. ESTERMANN, Washington, D.C.
J. C. FISHER, Schenectady
F. HERMAN, Princeton
CONYERS HERRING, New Jersey
A. R. VON HIPPEL, Cambridge, Mass
J. H. HOLLOMON, Schenectady
W. V. HOUSTON, Houston
H. B. HUNTINGTON, Troy
H. M. JAMES, Purdue
C. KITTEL, Berkeley, Calif.
W. KOHN, Pittsburgh
J. A. KRUMHANSL, Cleveland
A. W. LAWSON, Chicago
H. W. LEVERENZ, Princeton
O. T. MARZKE, Pittsburgh
B. T. MATTHIAS, New Jersey
L. R. MAXWELL, Silver Spring
JOSEPH E. MAYER, Chicago
E. W. MONTROLL, Maryland
DAVID PINES, Princeton
GEORGE T. RADO, Washington, D.C.
H. REISS, New Jersey
J. R. REITZ, Cleveland
A. ROSE, Princeton
O. C. SIMPSON, Argonne
R. SMOLUCHOWSKI, Pittsburgh
F. H. SPEDDING, Iowa
D. TURNBULL, Schenectady
J. H. VAN VLECK, Harvard
B. E. WARREN, Cambridge, Mass.
EUGENE P. WIGNER, Princeton
B. H. ZIMM, Schenectady

Canada

R. E. BURGESS, Vancouver
D. K. C. MACDONALD, Ottawa
W. B. PEARSON, Ottawa

United Kingdom

A. CHARLESBY, Shrivenham, Berks.
W. J. DUNNING, Bristol
F. C. FRANK, Bristol
H. K. HENISCH, Reading
H. JONES, London
J. W. MITCHELL, Bristol
A. B. PIPPARD, Cambridge
M. H. L. PRYCE, Bristol
R. A. SMITH, Malvern
K. W. H. STEVENS, Nottingham
F. C. TOMPKINS, London

France

E. F. BERTAUT, Grenoble
A. GUINIER, Orsay
LOUIS NÉEL, Grenoble
LOUIS WEIL, Grenoble

Germany

M. BORN, Bad Pyrmont
ULRICH DEHLINGER, Stuttgart
R. HILSCH, Göttingen
G. LEIBFRIED, Aachen
E. MOLLWO, Erlangen
H. PICK, Stuttgart
M. VON LAUE, Berlin
H. WELKER, Erlangen

Italy

F. G. FUMI, Pavia

Czechoslovakia

J. TAUC, Praha

Japan

TOSHINOSUKE MUTO, Tokyo

The Netherlands

A. MICHELS, Amsterdam
G. W. RATHENAU, Amsterdam

Sweden

J. O. LINDE, Stockholm
PER-OLOV LÖWDIN, Uppsala

Switzerland

G. BUSCH, Zurich
P. SCHERRER, Zurich

U.S.S.R.

G. S. ZHDANOV, Moscow

PERGAMON PRESS NEW YORK · LONDON · PARIS LOS ANGELES

Vol. 18
1961

Vol.
19

CONTENTS LISTS FOR VOLUME 18, NOS. 1–4

Volume 18 Number 1

Plastic Crystals and Rotation in the Solid State

	page
J. TIMMERMANS: Preface	iii
J. TIMMERMANS: Plastic crystals: a historical review	1
E. R. ANDREW: Nuclear magnetic resonance in solids containing small molecules	9
J. G. POWLES: Nuclear resonance effects in some molecular crystals having thermal transitions in the solid state	17
W. J. DUNNING: Crystallographic studies of plastic crystals	21
J. A. POPLE and F. E. KARASZ: A theory of fusion of molecular crystals—I. The effects of hindered rotation	28
C. P. SMYTH: Dielectric evidence of molecular rotation in solids	40
L. A. K. STAVELEY: Thermodynamic studies of molecular rotation in solids	46
G. B. GUTHRIE and J. P. MCCULLOUGH: Some observations on phase transformations in molecular crystals	53
J. G. ASTON: Rotational transitions in mixed crystals and surface films	62
W. C. PRICE and G. R. WILKINSON: The study of molecular motion in crystals by infra-red spectroscopy	74
F. A. RUSHWORTH: Nuclear magnetic resonance and diffusion in solids	77
J. S. ROWLINSON: Comments on the papers of (a) J. A. POPLE and F. E. KARASZ, (b) L. A. K. STAVELEY. Reply by J. A. POPLE and F. E. KARASZ	78 78
MANSEL DAVIES and C. CLEMETT: Energy and apparent entropy terms for quasi-spherical molecular rotations	80
J. H. VAN DER WAALS: Some observations on clathrates	82
E. F. WESTRUM, JR.: The thermophysical properties of three globular molecules	83
B. WEINSTOCK: Rotation and molecular distortion in the condensed phases of hexafluoride molecules	86
A. R. UBBELOHDE: Systematic studies of barriers to rotation in crystals	90

Volume 18 Numbers 2/3

H. KRONMÜLLER und A. SEEGER: Die Einmündung in die ferromagnetische Sättigung—II. Theorie des Einmündungsgesetzes in plastisch verformten kubisch-flächenzentrierten Einkristallen	93
R. F. BREBRICK: Composition stability limits of binary semiconductor compounds	116
M. LAMBERT, Ch. MAZIÈRES et A. GUINIER: Precipitation de lithium dans les monocristaux de fluorure de lithium irradiés aux neutrons thermiques	129
T. P. MCLEAN and E. G. S. PAIGE: Electron–hole scattering and minority carrier mobility in germanium	139
M. T. BÉAL: Variation du pouvoir thermoélectrique des alliages métalliques du type CuZnβ en fonction de l'ordre	150
M. T. BÉAL: Sur la résistivité électrique des alliages du type Cu_3Au en fonction de l'ordre	156
LING Y. WEI: Diffusion of silver, cobalt and iron in germanium	162
R. H. KERNOHAN and M. S. WECHSLER: Neutron irradiation of Cu–Al at elevated temperatures	175
JEAN-CLAUDE SOHM: Ionisation par choc des impuretés dans le silicium	181
Y. A. ROCHER et J. FRIEDEL: Aspect phenomenologique de quelques propriétés physiques de Plutonium et des solutions solides Plutonium–Aluminium δ	196
R. J. FRIAUF: Ionic conductivity of thallium chloride	203
J. H. WERNICK and S. E. HASZKO: Manganese rare earth compounds with the $MgZn_2$ structure	207
A. LANDESMAN: Polarisation dynamique en bas champ des protons du paradichlorobenzene	210
D. M. MATTOX and L. GILDART: Energy gaps in bismuth trioxide	215
A. GOLD: Impurity states in solid neon	218
W. L. MEDLIN: Thermoluminescence in anhydrite	238
E. E. HAVINGA: The temperature dependence of dielectric constants	253
Letters to the Editor:	
J. R. KLAUDER and J. E. KUNZLER: Concerning the Fermi surface topology of metals and open orbits from magnetoresistance and Hall effect data	256
H. N. SPECTOR: The existence of Kramers–Kronig relations for the magnetoconductivity tensor	258

Vol. 18
1961

page

D. L. GOLDWATER: The electrolysis of thorium oxide crystals 259

J. AUTH: Uber den Einfluss von Temperatur und äusserer Umgebung auf den Photo-Magneto-Elektrischen (PEM-) Effect bei CdS 261

SHOJI MAKISHIMA, TAKESHI TOMOTSU, MASAO HIRATA, RYOZO KAMBE and SHIGEO SHIONOYA: Polarization of low temperature luminescence from thallium-containing sodium nitrite single crystals 262

A. BERGSTEIN and L. ČERVINKA: To the structure and oxygen content of copper and copper–manganese errite 264

T. TIMUSK: Room temperature luminescence in pure alkali halides 265

J. L. MEIJERING: On the thermodynamics of the Au–Pt system 267

J. C. SLONCZEWSKI: Magnetocrystalline anisotropy of cobalt-substituted manganese ferrite 269

Book Review:

K. MENDELSSOHN: "Cryophysics" (reviewed by H. MEYER) 272

Erratum:

A. MANY, N. B. GROVER, Y. GOLDSTEIN and E. HARNIK: Discussion 272

Volume 18 Number 4

S. FONER, H. MEYER and W. H. KLEINER: Low temperature paramagnetic resonance of trapped O_2 . . 273

L. GILDART, J. M. KLINE and D. M. MATTOX: Some semiconducting properties of bismuth trisulfide . . 286

R. A. SWALIN: Theoretical calculations of the enthalpies and entropies of diffusion and vacancy formation in semiconductors 290

A. HALPERIN and J. NAHUM: Some optical and electrical properties of semiconducting diamonds . . 297

G. EREZ and P. S. RUDMAN: Long-range order in Fe–Al alloys—II. Thermo-electric power 307

D. LIBBY and M. G. ORMEROD: Electron spin resonance spectrum of stretched polyethylene 316

E. FAWCETT: The Fermi surface areas of magnesium, zinc and cadmium 320

R. I. BEECROFT and C. A. SWENSON: An experimental equation of state for sodium 329

A. GLASNER and R. REISFELD: The diffusion constants of thallous (Tl^+) and lead (Pb^{++}) ions in potassium chloride 345

Book Reviews:

R. A. SMITH: "Semiconductors" (reviewed by W. PAUL) 356

L. JOLLY: "Synthetic Inorganic Chemistry" (reviewed by F. G. A. STONE) 357

"Photochemistry in the Liquid and Solid States" (reviewed by V. J. LINNENBOM 358

C. L. ANDREWS: "Optics of the Electromagnetic Spectrum" (reviewed by R. H. MILBURN) 359

Tôme 18 Nº 1

J. TIMMERMANS: Préface iii

J. TIMMERMANS: Plastiques cristallisés. Revue historique 1

E. R. ANDREW: Résonance magnétique nucléaire dans des solides contenant de petites molécules . . 9

J. G. POWLES: Effets de résonance nucléaire dans quelques cristaux moléculaires ayant une transition excitable thermiquement à l'état solide 17

W. J. DUNNING: Etudes cristallographiques des plastiques cristallisés 21

J. A. POPLE et F. E. KARASZ: Une théorie de la fusion des cristaux moléculaires—I. Les effets du blocage de la rotation 28

C. P. SMYTH: Preuve par l'étude des propriétés diélectriques de la rotation moléculaire dans les solides . 40

L. A. K. STAVELEY: Etude thermodynamique de la rotation moléculaire dans les solides 46

G. B. GUTHRIE et J. P. MCCULLOUGH: Quelques observations sur les changements de phase des cristaux moléculaires 53

J. G. ASTON: Transitions de rotation dans les solutions solides et les films 62

W. C. PRICE et G. R. WILKINSON: Etude de la rotation moléculaire dans les cristaux par spectroscopie infrarouge 74

F. A. RUSHWORTH: Résonance magnétique nucléaire et diffusion dans les solides 77

page

J. S. ROWLINSON: Commentaires sur les articles de (a) POPLE et KARASZ, (b) STAVELEY 78
Réponse de POPLE et KARASZ 78
M. DAVIES et C. CLEMMETT: Termes d'énergie et d'entropie apparente pour les rotations des molécules presque sphériques 80
J. H. VAN DER WAALS: Quelques observations sur les clathrates 82
E. F. WESTRUM, JR.: Les propriétés thermophysiques de trois molécules quasi-sphériques 83
B. WEINSTOCK: Rotation et distorsion moléculaire des molécules d'hexafluorure en phase condensée . . 86
A. R. UBBELOHDE: Remarques en guise de conclusion 90

Tôme 18 Nos 2/3

H. KRONMÜLLER et A. SEEGER: Approche de la saturation ferromagnétique—II. Théorie pour les monocristaux cubiques à faces centrées plastiquement déformés 93
R. F. BREBRICK: Limites de stabilité de composés semiconducteurs binaires en fonction de la composition . 116
M. LAMBERT, Ch. MAZIÈRES et A. GUINIER: Précipitation de lithium dans les monocristaux de Fluorure de lithium irradiés aux neutrons thermiques 129
T. P. MCLEAN et E. G. S. PAIGE: 139
M. T. BÉAL: Variation du pouvoir thermoélectrique des alliages métalliques du type CuZnβ en fonction de l'ordre 150
M. T. BÉAL: Sur la résistivité électrique des alliages du type Cu_3Au en fonction de l'ordre 156
LING Y. WEI: Diffusion de l'argent, du cobalt et du fer dans le germanium 162
R. H. KERNOHAN et M. S. WECHSLER: Irradiation aux neutrons de CuAl à haute température . . . 175
JEAN-CLAUDE SOHM: Ionisation par choc des impuretés dans le silicium 181
Y. A. ROCHER et J. FRIEDEL: Aspect phenomenologique de quelques propriétés physiques de Plutonium et des solutions solides Plutonium–Aluminium – 196
R. J. FRIAUF: Conductibilité ionique du chlorure de thallium 203
J. H. WERNICK et S. E. HASZKO: Composés manganèse–terres rares ayant la structure de $MgZn_2$ . . 207
A. LANDESMAN: Polarisation dynamique en bas champ des protons du paradichlorobenzene . . . 210
D. M. MATTOX et L. GILDART: Bandes d'énergie interdites dans le trioxyde de Bismuth 215
A. GOLD: Niveaux d'impureté dans le néon solide 218
W. L. MEDLIN: Thermoluminescence de l'anhydrite 238
E. E. HAVINGA: Dépendance en température des constantes diélectriques 253

Lettres au Rédacteur:

J. R. KLAUDER et J. E. KUNZLER: Sur la topologie de la surface de Fermi des métaux et les orbites ouvertes d'après les données de magnétorésistance et d'effet Hall 256
H. N. SPECTOR: Existence de relations de Kramers-Kronig pour le tenseur de magnéto-conductance . 258
D. L. GOLDWATER: L'électrolyse des cristaux d'oxyde de Thorium 259
J. AUTH: Sur l'influence de la température et de l'environnement extérieur sur l'effet photo-magneto-électrique (P.E.M.) dans CdS 261
S. MAKISHIMA, T. TOMOTSU, M. HIRATA, R. KAMBE et S. SHIONOYA: Polarisation de la luminescence à basse température de monocristaux de nitrite de sodium contenant du thallium 262
A. BERGSTEIN et L. ČERVINKA: Structure et contenu en oxygène des ferrites de cuivre et cuivre-manganèse. 264
T. TIMUSK: Luminescence à la température ambiante des halogénures alcalins purs 265
J. L. MEIJERING: Sur la thermodynamique des systèmes Au–Pt 267
J. C. SLONCZEWSKI: Anisotropie magnétocristalline des ferrites de Manganèse avec du cobalt substitutionnel 269

Revue de Livre:

K. MENDELSSOHN: "Cryophysics" (revu par H. MEYER) 272

Erratum:

A. MANY, N. B. GROVER, Y. GOLDSTEIN et E. HARNIK: Discussion 272

Tôme 18 No 4

S. FONER, H. MEYER et W. H. KLEINER: Résonance paramagnétique à basse température de O_2 piégé . 273
L. GILDART, J. M. KLINE et D. M. MATTOX: Quelques propriétés du trisulfure de bismuth semi-conducteur 286

Vol. 18
1961

page

R. A. SWALIN: Calcul théorique des enthalpies et entropies de formation et de diffusion de lacunes dans les semi-conducteurs 290
A. HALPERIN et J. NAHUM: Quelques propriétés électriques et optiques des diamants semi-conducteurs . . 297
G. EREZ et P. S. RUDMAN: Ordre à longue distance dans les alliages Fe–Al—II. Pouvoir thermoélectrique . 307
D. LIBBY et M. G. ORMEROD: Spectre de la résonance des spins électroniques de polyéthylène étiré . . 316
E. FAWCETT: L'aire de la surface de Fermi du Magnésium, du Zinc et du Cadmium 320
R. I. BEECROFT et C. A. SWENSON: Une équation d'état expérimentale pour le Sodium 329
A. GLASNER et R. REISFELD: Constantes de diffusion des ions thallium (Tl^{+}) et plomb (Pb^{++}) dans le chlorure de potassium 345

Revue des livres:
R. A. SMITH: "Semiconductors" (revu par W. PAUL) 356
L. JOLLY: "Synthetic Inorganic Chemistry" (revu par F. G. A. STONE) 357
"Photochemistry in the Liquid and Solid States" (revu par V. J. LINNENBOM) 358
C. L. ANDREWS: "Optics of the Electromagnetic Spectrum" (revu par R. H. MILBURN) 359

Band 18 Nr. 1

J. TIMMERMANS: Vorwort iii
J. TIMMERMANS: Plastische Kristalle. Ein historischer Rückblick 1
E. R. ANDREW: Kernmagnetische Resonanz in Festkörpern mit kleinen Molekülen 9
J. G. POWLES: Kernmagnetische Effektes in einigen Molekülkristallen, die mangelhafte Umwandlungen im festen Zustande besitzen 17
W. J. DUNNING: Kristallographische Untersuchungen plastischer Kristalle 21
J. A. POPLE und F. E. KARASZ: Eine Theorie der Bildung von Molekülkristallen—I. Der Einfluss der behinderten rotation 28
C. P. SMYTH: Dielektrischer Nachweis der Molekülrotation in Festkörpern 40
L. A. K. STAVELEY: Thermodynamische Untersuchungen der Molekülrotation in Festkörpern 46
G. B. GUTHRIE und J. P. MCCULLOUGH: Einige Beobachtungen über Phasentransformationen in Molekülkristallen. 53
J. G. ASTON: Rotationsumwandlungen in Mischkristallen und Oberflächenschichten. 62
W. C. PRICE und G. R. WILKINSON: Die Untersuchung der Molekülbewegung in Kristallen mit der Infrarot-Spektroskopie 74
F. A. RUSHWORTH: Kernmagnetische Resonanz und Diffusion in Festkörpern 77
J. S. ROWLINSON: Bemerkungen zur Veröffentlichung von (a) POPLE und KARASZ, (b) STAVELEY . . 78
Erwiderung von POPLE und KARASZ 78
M. DAVIES und C. CLEMMETT: Energie und Scheinbare Entropieglieder bei quasisphärischen Molekülrotationen 80
J. H. VAN DER WAALS: Einige Beobachtungen an Clathraten 82
E. F. WESTRUM, JR.: Die thermophysikalischen Eigenschaften von drei kugelförmigen Molekülen. . . . 83
B. WEINSTOCK: Rotation und molekulare Verzerrungen in der kondensierten Phasen der Hexafluorid-Moleküle 86
A. R. UBBELOHDE: Zusammenfassende Bemerkungen 90

Band 18 Nr. 2/3

H. KRONMÜLLER und A. SEEGER: Die Einmündung in die ferromagnetische Sättigung—II. Theorie des Einmündungsgesetzes in plastisch verformten kubisch-flächenzentrierten Einkristallen 93
R. F. BREBRICK: Stabilitätsgrenze der Zusammensetzung binärer Halbleiter-Verbindungen. 116
M. LAMBERT, Ch. MAZIÈRES und A. GUINIER: Ausscheidung des Lithiums in Einkristallen des Lithiumfluorids, welches mit thermischen Neutronen bestrahlt wurde 129
T. P. MCLEAN und E. G. S. PAIGE: Streuung von Elektronen an Defektelektronen und die Beweglichkeit der Minoritätenladungsträger in Germanium 139
M. T. BÉAL: Die Abhängigkeit der thermoelektrischen Kraft der metallischen Verbindungen des Typs CuZnβ von der Ordnung 150

page

M. T. BÉAL: Über den elektrischen Widerstand der Legierungen vom Typ Cu_3Au in Abhängigkeit von der Ordnung . . . 156

LING Y. WEI: Diffusion von Silber, Kobalt und Eisen in Germanium . . . 162

R. H. KERNOHAN und M. S. WECHSLER: Bestrahlung von Cu–Al mit Neutronen bei erhöhten Temperaturen . 175

JEAN-CLAUDE SOHM: Stossionisation von Verunreinigungen in Silizium . . . 181

Y. A. ROCHER und J. FRIEDEL: Phänomenologische Betrachtung einiger physikalischer Eigenschaften des Plutoniums und der festen δ-Legierungen des Plutonium-Aluminium . . . 196

R. J. FRIAUF: Ionenleitfähigkeit von Thalliumchlorid . . . 203

J. H. WERNICK und S. E. HASZKO: Verbindungen der Struktur $MgZn_2$ von Mangan mit seltenen Erden . . 207

A. LANDESMAN: Dynamische Polarisation der Protonen bei kleinen Feldstärken in Paradichlorbenzol . . 210

D. M. MATTOX und L. GILDART: Energielücken in Wismuttrioxyd . . . 215

A. GOLD: Verunreinigungen in festem Neon . . . 218

W. L. MEDLIN: Thermolumineszenz in Anhydrit . . . 238

E. E. HAVINGA: Die Temperaturabhängigkeit der dielektrischen Konstanten . . . 253

Briefe an den Herausgebar:

J. R. KLAUDER und J. E. KUNZLER: Über die Fermioberfläche bei Metallen und offene Elektronenbahnen aus Messungen des magnetischen Widerstandes und des Halleffektes . . . 256

H. N. SPECTOR: Die Existenz der Kramers-Kronig Beziehung für den magnetischen Leitfähigkeitstensor . 258

D. L. GOLDWATER: Die Elektrolyse von Thoriumoxydkristallen . . . 259

J. AUTH: Uber den Einfluss von Temperature und äusserer Umgebung auf den Photo-Magneto-Elektrischen (PEM-) Effect bei CdS . . . 261

S. MAKISHIMA, T. TOMOTSU, M. HIRATA, R. KAMBE und S. SHIONOYA: Polarisation der Tieftemperatur-Lumineszenz von Natriumnitrit-Einkristallen die Thallium enthalten . . . 262

A. BERGSTEIN und L. ČERVINKA: Über die Struktur und den Sauerstoffgehalt von Kupfer und Kupfer-Mangan Ferriten . . . 264

T. TIMUSK: Lumineszenz bei Raumtemperatur in reinen Alkalihalogeniden . . . 265

J. L. MEIJERING: Über die Thermodynamik des Au-Pt-Systems . . . 267

J. C. SLONCZEWSKI: Die magnetokristalline Anisotropie von kobaltsubstituierten Manganferriten . . 269

Büchbesprechung:

K. MENDELSSOHN: "Cryophysics" (besprochen von H. MEYER) . . . 272

Erratum:

A. MANY, N. B. GROVER, Y. GOLDSTEIN und E. HARNIK: Diskussion . . . 272

Vol. 18
1961

Band 18 Nr. 4

S. FONER, H. MEYER und W. H. KLEINER: Paramagnetische Resonanz von eingefangenem O_2 bei tiefen Temperaturen . . . 273

L. GILDART, J. M. KLINE und D. M. MATTOX: Einige Halbleitereigenschaften von Wismuttrisulfid . . 286

R. A. SWALIN: Theoretische Berechnung der Enthalpien und Entropien der Diffusion und Bildung von Leerstellen in Halbleitern . . . 290

A. HALPERIN und J. NAHUM: Einige optische und elektrische Eigenschaften von halbleitenden Diamanten . 297

G. EREZ und P. S. RUDMAN: Fernordnung in Fe–Al Legierungen—II. Die Thermoelektrische Kraft . . 307

D. LIBBY und M. G. ORMEROD: Das Elektronenspin Resonanzspektrum von gezogenem Polyäthylen . . 316

E. FAWCETT: Die Fermioberflächen von Magnesium, Zink und Cadmium . . . 320

R. I. BEECROFT und C. A. SWENSON: Eine experimentelle Zustandsgleichung für Natrium . . . 329

A. GLASNER und R. REISFELD: Die Diffusionskonstanten von Thallium-(Tl^+) und Blei-(Pb^{++}) Ionen in Kaliumchlorid . . . 345

Büchbesprechungen:

R. A. SMITH: "Semiconductors" (besprochen von W. PAUL) . . . 356

L. JOLLY: "Synthetic Inorganic Chemistry" (besprochen von F. G. A. STONE) . . . 357

"Photochemistry in the Liquid and Solid States" (besprochen von V. J. LINNENBOM) . . . 358

C. L. ANDREWS: "Optics of the Electromagnetic Spectrum" (besprochen von R. H. MILBURN) . . 359

Том 18 На. 1

page

И. Тиммерманс: Предисловие iii
И. Тиммерманс: Пластические кристаллы. Исторический обзор 1
Е. Р. Андрю: Ядерный магнитный резонанс в твердых телах, содержащих малые молекулы 9
И. Г. Поулес: Ядерные резонансные эффекты в некоторых молекулярных кристаллах, имеющих тепловые переходы в твердом состоянии 17
В. Даннинг: Кристаллографические исследования пластических кристаллов . . 21
Дж. Попл, Ф. Карасс: Теория спекания молекулярных кристаллов. 1. Эффект затрудненного вращения. 28
К. Смит: Диэлектрические свидеталрства молекулярного вращения в твердых телах . 40
Л. А. К. Ставлей: Термодинамические исследования молекулярного вращения в твердых телах 46
Г. Б. Гутри, Дж. МакКуллоу: Некоторые наблюдения фазовых переходов в молекупярных кристаллох 53
Дж. Астон: Вращательные переходы в смешанных кристаллах и поверхностные пленки 62
В. Прайс, Г. Р. Вилкинсон: Исследование молекулярного движения в кристаллах с помощью инфра-красной спектроскопии 74
Ф. А. Рушворт: Ядерный магнитный резонанс и диффузия в твердых телах. . . . 77
Дж. С. Роулинсон: Замечания о статьях (а) Попла и Карасса 78
(б) Ставлея. Ответ Попла и Карасса 78
М. Девис, К. Клеметт: Энергия и кажущаяся энтропия для квази-сферического молекулярного вращения 80
Дж. ван дер Ваальс: Некоторые наблюдения клатратов 82
Е. Ф. Веструм мл.: Термофизические свойства трех глобулярных молекуи. . . . 83
Б. Вейнштох: Вращение и молекулярные нарушения в конденсированных фазах гексафлюорита 86
А. Р. Уббелоде: Заключительные замечания 90

Том 18 На. 2/3

Г. Кронмюлер и А. Зегер: Разгрузка в ферромагнитную насыщенность—II Теория закона разгрузки пластически формированных кубовидных гранецентрированных ионокристаллов 93
Р. Ф. Бребрик: Пределы стабильности соединения двойных Полупроводниковых смесей 116
М. Ламберт, Ш. Мазиер, и А. Гиние: Осаждение лития в ионокристаллах фтористого лития облучённых тепловыми нейтронами 129
Т. П. МакЛин и Е. Пэйдж: Рассеяние электронов на дурках и подвижность малочисленных носителей в германии 139
М. Т. Биил: Изменение термоэлектрической силы в металлических соединениях типа βCuZn в зависимости от степени упорядочения 150
М. Т. Биил: Об электрическом сопротивлении соединений типа Cu_3Au в зависимости от степени упорядоченности 156
Л. Вей: Диффузия серебра, кобальта и железа в германии 162
Р. Г. Керноган и М. С. Векслер: Облучение нейтронов Cu–Al при высоких температурах 175

page

Жан-Клод Сом: Ионизация загрязнении ударом в кремноземе 181

И. А. Роше и Ж. Фридель: Феноменологические аспекты некоторых свойств плутония и твердых растворов плутония и алюминия 196

Р. Фриауф: Ионная проводимость хлорида таллия 203

Дж. Верник и С. Хазко: Соединения марганца с редкоземельными элементами со структурой типа $MgZn_2$ 207

А. Ландесман: Динамическая поляризация протонов в парадихлорбензене в слабых полях 210

Д. М. Маттокс, Л. Гилдарт: Энергетические щели в триокиси висмута 215

А. Голд: Состояния примесей в твердом чеоне 218

В. Л. Медлин: Термолюминесценция ангидрита 238

Е. Е. Хавинга: Температурная зависимость диэлектрическох постоянных 253

Письма в редакцию:

Ж. Р. Клаудер и Ж. Е. Кунцлер: К конфигурации поверхности "Ферми" металлов и открытых орбит от магнитного сопротивления и данных "Холл-эффекта" . . 256

Г. Н. Спектор: Существование соотношений Крамерса-Кронига для тензора магнито-проводимости 258

Д. Л. Голдуотер: Электролиз кристаллов окиси тория 259

И. Аут: О влиянии температуры и внешних условий на фотоэлектромагнитный эффект в CdS 261

Ш. Макишима, Т. Томотсо, М. Хирата, Р. Камбе, Ш. Шионойя: Поляризация низкотемпературной люминесценции монокристаллов нитрита натрия, содержащию таллий. 262

А. Бергштейн, Л. Червинка: О структуре и содержании кислорода в медно-марганцевом феррите 264

Т. Тимуск: Люминесценция чистых щелочногалоидных соединений при комнатной температуре 265

Дж. И. Мейеринг: К термодинамике системы Au–Pt 267

И. Слончевский: Магнитная анизотропия марганцево-замещенного феррита . . 267

Рецензия на книгу:

К. Мендецсон: "Cryophysics" (рецензент Г. Мейя) 272

Опеуатка 272

Том 18 На. 4

С. Фонер, Г. Майер, В. Клейнер: Низкотемпературный парамагнитный резонанс в захваченном O_2 273

Л. Гилдарт, Дж. Клин, Д. М. Маттокс: Некоторые полупроводниковые свойства трисульфида висмута 286

Р. А. Свалин: Теоретическое вычисление энтгальпии и энтропии диффузии и образования вакансий в полупроводниках 290

А. Гальперин, Дж. Нахум: Некоторые оптические и электрические свойства полупроводящих алмазов 297

Г. Эрец, П. С. Рудман: Дальний порядок в сплавах Fe–Al—II. Термоэлектродвижущая сила 307

Vol. 18
1961

page

Д. Либби, М. Ормерод: Спектр электронного спинового резонанса в растянутом полиэтилене 316

Е. Фосетт: Площади поверхностей Ферми магния, цинка и кадмия 320

Р. Беекрофт и К. Свенсон: Эмпирическое уравнение состояния натрия 329

А. Гласнер, Р. Рейсфельд: Коэффициенты диффузии ионов таллия и свинца в хлориде калия 345

Рецензии на книги:

Р. А. Смит: "Semiconductors" (рецензент У. Пол) 356

Л. Жолли: "Synthetic Inorganic Chemistry" (рецензент Ф. Дж. А. Стон) . . 357

"Photochemistry in the Liquid and Solid States" (рецензент В. ДЖ. Линненбом) . 358

С. Л. Андруз: "Optics of the Electromagnetic Spectrum" (рецензент Р. Г. Милбурн) . 359

AUTHOR INDEX TO VOLUME 18

(B) denotes book review (E) denotes erratum

Andrew, E. R. 9
Aston, J. G. 62
Auth, J. 261
Béal, M. T. 150, 156
Beecroft, R. I. 329
Bergstein, A. 264
Brebrick, R. F. 116
Červinka, L. 264
Clemett, C. 80
Davies, M. 80
Dunning, W. J. 21
Erez, G. 307
Fawcett, E. 320
Foner, S. 273
Friauf, R. J. 203
Friedel, J. 196
Gildart, L. 215, 286
Glasner, A. 345
Gold, A. 218
Goldstein, Y. 272 (E)
Goldwater, D. L. 259
Grover, N. B. 272 (E)
Guinier, A. 129
Guthrie, G. B. 53
Halperin, A. 296
Harnik, E. 272 (E)
Haszko, S. E. 207
Havinga, E. E. 253
Hirata, M. 262
Kambe, R. 262
Karasz, F. E. 28, 78
Kernohan, R. H. 175
Klauder, J. R. 256
Kleiner, W. H. 273
Kline, J. M. 286
Kronmüller, H. 93
Kunzler, J. E. 256
Lambert, M. 129
Landesman, A. 210
Libby, D. 316
Linnenbom, V. J. 358 (B)
Makishima, S. 262
Many, A. 272 (E)
Mattox, D. M. 215, 286
Mazières, Ch. 129
McCullough, J. P. 53
McLean, T. P. 139
Medlin, W. L. 238
Meijering, J. L. 267
Meyer, H. 272, 273 (B)
Milburn, R. H. 359 (B)
Nahum, J. 297
Ormerod, M. G. 316
Paige, E. G. S. 139
Paul, W. 356 (B)
Pople, J. A. 28, 78
Powles, J. G. 17
Price, W. C. 74
Reisfeld, R. 345
Rocher, Y. A. 77
Rowlinson, J. S. 78
Rudman, P. S. 307
Rushworth, F. A. 77
Seeger, A. 93
Shionoya, S. 262
Slonczewski, J. C. 269
Smyth, C. P. 40
Sohm, J–C. 181
Spector, H. N. 258
Staveley, L. A. K. 46
Stone, F. G. A. 357 (B)
Swalin, R. A. 290
Swenson, C. A. 329
Timmermans, J. iii, 1
Timusk, T. 265
Tomotsu, T. 265
Ubbelohde, A. R. 90
Waals, van der, J. H. 82
Wechsler, M. S. 175
Wei, L. Y. 162
Weinstock, B. 86
Wernick, J. H. 207
Westrum, E. F., Jr. 83
Wilkinson, G. R. 74

J. Phys. Chem. Solids Pergamon Press 1961. Vol. 18, No. 1, pp. 1–8. Printed in Great Britain.

PLASTIC CRYSTALS: A HISTORICAL REVIEW

PROFESSOR J. TIMMERMANS

Sometime Professor of Physical Chemistry, Free University of Brussels

Vol. 18
1961

IN THIS short historical survey, I hope to give, to the best of my ability, the early experimental evidence concerning plastic crystals, and I apologize in advance if there remain some important gaps in my text, since I am a specialist in the study of physical properties of organic compounds, but am not so learned, either in inorganic chemistry or in theoretical physics.

Some twenty-five years ago, while collecting data for my book: *Les Constantes Physiques des Composés Organiques Cristallisés*, I saw directly, when I came to the chapter on the stoichiometry of the heat of melting, that the molecular heat of fusion and freezing temperature increase in ascending a homologous series. I tried to nullify this effect by dividing the values of the molecular heat by the absolute temperature of melting to obtain the molecular entropy of melting. There was, however, still no constancy of the melting entropy in a homologous series. However, some peculiar compounds, of usually relatively simple constitution, had a very low entropy of melting. These compounds were "globular", that is they were either symmetrical around their centre (CH_4, CCl_4, pentaerythritol, etc.); or would give a sphere by rotation around an axis (cyclohexane, camphor, etc.). All these compounds had an entropy of melting lower than 5 e.u. (cal deg^{-1} $mole^{-1}$), a quantity I represent by the symbol σ, and so far this arbitrary limit has not been exceeded. Thus cyclohexane with σ equal to 2·27, is globular, while methylcyclohexane with σ equal to 11·00 is non-globular; the reason seems to be that in methylcyclohexane, the lateral CH_3-group would stop the rotation.

The comparative study of many other properties of organic crystals revealed that such compounds had many other remarkable values of their constants. Usually their melting point is relatively high. While n-pentane melts at −141°C, tetramethylmethane melts at −16°C. However, they have a transition point lower down, with a high value of the entropy of transition (for $C(CH_3)_4$, this is at −133° with $\sigma = 4{\cdot}40$).

Table 1 classifies certain organic compounds from this point of view as either globular (column 1) or non-globular (column 2).

With a high melting point goes a high saturated vapour pressure of the plastic crystals. The triple point ($V+L+S$) may be higher than atmospheric pressure, so that sometimes, under ordinary pressure, the crystals sublime directly—as C_2Cl_6 does—instead of melting first.

Between the melting and the transition points, they crystallize almost all in the cubic system, the system with the highest symmetry, and take another form below the transition points; (cyclopentane, although globular, is hexagonal). In some cases the transition takes place in two steps, as with hexachloroethane and hydrogen chloride. Fig. 1 illustrates this for a globular molecule $C(CH_3)_4$ (one transition) and a non-globular molecule, normal-C_5H_{12}, which has no transition in the crystal.

This similarity in the symmetry of globular compounds explains how it is possible that substances so different from the chemical point of view as methane and argon are able to give a continuous series of mixed crystals. It explains also that the two stereochemical antipodes of such compounds give, not a racemate, but a series of mixed crystals, with constant melting point, as has formerly been found for camphor (see Fig. 2). Prof. ASTON will tell us more about this question.

The American School of physical chemists has collected very numerous data on the change of specific heat of crystals on heating. And so one

finds that—in cyclopentane for example—the specific heat of the plastic crystals rises on lowering of the temperature, instead of falling as usual. This is shown in Fig. 3. where the heat capacity (C_p) of cyclopentane is plotted against the temperature.

In some cases, as with methyl alcohol, the transition from ordinary to plastic crystals by heating is preceded by a very high value of C_p just under the transition point as is shown in Fig. 4.

In another direction, SMYTH and his collaborators, in particular, have studied the change of dielectric constant with temperature, and here also plastic crystals behave in a peculiar way. Usually when freezing, the dielectric constant of a substance falls markedly; but, with many plastic crystals the dielectric constant continues to rise on lowering the temperature, the curve for the plastic state being almost continuous with the curve for the liquid, and falling sharply only at the transition point. This is illustrated in Fig. 5 for methyl chloroform.

And finally, Dr. MICHILS, for his doctoral dissertation, has made comparative measurements

Table 1. *Classification of Molecules*

Globular compounds	Non-globular compounds
Inorganic Substances	
A, Xe	—
HCl	HF
H_2S	H_2O
H_3P	H_3N
H_4Si	Cl_4Si
CO	CO_2
DCl	D_2O
SF_6	—
Organic Substances: Fatty Series	
CH_4, CD_4, CH_3D	C_2H_6
C_2H_2	CH = CH
$C(CH_3)_4$	$C(C_2H_5)_4$
CF_4, CCl_4, CBr_4	CH_2Cl_2
$CCl(CH_3)_3$, $CCl_2(CH_3)_2$	$CHCl_3$
CCl_3CH_3, $CClF_2CH_3$	$CClH_3$
$CCl(CH_3)_2NO_2$	CCl_2HCH_2Cl
$C(NO_2)_4$	$CH(NO_2)_3$
$C(SCH_3)_4$	$C(SC_2H_5)_4$
C_2Cl_6, C_2F_6, C_2F_5Cl	C_2HCl_5
$C_2(CH_3)_6$, $C_2Cl(CH_3)_5$	—
$C(CH_3)_3C_2H_5$, $CH(CH_3)_2CH(CH_3)_2$	—
$CH(CH_3)_2C(CH_3)_2C_2H_5$	—
$C(CH_3)_3C(CH_3)_2C_2H_5$	$C(CH_3)_3CH(CH_3)C_2H_5$
$C(CH_3)_3CH(CH_3)CH(CH_3)_2$	—
$C(CH_3)_3CH = CH_2$	$CH_3CH_2CH = CHCH_2CH_3$
$CH_3CH = CHCH = CHCH_3$	—
CH_3OH, CH_3OD	C_2H_5OH
$(CH_3)_3COH$, $(CH_3)_3CSH$	—
$CH_3CH(OH)_2$	—
$(CH_3)_2C_2H_5COH$	$CH(CH_3)_2CH_2CO_2H$
$C(CH_3)_3CO_2H$, CCl_3CO_2H	CH_2ClCO_2H
$CC1_3C_6H_5$	$CH_2ClC_6H_5$
$(CNCH_2)_2$	Malonitrile, Glutaronitrile.

Table 1 (continued)

Globular compounds	Non-globular compounds
Heterocyclics	
Azocyclohexane Endomethylene piperazine Tropinone Camphor anhydride Tetrahydrofurane Thiocyclohexane	Piperidine Piperazine Thiophene Cineol Furane Dioxane
Cyclic Series	
Polymethylenes	
In C_4: Perfluorcyclobutane In C_5: 1,1 and 1,2-*cis*-Dimethylcyclopentane 1,1,2-*trans*-Trimethylcyclopentane Cyclopentanol, Cyclopentadienol Cyclopentyl chloride, Perfluorcyclopentane In C_6: Cyclohexane, Cyclohexylchloride Cyclohexanol, Cyclohexanone, α-Hexachlorcyclohexane, Cyclohexene 1,3-Cyclohexadiene, 1,4-Cyclohexadione Cyclohexylfluoroform, 1,1 and 1,2-*cis* Dimethylcyclohexane In C_8 and C_9: Ketone	Cyclobutanone Methylcyclopentane, 1,3 and 1,2-*trans* Dimethylcyclopentane Cyclopentene, Cyclopentanone, Cyclopentylamine, Cyclopentylnitrile, Cyclopentanone, Methylcyclopentanol Methylcyclohexane, 1,3, 1,4 and 1,2- *trans*-Dimethylcyclohexane β-Hexachlorcyclohexane, Cyclohexylamine Cyclohexanoxime Menthane
Condensed Cyclics	
Decahydronaphthalene Dicyclopentadiene Dihydro and tetrahydrodicyclopentadiene-α : Alcohol, Ketone, Oxide and Bioxide Tetrahydrohydrindane	Tricyclopentadiene
Bridged Cyclics	
Endomethylenecyclohexane, Camphene Camphenilane, Isocamphane, Camphenilone Norcamphor, Norpinane, Pinane, Tricyclene Endoethylenecyclohexane	Fenchane : Alcohol and Ketone
Camphor Group	
Camphane, Isobornylane, Bornylene, Bornyl and Isobornyl chloride, 2,6 and 2,10 Dichlorcamphane, Borneol and Isoborneol, Bornylamine, Camphor, Thiocamphor, 2,3-Camphanedione, 3-Cyanocamphor, Camphoroxime and Camphorquinone.	3-Camphor : Chloride, Bromide, Sulfone, Sulfonamide, Sulfoxide, and Sulfochloride

Vol. 18
1961

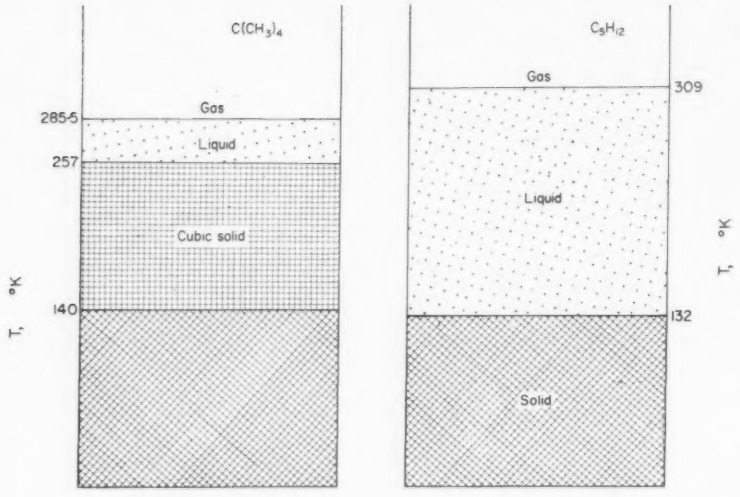

FIG. 1. Phases for neopentane (globular) compared with those for normal pentane (non-globular).

Vol. 19

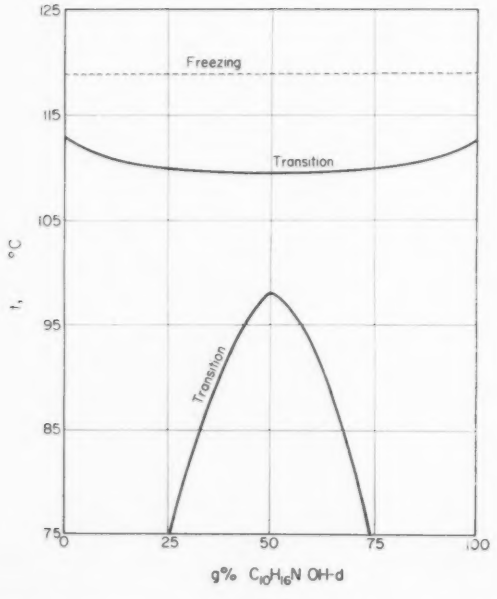

FIG. 2. Freezing-point–composition diagram for solid solutions of D- and L- camphoroxime.

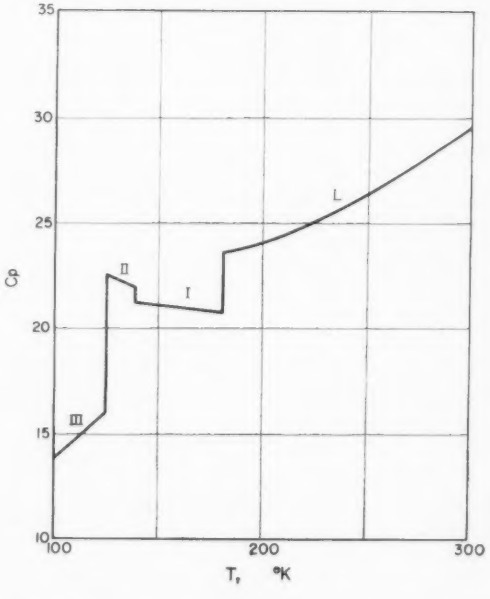

FIG. 3. Heat capacity–temperature curve for cyclopentane (a globular molecule).

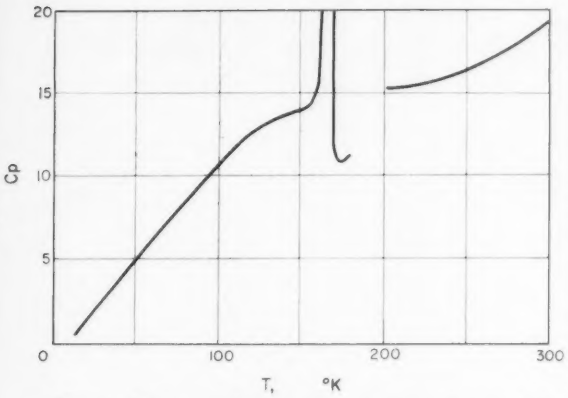

FIG. 4. Heat capacity–temperature curve for methyl alcohol (a globular molecule)

of the plasticity of these unusual substances, a few degrees higher and lower than their transition point, and has found that, for example with C_2Cl_6, they flow through a hole under a pressure which is more than ten times smaller in the plastic state than below the transition temperature.

Examples are given in Table 2 for the substances shown in column 1 along with entropy of fusion shown in column 2. The third and fourth columns give, respectively, the crystal form for the crystals stable above (I) and below (II) the transition. The fifth and sixth columns give the pressure to produce flow through a hole of forms I and II respectively. The example of 1,4-dichlorobenzene is of a case where evidently the form above the transition is not a plastic crystal as indicated by the high entropy of fusion, 13·4 e.u. In this case there is little difference between the two pressures. In all cases, where the entropy of fusion is lower than 5 e.u, the form stable above the transition flows at a pressure at most one half of that required for the form stable below.

Later on, I did find that formerly a few authors had observed some of the characteristics of plastic crystals, without realizing the importance of the subject, or at least in considering them as very special phenomena.

BRUNI and his co-workers have measured the molecular lowering of the freezing point of cyclohexane as a solvent, and I remember how struck we were, both my colleague at Brussels the late Professor CHAVANNE, and myself, when a student prepared pure cyclohexane from benzene, by the catalytic method of hydrogenation of Sabatier, and confirmed BRUNI's high value of the molecular lowering of the freezing point. Some

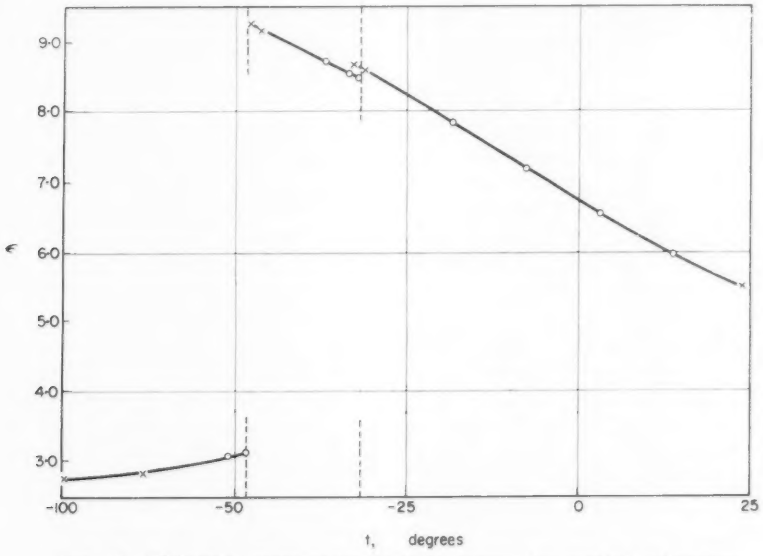

FIG. 5. Dielectric constant–temperature curve for methyl chloroform (a globular molecule).

Vol. 18
1961

Table 2. Comparison of flow properties of plastic and non-plastic crystals.

Substance	Q/T, cal deg^{-1} mole^{-1}	Crystall. form I	Crystall. form II	P, Kg/cm^2	
				Form I	Form II
CBr_4	2·4	Cubic	Monocl.	247	1,500
C_2Cl_6	4·3	Cubic	Triclin.	about 250	3,600
$C_2(CH_3)_6$	4·5	Cubic	—	—	—
Camphor-D	2·8	Cubic	Rhomb.	247	454
Borneol-D	4·1	—	—	240	864
Camphor anhydride	4·0	—	Orthor.	760	1,500
Camphoroxime	1·3	—	—	—	1,940
D-Bromcamphor-α	27·6	Cubic	Monocl.	1,960	—
Fenchylic alc. D	5·8	—	—	650	—
Naphthalene	13·3	Monocl.	—	2,240	—
Hexamethylbenzene	11·0	Triclin.	—	2,800	—
1-4-Dichlorbenzene	13·4	Monocl. I	Monocl. II	740	1,150
Dotriacontane	55·7	Orthor.	—	1,200	—
Stearic acid	39	Monocl.	Monocl.	1,120	—

years later, camphor was also used as a solvent by organic chemists, because the high value of that lowering has made possible the measurement of molecular weights with ordinary thermometers.

During the thirties, PAULING and later BERNAL explained some anomalies of ammonium salts by making the assumption of rotation of the molecules inside the crystal.

Our colleague PIRSCH, some 25 years ago, in a systematic survey of cyclic polymethylenes and their derivatives has discovered many other compounds of the plastic crystals series.

And just before the war, some of our Japanese colleagues had begun the study of this same kind of crystals by electronic microscopy, the last paper of this group of research workers being that of Professor NITTA, of Osaka: they found by this method that in the plastic state crystals give diagrams similar to those of liquids and not to those of real crystals.

And finally, a few years ago, my collaborator Dr. TRAPPENIERS, who is now Professor of Physical Chemistry in Gröningen (Netherlands), made a very interesting contribution to the problem, in combining the views of my colleague at Brussels, Professor PRIGOGINE, with my own notions about plastic crystals. Accepting the freezing diagram, under high pressure, of BRIDGMAN for CCl_4 as standard, he applied the idea of corresponding states to the similar diagram for CBr_4, taking their triple points as corresponding states: I had myself compared these two diagrams of BRIDGMAN many times, thinking that it was impossible that two such isomorphous compounds would not be similar also under high pressure, but without avail. With his theory, TRAPPENIERS found that in the diagram of BRIDGMAN there was a gap, in which there was a transition curve that this author was unable to detect fifty years ago because the difference of volume of the two phases was too small. TRAPPENIERS was able to detect it, almost exactly in the region where it was expected, by using a sensitive method of piezometric analysis developed in my own laboratory. The phase diagrams for CCl_4 and CBr_4 are compared in Fig. 6. This is, to my knowledge, the first time that the theory of corresponding states has been quantitatively applied, with success, to crystals.

In considering this large domain, I think that we are able to make certain general conclusions. The phenomenon of melting is not very easy to understand because our theoretical knowledge of the inner state of liquids is much more superficial than for crystals and gases. At the end of the last century, the discovery of liquid crystals had proved that the melting process is a superposition of two different effects, although both result from the thermal movements of molecules. When the temperature is high enough, the thermal energy becomes so great that the crystal boundaries

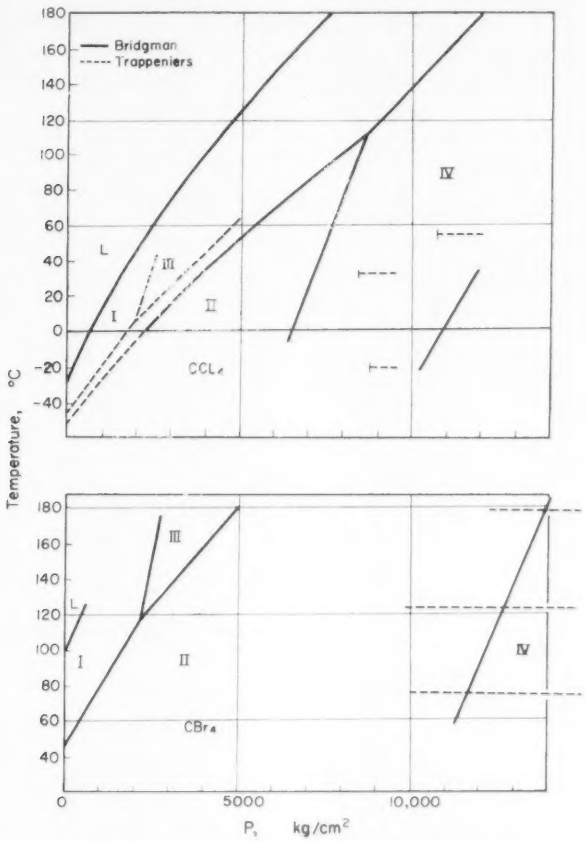

FIG. 6. Temperature–pressure equilibrium diagrams for CCl_4 and CBr_4.

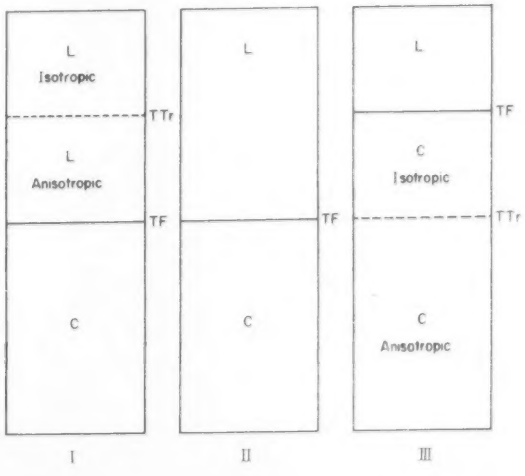

FIG. 7. Phases for systems giving: I. crystal, anisotropic liquid and isotropic liquid; II. crystal and liquid; III. anisotropic crystal, isotropic crystal and liquid (C = crystal; L = liquid).

Vol. 18
1961

are broken and the substance liquefies; if there is room, the free molecules then begin to turn in all directions, giving an isotropic liquid, as usual. The compounds which give anisotropic liquids are generally very long molecules which, because of double bonds, are unable to bend, having the shape of a string, and which need much space to rotate freely. Therefore, some directions in the liquids are privileged and it remains anisotropic, till the higher transition point where, by expansion, it becomes isotropic.

In the plastic crystals, on the contrary, the freedom to rotate exists already in the crystal state, because they are globular in shape, but the coherence of the crystal is broken only at a higher temperature, the melting point. In the two cases, the liquefaction and the isotropy do not happen at the same temperature. In liquid crystals, by heating, the fluidity comes first, but in plastic crystals, the isotropy comes first. This is illustrated in Fig. 7. They are complementary from this point of view, as I pointed out, in my first paper on the subject, in forging the nomenclature of the globular compounds, or plastic crystals.

Vol.
19

J. Phys. Chem. Solids Pergamon Press 1961. Vol. 18, No. 1, pp. 9–16. Printed in Great Britain.

NUCLEAR MAGNETIC RESONANCE IN SOLIDS CONTAINING SMALL MOLECULES

E. R. ANDREW

Department of Physics, University College of North Wales, Bangor, Caernarvonshire

Abstract—The reorientation and diffusion of molecules in the solid state may be revealed through the narrowing which they cause of the nuclear magnetic resonance spectrum. It is shown in outline how the nature of the motion can be determined and how, through measurements of the spin–lattice relaxation time, the kinetics of the motion may be investigated. Examples are given of rotational motion in solids containing small molecules. The effect of macroscopic rotation of a crystal is also described. A table is given of organic molecular solids in which self-diffusion has been established by nuclear magnetic resonance work. All have at least one phase transition in the solid state: for most of them the entropy of transition is much greater than the entropy of melting. All are compact, globular molecules and show considerable rotational freedom in the solid state.

Vol. 18
1961

OVER THE past twelve years nuclear magnetic resonance has proved to be a valuable tool in studying the motion of atoms and molecules in the solid state. Briefly summarized, the main information that is obtained is as follows:

(a) It is possible to tell whether a molecule or group is performing a rotational motion. The rotation is often not free, but consists rather in the reorientation of the molecule or group between a number of equilibrium positions. The method is sensitive; the threshold frequency for detection of the motion is usually a few kc/s. The method can be applied to both polar and non-polar molecules.

(b) The nature of the rotational motion can usually be established. One can determine whether the whole molecule reorients or only a part of it, and whether the motion is about one axis or is more general.

(c) The temperature-dependence of the rate of the motion can generally be determined.

(d) The diffusion of atoms, ions and molecules can be detected, and in favourable cases the rate of migration and its temperature dependence may be determined.

This knowledge is extracted from two pieces of experimental information, namely the nuclear magnetic resonance spectrum and the nuclear spin–lattice relaxation time. A full investigation of any solid will embrace measurements of both over as wide a range of temperature as possible. The temperature-dependence of the spectrum frequently suffices to establish the existence and nature of the motion; the kinetics of the motion are determined from the spin-lattice relaxation time.

It is well-known that the nuclear magnetic resonance spectrum of a solid is usually much broader than that of a liquid. For a solid the spectral breadth is generally of the order 10^3 c/s (or of the order of one gauss in terms of field strength) whereas for a liquid the breadth may be only one c/s or so wide (or one milligauss or so in terms of field strength). Although there are many sources of spectral broadening in solids the mechanism which predominates in most of our examples is the magnetic dipolar interaction between the nuclei. Molecular motion modifies and in general reduces the average dipolar interaction, causing a narrowing of the observed spectrum; observation of spectral narrowing thus serves to indicate the existence of the motion.

A simple example is provided[1] by 1,2-dichloroethane, for in this material the protons occur in fairly well-separated pairs. Consider one pair of protons, whose internuclear vector $\mathbf{r}$ is inclined at an angle θ to the applied field $\mathbf{H}_0$. Using a classical argument, one nuclear dipole μ would subject its neighbour to a local magnetic field whose component parallel to $\mathbf{H}_0$ is $\mu\mathbf{r}^{-3}$ $(3\cos^2\theta - 1)$. If the dipole can take up either of two orientations parallel

and antiparallel to $\mathbf{H}_0$, we might expect that a single crystal containing many similarly-oriented pairs would have a spectrum consisting of two lines; when measured with fixed frequency these lines would be found at $H_0 \pm \mu r^{-3}(3\cos^2\theta - 1)$. This simple argument does give the right form of the spectrum and the correct angular dependence, though a perturbation calculation, carried out by PAKE[2], provides a factor $\frac{3}{2}$ in the separation of the doublet. The angular factor plays an important role in our discussion, and it is therefore worth seeing that it does in fact arise from a proper calculation.

The dipolar interaction between each pair of protons has the form

$$\mathcal{H}_1 = \mu^2 r^{-3}[\boldsymbol{\sigma}(1)\cdot\boldsymbol{\sigma}(2) - 3(\boldsymbol{\sigma}(1)\cdot\mathbf{p})(\boldsymbol{\sigma}(2)\cdot\mathbf{p})], \tag{1}$$

where $\mathbf{p}$ is a unit vector along $\mathbf{r}$, and $\boldsymbol{\sigma}(1)$ and $\boldsymbol{\sigma}(2)$ are the two nuclear spin operators. Expanding the scalar products in (1), and omitting terms which are not diagonal in the Zeeman representation we get [2]

$$\mathcal{H}_1^1 = \tfrac{1}{2}\mu^2 r^{-3}(3\cos^2\theta - 1)[\boldsymbol{\sigma}(1)\cdot\boldsymbol{\sigma}(2) - 3\sigma_z(1)\sigma_z(2)]. \tag{2}$$

Taking triplet spin functions the three perturbed energy eigenvalues are

$$E_m = -2m\mu H_0 + \mu^2 r^{-3}(3\cos^2\theta - 1)(2 - 3m^2), \quad m = 0, \pm 1. \tag{3}$$

Transitions between adjacent levels thus lead to the two resonance lines given by

$$h\nu = 2\mu[H_0 \pm \tfrac{3}{2}\mu r^{-3}(3\cos^2\theta - 1)]. \tag{4}$$

Doublets of this form were observed by PAKE[2] in single crystal hydrates. If a polycrystalline specimen is used the observed spectrum is the sum of the doublets from crystallites of all orientations, whose separations range from zero to $3\mu r^{-3}$. The spectrum of 1,2-dichloroethane at 90°K was thus found by GUTOWSKY and PAKE[1] to be a broad double-humped curve, the separation between the peaks being 12 G or approximately $3\mu r^{-3}$. Between 160° and 180°K the spectrum was found to narrow to half this width, though retaining the same shape. Little change occurred on further heating until the melting point was reached, when the very narrow spectrum, characteristic of liquids, was observed.

The halving of the spectral width in the vicinity of 170°K is ascribed to reorientation of each molecule about its axis of least moment of inertia, which is normal to both proton-pair directions. The angle θ is now a function of time, and using the geometry of Fig. 1 we may write

$$(3\cos^2\theta - 1) = -\tfrac{1}{2}(3\cos^2\alpha - 1) + \tfrac{3}{2}\sin^2\alpha\cos 2\theta(t). \tag{5}$$

When the rotational motion is sufficiently rapid the mean dipolar interaction must be considered.

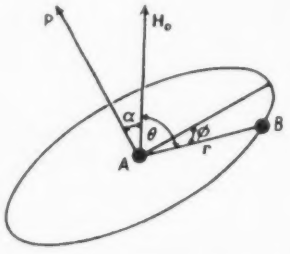

FIG. 1. Diagram illustrating the rotation of a pair of nuclei A and B about an axis AP normal to the line joining them. The applied magnetic field $\mathbf{H}_0$ makes an angle α with the axis of rotation. (Reproduced from the article by ANDREW E. R. and NEWING R. A., *Proc. Phys. Soc. Lond.* **72**, 959 (1958), by kind permission of the Institute of Physics and the Physical Society).

If the reorientation has at least 3-fold symmetry the mean value of $(3\cos^2\theta - 1)$ is given by the first term on the right in (5), since the mean of the second term is zero. The mean interaction is therefore obtained by replacing $(3\cos^2\theta - 1)$ in (2) by $-\frac{1}{2}(3\cos^2\alpha - 1)$. The spectrum for similarly oriented pairs is therefore a doublet given by

$$h\nu = 2\mu[H_0 \pm \tfrac{3}{4}\mu r^{-3}(3\cos^2\alpha - 1)]. \tag{6}$$

The angular dependence is the same as for the static pairs; the spectrum for polycrystalline material containing rotating molecules should, in agreement with observation, have the same shape but half the width of that for polycrystalline material containing static molecules. In 1,2-dichloroethane the axis of reorientation is not an axis of symmetry, but the approximate halving of spectral width

suggests that the rotational motion is nevertheless fairly symmetrical about the axis.

If the axis of rotation is not normal to the internuclear vector but is inclined at an angle γ with respect to it, then expression corresponding to (5) is

$$(3\cos^2\theta-1) = \tfrac{1}{2}(3\cos^2\alpha-1)(3\cos^2\gamma-1)+ \\ +\tfrac{3}{2}\sin 2\alpha \sin 2\gamma \cos\theta\,(t) \\ +\tfrac{3}{2}\sin^2\alpha \sin^2\gamma \cos 2\theta\,(t). \qquad (7)$$

The mean value is given by the first term on the right; the factor by which the spectral width is reduced is therefore $\frac{1}{2}|3\cos^2\gamma-1|$ for polycrystalline material.

When the molecule contains more than two interacting nuclei the part of the Hamiltonian expressing the dipolar interactions is the sum of terms such as (1) or (2) from each pair in the system. The perturbation problem has been solved for systems of three and four nuclei but becomes difficult for larger systems. In these situations VAN VLECK'S[3] classic calculation by a diagonal sum method of the mean square width and other even moments of the spectrum is of great value. The mean square width (second moment) for material containing only one magnetic species of nucleus is given by

$$S = \tfrac{9}{4}\mu^2 \sum_n (3\cos^2\theta_n-1)^2 r_n^{-6}, \qquad (8)$$

where the sum is taken over all neighbours of a representative nucleus; this expression clearly gives the right answer for the doublet spectrum of pairs of nuclei given by (4). With polycrystalline material the angular term in (8) must be replaced by its isotropic average, giving

$$S = \tfrac{9}{5}\mu^2 \sum_n r_n^{-6}. \qquad (9)$$

Such sums converge rapidly and may be readily calculated; comparison between theoretical and experimental values of S can yield useful structural information. When molecules are reorienting it would appear therefore that we should replace every factor $(3\cos^2\theta_n-1)$ in (8) by its mean using (7); thus for polycrystalline material every term in the sum in (9) is to be multiplied by its reduction factor $[\frac{1}{2}(3\cos^2\gamma_n-1)]^2$. The procedure works well, and the correctness of any postulated motion may be tested by comparing the calculated reduced second moment with that found experimentally.

Benzene provides a good example. In the solid state each molecule is found[4] to reorient about its hexad axis, which is normal to all intra-molecular proton pair directions. The second moment should therefore be reduced by a factor 1/4. The observed reduction (Fig. 2) is somewhat greater, and the slight discrepancy is accounted for by consideration of the intermolecular contributions to the sum in (9).

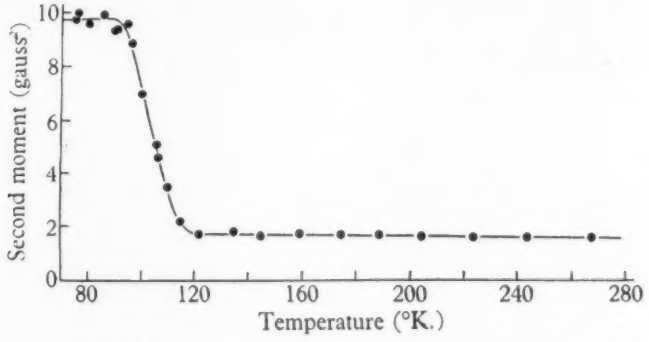

FIG. 2. Variation with temperature of the second moment of the recorded proton magnetic resonance spectrum for polycrystalline benzene.[4] As explained in the text only the horizontal portions of the graph below 90°K and above 120°K have quantitative significance. (Reproduced from *Nuclear Magnetic Resonance* by E. R. ANDREW, Cambridge University Press, p. 171, by kind permission of the publishers).

Vol. 18
1961

The more general the motion, the smaller is the average of $(3\cos^2\theta - 1)$, and the narrower does the resonance spectrum become. Some materials exhibit well-defined successive drops in linewidth and second moment. One example is solid cyclohexane[5] (Fig. 3). The first fall in second moment between 150° and 175°K is quantitatively accounted for by reorientation of the cyclohexane molecules about their triad axes. The second fall hand while the entropy of melting of benzene is 8·6 e.u., that of cyclohexane is only 2·2 e.u. though its entropy of transition is 8·6 e.u. Similarly the increase in molar volume of benzene on melting is 14 per cent while for cyclohexane it is only 5 per cent, though the increase at the transition is 8 per cent. While the lower phase of solid cyclohexane is comparable with that of solid benzene, there is clearly much greater molecular

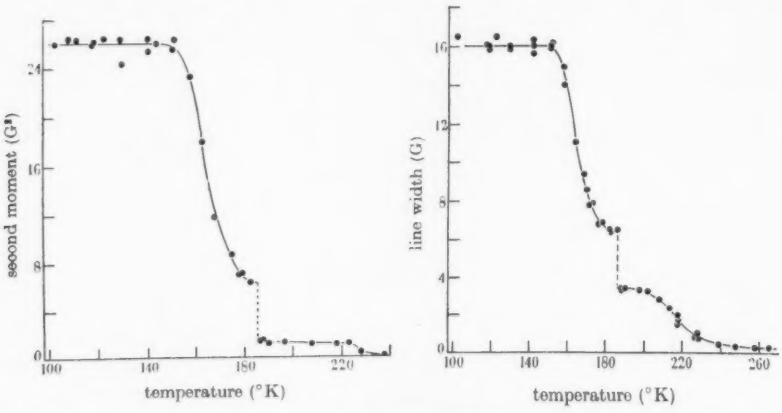

FIG. 3. Variation with temperature of the line width and the second moment of the proton magnetic resonance absorption spectrum for polycrystalline cyclohexane.[5] (Reproduced from *Nuclear Magnetic Resonance* by E. R. ANDREW, Cambridge University Press, p. 172, by kind permission of the publishers).

accompanying the first-order phase change at 186°K is caused by an almost isotropic reorientation of the molecules. The isotropic average of $(3\cos^2\theta - 1)$ is zero, and therefore the contribution of intramolecular pairs to the sums in (8) and (9) becomes very small; the relative motion of protons in different molecules is not isotropic however, and these residual intermolecular interactions account for the second moment of 1·4 G^2 just above 186°K. Above 220°K, and still well below the melting point, even this contribution disappears. This implies an isotropic relative motion of protons in different molecules, and indicates that self-diffusion of the molecules is taking place.

A comparison of the behaviour of benzene and cyclohexane is of some interest since they are both non-polar hydrocarbons of similar molecular weight and, within a degree, have the same melting points and boiling points. On the other freedom in the upper phase, and this is doubtless associated with the more globular shape of the molecules.

Some more recent examples of three successive reductions in spectral width are provided by hexamethyldisilane[6], 2,2- and 2,3-dimethylbutane[7] (Fig. 4). Although in these and many other solids phase transitions with considerable entropy release reflect the considerable freedom of the molecules, it is worth noting that in others, as for example benzene, nuclear magnetic resonance has detected molecular reorientation without there being any such obvious thermal indication.

The procedure for calculating the motionally-reduced second moment needs some justification, since it has been argued[8] on theoretical grounds that the second moment should remain invariant. Our procedure was to replace the factor

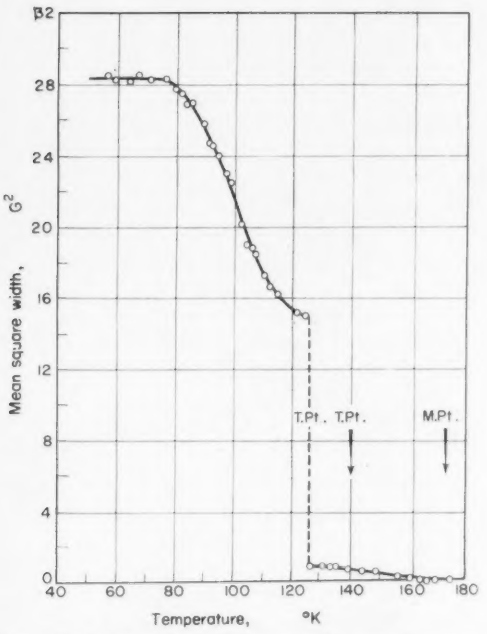

FIG. 4. Variation with temperature of the second moment of the proton magnetic resonance absorption spectrum for polycrystalline 2,2-dimethylbutane.[7]

$(3\cos^2\theta - 1)$ in the perturbation Hamiltonian (2) by its average value given by the first term in (7), omitting the time-dependent terms whose mean is zero. It is the omission of these time-dependent terms which leads to the apparent discrepancy. If the rotation were uniform we could replace $\theta(t)$ by $\omega_r t$ in (7), where ω_r is the angular velocity of rotation. These terms now provide a periodic perturbation which endows the resonance spectrum with sidebands set at frequencies $n\omega_r$, where n is any integer, on either side of the central spectrum. The analysis of this problem is formally similar to that in which the main field is modulated, a perturbation which also generates sidebands; the perturbation may be regarded as frequency-modulating the Larmor frequency. When these sidebands are included, the second moment does indeed remain invariant[9].

These sidebands were revealed by experiments which we carried out recently[10]. The ^{23}Na resonance was observed in a crystal of sodium chloride which was rotated macroscopically at high speed. All nuclear pairs rotate at the same uniform speed. If in particular we choose α, the angle between the axis of rotation and the applied field, to be $\cos^{-1}(1/\sqrt{3})$ or 54°44′, then equation (7) shows that the mean value of $(3\cos^2\theta - 1)$ is zero at high speed just as in the case of isotropic reorientation. In Fig. 5 are shown derivative recordings for the static crystal, and for the crystal rotated at 810 c/s. In the latter case a narrow central line is obtained flanked by sidebands, the first three of which are visible on either side. When the sidebands are included, the second moments of both spectra are the same. As the speed of rotation is increased the sidebands move out and their intensity falls approximately as ω_r^{-2} in order to preserve their contribution to the second moment; at very high speeds they become unobservably weak and we are just left with the narrowed central line. The experiment confirms quite clearly the theoretical criterion that a spectrum is narrowed when the rate of motion is of the order of the spectral width, in practice of order 10^3 c/s.

When molecules reorient within a solid the rotation is not uniform but has a random character expressible as a Fourier distribution of rotational frequencies up to frequencies of order $1/\tau_c$, where τ_c is the correlation time of the random motion.

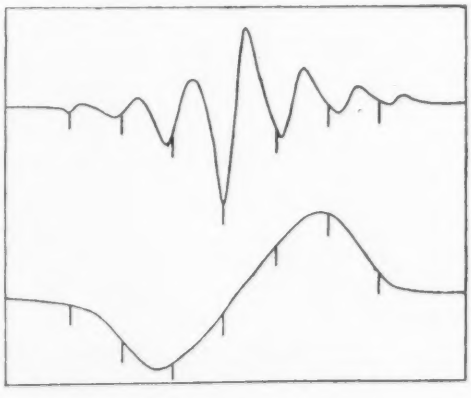

FIG. 5. The upper curve is the derivative spectrum for ^{23}Na in a crystal of sodium chloride rotated at 810 c/s about an axis making an angle 54°44′ with the direction of the applied field. The lower curve is the derivative spectrum for the static crystal. The marks are 790 c/s apart. (Reproduced from the article by ANDREW E. R., BRADBURY A. and EADES R. G., *Nature, Lond.* **183,** 1802 (1959) by kind permission of the editors).

Vol. 18
1961

The sidebands are therefore thinly distributed over a range of frequencies, and if $1/\tau_c$ greatly exceeds the linewidth the sidebands are unobservably weak. Though their inclusion would render the second moment independent of the rate of motion, in practice only the narrowed central portion of the spectrum is recorded. It must therefore be noted that in diagrams such as Figs. 2, 3 and 4 only the horizontal portions, representing rigid or reduced second moments are significant; the second moment in the falling portions in which spectral narrowing is actually taking place are dependent on the sensitivity of the apparatus, since this determines the ability of the apparatus to record the sidebands as they disappear in the wings of the spectrum. Attempts to calculate the temperature-dependence of τ_c from this falling portion are therefore fraught with considerable uncertainty.

The best way of obtaining the temperature-dependence of τ_c is through measurement of the temperature-dependence of the nuclears pin–lattice relaxation time T_1. The fluctuating interaction caused by molecular motion effects transition through the non-diagonal terms in $\mathscr{H}_1$, and attempts to restore thermal equilibrium between the spin system and the lattice. At temperatures for which $1/\tau_c$ is of the same order as the resonance frequency this interaction is particularly effective and T_1 is shortest; at either higher or lower temperatures T_1 is longer. From the theoretical dependence of T_1 on τ_c, measurements of the tem-

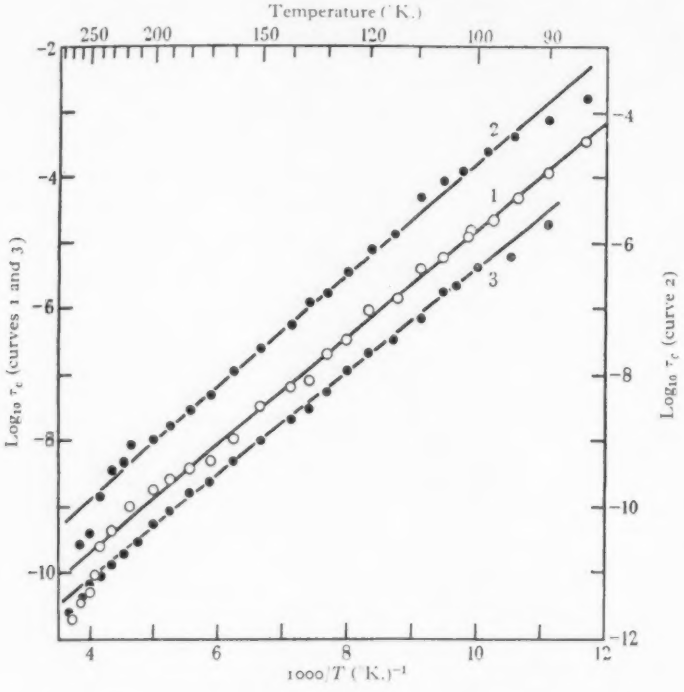

FIG. 6. Plot of $\log_{10}\tau_c$ against $1/T$ for polycrystalline benzene. Curve 1, C_6H_6; curve 2, C_6H_5D; curve 3, 1,3,5-$C_6H_3D_3$; from the slopes of the straight lines the barrier heights were all found to be $3{\cdot}7 \pm 0{\cdot}2$ kcal/mole.[5] (Reproduced from *Nuclear Magnetic Resonance* by E. R. ANDREW, Cambridge University Press, p. 179, by kind permission of the publishers).

perature-dependence of T_1 can be converted to give the temperature-dependence of τ_c. Often a plot of log τ_c against the reciprocal of temperature gives a straight line (for example benzene, Fig. 6) enabling an activation energy to be determined for the reorientation.

When one seeks to summarize the nuclear magnetic resonance information for small molecules one is struck by the dearth of accurate data for many of the smallest. Several investigations have been made of solid hydrogen [11–16] and some attention has been paid to methane[17,18]; both exhibit considerable rotational freedom in the solid state and also provide examples of self-diffusion. The hydrogen halides, H_2S and H_2Se were examined in the solid state by ALPERT[19] twelve years ago and showed clear evidence of motional narrowing; a re-examination of these materials would probably now be worthwhile. Solid ammonia, ethane, ethylene and disilane have not been examined systematically and many related compounds not at all, probably because the interesting region of temperature for many of these materials lies between 40° and 100°K. Of those small molecules, particularly non-polar molecules, which have been examined it may be generalized that if there is some symmetry or roughly globular shape without protruding side groups, then some form of restricted rotation is usually observed. Methyl groups in particular are usually found to exhibit reorientation about their three-fold axes. Where almost isotropic rotational motion is found, self-diffusion is frequently found also[20]. The table lists organic molecular solids which have been found by the nuclear magnetic resonance method to exhibit self-diffusion. All have one or more phase-transitions, and the entropy of transition is often much greater than that of melting. The molecules are all rather compact and more or less globular in shape.

Table 1. *Organic molecular solids exhibiting self-diffusion.*

Compound	n.m.r. reference	melting point, °K	transition point, °K	entropy melting, e.u.	entropy transition, e.u.
methane	17, 18	91	20	2·5	λ
neopentane	1, 21, 22	257	140	3·0	4·4
2,2-dimethylbutane	7	174	127	0·8	10·2
			141		0·5
2,3-dimethylbutane	7	144	136	1·3	11·4
cyclopentane	23	179	122	0·8	9·5
			138		0·6
cyclopentene	24	138	87	5·8	1·3
cyclohexane	5	280	186	2·2	8·6
cyclohexanol	25	298	263	1·4	7·5
methyl alcohol	1, 26	176	157	4·0	λ
hexafluoroethane	1	173	104	3·7	8·6
methyl chloroform	1, 21, 22	240	224	4·3	8·0
2,2-dichloropropane	22	239	187	3·3	>4
t-butyl chloride	21, 22	248	183	1·9	2·3
			220		6·4
t-butyl bromide	21	257	209	1·8	6·5
			232		1·1
hexamethyldisilane	6	288	222	2·5	10·5

REFERENCES

1. GUTOWSKY H. S. and PAKE G. E., *J. Chem. Phys.* **18,** 162 (1950).
2. PAKE G. E., *J. Chem. Phys.* **16,** 327 (1948).
3. VAN VLECK J. H., *Phys. Rev.* **74,** 1168 (1948).
4. ANDREW E. R. and EADES R. G., *Proc. Roy. Soc.* **218A,** 537 (1953).
5. ANDREW E. R. and EADES R. G., *Proc. Roy. Soc.* **216A,** 398 (1953).

Vol. 18
1961

6. YUKITOSHI T., SUGA H., SEKI S. and ITOH J., *J. Phys. Soc. Japan* **12,** 506 (1957).
7. EADES R. G., EL SAFFAR Z. M. and LLEWELLYN J. P., to be published.
8. PAKE G. E., *Solid State Physics* **2,** 1 (1956).
9. ANDREW E. R. and NEWING R. A., *Proc. Phys. Soc. Lond.* **72,** 959 (1958).
10. ANDREW E. R., BRADBURY A. and EADES R. G., *Arch. Sci. Genève* **11,** 223 (1958); *Nature, Lond.* **182,** 1659 (1958), **183,** 1802 (1959).
11. HATTON J. and ROLLIN B. V., *Proc. Roy. Soc.* **199A,** 222 (1949).
12. REIF F. and PURCELL E. M., *Phys. Rev.* **91,** 631 (1953).
13. SUGAWARA T., MASUDA Y., KANDA T. and KANDA E., *Sci. Rep. Tohoku Univ.* **A7,** 67 (1955).
14. TOMITA K., *Proc. Phys. Soc. Lond.* **68,** 213 (1955).
15. BLOOM M., *Physica* **23,** 767 (1957).
16. SMITH G. W. and HOUSLEY R. M., *Phys. Rev.* **117,** 732 (1960).
17. THOMAS J. T., ALPERT N. L. and TORREY H. C., *J. Chem. Phys.* **18,** 1511 (1950).
18. TOMITA K., *Progr. Theor. Phys. Osaka* **8,** 138 (1952); *Phys. Rev.* **89,** 429 (1953).
19. ALPERT N. L., *Phys. Rev.* **75,** 398 (1949).
20. ANDREW E. R., *Report of* 1954 *Bristol Conference on Defects in Crystalline Solids* **60** (1955).
21. POWLES J. G. and GUTOWSKY H. S., *J. Chem. Phys.* **21,** 1695 (1953).
22. STEJSKAL E. O., WOESSNER D. E., FARRAR T. C. and GUTOWSKY H. S., *J. Chem. Phys.* **31,** 55 (1959)
23. RUSHWORTH F. A., *Proc. Roy. Soc.* **222A,** 526 (1954).
24. LAWRENSON J. I. and RUSHWORTH F. A., *Proc. Phys. Soc. Lond.* **72,** 791 (1958).
25. AVERBUCH P., *C. R. Acad. Sci. Paris* **244,** 3147 (1957).
26. COOKE A. H. and DRAIN L. E., *Proc. Phys. Soc. Lond.* **65,** 894 (1952).

Vol. 19

J. Phys. Chem. Solids Pergamon Press 1961. Vol. 18, No. 1, pp. 17–20. Printed in Great Britain.

NUCLEAR RESONANCE EFFECTS IN SOME MOLECULAR CRYSTALS HAVING THERMAL TRANSITIONS IN THE SOLID STATE

J. G. POWLES

Physics Department, Queen Mary College, University of London

I SHOULD like to discuss the relaxation of nuclear magnetism in some molecular crystals having thermal transitions. The reader is referred to a recent review[1] and the previous paper (E. R. ANDREW, this Conference) for a more general discussion of the effects of molecular motion in magnetic resonance.

The thermal transitions under discussion and the corresponding solid state phases have been studied in a variety of ways and are more common in molecular crystals than might generally be supposed (see Ref. (2) and J. TIMMERMANS, this Conference). The method of measurement most directly comparable to nuclear magnetic resonance (n.m.r.) is that of dielectric polarization. I illustrate this with reference to a series of tetrasubstituted methanes for which fairly extensive n.m.r. measurements[3,4] and dielectric measurements are available.[5–8] Fig. 1 shows the values of the proton resonance line width (δH)[3] and spin–lattice relaxation time (T_1)[4] for methyl chloroform. The line narrowing centred at about $-130°C$ is due to methyl group C_3 reorientation. The manner of the reorientation of the CH_3 group has received considerable attention[28,29,4] but will not be discussed here. The line narrowing at $-70°C$ may be connected with an additional motion such as that of $-CCl_2CH_3$ becoming effective. (t.p.) is a weak and rather doubtful thermal λ point and little effect on δH is observed nor on T_1 except that it seems difficult to preserve the high temperature phase below it (Fig. 1, upper T_1 curve). At t.p., an important λ point occurs and there is a considerable change in both δH and T_1. This is also the temperature at which the dielectric constant rises and so the whole molecule no doubt becomes free to reorient at a considerable rate here. The rate of molecular reorientations must be much greater than about 10^4 c/s and must be about more than one axis. It is also necessary for the jump rate controlling self diffusion to be greater than a critical value, possibly about 10^2 c/s

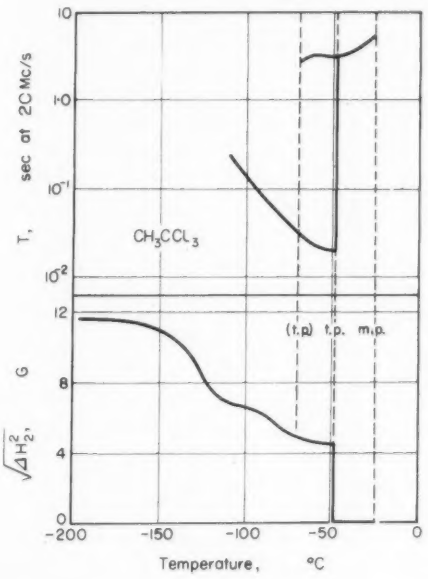

FIG. 1.

here. The T_1 data suggest that the rate of molecular reorientation jumps abruptly from a value below about 10^7 c/s to a value above. An interesting speculation arising from the T_1 behaviour in the supercooled high temperature solid phase is that it "knows" it is supercooled since the $T_1(T)$

behaviour is different from that in the stable temperature range. No n.m.r. measurements have been made in the liquid but the dielectric measurements[8] suggest that the change in thermal motion may not be large. A study of the effect of melting in these crystals by n.m.r. should be relatively easy and they will probably confirm that the melting is a relatively insignificant process as far as molecular reorientation is concerned. Information about the motion of the —C—Cl bonds can be obtained from the chlorine quadrupole magnetic resonance since this affects the resonant frequency. Reorientation of C—Cl by large angles should cause the resonance to "fade out" as indeed it does at about −100°C in methyl chloroform[8]. Valuable information about the same motion is also obtainable from measurements of the quadrupole T_1 and T_2 by the transient method[10]. In fact the T_2 shows an appreciable fall around −125°C possibly indicating C—Cl reorientation but at what rate is difficult to say[11]. In the polar tetrasubstituted methanes which have been measured there is a considerable change in both δH and T_1 at the transition for which the dielectric constant rises. On the other hand at an important thermal transition where there is no apparent change in dielectric properties there is no change in δH or T_1 e.g. in t-butyl chloride. It is interesting to compare t-butyl chloride and t-butyl bromide. In the bromide δH falls (and ϵ_0 rises) at the lower of the two transitions in the solid state and in the chloride this happens at the upper transition, the lower one having no effect on δH[3] and causing no discontinuity in T_1[4]. In neopentane (Fig. 2) the thermal transition does not affect δH but causes a discontinuous rise in T_1. This is understandable because δH and T_1 are sensitive to very different rates of motion. If we assume that the rate of molecular reorientation is greater than about 10^7 c/s below the transition (since $T_1(T)$ has positive slope) then the motion is already completely effective in narrowing δH, in this case to a comparatively large intermolecular value of one gauss. At the thermal transition a sudden increase in rate of motion, by a factor possibly of about 10^2 raises the value of T_1 but still, of course does not affect δH. At sufficiently higher temperature the self diffusion becomes effective in reducing δH and then this slow ($< \nu_r$) motion reduces T_1.

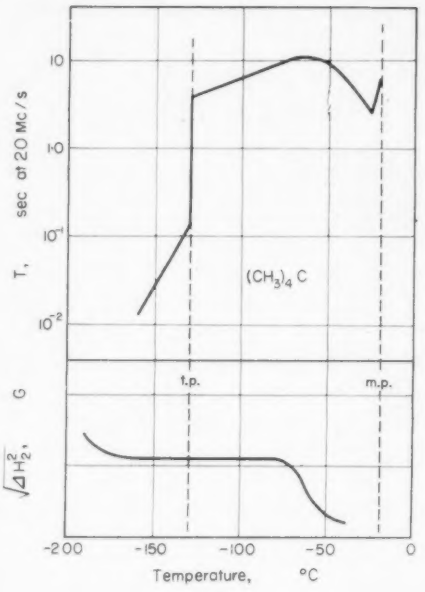

FIG. 2.

Some solid state transitions in solutions have also been detected by n.m.r.[3]

In methyl alcohol[12] (Fig. 3) the λ point results in a discontinuity in T_1 but the melting point has no apparent effect showing the relative insignificance of melting in determining the n.m.r. parameters in this crystal.

Relatively few molecules with phase transitions in the solid have been investigated. We exclude

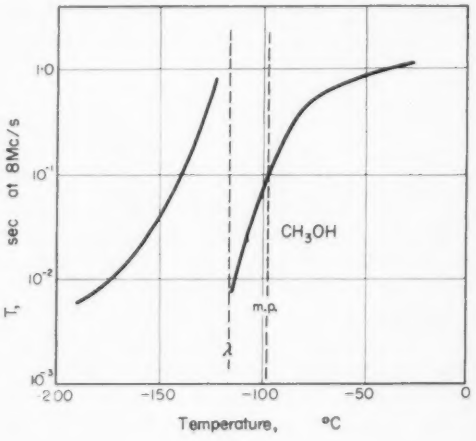

FIG. 3.

hydrogen and methane since the reorientation processes here are probably rather different in nature. An important group, the hydrogen halides, were studied some time ago[13] and these measurements would bear repeating with the improved techniques available now. There is a discontinuous fall in δH at the sharp transition in HCl but not to so low a value as might have been expected from the dielectric properties[14]. Similarly in HBr the important λ point at $-184°C$, where there is known to be a considerable change in dielectric correlation frequency[15,16], seems to have little effect on δH as do the other two transitions. Similarly for HI.

The n.m.r. effects of the thermal transitions in cyclopentane[17], cyclopentene[18], cyclohexane[19] and cyclohexene[20] have been investigated. Some peculiar effects have been found in cyclic dimethyl siloxanes.[33]

If we pass to long molecules the situation may possibly be expected to be simpler since one imagines that such molecules reorient most easily about one axis only, that of the chain, although the actual motion is undoubtedly more complex. In some long chain paraffins there is a phase transition in the solid[23] at which a limited line narrowing occurs e.g. in n-octacosane and dicetyl[21]. A simple explanation in terms of reorientation of some or all of the molecules about their long axes does not work too well[21,22]. However these materials are difficult in that the upper phase only exists in a small temperature interval, there is the possibility of various crystalline forms[23] and small traces of impurity molecules can have important effects, particularly in n.m.r.

When we pass to really long molecules the difficulties multiply because we do not have 100 per cent crystallinity and generally speaking it is more difficult to observe the n.m.r. signal from the crystalline regions than from the amorphous ones. We must also of course take care to distinguish clearly real thermal transitions from glass transitions and so forth which are presumably related to the amorphous regions. Even the concept of melting in the crystalline part of a polymer needs care. There seems to be only one polymer which has thermal transitions, polytetrafluoroethylene (PTFE) and these occur at 20°C and 30°C[24]. It seems likely that these have no effect on δH[25,26] although the difficulties mentioned above are predominant. In most polymers the crystalline melting occurs over a range of temperatures. However in polydimethyl siloxanes the temperature range is quite narrow and then the "melting" has a considerable effect on δH (or T_2)[27]. T_1 in the crystalline phase has not been measured. Other linear polymers such as polymethylene melt sharply but the crystal melting region has not been investigated in detail.

In ammonium bromide the important λ point is reported to have no effect on either δH or T_1[12] and hardly affects δH in the chloride and iodide[31,32], but we shall not discuss this and other examples in *ionic* crystals having solid state transitions.

The present need in this field is for a knowledge of both T_1 and T_2 in all the phases in the solid as well as the liquid state and preferably T_1 for various resonant frequencies. This information is most helpful for protons, when there are some in the molecule, but should really include n.m.r. data for all the magnetic nuclei since they interact together to a greater or lesser extent. When a nucleus such as chlorine occurs its nuclear electric quadrupole relaxation is also of direct interest as already mentioned for methyl chloroform. In due course no doubt more complex n.m.r. measurements such as rotary saturation and double resonance will be valuable.

It should be mentioned that there is at least one instance of a new phase in a molecular crystal being discovered by nuclear quadrupole resonance[30]. Nuclear resonance may well prove valuable in the same way.

Vol. 18
1961

REFERENCES

1. Powles J. G., *Arch. Sci. Genève* (8th Colloque AMPERE) **12,** 87 (1959).
2. Smyth C. P., *Dielectric Behaviour and Structure*, p. 142. McGraw-Hill, New York (1955).
3. Powles J. G. and Gutowsky H. S., *J. Chem. Phys.* **21,** 1695, 1704 (1953).
4. Stejskal E. O., Woessner D. E., Farrar T. C. and Gutowsky H. S., *J. Chem. Phys.* **31,** 55 (1959).
5. Baker W. O. and Smyth C. P., *Ann. N.Y. Acad. Sci.* **40,** 447 (1940).
6. Kushner L. M., Crowe R. W. and Smyth C. P., *J. Amer. Chem. Soc.* **72,** 1091 (1950).
7. Crowe R. W. and Smyth C. P., *J. Amer. Chem. Soc.* **72,** 4009 (1950).
8. Powles J. G., Williams D. E. and Smyth C. P., *J. Chem. Phys.* **21,** 136 (1953).

9. GUTOWSKY H. S. and MCCALL D. W., *J. Chem. Phys.* **32,** 548 (1960).
10. BLOOM M., HAHN E. L. and HERZOG B., *Phys. Rev.* **97,** 1699 (1955).
11. BLOOM M., Ph.D Thesis, University of Illinois (1954).
12. COOKE A. H. and DRAIN L. E., *Proc. Phys. Soc. Lond.* **65,** 894 (1952).
13. ALPERT N. L., *Phys. Rev.* **75,** 398 (1949).
14. PHILLIPS C. S. E., *J. Phys. Radium* **13,** 216 (1952).
15. POWLES J. G., *J. Phys.* **13,** 121 (1952).
16. BROWN N. L. and COLE R. H., *J. Chem. Phys.* **20,** 196 (1952).
17. RUSHWORTH F. A., *Proc. Roy. Soc.* **A222,** 526 (1954).
18. LAWRENSEN I. J. and RUSHWORTH F. A., *Arch. Sci. Genève* (8th Colloque AMPERE) **12,** 116 (1959).
19. ANDREW E. R. and EADES R. G., *Proc. Roy. Soc.* **A216,** 398 (1953).
20. EADES R. G., FINCH N. D. and EL SAFFAR Z. M., *Arch. Sci. Genève* (8th Colloque AMPERE), **12,** 109 (1959).
21. ANDREW E. R., *J. Chem. Phys.* **18,** 607 (1950).
22. POWLES J. G. and KAIL J. A. E., to be published.
23. DANIEL V., *Phil. Mag. Suppl.* **2,** 450 (1953).
24. FURUKAWA G. T., MCCOSKEY R. E. and KING G. J., *J. Res. nat. Bur. Stand.* **49,** 273 (1952).
25. SMITH J. A. S., *Disc. Faraday Soc.* **19,** 207 (1955).
26. POWLES J. G. and KAIL J. A. E., *J. Polymer Sci.* **31,** 183 (1958).
27. POWLES J. G. and HARTLAND A., *Nature, Lond.* **185,** 111 (1960).
28. POWLES J. G. and GUTOWSKY H. S., *J. Chem. Phys.* **23,** 1692 (1955).
29. STEJSKAL E. O. and GUTOWSKY H. S., *J. Chem. Phys.* **28,** 388 (1958).
30. ROSSET J. and BUYLE-BODIN, M., *Arch. Sci. Genève* (8th Colloque AMPERE) **12,** 179 (1959).
31. GUTOWSKI H. S., PAKE G. E. and BERSOHN R., *J. Chem. Phys.* **22,** 643 (1954).
32. BERSOHN R. and GUTOWSKI H. S., *J. Chem. Phys.* **22,** 651 (1954).
33. ROCHON E. G. and LECLAIR H. G., *J. Inorg. Nucl. Chem.* **1,** 92 (1955).

Vol
19

J. Phys. Chem. Solids Pergamon Press 1961. Vol. 18, No. 1, pp. 21–27. Printed in Great Britain.

CRYSTALLOGRAPHIC STUDIES OF PLASTIC CRYSTALS

W. J. DUNNING

Department of Physical and Inorganic Chemistry, University of Bristol

INTRODUCTION

IN THE study of crystal structure by X-ray diffraction methods, it was recognized very early that crystals are not ideally perfect. First there are the static imperfections, one dimensional, two dimensional and three dimensional, exemplified by point defects such as impurities and vacancies, by edge and spiral dislocations, and by stacking faults. Secondly, there are the imperfections which may be conceived as the loss of order in an ideal perfect crystal. HERRMANN and KRUMMACHER[1] in 1932 postulated that there were nineteen ways in which order could be lost and they characterized the kind of diffraction pattern which would result from every degree of order; as order is lost sharp diffraction maxima degenerate into streaks, patches and three dimensional diffuse volumes in reciprocal space. We are not concerned here with all these possibilities but mainly with the effects of thermal motions in rendering indefinite the positions of the atoms or molecular groups about mean positions in the lattice.

X-RAY STUDIES

A good deal of work has been carried out on the study of the effect of thermal motions on the intensities of Bragg reflections from a crystal. The effect can be understood since the frequency of X-rays is about 10^{18} sec^{-1} and that of the thermal motion 10^{13} sec^{-1} or less; hence the radiation sees a lattice in which atoms or groups are randomly displaced with respect to the mean geometrical planes. The radiation scattered by the displaced atoms is out of phase and this modifies the contributions of the atoms to the structure amplitude. The actual intensity I of the diffracted beam is related to the intensity I_R, which it would have if the atoms were at rest, by the Debye factor

$$I = I_R \exp\left(-\frac{B \sin^2\theta}{\lambda^2}\right),$$

where $B = 8\pi^2 \overline{u^2}$. In this $\overline{u^2}$ is the mean square amplitude of vibration in a direction normal to the reflection plane. Since $\sin^2\theta$ enters into this equation, it is to be expected that such disorder will affect reflections of high order more than those of low order and there will be a fall off in intensity at high angles near the edge of the film.

In many crystals, groups of atoms held together by strong covalent forces behave like rigid bodies and execute against the weak van der Waals forces oscillations or librations which are relatively large compared with the intramolecular atomic movements. As the temperature increases, the thermal movement increases the amplitude of the oscillations and librations. In the case of face-centred and body-centred cubic elements, it is thought[2] that when the oscillation amplitude reaches a certain fraction ($\sim 0{\cdot}2$) of the interatomic distance, melting occurs; similarly when the angular amplitude of libration of a group around an axis or point reaches some critical value, the group becomes orientationally disordered or rotates and the crystal undergoes a transition.

The onset of such a transition should be foreshadowed in the low temperature form by an increase in the B factor as the transition temperature approaches. Such a detailed study has not been made on a substance the high temperature form of which constitutes a "plastic crystal" (using Timmermans'[3] terminology) and would probably prove difficult to do. Nevertheless, ABRAHAMS and LIPSCOMB[4] have found analogous results in the high temperature form of thiophene. They found that just below the melting point the thiophene molecules are orientationally disordered around an axis normal to their molecular planes and have a B factor considerably larger than is usually found in organic crystals; this they consider is due to the large degree of thermal motion. In the high temperature form of HCN ($C_{4v}^9 - 14$ mm) DULMAGE and LIPSCOMB[5] found a very large

temperature factor corresponding to a large amplitude of libration normal to the c axis. Some caution appears to be necessary in relating large B factors solely to thermal motion since ROBERTSON *et al.*[6] have found that large B factors in circumanthracene $C_{40}H_{16}$ result from impurity molecules in the lattice.

The thermal expansion coefficients can be related[2] to the magnitude of the thermal vibrations. Since the latter are not necessarily the same in all directions, the coefficients may be anisotropic and their variation with temperature will reflect the changes in the motions of the molecules[7]. As the temperature is increased the librational amplitude attains a critical value and the molecules tend to turn from one (110) plane into the other $(1\bar{1}0)$ plane; this corresponds to the transition point and a discontinuous change in the a/b ratio. Thus the molecules become increasingly disordered with respect to the {101} plane and towards the melting point may approach free rotation.

The refinement of a structure of the low temperature form of plastic crystals may be possible if the atomic motions have not reached an extreme degree and should show on the electron density

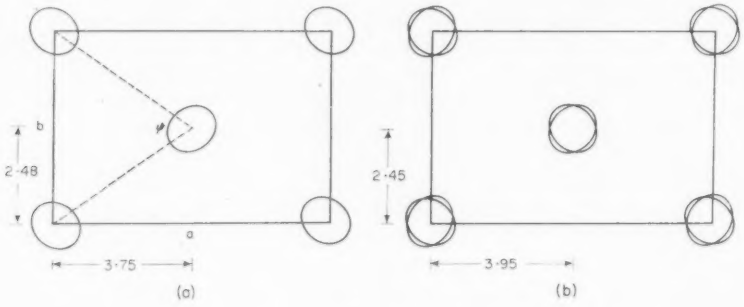

FIG. 1

MUELLER[8] studied a number of orthorhombic modifications of the n-paraffin series C_nH_{2n+2} between room temperature and the melting points and found that as the temperature rises the a axis increases at a greater rate than the b axis. The chains are zig-zag and may be depicted in projection along c as ellipses. Fig. 1(a) illustrates the arrangement at room temperature and Fig. 1(b) is the pattern near the melting point. For $n \geqslant 24$ these hydrocarbons undergo a sudden transition 5 or 10° below the melting point to a second orthorhombic form still similar to Fig. 1(a) but with different a and b axes. Between the transition point and the melting point the angle ψ approaches 60° and the structure becomes hexagonal or pseudo-hexagonal. There is a large expansion in a and a decrease in b. These are the transitions studied by GARNER[9]. The moment of inertia of the chains about the long molecular axis is small and at lower temperatures librations of large angular amplitude take place around this axis. maps contours indicative of large librations. No investigation of this sort has been carried out on "molecules globulaires", though TAUER and LIPSCOMB[10] have shown that in the orthorhombic form of CH_3OH stable above the λ-point, the electron density maps projected along the c-axis indicate that the contours for the CH_3 group are elliptical. This ellipticity arises from an exaggerated decline of reflections with increasing h index traceable to an anisotropic temperature factor with a maximum vibration normal to (100).

Plastic crystals in the form stable at the highest temperatures just below the melting point give X-ray diffraction photographs which frequently have only a very small number of reflections; this is due to the very rapid fall-off in intensity with increasing reflection angle. In addition there is considerable background blackening masking many of the weaker reflections. Whilst both these effects confirm that the crystal is highly disordered, it also means that there is a restriction on the

amount of information which can be used in a structure determination. An extreme case is to be found in the high temperature form of cyclobutane[11] where rotation photographs showed only (110) and (200) reflections: these just suffice to specify a body-centred cubic unit cell. Carbon tetrachloride just below the melting point diffracts very poorly and prolonged exposures are necessary; above the heavy background only five reflections were observed[12]. POST *et al.*[13] found only strong (111), (200) and weak (220) (222) reflections on an oscillation diagram of neohexane (2,2 dimethyl butane). Seven reflections were recorded for neopentane[14] and nine reflections for adamantane (symmetrical tricyclodecane)[15]. In the case of chinuclidin, $CH(CH_2CH_2)_3N$, NOWACKI[16] reported ten reflections observed against strong background blackening. The systematic absences characterized a face-centred cubic unit cell but not the space group. The number of reflections and their relative intensities were not sufficient to decide whether the molecules were rotating freely or were statistically disordered in orientation. An investigation of the effect of temperature on the X-ray diffraction of the cubic forms would provide some information on this point. It is possible that nearer to its melting point (268°C) the diffraction of adamantane would show fewer lines than at room temperature; this appears to be the case with cyclohexane[17].

PAULING[18], who was the first to recognize the possibility of rotational disorder of molecules in crystals, pointed out that the rotation of molecules like NH_3 and H_2O about symmetry axes would explain why these molecules can occupy positions in crystals the symmetry elements of which are incompatible with those of the non-rotating molecule. Thus in $Ni(NH_3)_6Cl_2$ the NH_3 molecules lie on four-fold axes and in alum the H_2O molecules lie on three-fold axes; rotation would give the molecules an effective infinite symmetry axis. In many plastic crystals the symmetry of the static molecule is not appropriate to the lattice. For example, tertiary butyl chloride[19] above its transition point crystallizes in a face-centred cubic lattice with only one molecule per lattice point. Since the stationary molecule possesses only a three-fold symmetry axis, it is assumed that the two-fold axis, needed by a molecule at a lattice point, results from rotation about a point on the C—Cl bond. Similar considerations[16] suggest that the trigonal symmetry of chinuclidin molecules may be brought into conformity with the cubic symmetry of their positions in the crystal by assuming either a free rotation or a statistical disordered distribution of the molecular axes parallel to the four space diagonals of the elementary cube.

An extensive study of cubic $C(NO_2)_4$ has been made by ODA and MATSUBARA[20] who found the diffraction pattern consistent with the space group $T_d^3-I\bar{4}3m$. It was assumed that the molecules (symmetry $S_4-\bar{4}$) acquire a statistical symmetry $D_{2d}-\bar{4}2m$ by having their molecular $\bar{4}$ axes distributed along the three principal axes of the unit cubic cell, the C—N bonds being parallel to the body diagonals and the oxygen pairs rotating around the C—N bonds. Laue photographs of this crystal showed a halo ring and some diffuse spots. The halo was accounted for by the assumed free rotation of the oxygen pairs in conjunction with a calculation based on that of BIJVOET and KETELAAR[21]. The diffuse spots could be explained using MATSUBARA's theory[22] for the diffuse scattering of disordered crystals.

STERIC CONSIDERATIONS

In the many cases where the X-ray information is sparse and comparison of the calculated and observed intensities of reflections is not decisive in distinguishing between free rotation and statistical disorder in orientation, steric arguments may be helpful. The crystal system can be found and usually is found to be cubic; whether it is simple, body-centred or face-centred can be established usually unequivocally and the lattice constant can be determined with reasonable accuracy. The size and shape of the molecules in the unit cell can be obtained from electron diffraction studies or derived from known bond lengths, angles and van der Waals radii. Thus the spatial requirements for free rotation can be compared with the space available in the crystal. In the gaseous state the molecules would rotate about their centres of mass but this may be modified in the crystal by the potential energy field.

In cubic CCl_4[12], the centres of the molecules are only 5·9 Å apart: since the diameter of a rotating molecule is 7·1 Å, it may be concluded that free rotation would be subject to steric

Vol. 18
1961

hindrance. SCHWARTZ *et al.*[19] found for t-butyl chloride and t-butyl bromide that the distances between molecular centres in the crystal were 5·94 Å and 6·20 Å respectively, and state that freely rotating molecules would sweep out spherical volumes of diameter 7·5 Å. In the case of cyclobutane[11], the intermolecular distance of 5·25 Å is substantially smaller than the van der Waals diameter, whilst for cyclopentane[13] the minimum distance between centres of carbon atoms in adjacent molecules in the crystal is only 3·2 Å compared with 4·0 Å, the van der Waals distance between two CH_2 groups. The distance between molecular centres in cubic cyclohexane is 6·1 Å which is less than the diameter 6·5 Å of the sphere of rotation. The same situation holds for chinuclidin, adamantane[15] and $C(SCH_3)_4$[23]. Table 1

Table 1

	d_{cryst}, Å	D_{max}, Å	form
Cyclobutane	5·25	6·22	planar
		5·1	puckered
Cyclopentane	5·83	6·61	planar
Cyclohexane	6·19	6·57	boat
Cyclohexanol	6·24	7·01	boat-flagpole
Chinuclidin	6·35	7·22	
Adamantane	6·68	7·55	
D-L-camphor	7·14	8·45	

lists for a number of compounds the value of the distance, d_{cryst}, between molecular centres in the crystal, together with the maximum diameter, D_{max}, of the molecule (i.e. assuming spherical rotation of the molecule); where the molecule may exist in a number of forms, e.g. chair or boat, the most compact form has been taken. For all these compounds in the cubic form it appears that space in the crystal will not allow the molecules to rotate freely and that one is dealing with a disordered structure[24]; in order to reorient themselves some co-operative fluctuation in the positions of neighbouring molecules is necessary.

In Table 2 there is given a list of substances with their crystal structures in the plastic form, together with the lattice constants and numbers of molecules in the unit cells. ZENER[25] has discussed the relative stability of body-centred, face-centred and close-packed cubic structures in pure metals and noted the susceptibility of body-centred cubic packing to mechanical instability in relation to (110) [$\bar{1}$10] type shear. It is likely that in plastic crystals similar considerations play a part in deciding the type of packing.

OPTICAL PROPERTIES

If, on passing above the transition point, the statistical symmetry of a non-equant group is increased, this is reflected in an enhanced symmetry of the crystal and should result in a change in the optical properties of the crystal. Thus MUELLER[8], in his studies of the higher paraffins, found that the onset of statistical disorder in the {110} planes changed the character of the birefringence from biaxial to uniaxial. Cyclopentane[13] is hexagonally close packed and hence uniaxial above its transition temperature; when cooled below this temperature, it changed to a polycrystalline form of lower optical symmetry. It is found for most "molecules globulaires" that the phase stable at the highest temperatures immediately below the melting point is isotropic in optical properties; this is in conformity with the cubic structure which these plastic crystals exhibit, and on passing below the transition temperature they become birefringent. For example, $C(SCH_3)_4$, investigated by PERDOK and TERPSTRA[23], was found to be optically isotropic from the melting point 65·7°C down to the transition point 45·5°C, whilst the phase stable from this latter temperature down to 23·2°C was found to be doubly refracting. Other examples in which the optical properties were noted are given in Table 3.

PLASTICITY AND VACANCIES

One of the most striking properties of the disordered crystalline forms of these "composés globulaires" is their plasticity. Some studies have been carried out by MICHILS[26] and these materials would serve as model substances for testing many of the theories of metallurgists.

The plastic flow of these crystals may be analogous to the high temperature creep at low stresses which copper and gold show a hundred or so degrees below their melting points. NABARRO[27] and later HERRING[28] have suggested that such creep results from the diffusion of vacancies from one side of a crystal or grain to the

Table 2

Substance	Crystal structure	No. of molecules in unit cell	Lattice constant
	Tetrahedral molecules		
CCl_4	f.c.c.	4	8·34
CBr_4	T_h^6 ($Pa3$)	8	11·34
	or T_d^1 ($P\bar{4}3m$)	1	5·67
CI_4	O_h, T_d or O	1	9·14
$C(Me)_4$	O_h^7 ($Fd3m$)	8	11·25
$C(SMe)_4$	b.c.c.	2	8·15
$(Me)_3CCl$	f.c.c.	4	8·40
$(Me)_3CBr$	f.c.c.	4	8·70
$(Me)_3CSH$	f.c.c.	4	8·82
$C(NO_2)_4$	T_d^3 ($I\bar{4}3m$)	2	7·08
SiF_4	T_d^3 ($I\bar{4}3m$)	2	5·41
SiI_4	T_h^6 ($Pa3$)	8	11·99
	Octahedral molecules		
$Cl_3C.CCl_3$	O_h^9 ($Im3m$)	2	7·43
$Me_3C.C.Me_3$	b.c.c.	2	7·69
$Me_3C.CMeCl_2$	b.c.c.	2	7·38
$Me_3C.CMe_2Cl$	b.c.c.	2	7·62
$Me_2ClC.CClMe_2$	b.c.c.	2	7·58
$Me_2ClC.C.Cl_2$	b.c.c.	2	7·4
$Br_3C.CBr_3$	b.c.c.	2	—
$Me_3Si.SiMe_3$	b.c.c.	2	8·47
$Me_3C.COOH$	O_h^5 ($Fm3m$)	4	8·82
	Cyclic molecules		
cyclobutane	b.c.c.	2	6·06
cyclopentane	hexagonal	2	5·83
			9·35
cyclohexane	f.c.c.	4	8·76
thiacyclohexane	f.c.c.	4	8·69
cyclohexanol	O_h^5 ($Fm3m$)	4	8·83
cyclohexanone	f.c.c.	4	8·61
chlor-cyclohexane	b.c.c.		9·05
cycloheptatriene	cubic	8	10·6
	Cage molecules		
chinuclidin	f.c.c.	4	8·977
sym-tricyclodecane	T_d^2 ($F\bar{4}3m$)	4	9·426
D-L-camphor	f.c.c.	4	10·1
D-L-camphene	b.c.c.	2	8·00
borneol	f.c.c.	4	10·25
bornyl chloride	f.c.c.	4	10·39

Vol. 18
1961

Table 3. Observations of optical isotropism in crystalline phases stable immediately below the melting point

HCl, HBr, HI	KRUIS and KAISCHEW[32]
CCl_4	POST[13]
$C(CH_3)_4$	WAHL[33]
$C(SCH_3)_4$	PERDOK and TERPSTRA[23]
$C_2(CH_3)_6$	WEST[34]
1,1,1,2 tetrachloro-2-methyl propane	KOIDE, ODA and NITTA[35]
t-butyl chloride, bromide	SCHWARTZ *et al.*[19]
cyclohexane, cyclohexanol	HASSEL and SOMMERFELDT[17]
cyclohexanone, chlorcyclohexane	
2 chloro-2,3,3, trimethyl butane	KOIDE *et al.*[36]
chinuclidin	NOWACKI[16]
adamantane	ULLRICH[31]

other. They find that the creep rate $\dot{\gamma}$ is given by

$$\dot{\gamma} = \frac{D}{l^2} \sinh\left(\frac{2pV}{kT}\right) \simeq \frac{2pVD}{l^2kT}$$

where D is the diffusion coefficient of the vacancies, V the volume of a molecule, l the dimension of the crystal or grain and p the stress.

In pure potassium metal the number of vacancies is about one per thousand atom sites[29]. Since the heat of sublimation of potassium is roughly twice that of the organic plastic crystals, the number of vacancies in the latter may be at least comparable. A possible method of calculating the vacancy density is by comparing the density obtained from X-ray data with that obtained by conventional means. Without special precautions being taken this might lead to serious error; a tentative figure of 1·25 per cent can be obtained from PERDOK and TERPSTRA's densities for cubic $C(SCH_3)_4$, 1·219 g ml^{-3} from X-ray measurements and 1·204 for the conventional density.

SURFACE FEATURES AND RATE OF GROWTH

The surfaces of camphor and of CBr_4 cubic crystals when subliming slowly show the development of pits which are probably located at the terminations of dislocations in the surface. GILLILAND has examined the surfaces of crystals of camphor and of CBr_4 during growth. Fig. 2 is a photograph of a large growth step on the surface of camphor at about 27°C; at the centre there is a deep pit, probably indicating that a screw dislocation of large Burger's vector and large strain energy emerges at this point. As the temperature is raised towards the transition point (about 105°C), the spiral remains visible up to 90°C, above which it is no longer visible. It was not clear whether or not the dislocation at its centre moved to the periphery of the surface or whether the large step dissociated into smaller steps.

By measuring the rate of forward movement of the edges of crystals, BRADLEY and DRURY[30] determined the rates of growth of the monoclinic and cubic forms of CBr_4. They found that the rate of growth of the monoclinic form was about ten times greater than that of the cubic form for the same supersaturation. The cause of this difference is obscure but is most likely due to the growth steps being higher ($\sim$ 10 times) on monoclinic crystals than on cubic. This is not unreasonable because strains in the growing crystal would be relieved by dislocations possibly of large Burger's vector in monoclinic crystals whilst stresses in the plastic cubic form could be relieved by the plastic flow arising from the diffusion of vacancies. Further, it is likely that screw dislocations of large Burger's vector would be more stable in the monoclinic form than in the cubic where mobility of vacancies could cause a large dislocation to split into an array of small dislocations with a reduction in the rate of growth.

Acknowledgement—My thanks are due to Dr. C. W. BUNN for helpful discussion.

REFERENCES

1. HERRMANN K. and KRUMMACHER A. H., *Z. Kristall.* **81,** 317 (1932).
2. CARTZ L., *Proc. Phys. Soc. Lond.* **B68,** 951 (1955).

Vol. 18
1961

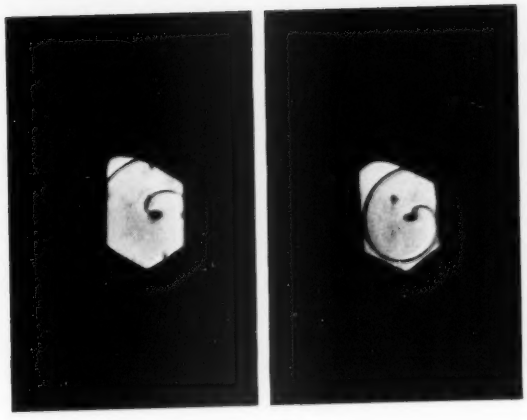

FIG. 2

[facing page 26.

BLANK
PAGE

Vol.
19

3. TIMMERMANNS J., *J. Chim. Phys.* **35,** 331 (1938).
4. ABRAHAMS S. C. and LIPSCOMB W. N., *Acta Cryst., Camb.* **5,** 93 (1952).
5. DULMAGE W. J. and LIPSCOMB W. N., *Acta Cryst., Camb.* **4,** 330 (1951).
6. ROBERTSON J. M., ROSSMANN M. G. and TROTTER J., *Acta Cryst., Camb.* **10,** 803 (1957).
7. LONSDALE K., *Z. Kristall.* **112,** 188 (1959).
8. MUELLER A., *Proc. Roy. Soc.* **A127,** (1930) 417; **A138,** 514 (1932); *Nature, Lond.* **129,** 436 (1932).
9. GARNER W. E., *J. Chem. Soc.* 1533 (1931).
10. TAUER K. J. and LIPSCOMB W. N., *Acta Cryst., Camb.* **5,** 606 (1952).
11. CARTER G. F. and TEMPLETON D. H., *Acta Cryst., Camb.* **6,** 805 (1953).
12. POST B., *Acta Cryst., Camb.* **12,** 349 (1959).
13. POST B., SCHWARTZ R. S. and FANKUCHEN I., *J. Amer. Chem. Soc.* **73,** 5113 (1951).
14. MONES A. H. and POST B., *J. Chem. Phys.* **20,** 755 (1952).
15. GIACOMELLO G. and ILLUMINATI G., *Gazz. chim. Ital.* **75,** 246 (1945); see also NOWACKI W., *Helv. Chim. Acta.* **28,** 1233 (1945).
16. NOWACKI W., *Helv. Chim. Acta* **29,** 1798 (1946).
17. HASSEL O. and SOMMERFELDT A. M., *Z. Phys. Chem.* **B40,** 391 (1938).
18. PAULING L., *Phys. Rev.* **36,** 430 (1930).
19. SCHWARTZ R. S., POST B. and FANKUCHEN I., *J. Amer. Chem. Soc.* **73,** 4490 (1951).
20. ODA T. and MATSUBARA T., *X-rays* **6,** 27 (1950); *Bull. Chem. Soc. Japan,* **27,** 273 (1954); see also ODA T., IIDA T. and NITTA I., *J. Chem. Soc. Japan,* **64,** 616 (1943); ODA T. and WATANABE T., *J. Chem. Soc. Japan* **65,** 154 (1944); ODA T. and NITTA I., *J. Chem. Soc. Japan* **64,** 621 (1943); NITTA I., *Z. Kristall.* **112,** 234 (1959).
21. BIJVOET J. M. and KETELAAR J. A. A., *J. Amer. Chem. Soc.* **54,** 625 (1932).
22. MATSUBARA T., *X-rays* **6,** 15 (1950).
23. PERDOK W. G. and TERPSTRA P., *Rec. trav. chim.* **65,** 493 (1946); PERDOK W. G., *Helv. Chim. Acta* **30,** 1782 (1947).
24. ZERNIKE F., *Ned. Tijdschr. Natuurk.* **8,** 55 (1941).
25. ZENER C., *Phys. Rev.* **71,** 846 (1947); *Trans. Amer. Inst. Min. (Metall.) Engrs.* **203,** 619 (1955).
26. MICHILS A., *Bull. Soc. Chem. Belg.* **57,** 575 (1949).
27. NABARRO F. R. N., *Rep. Conf. Strength of Solids,* Vol. 47. Physical Society, London (1947).
28. HERRING C., *J. Appl. Phys.* **21,** 437 (1950).
29. MACDONALD D. K. C., *Report of Bristol Conference on Defects in Crystalline Solids,* p. 283. Physical Society, London (1955).
30. BRADLEY R. S. and T. DRURY, *Trans. Faraday Soc.* **55,** 1848 (1959).
31. ULLRICH M., LANDA S. and MACHÁČEK V., *Coll. Trav. Chim. Tchécosl.* **5,** 1 (1933).
32. KRUIS A. and KAISCHEW R., *Z. Phys. Chem.* **41,** 427 (1938).
33. WAHL W., *Proc. Roy. Soc.* **88,** 356 (1913).
34. WEST C. D., *Z. Kristall.* **88,** 195 (1934).
35. KOIDE T., ODA T. and NITTA I., *Bull. Chem. Soc. Japan* **29,** 738 (1956).
36. KOIDE T., TAKEUCHI S., ODA T., YAMADA Y. and TAGUCHI I., *Bull. Chem. Soc. Japan* **30,** 680 (1957).

Vol. 18
1961

J. Phys. Chem. Solids Pergamon Press 1961. Vol. 18, No. 1, pp. 28–39. Printed in Great Britain.

A THEORY OF FUSION OF MOLECULAR CRYSTALS I. THE EFFECTS OF HINDERED ROTATION

J. A. POPLE and F. E. KARASZ

National Physical Laboratory, Teddington, England

Abstract—A theory of fusion is developed which allows for order–disorder phenomena in both the orientations and positions of molecules. The two-lattice model used by LENNARD-JONES and DEVONSHIRE is extended so that molecules may take up two orientations on any site. By introducing a physically realistic coupling between orientational and positional disorder, a theory results which gives a solid state rotational transition and a melting transition. For small rotational barriers, the transitions are separate, while for larger barriers they coalesce. The theory makes quantitative predictions about the effects of solid rotational transitions on the thermodynamics of melting, which are in approximate agreement with experimental data.

1. INTRODUCTION

ALTHOUGH the main qualitative distinction between the solid and liquid phases has long been attributed to the disappearance of the long-range order of the crystal structure, there are few theories able to give a satisfactory quantitative description of the thermodynamic changes involved. Most of these are concerned with the simplest type of monatomic crystal (particularly the inert gas crystals) and do not treat the diverse features observed in the melting of molecular crystals which is usually critically dependent on factors such as molecular shape and specific molecular association.

Probably the most successful treatment of the melting of inert gas crystals is the work of LENNARD-JONES and DEVONSHIRE[1,2] based on the cell model they had previously developed for the theory of condensation[3] (the liquid–vapour transition). These authors allowed for the possibility of increasing disorder in the positions of molecules in a crystal by permitting them to occupy sites on one of two equivalent interpenetrating lattices, referred to as α-sites and β-sites. The lowest energy configuration is that in which the particles all occupy α-sites or all β-sites corresponding to a state of perfect order. With increasing temperature, the number of particles on interstitial sites (e.g. β-sites in a crystal where mainly α-sites are occupied) increases, until a critical condition is reached where the long-range order is destroyed and the two kinds of site are equally populated. By using the statistical mechanical methods developed for handling co-operative problems of this sort and making the energy of particles on neighbouring α and β sites vary appropriately with the volume, LENNARD-JONES and DEVONSHIRE were able to develop a quantitative theory of the thermodynamics of the melting transition. They found that the predictions of the theory agreed well with many features of the experimental data for spherical or almost spherical molecules.

The LENNARD-JONES and DEVONSHIRE theory is unsatisfactory when applied to the melting of molecular crystals in which the intermolecular forces deviate appreciably from spherical form and the possibility of hindrance to rotation in the solid and liquid states has to be taken into account. As the theory is based on a simple central force law of given shape (actually the 6–12 potential field), it implies a law of corresponding states, according to which such quantities as the entropy of melting (at the triple point) and the ratio of triple point temperature to critical temperature should be the same for all substances. In fact, wide and systematic variations in such quantities are found which cannot be interpreted in terms of this simple theory.

The thermodynamic data on the melting of molecular crystals has been discussed qualitatively by a number of authors. EUCKEN[4] and UBBELOHDE[5] have pointed out that there are large

differences between substances which undergo phase transitions associated with rotational motion before reaching the melting point and substances where the hindrance to rotation is larger and the disorientation of the molecules cannot take place until the liquid state is reached. The first class (which must have relatively low rotational barriers in the crystal) usually have lower entropies of melting than the inert gases. The second class, however, have much higher entropies of melting, presumably because a greater increase in rotational freedom takes place with the transition. For substances such as water, which are associated as liquids, a great deal of the relative orientational order is retained in the liquid state and the entropies of fusion are again smaller.

As these empirical studies of experimental data suggest important connections between the thermodynamics of melting and orientational order in solids and liquids, it seems worthwhile to attempt an extension of the LENNARD-JONES and DEVONSHIRE theory to take account of rotational degrees of freedom in at least an approximate manner. In this paper we shall present such an extended theory in which the model used by LENNARD-JONES and DEVONSHIRE to describe the breakdown in positional order is combined with the rather similar model that has been used for theories of rotational transitions in solids. By introducing a relation between the processes in a physically realistic manner, a model results which can be used to study quantitatively the effects of rotational disordering on the thermodynamics of the melting process itself.

It should be emphasized at the outset, of course, that a simple model of the kind considered here cannot give an adequate description of the very diverse kinds of molecular motion that can occur in a variety of crystal structures, so that the theory can hardly apply in detail to any one particular material. Nevertheless, there is sufficient regularity in the experimental data to suggest that an approximate over-all theory should be able to interpret the trends in a reasonably quantitative manner.

2. A MODEL FOR DESCRIBING POSITIONAL AND ORIENTATIONAL ORDER–DISORDER

The method we shall use is an extension of the model used for monatomic substances adopted by LENNARD-JONES and DEVONSHIRE[2] and we shall follow their notation closely. They begin with a description of an assembly of N molecules each vibrating in a cell, the cells forming a regular lattice structure. The partition function for such an assembly, which is perfectly ordered, can be written f^N where f is the partition function for one particle vibrating in the cell potential field determined by its neighbours. Although this model was first developed for describing condensation, LENNARD-JONES and DEVONSHIRE pointed out the condensed state really corresponded to an ordered solid so that the solid/liquid transition could not be described without giving the system more flexibility.

To allow for the possibility of disorder in the arrangement of the cells, LENNARD-JONES and DEVONSHIRE suppose that the molecules could be centred on sites which could be of two kinds, α-sites and β-sites. The α-sites are the normal ones, so that in the equilibrium configuration of the solid (at zero temperature), the molecules are distributed over the N available α-sites. The second N abnormal or interstitial sites (β-sites) form a second lattice interpenetrating the first and symmetrically related to it. This means that the configuration in which all molecules occupy β-sites is also an equilibrium arrangement; the role of normal and abnormal sites is reversed. LENNARD-JONES and DEVONSHIRE specifically use two interpenetrating face-centred cubic lattices, since the inert gases (except helium) have the face centred cubic structure in the solid form. We need not specify the exact nature of the lattices however, since only limited information about them is required for the approximation to which we shall work. We shall assume that each α-site is surrounded by z equivalent neighbouring β-sites and each β-site by z α-sites. We shall also write z' for the number of α-sites closest to any given α-site or the number of β-sites closest to any given β-site.

The model of two interpenetrating lattices is capable of showing two condensed phases with properties analogous to solids and liquids. If, for a sufficiently large assembly, the free energy is smallest for a distribution in which the particles lie mainly on α-sites (or mainly on β-sites), the system possesses long-range positional order and corresponds to a solid. If, on the other hand, both kinds of site are equally populated, the system is disordered and corresponds to a liquid.

Vol. 18
1961

In their quantitative development of the theory, LENNARD-JONES and DEVONSHIRE introduce a repulsive energy W between molecules of neighbouring α and β sites, since a positive energy is required to move a particle in an α-lattice onto an interstitial β-site. If $N_{\alpha\beta}$ is the number of such neighbouring pairs in any particular configuration of the N particles among the $2N$ sites, the partition function for the whole assembly is written.

$$Z = \sum f^N \exp(-N_{\alpha\beta}W/kT) \qquad (2.1)$$

where Σ represents the summation over all configurations and f is the partition function per molecule in a state of perfect order where all molecules occupy α-sites. The function f itself is treated as a function of volume per molecule and temperature only, so that the factor f^N can in fact be taken outside the summation in (2.1). The treatment then proceeds by using an approximate form for f and taking the repulsive energy W to be an appropriate function of volume and using the zeroth or first-order approximation to evaluate the partition sum.

We now wish to modify this model so that account is taken of the orientation of the molecules and the energies of different relative orientations of neighbours. For this purpose, we shall suppose that each molecule can take up one of two orientations on any site. This means that there are then four possibilities for any molecule which can be denoted by α_1, α_2, β_1 and β_2. We shall further suppose that these orientations are such that, in the equilibrium configuration of the solid, all particles will occupy sites and orientations of the same type (e.g. all α_1). It is not meant to imply by this that all molecules have any particular relative orientation (such as all being parallel) but only that the total solid angle available to each molecule can be divided into two parts labelled 1 and 2 and that in the equilibrium configuration of the solid, at low temperatures, all molecules occupy their region 1, or alternatively all occupy region 2.

Just as LENNARD-JONES and DEVONSHIRE introduced a repulsive energy W for molecules on neighbouring α- and β-sites to allow for the higher energy of interstitial (β) sites in a mainly α-lattice, so we now introduce a second repulsive energy W' to allow for the higher energy of molecules in unfavourable relative orientations. In fact the energy W' will be associated with each pair of α_1 and α_2 molecules in neighbouring positions on an α-lattice (and similarly for neighbouring β_1 and β_2 molecules on a β-lattice). Thus $z'W'$ is the energy required to turn one molecule from α_1 to α_2 when the remainder of the lattice is α_1.

One further point of great importance which should be taken into account is the following. If we have a perfect lattice all in α_1 configurations and one molecule is then rotated into the unfavourable α_2 orientation, a strain is set up in the vicinity of this particular site. As a result of this there will be an increased tendency for molecules in this region to move onto interstitial positions. This introduces a coupling between the two processes of disorientation and has important physical consequences. In terms of our model, it means a lower relative energy for surrounding β-sites. This will be taken into account in the simplest possible manner by assuming that the energy W of α–β neighbours is independent of orientation, so that β-sites near a misorientation in a mainly α-lattice are favoured by not experiencing the repulsive W' term. A similar effect will apply to α-sites surrounding a β-misorientation in a mainly β-lattice.

If $N_{\alpha_1\alpha_2}$ is the number of relative misorientations on neighbouring α-sites and $N_{\beta_1\beta_2}$ is defined similarly, the new partition function can be written

$$Z = f^N \Omega$$
$$= f^N \sum \exp[-(N_{\alpha\beta}W + N_{\alpha_1\alpha_2}W' + N_{\beta_1\beta_2}W')/kT] \qquad (2.2)$$

where the sum is now over all orientations as well as over arrangements of particles on α- and β-sites. This analysis of this partition function should now predict order–disorder behaviour for both position and orientation and their interrelation. In fact the analysis of the summation part Ω in (2.2) can be discussed as a separate problem of a co-operative type and we shall deal with this in the next section.

3. APPROXIMATE SOLUTION OF THE CO-OPERATIVE ORDER–DISORDER PROBLEM

The partition function Ω in (2.2) can be evaluated approximately by an extension of the simple Bragg–Williams treatment of co-operative

problems of this sort used by LENNARD-JONES and DEVONSHIRE[2]. We introduce a degree of positional order Q, which is the fraction of particles on α-sites. Similarly we write S for the orientational order defined as the fraction of molecules in 1-orientations. Then the total Ω may be written as a sum of partition functions for given Q and S

$$\Omega = \sum_{Q,S} \Omega(Q, S) \tag{3.1}$$

$$\Omega(Q, S) = \sum^{(Q,S)} \exp\left[-(N_{\alpha\beta}W + N_{\alpha_1\alpha_2}W' + N_{\beta_1\beta_2}W')/kT\right] \tag{3.2}$$

where $\Sigma^{(Q,S)}$ is the sum over configurations in which there are NQS molecules in α_1 positions, $NQ(1-S)$ in α_2 positions, $N(1-Q)S$ in β_1 positions and $N(1-Q)(1-S)$ in β_2 positions. Since the complete partition function is sharply peaked, we seek only the maximum of $\Omega(Q, S)$. If this is at $Q = S = \frac{1}{2}$, both positions and orientations are completely disordered. If the maximum occurs for other values of Q and S, long-range order exists for the positions or orientations, or both.

The Bragg-Williams (or zeroth) approximation to this problem is to replace the exponent in (3.1) by its average value, so that the sum becomes equal to $\gamma(Q, S)$, the number of terms for given Q and S. Thus

$$\Omega(Q, S) = \gamma(Q, S)\exp\{-[zNWQ(1-Q) + Z'NW'S(1-S)(1-2Q+2Q^2)]/kT\}$$

The number of ways of arranging the particles for given Q and S is

$$\gamma(Q, S) = \left\{\frac{N!}{[NQ]![N(1-Q)]!}\right\}^2 \frac{[NQ]!}{[NQS]![NQ(1-S)]!} \times \frac{[N(1-Q)]!}{[N(1-Q)S]![N(1-Q)(1-S)]!} \tag{3.3}$$

so that, using Stirling's theorem, we have to maximize

$$N^{-1}\log\Omega = -2Q\log Q - 2(1-Q)\log(1-Q) - S\log S - (1-S)\log(1-S) - \frac{zW}{kT}Q(1-Q) - \frac{z'W'}{kT}S(1-S)(1-2Q+2Q^2) \tag{3.4}$$

The conditions for this expression to have a stationary value are

$$\log\frac{Q}{1-Q} = \left[\frac{zW}{2kT} - \frac{z'W'}{kT}S(1-S)\right](2Q-1) \tag{3.5}$$

$$\log\frac{S}{1-S} = \frac{z'W'}{kT}(1-2Q+2Q^2)(2S-1) \tag{3.6}$$

Equation (3.5) reduces to the corresponding result in the LENNARD-JONES and DEVONSHIRE theory if $W' = 0$.

Clearly the ratio

$$\nu = \frac{z'W'}{zW} \tag{3.7}$$

is a measure of the relative energy barriers for the rotation of a molecule and for its diffusion to an interstitial site. It is the key parameter in the present theory and we shall investigate the effect it has on the predicted thermodynamic properties of melting.

The point $Q = S = \frac{1}{2}$ is always a solution of equations (3.5) and (3.6). At high enough temperatures (small zW/kT), it is the only solution and maximizes $\log\Omega$. This corresponds to the situation in which there is a breakdown in the long-range order in both the positions and orientations of the molecules. For larger zW/kT, the values of Q and S maximizing $N^{-1}\log\Omega$ may differ from $\frac{1}{2}$, corresponding to some order in position or orientation. These values have been found for a series of values of the parameters γ and zW/kT by solving equations (3.5) and (3.6) for stationary points and comparing the corresponding values of the right hand side of (3.4). From this point, the symbols Q and S will be understood to refer to these values maximizing the partition function.

Vol. 18
1961

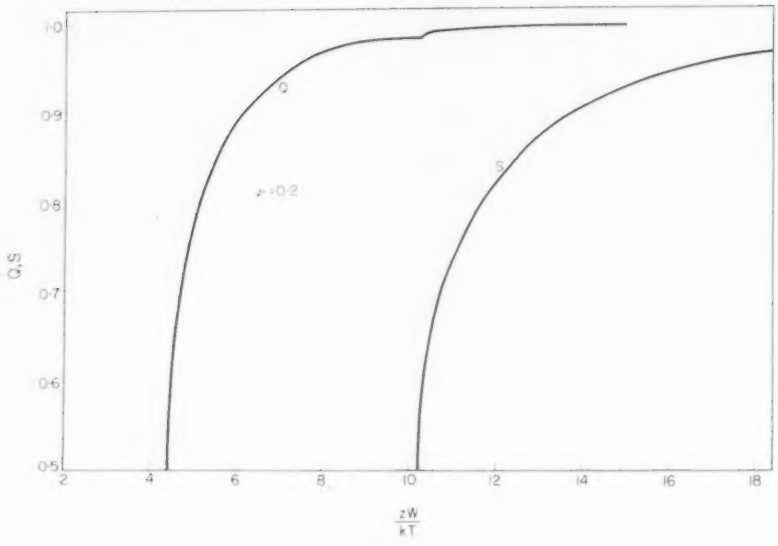
1·0
0·9
0·8
0·7
0·6
0·5
Q,S
Q
S
ν=0·2
2
4
6
8
10
12
14
16
18
zW/kT

FIG. 1(a)

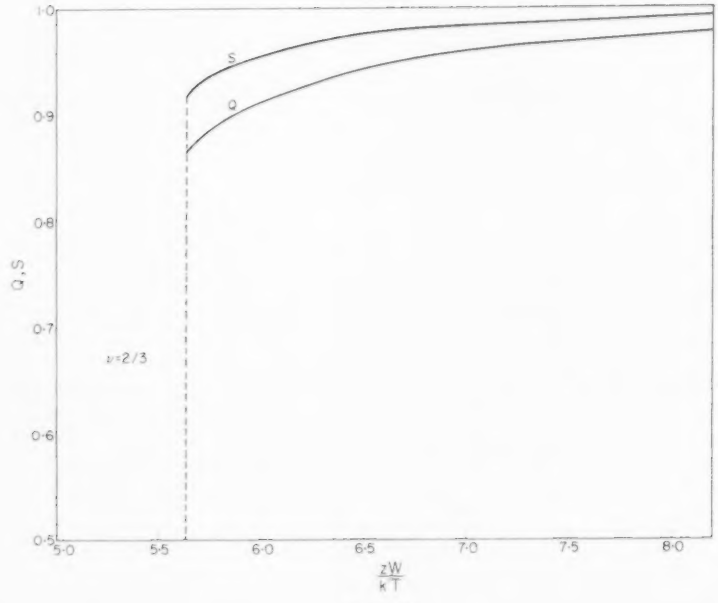
1·0
0·9
0·8
0·7
0·6
0·5
Q,S
S
Q
ν=2/3
5·0
5·5
6·0
6·5
7·0
7·5
8·0
zW/kT

FIG. 1(b)

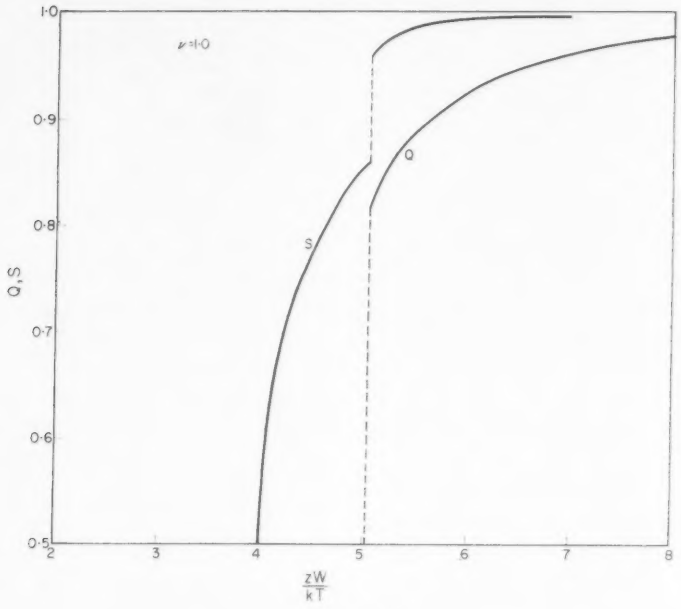

FIG. 1(c)

FIG. 1. Variation of positional order Q and orientational order S with zW/kT for various ν.

The kind of behaviour found in Q and S as a function of zW/kT varies with the parameter ν. For small ν, $Q = S = \frac{1}{2}$ at low zW/kT and as the latter parameter is increased Q first moves away from the value $\frac{1}{2}$. There is then a region of zW/kT in which the orientations are disordered ($S = \frac{1}{2}$) but the positions are ordered ($Q \neq \frac{1}{2}$). Eventually the value of S also moves away from $\frac{1}{2}$ as shown in Fig. 1(a). For larger values of ν, the absolute maximum of the partition function moves suddenly away from $(\frac{1}{2},\frac{1}{2})$ to some point at which $S \neq Q \neq \frac{1}{2}$. This is illustrated in Fig. 1(b). Finally for even larger ν, the situation is reversed and S leaves the value $\frac{1}{2}$ for smaller zW/kT (Fig. 1(c)).

4. EVALUATION OF THE THERMODYNAMIC PROPERTIES OF MELTING

Having found the values of the order parameters Q and S in the manner outlined in the previous section, we can write down the Helmholtz free energy A from the partition function and then examine the conditions under which the theory predicts phase changes. A is conveniently split into two parts

$$A = A' + A'' \tag{4.1}$$

$$A'/NkT = -\log f \tag{4.2}$$

$$A''/NkT = -N^{-1}\log\Omega(Q, S) \tag{4.3}$$

The first part A' gives the partition function for the completely ordered system, whereas the second part A'' gives the contribution due to the disordering of the positions and orientations of the molecules. Other thermodynamic functions can be derived from the free energy and also expressed as a sum of two parts in this way. To study the equation of state, we need the pressure which is given by

$$p = p' + p'' \tag{4.4}$$

$$p' = -(\partial A'/\partial v)_T;\ p'' = -(\partial A''/\partial v)_T \tag{4.5}$$

The free-volume theory may now be used to evaluate the single particle partition function f.

Vol. 18
1961

This is written in the form

$$f = f_{\text{kinetic}} v_f^* \exp(-\Phi_0/NkT) \qquad (4.6)$$

where f_{kinetic} is the partition function for kinetic energy (independent of volume and so not contributing to the pressure), v_f^* is an average free volume of each particle in its cell and Φ_0 is the potential energy of the central forces when all particles are in their equilibrium positions.

The free-volume theory has been extensively developed in terms of the 6–12 intermolecular energy law according to which the interaction energy of a pair of particles at a separation τ is given by

$$u(r) = 4\epsilon_0[(r_0/r)^{12} - (r_0/r)^6] \qquad (4.7)$$

where $-\epsilon_0$ is the energy minimum and r_0 the separation for zero interaction (balance between attractive and repulsive energies). The thermodynamic functions derivable from A' for the spherically-smoothed three-shell cell field have been tabulated by WENTORF *et al.*[6] and we shall use their values (slightly extrapolated to lower temperatures where necessary). These authors use a standard volume v_0 equal to the volume of the assembly if the particles occupy a face-centred lattice where the distance between nearest neighbours is equal to the distance minimizing $u(r)$, that is $r = 2^{1/6}r_0$. Then they tabulate the compressibility factor $pv/Nk\tau$ as a function of a reduced temperature kT/ϵ_0 and a reduced volume v/v_0.

To evaluate the other contribution to the pressure, we need to specify the variation of the energies W and W' with volume. Supposing these to be determined primarily by repulsion forces (with energies approximately proportional to r^{-12}) we take both these energies in the form

$$\left.\begin{aligned} W &= W_0(v_0/v)^4 \\ W' &= W_0'(v_0/v)^4 \end{aligned}\right\} \qquad (4.8)$$

where W_0 and W'_0 are constants proportional to ϵ_0. This means that the non-dimensional parameter $\nu(= z'W'/zW)$ is supposed independent of temperature and volume and is thus characteristic of the material. LENNARD-JONES and DEVONSHIRE[2] adjust the ratio W_0/ϵ_0 empirically to give the correct melting temperature of argon. We shall follow this and predict the melting properties of other substances as the parameter ν moves through a range of values. (The ratio W_0/ϵ_0 is found to be 0·977 which differs slightly from the LENNARD-JONES and DEVONSHIRE value because the modified tables of WENTORF *et al.*[6] have been used.)

The pressure p'' is now given by

$$\frac{p''v_0}{NkT} = \frac{v_0}{N}\left[\frac{\partial}{\partial v}\log\Omega(Q, S)\right]_T$$
$$= 4\frac{v_0}{v}\frac{zW}{kT}\{Q(1-Q)+\nu S(1-S)(1-2Q+2Q^2)\} \qquad (4.9)$$

using (3.4), (4.8) and the conditions $\partial\Omega/\partial S = \partial\Omega/\partial Q = 0$ which were used to maximize $\log\Omega(Q, S)$. This equation gives $p''v_0/NkT$ as a function of (v/v_0), kT/ϵ_0 and ν, so that by adding to $p'v_0/NkT$ we obtain a complete isotherm.

The isotherms obtained in this way show one or two kinks when the two kinds of long-range order disappear. Only one kink is found if the two sorts of order disappear together as in Fig. 1(b). In the model used, first order melting transitions are predicted and the temperature has to be adjusted to give equal areas above and below the zero-pressure line. Two typical isotherms are shown in Fig. 2. In Fig. 2(a), it is possible for two phases to exist in equilibrium represented by the points A and B provided that the total (algebraic) area under the curve between these points is zero. The point A corresponds to the solid ($Q \neq \frac{1}{2}$) and B to the liquid ($Q = \frac{1}{2}$). In this case $S = \frac{1}{2}$ at the point A so that the solid at the melting point has its molecules orientationally disordered. In other words, a transition occurs in the solid at some temperature below the melting point. Clearly for another lower temperature, an isotherm could be obtained for which it could be possible to have two solid phases in equilibrium corresponding to a solid-transition temperature. However, we shall not pursue the description of solid transitions given by the theory any further in this paper.

For larger values of ν, the two kinks in the curve where the two kinds of order disappear become closer together as illustrated in Fig. 2(b). In this case the melting isotherm is such that the two types of disordering (positional and orientational) both occur together in a single first-order transition at the point C, $S \neq Q \neq \frac{1}{2}$ and at D, $S = Q = \frac{1}{2}$. For a material characterized by this value of ν, there will be no solid state transition below the

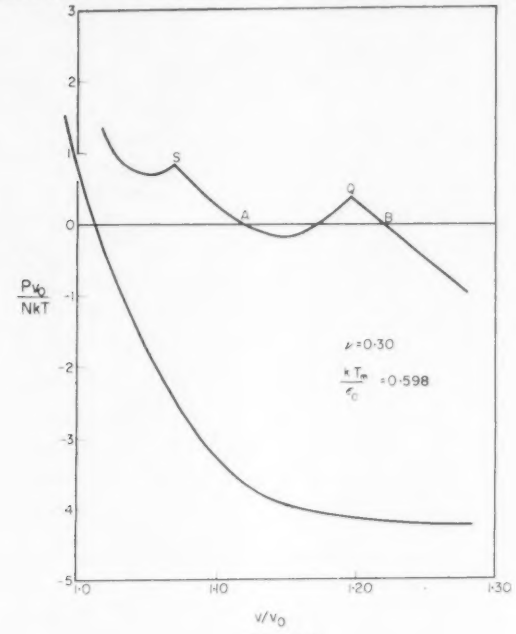

FIG. 2(a)

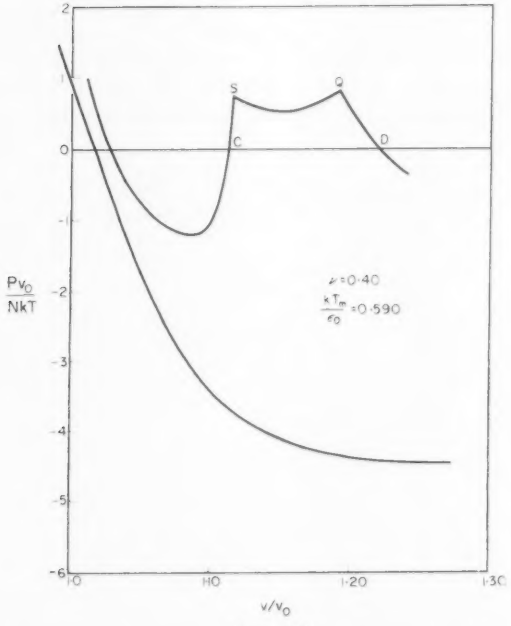

FIG. 2(b)

FIG. 2. Theoretical melting isotherms (a) for $\nu = 0{\cdot}3$ and (b) $\nu = 0{\cdot}4$.

Vol. 18
1961

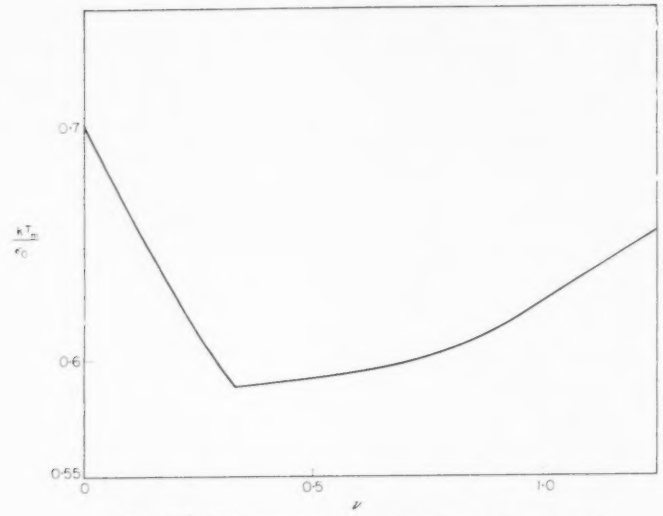

FIG. 3. Reduced temperature of melting as a function of ν.

melting point. The critical value of ν which gives the change from one case to the other is estimated to be $\nu = 0{\cdot}325$, when the solid rotation transition temperature and the melting temperature first coincide.

For a larger value of ν, the two kinks in the isotherms will coincide and then there will be a change to a situation in which the point at which S becomes $\frac{1}{2}$ is at higher volume than the corresponding point for Q. Eventually for still larger values of ν, the theory predicts a separation again into two thermodynamic transitions, the melting occurring at lower temperatures. This is analogous to the properties of liquid crystals but we shall not study this range of ν in the present paper.

Having found the melting isotherm at zero

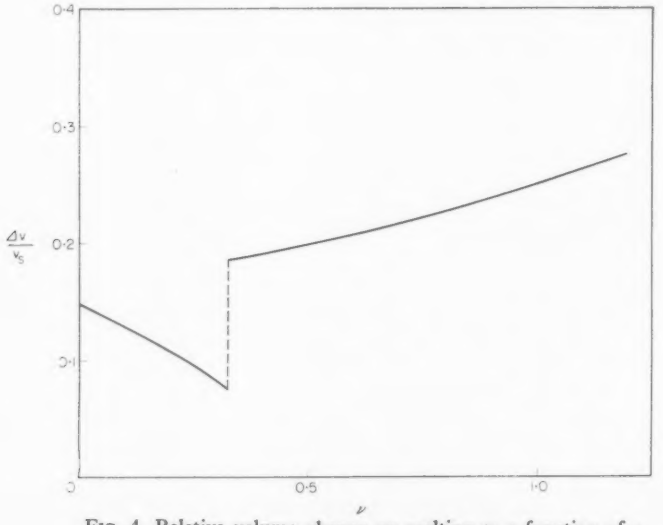

FIG. 4. Relative volume change on melting as a function of ν.

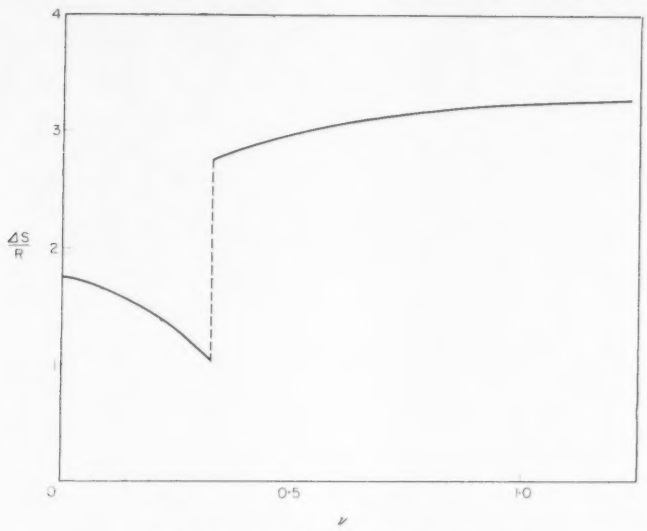

FIG. 5. Entropy of melting as a function of ν.

pressure, for a number of values of ν, the theory can now be used to predict other thermodynamic properties. For example the relative volume change $\Delta v/v_s$, where v_s is the solid volume at the melting temperature, can be obtained immediately. Similarly the entropy of melting ΔS can be found by calculating the entropies of the two phases in equilibrium from

$$S = S' + S'' = -(\partial A'/\partial T)_v - (\partial A''/\partial T)_v \qquad (4.10)$$

These calculations have been carried out for a series of values of ν with the results shown in Figs. 3, 4 snd 5.

5. DISCUSSION

The results derived in the previous section clearly show the trends observed in experimental data, although the latter are somewhat scattered and there are a number of anomalies. For $\nu = 0$, the points on the curves of Figs. 3, 4 and 5 correspond to the original theory of LENNARD-JONES and DEVONSHIRE[2]. The melting temperature for argon was adjusted empirically and the values of $\Delta v/v_s$ and $\Delta s/Nk$ then predicted successfully. (Our numerical results differ somewhat from those of the original paper as improved free-volume tables are used.)

As ν increased from zero to the value 0·325, the theory predicts the changes observed in materials with solid rotational transitions fairly well. In the first place, the reduced melting temperature kTm/ϵ_0 falls. This cannot be directly compared with experimental data, of course, but if we assume that ϵ_0 is proportional to the critical temperature T_c, we have a theory for changes of T_m/T_c*. Alternatively, another approximately valid relation is the constancy of the ratio of boiling (1 atm) and critical temperatures, so that the theory gives an increased liquid range as usually observed. Qualitatively this can be interpreted as a destabilization of the crystal lattice by the relative misorientations of molecules (above the solid transition temperature) leading to increased occupation of interstitial sites and earlier melting. The predicted lowering of the relative volume change, which is also in agreement with most experimental data, arises principally from increased solid volumes caused by the misorientation of molecules above the solid transition temperature. The fall in entropy of melting (again observed experimentally) is closely associated with this,

* In a full theory, account should be taken of changes in T_c itself due to the order–disorder effects. However such changes in T_c will be much smaller than those in T_m and we shall neglect them.

Vol. 18
1961

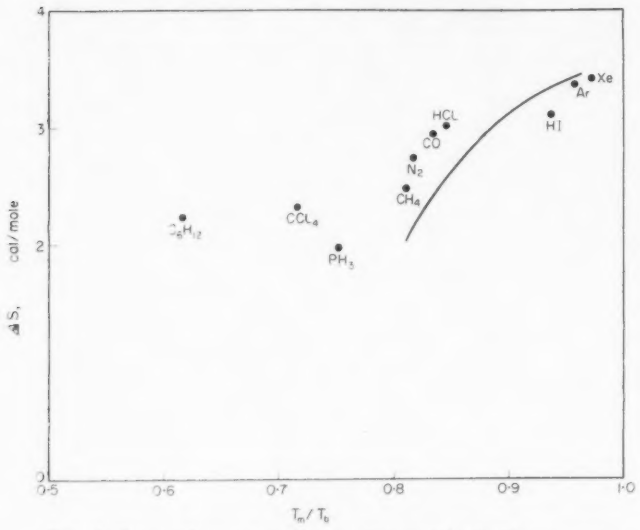

FIG. 6. Comparison of entropies and melting/boiling temperature ratios with theoretical prediction.

the principal reduction being in $\Delta S'$ representing changes in free volume.

Since we cannot expect to estimate the parameter ν for any substance with any accuracy with our present knowledge of intermolecular forces, the best way to test the theory quantitatively is to plot these experimental quantities against each other and compare with the predicted theoretical relationship. In Fig. 6, the entropy of melting is plotted against the ratio of melting to boiling temperatures for a number of substances with rotational transitions in the solid state (data

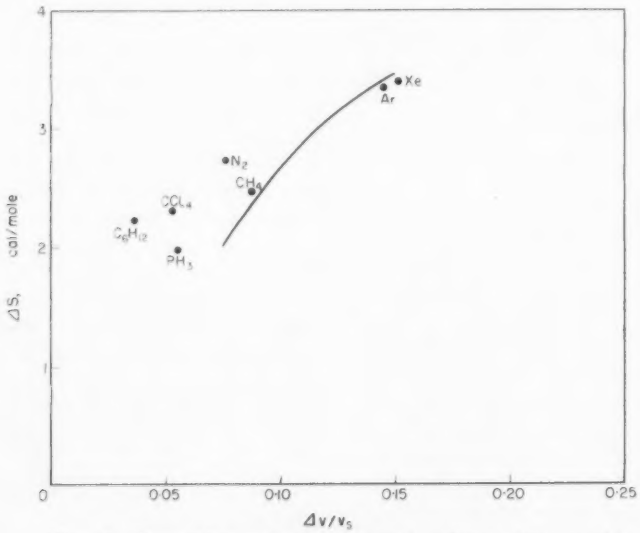

FIG. 7. Comparison of entropies and volume changes with theoretical prediction.

from EUCKEN[4]). The theoretical curve is obtained from Fig. 3 (up to $\nu = 0{\cdot}325$) together with the approximate relationship $kT_b = 0{\cdot}73\,\epsilon_0$ (close to the value for argon). As the theory contains no adjustable parameter other than the one used to fit the inert gas data, the agreement is reasonably satisfactory. The greatest deviation is for cyclohexane, where several types of rotation may occur. Fig. 7 shows a similar plot for entropies and relative volume changes. These correlations were noted empirically by EUCKEN[4] and now receive some quantitative support.

If ν is greater than the critical value 0·325, the theory predicts the correct qualitative changes for substances which show no rotational transitions in the solid state. Both volume changes and entropy changes are sharply increased, since the melting transition now covers the changes associated with both transitions previously. Further, the ratio of melting to boiling temperatures is still less than for the inert gases as is usually observed. This is again due to destabilization of the crystal lattice by relative misorientations, even though this is no longer associated with loss of orientational long-range order. Quantitatively the theory is rather less satisfactory for substances in this class. Relative volume changes are predicted to increase to the order of 18–25 per cent, although changes of this order are relatively rare. Entropies of melting are predicted to increase to the order of 6 cal/mole deg. In practice, a wide range of entropies is observed generally with larger values of the order of 9 cal/mole deg.[4] This limitation of the theory can probably be traced to the restriction of only two possible orientations per site. For many crystal lattices, there can be a considerably larger number of orientations among which disordering can take place, thereby making a larger contribution to the entropy of melting.

Acknowledgements—The work described above has been carried out as part of the research programme of the National Physical Laboratory, and this paper is published by permission of the Director of the Laboratory.

The authors acknowledge the help of Miss V. WAINWRIGHT and Miss P. M. NOYES in the computational work.

REFERENCES

1. LENNARD-JONES J. E. and DEVONSHIRE A. F., *Proc. Roy. Soc.* **A169,** 317 (1939).
2. LENNARD-JONES J. E. and DEVONSHIRE A. F., *Proc. Roy. Soc.* **A170,** 464 (1939).
3. LENNARD-JONES J. E. and DEVONSHIRE A. F., *Proc. Roy. Soc.* **A163,** 53 (1937).
4. EUCKEN A., *Z. angew. Chem.* **55,** 163 (1942).
5. UBBELOHDE A. R., *Quart. Rev. Chem. Soc., Lond.* **4,** 356 (1950).
6. WENTORF R. H., BEUHLER R. J., HIRSCHFELDER J. O. and CURTISS C. F., *J. Chem. Phys.* **18,** 1484 1950.

Vol. 18
1961

J. Phys. Chem. Solids Pergamon Press 1961. Vol. 18, No. 1, pp. 40–45. Printed in Great Britain.

DIELECTRIC EVIDENCE OF MOLECULAR ROTATION IN SOLIDS*

C. P. SMYTH

Frick Chemical Laboratory, Princeton University, Princeton, N.J.

Abstract—Measurements of dielectric constant as a function of temperature give clear evidence of molecular rotation in many crystalline phases comparable to the rotation in liquids and in a few organic glasses which have been studied. The effect of molecular shape upon rotation is examined, it being shown that spheroidal and cylindrical molecules may rotate. The rotation may be presumed usually to consist of rotational jumps between potential energy minima. Rotational freedom depends upon the closeness of the approach to one of the ratios of the molecular radii in different directions, but is influenced by the closeness of the molecular packing.

Many solids which show a rotational transition point are soft, waxy, and translucent in this rotator phase between the transition point and the melting-point and brittle below the transition point. A number of solids which show anomalous dielectric dispersion like that found in liquids and organic glasses, but no rotational transition, are brittle. It appears that plasticity may result from the increase in volume per molecule occurring when slightly unsymmetrical molecules begin to rotate at a transition point. Dielectric relaxation measurements show that the internal friction resisting molecular rotation in the crystal is, in some cases, about the same as in the liquid state, and, in some cases, much less.

1. INTRODUCTION

A MAJOR portion of the dielectric investigations of molecular rotational freedom in crystals has been summarized and discussed previously.[1] The present paper aims to evaluate and interpret certain aspects of the earlier results as well as to discuss more recent information.

2. DIELECTRIC CONSTANT AS EVIDENCE OF MOLECULAR ROTATION

The crystallization of a liquid normally so reduces the freedom of motion of its molecules that they are unable to turn in an externally applied electric field. If the molecules are non-polar, their freezing in the crystal lattice has only a small effect upon the dielectric constant of the material, the small increase accompanying the increase in the number of molecules per unit volume in the solid phase. If, however, the molecules have dipole moments, their freezing in the crystal lattice eliminates their usually large contribution to the dielectric constant, which, consequently, drops sharply on freezing to a low value, commonly between 2 and 3. As in the case of the non-polar materials, this low value arises from the displacement of charge induced in the molecules[1]. However, for many solids consisting of dipolar molecules possessing more or less spatial symmetry, dielectric constants similar in size and temperature dependence to those of the liquid phase have been found over a range of temperature. Since the high dielectric constants of liquids consisting of dipolar molecules are known to be due to the rotational orientation of the molecules in the alternating electric field used in measuring the dielectric constant, these high dielectric constants of dipolar molecular solids show the existence of molecular rotation in the solid. This does not mean that the molecules are necessarily rotating freely as in the gaseous state, but only that the potential energy barriers hindering their rotation are sufficiently low to permit frequent rotational passage.

* This research was supported in part by the Office of Naval Research and in part by the Office of Ordnance Research, U.S. Army. Reproduction, translation, publication, use or disposal in whole or in part by or for the United States Government is permitted.

If molecular rotation is possible only around the molecular axis in which the dipole lies, it does not affect the orientation of the dipole and, consequently, the dielectric constant does not give positive evidence of molecular rotation. This is the case, for example, with acetonitrile, methyl iodide, and nitromethane[1], for which nuclear magnetism measurements indicate the onset of rotation at 90°K, and, possibly, for t-butyl chloride[1] between 183 and 219·7°K. Change in dielectric constant accompanying change from one solid phase to another gives evidence of the transition, as in the 183·0°K transition for t-butyl chloride or in the transition for the non-polar carbon tetrachloride,[1] but, unless molecular rotation can occur above the temperature of the transition with a dipole turning about the axis of rotation, the dielectric constant does not give direct evidence of the rotation. Fortunately, molecular rotation so often involves turning of an electric dipole around the axis of rotation that measurement of dielectric constant, particularly, as a function of temperature, provides a useful tool for the investigation of the phenomenon in solids.

When a dipolar liquid is supercooled to a glass, it shows anomalous dispersion at radio frequencies very similar to that observed in the ordinary liquid range at microwave frequencies. In both cases, the mechanism is the relaxation of the rotational orientation of the molecules. This behavior has been studied particularly in the cases of branched-chain alkyl halides[1,2] and alcohols[1,3]. The branched-chain alkyl halide molecules, in contrast to those of the straight-chain alkyl halides, seem to have difficulty in fitting their irregular shapes into a crystal lattice. A similar difficulty is encountered by alcohol molecules, probably because of the molecular chains formed by hydrogen bonding. In liquids and glasses, molecular rotation is hindered by the intermolecular forces, which, as the frequency of the alternating field used in the dielectric constant measurement is increased or the temperature is lowered, cause the molecular dipole orientation to lag more and more behind the field until it disappears. The result is the familiar anomalous dielectric dispersion or gradual decrease in dielectric constant from the static or low-frequency value to the optical value, the square of the optical refractive index. The abrupt process of freezing a pure liquid gives no opportunity for such dispersion. If the polar molecules are very unsymmetrical, their packing in a crystal lattice prevents their rotation and the dielectric constant drops sharply from the static value to one close to the optical value. If the molecular shapes approach that of a sphere, the radio frequency and, sometimes, the microwave frequency dielectric constant of the crystalline solid behaves like that of the liquid for some distance below the freezing point because of molecular rotational freedom. Usually, with decreasing temperature, the rotational freedom disappears sharply at a transition point and the dielectric constant drops abruptly to a value close to that of the optical dielectric constant. It is often convenient to refer to such a transition as a "rotational transition" and to the phase existing above it as a "rotator phase". For a few crystalline solids, anomalous dispersion has been found like that in liquids and glasses.

3. EFFECT OF MOLECULAR SHAPE ON ROTATION IN CRYSTALS

(a) *Spheroidal molecules*

The simple hydride molecules[1,4] HCl, HBr, HI, H_2S, H_2Se, AsH_3, and others like them, which have been shown to rotate over considerable ranges of temperature in the solid state, may be regarded as spheres distorted by the protons, or, perhaps, as spheres with a bulge for each proton. The much larger molecules of camphor and some of its derivatives do not depart sufficiently from spherical form to prevent rotation in the crystal.

The tetrasubstituted methanes show a wide variety of rotational behavior according to the relative sizes of the substituents. The molecules of the methanes with four small atoms or groups replacing the hydrogens may be described as having the shape of a tetrahedron with small spheres at the corners or as a tetrahedron with rounded corners and indented edges, a symmetry sufficiently close to spherical to permit rotation over a considerable range of temperature. The four symmetrical tetrahalogenated methanes, CX_4, show transitions which, from their analogy to those found for dipolar tetrasubstituted methanes, may be presumed to be rotational[5]. Replacement of chlorine in CCl_4 by methyl gives dipolar molecules, CH_3CCl_3, $(CH_3)_2CCl_2$, and $(CH_3)_3CCl$, which

have been found by dielectric constant measurements to rotate below the freezing points. $(CH_3)_3CBr$ and $(CH_3)_3CI$ show similar behavior, although, for the latter, the relaxation time for the rotation process is much longer.

Measurements have been made on ten different tetrahalogenated methanes with fluorine, chlorine, and bromine as the halogens and at least two different halogens in each molecule to produce a molecular dipole moment[5]. The rotational behavior of the molecules was examined in the light of the lengths of the carbon–halogen radii C–X calculated as the sum of the two bond radii plus the van der Waals radius of the halogen, that is, the distance from the carbon nucleus to the hypothetical surface of the halogen atom. These C–X values slightly revised in terms of recently published van der Waals radii values[6], together with an analogous C–CH_3 value are as follows:

C–F, 2·76 Å; C–Cl, 3·56; C–Br, 3·86;
C–I, 4·25; C–CH_3, 3·54.

The closeness of the C–CH_3 and the C–Cl radius values shows why the tetrasubstituted methyl chloromethanes rotate so easily in the crystal. $CClBr_3$, CCl_2Br_2, and CCl_3Br, where the ratio of the two C–X values is 1·09, clearly show molecular rotation, but CF_2Cl_2, and $CFCl_3$, where the ratio is 1·29, CF_2Br_2 and CF_3Br, where the ratio is 1·40, and CF_2BrCl, show no rotation. CF_3Cl and CBr_3F show such sharp drops on freezing as to suggest that their transitions just below the freezing point correspond to cessation of molecular rotation about the symmetry axis in which the molecular dipole lies. In $(CH_3)_3CBr$, which shows rotation, the ratio of the two radii is 1·09 as in the chlorobromo compounds, which show rotation. A ratio of 1·20 in $(CH_3)_3CI$ permits rotation with some difficulty, while asymmetry to the extent of 1·29 and 1·40 prevents rotation. The nitro group is wider than the chlorine atom or the methyl group, but the models indicate approximately the same molecular radius for C–NO_2. Consistent with this is the molecular rotation found for $(CH_3)_3CNO_2$, $(CH_3)_2C(NO_2)_2$, $(CH_3)_2CCl(NO_2)$, and $(CH_3)_2CBr(NO_2)$, although the large dipole moment associated with the nitro group might be expected to increase the intermolecular forces somewhat.

(b) *Cylindrical molecules*

The disappearance of molecular rotation with increasing departure of the molecules from nearly spherical form might seem to imply the restriction of rotation in the crystalline state to nearly spherical molecules. However, long, more or less cylindrical molecules have often been found to rotate around the axis of the cylinder[1]. Many substances of the general formula $CH_3(CH_2)_nX$, where X = CH_3, Br, or OH, show rotation around the axis of the chain when n is large. Thus, many straight-chain hydrocarbons from $C_{18}H_{38}$ to $C_{44}H_{90}$ show transitions with rising temperature to a phase of hexagonal symmetry, in which the molecules are thought to rotate around the axes of their chains[1]. Several short-chain alkyl bromides have been found to show phase transitions in the crystalline state, but their dielectric constants have given no evidence of any considerable molecular rotational freedom. For n = 4,6,7,8,9,10,11,12,14, and 17 in $CH_3(CH_2)_nBr$, no rotation has been found, but for n = 21 and 29, rotation around the long axis of the extended chain has been found to occur, a low-frequency absorption arising from rotational jumps between a deep potential energy minimum and one of several shallow minima and a high-frequency absorption arising from jumps between two shallow minima[1,7]. The long, straight-chain alcohol molecules, which are hydrogen-bonded end-to-end, show no rotation for n-$C_8H_{17}OH$, n-$C_{10}H_{21}OH$, and pure n-$C_{12}H_{25}OH$, but rotation with apparent proton transfer is found above a monotropic transition for n-$C_{14}H_{29}OH$, n-$C_{16}H_{33}OH$, n-$C_{22}H_{45}OH$ and others.[1] Many long-chain esters and ethers also give evidence of molecular rotation or segment orientation by rotational twisting.[1,8] MEAKINS[8] has found that the energy barrier hindering rotation from one equilibrium position in the lattice to another increases linearly with chain length. Phase metastabilities often complicate the interpretation of the behaviors of the substances of higher molecular weights. It would appear that the shorter molecules in a series may not acquire the energy necessary to rotate over hindering potential barriers before the melting point is reached.

(c) *Oblate spheroidal molecules*

Because the benzene molecule is non-polar, the dielectric constant gives no evidence as to its

possible rotation in the crystal, but there is an indication of such rotation in the results of nuclear magnetic resonance measurements.[1] Dielectric constant measurements have been made on a large number of poly-substituted benzenes with methyl and chlorine as the substituents.[1,11] When there are fewer than five substituents, the molecules can pack in the lattice in such a way as to prevent rotation. When there are five substituents, the molecules rotate above a transition temperature, but when there are six substituents, the crystalline solids show no transition but rotation with anomalous dispersion at radio frequencies like that shown by organic glasses[1] and by polar liquids at microwave frequencies. In the tetrasubstituted methanes, replacement of a chlorine or methyl by a nitro group increases the difficulty of rotation. In the penta- and hexasubstituted benzenes, the effect is more pronounced. 1,2,3,4-tetramethyl-5, 6-dinitrobenzene and 5-nitro-3,4-dichloro-*o*-xylene show rotation above a transition point, but four penta- or hexa-substituted benzenes with the nitro group as one of the substituents show no rotation. Replacement of methyl by ethyl blocks rotation by a protrusion.

Vol. 18
1961

For the hexamethylbenzene molecule, calculation gives a van der Waals diameter of 9·66 Å in the plane of the ring. X-ray analysis[9] shows that the molecules lie in successive layers with their molecular ring planes tilted by just over 1° out of the (001) crystal planes in which these layers lie. As the distance between these planes is only 3·66 Å, it is evident that molecular rotation can occur only in or nearly in these planes, that is, approximetely around an axis perpendicular to the plane of the ring and through its center. The evident steric hindrance to rotation by turning out of the plane is so great for this crystal lattice that it appears safe to attribute practically all molecular rotation in these penta- and hexasubstituted benzenes to motion approximately in the plane of the ring. In the pentasubstituted methyl chlorobenzene molecules, the ratio of the van der Waals radius across a substituted position to that across the unsubstituted position is 1·43. This is a larger ratio than that which prevents rotation in the tetrasubstituted methanes, but, although both types of molecule are distorted spheres, the shapes and the consequent lattice packing are so different in detail that the factors determining molecular rotation or non-rotation should be quite different. It must be remembered that the axis of rotation does not necessarily pass through the central carbon atom of the methanes or through the center of the benzene ring but rather through a point somewhere between the geometrical center and the center of gravity of the molecule.

The actual rotational process in the crystal lattice is probably a series of jumps over the barriers between potential energy minima. In the lattices of the fairly symmetrical hexasubstituted benzenes, the levels of the potential energy minima should not be very different from one another and the barriers between them should not be high. The liquid- or glass-like dielectric dispersion observed for these crystals is, therefore, not surprising. The unsubstituted position of the penta-substituted molecules should raise the potential barriers to such a height that a co-operative loosening of the lattice with consequent increase of volume analogous to that occurring at the melting point may be necessary for rotation. The result is a sharp rotational transition accompanied by change of energy, volume, and usually crystal form.

4. WAXINESS

In many cases, the solid phases in which dielectric measurements showed the existence of molecular rotation were not handled in such a way as to make possible observation of their mechanical properties. The rotator phases of the tetrasubstituted methanes, the camphors, and the camphor derivatives discussed in the next section were observed to be waxy. WHITE and BISHOP[10], who investigated a large number of polymethylene compounds and camphor derivatives, found that crystals in which there was no molecular rotation at room temperature were relatively hard and brittle, while those in which the molecules rotated at room temperature were soft and waxy. WHITE *et al.*[11] found for several of the penta-substituted benzenes which have been discussed that the solids were brittle below the rotational transitions and waxy above them. However, for the hexasubstituted benzenes, which showed anomalous dispersion in the crystalline state but no transition, the solids were found[11] to be brittle at room temperature, although the dielectric constants were high. Several derivatives of camphane which

showed anomalous dispersion but no transition were found to be waxy and translucent like the high temperature forms of the solids which showed transitions. It was stated[11], however, that "there was some evidence that the failure of the transition to appear was due to the presence of solid solutions of optical isomers or to the existence of the high temperature form in a metastable state at temperatures below that of its presumed transition". In any event, it seems certain that many solid phases showing molecular rotation above a transition are waxy, while at least several showing anomalous dispersion and molecular rotation are brittle. Quantitative measurements[12] showed that for tetrabromomethane, hexachloroethane, *d*-camphor, and camphoric anhydride, the pressure required to deform by a standard amount a sample in the non-rotator phase was from 2 to 14 times as great as that required in the rotator phase. It has been suggested[13] that the waxiness of the rotator phase above a transition is due to the greater volume occupied by a somewhat unsymmetrical molecule when rotating. The hexa-substituted chloro- and methyl benzene molecules are so symmetrical around the axis through the center of the ring and perpendicular to its plane that rotation can occur without appreciable increase in volume and consequent increase in the molecular mobility, which might cause waxiness.

5. INTERNAL VISCOSITY

In liquids, dipole orientation, which occurs by molecular rotation, has been studied as a relaxation process, which, for a spherical molecule in a continuous viscous fluid, has a relaxation time proportional to the cube of the molecular radius and to the internal friction coefficient, or internal viscosity of the fluid.[14] Since the molecular radii of the spheroidal tetrasubstituted methanes could be calculated, it was possible to calculate the internal viscosities of these substances in the liquid state[15] from the molecular relaxation times determined for the liquids[16]. The values of the internal viscosities thus obtained were only 0·008 to 0·06 of the macroscopic or measured viscosities of the liquids and little parallelism was observed between the values of the internal viscosity and those of the macroscopic viscosity.

The dielectric constants and losses at a wavelength of 3·2 cm were measured over a range of temperature for several of these substances in the solid state.[1,13] For $(CH_3)_3CCl$, the solid rotator phase above the higher transition point showed a dielectric constant hardly distinguishable from that at low frequency and a loss so close to zero that no significant value could be calculated for the relaxation time, showing that the internal viscosity or resistance to molecular rotation was far less than in the liquid state. Just below the freezing-point, $(CH_3)_3CBr$, $(CH_3)_2CCl_2$, and CH_3CCl_3 showed almost as low a loss and high a dielectric constant as $(CH_3)_3CCl$, indicating much less resistance to rotation than in the liquid, but decreasing temperature raised the resistance to rotation until, at 20–25° below the freezing-point, the internal viscosity was about equal to that of the liquid just above the freezing-point. The results[13] on CBr_2Cl_2 are harder to interpret because of the smallness of the molecular dipole moment, but the high dielectric constant and small loss of the solid just above the rotational transition temperature 35° below the freezing-point indicate an internal viscosity not far from that of the liquid just above the freezing-point. $(CH_3)_2CClNO_2$ and $(CH_3)_2C(NO_2)_2$ show an internal viscosity close to that of the liquid and increasing only a little with decreasing temperature over a range of 40–55°.

The large molecules[13] of D,L-camphene, D-camphor, D,L-camphor, and D,L-isoborneol seem to encounter nearly the same resistance to rotation in the solid state just below the freezing-point as they do in the liquid, the resistance increasing gradually with decreasing temperature. In D-camphoric anhydride the molecules seem to possess slightly less rotational freedom in the solid than in the liquid just above the freezing-point but they lose little of this freedom as the temperature decreases over an 85° range to the transition point.

6. CONCLUSIONS

The factors determining molecular rotation or non-rotation in solids are more or less interdependent. The greater the symmetry about a molecular axis, the greater is the probability of rotation around that axis or around an axis parallel and close to it. Increase in the size of one part of a fairly symmetrical molecule, as by replacement of a methyl group by an ethyl, tends to block rotation by the introduction of a high and,

Vol. 19

perhaps, insurmountable potential energy barrier. To a much lesser extent, differences in polarizability between different parts of a molecule, as between a fluorine and a bromine atom, and large molecular dipole moments may contribute to the hindering potential barriers. Among solids which show molecular rotation, tremendous differences in molecular mobility are observed, as between the hexasubstituted benzenes, which show dielectric relaxation times of the order of 10^{-3} to 10^{-5} sec and t-butyl chloride, the relaxation time of which is much shorter than 10^{-12} sec. Waxiness or plasticity of crystalline phases tends to be associated with short dielectric relaxation times and may be speculatively attributed to increased free volume possessed by molecules above rotational transitions.

REFERENCES

1. SMYTH C. P., *Dielectric Behavior and Structure*, Chapter 5. McGraw-Hill, New York (1955).
2. DENNY D. J. and COLE R. H., *J. Chem. Phys.* **27,** 259 (1957).
3. DAVIDSON D. W. and COLE R. H., *J. Chem. Phys.* **19,** 1484 (1951); HASSION F. X. and COLE R. H., *ibid* **23,** 1756 (1955); DANNHAUSER W. and COLE R. H., *ibid* p. 1762; DENNEY D. J. and COLE R. H., *ibid* p. 1767.
4. COLE R. H. and HAVRILIAK S. Jr., *Disc. Faraday Soc.* **23,** 31 (1957).
5. MILLER R. C. and SMYTH C. P., *J. Amer. Chem. Soc.* **79,** 20 (1957).
6. PAULING L., *The Nature of the Chemical Bond*, 3rd Ed., p. 260. Cornell University Press, Ithaca, N.Y. (1960).
7. See also HOFFMAN J. D., *Arch. Sci. Genève* **12,** 36 (1959).
8. MEAKINS R. J., *Trans. Faraday Soc.* **55,** 1694, 1701 (1959).
9. ROBERTSON J. M., *Organic Crystals and Molecules*, p. 178. Cornell University Press, Ithaca, N.Y. (1953).
10. WHITE A. H. and BISHOP W. S., *J. Amer. Chem. Soc.* **62,** 8 (1940).
11. WHITE A. H., BIGGS B. S. and MORGAN S. O., *J. Amer. Chem. Soc.* **62,** 16 (1940).
12. MICHILIS A., *Bull. soc. chim. Belg.* **57,** 575 (1948).
13. WILLIAMS D. E., Ph.D. Thesis, Princeton University, 1956;
    WILLIAMS D. E. and SMYTH C. P., to be published.
14. SMYTH C. P., *Dielectric Behavior and Structure*, Chapter 2. McGraw Hill, New York (1955).
15. SMYTH C. P., *J. Phys. Chem.* **58,** 580 (1954).
16. MILLER R. C. and SMYTH C. P., *J. Chem. Phys.* **24,** 814 (1956).

Vol. 18
1961

J. Phys. Chem. Solids Pergamon Press 1961. Vol. 18, No. 1, pp. 46–52. Printed in Great Britain.

THERMODYNAMIC STUDIES OF MOLECULAR ROTATION IN SOLIDS

L. A. K. STAVELEY

The Inorganic Chemistry Laboratory, Oxford University

INTRODUCTION

THE POSSIBILITY that molecules and ions might rotate in crystal lattices seems to have been first raised by SIMON[1] to account for transitions in solids at which a low-temperature form of comparatively low symmetry changes into a high-temperature form of higher symmetry. Partly because of the development of this idea by PAULING[2], and partly because some of the facts about transitions (both sharp and gradual) can be plausibly explained if it is assumed that the passage from the low-temperature form to the high-temperature form is associated with the onset of free rotation of molecules or ions, belief in the reality of such free rotation became rather widespread, and many transitions in solids came to be described as rotational transitions. Though the energy barrier preventing the free rotation of a molecule or ion in a lattice is often relatively low, so that these particles can rapidly switch from one orientation to another, nevertheless the number of solids for which it has been convincingly established that the molecules or ions rotate in them with virtually the same complete freedom as molecules in the gaseous phase is still very small.

CLATHRATES

One method of investigating the motion of molecules or ions in a lattice consists simply in an analysis of the heat capacity of the solid, since in general the contribution to the heat capacity will differ according to whether the particles are freely rotating or executing torsional oscillations. The method can be applied in a particularly direct way to the so-called clathrates. Typical clathrates are those formed by quinol. This substance can crystallize in a stable α-form or an unstable β-form, both being hydrogen-bonded structures. In the β-form there are quite large holes (~ 8 Å diameter) regularly situated throughout the lattice, there being one hole to three quinol molecules. By producing the β-quinol in the presence of sufficiently small molecules (e.g. by carrying out the crystallization in the presence of, say, argon, nitrogen, or methane under pressure), these molecules can be trapped in the cavities. Since a hole cannot accommodate more than one molecule, the existence of such clathrates makes it possible to study the behaviour of molecules trapped individually in almost spherical cells. If the molecules are small enough, the holes are not distorted. If it is assumed that the trapped molecules do not affect the heat capacity of the quinol lattice itself, then the contribution C_A made by a mole of them to the heat capacity of the clathrate is given by the difference in C_p of three moles of β-quinol (with the holes empty) and C_p for the same amount of β-quinol with all the holes filled. Since the pure β-quinol is rather unstable, but much less so if even a few of the holes are filled, and since it is not always possible to fill *all* the holes, in practice it is better to make C_p measurements on two or preferably more clathrates of different compositions, and to derive C_A from isothermal plots of the heat capacity against the fraction of holes filled. This has been done for the methane clathrate from 14 to 298°K.[3] To examine the rotational or torsional movement of the methane molecules it is then necessary to allow for the contribution C_{vib} made to C_A by the vibrational (or quasi-translational) movement of each molecule within its cell. This can be done by the theory of VAN DER WAALS[4] (essentially an application of the Lennard-Jones–Devonshire cell model), the reliability of which we have adequately

confirmed by studies of the argon and krypton clathrates,[5] for which, of course, $C_A = C_{\text{vib}}$. The results for the methane clathrate are shown in Fig. 1, from which it can be seen that when C_{vib} has been subtracted from C_A (and a small allowance made for the contribution C_{int} from the internal vibrations of the methane molecules), the remainder, C_{rot}, has from about 150°K upwards (and possibly at still lower temperatures) the value of $\frac{3}{2}R$, within experimental error, thus showing that at higher temperatures the molecules are virtually rotating freely. (The analysis of C_A cannot be reliably extended to lower temperatures as VAN DER WAALS' treatment only holds in the "classical" region). A study has also been made, but by a different method, of the oxygen clathrate. MEYER *et al.*[6] showed that the magnetic susceptibility of the oxygen from 0·25 to 20°K could be accounted for if the rotation of the molecules is hindered by an energy barrier of 128 cal/mole. This means that the trapped molecules must have almost complete rotational freedom at ordinary temperatures. Thus the methane and oxygen quinol clathrates provide examples of lattices in which molecules may really be said to rotate, and other quinol clathrates with small molecules are probably similar in this respect. Molecules as large as methyl alcohol and acetonitrile can occupy the holes in β-quinol, but now there is some distortion of the cavities and the rotation of the molecules in them may be seriously impeded.

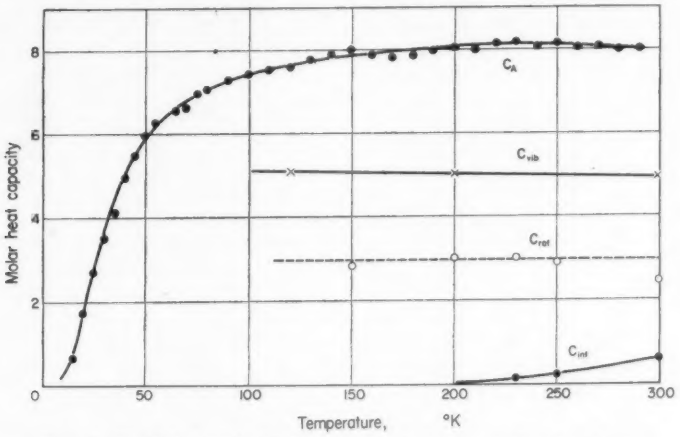

FIG. 1. Graphical analysis of the contribution per mole of methane to the heat capacity of the methane–quinol clathrate. Upper curve, full circles, the total contribution C_A. Crosses, the calculated contribution from the vibration of the methane molecules in the cavities, C_{vib}. Bottom curve, full circles, the contribution from the internal vibrations of the methane molecules, C_{int}. Open circles, C_{rot}, $= C_A - C_{\text{vib}} - C_{\text{int}}$. The dotted line is drawn at $\frac{3}{2}R$.

AMMONIUM SALTS

The particle which has been most thoroughly investigated with regard to its possible rotation in crystal lattices is the ammonium ion, especially in the ammonium halides. In the simple cubic forms of these salts the ammonium ion does not freely rotate, but in the face-centred forms stable at higher temperatures it undergoes almost free rotation about one N–H bond. This ion might however achieve something approaching free three-dimensional rotation in lattices in which the field of force acting on it is very symmetrical. We have recently tried to elucidate its motion in ammonium stannichloride and stannibromide.[7] These salts are isomorphous with the rubidium compounds and the ammonium and rubidium salts with the same anion have almost identical lattice dimensions. It is therefore reasonable to suppose that the quantity

$$\Delta C_p = C_p(\text{NH}_4\text{ salt}) - C_p(\text{Rb salt}) - C_{\text{int}}$$

(C_{int} being the small calculable contribution from

Vol. 18
1961

the internal vibrations of the ammonium ions) is the heat capacity contribution from the torsional oscillation or rotation of the ammonium ions, (at least at higher temperatures at which the lattice vibrations effectively make their limiting maximum contribution). The stannichloride and stannibromide were chosen for study because the ammonium ion has a very symmetrical environment in both salts, having as nearest neighbours twelve equidistant halogen atoms which cannot carry such high charges as monatomic halogen ions. The plot of ΔC_p against temperature for the stannichloride is shown in Fig. 2. The mini-

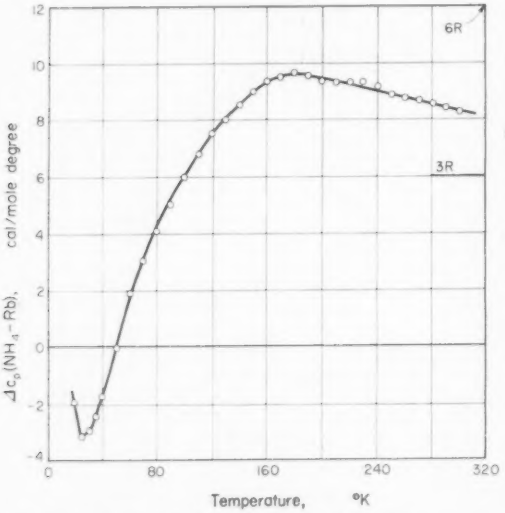

FIG. 2. Plot of $\Delta C_p(NH_4-Rb)$ against temperature. $\Delta C_p(NH_4-Rb)$ is the difference between the molar heat capacities of ammonium stannichloride and rubidium stannichloride, less the contribution from the internal vibrations of the ammonium ions.

mum at low temperatures is due to the difference in the contribution from the lattice vibrations arising from the difference in mass of the cations. At higher temperatures ΔC_p passes through a maximum and then falls, reaching at room temperature a value about half-way between $3R$ and $6R$. (Ammonium stannibromide has a λ-point at 144·8°K. Above this, ΔC_p follows much the same course as for the stannichloride.) The passage of ΔC_p through a maximum and its subsequent decrease towards $3R$ is the behaviour to be expected if the barrier to rotation of the ammonium ions is fairly low. Since ammonium stannichloride has no transition the system is a comparatively simple one in which the barrier to rotation should not change much with temperature. In this respect the ammonium ion in such a salt is more like the molecule trapped in the clathrate than the molecule in a one-component solid such as solid methane or carbon tetrachloride, where the rotation of any one molecule must naturally affect and be affected by the behaviour of its neighbours.

METHANE

The difference or comparative methods just described cannot be applied when the lattice contains one kind of particle only (as in a one-component molecular solid), but in principle whether the molecules in such solids are rotating or not can be investigated by analysing the heat capacity at constant volume C_v. It is therefore necessary to know C_p, the coefficient of expansion α, and the isothermal compressibility β, so that C_v can be derived from the relation

$$C_p - C_v = T\alpha^2 V/\beta$$

Values of α and more particularly of β are unfortunately seldom available for molecular solids. Nevertheless, an early application of this method was made by EUCKEN and VEITH[8] to methane, using some rather meagre information on the lattice dimensions to assess α, and one direct value of $(\partial p/\partial T)_v$. On deducting from the values of C_v the contribution from the lattice vibrations (evaluated from a plausible estimate of the Debye frequency), the residual heat capacity C_{rot} agreed closely with that calculated for the rotational heat capacity of gaseous methane, assumed to be the equilibrium mixture of the three types of molecule. C_{rot} is 3·5 cal/mole deg at 30°K and *decreases* with increasing temperature. At the melting-point it is within a few per cent of the limiting classical value of $\frac{3}{2}R$, indicating that the molecules are undergoing almost free rotation. The molecular movement in solid tetradeuteromethane (considered in preference to CH_4 owing to the smaller susceptibility of CD_4 to quantum effects) has recently been the object of a very thorough theoretical study by JAMES and KEENAN.[9] They conclude that even in the high-temperature phase of CD_4, owing to octupole–octupole interaction rotation of the molecules is not completely free, though from the heat capacity

Table 1. *Some properties of nitrogen and carbon monoxide*

	N_2	CO
Melting-point	63·14	68·09°K
ΔS_m	2·73	2·93 cal/mole deg
Transition temperature	35·61	61·55°K
ΔS_{tr}	1·54	2·46 cal/mole deg
Critical temperature	126	134°K
Critical volume	90	90 cm^3/mole
Critical pressure	33·5	35 atm
Quadrupole moment (a)	1·29	$1{\cdot}62\times10^{-26}$ e.s.u.
(b)	1·27	$1{\cdot}71\times10^{-26}$ e.s.u.

(a) From microwave collision broadening.

(b) From lattice energy calculations.

analysis for CH_4 it seems certain that the energy barrier to rotation must be small. They reach the interesting conclusion that in phase II of CD_4 (the phase stable below the upper transition temperature), one molecule in four rotates quite freely; its nearest neighbours oscillate, but do not rotate.

It is worth noting that the entropy of fusion ΔS_m of CH_4 (2·48 e.u.) is nearly 1 e.u. smaller than that of the rare gases, and that ΔS_m for SiH_4 and GeH_4 is still lower (1·80 and 1·86 e.u. respectively). Probably in the high-temperature forms of the last two hydrides molecular rotation is also virtually free.

NITROGEN AND CARBON MONOXIDE

An attempt can also be made to analyse the heat capacity of solid nitrogen. In Table 1 some properties of this element are compared with those of carbon monoxide. There is a close similarity between these two substances, and any conclusions reached about the molecular movement in solid nitrogen will probably also apply to carbon monoxide. Both substances show a transition below which they exist in a face-centred cubic α-form in which the molecules are orientationally ordered. In the high-temperature hexagonal β-forms the molecules are either rotating or at least orientationally disordered. It is worth noting that the $\alpha \rightarrow \beta$ transition temperature for carbon monoxide is considerably higher than that for nitrogen. From recent experimental work by SWENSON[10] on the effect of pressure on solid nitrogen an estimate can be made of the compressibility at zero pressure. At 53°K, this is $7{\cdot}2\times10^{-5}$ atm^{-1}. As SWENSON himself indicates, the values of the limiting compressibilities to be derived from his work are probably not very accurate. But since a direct determination[11] of the compressibility of nitrogen at a much lower temperature (4°K) gave a value of $5{\cdot}2\times10^{-5}$ atm^{-1}, and since the compressibility should decrease with falling temperature—that of argon drops by 30 per cent from 77 to 65°K—it is unlikely that the figure quoted for 53°K is seriously too small. Combining this with a value of α of $1{\cdot}73\times10^{-3}$ derived from density measurements,[12] (C_p-C_v) at 53°K is found to be 1·54 cal/mole deg, which gives $A = 2{\cdot}76\times10^{-4}$ in the equation $C_p-C_v = ATC_p^2$. Using this equation and GIAUQUE and CLAYTON's C_p values,[13] C_v has been estimated at 40, 50 and 60°K. The contribution C_1 from the lattice vibrations has been evaluated from a Debye function with $\theta_D = 79°$, this value being derived from the equation

$$\theta_D = 163\sqrt{(T_m/MV^{2/3})}$$

(T_m = melting-point, M = molecular weight, V = molar volume), which gives good agreement with the experimental θ_D values for argon, krypton, and xenon.[14]

The results of this analysis for the β-form of nitrogen are shown in Table 2. Admittedly this analysis is rather rough, but the values of C_{rot} are so far above that of ~ 2 cal/mole deg for free rotation that it is unlikely that the uncertainties in α, β, and θ_D falsify the obvious conclusion that even in the β-form of nitrogen the molecules do not rotate, but rather still undergo torsional

Vol. 18
1961

Table 2. Analysis of the heat capacity (in cal/mole deg) of the β-form of solid nitrogen. C_1 = contribution from the lattice vibrations. $C_{res} = C_v - C_1$

T	40	50	60°K
C_p	9·03	9·92	10·92
C_v	8·13	8·56	8·96
C_1	4·94	5·27	5·47
C_{res}	3·2	3·3	3·5

oscillations. This inference is consistent with the fact that the volume change for the $\alpha \rightarrow \beta$ transition is so small,[10] $\sim 0{\cdot}22$ cm³/mole, that it could scarcely be expected to make any difference to the movement of the molecules. (For carbon monoxide, the volume change at the transition is $\sim 1{\cdot}0$ cm³/mole.) The molar volume of β-N_2 at 60°K is 29·3 cm³. That for freely rotating molecules (estimated[15] from the distance of closest approach in α-N_2 at 4°K) would be 39 cm³.

The tendency for homopolar diatomic molecules to adopt preferred orientations with respect to each other could arise either from anisotropy in the dispersion forces or from quadrupole–quadrupole interactions. (The same is true for carbon monoxide molecules, for which the *dipole* moment is so small that its orientating influence is quite negligible). According to the calculations of JENSEN and DE WETTE,[16] it is the quadrupole effect which is the more important. DE WETTE[17] has shown that the transition temperature has a sensitive dependence on the quadrupole moment and that the difference in the latter for nitrogen and carbon monoxide (see Table 1) could account for the considerable difference in the transition temperatures.

Information on the rotational movement of the molecules of a substance in the *liquid* state may help in elucidating their motion in the solid, in that if it can be shown that rotation in the liquid state is not free, then *a fortiori* it must be hindered in the solid. Some insight into the relative degrees of order and molecular freedom in different liquids may be gained by a comparison of their entropies of vaporization. According to Hildebrand, the comparison should be made at a fixed value of the molar volume of the vapour, i.e. at a fixed value of p/T, where p is the vapour pressure of the liquid at T°K. In Fig. 3, the entropies of vaporization of nitrogen, oxygen, carbon monoxide,

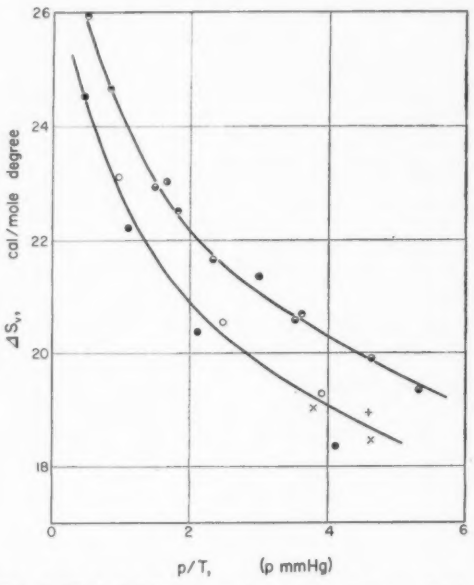

FIG. 3. Plot of ΔS_v (the molar entropy of vaporization) against p/T. (p = vapour pressure in mm Hg, T = absolute temperature). ◒ nitrogen; ◑ carbon monoxide; ◓ oxygen; ● germanium hydride; ○ methane; × xenon; + krypton.

methane, germanium hydride, krypton, and xenon are plotted against p/T. The points for the diatomic liquids tend to fall on one curve, and those for the substances with monatomic or tetrahedral molecules on another, lower curve. In liquid methane molecular rotation must be effectively free, since, as we have seen, this appears to be so even in the solid near the melting-point. The simplest explanation of Fig. 3 is therefore that in the diatomic liquids that part of the entropy associated with molecular rotation is significantly below the value for free rotation. At the melting-points of nitrogen and carbon monoxide the deficit is about 1·5 e.u.

Confirmation that in liquid nitrogen and carbon monoxide orientational forces are still important is provided by a recent study of the thermodynamic properties of liquid mixtures of these two substances. Their critical constants are

Table 3. Analysis of the heat capacity (in cal/mole deg) of carbon tetrabromide above and below the transition at 46·9°C. C_{int} = contribution from the lattice vibrations. $C_{v_{res}} = C_v - C_{int}$

t°C	C_p	C_v	C_{int}	$C_{v_{res}}$
0	28·25	24·94	13·23	11·7
37·69	31·70	25·57	14·05	11·5
55·32	32·98	25·78	14·33	11·45
70	33·12	25·68	14·55	11·1
85	33·70	25·60	14·76	10·8

so alike (Table 1) that on recent theories of solution,[18] based on the principle of corresponding states, it would be expected that nitrogen–carbon monoxide mixtures would be almost ideal. In fact, the equimolar mixture is formed with a 0·35 per cent increase in volume and has at 84°K a vapour pressure 3·3 per cent greater than the ideal value.[19] These departures from ideality (which are of the same order as those shown by, for example, argon–oxygen and argon–nitrogen mixtures) would therefore seem to depend on factors which have a much smaller influence on the critical constants. The tendency already noted for the molecules to adopt preferred orientations with respect to each other owing to quadrupole interactions could be important at lower temperatures but negligible in the relatively expanded condition of the fluids at the critical point.

Vol. 18
1961

CARBON TETRAHALIDES

Carbon tetrafluoride, tetrachloride, and tetrabromide all undergo transitions and have comparatively low entropies of fusion. The transition temperature for the tetrabromide (46·87°C) is conveniently situated for making thermodynamic measurements on both the high and low temperature forms. A few years ago we measured C_p, the coefficient of expansion α and the isothermal compressibility β for this substance above and below the transition and so estimated C_v.[20] The results are shown in Table 3. The lower three temperatures are those at which β was measured. The estimates of $(C_p - C_v)$ at the two higher temperatures were made from the relation $C_p - C_v = ATC_p'^2$, where $C_p' = C_p - C_{int}$, C_{int} being the contribution from the intramolecular vibrations, using the concordant values of A obtained by applying this relation to the data for the two higher temperatures at which β was measured. The values of $C_{v_{res}}$ in Table 3 give the sum of the contributions from the lattice vibrations and the torsional oscillations. It is clear that the molecules do not freely rotate even in the high-temperature form, which would require that the maximum value of $C_{v_{res}}$ would be $\frac{9}{2}R$, and in fact there is scarcely any change in $C_{v_{res}}$ at the transition even though this occurs with a volume increase of ~ 7 per cent. Nevertheless, there is a significant fall in $C_{v_{res}}$ as the melting-point is approached, which implies that the barrier to rotation cannot be very high. Probably the same state of affairs prevails in the other carbon tetrahalides, for there is a close correspondence in the thermodynamic characteristics of transition and fusion in these substances, as is shown by Table 4. It has in fact recently been stated[21] that the X-ray diffraction pattern of the high-temperature form of carbon tetrachloride cannot be satisfactorily accounted for quantitatively on the basis that the molecules are freely rotating. In any case, the molar volume of this form of the tetrachloride

Table 4. A comparison of the transitions in carbon tetrafluoride, tetrachloride and tetrabromide. T_{tr}/T_m is the ratio of the transition temperature to the melting-point. The entropy changes are in cal/mole deg

	CF_4	CCl_4	CBr_4
T_{tr}/T_m	0·852	0·901	0·881
ΔS_{tr}	4·64	4·86	4·98
ΔS_m	1·87	2·40	2·60

is less than that needed for true free rotation by somewhere between 20 and 40 per cent, depending on the estimates used for the van der Waals radius of the chlorine atom. Perhaps in solid neopentane near the melting-point there is a closer approach to free rotation since the molecules have no strongly polar bonds. It may be noted, however, that the molar volume of lead tetramethyl is less by 2 to 3 per cent than that of tin tetramethyl, both in the solid and liquid states,[22] in spite of the fact that the Pb–C bond is longer than the Sn–C bond. This is a clear indication of molecular interlocking, which must effectively prevent the molecules in the solids from gaining orientational freedom, since, unlike neopentane, the solid forms of lead and tin tetramethyl have no transitions and melt with entropies of fusion of 10·62 and 10·34 e.u. respectively.[23]

CONCLUSION

To sum up, the impression given by a consideration of the few systems where a thermodynamic analysis can be carried out is that it is possible for molecules to rotate in crystal lattices with almost complete freedom, examples being the oxygen and methane molecules in the quinol clathrates and the molecules in solid methane near the melting-point, but that such almost free rotation is probably rare, and is not necessarily guaranteed by a combination of a low entropy of fusion and a high degree of molecular symmetry. Nevertheless, there are undoubtedly numerous crystals in which in the form stable just below the melting-point the molecules have considerable orientational freedom. In such crystals the torsional movement of the molecules must be a co-operative matter of some complexity, which can scarcely be adequately treated as hindered rotation with an almost constant energy barrier. Possibly molecular reorientation in such lattices is connected with the comparative ease of diffusion known to prevail in solids of low entropy of fusion, in that two molecules simultaneously rotate round a common centre, thereby changing places in a manner recalling Eyring's theory of viscous flow in liquids.

REFERENCES

1. Simon F. and von Simson C., *Z. Phys.* **21,** 168 (1924).
2. Pauling L., *Phys. Rev.* **36,** 430 (1930).
3. Parsonage N. G. and Staveley L. A. K., *J. Mol. Phys.*, in press.
4. van der Waals J. H., *Trans. Faraday Soc.* **52,** 184 (1956).
5. Parsonage N. G. and Staveley L. A. K., *J. Mol. Phys.* **2,** 212 (1959) (argon); Parsonage N. G., Grey N. R. and Staveley L. A. K., unpublished results (krypton).
6. Meyer H., O'Brien M. C. M. and van Vleck J. H., *Proc. Roy. Soc.* **243A,** 414 (1958).
7. Morfee R. G. S., Staveley L. A. K., Walters S. T. and Wigley D. L., *J. Phys. Chem. Solids* **13,** 132 (1960).
8. Eucken A. and Veith H., *Z. Phys. Chem.* **34B,** 275 (1936); **38B,** 393 (1937).
9. James H. M. and Keenan T. A., *J. Chem. Phys.* **31,** 12 (1959).
10. Swenson C. A., *J. Chem. Phys.* **23,** 1963 (1955).
11. Stewart J. W., *Phys. Rev.* **97,** 578 (1955).
12. Dokoupil Z., van Soest G. and Swenker M. D. P., *Appl. Sci. Res. Hague* **5,** 204 (1955).
13. Giauque W. F. and Clayton J. O., *J. Amer. Chem. Soc.* **55,** 4875 (1933).
14. Clusius K., *Z. Phys. Chem.* **31B,** 459 (1935).
15. Bolz L. H., Boyd M. E., Mauer F. A. and Peiser H. A., *Acta Cryst., Camb.* **12,** 247 (1959).
16. Jansen L. and de Wette F. W., *Physica* **21,** 83 (1955).
17. de Wette F. W., *Physica* **22,** 644 (1956).
18. Prigogine I., *The Molecular Theory of Solutions.* North Holland Publishing Co., Amsterdam (1957).
19. Herrington T. M. and Staveley L. A. K., unpublished work.
20. Marshall J. G., Staveley L. A. K. and Hart K. R., *Trans. Faraday Soc.* **52,** 19 (1956).
21. Post B., *Acta Cryst., Camb.* **12,** 349 (1959).
22. Williams D. J. W. and Staveley L. A. K., unpublished work.
23. Staveley L. A. K., Warren J. B., Paget H. P. and Dowrick D. J., *J. Chem. Soc.* 1992 (1954).

Vol. 196

J. Phys. Chem. Solids Pergamon Press 1961. Vol. 18, No. 1, pp. 53–61. Printed in Great Britain.

SOME OBSERVATIONS ON PHASE TRANSFORMATIONS IN MOLECULAR CRYSTALS

G. B. GUTHRIE and J. P. McCULLOUGH

Abstract—This paper illustrates the use of calorimetric data in interpreting phase behavior in molecular crystals. Values of entropy of transition are used to estimate the number of distinguishable molecular orientations in a disordered phase, and symmetry and steric considerations are used to find a reasonable description of these orientations. As the number of molecular orientations in a plastic crystal is 10 or higher, it is proposed that orientations occur in which less than the full molecular symmetry is displayed at lattice sites. Thus, a molecule of tetrahedral symmetry may assume two orientations in which the common molecular and lattice symmetry elements belong to the T_d point group and an additional eight with the elements of C_{3v}. From this consideration, the entropy of transition for typical tetrahedral molecules is calculated to be R ln 10 (4·58 cal deg^{-1} mole^{-1}), in accord with experimental evidence. Molecules of approximately tetrahedral shape but less than tetrahedral symmetry form plastic crystals with disorder corresponding to the same ten orientations plus additional disorder due to the lower molecular symmetry.

INTRODUCTION

A PHASE transformation in a molecular crystal is a little like the elephant in the fable of the blind men—it shows different aspects depending on how it is approached. Thus, complete understanding of a phase transformation requires investigation of its various aspects by various approaches. Only a few phase transformations have been studied thoroughly enough by enough methods that the molecular processes involved may be described satisfactorily. Studies of crystal structure, dielectric constant, volumetric behavior, nuclear magnetic resonance spectrum, and thermal properties usually are needed to elucidate the most important aspects of a phase change in a molecular crystal. Seldom are more than one or two of these techniques available in one laboratory for study of a particular substance.

Studies of the change of thermal properties in the course of a phase change give valuable information about some aspects of phase behavior. As part of a program primarily to determine entropy values by the Third Law, the Bureau of Mines has made precise calorimetric studies of about thirty pure organic substances that undergo solid–solid phase transformations.[1] Some of the results obtained by the Bureau during the last 17 years will be used in speculations about the nature of "plastic crystals and rotation in the solid state." Ordinarily, such speculations based mostly on thermal data are avoided in public, but they are made here to show what can be done and to suggest fruitful subjects for research by non-thermal methods.

CALORIMETRIC STUDIES OF PHASE TRANSFORMATIONS

Most of the experimental data on which this paper is based were determined by the method of adiabatic calorimetry described by HUFFMAN and coworkers.[2] Precise measurements were made of heat capacity and the latent heats and temperatures of phase changes in the range 10–400°K. From the results, the enthalpy, entropy and free energy of crystalline and liquid phases were calculated. Such thermodynamic data characterize phase transformations in a precise quantitative way and provide a sensitive tool for use in both formulating and testing theoretical interpretations of transformation processes.

Thermal data are particularly useful in interpreting solid–solid transitions in which order–disorder effects are predominant. For such transitions the entropy change approximates R ln Q, where Q is the ratio of the number of states of disorder statistically occupied in the two phases.

If the number of states of disorder is known for any phase (usually the ordered phase at 0°K), the approximate numbers of states, N, in any other phase can be deduced. The problem of interpretation thus consists of finding, by stochastic means, a reasonable set of N states of disorder distinguished by displacement of the molecular center of gravity, over-all molecular orientation, and internal molecular conformation. To illustrate the method clear-cut examples of order–disorder transitions involving over-all orientational and conformational disorder will be discussed first.

INTERPRETATION OF SIMPLE ORDER–DISORDER TRANSITIONS

Thermal data for transitions observed in benzothiophene[3] and cyclopentyl-1-thiaethane[4] are listed in Table 1, along with values of N deduced from consideration of the molecular symmetry and observed entropy changes. Benzothiophene undergoes a non-isothermal transition in the range 250–262°K with an entropy change equal to $R \ln 4$ (2·75 cal deg^{-1} mole^{-1}) within experimental error. The disorder in the high temperature phase has been interpreted[3] by assuming that the molecule acquires the pseudo-symmetry of naphthalene by occupying at random any one of four distinguishable orientations obtained by rotation about two perpendicular axes.

The transformation process in benzothiophene involves changes in the over-all orientation of the molecule at a lattice site, but that in cyclopentyl-1-thiaethane probably involves a different kind of orientational disorder. The entropy of transition in this compound is about $R \ln 2 = 1{\cdot}38$ cal deg^{-1} mole^{-1}. A likely interpretation of this transformation is that it involves a statistical distribution of molecules in the high-temperature phase between two *skew* conformations obtained by restricted rotation of the thiaethyl (—SCH_3) group relative to the cyclopentyl group. This disordering may be called intramolecular orientational disorder or conformational disorder.

The transitions in these two compounds are typical of the simple order–disorder phenomena that can be interpreted with thermal data alone.

INTERPRETATION OF TRANSITIONS IN PLASTIC CRYSTALS

Before speculating about molecular disorder in plastic crystals, it is instructive to examine the data on entropy of phase transformation for a group of tetrahedral, or neopentane-like, molecules, summarized in Table 2. This summary shows that the total entropy of phase change is about the same for most members of the group. The same is true of other groups of molecules with similar shapes, such as the oblate ellipsoidal like cyclohexane, the prolate ellipsoidal like 2,2,4,4-tetramethylbutane, and the pear-shaped like 2,2-dimethylbutane. The fact that the entropy of phase change is about constant in each group means that, in general, similarly shaped molecules can assume the same number of distinguishable orientations in the liquid and, therefore, in plastic crystals with low entropies of fusion.

Thus, it should be possible to find a set of distinguishable orientations characteristic of each kind of molecule. The high entropy of transition typical of plastic crystals indicates that the number of such orientations, N, is too large to be explained by the simple method used for benzothiophene. One method of finding larger sets of reasonable orientations will now be described.

Table 1. *Simple order–disorder transitions*

Compound	T_t[a], °K	ΔS_t[b], cal deg^{-1} mole^{-1}	N[c]	$R \ln N$, cal deg^{-1} mole^{-1}
Benzothiophene	262[d]	2·75	4	2·75
Cyclopentyl-1-thiaethane	165·0	1·30	2	1·38

[a] The transition temperature. [b] The entropy of transition. [c] The ratio of the number of distinguishable orientations available to a molecule in the two phases. [d] Temperature of complete transformation for non-isothermal transition.

Table 2. Phase transformation data for tetrahedral molecules

Substance	$\Sigma\Delta S_t^a$, cal deg^{-1} mole^{-1}		$\Sigma\Delta S_t + \Delta S_m^b$, cal deg^{-1} mole^{-1}	
	observed	corrected[c]	observed	corrected[c]
Carbon tetrachloride	4·91	4·91	7·31	7·31
Carbon tetrabromide[d]	4·98	4·98	7·59	7·59
Neopentane	4·40	4·40[e]	7·44	7·44[e]
Methylfluoroform	0·45	<0	10·60	7·85
Methylchloroform	7·95	5·20	9·82	7·07
2-Methyl-2-propanethiol	8·56	3·62[e]	10·72	5·78[e]

[a] Sum of transition entropies. [b] Entropy of fusion. [c] Corrected for symmetry. [d] Ref. (7) and HILDEBRAND J. H. and SCOTT R. L., *Solubility of Non-Electrolytes*, p. 59. Reinhold (1950). [e] Does not include an estimate of the entropy of transition associated with regions of high heat capacity.

Method of finding distinguishable orientations in crystal lattices

About each lattice site in a crystal there is a volume or cavity shaped by the spheres of influence of molecules at nearest neighboring lattice sites. A molecule will fit into this cavity with its knobs and ridges fitting into the pits and valleys of the cavity like a key and lock. The angular locations of the pits and valleys of the cavity may be described in terms of the symmetry elements of the lattice; and the directions of the knobs and ridges of the molecules may be described by the *approximate* symmetry elements of the outermost atoms of the molecule. Thus, molecular orientations that are energetically favorable usually will be among those for which the approximate symmetry elements of the molecule are aligned with the symmetry elements of the lattice. That is, for favorable orientations the *effective* point symmetry of the molecule will be a sub-point group of the crystal symmetry at the lattice site.

The number of possible distinguishable orientations can thus be estimated from symmetry considerations. However, steric factors will cause some orientations to be energetically favored over others. In general, the more favorable orientations will be those with more correspondence between lattice and molecular symmetry elements. The method of finding available distinguishable orientations proposed here consists of finding the total number of ways the approximate symmetry elements of a molecule can be aligned with those of a lattice site without unfavorable steric interactions with neighboring molecules. This method will be illustrated, first, with an interpretation of the phase transformation in a globular molecule; next, with an interpretation for tetrahedral molecules in general; and finally, with a detailed discussion for a specific tetrahedral molecule.

Application to bicyclo(2,2,1)heptane

Bicyclo(2,2,1)heptane undergoes two nonisothermal transitions.[4] The temperatures at which maximum energy absorption occurs and the entropies of transition are: 131·5°K and 7·53 cal deg^{-1} mole^{-1}; and 305·8°K and 0·06 cal deg^{-1} mole^{-1}.

The symmetry of bicycloheptane is C_{2v}, but this nearly spherical molecule has the *approximate* D_{3h} symmetry of one conformation of bicyclo(2,2,2)octane. Although the crystal structure of bicycloheptane is not known, it probably forms a plastic crystal of the cubic type with each molecule located at a site of O_h symmetry. The most likely distinguishable orientations of a D_{3h} molecule at an O_h lattice site are those with the 3-fold molecular axis aligned with each of the four 3-fold axes of the lattice. As the molecular axis may be aligned with each lattice axis in two ways differing by 60° rotation about the 3-fold molecular axis, there are eight such orientations. Other orientations will align dissimilar symmetry elements and should be less favorable energetically; that is, the fit of molecular knobs and ridges to lattice pits and valleys will be poorer.

Vol. 18
1961

Because the symmetry of bicycloheptane actually is C_{2v}, this molecule has three orientations for each orientation of a D_{3h} molecule. Therefore, it is postulated that molecules in the high temperature phase are randomly oriented among $3 \times 8 = 24$ distinguishable positions. The calculated entropy of transition is $R \ln 24 = 6{\cdot}32$ cal deg^{-1} mole^{-1}, about 1 cal deg^{-1} mole^{-1} less than observed. Part of the additional observed entropy may be due to the availability of distinguishable orientations other than those considered. However, some entropy increase must be included for increased over-all libration of molecules at lattice sites in the high temperature phase. For a molecule as nearly spherical as bicycloheptane, a librational entropy of 1 cal deg^{-1} mole^{-1} is not unreasonable.

The very small transition at 306·5°K cannot be interpreted from thermal data, but it may represent a transition between body- and face-centered cubic lattices, which does not involve an increase in the number of distinguishable molecular orientations.

Application to tetrahedral molecules

The tetrahedral, or neopentane-like, molecules form a group of plastic crystals with phase behavior that can be interpreted by the method just described. Such molecules may be expected to form close-packed crystals in the cubic or hexagonal systems. To obtain the number of distinguishable orientations available to a molecule in these crystal systems, the orientations of a strictly tetrahedral molecule will be considered first. There are four sets of orientations in which two or more corresponding symmetry elements coincide in the cubic system and one such set in the hexagonal system. They are described as follows:

Cubic T_d Set. Each 3-fold axis of the tetrahedron is aligned with a 3-fold axis of the cubic lattice, each 2-fold axis is aligned with a 4-fold axis of the lattice, and all six tetrahedral mirror planes coincide with the diagonal mirror planes of the lattice. This set of common symmetry elements has T_d symmetry. Fig. 1(a) shows one of two such distinguishable orientations.

Cubic D_{2d} Set. One 2-fold tetrahedral axis is aligned with a 4-fold lattice axis, the other 2-fold tetrahedral axes are aligned with 2-fold lattice axes, and the tetrahedral mirror planes are aligned with two vertical and four diagonal mirror planes of the lattice. The symmetry of these common elements is D_{2d}. There are six orientations in this set, one of which is shown in Fig. 1(b).

Cubic C_{3v} Set. Another set of orientations involves coincidence of one 3-fold tetrahedral axis with a 3-fold lattice axis. Members of this set are obtained by rotating one of the T_d orientations by 60° about one 3-fold axis so that three tetrahedral mirror planes coincide with diagonal mirror planes of the lattice. The symmetry of this set of common elements is C_{3v}. There are eight such distinguishable orientations, one of which is shown in Fig. 1(c).

Cubic C_{2v} Set. A 2-fold tetrahedral axis is aligned with a 2-fold lattice axis and the two corresponding tetrahedral mirror planes coincide with a horizontal and a diagonal mirror plane of the lattice. These elements form the point group C_{2v}, and there are twelve distinguishable orientations, one of which is shown in Fig. 1(d).

Hexagonal C_{3v} Set. There is only one acceptable set of distinguishable orientations of a tetrahedron in a hexagonal closest-packed structure. One 3-fold tetrahedral axis is aligned with a 6-fold axis of the lattice, and three tetrahedral mirror planes coincide with lattice mirror planes, forming a group with C_{3v} symmetry. One member of the set of four such orientations is shown in Fig. 1(e).

Each of the foregoing sets of orientations involves coincidence of two or more symmetry elements and fixed location of the molecular centers. Although other sets of orientations may be obtained by relaxing these restrictions, the five sets described are enough to discuss the phase behavior of tetrahedral molecules. The pseudo-symmetry of each complete set is that of the lattice site, but except for the T_d set, the individual members of each set display less than the full molecular symmetry. Inclusion of orientations in which a molecule does *not* display its full symmetry is the key to finding enough orientations to account for the high degree of disorder in plastic crystals.

There is no direct way of obtaining quantitative estimates of the relative stability of systems in the four cubic sets of orientations, but qualitative estimates may be made from steric and symmetry considerations. Steric considerations show that the T_d, C_{3v} and C_{2v} sets probably are favorable orientations in a face-centered lattice but that the D_{2d} set probably is favored in a body-centered lattice. Of

Vol. 19

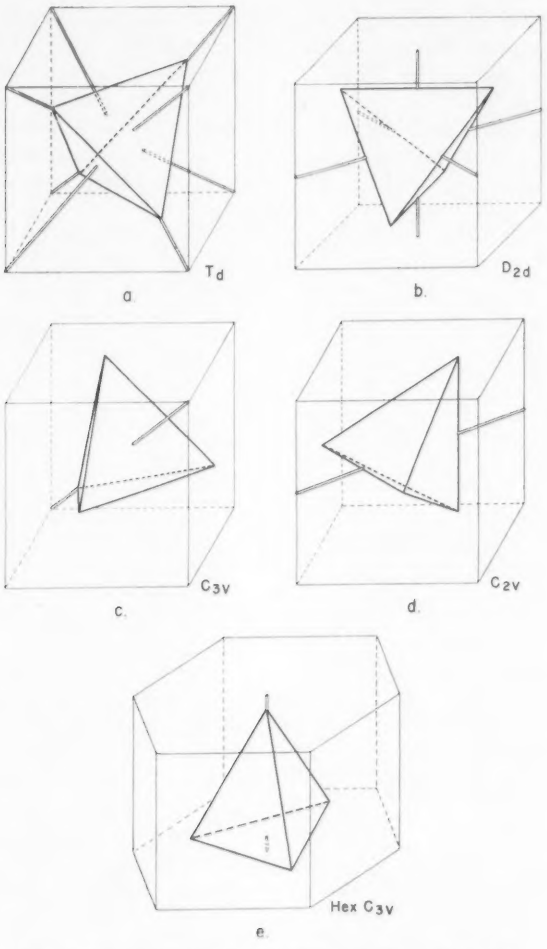

FIG. 1. Representative orientations of tetrahedral molecules at lattice sites.

the sets most likely for a face-centered lattice, the order of relative stability is assumed to be $T_d > C_{3v} > C_{2v}$, in the order of decreasing correspondence of molecular and lattice symmetry elements. These assumptions will be used in the following discussion of the phase behavior of tetrahedral molecules.

Most of the tetrahedral compounds in Table 2 undergo a single solid–solid phase transformation and, except methylfluoroform, form a plastic crystal probably of face-centered cubic structure.[5] The entropy of transition in carbon tetrachloride[6] and carbon tetrabromide[7] is just under 5 cal deg^{-1} mole^{-1}. If allowance is made for the significant "pretransition" that occurs in neopentane,[8] the total entropy of transition in this compound also is near 5 cal deg^{-1} mole^{-1}. Further, the entropy of transition in methylchloroform[9] is about the same if $R \ln 4 = 2{\cdot}75$ cal deg^{-1} mole^{-1} is subtracted to allow for the extra disorder this molecule can acquire by random orientation of the methyl group toward the corners of a tetrahedron. Methylfluoroform and 2-methyl-2-propanethiol are special cases that will be discussed later.

Vol. 18
1961

From the foregoing considerations, it is concluded that the entropy of transition in a typical tetrahedral molecule is about 5 cal deg^{-1} mole^{-1}, or of the order of $R \ln 12$ (4·94 cal deg^{-1} mole^{-1}). Thus, the maximum disorder of molecular tetrahedra that can occur will involve random orientation among 12 distinguishable positions. The cubic C_{2v} set of orientations would allow this much disorder, but the entropy remaining is too small to account for the increased librational freedom that surely is gained by transition to a plastic phase. Further, the C_{2v} set is least favored sterically of the cubic sets. Therefore, it is proposed that the orientational disorder in these plastic crystals corresponds to the 10 distinguishable orientations of the combined T_d and C_{3v} sets. The entropy of transition in a typical tetrahedral molecule is thus divided into $R \ln 10 = 4{\cdot}58$ cal deg^{-1} mole^{-1} due to orientational disorder and about 0·4 cal deg^{-1} mole^{-1} due to increased over-all libration.

Methylfluoroform does not fit the foregoing interpretation for typical tetrahedral molecules. Probably the small size of the fluorine atom and the more polar nature of the C–F bond restrict the number of stable orientations. However, the fact that the sum of entropies of fusion and transition in methylfluoroform is about the same as those of the other compounds shows that it is equally disordered in the liquid phase.

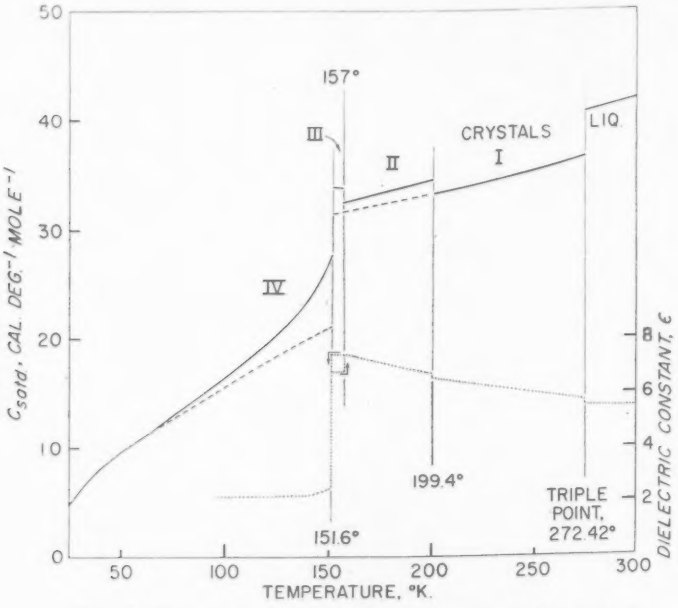

FIG. 2. Heat capacity and dielectric constant of 2-methyl-2-propanethiol: solid lines, observed heat capacity: dashed lines, estimated "normal" heat capacity, and dotted lines, dielectric constant.

Application to 2-methyl-2-propanethiol

An interesting but more complex example of phase behavior in tetrahedral molecules is given by the results for 2-methyl-2-propanethiol[11] summarized in Table 3 and Fig. 2. KONDO[12] has studied the dielectric constant of this compound between 100 and 325°K. He also reports that the high temperature phase, crystals I, is face-centered-cubic, with $a_0 = 8{\cdot}80$Å, and that it is highly disordered. KONDO's dielectric constant data are plotted with the thermal data in Fig. 2.

This compound undergoes three isothermal transitions in the solid state. Also, the heat capacity curve of crystals IV shows significant effects of pretransition, and the curves for crystals III and

Table 3. Phase behavior and disorder in 2-methyl-2-propanethiol

Phase	Crystal Structure	Transition Temp., °K	ΔS[a]	$\Sigma\Delta S$[a] observed	$\Sigma\Delta S$[a] disorder calculated
IV	Ordered		1·05[b]		
		151·6	6·41		$R \ln (4\times3)2$
			——	7·46	= 6·31
III	h.c.p.[c]		0·08		
		157·0	0·99		$R \ln (4\times3)6$
			——	8·53	= 8·50
II	b.c.c.[c]		0·25[b]		
		199·4	1·16		$R \ln (4\times3)\,10$
			——	9·94	= 9·51
I	f.c.c.				
		274·42	2·16		
			——	12·10	
Liquid					

[a] Cal deg^{-1} mole^{-1}. [b] $\int \Delta C d \ln T$, where ΔC is the excess heat capacity above "normal". [c] Proposed.

Vol. 18
1961

II are abnormally high. These regions of high heat capacity are due to increasing molecular libration and possibly some disordering, the net result of which is to increase the disorder of crystals I. To account for the entropy of disorder gained in the regions of high heat capacity, the "excess" entropy was calculated by extrapolating a "normal" heat capacity curve for both crystals IV and I to 151·6°K., the temperature of the major transition. In this way, the sum of the entropies of fusion, transition and "excess" entropy was made comparable to the entropy of transition and fusion of a typical tetrahedral molecule with a single transition at 151·6°K. The "excess" entropy ascribed to each region of high heat capacity is shown in Table 3.

The total entropy of disorder in crystals I can be explained in terms of the disorder typical of tetrahedral molecules. In crystals I, the molecules are randomly distributed among the 10 orientations of the T_d and C_{3v} sets favored for face-centered-cubic crystals. In addition, there are four orientations of the thiol group and three orientations of the thiol hydrogen for each of the ten tetrahedral orientations. The total number of distinguishable molecular orientations is $10\times4\times3 = 120$, and the calculated entropy of disorder is $R \ln 120 = 9{\cdot}51$ cal deg^{-1} mole^{-1}, in good agreement with the total observed entropy of transition, 9·94 cal deg^{-1} mole^{-1} (Table 3).

With the help of the dielectric constant data, similar but a little more speculative descriptions can be given of the disorder in the low-temperature phases. The dielectric constant data for crystals II show a small increase in density and no effect of decreased molecular freedom, but the entropy data show that the disorder in crystals II is about half that in crystals I. If it is assumed that the structure obtained by packing molecules of crystals II in the six orientations of the D_{2d} set of a body-centered crystal is more dense than that with molecules in the ten orientations of a face-centered crystal (T_d and C_{3v} sets), these facts are consistent. The D_{2d} set allows about as much molecular freedom as the T_d and C_{3v} sets, and the calculated entropy of disorder is $R \ln (4\times3\times6) = 8{\cdot}50$ cal deg^{-1} mole^{-1}, as compared with the observed, 8·53 cal deg^{-1} mole^{-1}.

The transition between crystals II and III was not found to be reversible in the dielectric constant studies, but the results obtained from heating experiments show that the effective dipole moment in crystals III is about 15 per cent less than in crystals II. The entropy data show that

the degree of disorder in crystals III is about half that in crystals II. The disorder possible in crystals I and II allows reorientation of the molecular tetrahedra so that the direction of the molecular dipole may change as much as 180° under the influence of an electric field. If the orientations of the molecules in crystals III are restricted to a half-set of the hexagonal C_{3v} set that does not include inversion of molecular tetrahedra, oscillation of the molecular dipoles would be restricted to the corners of a tetrahedron, or to 108·5°. The effective dipole moment would then be only 81 per cent of that effective if inversion of molecular tetrahedra occurs as in crystals I and II. On this basis, the disorder in crystals III is assumed to correspond to the 12 distinguishable orientations of a molecule at each of the two distinguishable positions of the hexagonal C_{3v} half-set that excludes inversion of molecular tetrahedra. The calculated entropy of disorder, $R \ln (4 \times 3 \times 2) = 6{\cdot}31$ cal deg^{-1} mole^{-1}, does not agree very well with the observed, 7·45 cal deg^{-1} mole^{-1}. More satisfactory agreement with the calorimetric data would be obtained if crystals II were assumed to be cubic with disorder corresponding to the cubic D_{2d} half-set that excludes inversion of tetrahedra. However, access to all three orientations in the D_{2d} sub-set allows enough over-all molecular freedom that the effective dipole moment in crystals III would not be expected to be significantly lower than in crystals II. Only if the frequency with which one member of the D_{2d} sub-set converts to another is below the lowest frequency used by KONDO would the dielectric constant show the observed decrease.

The transition from crystals III to IV obviously involves attainment of complete orientational order, except for the disorder associated with the pre-transition effects shown by both the heat capacity and dielectric constant data.

The nature of "rotation" in plastic crystals

The results of this study show clearly that "rotation" in plastic crystals is not necessarily rotation in the sense normally used in molecular physics. Because the behavior of the molecular crystals discussed can be described adequately in terms of orientational disorder, the molecules evidently librate about discrete, distinguishable positions in the crystal lattice. Of course, re-orientation of molecules occurs, but with such high frequency that nuclear magnetic resonance and X-ray measurements cannot distinguish between free rotation and random orientation, as ANDREW has pointed out.[13] The distinction between rotation in the usual molecular sense and restricted rotation from one preferred orientation to another is important in understanding the phase behavior of molecular crystals.

CONCLUSIONS

The foregoing discussion has shown that reasonable interpretations of phase behavior can be made primarily on the basis of thermal data and considerations of symmetry and steric factors. The interpretations are quite speculative for highly disordered crystals, but no presently known method of analysis is less speculative. The unique contribution of entropy data to the study of highly-disordered crystals is the provision of a quantitative measure of the *degree* of disorder. With more extensive structural and molecular data from non-thermal studies, descriptions of the *kind* of disorder could be made less speculative. Thus, studies of the compounds discussed here, and others that can be discussed in similar terms, by X-ray, dielectric constant and nuclear magnetic resonance methods would be particularly helpful in obtaining better descriptions of phase transformations in molecular crystals.

REFERENCES

1. McCULLOUGH J. P., *Transitions in Hydrocarbons and Related Substances*. Paper No. 34, IUPAC Symposium on Thermodynamics, Wattens, Tirol, 1959, to be published.
2. HUFFMAN H. M., *Chem. Rev.* **40,** 1 (1947); HUFFMAN H. M., TODD S. S. and OLIVER G. D., *J. Amer. Chem. Soc.* **71,** 584 (1949); SCOTT D. W., DOUSLIN D. R., GROSS M. E., OLIVER G. D. and HUFFMAN H. M., *ibid.* **74,** 883 (1952).
3. FINKE H. L., GROSS M. E., MESSERLY J. F. and WADDINGTON G., *J. Amer. Chem. Soc.* **76,** 854 (1954).
4. Unpublished results of this Laboratory.
5. WYCKOFF R. G., *Crystal Structures*. Interscience, New York, (1948–59).
6. HICKS J. F. G., HOOLEY J. G. and STEPHENSON C. C., *J. Amer. Chem. Soc.* **66,** 1064 (1944).
7. MARSHALL J. G., STAVELEY L. A. K. and HART K. R., *Trans. Faraday Soc.* **52,** 19 (1956).
8. ASTON J. G. and MESSERLY G. H., *J. Amer. Chem. Soc.* **58,** 2354 (1936).

9. RUBIN T. R., LEVEDAHL B. H. and YOST D. M., *J. Amer. Chem. Soc.* **66,** 279 (1944).
10. RUSSELL H., GOLDING D. V. R. and YOST D. M., *J. Amer. Chem. Soc.* **66,** 16 (1944).
11. MCCULLOUGH J. P., SCOTT D. W., FINKE H. L., HUBBARD W. N., GROSS M. E., KATZ C., PENNINGTON R. E., MESSERLY J. F. and WADDINGTON G., *J. Amer. Chem. Soc.* **75,** 1818 (1953).
12. Communication from S. KONDO. See also, KONDO SEIICHI, *Memoirs of Osaka University of Liberal Arts and Education*, Series B, No. 6, p. 25 (1947).
13. ANDREW E. R., *J. Chem. Phys.* **18,** 607 (1950).

Vol. 18
1961

J. Phys. Chem. Solids Pergamon Press 1961. Vol. 18, No. 1, pp. 62–73. Printed in Great Britain.

ROTATIONAL TRANSITIONS IN MIXED CRYSTALS AND SURFACE FILMS*

J. G. ASTON†

1. INTRODUCTION

IT IS the purpose of the present paper to present some of the typical properties of systems which are mixtures of two pure compounds, at least one of which, immediately below its melting point, forms plastic crystals. Familiarity with the earlier papers presented at this symposium is assumed.

The information to be obtained from mixtures is of two kinds: (a) The effect of diluents (such as rare gases) causes a more uniform potential field around a globular molecule and hence greater freedom to rotate. If the second substance is insoluble in all phases (e.g. an absorbent such as TiO_2) an effect equivalent to dilution is obtained by dilution in one dimension as a monolayer is approached and finally in the other two dimensions of the monolayer. From the results conclusions can be reached about the behaviour of the pure substances. (b) It is possible to detect co-operative effects between neighbors in the pure substances through *increased* co-operative effects in the mixture, i.e. in the mixture co-operative transitions require lower energies than in the parent compound.

First a few solid–liquid phase diagrams, above the rotational transitions, will be discussed. Some complicated cases have been chosen deliberately in order to draw attention to unsolved difficulties. This will be followed by a discussion of the types of transitions in typical mixtures and the values of the transition temperatures for which the effect of mixing seems clear and where the nature of the rotation seems to be revealed. Finally the transition temperature of carbon tetrafluoride in bulk and in films will be discussed with respect to the n.m.r. line broadening.

* Contribution from the Low Temperature Laboratory of the Pennsylvania State University and from the Mathematical Institute of Oxford University.

† Guggenheim Fellow 1959–60 associated with the Mathematical Institute of Oxford University.

2. PHASE DIAGRAMS

The solid–liquid phase diagram of methane dissolved in krypton is a simple case and indicates a continuous series of solid solutions.[1]

In the solid solutions, which are rich in methane, the rotational transition of methane is evident. This transition becomes more smeared out and appears at increasingly lower temperatures as the concentration of methane is decreased.[2]

There is little doubt that the methane is relatively free to rotate in the solid solutions as will be seen presently, thus causing the methane molecule with its high symmetry to behave like a rare gas molecule. STEPHENSON[3] has shown that dilution of ammonium nitrate by potassium nitrate greatly increases the freedom of the ammonium ion to rotate.

On the other hand mixtures of carbon tetrachloride and cyclohexane, both of which form plastic crystals, do not form solid solutions at all.[4]

The phase diagram is shown in Fig. 1, where the melting points of the mixtures are plotted against composition. On the diagram are also plotted the temperatures of a transition which is undoubtedly that of the solid carbon tetrachloride in the mixture since it occurs always at the same temperature, namely, approximately that of the transition temperature for pure carbon tetrachloride (227°K). Had the measurements been carried to lower temperatures there is little doubt that a transition corresponding to that for cyclohexane (182°K.) also would have been observed. The apparent continuity of the freezing point curve at the eutectic is presumably not real. It is due to lack of data near the eutectic.

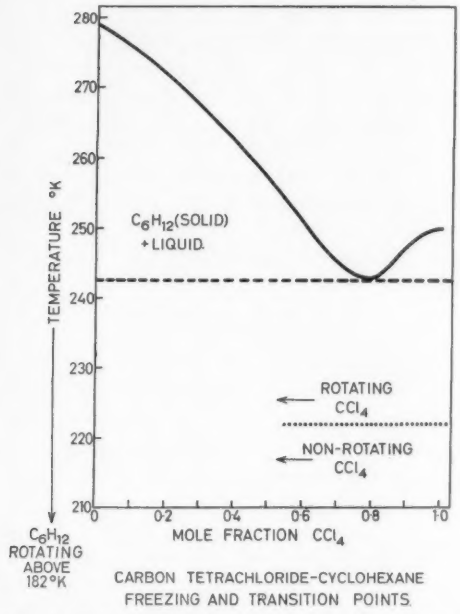

FIG. 1. Solid–liquid equilibria for the system carbon tetrachloride and cyclohexane. [Constructed from Ref. (4).]

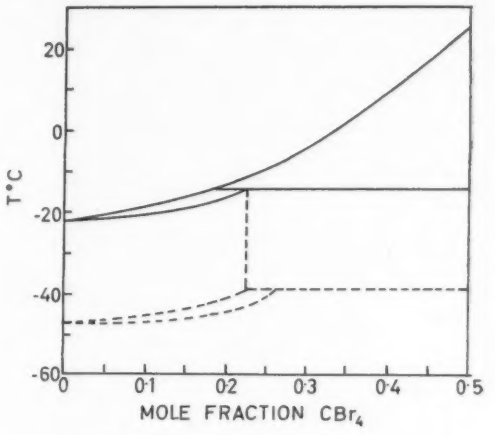

FIG. 2. Solid–liquid equilibria for the system carbon tetrachloride and carbon tetrabromide. [Constructed from Ref. (6).]

It has already been shown that the barriers to rotation in carbon tetrachloride must be quite high.[5] This is possibly connected with the inability of this pair to form solid solutions.

The behavior of the system carbon tetrachloride and carbon tetrabromide is quite complicated,[6] presumably for the same reason.

The phase diagram is shown in Fig. 2 (temperature–composition). On cooling solutions containing less than fifty per cent carbon tetrabromide, the non-rotating form of carbon tetrabromide separates in the pure state but at about −15°C a solid solution containing carbon tetrachloride starts to separate. Thus solutions with less carbon tetrachloride than that in the initially appearing solid solution (23 mole per cent CBr_4) yield a triple point of liquid solution, solid carbon tetrabromide and solid solution (23 per cent CBr_4); these, on further cooling yield a solid solution of 23 per cent CBr_4 and excess solid CBr_4. This solid solution has a transition point at −39°C (somewhat above that of carbon tetrachloride). It is somewhat difficult to interpret this transition as a rotational transition. As the solid solutions approach the composition of pure carbon tetrachloride the transition occurs at decreasingly lower temperatures until that of pure carbon tetrachloride −47°C is approached. At the transition a phase richer in carbon tetrabromide separates of composition shown by the lower dotted line.

In Fig. 3 is shown the temperature–composition phase diagram for the system carbon tetrachloride–t-butylchloride,[7] which was obtained by observations of the dielectric constant. The dielectric constant data presumably detect rotation but cannot detect the extent of hindrance.

t-Butylchloride has two rotational transitions. One of these occurs at 218·8°K and is associated with rotation (according to the dielectric constants) while the other at 183°K is apparently not associated with rotation. Carbon tetrachloride has a single rotation transition at 225°K[8] which has often been associated with rotation as is borne out by the dielectric constants.

The curve showing the change of melting point with composition is actually a superposition of the solidus and liquidus curves which are so close together as to be inseparable; the composition of the solid separating differs very little from that of the liquid. The minimum at approximately the composition of the equimolar mixture is approximately only 8 degrees below the melting points of

Vol. 18
1961

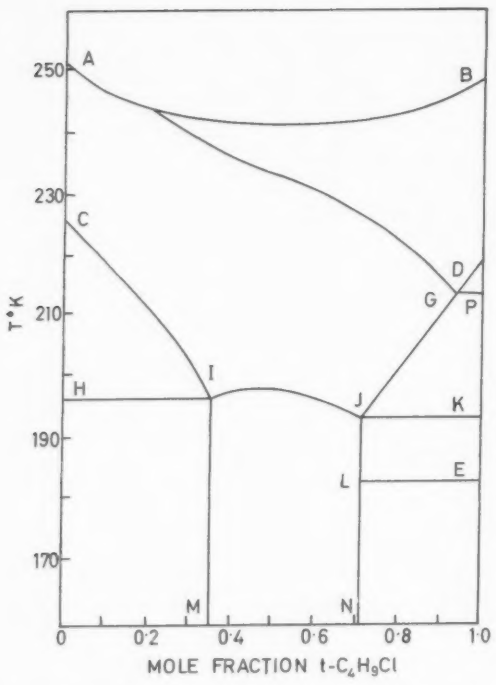

Fig. 3. Carbon tetrachloride and butyl chloride. [Constructed from Ref. (7).]

the pure components indicating solid solution formation with little intermolecular interaction. Thus the extremely complicated nature of the transitions is somewhat surprising. Below HIJK there is no rotation while in the area AGJIC there is presumably rotation modified by the presence of the t-butylchoride. The curve branching from the *solidus* curve AB originates, apparently, in some sort of triple point.

In the area CIH is solid solution and the non-rotating carbon tetrachloride that has separated. In the area DGP is solid solution and the non-rotating t-butyl chloride that has separated. In the area PGJK there is also non-rotating butyl chloride and a solid solution with a lower degree of rotation. The line LE represents the non-rotational transition in the carbon tetrachloride in equilibrium with composition N.

It appears that on mixing t-butyl chloride with carbon tetrachloride rotation of both is possible at lower temperatures in a modified way. The effects just described are complicated compared to the simple effect on mixing D- and L-nitrocamphor.

The effect of the laevo variety on the ability of D-3-nitrocamphor to rotate in the solid state is very much greater and more clear cut. In the previous example, the transition points are in no case lowered by more than 25° while with D-3-nitrocamphor the effect is a lowering of about 100° on mixing with an equimolar mixture of the laevo variety.[9]

WHITE and BISHOP demonstrated this by measurement of the dielectric constant at frequencies ranging from 1 to 100 kilocycles. In the D-variety the transition is at about 50°C while in the racemic mixture it is at about −50°C. Measurements of the dielectric constant show large decreases at these temperatures respectively but in the racemic mixture there is anomalous dispersion. It would seem that in the case of the racemic mixture the molecules must rotate in pairs.

Mixtures of cyclopentane and 2,2-dimethylbutane show a similar behaviour. Fig. 4(a) shows the temperature composition diagram for this system. This diagram is not complete but on it is also shown points joined by lines which indicate temperatures of sharp line narrowing in the nuclear magnetic resonance line.[10]

Both components have an upper and a lower transition as can be seen from the heat capacity–temperature curves of cyclopentane and 2,2-dimethylbutane shown in Figs. 5(a) and 5(b) respectively.

An upper transition was evident in the mixtures very rich in cyclopentane, but was too close to the melting point to be detected in most mixtures, thus no curve corresponding to it is shown on the diagram. A lower transition however was clearly evident in all mixtures containing over 70 per cent cyclopentane. This is represented by the solid curve, d, in Fig. 4(a). At the temperatures indicated by this curve almost pure cyclopentane in the non-rotating form apparently separates from the mixture at temperatures only slightly lower than the transition point of the pure compound. This must mean that 2,2-dimethylbutane is almost insoluble in the crystalline form of cyclopentane which is stable below the lower transition. According to the maximum in the solidus and liquidus

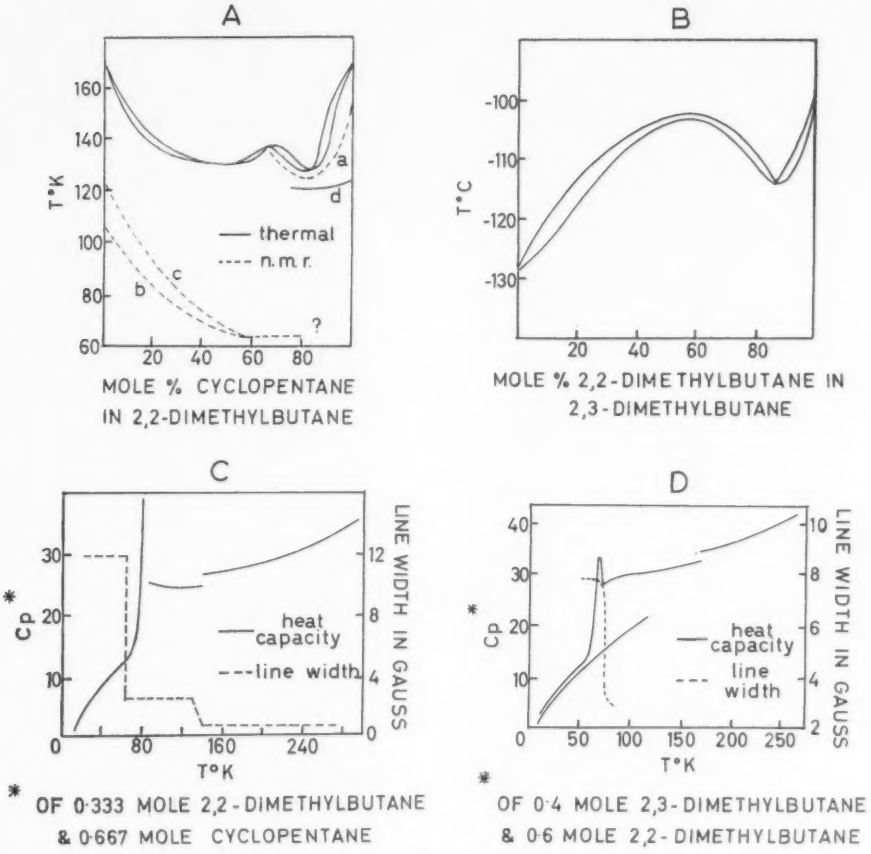

FIG. 4.

(a) Cyclopentane and 2,2-dimethylbutane. [Constructed from Ref. (9).]

(b) 2,3-Dimethylbutane and 2,2-dimethylbutane [constructed from data by FINK H. L., CINES M. R., FREY F. E. and ASTON J. F., *J. Amer. Chem. Soc.* **69**, 1501 (1947).]

(c Molar heat capacity of cyclopentane (0·667 mole) and neohexane (0·333 mole) [Constructed from Ref.(14).]

(d) Molar heat capacity of 2,3-dimethyl (0·40 mole) and 2,2-dimethylbutane (0·6 mole) [Constructed from Ref. (10).]

curves, there is apparently a "molecular compound" formed of 2 moles of cyclopentane to one mole of 2,2-dimethylbutane. In this compound the crystal form of cyclopentane stable below the lower transition is only slightly soluble. The nuclear magnetic resonance experiments clearly indicate that this compound has a rotational transition which is complete at about 65°K. The dotted curve, b, in Fig. 4(a) indicates sharp line narrowing at 65°K for mixtures containing above 60 mole per cent cyclopentane. The further line narrowing indicated by the dotted curve a is connected with the upper transition. Thus in the molecular compound, $(C_5H_{10})_2$ (C_5H_{12}), the lower transition has been lowered by nearly 60° and in the next section it will be shown to have changed

Vol. 18
1961

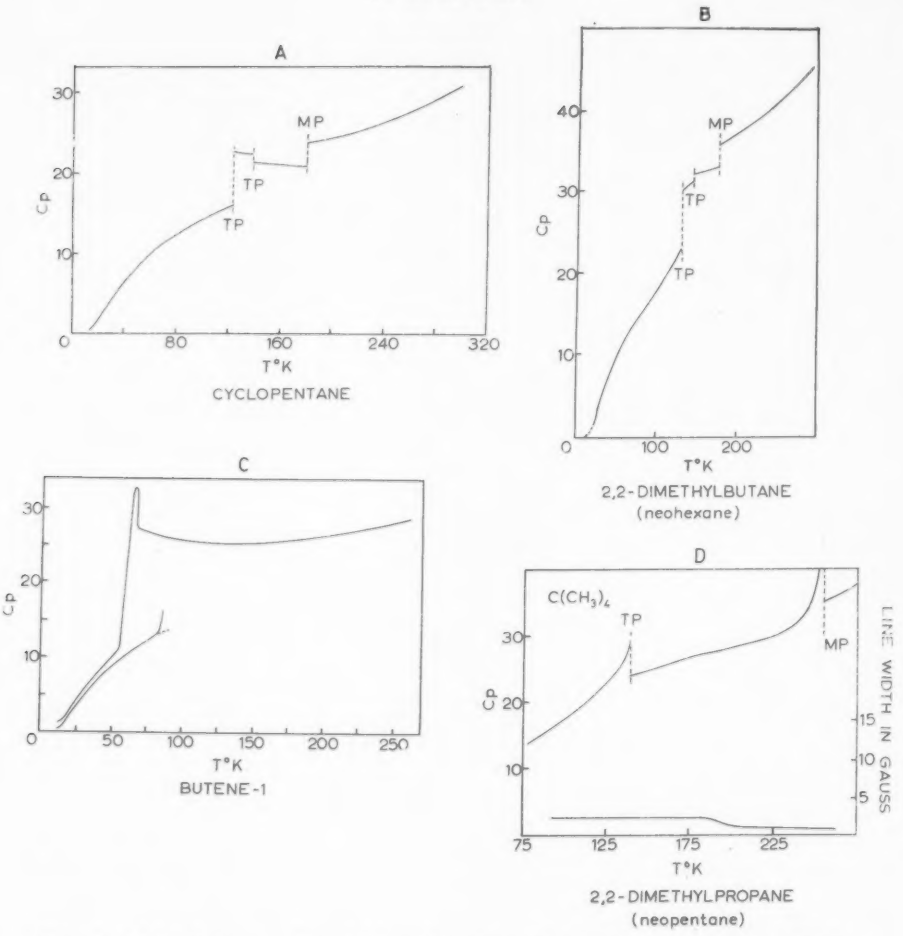

FIG. 5. Molar heat capacity of (a) cyclopentane [Constructed from ASTON J. G., FINK H. L. and SCHUMANN S. C., *J. Amer. Chem. Soc.* **65,** 341 (1943)].

(b) 2,2-dimethylbutane [Constructed from KILPATRICK J. E. and PITZER K. S., *J. Amer. Chem. Soc.* **68,** 1066 (1946)].

(c) Butene-1 [Constructed from ASTON J. G., FINK H. L., BESTUL A. B., PACE E. L. and SZASZ G. J., *J. Amer. Chem. Soc.* **70,** 53 (1948)].

(d) 2,2-Dimethylpropane [Constructed from H. L. GUTOWSKI and G. E. PAKE, *J. Chem. Phys.* **18,** 162 (1950)]. Upper curve—C_p, lower curve—line width in G.

its nature. The upper transition has apparently become raised to above the melting point (see next section). The unit appears to rotate as a whole above 65°K.

A similar study of mixtures of 2,2-dimethylbutane and 2,3-dimethylbutane yields the same sort of melting point composition diagram[11] with a maximum at 40 mole per cent 2,3-dimethylbutane as is shown in Fig. 4(b). The fact that the two curves do not touch at the maximum is due to impurity. There is rotation in the solid state at all compositions immediately below the melting point but in this case due to supercooling there is no rotational transition.

3. NATURE OF PHASE TRANSITIONS AND HEAT CAPACITIES

Methane–Krypton; Modification of barriers.

The thermodynamic nature of the phase transtions in which ordinary crystals change into "plastic crystals" is revealed in the curves of heat capacity plotted against the temperature. Some of these transitions are of the same type as the solid–liquid transition and occur at constant temperature (first order transitions). Others are apparently second order.[12]

Second order transitions seem to be characteristic of compounds with molecules whose envelope is very nearly spherical (e.g. methane, carbon tetrafluoride and tetramethyl methane). The heat capacity curve for tetramethyl methane is shown in Fig. 5(d) and for carbon tetrafluoride in Fig. 8. In such compounds the transition starts at temperatures well below the maximum in the heat capacity curve. When the envelope is nearly spherical molecules can rotate without greatly disturbing the crystalline lattice. However, after a few molecules have started to rotate it becomes progressively easier to rotate others since potential fields have been smoothed out due to rotation of neighbors (first or second). Thus as the temperature is increased more and more thermal energy goes into molecular rotation. This is evident by an "abnormal" rise in the heat capacity several degrees before the maximum which is characteristic of second order transitions.

When the molecules have envelopes which are spheres distorted in a significant manner (e.g. cyclopentane, 2,2-dimethylbutane), rotation of even a few molecules so distorts the crystal structure that all molecules rotate at once. Heat capacity curves for cyclopentane and 2,2-dimethylbutane are shown in Figs. 5(a) and (b) respectively. In both cases there are two transitions of the first order.

The role of the molecular environment in determining the nature of "rotational" transitions has been qualitatively substantiated[13] by studying the heat capacity of solid solutions of krypton in methane in the neighborhood of the second order transition. Since it would be expected that the potential field would be more uniform round a krypton atom than round a methane molecule solution of krypton in methane should reduce the barriers hindering rotation of the methane. Thus, while a methane molecule in the pure crystal would only experience barriers sufficiently low to rotate relatively freely when its nearest neighbors were rotating, methane molecules might be expected to have sufficiently low barriers when its nearest neighbors were krypton atoms.

Fig. 6 shows the heat capacity curve of solutions of 0·00 (curve a), 7·45 (curve b) and 15·6 (curve c)

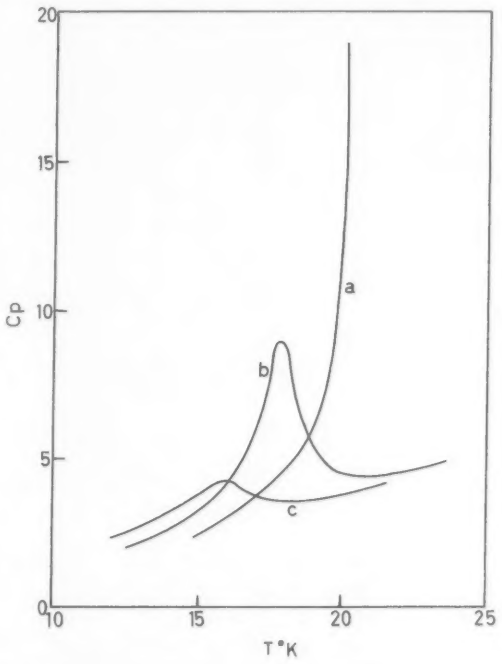

FIG. 6. Molar heat capacity of solid solutions of krypton in methane [Constructed from Ref. (12).] (a) 0·0 mole per cent (b) 7·45 mole per cent (c) 15·6 mole per cent krypton.

mole per cent krypton dissolved in methane. Qualitatively the effect of the dissolved krypton is to lower the temperature of the maximum and increase the temperature range. The compositions studied by EUCKEN and VEITH ranged up to 71·94 per cent krypton.

By making reasonable assumptions, EUCKEN and VEITH calculated values of the molar heat capacity of methane due to rotation. First of all values of C_v were calculated using the formula

$$C_v = C_p - ATC_p^2 \qquad (1)$$

A reasonable way of calculating A was deduced from the heat capacity of argon–krypton mixtures. The value of C_v per mole of methane was then calculated from the formula

$$C_v = xC_M + (1-x)C_A \qquad (2)$$

where x is the mole fraction of methane, C_M and C_A the respective molar heat capacities at constant volume of methane and krypton respectively.

Above the rotational transition, $3R/2$ was subtracted from C_M in the pure methane, to get the heat capacity contribution, C_s, due to motion of the centers of gravity of the methane molecules in the lattice. From each of the values a Debye θ was calculated. The values of θ, thus obtained, were extrapolated to the transition point. The value of 140 degrees found for θ was in excellent accord with that calculated from the Lindemann melting point formula.

With this value of θ, values of C_s, the heat capacity due to the lattice vibrations of the methane molecules were calculated and subtracted from C_M to get C_R, the rotational heat capacity, below 20°K. Above 20°K the values of C_s computed as above for pure methane were subtracted to get C_R.

Fig. 7 shows the rotational heat capacity C_k deduced in this manner for (d) 32·21 per cent (e) 50·22 per cent and (f) 71·94 per cent krypton as a function of temperature. Above 20°K in all cases the value of C_R approaches $3R/2$, the value for free rotation *as it should from the method of calculation.* Below 20°K the values go through a maximum. This is characteristic of the heat capacity curves for a hindered rotor.[14]

It is evident that the presence of the krypton lowers the barriers to rotation thus allowing the transition to start at lower temperatures.

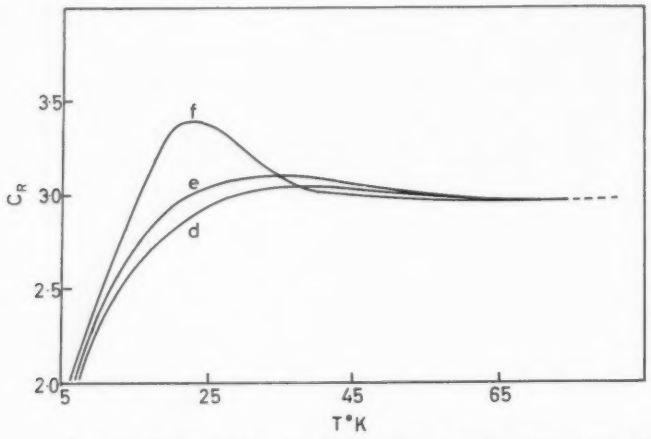

FIG. 7. Molar rotational heat capacity of methane [constructed from Ref. (12)] with certain percentages of krypton. (d) 32·21 mole per cent, (e) 50·22 mole per cent. (f) 71·94 mole per cent.

Short range co-operative effects: Modification of cyclopentane transitions.

It is unfortunate that no heat capacity data are available on the CCl_4–t-butylchloride mixtures previously discussed. Such measurements would reveal modifications in the nature of the transitions occurring in the pure compound. There is little doubt that the effect would be highly complex. On the other hand the behavior of the mixture of 2 moles of cyclopentane and one mole of 2,2-dimethylbutane is extraordinarily simple.

It has already been pointed out that in the mixture the transition begins below 65°K. The heat capacity–temperature curve is shown in Fig. 4(c).[15]

The single transition point and the melting point are clearly evident. The transition point is quite clearly of the second order and the transition

Vol. 196

is complete at 83°K. On the same graph are shown the widths of the nuclear magnetic resonance absorption line as a function of temperature. There is a sudden narrowing of the line to a width of about 2 G at about 65°K, the temperature at which the second order transition begins.

There is no evidence of the two first order transitions which are present in each component and for purposes of comparison, the heat capacity temperature curves are shown in Figs. 5(a) and (b) for the components. Not only is there a great lowering in the temperatures at which rotation can occur but the entire nature of the transition is changed. There is little doubt that two molecules of cyclopentane and one of 2,2-dimethylbutane rotate as a unit. Rotation of this unit does not require as much co-operation from neighboring molecules outside the unit as is required for rotation in the pure components and the potential field surrounding it is highly symmetrical.

Glassy transitions

The plastic crystals of 2,3-dimethylbutane are easily supercooled[16] but on warming the supercooled plastic crystals the rotational transition sets in. When sufficient 2,2-dimethylbutane is added this method of initiation of the transition fails (see above), and it is possible to study the heat capacity of the supercooled plastic crystals.[10]

The heat capacity–temperature curve is shown in Fig. 4(d) for a mixture of 40 mole per cent 2,3-dimethylbutane and 60 mole per cent 2,2-dimethylbutane.[10] The melting point is clearly evident but in the region where a rotational transition might be expected (60°K) there is a sharp rise in the heat capacity curve followed by a small maximum. Such a heat capacity curve is characteristic of a glass.

For comparison the heat capacity curve of supercooled butene-1 is shown in Fig. 5(c). In the case of supercooled butene-1 there is no melting point following the glassy transition for this transition occurs in the supercooled liquid. It should be carefully noted, however, that there is ***melting at a single temperature*** following the sharp rise of heat capacity in the case of the 40 mole per cent 2,3-dimethylbutane–60 mole per cent 2,2-dimethylbutane mixture. Thus the glassy transition is occurring in a plastic crystal.

In Fig. 4(d) the width of the nuclear magnetic resonance absorption line is also plotted against temperature. There is narrowing to a width of the order of 2G at the temperature of the glassy transition showing that freedom of motion in the plastic crystal is greatly increased at this point.

4. PHASE TRANSITIONS IN SURFACE LAYERS

It has been seen, in the last section, that dilution of methane with krypton has a smoothing effect on the potential field surrounding methane molecules and thereby reduces barriers to rotation. In a previous paper of this symposium it has been shown that the same effect can be produced by confining the methane molecules to the cells of a quinol clathrate.[17]

The interaction between the methane molecules is thereby reduced. By studying the nuclear magnetic resonance absorption line narrowing of absorbed layers it has been shown that freedom for rotation and migration of molecules that form plastic crystals is greatly increased in the outer layers of a crystal. Carbon tetrafluoride absorbed in titanium dioxide has been extensively investigated.[18]

First it should be pointed out that carbon tetrafluoride is a simpler substance to study than methane from the standpoint of the narrowing of the nuclear magnetic resonance line.[19]

In the case of methane there are two complications. The first of these is that the narrowing due to rotation is relatively small since it is the effect of neighboring molecules (external effect) that is largely responsible for the broadening of the line rather than the protons in the absorbing molecule. The second complication is that the internal broadening is reduced by a process involving the frequency of reorientation rather than by a process involving rotation against barriers.[20]

For tetramethylmethane reorientation of methyl groups narrows the line at much lower temperatures than the transition where rotation of the entire molecule sets in, as can be seen from the lower curve in Fig. 5(d) so that such an effect for methane is quite reasonable.[21]

According to theoretical calculations, the effect of fluorine nuclei in the absorbing molecule (internal effect) on the line width of carbon tetrafluoride accounts for over three quarters of the observed line width (second moment of

Vol. 18
1961

12 G²)[18] at temperatures below the early stages of the rotational transition. At temperatures where the abnormal rise in the heat capacity is apparent hindered rotation occurring at the early stages of the rotational transition (60°K) averages out the internal effect leaving only that of the nearest neighbors (2 G²). This can be seen from Fig. 8 in

Here there is no narrowing due to reorientation at temperatures below those where the abnormal rise in heat capacity is first observed. The mass of the fluorine atoms apparently reduces the reorientation frequency sufficiently to prevent this.[18]

In Figs. 9(b), (c) and (d) are shown the width

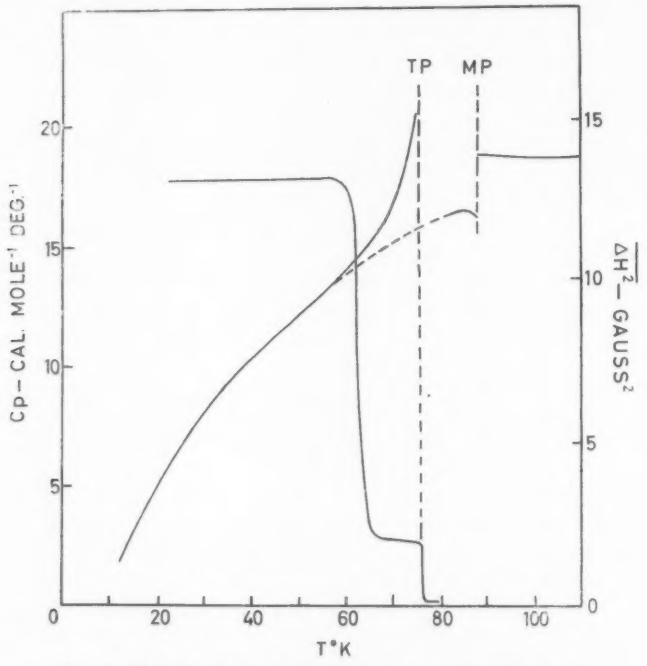

FIG. 8. Molar heat capacity and n.m.r. second moments of carbon tetrafluoride [Constructed from Ref. (18) and EUCKEN A. and SCHRODER E., *Z. Phys. Chem.* B**41**, 307 (1938).]

which the n.m.r. second moments and heat capacities are plotted as a function of temperature. There is a region where the second moment falls from 13 G² to 2 G² (i.e. from 55–65°K). In this region the line structure is complicated and the line can be resolved into two components. One line is of width about 12 G and the other of width between 4 and 5 G as measured between the points of maximum and minimum slope. The former will be designated III and the latter II. Above the transition there is a single narrow line of width considerably less than 1 G. This will be designated I. The width of these components as a function of temperature is shown in Fig. 9(a).

of these components as a function of temperature for films of carbon tetrafluoride on titanium dioxide when the number of molecular layers present was 8·97(b), 3·23(c) and 1·09(d).

To fully understand the meaning of the components of the *line* it is necessary to compare second moments (ΔH^2),[22] calculated for the part of the line attributed to each component, with values calculated theoretically. For this purpose, line shape derivatives for each component were deduced from the observed line shape derivatives in an arbitrary but obvious way and integration made of these over the observed temperature range. Figs. 10(a) and (b) show the values of ΔH^2

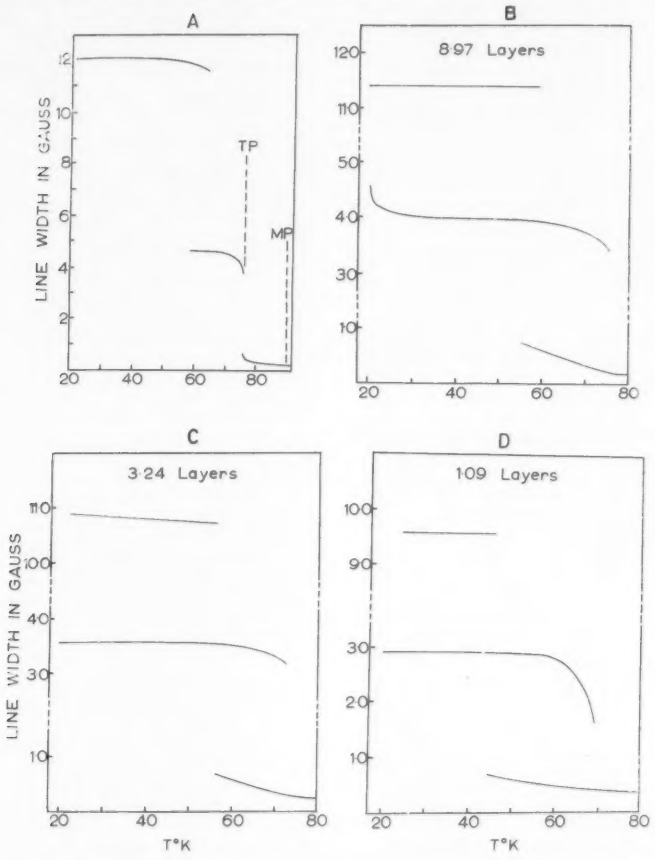

Fig. 9. Line width for n.m.r. components for carbon tetrafluoride in (a) polycrystalline phase (b) 8·97 monolayers, (c) 3·24 monolayers, (d) 1·09 monolayers, (b, c and d on titanium dioxide) [Constructed from Ref. (17).]

as a function of temperature for 3·24 and 1·09 layers respectively.

For the theoretical calculation the distance between the centres of the CF_4 molecules was calculated from the density data to be $4{\cdot}97 \times 10^{-8}$ cm assuming hexagonal close packing. Adjacent CF_4 molecules were assumed to be tetrahedral and randomly oriented with an internal distance between fluorine atoms of $2{\cdot}15 \times 10^{-8}$ cm. Assuming a polycrystalline substance with no rotation or orientation the formulae used were those given by VAN VLECK.[23]

For the broadening produced by fluorine atoms within the same molecule the calculated value of ΔH^2 was 9·52 G^2 while the additional broadening due to neighboring randomly oriented molecules within the crystal is 2·52 G^2. Providing at least two layers are present the latter value can be shown to be essentially unchanged and the former value is unchanged under any circumstances where there is no rotation or reorientation. For a monolayer the broadening due to neighboring molecules is calculated to be about 1 G^2 with a surface spacing consistent with the above assumptions. Thus a value of the second moment for the domains in the crystal undergoing no rotation or reorientation of about 12 G^2 is to be expected. For a monolayer this value would be

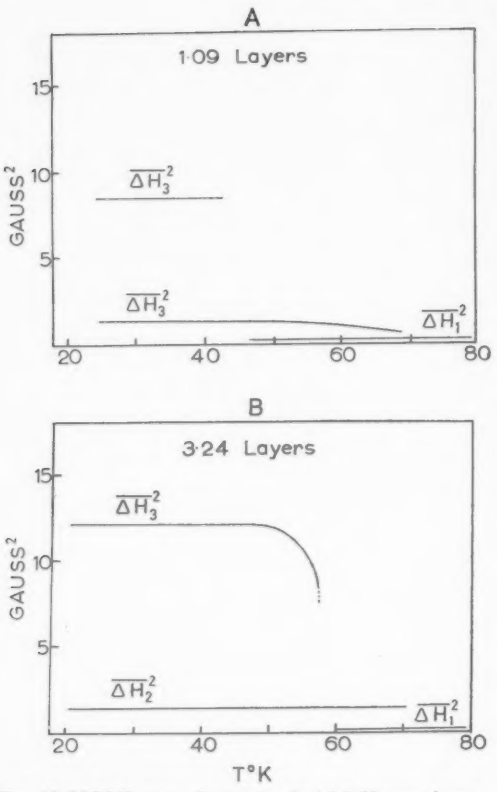

FIG. 10. N.M.R. second moments in (a) 1·09 monolayers, (b) 3·24 monolayers of carbon tetrafluoride on titanium dioxide [Constructed from Ref. (17).]

expected to fall to about 10·5 G². Reference to Figs. 10(a) and (b) shows clearly that the broad component III has the value of the second moment expected for a rigid lattice in the 3·24 layers and in the monolayer as well as in the bulk (see Fig. 8).

If it is assumed that relatively free rotation occurs in the early stages of the transition in certain parts of the crystal while in others the molecules do not rotate at all, the parts in which there is relatively free rotation will contribute a component to the line of width due only to the action of nearest neighbors, the internal contribution to the line width having averaged to zero. Thus the component of intermediate width, II, is to be attributed to such domains. As can be seen the second moment for this component in the 3·24 layers is about 1·3 G² while that in the 1·09 layers is about the same amount in good agreement with expectations.

Reference to the second moments for bulk carbon tetrafluoride, as shown in Fig. 8, shows that soon after the start of the transition at 60°K the broad line, III, has entirely disappeared and been replaced by the line, II, whose width stays almost unchanged until the transition is complete. After the transition, the component, I, has a second moment less than 1 G² and the component II has disappeared. Thus there must be considerable self diffusion as well as rotation above the transition.

In the 8·97 and 3·24 layers the component, II, of intermediate width, is present at all temperatures below 70°K, as is evident from Figs. 9(b) and (c); i.e. below the transition point of the bulk (see Fig. 9a). This indicates that rotation in the outer layer is present at all temperatures above 20°K. In the 8·97 layers there is evidence of broadening at 25°K. Exactly the same situation maintains in the 1·09 layers (see Figs 9(d) and 10(b)). It is also of interest that the narrow component, I, is present down to 60°K in the 3·24 monolayers and to 45°K in 1·04 monolayer (see Figs. 9(c) and (d)). This indicates that diffusion is easier in films than in bulk as is to be expected. In the 8·97 and 3·24 monolayers the component III is always present below 60°K. In the former it is almost constant at 11·5 G which is very little below that of the bulk. In the latter the width is almost constant at 10·5 G. The reduced width is due to the smaller nearest neighbor broadening. That there are pronounced regions of more than one monolayer on the surface in the 1·09 monolayer data average is shown by the presence of component III at all temperatures below 45°K with a somewhat reduced width of 9·5 G. This is to be expected from theories of physical absorption such as that of BRUNAUER *et al.* These results on the films are exactly what would have been predicted from the heat capacity measurements on methane in the quinol clathrate.[16]

The reasonableness of the results in the films confirms the identification of the line compounds I, II and III in the bulk. Once this identification is made rotation in the bulk during most of the transition seems to be well established, as well as considerable migration above, in agreement with the initial assumption.

REFERENCES

1. STACKELBERG M. V., QUATRAM F. and ANTWEILER H. J., *Z. Electrochem.* **42,** 552 (1936).
2. EUCKEN A. and VEITH H., *Z. Phys. Chem.* **34,** 275 (1936).
3. STEPHENSON C. C., private communication.
4. TIMMERMANS J., *Bull. Soc. Chem. Belg.* **37,** 409 (1928).
5. STAVELEY L. A. K., *J. Phys. Chem. Solids* **18,** 46 (1960). (1960).
6. SACHMANN H., *Z. Phys. Chem.* **204,** 299 (1955).
7. CONNOR W. P. and SMYTH C. P., *J. Amer. Chem. Soc.* **63,** 3424 (1941).
8. JOHNSON H. L. and LONG E. A., *J. Amer. Chem. Soc.* **56,** 31 (1934).
9. WHITE A. W. and BISHOP W. S., *J. Amer. Chem. Soc.* **62,** 8 (1940).
10. ASTON J. G., BOLGE B., TRAMBAROLO R. and SEGALL H., *J. Chem. Phys.* **22,** 460 (1954).
11. ASTON J. G., SEGALL H. and FUSCHILLO N., *J. Chem. Phys.* **24,** 1061 (1956); See also FINK H. L., CINES M. R., FREY F. E. and ASTON J. G., *J. Amer. Chem. Soc.* **60,** 1501 (1947).
12. EHRENFEST P., *Koninkl. Ned. Akad. Wetenschep. Proc.* **36,** 153 (1933); *Leiden Comm. Suppl.* 75b.
13. EUCKEN A. and VEITH H., *Z. Phys. Chem.* B**34,** 296 (1936).
14. PITZER K. S., *J. Chem. Phys.* **5,** 473 (1937).
15. SELBY R. N. and ASTON J. G., *J. Amer. Chem. Soc.* **80,** 5070 (1958).
16. SEGALL G. and ASTON J. G., *J. Chem. Phys.* **23,** 528 (1955).
17. STAVELEY L. A. K., *J. Phys. Chem. Solids,* **18,** 46 (1960).
18. STOTTLEMEYER Q. R., MURRAY G. R. and ASTON J. G., *J. Amer. Chem. Soc.* **82,** 1284 (1960).
19. ASTON J. G., STOTTLEMEYER Q. R. and MURRAY G. A., *J. Amer. Chem. Soc.* **82,** 1281 (1960).
20. ANDREW E. R., this journal, p. 9; POWLES J. G., this journal, p. 17; ANDREW E. R., *Nuclear Magnetic Resonance,* p. 167. Cambridge University Press (1954).
21. TOMITA K., *Phys. Rev.* **89,** 429 (1953).
22. ANDREW E. R., *Nuclear Magnetic Resonance,* p. 31. Cambridge University Press (1954).
23. VAN VLECK J. H., *Phys. Rev.* **74,** 1169 (1948).

Vol. 18
1961

J. Phys. Chem. Solids Pergamon Press 1961. Vol. 18, No. 1, pp. 74–76. Printed in Great Britain.

THE STUDY OF MOLECULAR MOTION IN CRYSTALS BY INFRA-RED SPECTROSCOPY

W. C. PRICE and G. R. WILKINSON

Physics Department, Kings College, Strand, London, W.C.2.

INFRA-RED spectroscopy is concerned essentially with the study of transitions between vibrational and rotational energy levels.[1] In crystals, however, the possibility of observing rotational transitions is remote except in very favourable circumstances. In considering the infra-red absorption spectra of molecular crystals it is convenient to classify the atomic vibrations as follows.

(a) The internal vibrational modes of atoms within a molecule, the frequency of which depend upon the atomic masses and interatomic forces. For non-linear molecules containing N atoms there are $3N-6$ normal modes of vibration. These may be readily classified using group theoretical methods.[2] These normal modes persist with little modification in going from the gas to liquid to crystalline phase.

(b) Librational or torsional modes involve the rotational movement of a part of e.g. a CH_3 group or the whole molecule about its principal moments of inertia.

(c) In "lattice modes" the molecules move as a whole with respect to one another. The frequency distribution of these modes $g(\nu)$ depend upon the mass of the molecule and intermolecular forces.

As the energy levels of a crystal are really a property of the entire system this classification is only an approximation. However, it is very convenient in analysing the vibrations of a molecular crystal to consider the similarities between the gas, liquid or solution and crystal spectra. The degree of thermal excitation at a temperature T of a mode with frequency ν depends upon the ratio ν/T.

All crystals have absorption bands which occur in the infra-red region of the electromagnetic spectrum, and the quantity which may be measured is the absorption coefficient as a function of frequency. In many crystals this is anisotropic and hence may be studied with polarized radiation. In the case of a well defined e.g. approximately Lorentzian band it is possible to specify its integrated intensity and also its half width $\Delta\nu_{\frac{1}{2}}$ which is proportional in simple cases to $1/\tau$ where τ is the lifetime of the excited state. The lifetimes of excited states are frequently limited by molecular motion. In molecular crystals $\Delta\nu_{\frac{1}{2}}$ is usually of the order of 10 cm^{-1} and hence τ must be about 10^{-12} sec. All the measurable quantities depend upon temperature and hence it is necessary to observe the absorption spectrum over a wide temperature range.

The internal vibrational energy levels of a molecule depend on its environment. Whilst the intensity of the infra-red absorption depends upon the symmetry of the atoms within the molecule and also on the symmetry of the arrangement of the molecules within the unit cell, small changes in configuration thus lead to changes in the infra-red spectrum and hence provide information on the movement of atoms within the crystal. Infra-red observations are hence complementary to other spectroscopic studies and to dielectric, diffraction and thermodynamic studies. Here we review some examples from work in our laboratory which illustrate the use of infra-red radiation in this field of investigation. Fuller details and spectra are published elsewhere.

The motion of the ammonium ion in different crystals has been the subject of study by many investigations using a variety of physical methods. The chief infra-red work on this ion has been by HORNIG[3] and co-workers. In our work[4] we have isolated a small percentage of NH_4^+ ions in CsCl, CsBr and in CsI lattices. The ammonium ion very readily replaces the caesium and hence as only about one per cent replacement is used the interaction between the ammonium ions is small. The

infra-red absorption of all the ammonium salts reveal two sharp absorption bands at low temperature which are interpreted as combination frequencies of a torsional mode with two different internal vibrational modes. The identification of these torsional modes has been aided by the use of the N^{15} isotope as well as the deuterated species ND_4^+. The torsional frequencies that we find for the NH_4^+ ion in the different caesium halides are

CsCl	CsBr	CsI
350 cm^{-1}	310 cm^{-1}	260 cm^{-1}

BH_4^- isolated in different alkali halides[4, 5] has very narrow absorption bands at liquid helium temperature, however, there is no indication of the corresponding combination bands which involve the torsional mode.

In clathrates the holes in which small "gaseous" molecules may be trapped are frequently relatively large and hence they might appear to be ideal cases for the study of free quantised rotation using infra-red radiation to induce transitions between the rotational states. However, in order to observe such transitions it is important that the molecule should not "collide" with the "cavity walls" during the period taken to complete a single rotation; this is of the order of 10^{-11} sec. As this time is of the same order of magnitude as the translational vibrational period of the molecule in the site, it is not surprising that the rotational transitions have not been observed. At very low temperatures it is feasible that in certain cases the transitions may be observable and further investigations in this field are clearly desirable. A further example of molecules isolated in a lattice is that of H_2O and OH^- in crystalline quartz.[6] At room temperature these give rise to a broad absorption band in the 3300 cm^{-1} region, however, on cooling to liquid nitrogen temperature the movement of these OH groups is very much reduced and a large number of sharp absorption bands appear. These result from the isolation at different sites within the crystal lattice. By using polarized infra-red radiation it has been found that all the O–H bonds are aligned perpendicular to the optic axis of the quartz crystal. In all the examples cited above cooling leads to a very marked reduction in the band half-widths thus showing that the vibrational relaxation times increase on lowering the temperature.

A notable example of a change in molecular symmetry leading to a marked alteration in spectrum is hexamethyl benzene.[6] The polarized infra-red spectrum of $C_6(CH_3)_6$ for different crystal faces has been studied over a wide temperature range and the change in the spectrum is interpreted as resulting from an ordering of the methyl groups about the

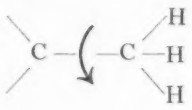

axes. At higher temperatures the methyl groups have a disordered configuration but, on cooling they apparently become more highly ordered and hence permit the molecules to pack more closely together. Similar conclusions have been drawn by SCHNEPP[7] and by WOLF[8] from a study of the near ultra-violet absorption spectrum. Another example of an infra-red study on the reorientation of methyl groups is that of dimethyl triacetylene. This molecule crystallizes with all the acetylene bonds parallel to one another and neighbouring CH_3 groups with the same axes are arranged in the staggered configuration at low temperature.

The vibrational spectrum $g(\gamma)$ of molecules moving relative to one another in modes which are analogous to the lattice modes in simple monatomic and diatomic lattices is not readily obtained directly in molecular crystals on account of the fact that there is no large periodic variation in electric charge as occurs in ionic crystals. However HEXTER[9] has shown that if the infra-red spectrum of iodoform CI_3H is obtained with the direction of propagation of the radiation along that crystal direction to which all the C–H bonds are parallel then the absorption due to the C–H stretching vibration is weak and that "wings" can be observed on either side of the C–H absorption near 3000 cm^{-1}. These appear to be the sum and difference combinations of the lattice spectrum $g(\gamma)$ with the C–H stretching mode. The high frequency[6] cut-off of this mode occurs at 50 cm^{-1}. The changes that occur in the spectrum on cooling down to liquid helium temperature have been observed and the difference spectrum i.e. the low frequency wing disappears as the lattice modes are frozen out.

Polarized infra-red studies on many different polymers have been carried out and phase

Vol. 18
1961

transitions have been observed in several of these. Polytetrafluorethylene (PTFE) is crystalline below 20°C, however at this temperature there is a first order transition. This has been shown[10] to be the result of a screw transition. The PTFE molecular chains are compact helixes and hence can slip past or roll around one another very easily. The transition results in a marked change in the infra-red absorption at 630 cm^{-1} as the temperature is raised through the transition point. The "plasticity" as well as the structure of biopolymers depends very markedly on their water content. One of the most interesting examples of this is the nucleic acid DNA. The crystal displays a high degree of crystallinity when exposed to a high humidity. In this form all the planes of the purine and pyrimidine base pairs are perpendicular to the helix axis. On removing the water these tilt and become disordered. The infra-red absorption spectra of the vibrations of the atomic groups in the bases have been studied using polarized radiation[12] and from the measurement of the dichroic ratio which is the ratio of the absorptions measured with the electric vector of the radiation (1) perpendicular and (2) parallel to the axis, an estimate of the tilting movement of the bases has been obtained.

The above examples are intended to give some indication of the type of problems which have been investigated and the general conclusions on the results that have been obtained. However, at present the interpretation of the infra-red spectra of molecular crystals is hampered by the lack of a really satisfactory theory of the coupling between similar vibrational groups in adjacent molecules and also by requiring a more complete theory of the factors which influence the contours including the line widths of the absorption bands. Much further work is needed on vibrational relaxation processes in molecular crystals i.e. the mechanism of energy transfer between internal and lattice modes before the wealth of accurate experimental data which is now being accumulated can be used to give qualitative information on molecular motions in crystals.

REFERENCES

1. Herzberg G., *Infra-red and Raman Spectra of Polyatomic Molecules*. Van Nostrand, New York (1945).
2. Wilson E. B., Decius J. C. and Cross P.C., *Molecular Vibrations*. McGraw-Hill, New York (1955).
3. Hornig D. F. and Wagner E. L., *J. Chem. Phys.* **18,** 296 (1950).
4. Price W. C., Sherman W. F. and Wilkinson G. R., *Proc. Roy. Soc.* **5,** 255 (1960).
5. Price W. C., Sherman W. F. and Wilkinson G. R., *Spectrochim. Acta* (1960), to be published.
6. Price W. C., Inglis S. A., Senior W. A., Smart C. and Wilkinson G. R., *Spectrochim. Acta* (1960), to be published.
7. Schnepp O. and McClure D. S., *J. Chem. Phys.* **26,** 83 (1957).
8. Wolf H. C., *Z. Naturf.* **13**a, 336 (1958).
9. Hexter R. M. and Cheung H., *J. Chem. Phys.* **24,** 1186 (1955).
10. Klug A. and Franklin R. E., *Disc. Faraday Soc.* **25,** 106 (1958).
11. Robinson T. S. and Price W. C., *Proc. Phys. Soc.* **66,** 969 (1953).
12. Wilkinson G. R., Price W. C. and Bradbury E. M., *Spectrochim. Acta* **14,** 284 (1959).

J. Phys. Chem. Solids Pergamon Press 1961. Vol. 18, No. 1, p. 77. Printed in Great Britain.

NUCLEAR MAGNETIC RESONANCE AND DIFFUSION IN SOLIDS

F. A. RUSHWORTH

University of St. Andrews, Aberdeen

Vol. 18
1961

THE EVIDENCE from the nuclear magnetic resonance spectra of several molecular solids strongly suggests a diffusion process at temperatures several degrees below the melting points.[1] These molecules are usually "globular" in character and it is found that free spherical rotation alone is not sufficient to cause the amount of line-narrowing which is observed.

Broadening of a nuclear magnetic resonance absorption line is due to magnetic interaction between neighbouring nuclei. The calculation of the expected value for the second moment of an absorption line is conveniently split into two parts, the intramolecular contribution due to interactions between nuclei in the same molecule and the intermolecular contribution due to interactions between nuclei in different molecules. Free spherical rotation of a molecule will, if fast enough, reduce the intramolecular contribution to a negligible value. The effect of such motion on the intermolecular contribution to the second moment is not easy to estimate, but various calculations all give values between 1·0 and 1·5 G^2. The total second moment of the absorption line due to free spherical rotation of these "globular" molecules on their own sites should not, therefore, fall much below 1·0 G^2. Experimentally, however, the second moments of these narrow lines are considerably smaller than this, and values of less than 0·01 G^2 have been quoted. This additional narrowing can be explained by movement of whole molecules relative to each other at a rate faster than the line-width expressed as a frequency. Self-diffusion is therefore suggested at a rate of at least 10^4 displacements per second, and it is difficult to visualize any other kind of mechanism which would cause this effect.

Accurate pictures of the shapes of these narrow lines are not normally obtained for two reasons. Firstly it would involve the use of a magnet of high homogeneity with all its ancillary equipment, and such magnets are not generally used for broad-line work since they are not essential to the study of broad lines. Secondly the method of detection of broad lines involving the use of field modulation and a lock-in detector is normally unsuitable for very narrow lines since the line-shapes are broadened and distorted when the line-widths are of the order of the modulation frequency. It would certainly be very interesting to examine the shapes of these very narrow solid lines using high resolution techniques.

REFERENCES

1. ANDREW E. R., *Defects in Crystalline Solids* p. 60. Report of 1954 Bristol Conference. Physical Society, London.

J. Phys. Chem. Solids Pergamon Press 1961. Vol. 18, No. 1, pp. 78–79. Printed in Great Britain.

COMMENTS ON THE PAPERS OF (a) J. A. POPLE AND F. E. KARASZ, (b) L. A. K. STAVELEY

J. S. ROWLINSON
Manchester University

(a) Dr. POPLE and Dr. KARASZ have taken the very crude model of a freezing liquid proposed for spherical molecules by LENNARD-JONES and DEVONSHIRE and have extended it in a most elegant way to account qualitatively for the lowering of the melting point with increasing asymmetry.

I would like first to observe that the model of LENNARD-JONES and DEVONSHIRE cannot be accurate as it would require the separation of nearest neighbours in the crystal to be substantially larger than that in the liquid (the ratio would be about $2^{1/3}$). In fact, the separation is almost unaltered on freezing, and any change is certainly a decrease.

Secondly, I would like to ask if there is any correlation between the melting temperatures (and the transition temperatures of the plastic crystals which are also predicted by this theory) and the various parameters which have been derived from the thermodynamic properties of the fluids (by PITZER, by RIEDEL and by COOK and ROWLINSON) to represent the molecular eccentricity?

(b) Mr. STAVELEY has shown that methane has a greater freedom of rotation in the crystalline state than have nitrogen and oxygen. A recent analysis[1] of the configurational heat capacities of the liquids has shown that this difference persists into the liquid state. Liquid methane has no observable configurational heat capacity of rotation either at constant volume or at constant pressure. Diatomic molecules have observable heat capacities which increase in the order oxygen, nitrogen, carbon monoxide.

REFERENCES

1. ROWLINSON J. S., *Liquids and Liquid Mixtures*, pp. 289–91. Butterworths, London (1959).

REPLY BY J. A. POPLE AND F. E. KARASZ

We agree with Dr. ROWLINSON that the model of LENNARD-JONES and DEVONSHIRE has a number of deficiencies as a precise theory of melting. This is reflected in the need to choose W_0 empirically (W_0 being proportional to the energy required to move an atom onto an interstitial site at low temperatures). Any attempt to calculate this without allowing for movement away from α or β sites gives a much larger value, so that many of the limitations are hidden beneath this empirical value. Within these limitations, however, the LJD theory was very successful in correlating properties and our aim has been to extend the theory rather than refine it.

As our parameter ν and the $\delta(T_c)$, for example, of COOK and ROWLINSON[1] are both measures of deviation of molecular interactions from spherical symmetry, there should certainly be a correlation between $\delta(T_c)$, and ν, or some physical property which itself is dependent on ν. We have plotted, therefore, values of $\delta(T_c)$ against T_m/T_b (T_m/T_c would be more correct) and find that there is, indeed, such a correlation, though as one might expect, there is considerable scatter. [The $\delta(T_c)$ values are those derived from vapour pressure measurements[2], supplemented with our own calculations for HCl, HI, and PH_3; data from International Critical Tables.]

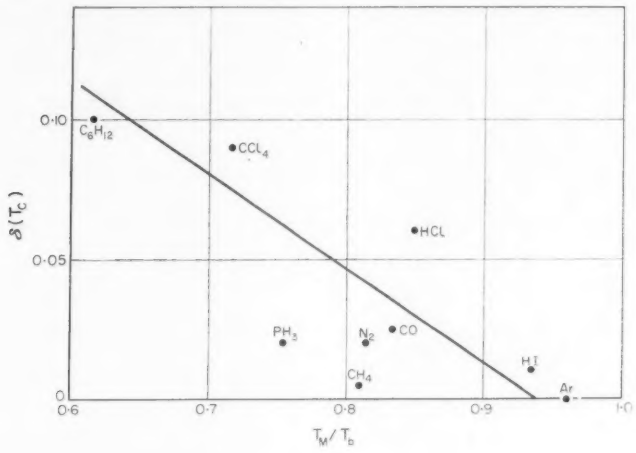

FIG. 1

It might be noted that the direction of the deviations of methane and, to a lesser degree, phosphine, is a reflection of their greater non-ideality at high densities, indicating a more specialized interaction in the solid or liquid state.

Though the theory will predict transition temperatures we have yet to extend our work in this direction and are therefore at the present unable to correlate these with $\delta(T_c)$.

Vol. 18
1961

REFERENCES

1. COOK D. and ROWLINSON J. S., *Proc. Roy. Soc.* **A219,** 405 (1953).
2. ROWLINSON J. S., *Liquids and Liquid Mixtures.* Butterworths, London (1959).

J. Phys. Chem. Solids Pergamon Press 1961. Vol. 18, No. 1, pp. 80–81. Printed in Great Britain.

ENERGY AND APPARENT ENTROPY TERMS FOR QUASI-SPHERICAL MOLECULAR ROTATIONS

MANSEL DAVIES and C. CLEMETT

University College of Wales, Aberystwyth

A NUMBER of contributors emphasized the ability of "globular" molecules to rotate as readily in the solid as in the liquid state: in many cases data were presented which showed only insignificant changes in passing through the melting-point. It is obviously important to assess this freedom quantitatively. For polar molecules, measurements of the relaxation time (or times) in the solid provide one such means, and it is customary to use an Arrhenius type expression for the rotational activation enthalpy, ΔH.

$$\frac{1}{\tau} = A \exp(-\Delta H/RT) \qquad (1)$$

There is some uncertainty as to the adequacy of this expression especially when ΔH is small (<6 kcal/mole). Chemists are familiar with this limitation in the form of ΔC_p or similar terms, which can themselves be temperature dependent, leading to variations in ΔH (apparent): such terms are the more obvious the smaller ΔH.

For quasi-spherical molecules the available dielectric data (over ranges of ca. 40°C in solid or liquid phases) do not suffice to establish departures from (1). Professor ANDREW presented n.m.r. data for benzene rotations (about an axis perpendicular to the plane of the ring) which showed good conformity to (1) over more than a 100°C range. Accordingly, it is worth considering the available dielectric data in this sense.

For the factor A absolute rate theory arrives at different values according to the model envisaged for the restricted rotation. The most frequently used value is Eyring's $A = (kT/h) \exp(\Delta S/R) = P.\ kT/h$ where ΔS is an arbitrary "entropy of activation" which is adjusted to fit the observations. The expression (kT/h) is in itself valid probably only in those cases where many degrees of freedom are involved and where many energy levels occur in the energy trough.

An alternative expression is that of Bauer

$$A = \left(\frac{kT}{2\pi I}\right)^{1/2} \exp(\Delta S/R) = \left(\frac{kT}{2\pi I}\right)^{1/2} \times \times \left[\frac{1}{\sigma_1} + \frac{1}{\sigma_2}\right] \times L = P \left[\frac{kT}{2\pi I}\right]^{1/2}$$

where σ_1 and σ_2 are configurational partition functions and L the "effective length" of the potential barrier. In a simple model due to Hoffmann these geometrical factors reduce to 2π. We shall test the assumption that

$$\left[\frac{1}{\sigma_1} + \frac{1}{\sigma_2}\right] L = 1.$$

The following table summarizes the data for a number of quasi-spherical molecules in the liquid state due to Smyth and coworkers and current measurements at Aberystwyth. It seems preferable to replace the ΔS term in the above relations by the non-committal numerical factor $P = \exp(\Delta S/R)$. One feature which is very obvious in this table is the smallness of the ΔH values: they are appreciably smaller than the $\Delta H(\eta)$ values normally associated with the viscosity process of liquids.

Omitting the example of succino-nitrile, whose molecule is far from being spherical, the average values are P(Eyring) = 0·18 ($\Delta S = -3{\cdot}4$ e.u.); P(Bauer) = 3·4 ($\Delta S = +2{\cdot}3$ e.u.). These P factors are much closer to unity than is usual for chemical rate processes, and these data scarcely indicate any preference between the two expressions. There is, however, apart from a slightly better numerical fit, somewhat better internal consistency in the Bauer factor for which the plot of

Table 1.

Compound	Eyring's relation		Bauer's relation	
	ΔH kcal/mole	P	ΔH kcal/mole	P
$(CH_3)_3.C.Cl$	0·67	0·11	0·96	2·0
$(CH_3)_3.C.NO_2$*	0·98 ± 0·2	0·11	1·29 ± 0·2	2·4
$(CH_3)_3.C.CN$*	1·78 ± 0·2	0·45	2·09 ± 0·2	7·7
$(CH_3)_2.C.Cl_2$	1·14 ± 0·3	0·18	1·45 ± 0·3	2·7
$CH_3.C.Cl_3$	1·21 ± 0·3	0·25	1·49 ± 0·3	3·8
$(CH_3)_2.C.(NO_2)Cl$(liq.)*	1·25 ± 0·2	0·12	1·56 ± 0·2	2·7
$(CH_3)_2.C.(NO_2)Cl$(solid)*	1·1	0·07	1·35	4·0
$(CH_2.CN)_2$(liq.)*	3·2 ± 0·4	1·0	3·5 ± 0·4	2·4
$(CH_2.CN)_2$(solid)*	2·1	0·09	2·4	2·1

* Studied at Aberystwyth.

ΔH against ΔS (apparent) gives an appreciably better approach to linearity than for the Eyring factors. The former plot gives, for $\Delta H = 0$, ΔS (apparent) ca. $-0{\cdot}3$ e.u.; the latter, ΔS (apparent) $= -5{\cdot}5$ e.u.

The purpose of this note is to raise the question of the correct form of A in particular cases and to emphasize the arbitrariness of the related ΔS terms unless the absolute rate factors can be fully justified.

Vol. 18
1961

J. Phys. Chem. Solids Pergamon Press 1961. Vol. 18, No. 1, p. 82. Printed in Great Britain.

SOME OBSERVATIONS ON CLATHRATES

J. H. VAN DER WAALS

Koninklijke/Shell Laboratorium, Amsterdam

IN CONNECTION with Mr. STAVELEY's interesting contribution on the specific heat of clathrates I should like to make two remarks.

Firstly, the seemingly simple problem of the rotational motion of a molecule encaged in a clathrate already exhibits the fundamental difficulty encountered in our discussion of rotation in solids: it is not strictly possible to write the potential energy of the encaged molecule as a sum of two terms, depending on the positional and orientational coordinates, respectively. In fact, the rotational contribution to the free energy will depend on the vibrational state corresponding to the "rattling" of the molecule in its cage. Or in a very simple picture: an oblong molecule will be forced to orient itself parallel to the wall of the cage when its centre approaches the wall. This loss of orientational freedom of polyatomic molecules in a clathrate is clearly borne out by their smaller entropy of clathration relative to that of monatomic gases.

Specific heat measurements may not be so sensitive to small potential barriers opposing free rotation. However, when describing the potential energy of an encaged molecule by a Lennard-Jones and Devonshire potential the specific heat provides a very sensitive experimental criterion for the distance parameter τ, whereas it hardly depends on the energy parameter ϵ. This can be understood when it is realized that the shape of the field within the cage rather resembles a very deep square well, in which the energy levels near the bottom—and thus the specific heat—only depend on the width of the well.

Secondly, Mr. STAVELEY referred to the susceptibility measurements on the oxygen clathrate started in Oxford and later continued at Harvard. Dr. MEYER has now followed up these investigations by low-temperature resonance experiments. He studied the O_2 clathrate by electron spin resonance and the N_2 clathrate by pure quadrupole resonance.[1] Such experiments give more detailed information on orientational freedom of the enclosed molecules than n.m.r. measurements can furnish. Describing the potential binding these diatomic molecules to the axis of the cage by a simple potential of the form $V = V_0\ (1-\cos 2\theta)$ it was found that

$$V_0 = 0{\cdot}06 \text{ kcal/mole for } O_2$$

$$V_0 = 0{\cdot}44 \text{ kcal/mole for } N_2;$$

the former value is in good agreement with that following from the susceptibility measurements.[2]

It is thought to be difficult to interpret these results qualitatively. Although the difference between the two molecules may seem considerable one should keep in mind that the above values are averages over the respective zero-point rattlings in the cages, and that the nitrogen molecules fit rather more tightly than those of oxygen. The given values of V_0, moreover, represent only a small fraction of the energy of binding of these molecules in the clathrate cages which is of the order of 5 kcal per mole.

REFERENCES

1. MEYER H. and SCOTT T. A., *J. Phys. Chem. Solids* **11,** 215 (1959).
2. MEYER H., O'BRIEN M. C. M. and VAN VLECK J. H., *Proc. Roy. Soc.* A**243,** 414 (1957).

J. Phys. Chem. Solids Pergamon Press 1961. Vol. 18, No. 1, pp. 83–85. Printed in Great Britain.

THE THERMOPHYSICAL PROPERTIES OF THREE GLOBULAR MOLECULES

E. F. WESTRUM, Jr.

Department of Chemistry, University of Michigan, Ann Arbor, Michigan

Abstract—The low temperature heat capacities of adamantane, hexamethylenetetramine and triethylenediamine have been determined from 5 to 350°K by adiabatic calorimetry. A transition at 208·6°K involving an entropy increment of 3·87 e.u. is associated with a slight modification of the crystalline arrangement and the molecular freedom in adamantane. Although a related transition also occurs in triethylenediamine at 353°K, none has yet been detected in hexamethylenetetramine.

Vol. 18
1961

1. ADAMANTANE AND HEXAMETHYLENETETRAMINE

OF THE many molecules which may be classified as "globular"[1] few approach geometrical or force field sphericity to the extent of adamantane,* which is the simplest saturated polycyclic hydrocarbon possessing a cage-like skeleton like that of the crystalline lattice of diamond. This interesting substance exists in a face-centered cubic array with a $T_d^2-F\bar{4}3m$ space group at room temperature according to NOWACKI[2] (although it is presently considered that this phase represents a disordered structure), melts at 270°C,[3] and moreover undergoes an apparently first order transition[4] to a body-centered tetragonal lattice at 208·62°K with the tentative unit cell dimension $a = 6{\cdot}641$ Å and $c = 8{\cdot}875$ Å.[5] A schematic diagram of its molecular structure is presented in Fig. 1(a). The compound was synthesized by the method of SCHLEYER[6] and its purity established by chemical X-ray diffraction and gas chromatography.

A closely related substance, hexamethylenetetramine,†[cf. Fig. 1(b)], which may be considered to be "derived" from adamantane by replacement of the four methine (CH) groups with nitrogen atoms, on the other hand apparently does not undergo transition to a plastic crystalline phase below 240°C and possibly not before decomposition or fusion. Its structure is that of a body-centered cubic lattice of space group $T_d^3-I\bar{4}3m$ with $a = 7{\cdot}02$ Å.[7] Like adamantane this substance is characterized by a relatively high melting point —about 280°C[8] because of the molecular symmetry and relatively strong intermolecular forces.

The heat capacities of these substances were determined by precise adiabatic calorimetry and are depicted in Fig. 2. Although the temperature dependence of the heat capacity is similar in general for both substances, the transition in adamantane is pronounced. Apparent heat capacities as high as 4500 cal/(deg mole) were observed at the peak. Thermal equilibrium was reached within an hour's time in the transition region. The enthalpy of transition of adamantane is 807 cal/mole and the entropy increment of transition is 3·87 e.u. In some respects these represent minimal values since the interpolated dashed line in Fig. 2 is used to represent the background or lattice heat capacity. Since the transformation is apparently a first order phase transition, separate extrapolations of the heat capacities of both the high and low temperature forms might have been more appropriate and would almost certainly have led to larger values of the increments; the proper extrapolations on this basis are quite ambiguous. A brief summary of the thermodynamic properties of these compounds is given in Table 1.

* $C_{10}H_{16}$, tricyclo[3,3,1,$1^{3,7}$]decane.

† $C_6N_4H_{12}$, 1,3,5,7-tetrazatricyclo[3,3,1,$1^{3,7}$]decane.

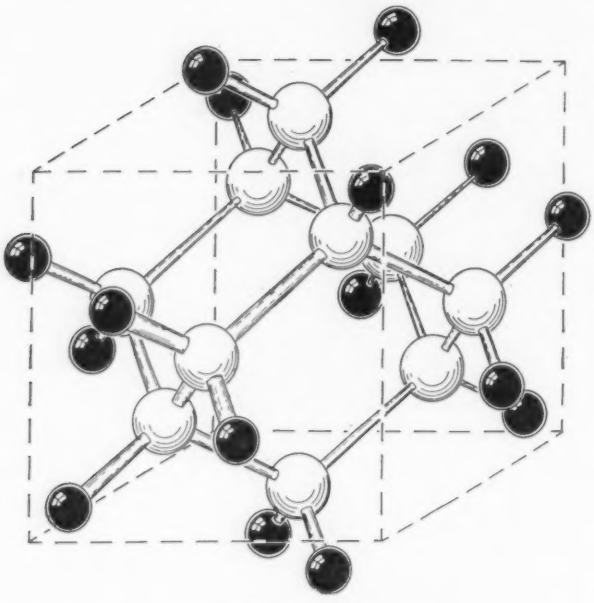

FIG. 1(a)

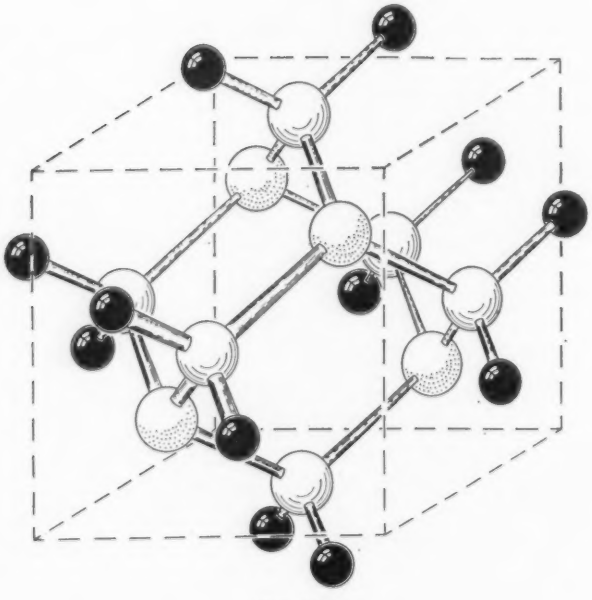

FIG. 1(b)

FIG. 1. The molecular structures of (a) adamantane and (b) hexamethylenetetramine.

Table 1. *Comparison of thermodynamic properties of adamantane* (*A*), *hexamethylenetetramine* (*HMT*) *and triethylenediamine* (*TED*) *at* 298·15°K *in cal*/(*deg mole*)

Compound	C_p	$S°$	$(H°-H_0°)/T$	$-(F°-H_0°)/T$
A	45·35	46·80	24·38	22·42
HMT	36·42	39·05	18·26	19·65
TED	36·61	37·67	18·52	19·14

Adamantane is the prototype for a considerable variety of diamondoid derivatives obtained by substituting nitrogen, oxygen, sulfur, and phosphorus into the skeleton. The most readily synthesized of these compounds having suitably

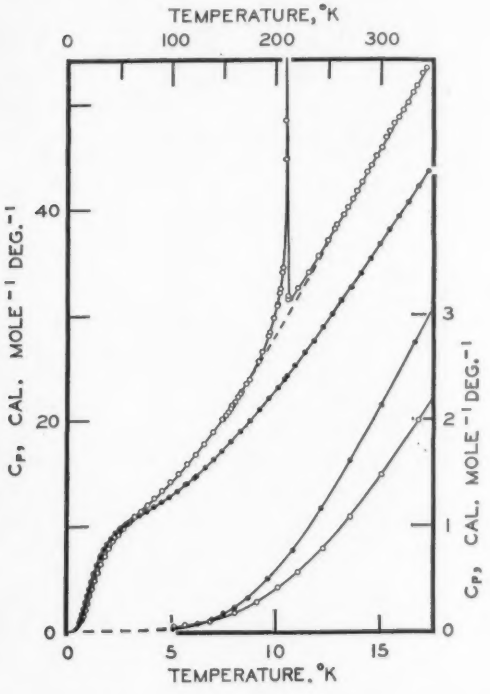

FIG. 2. Molal heat capacities of adamantane (○) and hexamethylenetetramine (●).

tailored symmetries are currently being examined by thermophysical techniques. The higher temperature heat capacities, energetics of pseudorotation and fusion transitions are also under study.

2. TRIETHYLENEDIAMINE*

This globular molecule possesses the shape of a symmetrical top rather than the sphericity characteristic of the diamondoid compounds. Triethylenediamine undergoes transition from a $C_{6_h}^2-P6_{3/m}$ space lattice[9] to a presumably more symmetrical structure at about 353°K, rather than at the temperature of 74°C (347°K) reported by FARKAS *et al.*[10] No anomalies are found in the heat capacity from 5 to 350°K. Thermodynamic functions of triethylenediamine are included in Table 1. The thermodynamics of the 353°K and fusion transitions are under investigation.

This work is being done with the collaboration of SHU-SING CHANG and is partially supported by the Division of Research of the U.S. Atomic Energy Commission.

* $C_6N_2H_{12}$, 1,4-diazabicyclo[2, 2, 2]octane.

REFERENCES

1. TIMMERMANS J., *Bull. Soc. Chim. Belg.* **44,** 17 (1935); *Industr. Chim. Belge* **16,** 178 (1951).
2. NOWACKI W., *Helv. Chim. Acta* **28,** 1233 (1945).
3. LANDA S., KRIEBEL S. and KNOBLOCH E., *Chem. Listy* **48,** 161 (1954).
4. CHANG S. S. and WESTRUM E. F., Jr., *J. Phys. Chem.* **64,** 1547 (1960).
5. NORDMAN C. E., unpublished data.
6. SCHLEYER P. V. R., *J. Amer. Chem. Soc.* **79,** 3292 (1957).
7. DICKINSON R. G. and RAYMOND A. L., *J. Amer. Chem. Soc.* **45,** 22 (1923); GONELL H. W. and MARK H., *Z. Phys. Chem.* **107,** 181 (1923); MARK H., *Ber.* **57B,** 1820 (1923); WYCKOFF R. W. G. and COREY R. B., *Z. Kristall.* **89,** 462 (1934); BRILL R., GRIMM G. H., HERMANN C. and PETERS C., *Ann. Phys. Lpz.* **34,** 383 (1939); SHAFFER P. A., Jr., *J. Amer. Chem. Soc.* **69,** 1557 (1947).
8. GRASSI G., *Gazz. Chim. Ital.* **36II,** 505 (1906).
9. SEKI S., unpublished data.
10. FARKAS A., MILLS G. A., ERNER W. E. and MAERKER J. B., *Industr. Engng. Chem.* **51,** 1299 (1959); *J. Chem. Eng. Data* **4,** 334 (1959).

J. Phys. Chem. Solids Pergamon Press 1961. Vol. 18, No. 1, pp. 86–89. Printed in Great Britain.

ROTATION AND MOLECULAR DISTORTION IN THE CONDENSED PHASES OF HEXAFLUORIDE MOLECULES*

B. WEINSTOCK†

The Argonne National Laboratory, Argonne, Illinois

STUDIES of the structure and physical properties of hexafluoride molecules reveal effects that are of pertinence to the question of rotation in the solid state. Present evidence also suggests that the highly symmetrical structure found for these molecules in the vapor phase is distorted in the condensed phases and that this structural alteration has a significant effect on the equilibrium thermodynamic properties of these compounds.

There are twelve known hexafluoride molecules each of which has the common distinction of being the most volatile compound of its element. Six of the elements that form hexafluorides are in the sixth column of the periodic table and use all of their valence electrons for the formation of the six fluorine bonds. The other six form two transition series in which there are non-bonding electrons besides the six fluorine bonds: ReF_6, OsF_6, IrF_6 and PtF_6 have $5d^1$, $5d^2$, $5d^3$ and $5d^4$ non-bonding electronic configurations respectively, and NpF_6 and PuF_6 have $5f^1$ and $5f^2$. These non-bonding electrons give rise to interesting electronic and magnetic properties that have been partially studied in both vapor and condensed phases.[1–4]

The structure of all of the hexafluoride molecules in the vapor phase has been established as that of a regular octahedron, symmetry O_h, both by vibrational spectroscopy[5–8] and electron diffraction studies.[9, 10] The metal to fluorine distances for six of them[10] in the two transition series are given in Table 1. Owing to their high symmetry and spherical-like contour, one might expect all of these molecules to be examples of Professor Timmermans' globular compounds. However, in Table 1, we see that the entropy of fusion for the three $5f$ hexafluorides of about 13 cal $mole^{-1}$ deg^{-1}[11] far exceeds the value of 5 cal $mole^{-1}$ deg^{-1} that Professor Timmermans has suggested as the limit for plastic crystals. This high value for the entropy of fusion is a consequence of the close packed arrangement of these hexafluoride molecules in the solid state, which makes the possibility of rotation very unlikely. The crystal structure has orthorhombic holohedral symmetry, space group $D_{2h}^{16}-P_{nma}$, which in

* Based on work performed under the auspices of the U.S. Atomic Energy Commission.

† Present address: Ford Motor Company, Scientific Laboratory, P.O. Box 2053, Dearborn, Michigan.

Table 1.

	WF_6	ReF_6	OsF_6	IrF_6	PtF_6
M–F distance, Å	1·833	—	1·831	1·830	—
	UF_6	NpF_6	PuF_6		
M–F distance, Å	1·996	1·981	1·971		
Entropy of fusion, cal $mole^{-1}$ deg^{-1}	13·6	12·8	13·7		
Triple point temperature, °C	64·05	55·1	51·6		

idealized form positions the fluorine atoms in parallel planes double hexagonally close packed (ABAC) with the metal atoms in the appropriate interstitial positions.[12–14] It is also very probable that free rotation does not even occur in the liquid state for these molecules since the rotational entropy in the vapor phase at their triple point temperatures is about 22 cal mole^{-1} deg^{-1} which is much greater than the entropy of fusion.

The 5*d* transition series hexafluorides, WF_6, ReF_6, OsF_6, IrF_6 and PtF_6, all show a transition in the solid state from the close packed orthorhombic structure to a less dense body centered cubic form.[15] This transition occurs at 3°C for PtF_6[16] and the entropy of transition calculated from vapor pressure data and the Clapeyron relation is 7·7 cal mole^{-1} deg^{-1}. The fusion triple point is at 61·3°C and the entropy of fusion 3·2 cal mole^{-1} deg^{-1}. Cubic PtF_6 and probably the other 5*d* hexafluorides would therefore qualify as plastic crystals. It is tempting to consider the solid–solid transition in PtF_6 as a consequence of the onset of rotation in the solid and the small entropy of fusion is in agreement with this view. However, the total entropy change associated with the two transitions is only 10·9 cal mole^{-1} deg^{-1}, which, similarly to the 5*f* hexafluorides, is substantially less than the rotational entropy of the molecules in the vapor phase (22·1 cal mole^{-1} deg^{-1} at the fusion point). It therefore seems likely that there is relatively little difference with regard to rotation between the cubic solid and the liquid and that free rotation does not occur in either case. The entropy associated with the solid–solid transition in PtF_6 is 7·7 cal mole^{-1} deg^{-1} = R ln 48. Since the symmetry number of this molecule is 24, a simple explanation for this transition similar to that offered by GUTHRIE for so many organic compounds is not readily apparent.[17]

Preliminary X-ray data with PtF_6 gives the value of 6·21 Å for a_0, the side of the unit cubic cell.[15] By assuming that the six Pt–F bonds are directed along the rectangular cubic axes a minimum value for the radius of PtF_6 of 3·10 Å is obtained. Using 1·83 Å for the Pt–F distance, the fluorine radius in the molecule is computed to be 1·27 Å. This is smaller than the ionic fluorine radius, 1·33–1·36 Å. However, there is a contraction to be expected in the fluoride radius because of the partial covalent nature of the bonds and also owing to the high charge on the central atom.[18] Such a contraction could account for some of this difference. Measurements of the orthorhombic solid density of PtF_6 as a function of temperature have been made to liquid nitrogen temperatures.[16] When these values are extrapolated linearly to absolute zero the density calculated is 0·0231 mole/cm^3. This value is in agreement with the value, 0·0226 mole/cm^3, that one calculates using 1·83 Å for the Pt–F distance and the idealized orthorhombic structure; i.e. the intermolecular F–F distance taken the same as the intramolecular F–F distance. The F–F distance in the regular octahedron is 1·29 Å. In the liquid the observed density is 0·0125 mole/cm^3. The density of a set of close packed spheres of radius 3·10 Å is 0·0099 mole/cm^3. This latter density would be expected for PtF_6 if the molecules were rotating freely in the liquid. These considerations suggest that free rotation does not occur in either the liquid or cubic solid but rather a hindered or correlated cog-wheel type rotation occurs.

The vapor pressures of UF_6, NpF_6 and PuF_6 shown in Fig. 1 have a very complicated character.[11] The vapor pressure of NpF_6 in the solid is greatest and in the liquid intermediate between that of UF_6 and PuF_6. Solid UF_6 at the lowest temperature is least volatile, crosses the vapor pressure of PuF_6 to an intermediate value and in the liquid is most volatile. These results are particularly curious since there are no irregularities apparent in the molecular weights, metal to fluorine distances, vibrational frequencies, and crystal densities to account for this complicated behavior. The crystal structures of the three molecules are the same and the lattice parameters are identical within the experimental uncertainty of 0·003 Å. The metal to fluorine distances decrease regularly in going through the sequence UF_6, NpF_6 and PuF_6, and, since their crystal spacings are the same, we can conclude that the van der Waals binding in the crystals decreases in the same order as the metal to fluorine distances. The observed melting points decrease similarly in agreement with this view, i.e. UF_6 melts highest and PuF_6 lowest. This concept, however, predicts that PuF_6 should be most volatile, contrary to the observations. In order to explain the complicated anomalous vapor pressure observations, it has been suggested that the octahedra are distorted

Vol. 18
1961

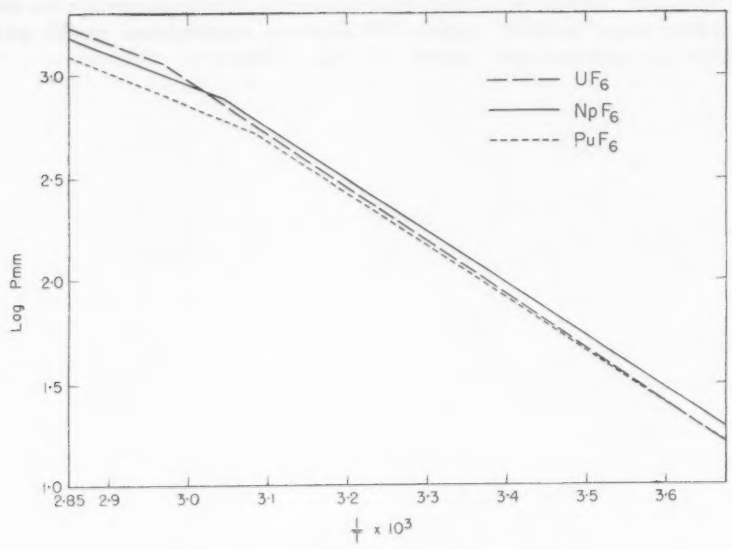

VAPOR PRESSURE OF UF_6, NpF_6, AND PuF_6.

FIG. 1

in the condensed phase and that this effect is different for the three molecules.[11] In the original vibrational spectra measurements with UF_6,[19] the Raman shifts for σ_1 and σ_2 observed for the pure liquid were markedly different from the values derived from infrared combination bands in the vapor, while the Raman shifts observed for σ_2 and σ_5 in a dilute solution of UF_6 in a fluorocarbon agreed with the values derived from the vapor. This large shift between the vibrational frequencies observed in the pure liquid compared to those observed in the vapor or dilute solution has been confirmed by measurement of the Raman spectrum of the vapor.[20] The vibrational frequencies are lower in the liquid than in the vapor and as a consequence there is a lowering of the vapor pressure for the system. Measurements of the partial pressure of UF_6 in fluorocarbon solutions show large positive deviations from Raoult's law. These deviations become as large as 40 per cent at UF_6 concentrations of 20 mole per cent or lower and are observed at temperatures above and below the triple point of UF_6. These observations are in agreement with the vibrational spectra results and suggest that molecular distortion does indeed have an important effect on the vapor pressures. These considerations lead to the prediction that in dilute solution the partial pressures of PuF_6, NpF_6 and UF_6 at the same temperatures and concentrations would decrease in that order, which is the inverse order of the vapor pressures of the pure liquids. The crossing of the vapor pressure of solid UF_6 and PuF_6 is in agreement with this view, since at lower temperatures the contribution of the vibrational modes to the partition function becomes less important and the vapor pressures should arrange themselves in an order with the one compound having the strongest van der Waals binding, UF_6, being the least volatile. The fact that NpF_6 is most volatile in the solid remains anomalous but is believed to be a consequence of the fact that of these three compounds only NpF_6 is paramagnetic.[1, 2] One possibility is that there is an interaction between the paramagnetic electron and the "crystalline field," that is different in the liquid than in the solid. The ground electronic state of the molecule would then be shifted by different amounts in liquid and solid relative to the state in the undistorted vapor molecule. In order to explain the excess volatility of solid NpF_6 on this basis this effect must be of the order of 30–100

cm^{-1}. It is interesting to note that the entropy of fusion of NpF_6 is lower than that both of UF_6 and PuF_6 by an amount of the order of 100 cm^{-1} (Table 1) in agreement with this possibility.

REFERENCES

1. Gruen D. M., Malm J. G. and Weinstock B., *J. Chem. Phys.* **24,** 905 (1956).
2. Weinstock B. and Malm J. G., *J. Chem. Phys.* **27,** 594 (1957).
3. Moffitt W., Goodman G. L., Fred M. and Weinstock B., *Mol. Phys.* **2,** 109 (1959).
4. Hutchison C. A., Jr. and Weinstock B., *J. Chem. Phys.* **32,** 56 (1960).
5. Gaunt J., *Trans. Faraday Soc.* **49,** 1122 (1953); **50,** 209 (1954).
6. Mattraw H. C., Hawkins N. J., Carpenter D. R. and Sabol W. W., *J. Chem. Phys.* **23,** 985 (1955).
7. Malm J. G., Weinstock B. and Claassen H. H., *J. Chem. Phys.* **23,** 2192 (1955).
8. Weinstock B., Claassen H. H. and Malm J. G., *J. Chem. Phys.* **32,** 181 (1960).
9. Glauber R. and Schomaker V., *Phys. Rev.* **89,** 667 (1953).
10. Schomaker V., Kimura M., Smith D. W. and Weinstock B. unpublished results.
11. Weinstock B., Weaver E. E. and Malm J. G., *J. Inorg. Nucl. Chem.* **11,** 104 (1959).
12. Hoard J. L. and Stroupe J. D., *X-ray Crystal Structure of* UF_6, Cornell Report A–1296 (1944).
13. Zachariasen, W. H., *The Transuranium Elements* (edited by Seaborg G. T., Katz J. J. and Manning W. M.) PPR, NNES, Div. IV, Vol. 14B, p. 1465. McGraw-Hill, New York (1949).
14. Florin A. E., Tannebaum I. R. and Lemons J. F., *J. Inorg. Nucl. Chem.* **2,** 368 (1956).
15. Siegel S., private communication.
16. Weinstock B., Malm J. G. and Weaver E. E., to be published.
17. Since the conference a report by Brady A. P., Clauss J. K. and Myers D. E., has come to my attention, WADC Technical Report 56–4 (September 1957); these authors have measured the heat capacity of MoF_6 and report a solid–solid transition at 263·6°K, $\Delta S = 7{\cdot}72$ cal $mole^{-1}$ deg^{-1}, and the melting point at 290·6°K, $\Delta S = 3{\cdot}65$ cal $mole^{-1}$ deg^{-1}. These numbers are quite in accord with the values for PtF_6.
18. Zachariasen W. H., *Z. Kristallogr.* **80,** 137 (1931).
19. Bigeleisen J., Mayer M. G., Stevenson P. C. and Turkevich J., *J. Chem. Phys.* **16,** 442 (1948).
20. Claassen H. H., Weinstock B. and Malm J. G., *J. Chem. Phys.* **25,** 426 (1956).

Vol. 18
1961

J. Phys. Chem. Solids Pergamon Press 1961. Vol. 18, No. 1, pp. 90–92. Printed in Great Britain.

SOME CONCLUDING REMARKS ON SYSTEMATIC STUDIES OF BARRIERS TO ROTATION IN CRYSTALS

A. R. UBBELOHDE

Imperial College, London

IT MAY be profitable to detail some of the unsolved problems that seem to call for urgent attention, both by more experimental work, and by the development of more accurate and more manageable theoretical models. For convenience these problems may be divided into three groups which refer respectively to thermodynamic properties, to relaxation times, and to mechanical properties, though of course new developments in any one group usually influence the other two.

THERMODYNAMIC PROBLEMS

Thermodynamic properties decidedly show the need for much more work on the effects of changes of pressure on rotational transitions. Various lines of evidence suggest that barriers to rotation are quite sensitive to increases in pressure of the order of a few hundred atmospheres. It is a great weakness in our present understanding of rotational transitions that effects of changes of temperature are known in very much greater detail than effects of changes of pressure. The well known instance of the lambda transition in methane which develops two peaks in place of one at increased pressures points to the kind of new information to be obtained. Comparisons between isotopic molecules can give closely related information about the detailed configuration of rotational barriers. Bonds between various atoms and hydrogen normally have a slightly greater Van der Waals repulsion envelope than the corresponding bonds to deuterium. This means that the isotopic molecules containing deuterium are contained in a lattice slightly more shrunk than is the case with the normal molecules containing hydrogen. Usually this shrinkage would be expected to increase the barriers to rotation in a way somewhat analogous to the effects of increase of pressure, though differences of moments of inertia and of nuclear spin can also change details of the thermodynamic transformations for isotopic molecules, because of quantum effects.

Another pressure variable about which systematic information is urgently required is the compressibility of the crystal in its two states. Modern techniques of measuring the velocity of sound should prove helpful for this requirement, whose fulfilment can for example lead to the calculation of transitions at constant volume rather than the usual constant pressure.

A second thermodynamic variable about which present information seems quite inadequate is the crystal density. Experimental densities are required accurate to about one part in 10^6, for comparison with theoretical densities calculated from precision values of the unit cell of the crystal lattice. For molecular crystals, such comparisons seem to be the most direct route available to determine whether the concentration of crystal defects becomes high—say of the order of 0·1 per cent—in the plastic state of the crystal under discussion. Possibly some kind of buoyancy method with helium, using very finely ground crystals, would help to discriminate between defects in thermal equilibrium in the high temperature state of the crystal, and pores and vacuoles whose significance is only trivial. As is well known, precision measurements of the space-occupancy of crystals when these are plastic is quite difficult.

A third thermodynamic problem arises in connection with studies of the effects of diluents on rotational transitions in crystals. There seem to be opportunities as yet unexploited for more refined studies on the modification of barriers to rotation by the addition of diluents in solid solution. Effects of diluents on some of the

non-thermodynamic properties are however probably even more revealing. Very little seems to be known about these at present.

A fourth thermodynamic problem is not perhaps of equal importance with the first three. Nevertheless it is interesting to inquire how many crystals with possibilities of rotational transitions show any residual entropy at 0°K due to frozen-in rotational disorder.

RELAXATION TIMES

The second group of problems arises from developments in the possibilities for measuring relaxation times in rotational transitions. Measurements of relaxation times by means of nuclear magnetic resonance, or dielectric relaxation, can presumably give much more detailed information about barriers to rotation than measurement of thermodynamic parameters which always present broad statistical averages. However, it seems that in this group of problems, too, there are many unanswered questions. Probably it can serve a useful purpose to try to define some of these questions as closely as possible in the light of current information, although further research may alter the best way of stating them.

As with studies of thermodynamic properties, the influence of pressure on the parameters characterizing rotational barriers in relation to relaxation times calls for systematic study. In some cases comparisons between isotopic molecules can amplify the information obtained from direct variations of pressure. Crystal defects could likewise have an important influence on relaxation times. Defects can be created or modified by adding diluents in solid solution. One would expect certain diluents to reduce the barriers and others to increase them.

Other important problems in connection with relaxation times associated with rotation in crystals refer to what may be called coupled or co-operative or synchronous molecular processes. It does not seem clear, for example, whether the "diffusion" effects that become apparent in some nuclear magnetic studies of rotational transitions, involve the same parameters as those controlling ordinary mass diffusion of the molecules, which are usually thought to involve hopping mechanisms. Do the specific molecules that are activated for rotation find it easier to hop from one site to another, or is the hopping diffusion completely uncorrelated with such rotational activation?

And again, various authors have referred somewhat loosely to the synchronous rotation of neighbouring molecules, comparing these to slack gear wheels, and so on. It seems highly desirable to formulate such suggestions with the maximum degree of quantitative precision, in order to permit fruitful experimental investigations. For example, the probability P_r of a rotational "flip" of a non-spherical molecule can normally be regarded as given by the reciprocal of a characteristic frequency of relaxation. If the "flips" are completely uncorrelated, as would seem to apply for rotators isolated in the crystal, fluctuation theory suggests a probability relationship of the form

$$P_r = a \exp(-\epsilon/kT)$$

where the barrier ϵ and the factor a may depend on such variables as the pressure, but do not involve what neighbouring molecules are doing. On the other hand, when "flips" are synchronized more or less closely, this involves the theory of co-operative fluctuations. Such theory has not been developed very far at present,* but a well known instance is the contrast between unimolecular or bimolecular chemical reactions, that can be treated by the theory of uncorrelated fluctuations, and chain chemical reactions. Very tentatively, the probability of co-operative flips might perhaps take the form

$$P_r = af(T) \exp(-\epsilon/kT)$$

where the factor $f(T)$ allows for the length of a chain of interdependent events. Our knowledge of reaction chains in chemistry suggests that the length of a co-operative chain in rotational flips is likely to decrease as more diluents are added or as the temperature is raised. By way of illustration, an expression of the form

$$P_r = a'\left[1-\frac{n}{N}\right]\left[\exp b\left(1-\frac{T}{T_c}\right)\right] \exp(-\epsilon'/kT)$$

where T_c is the peak transition temperature, and n/N is the fraction of lattice sites occupied by diluent molecules could represent the way co-operative fluctuations would vary for rotators in

* Some illustrative examples are discussed by UBBELOHDE A. R., *Trans. Faraday Soc.* **33,** 1198 (1937); **23,** 128 (1957).

crystals. More experiments on the role of diluents in affecting relaxation times, and on the precise temperature dependence of relaxation, could throw important light on how far rotational "flips" are at all co-operative.

Professor TIMMERMANS in his introductory remarks suggested that above the clearing point of liquid crystals the molecules in liquids are rotating freely. However, considerations about volume occupancy suggest that this is highly unlikely in any liquids when the molecular shape departs significantly from the spherical. Clusters of more or less parallelized molecules must be present, though their extent and degree of order is insufficient to lead to optical anisotropy for light of visible wave lengths. Presumably in such liquids molecular rotation is likewise frequently "synchronous". This can lead to highly anomalous entropies of activation S_η in reaction rate expressions such as those for the viscosity of the liquids:

$$\eta = \frac{hN}{V} \exp\left(-\frac{S_\eta}{R}\right) \exp\left(\frac{E_\eta}{RT}\right)$$

(cf. ANDREWS and UBBELOHDE A. R., *Proc. Roy. Soc.* **228A,** 435 (1954)).

MECHANICAL PROBLEMS

A third group of problems refers to the mechanical properties of crystals in which molecules are considered to undergo "rotation". It seems likely that the plastic property of many such crystals, referred to by Professor TIMMERMANS, must be associated with a comparatively large concentration of crystal defects, such as lattice vacancies. At a guess, marked plasticity would be expected for concentrations of vacancies of the order 0·1 to 1 per cent. If these vacancies are really present in thermal equilibrium in the crystals, the addition of diluents in solid solution, though it might reduce rotational barriers, could actually increase resistance to plastic flow by making it harder for vacancies to move along many lattice sites. It would be most interesting to determine whether such effects of diluents are at all prominent.

Vol.
19

J. Phys. Chem. Solids Pergamon Press 1961. Vol. 18, Nos. 2/3, pp. 93–115. Printed in Great Britain.

DIE EINMÜNDUNG IN DIE FERROMAGNETISCHE SÄTTIGUNG—II

THEORIE DES EINMÜNDUNGSGESETZES IN PLASTISCH VERFORMTEN KUBISCH-FLÄCHENZENTRIERTEN EINKRISTALLEN

H. KRONMÜLLER und A. SEEGER

Max-Planck-Institut für Metallforschung, Stuttgart, und Institut für theoretische und angewandte Physik der Technischen Hochschule Stuttgart

(*Received* 31 *December* 1959; *revised* 24 *June* 1960)

Zusammenfassung — Die vorliegende Arbeit befasst sich mit der quantitativen theoretischen Interpretation neuerer Messungen über die Einmündung in die ferromagnetische Sättigung in plastisch gedehnten Nickel- und Nickel-Kobalt-Einkristallen. Mit Hilfe der im Teil I dieser Arbeit entwickelten allgemeinen Theorie führen wir den Vergleich zwischen Experiment und Theorie für das an anderer Stelle für den Verfestigungsbereich II angegebene Versetzungsmodell durch. Ohne Anpassung von Parametern ergibt sich vorzügliche Übereinstimmung sowohl hinsichtlich des Absolutwerts der differentiellen Suszeptibilität als auch hinsichtlich ihrer Abhängigkeit von der Fliessspannung, der Messtemperatur und der magnetischen Feldstärke. In Einzelheiten wird gezeigt, dass in die magnetischen Messungen besonders empfindlich die Versetzungsanordnung innerhalb aufgestauter Versetzungsgruppen und das elastische Fernfeld zwischen Versetzungsgruppen entgegengesetzten Vorzeichens eingehen. Wir besprechen ferner eine Reihe von Verfeinerungen der Verfestigungstheorie, die jedoch das Endresultat nur wenig beeinflussen. Die vorliegenden Ergebnisse zeigen, dass die Suszeptibilitätsmessungen ein quantitatives Hilfsmittel für die Erforschung der Versetzungsanordnung in Ferromagnetika darstellen. In den hier untersuchten Fällen entscheiden diese Messungen zwischen den Theorien der Verfestigung durch den sog. Verfestigungswald oder durch weitreichende Spannungsfelder eindeutig zu Gunsten der letzteren.

Abstract—The present paper is concerned with the quantitative theoretical interpretation of recent measurements of the approach to ferromagnetic saturation in nickel and nickel–cobalt alloy single crystals deformed in tension. Employing the general theory given in part I of this work, the comparison between experiment and theory is based on the dislocation model that was developed elsewhere for the work-hardening in stage II of the stress-strain curve of f.c.c. single crystals. Without adjusting parameters, very good agreement with respect to the absolute magnitude of the differential susceptibility as well as to its dependence on flow-stress, temperature, and magnetic field is obtained. As is discussed in some detail, the magnetic measurements are particularly sensitive to the dislocation arrangement within the piled-up groups and to the long-range stress fields between piled-up groups of opposite sign. We also discuss a number of refinements in the theory of work-hardening, which, however, have little effect on the final result. The present results demonstrate that susceptibility measurements provide a quantitative tool for the study of dislocation distributions in ferromagnetic materials. In the particular cases studied, they decide the controversy between "forest" theories of work-hardening and the "long range stress field" theory definitely in favour of the latter.

1. EINLEITUNG UND ÜBERBLICK

Wie aus zahlreichen experimentellen Arbeiten bekannt ist,[1–6] nimmt die differentielle Suszeptibilität χ von Ferromagnetika im Gebiet der Einmündung in die Sättigungsmagnetisierung, also bei grossen Feldstärken H, mit der plastischen

Verformung des Materials stark zu. Übersichtliche Verhältnisse, die eine Korrelation mit den derzeitigen Vorstellungen über den Mechanismus der plastischen Verformung und Verfestigung von Kristallen gestatten, wurden jedoch erst gefunden, als Einkristalle untersucht wurden.[4,6] Messungen der Temperaturabhängigkeit der differentiellen Suszeptibilität von Nickeleinkristallen bewiesen,[6] dass, wie schon von BROWN[7,8] angenommen, die Erhöhung von χ durch plastische Verformung von der magnetischen Wirkung innerer Spannungen (also von Versetzungen) herrührt. Zur feineren Analyse der Versuchsergebnisse erwies es sich als zweckmässig, nicht wie frühere Autoren von der H-Abhängigkeit der differentiellen Suszeptibilität auszugehen, sondern von deren Variation mit der Fliessspannung τ des verformten Einkristalls. Es ergab sich vorzügliche Übereinstimmung mit der von der Stuttgarter Schule entwickelten und vertretenen Theorie der Verfestigung kubisch-flächenzentrierter Einkristalle.[9,6] Dies gilt sowohl für Ni-Einkristalle als auch für Einkristalle einer Legierung von 80 Prozent Ni und 20 Prozent Co, die eine besonders niedrige Kristallenergie besitzt und deswegen die Messung des Einmündungsgesetzes bis herab zu verhältnismässig kleinen Feldstärken gestattet.

Der Einmündungsbereich zeichnet sich vor allen Magnetisierungsvorgängen dadurch aus, dass in ihm *keine Bewegungen von Bloch-Wänden* stattfinden. Bei der theoretischen Deutung tritt die in der Theorie der Magnetisierungskurve sonst so störende ungenügende Kenntnis der Zahl, Art und Anordnung der Blochwände nicht auf. Unbekannt ist lediglich die *Verteilung der inneren Spannungen*. Man kann daher die Einmündungsmessungen dazu benützen, nähere Informationen über die Zahl und Anordnung der Quellen dieser inneren Spannungen, also der Versetzungen, abzuleiten. Wie die vorliegende Mitteilung zeigen wird, kann man auf diese Weise in der Tat eine Reihe von Fragen, über die in einem Teil der neueren Literatur Unklarheiten bestehen, einfach und überzeugend beantworten.

Im Teil I dieser Arbeit wurde gezeigt,[10] dass es durch eine Erweiterung und Weiterführung der von BROWN[8] benützten Rechenmethode möglich ist, die differentielle Suszeptibilität explizit in der Versetzungsverteilung (und natürlich Materialkonstanten wie den magnetostriktiven und elastischen Konstanten) auszudrücken.* In die Lösung geht dabei die Fourierzerlegung der räumlichen Versetzungsverteilung ein. Wie wir sogleich anschaulich erläutern werden, sind für die differentielle Suszeptibilität nicht alle Fourierkomponenten gleich wichtig. Den Hauptbeitrag liefern Versetzungen, die etwa im Abstand der sog. Austauschlänge $\kappa^{-1} = (C/HI_s)^{1/2}$ voneinander liegen (C = Konstante der Austauschenergie, siehe Teil I; I_s = Sättigungsmagnetisierung). Bei Nickel beträgt für $H = 2000$ Oe die Austauschlänge $\kappa^{-1} = 130$ Å; sie liegt also in jenem Bereich, der für die Versetzunganordnung in kaltverformten kubisch-flächenzentrierten Metallen wesentlich ist.

Die vorstehenden Bemerkungen über die Wechselbeziehungen zwischen *Austauschkopplung* und *Versetzungsanordnung* werden in Abschnitt 2 anschaulich erläutert werden. In Abschnitt 3 erinnern wir kurz an die Grundbegriffe der Theorie der Verfestigung,[15] soweit wir sie für das Verständnis der magnetischen Erscheinungen benötigen. Für letztere spielen vor allem die während der Verformung gebildeten aufgestauten Versetzungsgruppen eine wichtige Rolle. Dementsprechend behandeln wir in Abschnitt 4 ausführlich deren Spannungsfelder. Zusammen mit einigen weiteren Verfeinerungen der in Abschnitt 3 skizzierten einfachen Theorie führt dies in Abschnitt 5 auf eine verbesserte Berechnung des Verfestigungsanstiegs. Wir können einerseits auf diese Weise angeben, welche Versetzungsverteilung in unserem Modell bei gegebener Fliessspannung vorliegt. Andererseits ist damit auf Grund der in I entwickelten Theorie die differentielle Suszeptibilität festgelegt. Durch den Vergleich der berechneten Suszeptibilität (Abschnitt 6) mit den gemessenen Werten (Abschnitt 7) ist eine *Prüfung des zugrundegelegten Versetzungsmodells* möglich. Man bekommt eine gute Übereinstimmung mit unserem Modell. Eine nähere Diskussion (Abschnitt 8) zeigt, dass Verfestigungsmodelle von der Art der von BASINSKI[16] und HIRSCH[17] vorgeschlagenen weder in der Grössenordnung noch in Einzelheiten Übereinstimmung mit dem Experiment ergeben würden.

* Es handelt sich hier um eine Fragestellung aus dem Problemkreis des sog. *Mikromagnetismus* (BROWN), dem neuerdings verstärktes Interesse entgegengebracht wird.[11,12,13,14]

2. AUSTAUSCHKOPPLUNG UND VERSETZUNGSANORDNUNG

In diesem Abschnitt wollen wir anschaulich zeigen, wie die Spinverteilung im Einmündungsbereich von der Versetzungsanordnung abhängt und wie insbesondere die starke Wirkung von Versetzungsgruppen zustande kommt. Die Austauschkopplung zwischen benachbarten Elektronenspins versucht, starke räumliche Gradienten der Magnetisierungsrichtung nach Möglichkeit zu vermeiden und lokale Störungen in der Magnetisierungsrichtung, etwa durch Inhomogenitäten oder magnetostriktive Effekte, zu glätten.

Fassen wir zunächst eine flächenhafte Spannungsquelle in der Ebene $x = 0$ ins Auge, so wird die Magnetisierungsrichtung um einen Richtungskosinus

$$\gamma(x) = A \exp(-\kappa x) \tag{2.1}$$

gegenüber dem von den Spannungen unbeeinflussten Bereich ausgelenkt.* Es ist hierbei

$$\kappa = (HI_s/C)^{1/2} \tag{2.2}$$

Spannungsquellen innerhalb der Austauschlänge κ^{-1}, so besteht zwischen diesen eine magnetische Wechselwirkung. Die Magnetisierungsrichtung kann den einzelnen Spannungsquellen nicht mehr vollständig folgen und

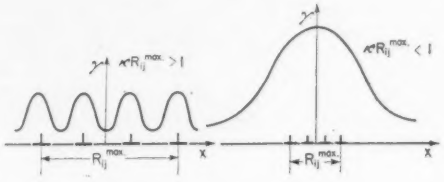

(a) (b)

ABB. 1(a). Schematische Darstellung des Einflusses weit auseinanderliegender Versetzungen auf die Magnetisierungsrichtung.

(b). Schematische Darstellung des Einflusses aufgestauter Versetzungen auf die Magnetisierungsrichtung.

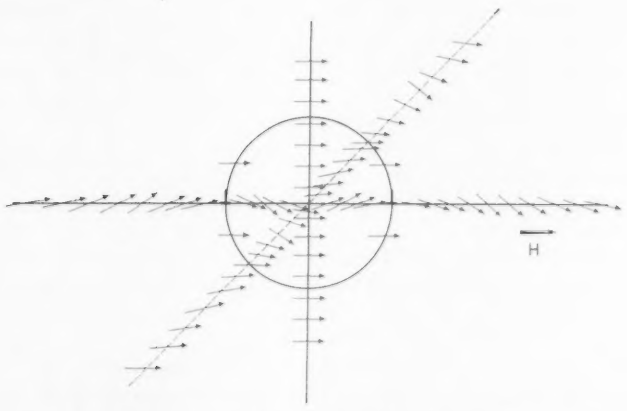

ABB. 1(c). Qualitativer Verlauf der Magnetisierung in der Nähe zweier Versetzungen. Dabei wurde $\kappa R_{ij} = 2$ gewählt und die Auslenkung aus der Feldrichtung etwa um den Faktor 5 vergrössert.

mit den schon in Abschnitt 1 erläuterten Bedeutungen der Konstanten. A ist eine durch die Stärke der Spannungsquelle festzulegende Integrationskonstante. Die Austauschlänge κ^{-1} ist dadurch charakterisiert, dass in der Entfernung κ^{-1} von der Spannungsquelle die Störung der Magnetisierungsrichtung auf das e^{-1}-fache abgefallen ist. Eine lokale Störung der Magnetisierungsrichtung wird also durch die Wirkung der Austauschkopplung in den Kristall hineingetragen. Liegen mehrere verhält sich im Grenzfalle so, als ob nur eine Spannungsquelle mit entsprechend grösserer Stärke vorhanden wäre. Wenn die gegenseitigen Abstände der Spannungsquellen grösser als κ^{-1} sind, so reicht das Auflösungsvermögen der Magnetisierung aus, um jede einzelne Spannungsquelle anzuzeigen. In Bild 1(a) und 1(b) ist am Beispiel von Versetzungen dieser Zusammenhang zwischen Abstand und Austauschlänge κ^{-1} schematisch dargestellt. Wie bereits ausgeführt, beträgt bei Ni κ^{-1} bei 2000 Oe etwa 130 Å. Von derselben Grössenordnung sind die mittleren Abstände der Versetzungen in plastisch verformten Einkristallen. Demnach ist zu erwarten, dass χ in starkem Masse von der Versetzungsanordnung abhängt und dass Messungen von χ experimentelle

* Gl. (2.1) gilt, wenn innere Streufelder vernachlässigt werden dürfen. In der ausführlichen Rechnung in Abschnitt 6 ist der Beitrag der inneren Streufelder voll berücksichtigt.

Aussagen hierüber gestatten. Insbesondere sollten die Suszeptibilitätsmessungen im Einmündungsgebiet eine Klärung der Frage gestatten, inwieweit im Innern eines plastisch verformten Einkristalls ein elastisches Fernfeld entsprechend Fig. 1(b) vorhanden ist, oder ob die Versetzungsstruktur eher einem Versetzungsnetzwerk entspricht, bei dem keine wesentliche Abweichungen von der statistischen Verteilung der Versetzungen in Form von Versetzungsgruppen auftreten. In Bild 1(c) wird am Beispiel zweier Stufenversetzungen der Einfluss elastischer Spannnugen, welche von Versetzungen herrühren, auf die Magnetisierungsrichtung qualitativ dargestellt.

3. VERFESTIGUNG UND VERSETZUNGSANORDNUNG KUBISCH-FLÄCHENZENTRIERTER KRISTALLE

In der Theorie der Verfestigung kubisch-flächenzentrierter Metalle pflegt man drei Verfestigungsbereiche I, II und III zu unterscheiden.[9] Wir befassen uns hier in erster Linie mit dem sog. Bereich II, in welchem der Verfestigungsanstieg $\theta_{II} = d\tau/da$ (τ = Fliessspannung, a = Abgleitung) den grössten Wert besitzt. Die Gründe hierfür sind, dass der Bereich II für das Verfestigungsverhalten der kubisch-flächenzentrierten Metalle am charakteristischsten ist, dass eine experimentell gut bestätigte Theorie der Verfestigung in diesem Bereich vorliegt,[9,15] und dass man die wesentlichsten Züge der Versetzungsanordnung in diesem Bereiche kennt.[9,18,19] Letzteres ist die Voraussetzung für die Berechnung der differentiellen Suszeptibilität χ im Einmündungsgebiet an Hand der in Teil I der vorliegenden Arbeit entwickelten Theorie. Während diese Berechnung von Unsicherheiten gänzlich frei ist, gehen in die Berechnung der Fliessspannung gewisse Mittelbildungen über das Schubspannungsfeld im Kristallinnern ein, deren genaue Form sich deduktiv schwer begründen lässt.* Es ist deshalb sehr willkommen, dass die Einmündungsmessungen eine strengere quantitative Prüfung der theoretischen Vorstellungen zulassen, als dies bisher möglich war. Wir wollen im vorliegenden Abschnitt zunächst kurz an die groben Züge des Verfestigungsmodells erinnern und die durch die verbesserten Prüfungsmöglichkeiten nahegelegten Verfeinerungen bis zu Abschnitt 5 zurückstellen.

Die Fliessspannung τ bei einer gegebenen Abgleitung setzt sich gemäss

$$\tau = \tau_S + \tau_G \tag{3.1}$$

aus einem von thermisch aktivierten Prozessen herrührenden (τ_S-) und einem athermischen (τ_G-) Anteil zusammen. In den uns interessierenden Fällen rührt τ_S vom sog. Versetzungswald her, d. h. von jenen Versetzungen, die die Gleitebene durchstossen. Zur Ermittlung des τ_S-Anteils sind Messungen der Temperaturabhängigkeit der Fliessspannung in Verbindung mit einer quantitativen Theorie erforderlich. Solche Messungen liegen zwar an Cu vor,[20,15,21] nicht aber an Nickel oder Nickel-Legierungen, doch dürften sich die Verhältnisse bei Nickel nicht wesentlich von denen bei Kupfer unterscheiden. Bei der Ableitung von τ_S aus den Messungen[20,15] waren allerdings, wie wir heute wissen,[22] die Bildungsenergien der Sprünge zu gross angesetzt worden, so dass der ermittelte Wert von τ_S zu gross war. Gemäss

$$\tau_G = \tau_G^{(w)} + \tau_G^{(i)} \tag{3.2}$$

setzt sich τ_G, das im Bereich II der Verfestigungskurve gross gegen τ_S ist, zusammen aus dem inneren Spannungsfeld $\tau_G^{(i)}$ der in der Gleitebene liegenden Versetzungen und einem Beitrag $\tau_G^{(w)}$, der von den weitreichenden elastischen Spannungen der Waldversetzungen herrührt und auf den besonders HIRSCH[17] und Mitarbeiter[23] hingewiesen haben. Eine Berechnung von $\tau_G^{(w)}$ durch SAADA[24] ergibt zusammen mit eigenen Abschätzungen, dass $\tau_G^{(i)}$ bei nicht zu hohen Temperaturen von der Grössenordnung von τ_S ist, und dass $\tau_S + \tau_G^{(w)}$ etwa den ursprünglich für τ_S allein angegebenen Wert[15] hat. Da, wie wir in Abschnitt 8 genauer besprechen werden, der Versetzungswald praktisch nichts zur magnetischen Suszeptibilität beiträgt, interessiert uns beim Vergleich von Theorie und Messungen das Verhältnis $\tau_G^{(i)}/\tau$. Dieses Verhältnis liegt nahe bei Eins, so dass wir es nach dem eben Gesagten ohne ernsten Fehler durch das früher[15] für Kupfer berechnete τ_G/τ-Verhältnis ersetzen und das Resultat auch auf Nickel anwenden können. Die im Rest der Arbeit angegebenen $\tau_G^{(i)}$-Werte sind auf diese Weise erhalten worden.

* Dies hängt damit zusammen, dass die zur „Ausmessung" der inneren Spannungen verwendeten „Probekörper" selbst wieder Versetzungen sind, und dass diese sich über Entfernungen bewegen, die vergleichbar mit oder grösser als die Wellenlänge der inneren Spannungen sind.

Die physikalische Bedeutung von $\tau_G^{(i)}$ ist folgende : Im Bereich II schreitet die Gleitung durch fortwährende Neubildung von Gleitlinien fort,[25] und zwar wohl durch Betätigung von Frank–Read-Quellen. Dabei muss die angelegte Spannung gross genug sein, um der Quellenversetzung bei ihrem ersten Umlauf die Überwindung der Gegenspannungen (im verformten Kristall sind dies vor allem die zu $\tau_G^{(i)}$ beitragenden), zu ermöglichen. Die kleinsten Werte nehmen diese Spannungen auf Gleitebenen an, die gerade in der Mitte zwischen zwei aufgestauten Versetzungsgruppen hindurchlaufen. Da das bei diesem ersten Umlauf überstrichene Gebiet einen Radius von der Grössenordnung der Wellenlänge der inneren Spannungen besitzt, ist die Bedingung für die Betätigung neuer Frank–Read-Quellen diejenige, dass $\tau^{(i)}$ gleich dem Maximum der Schubspannungen in dieser Gleitebene ist. Die Verhältnisse sind an anderer Stelle[9] an Hand von Beispielen für den unverformten Kristall diskutiert worden. Sie lassen sich auf den Bereich II übertragen, wenn man die im verformten Kristall vorhandenen Gruppen von n Versetzungen durch Überversetzungen des Burgersvektors nb ersetzt. Fassen wir beispielsweise die Bewegung von Schraubenversetzungen ins Auge und bezeichnen mit N' die Flächendichte der Versetzungsgruppen, so ergibt sich (G = Schubmodul, b = Betrag des Burgersvektors der einzelnen Versetzung)

$$\tau_G^{(i)} = \frac{\alpha}{2\pi} Gnb(N')^{1/2}, \tag{3.3}$$

wo α ein geometrischer Faktor der Grössenordnung 1 ist.

Die für die Berechnung des Verfestigungsanstiegs erforderliche Kenntnis der mit einer Vergrösserung von N' bzw. $\tau_G^{(i)}$ verbundenen Abgleitung kann man auf zwei Wegen bekommen. Man findet experimentell, dass sich der Zusammenhang zwischen Gleitlinienlänge L und Abgleitung a mit Hilfe zweier Konstanten Λ und a^* in der Form[25]

$$L = \frac{\Lambda}{a - a^*} \tag{3.4}$$

darstellen lässt. Identifiziert man L mit dem Laufweg der Versetzungen, so kann man die von den Versetzungen überstrichene Fläche und damit die Abgleitung berechnen. Man erhält auf diese Weise gute Übereinstimmung mit dem gemessenen Wert θ_{II}. — Der andere Weg besteht darin, die Rückspannung einer aufgestauten Versetzungsquelle zu berechnen und der experimentellen Tatsache Rechnung zu tragen, dass der verformte Zustand beim Entlasten „gerade noch" stabil ist. Man kann diese Bedingung so formulieren, dass die Rückspannung einer Gruppe am Ort ihrer Quelle gegenüber $\tau_G^{(i)}$ um einen Faktor β reduziert ist, wobei $\beta \approx 1/2$. Auch dieses Vorgehen liefert das lineare Verfestigungsgesetz im Bereich II und den richtigen Wert für θ_{II}.

In der vorstehenden Diskussion haben wir angenommen, dass wir die im Bereich II vorhandenen Gruppen von n Versetzungen als eine Versetzung n-facher Stärke behandeln können. Wie die Ausführungen von Abschnitt 2 zeigen, ist diese Näherung für die magnetischen Untersuchungen unzureichend. Wir werden vielmehr in Abschnitt 6 die Verteilungsfunktion der Versetzungen innerhalb einer Gruppe berücksichtigen. Dabei zeigt es sich, dass man gute Übereinstimmung mit den Experimenten bekommt, wenn man folgendes Modell zugrunde legt : Die Versetzungsanordnung im belasteten und entlasteten Zustand ist im wesentlichen gleich, nämlich diejenige einer Gruppe von n Versetzungen, die durch die Spannung $\beta\tau_G^{(i)}$ gegen ein Hindernis angepresst sind. Durch den oben eingeführten Faktor β wird in pauschaler Weise einerseits die verfestigende Wirkung der Spannungsfelder der Versetzungsgruppen berücksichtigt und andererseits die Stabilität der Gruppe als Ganzes beim Entlasten sichergestellt. Dank der eben erwähnten Stabilität ist zur Fixierung der einzelnen Versetzungen innerhalb der Gruppe kein sehr starker Mechanismus erforderlich. Es ist z.B. denkbar, dass diese Fixierung durch die von HIRSCH[17] und WHELAN[23] diskutierte Wechselwirkung einer Versetzungsgruppe mit einer schräg dazu verlaufenden Versetzung zustande kommt.

Die Berücksichtigung der Versetzungsanordnung n einer Gruppe beeinflusst auch etwas die Berechnung des Schubspannungsfeldes (Abschnitt 4) und der Abgleitung (Abschnitt 5). In Abschnitt 5, der der verfeinerten Berechnung des Verfestigungsanstiegs gewidmet ist, berücksichtigen wir ferner, dass die Versetzungen in der Gleitebene in der Form geschlossener Ringe liegen, die wir

durch Sechsecke approximieren. Grössen, die sich auf Versetzungen verschiedenen Charakters beziehen, unterscheiden wir durch Indizes. Wir schreiben z. B. in leicht verständlicher Weise in Gl. (3.4) L_1 und Λ_1 für Stufenversetzungen und L_2 und Λ_2 für Schraubenversetzungen. Ferner berücksichtigen wir die elastische Anisotropie durch Einführung anisotroper elastischer Koeffizienten und schliesslich die Streuung in den auftretenden Gleitlinien- und Aufstaulängen durch geeignete Mittelungen. Die Auswirkungen aller dieser Verfeinerungen sind jedoch gering, da sie sich gegenseitig fast vollständig kompensieren. Aus diesem Grunde werden wir sie nur bei der Auswertung der Messungen an reinem Nickel berücksichtigen und bei den Nickel–Kobalt-Legierungen mit dem ursprünglichen Modell[15] (Rechteckringe aus Stufen- und Schraubenversetzungen) begnügen.

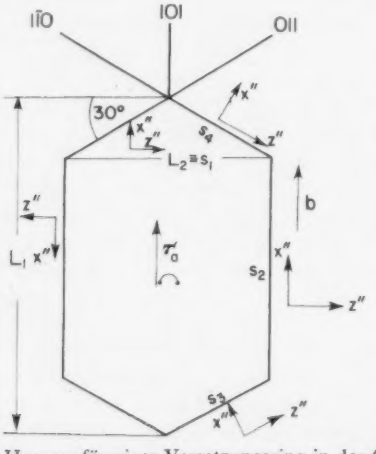

ABB. 2. Hexagonförmiger Versetzungsring in der (111)-Ebene mit den im Text verwendeten Bezeichnungen.

4. DAS SPANNUNGSFELD AUFGESTAUTER VERSETZUNGEN

Wie in Abschnitt 3 ausgeführt wurde, benötigen wir für das von uns gewählte Versetzungsmodell des verformten Zustands flächenzentrierter Kristalle (Abb. 2) die Kenntnis des Schubspannungsfeldes aufgestauter Versetzungsgruppen in einiger Entfernung von der Gruppe. Es ist für diesen Zweck ausreichend, nach LEIBFRIED[26] die Versetzungsverteilung in der Gruppe durch eine Dichtefunktion $D(x)$ zu beschreiben. Wir nehmen dabei an, dass sich die Versetzungen in z-Richtung erstrecken und als unendlich lang angesehen werden können.

Ist eine Gruppe von n Versetzungen, wie in Abb. 3 angegeben, über eine Länge $2a^{(m)}$ verteilt und durch eine wirksame Schubspannung τ_a gegen ein Hindernis angepresst, so gilt:

$$D(x) = \frac{n}{\pi a^{(m)}} \left(\frac{a^{(m)} - x}{a^{(m)} + x} \right)^{1/2} . \qquad (4.1)$$

$a^{(m)}$ bedeutet die halbe Aufstaulänge der Versetzungsgruppen. Dabei bezieht sich $m = 1$ auf 90°-Versetzungen (Stufenversetzungen), $m = 2$ auf 0°-Versetzungen (Schraubenversetzungen) und $m = 3$ auf 60°-Versetzungen. Wenn wir die elastische Anisotropie berücksichtigen und die von SEEGER und SCHÖCK[27]

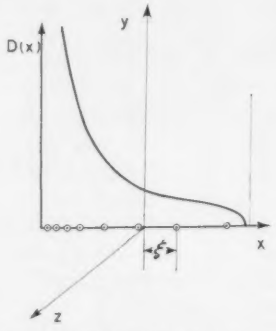

ABB. 3. Verlauf der Dichte $D(x)$ bei einer aufgestauten Versetzungsgruppe.

berechneten anisotropen elastischen Konstanten einführen, so gilt für Versetzungen, die sich in ⟨110⟩-Richtung erstrecken:

$$a^{(1),(2)} = \frac{nb}{2\pi\tau_a K_2^{(1),(2)}} \qquad (4.2a)$$

$$a^{(3)} = \frac{nb}{8\pi\tau_a K_2^{(1)}} \left(3 + \frac{K_2^{(1)}}{K_2^{(2)}} \right) . \qquad (4.2b)$$

τ_a ist nicht gleich der von aussen angelegten Schubspannung τ, sondern wie in Abschnitt 3 ausgeführt, gleich $\beta\tau_G^{(i)}$. Da wir uns in Abschnitt 4 bis 7 nur noch mit $\tau_G^{(i)}$ befassen werden, unterdrücken wir im folgenden den Index i. β ist ein geometrischer Faktor, der vom Anordnungsmuster der Gruppen abhängt und in pauschaler Weise die Abschirmung des äusseren Spannungsfeldes durch umliegende Versetzungsgruppen berücksichtigt. Aus Messungen des Bauschingereffektes folgt,[9] dass β von der Grössenordnung 1/2 ist.

Die Spannungskomponenten $\tau_{ik}^{v,m}$ der in Abb. 3 beschriebenen Versetzungsgruppe berechnen sich aus

$$\tau_{ik}^{v,m} = \int_{-a^{(m)}}^{a^{(m)}} \tau_i^{(m)}(x-\xi, y) D(\xi)\, d\xi . \qquad (4.3)$$

Hierbei bedeutet $\tau_{ik}^{(m)}$ die Spannungskomponente einer einzelnen Versetzung. Wir beschränken uns hier auf die Angabe der Schubspannung im Gleitsystem, die ja für die Fliessspannung massgebend ist. Durch Einsetzen von Gl. (4.1) in Gl. (4.3) findet man :

1. 0°-Versetzung :

$$\tau_G^{(2)} = \tau_{zy}^{v,(2)} = \tau_a - \frac{(x-a^{(2)})\delta_2 + y\delta_1}{\rho^2}\tau_a \tag{4.4}$$

2. 90°-Versetzung :

$$\tau_G^{(1)} = \tau_{xy}^{v,(1)} = \tau_a\Big[1 - \frac{(x-a^{(1)})\delta_2+3y\delta_1}{\rho^2} + \frac{2y^2}{\rho^6 xy}\Big\{((a^{(m)})^2+x^2+y^2)\times$$

$$\times[\delta_1\{\tfrac{1}{4}\rho^2(a^{(1)}-x)+xy^2\}-\delta_2 y\{x(a^{(1)}-x)+\tfrac{1}{4}\rho^2\}] - \frac{\rho^4}{4}[\delta_1(a^{(1)}-3x)+y\delta_2]\Big\}\Big] \tag{4.5}$$

wobei :

$$\delta_{1,2} = [\tfrac{1}{2}\rho^2 \pm \tfrac{1}{2}((a^{(m)})^2-x^2+y^2)]^{1/2}$$

$$\rho^2 = [\{(a^{(m)})^2-x^2+y^2\}^2+4x^2y^2]^{1/2}$$

3. 60°-Versetzung :

$$\tau_G^{(3)} = \tfrac{3}{4}\tau_G^{(1)} - \tfrac{1}{4}\tau_G^{(2)} \tag{4.6}$$

Wie in Abschnitt 3 beschrieben, benötigen wir für die Berechnung der Verfestigung die maximale Schubspannung $\tau_G^{\max}$ bei festem y. Sie ergibt sich aus der Extremalbedingung :

$$\frac{\partial}{\partial x}(\tau_G^{(m)})_{y=\text{const.}} = 0\,; \quad m = 1,2,3. \tag{4.7}$$

Der in Gl. (3.3) eingeführte geometrische Faktor $\alpha^{(m)}$ kann aus dieser Bedingung für die drei verschiedenen Versetzungstypen berechnet werden. Ist $(\tau_G^m)_{\max}$ die maximale Schubspannung des entsprechenden Versetzungstyps mit dem Burgersvektor nb, so gilt :

$$\alpha^{(m)} = \frac{(\tau_G^{v,m})_{\max}}{(\tau_G^m)_{\max}}\,. \tag{4.8}$$

Die nach Gl. (4.7) berechneten Kurven maximaler Schubspannung sind in Bild 4 dargestellt. Die Faktoren $\alpha^{(m)}$ sind in Bild 5 als Funktion von $y/a^{(m)}$ angegeben. Bei der Berechnung von $\alpha^{(3)}$ wurden für $K_2^{(1)}$ und $K_2^{(2)}$ die für Ni ermittelten Werte[15] verwendet. $\alpha^{(1)}$ und $\alpha^{(2)}$ sind unabhängig von $K_2^{(1)}$ und $K_2^{(2)}$. Aus Bild 5 ist ersichtlich, dass für $y/a^{(m)} > 0{,}5$ die Schubspannung $(\tau_G^{v,m})_{\max}$ mehr als 80 Prozent der einer Versetzung vom Burgersvektor nb beträgt. Demnach ist die in Abschnitt 3 bei der Berechnung des Verfestigungsanstiegs besprochene Näherung durchaus berechtigt.

Zum Schluss dieses Paragraphen wollen wir auf den engen Zusammenhang zwischen den Grössen α und β hinweisen. Für den mittleren Abstand zwischen gleichnamigen Versetzungsgruppen gilt :

$$R_0' = \frac{1}{\sqrt{(N_0 L_{1,2})}} = \frac{\alpha^{(2),(3)}}{2\pi\tau_G K_2^{(2),(1)}}\,. \tag{4.9}$$

Bei einem quadratischen Anordnungsmuster der Versetzungsgruppen gilt : $R'_0 = y\sqrt{(2)}$. Setzen wir in Gl. (4.2) für τ_a den Wert $\beta \cdot \tau_G$ ein, so erhalten wir durch Division mit Gl. (4.9) :

$$\alpha^{(m)}(z^{(m)}) \cdot \beta = \sqrt{(2)} \cdot z^{(m)}, \tag{4.10}$$

wobei $z^{(m)} = y/a^{(m)}$ gesetzt wurde.

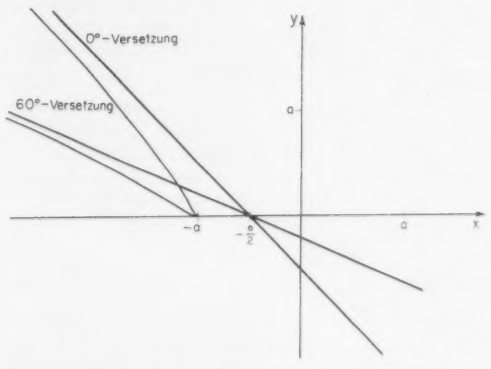

ABB. 4. Vergleich zwischen den Kurven maximaler Spannung einer aufgestauten Versetzungsgruppe (gekrümmte Kurven) und denen einer einzelnen Versetzung vom Burgersvektor nb im Punkte $x = -a/2$ (gerade Linien).

Gl. (4.10) entnimmt man, dass bei bekanntem β sowohl $\alpha^{(m)}$ als auch $y/a^{(m)}$ festgelegt sind. Für den oben begründeten Wert $\beta = 1/2$ finden wir :

$$\alpha^{(1)} = 0{,}91\,; \quad \alpha^{(2)} = 0{,}72;$$

$$\alpha^{(3)} = 0{,}85\,; \quad z^{(m)} = 0{,}3\text{–}0{,}4.$$

Vol. 18
1961

Diese Werte sollten sich für sämtliche kubisch-flächenzentrierten Metalle als gleich ergeben. Eine Prüfung dieser Gesetzmässigkeit ist durch direkte Messung des Verfestigungsanstiegs θ_{II} und der Gleitlinienlänge L_2 möglich. Wir werden diesen Vergleich im nächsten Abschnitt durchführen.

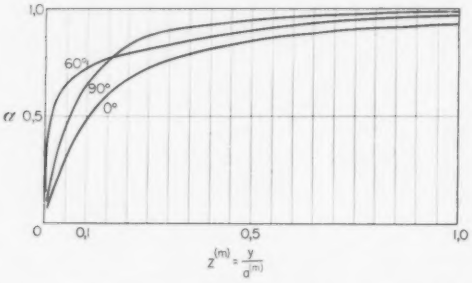

ABB. 5. Der geometrische Faktor $\alpha(y/a)$ für eine 0°-, 60°- und 90°-Versetzung.

5. VERFEINERTE BERECHNUNG DES VERFESTIGUNGSANSTIEGS

Zunächst wollen wir die von einer Versetzungsgruppe hervorgerufene Abgleitung berechnen. Dabei berücksichtigen wir, dass die Versetzungen Sechsecke bilden und eine endliche Aufstaulänge besitzen. Wir dürfen annehmen, dass die experimentell bestimmten Gleitlinienlängen etwa dem grössten der Versetzungsringe entsprechen. Seine Fläche beträgt :

$$F_{\max} = L_1 L_2 - L_2^2\sqrt{(3)}/6. \qquad (5.1)$$

Will man nun die endliche Aufstaulänge innerhalb der Versetzungsgruppen berücksichtigen, so hat man im 1. Glied von Gl. (5.1) L_2 durch $L_2 - a^{(1)}$ und im 2. Glied L_2^2 durch $L_2(L_2 + 4a^{(2)})$ zu ersetzen. Somit ergibt sich für die effektive Fläche :

$$F_{\text{eff}} = F_{\max} - a^{(1)}L_1 - 2\sqrt{(3)}L_2 a^{(2)}/3. \qquad (5.2)$$

Zwischen der differentiellen Abgleitung da und den bei dieser Abgleitung neu betätigten Quellen dN_0 besteht die Beziehung :

$$da = nbF_{\text{eff}}\, dN_0. \qquad (5.3)$$

Die Beziehung (5.3) muss noch dahingehend verfeinert werden, dass die Laufwege eine statistische Verteilung besitzen. Man kann sie wohl als eine Gaussverteilung um die experimentell bestimmbaren Mittelwerte L_1 und L_2 beschreiben. Es gilt dann für die Häufigkeitsverteilung $H(L)$ der Gleitlinienlängen :

$$H(L) = c \exp[-(\Delta L/h)^2], \qquad (5.4)$$

wobei $L = \bar{L}_{1,2} + \Delta L$ und c eine Normierungskonstante bedeutet.

$\bar{L}_1$ und $\bar{L}_2$ bedeuten die experimentell ermittelten Mittelwerte der Gleitlinienlängen L_1 und L_2.

Unseren experimentellen Verteilungskurven von L_2 bei Ni entnimmt man $h_2 = 0{,}4L_2$. Nehmen wir an, dass dieselbe Beziehung auch für L_1 gilt, so erhalten wir für die differentielle Abgleitung :

$$da = nbc \int_{-\infty}^{\infty} F_{\text{eff}} \exp[-(\Delta L/h)^2]\, d\Delta L$$

$$= \left(1 + \frac{h_2^2}{2\bar{L}_2^2}\right) nbF_{\text{eff}}\, dN_0\,. \qquad (5.5)$$

Für die nun folgende Berechnung des Verfestigungsanstiegs führen wir folgende Abkürzungen ein :

$$1 + h_2^2/2\bar{L}_2^2 = \alpha_L^2\,; \quad F_{\text{eff}} = F_0 \cdot \alpha_F^2, \qquad (5.6a)$$

wobei

$$F_0 = \bar{L}_1\bar{L}_2\,; \quad \alpha_F^2 = 1 - \frac{\bar{L}_2}{\bar{L}_1}\frac{\sqrt{(3)}}{6} - \frac{a^{(1)}}{\bar{L}_2} - \frac{2}{3}\sqrt{(3)}\frac{a^{(2)}}{\bar{L}_1}\,. \qquad (5.6b)$$

Die in α_L und α_F auftretenden unteren Indices weisen auf die Herkunft dieser Faktoren von der Längenverteilung und von der Ringform hin. Sowohl α_L als auch α_F ergeben sich im Bereich II als von der plastischen Verformung unabhängig. Aus den Beziehungen $da = nb(\alpha_L\alpha_F)^2\, dN_0$ und

$$\tau_G = \frac{\alpha^{(2),(3)} n}{2\pi K_2^{(2),(1)}} (N_0\bar{L}_{1,2})^{1/2} \qquad (5.7)$$

ergibt sich[15] der Verfestigungsanstieg

$$\theta_{II} = \frac{\alpha^{(2),(3)}}{2\pi K_2^{(2),(1)}\alpha_L\alpha_F}\left(\frac{nb}{3\Lambda_{1,2}}\right)^{1/2}. \qquad (5.8)$$

Zum Vergleich mit den Messungen setzen wir $\beta = 1/2$ und finden :

$$\text{Cu}: \alpha^{(2)} = 0{,}84\,; \quad \alpha^{(3)} = 0{,}89\,; \quad \frac{\Lambda_1}{\Lambda_2} = 3{,}2$$

$$\text{Ni}: \alpha^{(2)} = 0{,}80\,; \quad \alpha^{(3)} = 0{,}88\,; \quad \frac{\Lambda_1}{\Lambda_2} = 2{,}6.$$

Hierbei wurden folgende experimentell bestimmten Werte eingesetzt :

$$\text{Cu}: \theta_{II} = 13{,}5\ kp/\text{mm}^2,$$
$$n = 25,\ \Lambda_2 = 4\times 10^{-4}\text{cm}.$$
$$\text{Ni}: \theta_{II} = 23\ kp/\text{mm}^2,$$
$$n = 31,\ \Lambda_2 = 5{,}9\times 10^{-4}\text{cm}.$$

Vergleichen wir die auf diese Weise gefundenen Werte für $\alpha^{(3)}$ und $\alpha^{(2)}$ mit den oben von der Theorie geforderten Werten, so zeigt sich, dass im Falle von $\alpha^{(2)}$ die Abweichungen vom theoretischen Wert 10–15 Prozent betragen und im Falle von $\alpha^{(3)}$ nur 3–4 Prozent. Die Übereinstimmung zwischen Experiment und Theorie ist befriedigend. Sie könnte durch geringe Abänderungen der Annahmen über β und über die geometrische Anordnung der Versetzungsgruppen verbessert werden.

6. BERECHNUNG DER DIFFERENTIELLEN SUSZEPTIBILITÄT

Wir wollen nunmehr die in Teil I entwickelte allgemeine Methode auf die Berechnung der differentiellen Suszeptibilität $\chi(H)$ im Einmündungsbereich auf das in Abschnitte 3 und 5 beschriebene Versetzungsmodell anwenden. Wie in Teil I gezeigt wurde, ist zur Berechnung der differentiellen Suszeptibilität die Kenntnis der Grösse

$$\tilde{g}_\nu = \frac{1}{2C} \sum_{k,l} c^\nu_{kl} \tilde{\sigma}''_{kl} \tag{6.1}$$

erforderlich. Dabei bedeuten die $\tilde{\sigma}''_{kl}$ die Fouriertransformierten der elastischen Spannungen σ''_{kl} und die c^ν_{kl} Funktionen der magnetostriktiven Konstanten λ_{100} und λ_{111}. Die Koeffizienten c^ν_{kl} werden im Anhang A gemäss den in Teil I angegebenen Beziehungen für eine 0°-, eine 60°- und eine 90°-Versetzung berechnet. Da die 60°-Versetzung in eine 0°-Versetzung und eine 90°-Versetzung zerlegt werden kann, genügt es, die Fouriertransformierten der 0°- und 90°-Versetzung zu berechnen. Die Spannungen σ''_{kl} entnehmen wir einer Arbeit von DIETZE[28]. Das von ihm zur Berechnung der elastischen Spannungen zugrunde gelegte Modell ist in Abb. 6 dargestellt. In einem an der Oberfläche spannungsfreien Kreiszylinder vom Radius R_0 befindet sich im Abstande R_i vom Mittelpunkt eine der Zylinderachse parallele 0°- oder 90°-Versetzung, deren Gleitebene durch die Zylinderachse geht. Als Spezialfall $R_i \ll R_0$ ist darin auch die von BROWN[8] betrachtete Anordnung enthalten. Das oben beschriebene Modell ist im Einklang mit den wirklichen Verhältnissen, wenn wir den Radius

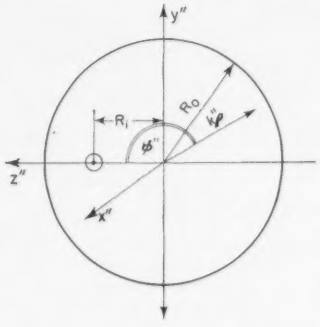

ABB. 6. Zur Definition von R_i und R_0 bei 0°-Versetzungen. Bei der 60°-Versetzung müssen in Fig. 6 z'' und $-x''$ vertauscht werden.

R_0 gleich dem mittleren halben Abstand der Versetzungsgruppen verschiedenen Vorzeichens wählen. Wir erreichen damit, dass unser Modell die Abschirmung des Spannungsfeldes einer Versetzungsgruppe durch die Gruppen in der Umgebung näherungsweise richtig wiedergibt. Die Berechnung der Fouriertransformierten liefert, falls sämtliche Glieder, die stärker als die Besselfunktion $J_0(kR_0)$ für $R_0 \to \infty$ gegen Null gehen, vernachlässigt werden* :

(a) Schraubenversetzung :

$$\begin{aligned}
\tilde{\sigma}''_{12} &= -\frac{2ib}{K_2^{(2)}(2\pi)^{3/2}} \frac{\sin \tfrac{1}{2}k''_x s_2}{k''_x k''_\rho} \cos\phi''[\exp(-i\mathfrak{k}'' \cdot \mathfrak{R}_i) - J_0(k''_\rho R_0)] \\
\tilde{\sigma}''_{13} &= \frac{2ib}{K_2^{(2)}(2\pi)^{3/2}} \frac{\sin \tfrac{1}{2}k''_x s_2}{k''_x k''_\rho} \sin\phi''[\exp(-i\mathfrak{k}'' \cdot \mathfrak{R}_i) - J_0(k''_\rho R_0)]
\end{aligned} \tag{6.2}$$

(b) 60°-Versetzung :

(i) Stufenanteil :

$$\tilde{\sigma}''_{11} = \mp \frac{ib_1}{K_2^{(1)}(2\pi)^{3/2}} \frac{\sin \tfrac{1}{2}k''_z s_{3,4}}{k''_z k''_\rho} (3\sin\phi'' - \sin 3\phi'')[\exp(-i\mathfrak{k}'' \cdot \mathfrak{R}_i) - J_0(k''_\rho R_0)]$$

$$\tilde{\sigma}''_{22} = \mp \frac{ib_1}{K_2^{(1)}(2\pi)^{3/2}} \frac{\sin \tfrac{1}{2}k''_z s_{3,4}}{k''_z k''_\rho} (\sin\phi'' + \sin 3\phi'')[\exp(-i\mathfrak{k}'' \cdot \mathfrak{R}_i) - J_0(k''_\rho R_0)]$$

* Es handelt sich hierbei um Glieder der Form $(R_i/R_0)^{2n} J_{2n}(kR_0)$, wobei $n \geqq 1$.

Vol. 18
1961

$$\tilde{\sigma}''_{33} = \mp \frac{ib_1}{K_2^{(1)}(2\pi)^{3/2}} \frac{\sin\frac{1}{2}k''_z s_{3,4}}{k''_z k''_\rho} 4 \sin\phi'' \left(1 - \frac{K_2^{(1)}}{K_2^{(2)}}\right)[\exp(-i\mathfrak{k}''\cdot\mathfrak{R}_l) - J_0(k''_\rho R_0)]$$

$$\tilde{\sigma}''_{12} = \mp \frac{ib_1}{K_2^{(1)}(2\pi)^{3/2}} \frac{\sin\frac{1}{2}k''_z s_{3,4}}{k''_z k''_\rho} (\cos\phi'' - \cos 3\phi'')[\exp(-i\mathfrak{k}''\cdot\mathfrak{R}_l) - J_0(k''_\rho R_0)] \tag{6.3}$$

(ii) Schraubenanteil:

$$\tilde{\sigma}''_{13} = -\frac{2ib_2}{K_2^{(2)}(2\pi)^{3/2}} \frac{\sin\frac{1}{2}k''_z s_{3,4}}{k''_z k''_\rho} \sin\phi''[\exp(-i\mathfrak{k}''\cdot\mathfrak{R}_l) - J_0(k''_\rho R_0)]$$

$$\tilde{\sigma}''_{23} = \frac{2ib_2}{K_2^{(2)}(2\pi)^{3/2}} \frac{\sin\frac{1}{2}k''_z s_{3,4}}{k''_z k''_\rho} \cos\phi''[\exp(-i\mathfrak{k}''\cdot\mathfrak{R}_l) - J_0(k''_\rho R_0)]. \tag{6.4}$$

Hierbei bezieht sich das obere Vorzeichen in Gl. (6.3) auf den Bogenteil s_3 und das untere auf den Bogenteil s_4. Wir verzichten auf die Angabe der Fouriertransformierten einer 90°-Versetzung, da diese sich aus Gl. (6.3) ergeben, indem b_1 durch b ersetzt wird. Ist a_0 die kubische Gitterkonstante, so gilt:

$$b = a_0/2\sqrt{(2)},\ b_1 = b\sqrt{(3)}/2,\ b_2 = b/2. \tag{6.5}$$

Ferner ist:

$$s_2 = L_1 - L_2\sqrt{(3)}/3,\ s_3 = s_4 = L_2\sqrt{(3)}/3 \tag{6.6}$$

Die Beziehungen (6.6) können aus Bild 2 anschaulich abgeleitet werden.

Für die weitere Berechnung müssen nach Gl. (2.15) von Teil I die Grössen $|\tilde{g}_x|^2$ und $|\tilde{g}_z|^2$, sowie der Ausdruck

$$A \equiv |\tilde{g}_x|^2 k_x^2 + |\tilde{g}_z|^2 k_z^2 + 2k_x k_z(\mathfrak{Re}\tilde{g}_x \cdot \mathfrak{Re}\tilde{g}_z + \mathfrak{Im}\tilde{g}_x \cdot \mathfrak{Im}\tilde{g}_z) \tag{6.7}$$

berechnet werden. Im Falle der 90°-Versetzung genügt es, $|\tilde{g}_x|^2$ und $|\tilde{}_z|^2$ zu kennen. Entsprechend unserem für die Berechnung des Verfestigungsanstiegs verwendeten Versetzungsmodell müssen die oben angegebenen. Grössen für die Linienteile s_2, s_3 und s_4 bestimmt werden. Eine Vereinfachung der Darstellung ergibt sich, wenn die Integration über k''_x bei der 0°-Versetzung bzw. die über k''_z bei der 60°-Versetzung zuerst ausgeführt wird. Das in den Fouriertransformierten Gl. (6.2–6.4) auftretende Glied

$$\frac{\sin\frac{1}{2}k''_{x,z}s_m}{k''_{x,z}}$$

lässt sich mit Hilfe der für $(\pi/s_m)^2 \ll \kappa^2$ anwendbaren Formel:

$$\int_{-\infty}^{\infty} \frac{\sin^2(\frac{1}{2}k''_{x,z}s_m)}{(k''_{x,z})^2} f(k''_{x,z})\, dk''_{x,z} = \tfrac{1}{2}\pi s_m f(0) \tag{6.8}$$

auswerten. (Integrale dieses Typs treten bei der Berechnung der differentiellen Suszeptibilität auf, wie man leicht an Hand der Beziehung Gl. (2.15) aus Teil I und den Fouriertransformierten Gl. (6.2–6.4) sieht. Für die bei uns auftretenden Gleitlinienlängen ist obige Ungleichung wie $10^6 \ll 10^{12}$ erfüllt). Wird die k''_x- bzw. die k''_z-Integration gemäss Gl. (6.8) ausgeführt, so sind in Gl. (2.15) von Teil I die Grössen $|\tilde{g}_{x,z}|^2$ und A durch folgende Ausdrücke zu ersetzen:

$$|\tilde{g}^m_{x,z}|^2 \equiv \frac{\epsilon_m b^2}{64C^2\pi^3 K_m^2 k''^2_\rho} B^m_{x,z}(\phi'') E(k''_\rho, R_{ij}) \tag{6.9a}$$

$$A^m \equiv \frac{\epsilon_m b^2}{64C^2\pi^3 K_m^2 k''^2_\rho} B^m_0(\phi'') E(k''_\rho, R_{ij}), \tag{6.9b}$$

wobei

$\epsilon_m = 1$ für $m = 1, 3, 4$; $K_m = K_2^{(2)}$ für $m = 2$

$\epsilon_m = 16$ für $m = 2$; $K_m = K_2^{(1)}$ für $m = 1, 3, 4$.

Die in Gl. (6.9a) und Gl. (6.9b) auftretenden Funktionen $B^m_{x,z}(\phi'')$ und $E(k''_\rho, Rij)$ lauten:

$$E(k''_\rho, R_{ij}) \equiv n - 2nJ_0(k''_\rho R_0) \sum_{i=1}^{n} \sum_{n'=0}^{\infty} \epsilon(-1)^{n'} J_{2n'}(k''_\rho R_i) \cos 2n'\phi'' + 2\sum_{i \neq j} \{J_0(k''_\rho R_{ij}) + 2\sum_{n'=1}^{\infty} (-1)^{n'} J_{2n'}(k''_\rho R_{ij}) \cos 2n'\phi''\} + n^2 J_0^2(k''_\rho R_{ij}) \tag{6.10}$$

$$B^m_{x,z,0}(\phi'') \equiv \tfrac{1}{2}\sum_{p=0}^{3} c^{1,3,0;m}_{2p;1}\cos 2p\phi'' + \tfrac{1}{2}\sum_{p=1}^{3} c^{1,3,0;m}_{2p;2}\sin 2p\phi''. \tag{6.11}$$

Die Konstanten $c^{1,3,0;m}_{2p;1}$ und $c^{1,3,0;1}_{2p;}$ werden im Anhang Aangegeben. Mit den Definitionen Gl. (6.9a–6.9b) lautet das gemäss Gl. (2.14) von Teil I zu berechnende Integral :

$$\tfrac{1}{2}(\overline{\gamma_1^2}+\overline{\gamma_3^2}) = \sum_m \frac{\epsilon_m s_m b^2}{128\pi^2 C^2 K_m^2 V}\int_0^\infty\int_0^{2\pi}\left\{\frac{B^m_x(\phi'')+B^m_z(\phi'')}{(k_\rho''^2+\kappa^2)^2}E(k''_\rho,R_{ij}) - \right.$$

$$\left. -\left(2h^2 - \frac{h^4(k_\rho''^2-(\sum_{k=1}^{3}\beta''^m_{2k}k''_k)^2)}{k_\rho''^4+k_\rho''^2(\kappa^2+h^2)-h^2(\sum_{k=1}^{3}\beta''^m_{2k}k''_k)^2}\right)\frac{B^m_0(\phi'')E(k''_\rho,R_{ij})}{(k_\rho''^2+\kappa^2)^2(k_\rho''^4+k_\rho''^2(\kappa^2+h^2)-h^2(\sum_{k=1}^{3}\beta''^m_{2k}k''_k)^2)}\right\}\frac{dk''_\rho\,d\phi''}{k''_\rho}. \tag{6.12}$$

Dabei läuft die Summe über m in Falle der Sechseckschleifen über $m = 2, 3, 4$ und im Falle der Rechteckschleifen über $m = 1, 2$. Das 1. Glied des Integrals der Gl. (6.12) kann in leicht ersichtlicher Weise in zwei Teilintegraltypen zerlegt werden :

$$= \frac{(-1)^{l+1}}{l!}\frac{d^l}{d(\kappa^2)^l}\left\{\frac{1}{\kappa^2}\left[2K_{2n'}(\kappa R_{ij}) - \right.\right.$$

$$\left.\left. - \sum_{m=0}^{n'}(-1)^m\frac{(2n'-m-1)!}{m!}(\tfrac{1}{2}\kappa R_{ij})^{2m-2n'}\right]\right\}. \tag{6.14}$$

Vol. 18
1961

$$I_1 = \int_0^\infty\{n - 2nJ_0(k''_\rho R_0)\sum_{i=1}^{n}\sum_{n'=0}^{\infty}\epsilon(-1)^{n'}J_{2n'}(k''_\rho R_i)\cos 2n'\phi'' +$$

$$+2\sum_{i\neq j}J_0(k''_\rho R_{ij})+n^2J_0^2(k''_\rho R_0)\}\frac{dk''_\rho}{k''_\rho(k_\rho''^2+\kappa^2)^2}$$

$$= \frac{1}{\kappa^4}\left(n\ln\frac{1}{2}\kappa R_0 - n\psi(1) - 2\sum_{i\neq j}\ln\frac{R_{ij}}{R_0} - 2K_0(\kappa R_{ij}) - \kappa R_{ij}K_1(\kappa R_{ij})\right). \tag{6.13}$$

Glieder, die für $R_0 \to \infty$ verschwinden, sind in Gl. (6.13) weggelassen. (In Gl. (6.13) und in den folgenden Gleichungen bedeuten die $K_i(z)$ die modifizierten Hankelfunktionen und $\psi(1) = -0{,}5772$. Wegen der im vorliegenden Abschnitt nicht erläuterten Symbole siehe Teil I der Arbeit. Die genaue Bedeutung der Doppelsummen über i und j wird unten besprochen werden.) Die verbleibenden Glieder sind vom Typ :

$$I_2 = I^l_{2n'}(\kappa R_{ij}) \equiv \int_0^\infty \frac{(-1)^{n'}J_{2n'}(k''_\rho R_{ij})}{k''_\rho(k_\rho''^2+\kappa^2)^{l+1}}\,dk''_\rho$$

Die Funktionen $I^2_{2n}(\kappa R_{ij})$ sind im Anhang B explizit angegeben und in Bild 13 dargestellt. Mit Gl. (6.13) und Gl. (6.14) ergibt sich für das 1. Glied von Gl. (6.12) :

$$\int_0^\infty\int_0^{2\pi}\frac{B^m_x(\phi'')+B^m_z(\phi'')}{(k_\rho''^2+\kappa^2)^2}E(k''_\rho,R_{ij})\frac{dk''_\rho\,d\phi''}{k''_\rho}$$

$$= \pi\sum_{\nu=1,3}\{c^{\nu;m}_0 I_1 + 2\sum_{p=1}^{3}c^{\nu;m}_{2p;1}I^{(1)}_{2p}(\kappa R_{ij})\}. \tag{6.15}$$

Die Methode zur Berechnung des 2. Gliedes der Gl. (6.12), das wir mit F_s^m/κ^4 abkürzen, wird im Anhang B entwickelt. Wie der Index s andeutet, rührt dieses Glied vom magnetostriktiven Streufeld her. Mit den so berechneten Integralen ergibt sich für die differentielle Suszeptibilität:

$$\chi = -\frac{1}{2}\frac{I_s^2}{C}\frac{d}{d\kappa^2}(\overline{\gamma_1^2}+\overline{\gamma_3^2}) = \frac{1}{H^3 I_s}\sum_{m,\nu} 2\left[\frac{\epsilon_m s_m b^2}{128\pi K_m^2 V}\left\{nc_0^{\nu;m}(\ln\tfrac{1}{2}\kappa R_0-\tfrac{1}{4}-\psi(1))+\right.\right.$$

$$\left.\left.+\sum_{i\neq j}F_s^{*m}-\sum_{i\neq j}\left(2c_0^{\nu;m}\ln\frac{R_{ij}}{R_0}-2\sum_{p=0}^{3}\kappa^6 c_{2p;1}^{\nu;m}I_{2p}^{(2)}(\kappa R_{ij})\right)\right\}\right], \tag{6.16}$$

wobei $F_s^{*m} = F_s^m - (\kappa^2/2)(F_s^m)'$ gesetzt wurde.

Die in Gl. (6.16) auftretenden Faktoren $A_m = \epsilon_m s_m b^2/128\pi K_m^2 V$ können mit Hilfe von Gl. (6.6) und Gl. (5.7) berechnet werden. Man findet:

$$A_m = \frac{\pi\tau_G^2}{(\alpha^{(2)}n)^2}d_m;\quad d_3 = d_4 = \left(\frac{\alpha^{(2)}}{\alpha^{(3)}}\right)^2\frac{\sqrt{(3)}}{3}\frac{1}{32}, \tag{6.17}$$

wobei $d_2 = 0{,}759$ und $d_3 = d_4 = 0{,}0146$ ist.
Mit den Abkürzungen

$$F_0 = \sum_{\nu,m} 2\,d_m c_0^{\nu;m} n(\ln\tfrac{1}{2}\kappa R_0-\tfrac{1}{4}-\psi(1)), \tag{6.18a}$$

$$F_w = \sum_{\nu,m} 4d_m\left(c_0^{\nu;m}\ln\frac{R_{ij}}{R_0}+\sum_{p=0}^{3}\kappa^6 c_{2p;1}^{\nu;m}I_{2p}^{(2)}(\kappa R_{ij})\right), \tag{6.18b}$$

$$F_s = \sum_m 2\,d_m F_s^{*m} \tag{6.18c}$$

erhalten wir schliesslich:

$$\chi H^3 = \frac{\pi\tau_G^2}{I_s(\alpha^{(2)}\cdot n)^2}[F_0+\sum_{i\neq j}(F_w+F_s)]. \tag{6.19}$$

Die Funktionen F_0, F_w und F_s sind für das 6-Eck-Versetzungsmodell im Falle von Ni in Bild 7 dargestellt. Die drei Anteile F_0, F_s und F_w besitzen eine anschauliche physikalische Bedeutung. So entspricht F_0 dem Fall, dass der Effekt jeder einzelnen Versetzung unabhängig von ihren Nachbarn betrachtet wird. Die Funktion F_w berücksichtigt die magnetoelastische Wechselwirkung der n Versetzungen in einer Gruppe. Der Anteil F_s trägt der Wirkung des magnetostriktiven Streufeldes Rechnung. Aus Bild 7 ist zu entnehmen, dass er etwa 30 Prozent des Wechselwirkungsgliedes F_w beträgt und somit bei quantitativen Überlegungen nicht vernachlässigt werden darf. F_s liefert einen negativen Beitrag zur Gesamtsuszeptibilität. Dies entspricht den physikalischen Erwartungen, da das magnetostriktive Streufeld bestrebt ist, die Auslenkungen der Magnetisierung aus der Feldrichtung möglichst klein zu halten.

Zur weiteren numerischen Durchführung der Summation über i, j muss die Wahrscheinlichkeitsdichte $W(R_{ij}/R_0)$ der in unserem Versetzungsmodell vorkommenden gegenseitigen Abstände bekannt sein. In unserem Modell beträgt der Abschirmradius

$$R_0 = \frac{1}{\sqrt{(2\pi)}}\frac{\alpha^{(2)}nb}{2\pi\tau_G K_2^{(2)}\beta} \tag{6.20}$$

und (in guter Näherung) der gegenseitige Abstand der i-ten und j-ten Versetzung nach ESHELBY *et al.*[29]

$$R_{ij} = \frac{\pi b(j^2-i^2)}{16K_2^{(2)}n\tau_G\beta}. \tag{6.21}$$

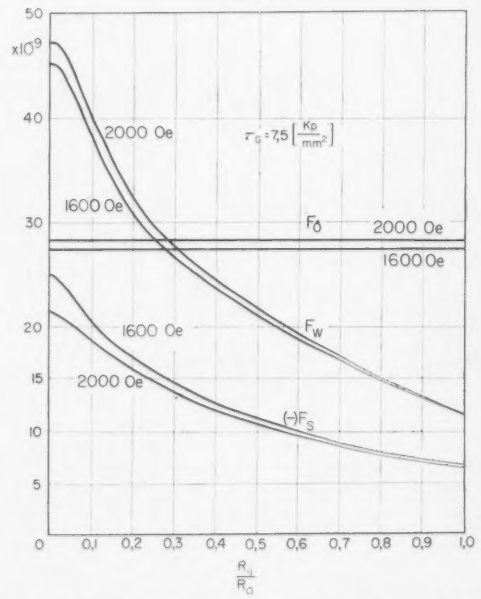

ABB. 7. Die Funktionen F_0, F_w und-F_s bei Nickel in Abhängigkeit von R_{ij}/R_0 für die Feldstärken 1600 (Oe) und 2000 (Oe).

Die Zahl der Versetzungen, über die zu summieren ist, ist durch die Bedingung $R_{ij} \leqq R_0$ gegeben. Aus Gl. (6.20) und Gl. (6.21) folgt:

$$j_{\max} = n\sqrt{(\alpha^{(2)})}\left(\frac{2}{\pi}\right)^{5/4}. \qquad (6.22)$$

Für $n = 31$ und $\alpha^{(2)} = 0{,}85$ ergibt sich $j_{\max} = 17$. Man

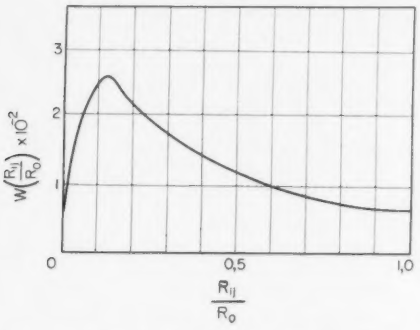

ABB. 8. $W(R_{ij}/R_0)$ für siebzehn Versetzungen einer aufgestauten Versetzungsgruppe.

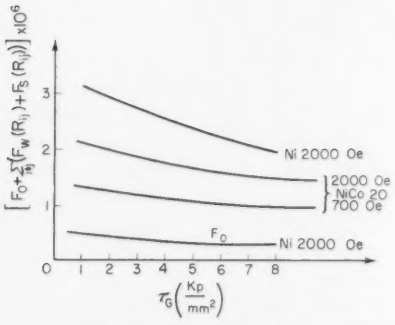

ABB. 9. Die Funktion $F_0 + \sum_{i \neq j} [F_w(R_{ij}) + F_s(R_{ij})]$ bei Nickel und einer Nickel–Kobalt 20-Legierung für verschiedene Feldstärken. Zum Vergleich der Grössenordnungen wurde für Ni auch die Funktion F_0 angegeben.

hat also innerhalb von R_0 17 Versetzungen zu berücksichtigen, für die $W(R_{ij}/R_0)$ in Bild 8 dargestellt ist. Die numerisch berechneten Integrale

$$\sum_{i \neq j}^{j_{\max}} F(R_{ij}/R_0) = \int_0^1 (F_s + F_w) W(R_{ij}/R_0)\, d(R_{ij}/R_0)$$

sind in Bild 9 als Funktion von τ_G angegeben. Aus der nunmehr bekannten τ_G-Abhängigkeit von

$$\sum_{i \neq j} F(R_{ij}/R_0)$$

können wir nach Gl. (6.19) die Funktion $(dX/d\tau_G)H^3$ numerisch bestimmen. Sie ist in Bild 10 für Nickel und zwei Werte des Parameters $\alpha^{(2)}$ dargestellt. Es zeigt sich, dass im Falle von Nickel die für das Sechseck-Modell berechnete differentielle Suszeptibilität χ nur geringfügig von der früher[6] für das Rechteck-Modell berechneten abweicht. Wir geben deshalb in Fig. 11 für die NiCo20-Legierung die für das Rechteckmodell und zwei Feldstärken ermittelten $(dX/d\tau_G)H^3$-Kurven an.

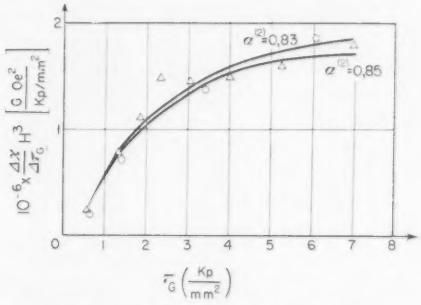

ABB. 10. Die Grösse $(dX/d\tau_G)H^3$ bei Nickel. Von den angegebenen Messpunkten bezieht sich △ auf die Verformungstemperatur 20°C und ○ auf die Verformungstemperatur −183°C. Die ausgezogenen Kurven sind die nach Gl. 6.19 numerisch berechneten.

7. VERGLEICH MIT DEN EXPERIMENTEN

Zum Vergleich der theoretischen Ergebnisse mit unseren Messungen gehen wir von den in Bild 10 und 11 dargestellten $(dX/d\tau_G)H^3$-Kurven

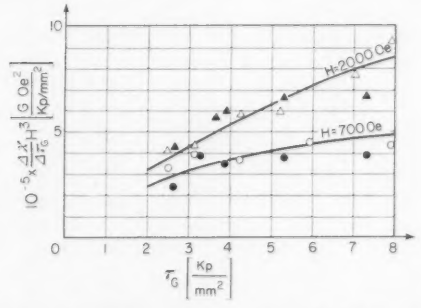

ABB. 11. Die Grösse $(dX/d\tau_G)H^3$ bei NiCo20. △, ○ Verformungstemperatur 20°C. ▲, ● Verformungstemperatur −183°C. Die ausgezogenen Kurven wurden nach Gl. 6.19 für das Rechteckmodell und $\alpha = 1$ numerisch berechnet.

Vol. 18
1961

aus. Die bereits früher[6] gemessenen $\chi(\tau)$-Kurven erlauben die Bestimmung der Grösse $[(\Delta\chi/\Delta\tau_G)H^3]$ für jede einzelne Verformungsstufe.* Die so gewonnenen Punkte sind in den Bildern 10 und 11 eingezeichnet. Im Falle von Nickel können die experimentellen Ergebnisse durch die Theorie am besten angenähert werden, wenn $0{,}82 < \alpha^{(2)} < 0{,}86$ gewählt wird. Bei der Nickel–Kobalt-Legierung ist eine grössere Streuung der experimentellen Punkte vorhanden, jedoch vermag auch hier die Theorie die Messungen sowohl qualitativ als auch quantitativ zu deuten. Ein wesentlicher Teil der Streuung ist durch die Art der Auswertung bedingt. Wie Abb. 12 der experimentellen Arbeit[6] zeigt, ist die Streuung in einem $\chi H^3 - \tau_G$ Diagramm viel geringer und nicht wesentlich von derjenigen von Nickel verschieden.

Eine weitere Möglichkeit für den quantitativen Vergleich von Theorie und Experimenten bietet die Feldstärkeabhängigkeit der differentiellen Suszeptibilität für einen bestimmten Verformungszustand, also für festes τ_G. Da mit der von uns[6] verwendeten Messanordnung nur Messungen bis zu Feldstärken von etwa 2300 Oe ausgeführt werden konnten, eignen sich für einen derartigen Vergleich besonders die Legierungen mit 80 Prozent Ni und 20 Prozent Co, bei denen wegen der niedrigen Kristallenergie der Einmündungsbereich bei Raumtemperatur schon bei etwa 600 Oe beginnt. Die ausgezogene Kurve in Abb. 12 gibt für eine solche Legierung den berechneten Verlauf von $(\chi - \chi_3)H^3$ als Funktion von H bei $\tau_G^{(i)} = 7{,}7$ *kp*/mm² sowie die zugehörigen Messpunkte (bei Raumtemperatur) an. Wiederum ist die Übereinstimmung zwischen experimentellen und theoretischen Werten sowohl dem absoluten Betrage nach als auch hinsichtlich der Variation mit der Feldstärke sehr gut.

Schliesslich wollen wir noch kurz die Temperaturabhängigkeit der differentiellen Suszeptibilität erwähnen. Diese ist im wesentlichen durch die Temperaturabhängigkeit einer ganz bestimmten Kombination der magnetostriktiven Konstanten gegeben (siehe Gl. A.1—A.3). Die Temperaturabhängigkeit von λ_{100} und λ_{111} ist zwar bei reinem Nickel, nicht aber bei den Nickel–Kobalt-Legierungen bekannt. Wie bereits früher[6] gezeigt wurde, ergibt sich bei reinem Nickel eine gute Übereinstimmung zwischen der errechneten und der gemessenen Temperaturabhängigkeit, die geradezu als Nachweis dafür angesehen werden kann, dass die untersuchten Effekte magnetostriktiven Ursprungs sind. Da λ_{100} und λ_{111} einen verschiedenen Temperaturgang aufweisen und die in die Theorie eingehende Kombination dieser Konstanten mit der Temperatur weniger variiert als die einzelnen Konstanten, kann die erwähnte Übereinstimmung zwischen Messung und Rechnung in gewissem Umfange als Bestätigung des von uns verwendeten Modells der Verteilung der inneren Spannungen angesehen werden.

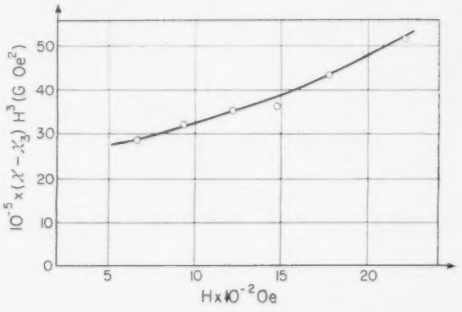

ABB. 12. Vergleich zwischen berechneter und gemessener Feldstärkeabhängigkeit der Grösse $(\chi - \chi_3)H^3$. χ_3 bedeutet die Suszeptibilität am Beginn von Bereich II der Verfestigungskurve. Die experimentellen Punkte wurden unserer früheren Arbeit[6] (Kurve 8 in Bild 10a) entnommen. Verformungstemperatur und Messtemperatur betrugen 20°C.

8. DISKUSSION

Das wesentliche Ergebnis der vorstehenden Ausführungen ist, dass die Messungen der differentiellen Suszeptibilität im Gebiet der Einmündung in die ferromagnetische Sättigung bei plastisch gedehnten Nickel- und Nickel–Kobalt-Einkristallen hinsichtlich ihrer Abhängigkeit von der Feldstärke, der Messtemperatur und der Vorverformung quantitativ durch dasselbe Versetzungsmodell gedeutet werden können, das auch die Verfestigung und das Gleitlinienbild kubisch-flächenzentrierter Kristalle richtig wiedergibt. Es ist damit gezeigt, dass solche Suszeptibilitätsmessungen in Verbindung mit der im Teil I gegebenen allgemeinen Theorie des Versetzungseinflusses

* Die hierbei erforderliche Reduktion der gemessenen τ-Werte auf τ_G wurde in Ziff.3 besprochen.

zum Studium der Versetzungsanordnung in ferromagnetischen Materialien verwendet werden können.

Wir wollen nunmehr die Frage diskutieren, welcher Aspekt des verwendeten Versetzungsmodells bestimmend für die gute Übereinstimmung zwischen Experiment und Theorie ist, und inwieweit auch andere Versetzungsmodelle die Beobachtungen deuten könnten.

Wie schon in Abschnitt 2 ausgeführt worden ist, sprechen die Suszeptibilitätsmessungen vor allem auf des elastische Fernfeld zwischen den Versetzungen an. Allgemein kann man sagen, dass dieses elastische Fernfeld klein ist, wenn die Versetzungen in einem Netzwerk derart angeordnet sind, dass unmittelbar benachbarte Versetzungen ihre Spannungsfelder gegenseitig abschirmen, und dass das Fernfeld gross ist, wenn aufgestaute Versetzungsgruppen vorhanden sind. Im letztgenannten Falle ist bei festgehaltener Austauschlänge κ^{-1} das elastische Fernfeld (und damit die Suszeptibilität) umso grösser, je grösser die Zahl n der Versetzungen in einer Gruppe ist und je grösser die Dichte dieser Versetzungsgruppen ist. Qualitativ das gleiche gilt auch für den $\tau_G^{(f)}$-Beitrag zur Fliessspannung. Sofern n hinreichend gross ist, hängen deshalb bei einer festgehaltenen Fliessspannung die von der Theorie gelieferten Suszeptibilitätswerte nicht sehr empfindlich von n ab. Wird jedoch n sehr verkleinert, so ändert sich die Versetzungsanordnung innerhalb des Abstandes $2\kappa^{-1}$ vom Kopf der Versetzungsgruppe, auf die es vor allem ankommt, so stark, dass die Suszeptibilität doch mit sinkendem n rasch abnimmt. Als Extremfall, auf den wir unten noch näher eingehen werden und der ein ganz anderes Erscheinungsbild liefert, kommt man schliesslich zu $n = 1$, also dem Fall einzelner, sich gegenseitig abschirmender Versetzungen.

Wir erläutern das Vorstehende an einem Beispiel, als das wir $\tau_G^{(f)} = 8\ kp/mm^2$ herausgegriffen haben. Wie oben besprochen, ergab sich aus Gleitlinienbeobachtungen bei Nickeleinkristallen $n = 31$, was auf einen Wert $j_{max} = 17$ für die Zahl der innerhalb des „Abschirmradius einer Gruppe" R_0 liegenden Versetzungen führte (Gl. 6.22). Halbiert man nun bei festgehaltenem $\tau_G^{(f)}$, also unter Vervierfachung der Flächendichte der Versetzungsgruppen, den Zahlenwert von n, so ergibt sich $j_{max} = 8{,}5$. Dann ergibt sich nach Gl. (6.18b) eine Verminderung von χH^3 (Gl. 6.19) um 30 Prozent. Diese Verminderung würde bereits die Übereinstimmung mit den Messergebnissen beeinträchtigen. Würde man n noch weiter verkleinern, so würden sehr radikale Änderungen in χH^3 auftreten, die sich nicht nur in einer starken Verminderung des Absolutwertes, sondern auch in einer ausgeprägten Veränderung der H- und der τ_G-Abhängigkeit äussern würden. Man kann somit sagen, dass durch die hier besprochenen ferromagnetischen Untersuchungen die Existenz von aufgestauten Versetzungsgruppen (bzw. des zugehörigen elastischen Fernfeldes) von der Grössenordnung, wie sie in der Theorie der Verfestigung auftreten, nachgewiesen wurde.

Von BASINSKI[16] und HIRSCH[17] sind neuerdings Vorschläge zur Deutung der Verfestigung kubisch-flächenzentrierter Kristalle gemacht worden, die darauf hinauslaufen, dass τ_S wie bei uns interpretiert wird, dass aber die Zunahme von τ_G während der Verformung allein der Vergrösserung der Dichte des Versetzungswaldes, also $\tau_G^{(w)}$ zugeschrieben wird. Die gesamte Versetzungsdichte ist etwa dieselbe wie in unserer Theorie. Jedoch ist die gegenseitige Anordnung der Versetzungen derart, dass $R_{ij} \approx R_0$, also der Abschirmradius etwa gleich dem Abstand benachbarter Versetzungen ist. Während in unserem Modell

$$\chi H^3 \sim \alpha^{(2)} \left(\frac{2}{\pi}\right)^{5/2} b^2 n \ln(\kappa R_0/2) \qquad (8.1)$$

gilt, hat man für das BASINSKI–HIRSCH'sche Modell

$$\chi H^3 \sim b^2 \ln(\kappa R_0'/2) \qquad (8.2)$$

mit $R_0' = n^{-1/2} R_0$. Den Gl. (8.1) und (8.2) gemeinsamen Proportionalitätsfaktor, der u.a. die Gesamtzahl der Versetzungen enthält, haben wir weggelassen, da es uns hier nur auf das Verhältnis der beiden Ausdrücke ankommt. Setzt man $n = 31$ ein, so ergibt sich χH_3 aus Gl. (8.2) um einem Faktor 20 kleiner als aus (8.1). Berücksichtigt man, dass BASINSKI eine ein wenig grössere Versetzungsdichte benützt wie wir, so reduziert sich die Diskrepanz auf einen Faktor 13. Dieser ist jedoch immer noch viel zu gross, um mit den experimentellen Ergebnissen verträglich zu sein. Wir können somit sagen, dass das BASINSKI–HIRSCH'sche Modell nicht einmal grössenordnungsmässig in der Lage ist, die Messungen zu deuten.

Versucht man die eben besprochene Diskrepanz dadurch zu beheben, dass man $n = 1$ annimmt, aber die Versetzungsdichte um einen Faktor 20 vergrössert, so ergeben sich (abgesehen von der Inkonsistenz mit anderen Untersuchungsmethoden) neue Schwierigkeiten. Es gilt dann $R_{ij} \approx R_0$, jedoch mit $\kappa R_{ij} < 1$. Man kann dann die ursprünglichen Rechnungen von BROWN[8] über die Wirkung von Versetzungsdipolen anwenden. Das gleiche Ergebnis erhält man auch ohne weiteres durch Spezialisierung aus unseren allgemeinen Formeln in Abschnitt 6. Es ergibt sich

$$\chi H^3 \sim N \cdot \overline{R_{ij}^2} H, \tag{8.3}$$

wo N die Versetzungsdichte ist. Da der Mittelwert $\overline{R_{ij}^2}$ proportional zu N^{-1} ist, liefert dieses Modell eine von der Verformung unabhängige Suszeptibilität, was den Messungen (auch an Vielkristallen) in eklatanter Weise widerspricht. Die Feldstärkenabhängigkeit von Gl. (8.3) würde in der Darstellung der Abb. 12 eine durch den Ursprung gehende Gerade liefern, was ebenfalls der Erfahrung widerspricht.

Abschliessend können wir also feststellen, dass keines der *ohne* die Vorstellung von *Versetzungsgruppen* arbeitenden Verfestigungsmodelle in der Lage ist, die Einmündungsmessungen auch nur näherungsweise zu deuten, während unsere von Versetzungsgruppen ausgehende Verfestigungstheorie ohne eine wesentliche Anpassung von Parametern vorzügliche Übereinstimmung mit den Experimenten liefert. Inwieweit die Theorie gegen die Grösse dieser Gruppen empfindlich ist, ist oben besprochen worden.

Anerkennung—Die Verfasser danken der Deutschen Forschungsgemeinschaft für die finanzielle Unterstützung der Arbeit.

ANHANG A

Zur Berechnung der in Gl. (6.11) definierten Fourierkoeffizienten $c_{22;1,2}^{1,3,0;m}$ sind die in Teil I erklärten Tensoren β_{ik}, β'_{ik} und β''_{ik} erforderlich. Im folgenden kennzeichnen wir die zu den Bogenteilen s_1, s_2, s_3, s_4 gehörenden Tensoren durch einen entsprechenden oberen Index. Aus den in Fig. 2 angegebenen Orientierungen der einzelnen Bogenteile ergeben sich für mittelorientierte Einkristalle folgende Tensoren:

$$\beta_{ik}^{(m)} = \begin{bmatrix} \frac{\sqrt{(30)}}{30} & -\frac{\sqrt{(30)}}{15} & \frac{\sqrt{(30)}}{6} \\ -\frac{2}{5}\sqrt{(5)} & \frac{\sqrt{(5)}}{5} & 0 \\ -\frac{\sqrt{(6)}}{6} & \frac{\sqrt{(6)}}{3} & \frac{\sqrt{(6)}}{6} \end{bmatrix}; \quad m = 1, 2, 3, 4$$

$$\beta'^{(1)}_{ik} = \beta'^{(2)}_{ik} = \begin{bmatrix} \frac{\sqrt{(2)}}{2} & 0 & \frac{\sqrt{(2)}}{2} \\ \frac{\sqrt{(3)}}{3} & \frac{\sqrt{(3)}}{3} & -\frac{\sqrt{(3)}}{3} \\ -\frac{\sqrt{(6)}}{3} & \frac{\sqrt{(6)}}{3} & \frac{\sqrt{(6)}}{6} \end{bmatrix}; \quad \beta''^{(1)}_{ik} = \beta''^{(2)}_{ik} = \begin{bmatrix} \sin\lambda & \cos\lambda & 0 \\ -\cos\lambda & \sin\lambda & 0 \\ 0 & 0 & 1 \end{bmatrix}$$

$$\beta'^{(3)}_{ik} = \begin{bmatrix} \frac{\sqrt{(6)}}{3} & -\frac{\sqrt{(6)}}{6} & \frac{\sqrt{(6)}}{6} \\ \frac{\sqrt{(3)}}{3} & \frac{\sqrt{(3)}}{3} & -\frac{\sqrt{(3)}}{3} \\ 0 & \frac{\sqrt{(2)}}{2} & \frac{\sqrt{(2)}}{2} \end{bmatrix}; \qquad \beta''^{(3)}_{ik} = \begin{bmatrix} \frac{3}{10}\sqrt{(5)} & \frac{1}{10}\sqrt{(30)} & -\frac{1}{2} \\ -\frac{1}{5}\sqrt{(10)} & \frac{1}{5}\sqrt{(15)} & 0 \\ \frac{1}{10}\sqrt{(15)} & \frac{\sqrt{(10)}}{10} & \frac{1}{2}\sqrt{(3)} \end{bmatrix}$$

$$\beta_{ik}^{\prime(4)} = \begin{bmatrix} \frac{\sqrt{(6)}}{6} & \frac{\sqrt{(6)}}{6} & \frac{\sqrt{(6)}}{3} \\ \frac{\sqrt{(3)}}{3} & \frac{\sqrt{(3)}}{3} & -\frac{\sqrt{(3)}}{3} \\ -\frac{\sqrt{(2)}}{2} & \frac{\sqrt{(2)}}{2} & 0 \end{bmatrix}; \qquad \beta_{ik}^{\prime\prime(4)} = \begin{bmatrix} \frac{3}{10}\sqrt{(5)} & \frac{1}{10}\sqrt{(30)} & \frac{1}{2} \\ -\frac{1}{5}\sqrt{(10)} & \frac{1}{5}\sqrt{(15)} & 0 \\ -\frac{1}{10}\sqrt{(15)} & -\frac{\sqrt{(10)}}{10} & \frac{1}{2}\sqrt{(3)} \end{bmatrix}.$$

Mit Hilfe der soeben definierten Tensoren $\beta_{ik}^{(m)}$ und der Beziehung (2.28) von Teil I finden wir :

(1) Die Koeffizienten für 0°- und 90°-Versetzungen :

$$\begin{aligned} c_{11}^{1;1,2} &= \frac{\sqrt{(6)}}{10}(\lambda_{100}+5\lambda_{111}) & c_{11}^{3;1,2} &= -\frac{\sqrt{(30)}}{10}(\lambda_{100}-\lambda_{111}) \\ c_{22}^{1;1,2} &= -\frac{3}{5}\sqrt{(6)}\lambda_{111} & c_{22}^{3;1,2} &= 0 \\ c_{33}^{1;1,2} &= -\frac{\sqrt{(6)}}{10}(\lambda_{100}-\lambda_{111}) & c_{33}^{3;1,2} &= -\frac{\sqrt{(30)}}{30}(3\lambda_{100}-\lambda_{111}) \\ c_{12}^{1;1,2} &= \frac{1}{5}(2\lambda_{100}+\lambda_{111}) & c_{12}^{3;1,2} &= -\frac{2}{5}\sqrt{(5)}(\lambda_{100}-\lambda_{111}) \\ c_{13}^{1;1,2} &= -\frac{\sqrt{(2)}}{5}(\lambda_{100}-\lambda_{111}) & c_{13}^{3;1,2} &= \frac{\sqrt{(10)}}{10}\left(\frac{2}{3}\lambda_{111}+\lambda_{100}\right). \end{aligned} \tag{A.1}$$

Hierbei entspricht der erste obere Index in den $c_{ik}^{\nu;m}$ dem in Teil I eingeführten und der zweite bezieht sich auf den entsprechenden Bogenteil.

(2) Die Koeffizienten für die 60°-Versetzung lauten :

$$\left.\begin{aligned} c_{11}^{1;3} &= \frac{\sqrt{(6)}}{10}(2\lambda_{100}+5\lambda_{111}) & c_{11}^{3;3} &= -\frac{\sqrt{(30)}}{10}(2\lambda_{100}+\lambda_{111}) \\ c_{22}^{1;3} &= -\frac{6}{5}\lambda_{111}\sqrt{(6)} & c_{22}^{3;3} &= 0 \\ c_{33}^{1;3} &= \frac{\sqrt{(6)}}{15}(2\lambda_{100}+5\lambda_{111}) & c_{33}^{3;3} &= \frac{\sqrt{(30)}}{10}\lambda_{111} \end{aligned}\right\} \tag{A.2}$$

$$\left.\begin{aligned} c_{12}^{1;3} &= \frac{\sqrt{(3)}}{10}(4\lambda_{100}-\lambda_{111}) & c_{12}^{3;3} &= \frac{\sqrt{(15)}}{5}(-2\lambda_{100}+\lambda_{111}) \\ c_{13}^{1;3} &= \frac{\sqrt{(2)}}{5}(6\lambda_{111}+\lambda_{100}) & c_{13}^{3;3} &= \frac{\sqrt{(10)}}{5}(2\lambda_{111}-\lambda_{100}) \\ c_{23}^{1;3} &= \frac{1}{10}(7\lambda_{111}-4\lambda_{100}) & c_{23}^{3;3} &= \frac{\sqrt{(5)}}{10}(4\lambda_{100}+5\lambda_{111}) \end{aligned}\right\}$$

Vol. 18
1961

$$
\left.
\begin{aligned}
c_{11}^{1;4} &= \frac{3}{2}\sqrt{(6)}\lambda_{111} & c_{11}^{3;4} &= \frac{3}{10}\sqrt{(30)}\lambda_{111}\\
c_{22}^{1;4} &= -\frac{6}{5}\sqrt{(6)}\lambda_{111} & c_{22}^{3;4} &= 0\\
c_{33}^{1;4} &= \frac{3}{10}\sqrt{(6)}\lambda_{111} & c_{33}^{3;4} &= -\frac{3}{10}\sqrt{(30)}\lambda_{111}\\
c_{12}^{1;4} &= \frac{8}{15}\sqrt{(3)}\lambda_{111} & c_{12}^{3;4} &= \frac{3}{10}\sqrt{(15)}\lambda_{111}\\
c_{13}^{1;4} &= -\frac{\sqrt{(2)}}{10}(4\lambda_{100}+5\lambda_{111}) & c_{13}^{3;4} &= \frac{\sqrt{(10)}}{10}(4\lambda_{100}-\lambda_{111})\\
c_{23}^{1;4} &= \frac{1}{10}(-8\lambda_{100}+5\lambda_{111}) & c_{23}^{3;4} &= \frac{\sqrt{(5)}}{10}(8\lambda_{100}+\lambda_{111}).
\end{aligned}
\right\} \qquad \text{(A.3)}
$$

Die Berechnung der in Gleichung A.1–A.3 definierten Koeffizienten erfolgt für Nickel mit den von CORNER und HUTCHINSON[30] gemessenen Werten $\lambda_{100} = 53{,}6\times10^{-6}$ und $\lambda_{111} = 21{,}8\times10^{-6}$. Bei der NiCo20-Legierung verwenden wir die von YAMAMOTO und NAKAMICHI[31] gemessenen Werte.

Die in Gl. (6.11) definierten Koeffizienten $c_{2p;1,2}^{1,3,0;m}$ lauten :

$$
\begin{aligned}
c_{0;1}^{\nu;m} &= (A^{\nu;m})^2+(B^{\nu;m})^2+(C^{\nu;m})^2+(D^{\nu;m})^2\\
c_{2;1}^{\nu;m} &= -(A^{\nu;m})^2+(C^{\nu;m})^2+\\
&\quad +2A^{\nu;m}B^{\nu;m}+2D^{\nu;m}C^{\nu;m}\\
c_{4;1}^{\nu;m} &= 2D^{\nu;m}C^{\nu;m}-2A^{\nu;m}B^{\nu;m}\\
c_{6;1}^{\nu;m} &= -(B^{\nu;m})^2+(D^{\nu;m})^2\\
c_{2;2}^{\nu;m} &= 2A^{\nu;m}C^{\nu;m}+2B^{\nu;m}C^{\nu;m}-2A^{\nu;m}D^{\nu;m}\\
c_{4;2}^{\nu;m} &= 2B^{\nu;m}C^{\nu;m}+2A^{\nu;m}D^{\nu;m}\\
c_{6;2}^{\nu;m} &= 2B^{\nu;m}D^{\nu;m}.
\end{aligned}
\qquad \text{(A.4)}
$$

Hierbei bedeuten die Konstanten $A^{\nu;m}$, $B^{\nu;m}$, $C^{\nu;m}$, $D^{\nu;m}$ für die Bogenteile s_1–s_4 jeweils eine spezielle Kombination der Konstanten $c_{ik}^{\nu;m}$:

1. 0°-Versetzung :

$$A^{\nu;2} = c_{13}^{\nu;2};\quad C^{\nu;2} = c_{12}^{\nu;2};\quad B^{\nu;2}\equiv 0;\quad D^{\nu;2}\equiv 0$$

2. 60°-Versetzung :

$$
\begin{aligned}
A^{\nu;m} &= \mp\frac{\sqrt{(3)}}{2}\left\{3c_{11}^{\nu;m}+c_{22}^{\nu;m}+\right.\\
&\quad \left.+4\left(1-\frac{K_2^{(1)}}{K_2^{(2)}}\right)c_{33}^{\nu;m}\right\}-2\frac{K_2^{(1)}}{K_2^{(2)}}c_{13}^{\nu;m}\\
B^{\nu;m} &= \mp\frac{\sqrt{(3)}}{2}(c_{22}^{\nu;m}-c_{11}^{\nu;m});\\
C^{\nu;m} &= \frac{2K_2^{(1)}}{K_2^{(2)}}c_{23}^{\nu;m}\mp\sqrt{(3)}c_{12}^{\nu;m}\\
D^{\nu;m} &= \mp\sqrt{(3)}c_{12}^{\nu;m};\quad m=3,4
\end{aligned}
\qquad \text{(A.5)}
$$

3. 90°-Versetzung : Diese Koeffizienten erhalten wir aus den Gleichungen A.4 und A.5, indem wir in Gl. A.5 für $\sqrt{(3)}$ den Wert 2 einsetzen und den Faktor $K_2^{(1)}/K^{(2)}\equiv 0$ setzen.

Wir verzichten auf eine explizite Angabe der beim Streufeldanteil auftretenden Koeffizienten $c_{2p;1,2}^{0;m}$ und geben nur ihre Fourierintegraldarstellung an.

1. 0°-Versetzung :

$$
c_{2p;1,2}^{0;2} = \frac{\epsilon}{2\pi}\int_0^{2\pi}\left\{\begin{aligned}&(c_{12}^{1;2}\cos^2\phi''-\tfrac{1}{2}c_{13}^{1;2}\sin 2\phi'')^2\cos^2\lambda+(\tfrac{1}{2}c_{12}^{3;2}\sin 2\phi''-c_{13}^{3;2}\sin^2\phi'')^2\\&+\cos\lambda\sin 2\phi''[c_{12}^{1;2}c_{12}^{3;2}\cos^2\phi''+c_{13}^{1;2}c_{13}^{3;2}\sin^2\phi''-\tfrac{1}{2}(c_{12}^{1;2}\cdot c_{13}^{3;2}+c_{12}^{3;2}\cdot c_{13}^{1;2})\sin 2\phi'']\end{aligned}\right\}\begin{pmatrix}\cos 2p\phi''\\ \sin 2p\phi''\end{pmatrix}d\phi''. \qquad \text{(A.6)}
$$

In Gl. A.6 und in den folgenden Fällen bezieht sich $\cos 2p\phi''$ auf $c^{0;2}_{2p;1}$ und $\sin 2p\phi''$ auf $c^{0;2}_{2p;2}$.

2. 60°-Versetzung :

$$c^{0;m}_{2p;1,2} = \frac{\epsilon}{2\pi}\int_0^{2\pi} \{3c^{1;m}_{2p;1,2} + c^{3;m}_{2p;1,2} \pm 2\cdot\sqrt{(3)}(c^{0;m}_{2p;1,2})'\}(b_1 + b_2\cos 2\phi'' + b_3\sin 2\phi'')\begin{pmatrix}\cos 2p\phi''\\ \sin 2p\phi''\end{pmatrix} d\phi''. \tag{A.7}$$

In Gl. A.6 und Gl. A.7 ist $\epsilon = 2$ für $p = 0$ und $\epsilon = 1$ für $p = 1, 2, \ldots$ Das in Gl. A.6 auftretende Glied $(c^{0;m}_{2p;1,2})'$ wird aus den $c^{;m}_{2p;1,2}$ dadurch gebildet, indem quadratische Glieder, z.B. $(A^{\nu;m}_{2p;1,2})^2$ durch $A^{1;m}A^{3;m}$ ersetzt werden und entsprechend gemischte Glieder, z.B. $2A^{\nu;m}B^{\nu;m}$ durch $A^{1;m}B^{3;m} + A^{3;m}B^{1;m}$. Die in Gl. A.7 auftretenden Konstanten b_i besitzen folgenden Wert:

$$b_1 = 1/8;\ b_2 = 1/40;\ b_3 = (6)^{1/2}/20.$$

3. 90°-Versetzung : In diesem Fall ist keine besondere Berechnung der $c^{0;1}_{2p;1,2}$ erforderlich, weil die spezielle Art des Tensors $\beta''^{(1)}_{ik}$ die Grösse $(\overline{\gamma_1^2} + \overline{\gamma_3^2})$ folgendermassen anzuschreiben gestattet :

Wie aus Gl. A.8 ersichtlich ist, sind die $c^{0;1}_{2p;1,2}$ mit den in Gl. A.4 für die 90°-Versetzung definierten $c^{1;0}_{2p;1,2}$ identisch. Für die numerische Rechnung erweisen sich die folgenden Abkürzungen als geeignet :

$$\overline{c^2_{2p;1,2}} = c^{1;2}_{2p;1,2} + c^{3;2}_{2p;1,2}$$

$$\overline{c^{3,4}_{2p;1,2}} = c^{1;3}_{2p;1,2} + c^{3;3}_{2p;1,2} + c^{1;4}_{2p;1,2} + c^{3;4}_{2p;1,2}$$

$$c^{0;3,4}_{2p;1,2} = c^{0;3}_{2p;1,2} + c^{0;4}_{2p;1,2}.$$

$$\tfrac{1}{2}(\overline{\gamma_1^2} + \overline{\gamma_3^2}) = \frac{\epsilon_1 s_1 b^2}{128\pi^2(K_2^{(1)})^2 V}\int_0^{2\pi}\int_0^{\infty}\left(\frac{B^0_z(\phi'')}{(k''^2_\rho + \kappa^2)^2} + \frac{B^0_x(\phi'')}{(k''^2_\rho + \kappa^2 + h^2\sin^2(\phi'' + \lambda))^2}\right)\frac{dk''_\rho\, d\phi''}{k''_\rho}. \tag{A.8}$$

Mit diesen Abkürzungen wurden für Nickel folgende Werte berechnet :

$$\overline{c^2_0} = 3{,}410\times10^{-9};\ \overline{c^2_{2;1}} = -2{,}120\times10^{-10};\ c^{0;2}_0 = 0{,}729\times10^{-9};$$

$$c^{0;2}_{2;1} = -1{,}175\times10^{-9};\ c^{0;2}_{4;1} = 0{,}736\times10^{-9};\ c^{0;2}_{2;2} = -1{,}175\times10^{-9};\ c^{0;2}_{4;2} = 0{,}589\times10^{-9}$$

$$\overline{c^{3,4}_0} = 17{,}082\times10^{-8};\ \overline{c^{3;4}_{2;1}} = -20{,}895\times10^{-8};\ \overline{c^{3,4}_{4;1}} = 3{,}062\times10^{-8}$$

$$\overline{c^{3,4}_{6;1}} = -1{,}099\times10^{-8};\ \overline{c^{3,4}_{2;2}} = 10{,}781\times10^{-8};\ \overline{c^{3,4}_{4;2}} = -9{,}871\times10^{-8}$$

$$\overline{c^{3,4}_{6;2}} = 3{,}720\times10^{-8};\ c^{0;3,4}_0 = 1{,}995\times10^{-8};\ c^{0;3,4}_{2;1} = -2{,}924\times10^{-8}$$

$$c^{0;3,4}_{4;1} = 1{,}207\times10^{-8};\ c^{0;3,4}_{6;1} = -0{,}457\times10^{-8};\ c^{0;3,4}_{8;1} = 0{,}083\times10^{-8}$$

$$c^{0;3,4}_{2;2} = -1{,}367\times10^{-8};\ c^{0;3,4}_{4;2} = -1{,}254\times10^{-8};\ c^{0;3,4}_{6;2} = 0{,}680\times10^{-8}$$

$$c^{0;3,4}_{8;1} = -0{,}237\times10^{-8}.$$

Für die NiCo20-Legierung ergaben sich folgende Koeffizienten :

$$\overline{c^2_0} = 2{,}004\times10^{-9};\ \overline{c^2_{2;1}} = 1{,}340\times10^{-9}$$

$$c^{0;2}_0 = 1{,}257\times10^{-9};\ c^{0;2}_{2;1} = -28{,}30\times10^{-9};\ c^{0;2}_{4;1} = 0{,}074\times10^{-9}$$

$$c^{1;1}_{0;1} = 27{,}02\times10^{-9};\ c^{1;1}_{2;1} = -28{,}30\times10^{-9};\ c^{1;1}_{4;1} = -1{,}735\times10^{-9};\ c^{1;1}_{6;1} = -8{,}79\times10^{-9}$$

Vol. 18
1961

$$c^{3;1}_{2;1} = -3{,}68\times10^{-9};\ c^{3;1}_{4;1} = 3{,}82\times10^{-9};\ c^{3;1}_{6;1} = 0{,}648\times10^{-9};$$

$$c^{1;1}_{2;1} = 2{,}15\times10^{-9};\ c^{1;1}_{4;2} = 9{,}04\times10^{-9};\ c^{1;1}_{6;2} = -2{,}15\times10^{-9}.$$

ANHANG B

Die in Abschnitt 6 definierte Funktion F^{*m}_s ist durch folgendes Integral gegeben :

$$F^{*m}_s = -\int_0^\infty \int_0^{2\pi} \frac{B^m_0(\phi'')E(k''_\rho,R_{ij})}{\sin^2(\phi''+\lambda)} \left(\frac{1}{(k''^2_\rho+\kappa^2)^3} - \frac{1}{(k''^2_\rho+\kappa^2+h^2\sin^2(\phi''+\lambda))^3}\right) \frac{dk''_\rho\, d\phi''}{k''_\rho}. \tag{B.1}$$

Hierbei ist für $m = 3{,}4$ $\cos\lambda = -\sqrt{(10/5)}$ und $\sin\lambda = \sqrt{15/5}$ zu setzen. Im Falle $m = 2$ ist in Gl. B.1 $\sin^2(\phi''+\lambda)$ durch $1-(\sin^2\phi'')/2$ zu ersetzen. Die Funktion F^*_s geben wir hier nicht an, da sie bereits Gl. A.7 zu entnehmen ist. Die in Gl. B.1 auftretende Schwierigkeit bei der ϕ''-Integration legt es nahe, zunächst die k''_ρ-Integration durchzuführen. Mit den in Abschnitt 6 angegebenen Integralformeln (6.13) und (6.14) finden wir :

$$F^{*m}_s = -\int_0^{2\pi} \frac{B_0(\phi'')}{\sin^2(\phi''+\lambda)} \left(\frac{1}{\kappa^6}F^{*m}_0(\kappa R_{ij}) - \frac{1}{\kappa'^6}F^{*m}_0(\kappa' R_{ij})\right) - 2\left(\frac{1}{\kappa^2}-\frac{1}{\kappa'^2}\right)\ln\frac{R_{ij}}{R_0} + \sum_p \epsilon\left(I^{(2)}_{2p}(\kappa R_{ij}) - I^{(2)}_{2p}(\kappa' R_{ij})\right) d\phi''. \tag{B.2}$$

Dabei bedeutet :

$$\kappa'^2 = \kappa^2 + h^2\sin^2(\phi''+\lambda);\ \epsilon = 2 \text{ für } p = 0$$

$$\text{und } \epsilon = 4 \text{ für } p \neq 0.$$

Die ersten beiden Glieder von B.2 sind elementar integrierbar und liefern :

$$F^{*m}_{s,1} = -\frac{1}{\kappa^4}\frac{h^2}{\kappa^2}\left(n\ln\frac{1}{2}\kappa R_0 - \frac{n}{4} - n\psi(1) - 2\sum_{i\neq j}\ln\frac{R_{ij}}{R_0}\right)\sum_{p;1,2} c^{0,m}_{2p;1,2}\sum_{t=1}^{3}\Phi^p_t \begin{pmatrix}\cos 2p\lambda \\ -\sin 2p\lambda\end{pmatrix}\kappa^{2t-2}. \tag{B.3}$$

In B.3 bezieht sich die Summation über 1 auf $\cos 2p\lambda$ und die Summation über 2 auf $-\sin 2p\lambda$. Dabei bedeutet :

$$\Phi^p_t = \int_0^{2\pi} \frac{\cos 2p\phi}{(\kappa^2+h^2\sin^2\phi)^t}\, d\phi$$

$$\Phi^p_1 = \frac{2\pi(\sqrt{(a^2-b^2)}-a)^p}{(b)^p\sqrt{(a^2-b^2)}} \tag{B.4a}$$

$$\Phi^p_2 = 2\pi\frac{(\sqrt{(a^2-b^2)}-a)^p}{(b)^p(a^2-b^2)}\left(p+\frac{a}{\sqrt{(a^2-b^2)}}\right) \tag{B.4b}$$

$$\Phi^p_3 = \pi\frac{(\sqrt{(a^2-b^2)}-a)^p}{(b)^p(a^2-b^2)}\times \times\left(3pa+\frac{3a^2}{\sqrt{(a^2-b^2)}}+(p^2-1)\sqrt{(a^2-b^2)}\right). \tag{B.4c}$$

In den Formeln B.4a–B.4c sind für die Konstanten a und b folgende Werte einzusetzen :

1. 0°-Versetzung :

$$a = \kappa^2+\frac{3}{4}h^2;\quad b = \frac{h^2}{4}$$

2. 60°-Versetzung :

$$a = \kappa^2+\frac{h^2}{2};\quad b = -\frac{h^2}{2}.$$

Die Koeffizienten $c^{0;3,4}_{2p;1,2}$ sind im Anhang A definiert.

Das dritte Glied des Integrals B.2 ist nicht geschlossen

integrierbar. Wir gehen deshalb auf die explizite Darstellung der Funktionen $I^{(2)}_{2p}(\kappa R_{ij})$ zurück und führen die Integration gliedweise durch. Nach Gl. (6.14) lauten die Funktionen $I^{(2)}_{2p}(\kappa R_{ij})$ (siehe Abb. 13) :

$$I^{(2)}_0(\kappa R_{ij}) = -\frac{1}{2\kappa^6}[(4-\kappa^2R^2_{ij})K_0(\kappa R_{ij})+\tfrac{3}{2}\kappa^2R^2_{ij}K_2(\kappa R_{ij})]$$

$$I^{(2)}_2(\kappa R_{ij}) = -\frac{1}{2\kappa^6}\left[3\kappa R_{ij}K_3(\kappa R_{ij})+\tfrac{1}{2}\kappa^2R^2_{ij}K_2(\kappa R_{ij})-\frac{24}{\kappa^2R^2_{ij}}+2\right]$$

$$I^{(2)}_4(\kappa R_{ij}) = -\frac{1}{2\kappa^6}\left[24K_4(\kappa R_{ij})+6\kappa R_{ij}K_3(\kappa R_{ij})+\tfrac{1}{2}\kappa^2R^2_{ij}K_2(\kappa R_{ij})-\frac{1152}{\kappa^4R^4_{ij}}+\frac{48}{\kappa^2R^2_{ij}}-1\right]$$

$$I^{(2)}_6(\kappa R_{ij}) = -\frac{1}{2\kappa^6}\left[(40+\tfrac{1}{2}\kappa^2R^2_{ij})K_6(\kappa R_{ij})+3\kappa R_{ij}K_5(\kappa R_{ij})-\frac{120\cdot1280}{\kappa^6R^2_{ij}}+\right.$$

$$\left.+\frac{4608}{\kappa^4R^2_{ij}}-\frac{72}{\kappa^2R^2_{ij}}+\frac{2}{3}\right]. \qquad \text{(B.5)}$$

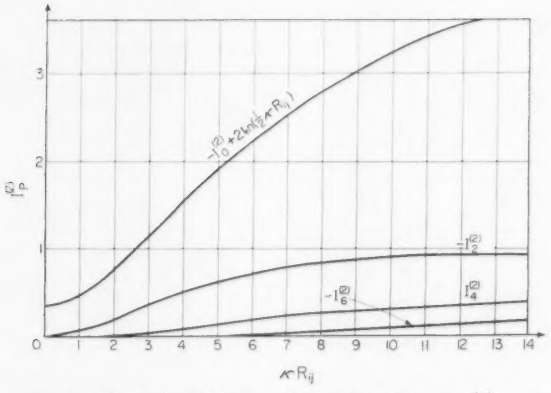

ABB. 13. Die nach (6.14) berechneten Funktionen $I^{(2)}_{2p}(\kappa R_{ij})$.

Mit Hilfe der Gl. B.5 erkennen wir, dass im Integral

$$F^{*m}_{s,2} = -\int_0^{2\pi}\frac{B_0(\phi'')}{\sin^2(\phi''+\lambda)}\left\{\sum_p \epsilon(I^{(2)}_{2p}(\kappa R_{ij})-I^{(2)}_{2p}(\kappa' R_{ij}))\right\}d\phi''$$

folgende Teilintegrale auftreten :

$$\int_0^{2\pi}\frac{B_0(\phi'')}{\sin^2(\phi''+\lambda)}\left\{\left(\frac{1}{\kappa^2R^2_{ij}}\right)^n\frac{1}{\kappa^6}-\left(\frac{1}{\kappa'^2R^2_{ij}}\right)^n\frac{1}{\kappa'^6}\right\}\cos 2p\phi''\,d\phi''$$

$$=\frac{h}{2R^{2n}_{ij}\kappa^{6+2n}}\sum_p\sum_{i=1}^{1=3+n}(\Phi^{p-n}_i+\Phi^{p+n}_i)c^{0;m}_{2p;1,2}\begin{Bmatrix}\cos 2p\lambda\\ -\sin 2p\lambda\end{Bmatrix}(\kappa)^{2i-2}, \qquad \text{(B.6)}$$

Vol. 18
1961

$$\int_0^{2\pi} \left\{ \frac{(\kappa R_{ij})^{4-n}}{\kappa^6} K_n(\kappa R_{ij}) - \frac{(\kappa' R_{ij})^{4-n} K_n(\kappa' R_{ij})}{\kappa'^6} \right\} \sum_{\nu=0}^{4} a_\nu^m \sin^{2\nu}(\phi''+\lambda)\, d\phi''. \tag{B.7}$$

In Gl. B.7 wurde für $B_0(\phi'')$ die Darstellung

$$B_0^m(\phi'') = \sum_{\nu=0}^{4} a_\nu^m \sin^{2\nu}(\phi''+\lambda)$$

eingesetzt. Es ist sofort ersichtlich, dass das mit a_0^m verbundene Integral besonders betrachtet werden muss. Mit Hilfe der Integraldarstellung

$$K_n(\kappa R_{ij}) = \tfrac{1}{2}(\kappa R_{ij})^n \int_0^\infty \exp[-\tfrac{1}{2}(t+(\kappa^2 R_{ij}^2)/t)]\, t^{-n-1}\, dt \tag{B.8}$$

erhalten wir für das erste Glied des Integrals B.7 :

$$I_0 = \frac{a_0^m (\kappa R_{ij})^{4-n} h^2}{\kappa^8} \int_0^{2\pi} \left(\frac{K_n(\kappa R_{ij})}{(\kappa')^{n+2}} (\kappa)^{n+2} + \right.$$

$$\left. + \kappa R_{ij} \cos^2\phi'' \frac{K_{n+1}(\kappa' R_{ij})(\kappa)^{n+1}}{(\kappa')^{n+1}} \right) d\phi''. \tag{B.9}$$

Auf diese Weise ist es gelungen, den in Gl. B.7 auftretenden Nenner $\sin^2(\phi''+\lambda)$ zu beseitigen. Wenden wir nun in Gl. B.9 das Additionstheorem der Besselfunktionen[32] an, so erhalten wir :

$$I_0 = \frac{(\kappa R_{ij})^4 h^2 a_0^m (2)^{3n}}{\kappa^8 (h R_{ij})^{2n}} (\Gamma(n) \sum_{q=0}^{\infty} (n+q) K_{n+q}(Z) I_{n+q}(z) H_q^{(1)} +$$

$$+ \frac{4\kappa^2}{h^2} \Gamma(n+1) \sum_{q=0}^{\infty} (n+q+1) K_{n+q+1}(z) I_{n+q+1}(z) H_q^{(2)}). \tag{B.10}$$

Hierbei bedeuten (C_l^m = Gegenbauersche Funktion) :

$$Z = \tfrac{1}{2}\kappa R_{ij}[1+\sqrt{(1+h^2/\kappa^2)}];$$

$$z = \tfrac{1}{2}\kappa R_{ij}[\sqrt{(1+h^2/\kappa^2)}-1]$$

$$H_q^{(1)} = \int_0^{2\pi} \frac{C_{2q}^n(\cos 2\phi'')}{\kappa^2 + h^2 \sin^2(\phi''+\lambda)}\, d\phi'' \tag{B.11}$$

$$= \sum_{\nu=0}^{2q} \frac{(n)_\nu (n)_{2q-\nu}}{\nu!(2q-\nu)!} \Phi_1^{[q-\nu]}$$

$$H_q^{(2)} = \int_0^{2\pi} \cos^2\phi'' C_{2q}^{n+1}(\cos 2\phi'')\, d\phi''$$

$$= \pi \left(\frac{(n)_q \cdot (n)_q}{(q!)^2} - \frac{(n)_{q-1}(n)_{q+1}}{(q-1)!\,(q+1)!} \right) \tag{B.12}$$

Bei der Integration der Glieder für $\nu > 0$ in Gl. B.7 können wir auf die Integraldarstellung nach Gl. B.8 verzichten und sofort auf $K_p(\kappa' R_{ij})/(\kappa' R_{ij})^p$ das bereits erwähnte Additionstheorem der Besselfunktionen anwenden; dann kann die ϕ''-Integration wieder mit Hilfe der in Gl. B.4 angegebenen Beziehungen durchgeführt werden.

LITERATUR

1. KAUFMANN R., *Phys. Rev.* **55,** 1142 (1939); KAUFMANN R., *Phys. Rev.* **57,** 1084 (1940).
2. BUHL O., *Z. Phys.* **126,** 84 (1949).
3. KNELLER E., *Beiträge zur Theorie des Ferromagnetismus* (Herausgegeben von KÖSTER W.) Springer-Verlag, Berlin (1956).
4. DIETRICH H. und KNELLER E., *Z. Metallk.* **47,** 672 (1956).
5. HUZIMURA T. H., *Sci. Rep. Tohôku Univ.* **A8,** 73 (1956).
6. KRONMÜLLER H., *Z. Phys.* **154,** 574 (1959).
7. BROWN W. F., *Phys. Rev.* **58,** 736 (1940).
8. BROWN W. F., *Phys. Rev.* **60,** 132 (1941).
9. SEEGER A., *Handbuch der Physik* Bd. VII/2. Springer Verlag, Berlin (1958).
10. SEEGER A. und KRONMÜLLER H., *J. Phys. Chem. Solids* **12,** 298 (1960).
11. BROWN W. F., *J. Phys. Radium* **20,** 101 (1959).
12. BROWN W. F., *J. Appl. Phys.* **30,** 62S (1959).

Vol. 19

13. AHARONI A., *J. Appl. Phys.* **30,** 70S (1959).
14. AHARONI A., FREI E. H. und SHTRIKMAN S., *J. Appl. Phys.* **30,** 79S (1959).
15. SEEGER A., DIEHL J., MADER S. und REBSTOCK R., *Phil. Mag.* **2,** 323 (1957).
16. BASINSKI Z. S., *Phil. Mag.* **4,** 393 (1959).
17. HIRSCH P. B., *Internal Stresses and Fatigue in Metals* p. 139 (edited by RASSWEILER G. M. and GRUBE W. L.) Elsevier, Amsterdam (1959).
18. MADER S. und SEEGER A., *Acta Met.* **8,** 513 (1960).
19. SEEGER A. und MADER S., *Trans. Ind. Inst. Metals* (im Druck).
20. REBSTOCK H., *Z. Metallk.* **48,** 206 (1957).
21. BERNER R., Diplomarbeit, Technische Hochschule Stuttgart 1957; DIEHL J. und BERNER R., *Z. Metallk.* **51,** 522 (1960).
22. SEEGER A., BERNER R. und WOLF H., *Z. Phys.* **155,** 247 (1959).
23. WHELAN M. J., *Proc. Roy. Soc.* A**249,** 144 (1958).
24. SAADA G., private Mitteilung; *Acta Met.* (im Druck).
25. MADER S., *Z. Phys.* **149,** 73 (1957).
26. LEIBFRIED G., *Z. Phys.* **130,** 214 (1951).
27. SEEGER A. und SCHÖCK G., *Acta Met.* **1,** 519 (1953).
28. DIETZE H., Diplomarbeit, Göttingen 1949.
29. ESHELBY J. D., FRANK F. C. und NABARRO F. R. N., *Phil. Mag.* **42,** 351 (1951).
30. CORNER W. D. und HUTCHINSON F., *Proc. Phys. Soc. Lond.* **72,** 1049 (1958).
31. YAMAMOTO M. und NAKAMICHI T., *J. Phys. Soc. Japan* **13,** 228 (1958).
32. WATSON G., *Theory of Bessel Functions.* Cambridge University Press (1952).

Vol. 18
1961

J. Phys. Chem. Solids Pergamon Press 1961. Vol. 18, Nos. 2/3, pp. 116–128. Printed in Great Britain.

COMPOSITION STABILITY LIMITS OF BINARY SEMICONDUCTOR COMPOUNDS

R. F. BREBRICK

U.S. Naval Ordnance Laboratory, White Oak, Silver Spring, Maryland

(*Received* 10 *May* 1960)

Abstract—The composition stability-limits of an essentially-ordered, non-degenerate, semiconductor crystal, MN, showing small deviations from stoichiometry, are investigated under the conditions (1) that clustering of atomic point-defects is unimportant, (2) the predominant atomic point-defects are M-vacancies and N-vacancies, (3) each M-vacancy is associated with one acceptor level and each N-vacancy with one donor level, and (4) the coexisting phase is one or the other of the pure elements M or N. Characterizing a limit of stability by the corresponding value of the net relative electron concentration, $(n-p)/2n_i$, it is found that the magnitude of the stability range is larger the more negative the standard free energy of formation of the compound and the larger the intrinsic disorder ratio. The latter is the square root of the Schottky constant for ionized vacancies divided by the intrinsic carrier concentration. The parameters determining the position of the stability range are also given.

The effects of singly ionized foreign donor and acceptor impurities on the limits of stability are considered for the same crystal model under the restriction that the foreign impurity does not significantly alter the Gibbs free energy per gram-atom of the coexisting phase. The behavior of the net relative electron concentration as a function of the concentration of ionized foreign impurities depends on the value of the former concentration in the pure compound and on the intrinsic disorder ratio. There is an asymmetry in the effects of donors and acceptors that can be large. Donor impurities are more effective in increasing the net relative electron concentration at a positive limit of stability ($n > p$) than acceptor impurities are in decreasing it. The converse holds at a negative limit of stability.

1. INTRODUCTION

A PURE CRYSTALLINE semiconductor compound can exist over a range of composition by the inclusion of atomic point defects. The latter are often associated with donor or acceptor levels in the forbidden gap of the electronic energy band structure so that electrical measurements can be used to detect composition changes whose magnitudes cannot be determined by conventional analytical techniques. KROGER and VINK[1,2] have extended the earlier theory of SCHOTTKY and WAGNER relating the concentrations of point defects in an essentially ordered compound showing small deviations from the stoichiometric composition. The experimental results on a number of compounds have been successfully interpreted[3,4,5] with the extended theory. For a given model of a non-degenerate semiconductor compound the appropriate mass action law equations and the equation for electrical neutrality are solved approximately by a graphical method. The concentration of each type of point defect is thereby obtained as a function of the temperature and (for a binary compound) partial pressure of one gaseous species of one crystal component. The various energies quantitatively characterizing the crystal model appear as parameters in this functional dependence. However, the theory is that of a single phase and in itself says nothing concerning the question of the range over which the phase is stable. It is the purpose here to examine this question.

In order to obtain specific results some assumptions concerning the thermodynamic properties of the semiconductor crystal and the phases coexisting at either limit of stability must be made. The treatment is simplified by considering those situations in which the coexisting phase is one or the other of the pure elements. The semiconductor

crystal, MN, is characterized by expressions for the chemical potentials of the crystal components M and N which follow from a statistical mechanical analysis.[6] As has been shown such an analysis leads to the mass action law equations used as a starting point by KROGER and VINK. The limits of stability for the semiconductor compound can then be obtained in terms of energy terms associated with the creation of the predominant point defects in the compound and the molar Gibbs free energies of the compound and the pure elements. The approach is different from that used for systems showing relatively wide ranges of stability in which nearest neighbor interaction and consequent possible clustering of atomic point defects limit the stability range.[7,8] In an essentially-ordered compound semiconductor the chemical potentials of the crystal components can be very strong functions of composition[6] and consequently the limits of stability can be attained before or near the point at which clustering becomes important. The effect of foreign atoms that act as donors or acceptors is then considered.

Vol. 18
1961

For simplicity an essentially-ordered binary semiconductor MN is considered. It is assumed that (1) the predominant point defects are vacancies in the two sublattices, (2) each M vacancy (N vacancy) is associated with one acceptor (donor) level, and (3) the semiconductor is non-degenerate. As is the case in the theory[1,2] relating the concentrations of point defects the results are formally the same if (1) is altered by considering certain other point defect pairs. The four possibilities arise by taking N vacancies or M interstitials to be associated with donor levels and either M vacancies or N interstitials to be associated with acceptor levels. Assumptions (2) and (3) seem to be necessary if the results are to be obtained in analytical form. The problem though simplified in this way is still physically interesting since a number of semiconductors fit the assumptions over a broad range of conditions.

2. CHEMICAL POTENTIALS OF SEMICONDUCTOR-CRYSTAL COMPONENTS

At each temperature the standard state relative to which all chemical potentials and free energies are measured is the monatomic gaseous elements each at one atmosphere and considered ideal unless stated otherwise. If the vapor phase in equilibrium with the semiconductor crystal, MN, is ideal, the chemical potentials of the M and N components as given respectively by equations. (A.8a) and (A.8b) of the Appendix can be written as

$$\mu_M = RT\ln P_M = RT\ln S/V_M + \\ + (E_f - E_a) - E_M - RT\ln K'_M - \mu^0_M \quad (1a)$$

$$\mu_N = RT\ln P_N = RT\ln S/V_N - \\ -(E_f - E_d) - E_N - RT\ln K'_N - \mu^0_N \quad (1b)$$

where P_M and P_N are respectively the partial pressures of gaseous, monatomic M-component and gaseous monatomic N-component in equilibrium with the crystal; V_M and V_N are respectively the concentrations of ionized M-vacancies and ionized N-vacancies; S is the constant concentration of lattice sites in each sublattice; E_f, E_a, and E_d are respectively the energies of the Fermi level, the acceptor level associated with each M-vacancy, and the donor level associated with each N-vacancy; K'_M and K'_N are respectively contributions of the lattice vibrations given by equation (A.6) of the Appendix for a simple Einstein model; and E_M and E_N are respectively the energies per mole to create unionized M-vacancies and unionized N-vacancies. More precisely E_M is the energy on a per mole basis to remove one M-atom from the crystal to infinity in its lowest quantum state leaving an unionized M-vacancy in the crystal, the concentrations of all other point defects being held constant except phonons which are allowed to assume an equilibrium distribution. The quantities μ^0_M and μ^0_N refer to respectively the ideal monatomic gases M and N and are the chemical potentials at one atmosphere measured relative to the infinitely dispersed atoms in their lowest quantum state. The composition dependence of the chemical potentials resides in their dependence on the concentration of ionized vacancies and on the Fermi level. The Fermi level for a non-degenerate semiconductor is given by the equation:

$$E_f = E^i_f + RT\sinh^{-1} y \quad (2)$$

where E^i_f is the intrinsic Fermi level[9] and y is given by

$$y \equiv (n-p)/2n_i \quad (3)$$

The concentrations of conduction band electrons and valence band holes are n and p respectively. The concentrations of electrons and holes in the intrinsic semiconductor are each given by n_i, the intrinsic carrier concentration. Thus the reduced variable y is the net relative concentration of electrons. The concentrations of ionized vacancies may be obtained in terms of y by means of the mass action law equation for ionized vacancies given by:

$$V_M V_N = k_s \tag{4}$$

and the equation for electrical neutrality given by

$$[(V_N - V_M)/2n_i] + D = y \tag{5}$$

where D is the concentration of ionized foreign donors less the concentration of ionized foreign acceptors all divided by twice the intrinsic carrier concentration and where it is assumed that the impurities are not multiply ionized. The result is

$$\ln(V_N/k_s^{1/2}) = -\ln(V_M/k_s^{1/2}) = \sinh^{-1}[(y-D)/\alpha] \tag{6}$$

where the "intrinsic disorder ratio" α is the square root of the Schottky constant, k_s, divided by the intrinsic carrier concentration, n_i. For a semiconductor which conducts primarily by electrons and holes rather than by ions the intrinsic disorder ratio cannot be too large. A typical range of values is illustrated[3] by PbS in which α varies from 0·05 to 0·7 for temperatures between 800° and 1350°K. Substituting equation (2) and (6) into equation (1a) one obtains,

$$\begin{aligned}\mu_M = {} & RT \sinh^{-1}[(y-D)/\alpha] + \\ & + RT \sinh^{-1} y + (E_f^i - E_a) - RT/2 \ln k_s - \\ & - E_M + RT \ln(S/K_M') - \mu_M^0.\end{aligned} \tag{7}$$

In what follows it will be useful to have an analogous expression for the difference in the chemical potentials given by

$$\begin{aligned}\mu_N - \mu_M = {} & -2RT \sinh^{-1}[(y-D)/\alpha] - \\ & - 2RT \sinh^{-1} y - (2E_f^i - E_a - E_d) + \\ & + (E_M - E_N) + RT \ln K_M'/K_N' + (\mu_M^0 - \mu_N^0)\end{aligned} \tag{8}$$

where $(E_M - E_N) - (2E_f^i - E_a - E_d)$ is the difference in the energy to create an M-vacancy and that to create an N-vacancy in the intrinsic crystal; and K_M'/K_N' is a temperature independent ratio of frequencies in the high temperature limit (equation A.7). The expressions for the chemical potentials given by equations (7) and (8) depend on composition only through the first two terms of the right-hand members. The intrinsic carrier concentration and the square root of the Schottky constant determine the magnitude of change in the concentration, $n-p$, necessary to alter significantly the chemical potentials. Since these constants are often very small relative to the concentration of atoms, very small changes in atom concentrations can exert large effects on the chemical potentials. The composition dependence of the chemical potential given by equation (7) reduces to that recently used[10] by WAGNER to analyze experimental results of the solid state coulometry technique when one considers a pure crystal, $D = 0$, and a much higher intrinsic disorder of atoms than electrons, $\alpha = \infty$.

The net relative electron concentration is chosen as a measure of crystal composition rather than the mole fraction of one crystal component since it corresponds more closely to what is measured experimentaly in semiconductor compounds showing only small deviations from stoichiometry. Provided all the donors and acceptors are ionized, the mole fraction of either component may easily be obtained for the pure crystal using equation (5) to obtain first the deviation from stoichiometry, $C_M - C_N$. For the impure crystal the net relative concentration of ionized foreign donors must also be known.

3. LIMITS OF STABILITY OF PURE COMPOUND

At constant temperature and pressure the criterion of thermodynamic equilibrium is that the chemical potential of each component of the system must be the same in each phase. This leads to the expression:

$$\mu_N - \mu_M = \left(\frac{\Delta F}{\Delta x}\right) \tag{9}$$

where $\Delta F = F' - F$; $\Delta x = x' - x$; F' is the free energy per gram atom of the coexisting phase; F is that of the binary-compound semiconductor; x' is the atomic fraction of component N in the coexisting phase; x is that in the semiconductor.

There are two equations of the form of equation (9), one for both the M-rich and N-rich limits of stability of the semiconductor compound. The coexisting phases will, of course, be different in the two cases. A well-known schematic representation[11] is given in Fig. 1, where the isothermal

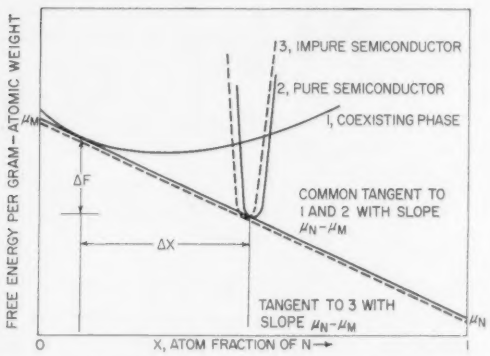

FIG. 1. Schematic diagram of isothermal free energies per gram-atomic weight of coexisting phase, pure semiconductor, and impure semiconductor as a function of composition. Dashed curves are in reference to impurity effects.

Gibbs free energy of one gram-atom of the semiconductor compound and that of one coexisting phase is plotted against the atom-fraction of component N. The equilibrium compositions of the two phases are determined by the point at which the free energy curves are tangent to a common straight line whose slope is $\mu_N-\mu_M$. A basic assumption in the theory of point defects in essentially ordered crystals is that the range of stability is small enough at any one temperature that the Gibbs free energy per gram atom is equal to one-half the sum of the chemical potentials of the M and N components of the compound MN and this sum is a function of temperature only. The individual chemical potentials and their difference can change significantly with composition, however, as seen by equations (7) and (8).

In order to proceed with equation (9) further consideration is restricted to those cases in which the phases coexisting with the semiconductor compound at either limit of stability are of "fixed" compositions. For concreteness consider these phases to be the pure elements M and N. "Fixed" composition then means that the M-rich phase in equilibrium with the compound contains so little of component N that the composition difference, Δx, appearing in equation (9) differs only negligibly from $-\frac{1}{2}$ and the gram-atomic free energy F' differs negligibly from that of the pure element M. Equation (9) can then be written as:

$$\mu_N-\mu_M = \pm\Delta F^*_{MN}+(F^0_N-F^0_M) \qquad (10)$$

where ΔF^*_{MN} is the change in Gibbs free energy in forming one mole of the compound MN from the elements; F^0_N is the molar Gibbs free energy of the element N relative to gaseous, monatomic N at one atmosphere and considered ideal, and F^0_M is the analogous quantity for element M. The upper sign of the first term of the right-hand member of equation (10) is to be taken for the M-rich limit of stability and the lower, negative sign, for the N-rich limit. Substituting equation (8) with the net relative donor concentration, D, set equal to zero into equation (10) gives the desired result as:

$$2RT(\sinh^{-1}y/\alpha+\sinh^{-1}y) = -\Delta F^*_{MN}+a; \quad M\text{-rich} \qquad (11a)$$

$$2RT(\sinh^{-1}y/\alpha+\sinh^{-1}y) = \Delta F^*_{MN}+a; \quad N\text{-rich} \qquad (11b)$$

where y in the upper equation is the value of the net relative electron concentration, $(n-p)/2n_i$, at the M-rich limit of stability, y in the lower equation is the value at the N-rich limit; and the parameter a is given by:

$$a = (E_M-E_N)-(2E^t_f-E_a-E_d)+ +RT\ln K'_M/K'_N+(F^0_M-F^0_N)+(\mu^0_M-\mu^0_N). \qquad (12)$$

Only negative values of the free energy of formation ΔF^*_{MN} are significant since only for these values is the compound a stable phase.

The limits of stability determined by equations (11) are wider apart the more negative ΔF^*_{MN} is and the larger the intrinsic disorder ratio, α, is. This is readily understood since the more negative the free energy of formation, the greater the excess of component M or N that can be incorporated into the crystal before the chemical potential of M or N is increased to that of the pure element. On the other hand, any increase in the net relative

Vol. 18
1961

electron concentration, y, must be compensated by an identical increase in $(V_M - V_N)/2n_i$ in the pure crystal (equation 5). This latter change is more effective in increasing the chemical potential of M in the crystal when the intrinsic disorder ratio is small, as can be seen from equation (7). Thus, in two semiconductor compounds with the same free energies of formation and the same intrinsic carrier concentrations, the limits of stability (as measured by net relative carrier concentrations) are wider apart in the compound that has the larger Schottky constant, i.e. in the compound in which less energy is required to create the atomic point defects.

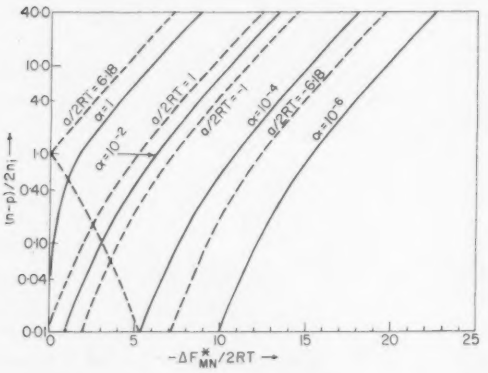

FIG. 2. Net relative electron concentration at a limit of stability as a function of the free energy of formation per gram-molecular weight of compound (equations 11 and 12). Solid curves are for a equal to zero and the labeled value of α; dashed curves are for the labeled values of $a/2RT$ and $\alpha = 10^{-2}$.

The position of the range of stability is determined by the sign and magnitude of the parameter a divided by $2RT$. Positive values of a tend to shift both limits of stability in the direction of increasing concentration of electrons and component M. Negative values do the opposite. The value of a is more positive the larger the energy to create an M-vacancy in the intrinsic crystal is than that required to create an N-vacancy. It is also more positive the larger the molar free energy of M measured relative of the infinitely dispersed atoms in their lowest quantum state is than that of N (last two terms of equation 12). The free energies of the elements relative to the standard state chosen here are simply

$$F_M^0 = RT \ln P_M^0; \qquad F_N^0 = RT \ln P_N^0$$

where P_M^0 is the partial pressure of gaseous monatomic, M-component in equilibrium with the pure element M and P_N^0 is the analogous quantity for the pure element N.

To illustrate some of the above points, the limits of stability given by equation (11) are plotted in Fig. 2 against the molar Gibbs free energy of formation for a few values of the parameters α and a. Only positive values of the net relative electron concentration are shown.

4. IMPURITY EFFECTS ON THE LIMITS OF STABILITY

Theory

In this section the assumption made in the last section that the semiconductor compound is in equilibrium with one or the other of its pure elements is discarded. As usual, it is assumed that the concentration of impurities in the semiconductor compound is small enough that the molar Gibbs free energy is negligibly different from that of the pure intrinsic compound. The limits of stability in the presence of an impurity are then related to those in the pure compound by the following:

$$\mu_M \text{ (with impurity)} = \mu_M \text{ (pure compound)} \tag{13a}$$

$$(\mu_N - \mu_M) \text{ (with impurity)} = (\mu_N - \mu_M) \text{ (pure compound)} \tag{13b}$$

If the impurity is imagined to be confined to the semiconductor compound, equation (13a) is exact. Moreover, a similar equation for component N and therefore equation (13b) are also valid. Such a partial equilibrium might be attained in practice when impurity diffusion is much slower than interdiffusion. However, equation (13b) can be a good approximation under less restrictive conditions as will be indicated qualitatively below. In this case (equation 13a) is also approximately true since the gramatomic free energy of the compound is approximately independent of composition for small impurity contents and deviations from stoichiometry. Suppose the impurity distributes itself between the semiconductor compound and the

coexisting M-rich phase. The atom fraction scale in Fig. 1 is now calculated ignoring the impurity. The isothermal Gibbs free energy per gram atom of the coexisting phase is assumed to be essentially unchanged but is now drawn for the equilibrium impurity content. The weak composition dependence of this free energy isotherm is due to the assumed high intrinsic disorder of the coexisting phase. The isothermal Gibbs free energy of the semiconductor compound must be shifted slightly since the chemical potentials of M and N, and therefore the slope of the free energy isotherm, for a given "atom fraction" are altered by the influence of electrically active impurities on the Fermi level (equation 5). In Fig. 1 this is shown arbitrarily as a horizontal shift of the isotherm with no change in shape. At some "atom fraction" the isotherm for the impure compound has the same slope as the isotherm for the pure compound at the M-rich limit of stability of the latter as shown in Fig. 1. At this composition the tangent to the isotherm for the impure compound is not generally simultaneously tangent to the isotherm for the coexisting phase. However, a simultaneous tangent will be found at a slightly different composition, the difference being smaller the larger the difference in the "atom fractions" of the coexisting phases and the stronger the composition dependence of the isotherm for the impure semiconductor compound. Therefore in practice one expects equations (13a) and (13b) to be a good approximation even when the impurity is present in both coexisting phases provided the impurity content is small and the temperature is far enough below the invariant melting point of the semiconductor compound.

Substituting equation (7) into equation (13a) and equation (8) into equation (13b) gives the common desired result:

$$\sinh^{-1}[(y-D)/\alpha]+\sinh^{-1}y = \sinh^{-1}y_0/\alpha+\sinh^{-1}y_0 \qquad (14)$$

where y_0 is the relative net electron concentration [equation (3)] at either limit of stability of the pure compound; and y is that at the corresponding limit of stability for the impure compound. The behavior of the limit of stability in the impure compound, y, is shown in Fig. 3 as a function of the net relative concentration of ionized donors in the compound for various values of y_0 (the intercept on the y-axis) and the intrinsic disorder ratio α. Unless there is a zero range of stability, there will be two curves, one for either limit of stability, associated with a particular compound at a given temperature. As seen from equation (14), for a given value of α the curve for one value of y_0 is related to that for $-y_0$ by a center of inversion through the origin. This is illustrated in Fig. 3 by the curves for y_0 equal to $+10$ and -10. For absolute values of y_0, larger than about 5, the parameter α is unimportant in the range zero to unity, which is probably typical of a large number of semiconductors with not too large a forbidden energy gap. The large asymmetry in the effects of donors and acceptors on a limit of stability is to be noted. If the net relative electron concentration is positive at one limit of stability of the pure semiconductor, the addition of donor impurities increases this concentration. For values of α between zero and unity the net relative electron concentration soon reaches one-half to one times the net relative donor concentration, depending on the exact value of α and y_0. The addition of acceptors on the other hand decreases the net relative electron concentration more slowly. Asymptotically the (negative) net relative electron concentration varies linearly with, but may be only a small fraction of, the (negative) net relative donor concentration, the fraction depending on the exact value of α and y_0. For values of y_0 greater than unity, the net relative concentration of ionized acceptors required to make the crystal intrinsic is approximately $2y_0^2$ for $\alpha \leqslant 1$. One would say qualitatively that at a positive limit of stability donor impurities are more effective in adding electrons to the crystal than acceptor impurities are in adding holes. The reverse of course holds at a negative limit of stability.

Alloy impurities

In the above foreign impurities which have one donor or acceptor level associated with each atom have been considered. Consider an "alloy" impurity which enters the lattice of the semiconductor compound substitutionally for either the M or N atom but has no impurity level associated with it. This might be the case when the valence shell of the impurity atom is similar to that of the substituted atom. Oxygen, selenium, and tellurium

Vol. 18
1961

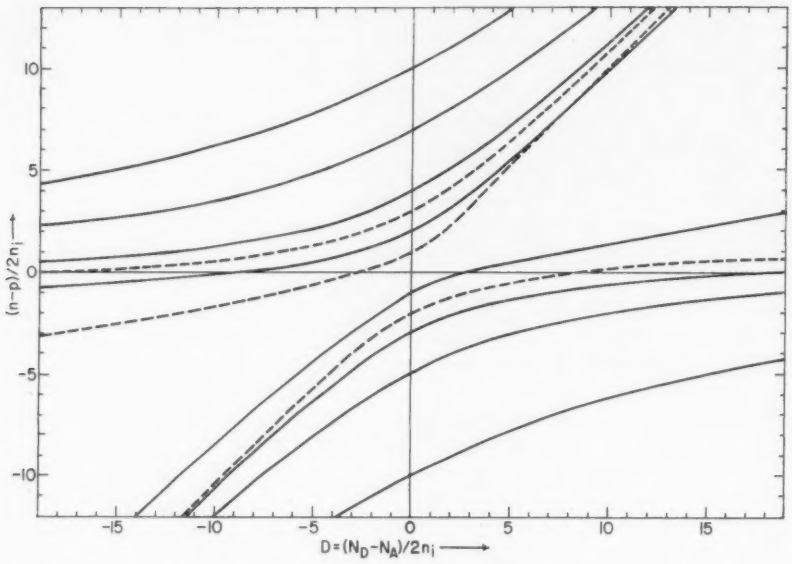

FIG. 3. Net relative electron concentration at a limit of stability as a function of the net relative concentration of ionized, foreign donor impurities. The solid lines are for a value of α of unity. The dashed lines are for a value of α equal to 10^{-2}.

impurities in lead sulfide would be expected to be examples. The concentration of impurity then does not enter equation (5) expressing the condition for electrical neutrality. Therefore, the effect of this type of impurity on the net relative electron concentration is given by equation (14) with D set equal to zero. In other words, the net relative electron concentration at a limit of stability is unchanged by the presence of the impurity! The impurity concentration must be small enough, of course, not to change significantly the basic properties of the host lattice or the free energy of the coexisting phase. The reason for the above result is as follows. In the approximation used here the chemical potentials of the crystal components are assumed fixed at a limit of stability independent of the impurity content. The impurity atoms occupy N-sites in the lattice, say. Since the chemical potential of component N depends on the concentration of N-vacancies and not on that of N-atoms, the same concentration of N-vacancies and donor levels and hence M-vacancies and acceptor-levels will result with and without the "alloy" impurity.

Internal structure of the solidus field

Impurity effects for crystal compositions within the limits of stability have been considered by KROGER and VINK[2] and an approximate graphical solution given. An analytical solution can be given for the special case considered here (assumption (2) in the Introduction). One asks how the net relative concentration of electrons is affected by the presence of electrically active impurities when the chemical potential of one crystal component is held fixed, i.e. when the partial pressure of one gaseous species of one component is held constant. Using equations (1a), (1b) and (7), the partial pressures are given by the equations:

$$(1/r)\ln(P_{M_r}/P^{i}_{M_r}) = (1/s)\ln(P^{i}_{N_s}/P_{N_s}) = \sinh^{-1}\left(\frac{y-D}{\alpha}\right) + \sinh^{-1} y \qquad (15)$$

where $P^{i}_{M_r}$ is the partial pressure of gaseous r-atomic M-component in equilibrium with the intrinsic crystal, $y = 0$; $P^{i}_{N_s}$ is the analogous quantity for gaseous, s-atomic M-component, and the other terms are as previously defined. If the

electronic energy band structure is neglected and all electrons are considered to belong to atoms or ions, only the first term of the right-hand member of equation (15) occurs with $D = 0$. (Ref. 8, p. 37.)

The partial pressures of the crystal components in equilibrium with the intrinsic compound have been obtained[12] in terms of the energy parameters of the crystal model and the free energy of formation of the compound. However, the chemical potentials relative to the atoms at infinite dispersion as given by equations (A.1a) and (A.1b) were incorrectly identified as chemical potentials relative to the monatomic gases at one atmosphere and considered ideal, equations (A.8a) and (A.8b). Moreover, the energies required to create lattice vacancies were incorrectly identified as indicated in the Appendix. The partial pressure of monatomic N-component in equilibrium with the intrinsic crystal is obtained from equations (1a) and (1b) and equation (2) of Ref. (12) as

$$2RT \ln P_N^i = F_{MN} + (E_M - E_N) - \\ -(2E_f^i - E_a - E_d) + RT \ln K_M'/K_N' + (\mu_M^0 - \mu_N^0) \quad (16)$$

where F_{MN} is the molar Gibbs free energy of the compound MN relative to the standard state of gaseous, monatomic components at one atmosphere and considered ideal. If the last term is ignored and if E_f^i is arbitrarily set equal to zero, equation (16) is equivalent to its analog, equation (6) of Ref. (12). However, the treatment here shows that the validity of equation (16) is independent of whether the semiconductor compound is simultaneously intrinsic and stoichiometric and that the energies to create atomic point defects enter as the difference in the energy to create an M-vacancy in the *intrinsic* compound and that to create an N-vacancy.

Equation (15) can be used to give the internal structure of the solidus field of the semiconductor as exhibited by lines of constant net carrier concentration.* The equation can also be used to determine the limits of stability, for the pure semiconductor regardless of the atomic ratio of M to N in the coexisting phases, provided the vapor phase is ideal and the appropriate partial pressures are known. In this sense equation (15) is a generalization of equations (11a) and (11b) and reduces to them when the coexisting phases are the pure elements.

Comparison with elemental semiconductors

The solubility of a given electrically active impurity in an elemental semiconductor is influenced by the presence of a second electrically active impurity in a manner somewhat analogous to the effect of impurities on the limits of stability in compound semiconductors. The theory has been given by REISS and FULLER[13] under the assumptions that the second impurity is present only in the semiconductor crystal and the influence of native atomic point defects is negligible. The experimental solubility of lithium in boron-doped germanium follows the theory quite well. KROGER and VINK[2] have given a discussion of the same problem using the graphical method. For comparison with the behavior of semiconductor compounds, the result of REISS and FULLER[13] is rewritten to give

$$\ln(y - D') + \sinh^{-1} y = \ln y_0 + \sinh^{-1} y_0 \quad (17)$$

where y_0 is the relative net electron concentration when the otherwise pure elemental semiconductor is saturated with a given impurity, and y is that when there is a fixed net relative concentration of ionized foreign donors, D', in the crystal, exclusive of that of the impurity whose solubility is in question. Equation (14) is the analogous result for the semiconductor compound giving a measure of the solubility of atomic point defects native in the pure crystal as a function of impurity content. The inverse hyperbolic sine terms common to both equations arises from a common dependence of the chemical potential of an impurity in an elemental semiconductor and that of a crystal component of a semiconductor compound on the Fermi level. The logarithmic terms in equation (17) follow from the dependence of the chemical potential of an impurity in an elemental semiconductor on the logarithm of the concentration of that impurity in the ionized state. This concentration is linearly related to the concentration, $y - D'$, through the equation for electrical neutrality. In the semiconductor compound the chemical potential of one

* Fig. 4 of Ref. (4) gives the experimentally determined internal structure for PbS. Since for PbS the donor and acceptor levels are all ionized the net carrier concentration is equal to the difference in the Pb and S concentrations.

Vol. 18
1961

of the crystal components depends not on the logarithm of the concentration of that component but on that of the ionized atomic point defect related to that component. In turn this latter concentration depends quadratically on the concentration, $y-D$, through the equation for electrical neutrality and the mass action law equation coupling the concentrations of the two predominant atomic point defects in the ionized state (equations 1, 4, 5, 6). As a result another inverse hyperbolic sine term enters equation (14) in both members.

5. COMPARISON WITH EXPERIMENT

Among compound semiconductors with ranges of stability small enough that the basic theoretical assumptions might be valid, PbS is probably the best understood. Attention will therefore be confined to it with some remarks about PbSe and PbTe. In all three compounds excess lead leads to n-type behavior so that the place exchange type of point defect is not predominant. The donor and acceptor levels associated with deviations from stoichiometry and the few impurities investigated systematically are ionized at room temperature and above so that the high temperature value of $(n-p)$ is unchanged by quenching to room temperature, (assuming quenching freezes the concentrations of atomic point defects). High temperature properties can therefore be simply interpreted in terms of room temperature electrical measurements. Finally there is only one donor or acceptor level associated with each point defect in PbS and this appears to be true for PbSe and PbTe also.

Internal structure of the solidus field for PbS

The internal structure of the PbS solidus field has been determined in pure and doped crystals between 1000° and 1223°K by BLOEM[3]. Analysis by the graphical method, equivalent in principle to fitting the experimental data with equation (15), gave the intrinsic carrier concentration as $n_i = 10^{15\cdot2}T^{3/2}\exp(-E/kT)$ with $E = 0{\cdot}33$ eV; the Schottky constant as $k_s = 10^{43\cdot4}\exp(-E/kT)$ with $E = 1{\cdot}75$ eV, and the partial pressure of diatomic sulfur in equilibrium with intrinsic PbS as $\log p^i_{S_2}(\text{atm}) = -[7{\cdot}48(10^3)/T]+5{\cdot}04$. The extrapolated value of $p^i_{S_2}$ agrees well with that calculated from the work of BREBRICK and SCANLON[14] at 773°K using the vapor pressure of sulfur given by WEST[15]. The extrapolated lines of constant net electron concentration, $n-p$, do not agree well, however. Knowing $p^i_{S_2}$ as a function of temperature and the free energy of formation of PbS the difference in the energies to create Pb-vacancies and S-vacancies in the intrinsic crystal and the quantity $\log(K'_{Pb}/K'_s)$ can be obtained.* The values are respectively $+0{\cdot}4$ eV and 2·0 with the free energy of formation used by BLOEM and KROGER[3,4], and respectively $+0{\cdot}3$ eV and 1·21 with the free energy of formation recently determined by STUBBLES and BIRCHENALL[17].

Limits of stability for PbS

The limits of stability of PbS have been determined[4] between 1000°K and 1400°K (the invariant melting point) on the Pb-rich, n-type side and 833° and 1400°K on the S-rich, p-type side. The maximum deviations from stoichiometry occur at about 1360°K on the Pb-rich side and 1110°K on the S-rich side; the corresponding room temperature carrier concentrations are respectively $1{\cdot}6\times10^{19}$ electrons/cm^3 and $6{\cdot}5\times10^{18}$ holes/cm^3. The limits of stability between 560 and 1000°K have been calculated using equation (15) with the values of k_s and $p^i_{S_2}$ obtained from the formulae above, the partial pressure of diatomic sulfur in saturated sulfur vapor,[15,17] the vapor pressure of lead,[18] the free energy of formation of PbS,[16,19] and intrinsic carrier concentrations below 800°K given by $n_i = 10^{13\cdot92}T^{3/2}\exp(-E/kT)$ with $E = 0{\cdot}129$ eV. The latter corresponds to a room temperature value[20] for n_i of 3×10^{15}, and a room temperature energy gap[21] of 0·37 eV which increases[22] by $3{\cdot}7\times10^{-5}$ eV per degree Kelvin as the temperature increases. The value of n_i given by this formula agrees with that given by the above expression from the work of BLOEM and KROGER at 800°K. The limits of stability obtained agree within a factor of two or less with the experimental data in the overlapping temperature range. At lower temperatures they agree with a linear extrapolation of the experimental values (Ref. 4, Table 1) obtained on a plot of the logarithm of the room temperature carrier concentration against reciprocal equilibrium temperature. The fact that the melt in equilibrium with S-rich PbS contains 5

* Using equation (16) and assuming K'_{Pb}/K'_s is temperature independent.

atomic per cent[4] or more Pb above about 800°K means that the calculated S-rich limit of stability should be somewhat high.

The limits of stability of PbS can also be understood in terms of equations (11) and (12). Of particular interest is the fact that the difference in the free energies of elemental lead and sulfur referred to the atoms at infinite dispersion (last two terms of equation 12) is positive,[19] being 0·34 eV at 300°K and 0·13 eV at 800°K. Along with the positive signs of the other quantities determining a in equation (12), this accounts for the fact that the range of stability lies primarily on the Pb-rich, n-type side of the stoichiometric composition in PbS. In contrast the corresponding differences for Pb and Se and Pb and Te vary respectively between $+0{\cdot}05$ and $-0{\cdot}04$ eV and $-0{\cdot}05$ and $-0{\cdot}11$ eV over the same temperature interval. Other things being equal, one therefore expects the range of stability to be shifted away from the Pb-rich side in going from PbS to PbTe. In PbTe the limits of stability have been determined between 673° and 1148°K and the stability range has been found to lie primarily on the Te-rich, p-type side.[23] In PbSe the limits of stability have been determined[24] for a temperature interval only some 30°C below the invariant melting point but would be expected to be more symmetrical about the stoichiometric composition at low temperatures than is the case for PbS or PbTe.

Impurity effects on the limits of stability on PbS, PbSe *and* PbTe

Ingots of PbS containing just enough excess lead to insure the presence of a second condensed phase have been fused with varying amounts of impurities, annealed between 813° and 1088°K under inert atmospheres in sealed tubes, quenched, and room temperature resistivity and thermoelectric power measured.[25] At room temperature the second phase did not substantially affect the electrical properties of the ingot. It was found that small amounts of selenium and tellurium impurities did not affect the electrical properties so that as expected they may be considered to be alloy impurities. The results for other impurities are given as room temperature thermoelectric power vs. weight per cent impurity added for an unspecified anneal temperature in the above range. They are in at least qualitative agreement with equation (14) for some impurities. It was found that the thermoelectric power of the n-type base material decreased linearly as the logarithm of the weight per cent of Cl and I between about 10^{18} and 10^{19} electrons/cm^3. On the other hand, the amount of Na, K, Rb, or Ag required to make the original (5×10^{17}–10^{18} electrons/cm^3 at room temperature) PbS intrinsic corresponded to 4×10^{19}, $4{\cdot}4\times10^{19}$, 1×10^{20}, and $1{\cdot}4\times10^{20}$ atoms/cm^3 respectively. From the work of BLOEM and KROGER[3,4] the net relative electron concentration (equation 3) in pure PbS at the Pb-rich limit of stability and the intrinsic disorder ratio are respectively 7·6 and 0·05 at 800°K and 3 and 0·3 at 1100°K. Inserting these values into equation (14) it is found that the net relative acceptor concentrations required to compensate PbS at its Pb-rich limit of stability are 115 at 800°K and 18 at 1100°K. Assuming no foreign donor impurities these numbers correspond to respectively 6×10^{19} and 2×10^{19} acceptors/cm^3.

Analogous experiments have been made[26] at the Pb-rich limit of stability of PbSe but are not discussed here because of a lack of data on the pure compound and a failure to specify the anneal temperature for which the quantitative results on impurity addition are given. Analogous experiments have also been made at 500°C at both the Pb-rich and Te-rich limits of stability of PbTe.[27] It was found that oxygen (added as 10^{19} to 10^{20} atoms/cm^3 of PbO or TeO_3), selenium, and sulfur impurities resulted in practically the same room temperature carrier concentrations as obtained with undoped PbTe, $4{\cdot}5\times10^{18}$ holes/cm^3 for Te-rich PbTe and 7×10^{17} electrons/cm^3 for Pb-rich PbTe. These are alloying impurities as discussed in Section IV. With the addition of bismuth or chlorine to PbTe at the Pb-rich limit of stability the room temperature electron concentration increased linearly. In the range 2×10^{18} to 20×10^{18} atoms/cm^3 of Cl, the room temperature concentration of electrons is approximately equal to that of added Cl. Addition of chlorine to PbTe at the Te-rich limit of stability was said to scarcely change the room temperature concentrations although no quantitative results are given. On the other hand addition of silver at the Te-rich limit of stability increased the room temperature concentration of holes. The latter was approximately 0·6 of the concentration of added Ag in the range 4×10^{18} to

Vol. 18
1961

20×10^{18} atoms Ag/cm^3. Equation (14) would predict that the hole concentration obtained at the Te-rich limit of stability at 500°C with a given concentration of foreign acceptors is higher than the electron concentration obtained at the Pb-rich limit of stability with the same concentration of foreign donors, in contrast to the experimental results with Cl and Ag. The discrepancy may be due to a preferential concentration of Ag in the Te-rich phase so that the concentration of added Ag is not the concentration of Ag in solid solution in PbTe.

Acknowledgement—The author wishes to acknowledge a helpful discussion with R. F. GREENE concerning the vibrational contributions to the partition function and the significance of the energy parameters discussed in the Appendix.

APPENDIX

Significance of energy parameters

The symbols used here differ slightly from those used previously by the author,[6,12] the change usually being a simplification. Moreover, a terminology that would imply an unnecessary restriction of the crystal model to crystals with purely ionic binding is avoided. No change in the equations describing the model are rendered necessary thereby. The chemical potentials of the crystal component are given by equations (18a) and (18b) of Ref. (6). In terms of the symbols used here they are

$$\mu_M = RT \ln S/V_M + E_f - \zeta_M + U - RT \ln K_M \tag{A.1a}$$

$$\mu_N = RT \ln S/V_N - E_f - \zeta_N + U - RT \ln K_N \tag{A.1b}$$

where S is the constant concentration of lattice sites in each sublattice; V_M and V_N are respectively the concentrations of ionized M-vacancies and ionized N-vacancies; E_f is the Fermi level; $2U$ is the lattice energy per mole of the perfect crystal relative to the infinitely dispersed atoms in their lowest quantum states, $RT \ln K_M$ and $RT \ln K_N$ are the contributions respectively of the M-atoms and the N-atoms to that part of the free energy of the crystal associated with lattice vibrations; and ζ_M and ζ_N comprise parts of the energies required to create respectively M-vacancies and N-vacancies. It is the purpose here to replace the energies ζ_M and ζ_N by simpler quantities and to illustrate the quantities K_M and K_N for a simple case. The meanings of the energies ζ_M and ζ_N have been inaccurately described by the author previously.[12]

The quantities K_M and K_N can be evaluated for a simple Einstein model of the lattice vibrations[28] in which the introduction of each M-vacancy (N-vacancy) results in the loss of three modes of frequency $\nu_M(\nu_N)$ and the replacement of a small number, r, of modes of the same frequency by an equal number of frequency $\nu_M'(\nu_N')$. In this case

$$RT \ln K_M = rF_{\nu_M'} - (3+r)F_{\nu_M} \tag{A.2a}$$

$$RT \ln K_N = rF_{\nu_N'} - (3+r)F_{\nu_N} \tag{A.2b}$$

where F_ν is the free energy per mole of a one-dimensional harmonic oscillator of frequency ν.[29]

The Boltzmann factor in the grand partition function from which equations (A.1a) and (A.1b) derive is $\exp(-\mathscr{E}/RT)$ where (equations 3 and 6 of Ref. 6)

$$\begin{aligned}\mathscr{E} = {} & V_{M^+}\{\zeta_M - U - E_a - (3+r)E_{\nu_M} + rE_{\nu_M'}\} + \\ & + V_M\{\zeta_M - U - (3+r)E_{\nu_M} + rE_{\nu_M'}\} + \\ & + V_{N^-}\{\zeta_N - U + E_d - (3+r)E_{\nu_N} + rE_{\nu_N'}\} + \\ & + V_N\{\zeta_N - U - (3+r)E_{\nu_N} + rE_{\nu_N'}\} + \\ & + nE_c - pE_v + S(2U + 3E_{\nu_M} + 3E_{\nu_N})\end{aligned} \tag{A.3}$$

The quantities not previously defined are: V_{M^+}, the concentration of un-ionized M-vacancies; V_{N^-}, the concentration of un-ionized N-vacancies; E_a, the energy of the acceptor level associated with each M-vacancy; E_d, that of the donor level associated with each N-vacancy; E_c and E_v, the energies of respectively the conduction and valence bands; and E_ν, the average energy per mole[29] of a one-dimensional harmonic oscillator of frequency ν. The oscillator terms are not present explicitly in equation (3) of Ref. (6) where the lattice vibrations were treated formally. They would follow on the basis of the above Einstein model. The coefficient of the concentration of lattice sites, S, in equation A.3 represents the energy of the crystal when phonons are the only point defects present. The other terms on the right-hand side represent the increase in the energy of the crystal on the introduction of the other point defects. By definition of the Boltzmann factor the energy required to create one un-ionized M-vacancy, E_M, is given by the coefficient of V_{M^+} in equation (A.3), i.e.

$$E_M \equiv \zeta_M - U - E_a - (3+r)E_{\nu_M} + rE_{\nu_M'} \tag{A.4a}$$

More precisely, E_M is the energy per mole to remove an M-atom from the crystal to infinity in its lowest quantum state leaving an un-ionized M-vacancy in the crystal, the concentrations of the other point defects remaining unchanged except for that of the phonons which are allowed to reach an equilibrium distribution.

The analogous energy required to create an un-ionized N-vacancy, E_N, is given by the coefficient of

V_N- in equation (A.3), i.e.

$$E_N = \zeta_N - U + E_d - (3+r)E_{\nu_N} + rE_{\nu'_N} \quad \text{(A.4b)}$$

The significance of the energy parameters is now established. This procedure can also be followed considering point defects other than the un-ionized vacancies, if it is remembered that the concentrations V_M, V_N, n, and p are coupled by a constraint of electrical neutrality (equation 2 of Ref. 6) and cannot be varied independently. For example, if the concentrations of ionized N-vacancies and conduction band electrons are both increased by unity the constraint is satisfied and the necessary energy is given by the sum of the coefficients of V_N and n in equation (A.3), i.e. it is given by equation (A.4b) if E_d is replaced by E_c. On the basis of the above discussion the energy required to create an un-ionized N-vacancy and then to allow the donor electron to seek its equilibrium energy or briefly, the energy required to create an N-vacancy, is given by $E_N + (E_f - E_d)$ while the analogous energy required to create an M-vacancy is given by $E_M - (E_f - E_a)$.

Substituting equations (A.2a) and (A.4a) into (A.1a) and equations (A.2b) and (A.4b) into (A.1b), the chemical potentials are given by

$$\mu_M = RT \ln S/V_M + (E_f - E_a) - E_M - RT \ln K'_M \quad \text{(A.5a)}$$

$$\mu_N = RT \ln S/V_N - (E_f - E_d) - E_N - RT \ln K'_N \quad \text{(A.5b)}$$

where

$$RT \ln K'_M = rT(S_{\nu_M} - S_{\nu'_M}) + 3TS_{\nu_M} \quad \text{(A.6)}$$

and S_ν is the entropy[29] per mole of a one-dimensional harmonic oscillator of frequency ν. The definition of K'_N follows from equation (A.6) if the subscript M is replaced by N. In the high temperature limit equation (A.6) reduces to

$$RT \ln K'_M = RT\{r \ln \nu'_M/\nu_M - 3(\ln h\nu_M/kT - 1)\}. \quad \text{(A.7)}$$

In the text it is found convenient to refer chemical potentials at each temperature to a thermodynamic standard state consisting of the monatomic gases M and N each at one atmosphere and considered ideal. Subtracting the expression for the chemical potential (referred to the atoms at infinite dispersion and in their lowest quantum state) of an ideal monatomic gas at one atmosphere from equations (A.5a) and (A.5b) gives the desired result as:

$$\mu'_M = RT \ln S/V_M + (E_f - E_a) - E_M - RT \ln K'_M - \mu^0_M \quad \text{(A.8a)}$$

$$\mu'_N = RT \ln S/V_N - (E_f - E_d) - E_N - RT \ln K'_N - \mu^0_N \quad \text{(A.8b)}$$

Explicit expressions for the chemical potentials of the monatomic gases at one atmosphere, μ^0_M and μ^0_N, are given elsewhere.[30] Numerical values for various temperatures can be easily obtained from tabulated "free energy functions" for monatomic gases.[19]

REFERENCES

1. KROGER F. A. and VINK H. J., *Solid State Physics* (edited by SEITZ F. and TURNBULL D.) Vol. III, p. 310. Academic Press, New York (1956).
2. KROGER F. A. and VINK H. J., *J. Phys. Chem. Solids* **5,** 208 (1958).
3. BLOEM J., *Philips Res. Rep.* **11,** 273 (1956).
4. BLOEM J. and KROGER F. A., *Z. phys. Chem.* **7,** 1 (1956).
5. KROGER F. A., VINK H. J. and VAN DEN BOOMGAARD J., *Z. phys. Chem.* **203,** 1 (1954).
6. BREBRICK R. F., *J. Phys. Chem. Solids* **4,** 190 (1958).
7. LACHER J. R., *Proc. Roy. Soc.* **A161,** 525 (1937).
8. REES A. L. G., *Chemistry of the Defect Solid State* Methuen, London (1954).
9. SHOCKLEY W., *Electrons and Holes in Semiconductors* p. 303. Van Nostrand, New York (1950).
10. WAGNER C., *J. Chem. Phys.* **18,** 62 (1950); WAGNER B. J. and WAGNER C., *J. Chem. Phys.* **26,** 1602 (1957); LORENZ G. and WAGNER C., *J. Chem. Phys.* **26,** 1607 (1957).
11. COTTRELL A. H., *Theoretical Structural Metallurgy* Chapter 10. Edward Arnold, London (1957).
12. BREBRICK R. F., *J. Phys. Chem. Solids* **11,** 43 (1959).
13. REISS H. and FULLER C. S., *J. Metals, N.Y.* **8,** 276 (1956).
14. BREBRICK R. F. and SCANLON W. W., *Phys. Rev.* **96,** 598 (1954).
15. WEST W. A., *Industr. Engng. Chem.* **42,** 713 (1950).
16. STUBBLES J. R. and BIRCHENALL C. E., *Trans Amer. Inst. Min. (Metall.) Engrs.* **215,** 535 (1959).
17. BRAUNE H., PETER S. and NEVELING U., *Z .Naturf.* **6a,** 32 (1951).
18. SMITHELLS C. J., *Metals Reference Book* Vol. II, p. 613. Interscience, New York (1955).
19. STULL D. R. and SINKE G. C., *Thermodynamic Properties of the Elements.* American Chemical Society, Washington (1956).
20. SCANLON W. W., *Solid State Physics* (edited by SEITZ F. and TURNBULL D.) Vol. IX, p. 83. Academic Press, New York (1959).
21. SCANLON W. W., *Phys. Rev.* **109,** 47 (1958).
22. PAUL W. and JONES R. V., *Proc. Phys. Soc. Lond.* **66B,** 194 (1953).
23. BREBRICK R. F. and ALLGAIER R. S., to be published in *J. Chem. Phys.*
24. GOLDBERG A. E. and MITCHELL G. P., *J. Chem. Phys.* **22,** 220 (1954).

Vol. 18
1961

25. FRITTS R. W. and KARRER S., U.S. Patent 2 811 721, October 29, 1957, Filed December 15, 1954.
26. FRITTS R. W. and KARRER S., U.S. Patent 2 811 270, October 29, 1957, Filed December 15, 1954.
27. KOVALCHIK T. L. and MASLAKOVETS Iu. P., *Zh. tekh. fiz. Mosk.* **26,** 2417 (1956); *Soviet Phys. Tech. Phys.* **1,** 2337 (1957).
28. MOTT N. F. and GURNEY R. W., *Electronic Processes in Ionic Crystals* p. 30. Oxford University Press (1950).
29. RUSHBROOKE G. S., *Statistical Mechanics* Chapter 2. Oxford University Press (1949).
30. FOWLER R. and GUGGENHEIM E. A., *Statistical Thermodynamics* p. 170. Cambridge University Press (1949).

Vol.
19

J. Phys. Chem. Solids Pergamon Press 1961. Vol. 18, Nos. 2/3, pp. 129–138. Printed in Great Britain.

PRECIPITATION DE LITHIUM DANS LES MONOCRISTAUX DE FLUORURE DE LITHIUM IRRADIES AUX NEUTRONS THERMIQUES

M. LAMBERT, Ch. MAZIERES et A. GUINIER

Faculté des Sciences, Orsay—Conservatoire National des Arts et Métiers, Paris, France

(*Received* 25 *July* 1960)

Résumé—Nous avions montré, au moyen des Rayons X, qu'il se produit une précipitation de lithium dans les cristaux de fluorure de lithium irradiés au moyen de neutrons thermiques. Il se forme d'abord des plaquettes d'épaisseur atomique puis, pour des doses de neutrons plus importantes, on observe la formation d'un lithium anormal c.f.c., orienté dans le réseau de fluorure de lithium, qui, par recuit, se transforme en lithium normal c.c. Ces résultats sont confrontés avec ceux d'une méthode complètement différente : microanalyse thermique différentielle (μA.T.D.) et au moyen des deux méthodes (diffraction des rayons X et μA.T.D.), on étudie les transformations par chauffage des amas de lithium.

Abstract—Earlier X-ray diffraction results have shown that lithium precipitation occurs in lithium fluoride by radiation damage. Thin plates of atomic thickness are produced and for larger neutron doses, anomalous f.c.c. lithium appears in epitaxy on the lithium fluoride lattice. By heating, this lithium is transformed into normal, b.c.c. lithium. These results are in good agreement with those found by a fundamentally different method, the differential thermal micro-analysis (μD.T.A.), and by means of the two methods (X-ray diffraction and μD.T.A.), we study the transformations of lithium inclusions on heating.

Vol. 18
1961

Les sels de lithium sont particulièrement adaptés à l'étude des défauts introduits dans un solide par irradiation grâce à la grande section efficace de la réaction Li^6 (n, α) H^3 : 70 barns pour des neutrons d'énergie 0,025 eV et à 20°C. Cette réaction libère une particule α d'énergie 2,1 MeV et un noyau de tritium d'énergie 2,7 MeV qui dissipent leur énergie en ionisant, puis en déplaçant les atomes, leur libre parcours moyen étant de 1/100 mm. Seitz[1] a évalué à 1900 le nombre d'atomes déplacés par fission dans un cristal de fluorure de lithium. Ce nombre est très grand; si ϕt représente le flux intégré de neutrons par cm^2 de cristal, σ la section efficace de la réaction nucléaire, la proportion d'atomes déplacés est alors :

$$\frac{1900}{2}\sigma\phi t \sim 7\times 10^{-20}\phi t$$

Si aucun autre phénomène n'intervenait, tous les atomes devraient être déplacés une fois pour une dose de $1{,}5\times 10^{19}$ neutrons par cm^2.

Ces défauts sont créés d'une manière homogène, ce qu'on ne pourrait réaliser avec des particules α seules. En effet, le libre parcours moyen des neutrons thermiques dans le fluorure de lithium est environ de 2,5 mm et les échantillons irradiés ont la forme de lamelles d'épaisseur voisine de 0,5 mm.

D'autre part, le fluorure de lithium est un des seuls sels de lithium non hygroscopique qu'on peut obtenir à l'état de beaux monocristaux de structure simple, type NaCl. Nous avons étudié également quelques cristaux d'hydrure de lithium, malheureusement ils se détériorent très vite au contact de l'air.

Dans tous les cas, l'effet primaire de l'irradiation est d'introduire à l'intérieur du cristal des défauts ponctuels : lacunes et atomes interstitiels. Le problème est de savoir comment ces défauts vont

se comporter, s'ils sont stables à la température où l'irradiation est faite, ou s'ils vont se détruire par annihilation mutuelle ou en donnant naissance à un autre type de défaut cristallin.

Pour les faibles taux d'irradiation, des mesures de dilatation linéaire effectuées au moyen de jauges de contrainte par BINDER et STURM[2] donnent une concentration en atomes interstitiels correspondant à 8600 atomes déplacés par fission. Ce nombre est très grand (supérieur à celui calculé par SEITZ); les défauts ponctuels formés sont donc stables à la température ambiante et lorsque leur concentration est faible. Les mêmes auteurs, par des mesures comparatives de paramètre cristallin et de densité[3], ont conclu à la formation à l'intérieur des cristaux irradiés d'un nombre égal de lacunes et d'atomes interstitiels, c'est-à-dire de défauts de Frenkel, pour des doses de neutrons inférieures à 6×10^{16} neutrons par cm^2.

Enfin, PERIO *et al.*[4] ont montré que lorsque la dose de neutrons varie de 10^{16} à 10^{19} neutrons par cm^2, l'augmentation relative de paramètre cristallin passe par un maximum pour un flux intégré de 3×10^{17} neutrons par cm^2, ce qui correspond à une saturation de la concentration en atomes interstitiels, la concentration maximum étant de l'ordre de 4 pour mille. Ces résultats ont été confirmés par les mesures de WILLIS et SMALLMAN[5].

Pour des doses de neutrons importantes, il était raisonnable de penser que si la température d'irradiation était suffisante, les différents défauts ponctuels formés allaient se rassembler pour donner naissance à des défauts plus gros sur lesquels il y a peu de renseignements théoriques. On a donc cherché à obtenir des données expérimentales dans ce domaine.

Un travail effectué au moyen des Rayons X par LAMBERT[6] a permis de détecter la présence dans les cristaux irradiés de plusieurs types de "gros défauts" correspondant à l'apparition de taches de diffusion et de diffraction supplémentaires sur les diagrammes. On peut distinguer deux sortes de "gros défauts": d'une part des cavités n'ayant aucune orientation privilégiée et dont la taille varie entre quelques Å et quelques centaines d'Å; d'autre part des rassemblements d'atomes de lithium dont l'orientation est bien définie dans le cristal qui les renferme.

L'objet de cet article est uniquement l'etude de la formation et des transformations des amas de lithium créés par irradiation; nous ne ferons que rappeler les résultats donnés par les Rayons X et nous les confronterons avec ceux donnés par une méthode complètement différente : la microanalyse thermique différentielle.

1. CLASSIFICATION DES DIFFERENTS TYPES DE STRUCTURE DES RASSEMBLEMENTS DE LITHIUM, FORMES PAR IRRADIATION

Les atomes interstitiels de lithium ne restent pas isolés dans le cristal mais se rassemblent en donnant des types différents d'amas, dont la taille et la structure varient à la fois en fonction du flux intégré de neutrons et de la température à laquelle l'echantillon a été porté pendant et après l'irradiation.

Les Rayons X ont permis de décrire les différents types d'amas de lithium susceptibles d'être rencontrés dans les cristaux irradiés[7,8] et de déterminer dans quelles conditions ils apparaissent.

Nous allons rappeler ces résultats mais sans les justifier : nous ne reporterons pas ici les calculs de diffraction, exposés dans le mémoire cité ci-dessus,[6] qui permettent de préciser la nature et la structure des amas et donnent, par comparaison avec les résultats des mesures quantitatives, un ordre de grandeur de la concentration en défauts des échantillons étudiés.

1.1 *Description des différents types d'amas de lithium*

1.1.1 *Plaquettes de lithium.* Les plaquettes constituent des défauts "plans" dans le réseau du fluorure de lithium : 1, 2 ou même 3 plans (200) successifs du fluorure de lithium sont remplacés par des plans de lithium. Le diamètre de l'atome neutre de lithium est de 3 Å, alors que la distance des plans (200) du fluorure est de 2,01 Å, cette insertion de plans de lithium correspond à un écartement local des plans du fluorure sans que le reste du cristal soit sérieusement perturbé. L'épaisseur de ces plaquettes de lithium varie entre 3 Å et une dizaine d'Å. Leur étendue, parallèlement aux plans (200) de LiF, est de quelques milliers d'Å^2.

1.1.2 *Lithium c.f.c.* A l'intérieur du réseau du fluorure de lithium, le lithium précipite sous une forme *anormale*, c.f.c., de paramètre 4,30 Å et

Vol. 18
1961

en épitaxie avec le fluorure de lithium : les axes [100] du lithium c.f.c. et du fluorure sont confondus. L'empilement des plans (111) de ce lithium n'est du reste pas parfait et présente certaines irrégularités.

Une forme de lithium analogue, c.f.c., de paramètre 4,40 Å, avait déjà été observée par BARRETT[9] lorsque des cristaux de lithium c.c. étaient comprimés à basse température. Le lithium c.f.c. formé était en épitaxie avec le lithium c.c. et BARRETT a déterminé l'orientation relative des deux formes de lithium. Nous reviendrons sur ce point au paragraphe 1.1.3.

Le paramètre du lithium c.f.c. apparu par irradiation est inférieur à celui donné par BARRETT, mais les conditions sont ici très différentes : les cristaux de lithium sont comprimés dans le réseau de fluorure de lithium de paramètre inférieur : 4,02 Å.

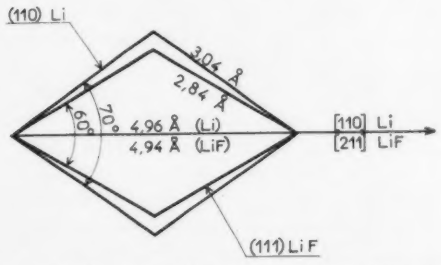

FIG. 1. Epitaxie du lithium c.c. dans le fluorure de lithium : orientation relative d'un plan (110) de lithium et (111) de fluorure de lithium.

1.1.3 *Lithium c.c.* Nous verrons que ce lithium c.c. n'apparaît pas directement par irradiation, mais provient du changement de phase du lithium c.f.c. Les cristaux de ce lithium normal sont en épitaxie dans le réseau du fluorure et nous avons vérifié à la précision de 1° la relation établie par NISHIYAMA dans le cas de la transformation martensitique du fer γ en fer α.[10]

$$\begin{cases} (110)\ \text{Li} \,//\, (111)\ \text{LiF} \\ \langle 110\rangle\ \text{Li} \,//\, \langle 211\rangle\ \text{LiF} \end{cases}$$

Il est à noter que cette relation d'épitaxie lithium c.c., fluorure de lithium est également une relation d'épitaxie entre lithium c.c. et lithium c.f.c. au sein du fluorure de lithium. Elle diffère de la relation établie par BARRETT dans le cas de la transformation, à basse température, de lithium normal en lithium c.f.c.[9] :

$$\begin{cases} (110)\ \text{c.c.} \,//\, (111)\ \text{c.f.c.} \\ \langle 110\rangle\ \text{c.c. formant un angle de } 3° \text{ avec } \langle 111\rangle\ \text{c.f.c.} \end{cases}$$

Ce n'est guère surprenant car les inclusions de lithium ne peuvent se comporter comme le métal libre. Elles sont soumises aux contraintes exercées par le réseau environnant.

1.1.4 *Sels de lithium.* Pour des doses de neutrons très importantes, en dehors de l'apparition des "gros défauts", il apparaît dans les cristaux des fissures qui laissent pénétrer les gaz atmosphériques; il se forme alors des composés du lithium : lithine, carbonate de lithium, toujours en épitaxie dans le réseau du fluorure.

1.2 *Conditions d'apparition et évolution de ces précipités de lithium en fonction de la dose de neutrons et du recuit.*

1.2.1 *Plaquettes.* On observe leur formation à partir d'une dose de neutrons de 3×10^{17} neutrons par cm^2.

Lorsque le flux intégré croît, les plaquettes s'épaississent, leur nombre augmente, mais leur surface reste voisine de 2.500 Å^2. Par contre, celle-ci augmente lorsqu'on recuit un cristal irradié (elle atteint 25.000 Å^2 par chauffage à 450°C); les plaquettes s'étendent alors dans toutes les directions, soit par diffusion d'atomes interstitiels isolés présents dans le cristal, soit à partir d'atomes appartenant à d'autres plaquettes. Ceci ne se produit qu'a partir d'une température voisine de 200°C, c'est-à-dire supérieure à la température de fusion du lithium métallique, lorsque la vitesse de diffusion des atomes de lithium est plus grande. En chauffant 100 heures à 250°C ou 100 minutes à 450°C, un cristal soumis au bombardement de 4×10^{17} neutrons par cm^2, on a fait disparaître complètement les plaquettes, vraisemblablement par suite de leur transformation en cristallites plus gros.

Du point de vue quantitatif, nous avons pu évaluer à environ 5 pour mille la concentration en volume des plaquettes de lithium dans un cristal ayant reçu 5×10^{18} neutrons par cm^2 et non recuit.

1.2.2 *Lithium c.f.c.* On n'observe la précipitation de ce lithium que pour des doses de neutrons supérieures à 5×10^{18} neutrons par cm^2.

Les cristaux ont une taille au moins égale à quelques centaines d'Å et leur concentration en volume est de quelques pour cent dans un cristal ayant reçu 6×10^{18} neutrons par cm^2.

Lorsqu'on porte l'échantillon à 200°C, ce lithium fond et après refroidissement on constate la formation de lithium normal c.c.

Une étude plus détaillée du changement de phase Li c.f.c., Li c.c. sera présentée plus loin.

1.2.3 *Lithium c.c.* Ce lithium provient donc du lithium c.f.c produit par irradiation; les cristaux sont plus gros que ceux de Li c.f.c., leur taille est supérieure à 1.000 Å. et augmente au cours du recuit des échantillons à des températures supérieures à 200°C.

2. ETUDE PAR MICROANALYSE THERMIQUE DIFFERENTIELLE (μA.T.D.)

2.1 *Principe et performances de la méthode.*

Le principe de l'analyse thermique différentielle (A.T.D.) est bien connu, mais la méthode employée ici est originale[11] en ce sens qu'on utilise de très faibles quantités de substance (de 1 à 100 microgrammes). L'échantillon de dimension moyenne: $\frac{1}{10}$ à $\frac{4}{10}$ de mm, est dèposé à l'intèrieur d'une fine soudure thermoèlectrique en forme de microcreuset. Cette soudure est montée en opposition avec une soudure identique extrèmement voisine, et l'ensemble indique la "température différentielle" grâce à un dispositif enregistreur à la fois sensible et à faible temps de résonse. Il n'est pas besoin de "corps de référence". Une troisième soudure indique la température "absolue". Les trois têtes de couples sont au coeur d'une enceinte métallique de dimension trés réduite.

La microanalyse thermique différentielle (μA.T.D.) présente les avantages suivants :

(1) Un excellent pouvoir de résolution d'effets thermiques rapprochés dans l'échelle des températures. Des phénomènes à cinétique rapide se produisant à des températures voisines de quelques centièmes de degré donnent des signaux parfaitement distincts sur les enregistrements. En somme, le dispositif présente un véritable caractère oscillographique avec une constante de temps de l'ordre de la $\frac{1}{2}$ seconde.

(2) Une forte sensibilité. Sur nos diagrammes, 30 cm en ordonnée représentent 1°C de température différentielle. Dans ces conditions, on peut encore déceler la transformation $\alpha \rightleftarrows \beta$ de la tridymite (soit 1 cal/g) sur un échantillon de masse 1 μg.

(3) Une bonne précision dans la détermination des températures des transformations (voir ci-dessous par exemple : la température de fusion du lithium est trouvée à 180,5°C en excellent accord avec les données récentes).

2.2 *Etude des amas de lithium dans les monocristaux de fluorure de lithium irradiés.*

2.2.1 *Plaquettes.* Nous avons essayé la technique de microanalyse thermique pour voir si les plaquettes de lithium ne donneraient pas lieu à un phénomène endothermique analogue à une fusion. Ces essais ont toujours apporté une réponse négative, soit parce que la méthode n'est pas assez sensible pour mettre un tel phénomène en évidence, soit parce qu'il est impropre de parler de fusion dans le cas d'un métal à "deux dimensions". Nous indiquons néanmoins ces résultats (négatifs) pour servir de comparaison avec ceux obtenus dans le cas de cristaux plus fortement irradiés.

Quant à la disparition des plaquettes par recuit, qui s'accompagne en principe d'une manifestation thermique, sa cinétique est certainement trop lente pour être saisie par la méthode.

2.2.2 *Lithium métallique.* Un premier chauffage, jusqu'à 220°C environ, d'un fragment de monocristal de fluorure de lithium irradié (6×10^{18} neutrons/cm^2) donne le tracé 1 (Fig. 2). Le refroidissement consécutif donne le tracé 2. Un nouveau cycle thermique identique donne les tracés 3 et 4, qu'on retrouve ensuite sans changement, si l'on réalise encore d'autres cycles semblables.

Nous interprétons les deux effets endothermiques A_1 et B_1 (tracé 1) comme les fusions respectives de deux formes distinctes du lithium métallique inclus dans le cristal de fluorure de lithium irradié. En effet, après un chauffage au-delà de 200°C et refroidissement, les rayons X montrent la présence de lithium normal c.c. dans le réseau; le tracé 3 (A.T.D.) est relatif à de tels échantillons : la situation du signal A_2, entre 170 et 180°C, ne

laisse pas de doute sur sa signification : c'est le signal de fusion de ce lithium cubique centré. Or dans le tracé 1 la situation du signal A_1 est exactement la même; il doit donc s'agir aussi de la fusion d'un peu de lithium présent sous la forme c.c.

Quant à B_1, ce signal n'apparaît qu'à un premier chauffage : Nous l'attribuons à la fusion des particules de lithium cubique à faces centrées, dont les rayons X ont montré la présence après l'irradiation aux neutrons et la disparition irréversible par chauffage à 200°C. L'A.T.D. indique donc comme point de fusion de cette forme anormale, une température supérieure d'une dizaine de degrés à celle de la forme habituelle. Ce résultat peut paraître inattendu; il convient néanmoins de ne pas perdre de vue les circontances très particulières dans lesquelles cette forme compacte, inhabituelle, de lithium s'est formée. En particulier, nous ignorons la pression à laquelle sont soumises, dans le réseau de fluorure de lithium, les particules de lithium c.f.c. La présence de A_1, c'est-à-dire de lithium sous forme normale, s'explique très bien par une transformation partielle de la phase c.f.c., au cours du chauffage, avant la fusion. Nous avons d'ailleurs essayé de mieux saisir cette transformation et nous verrons (§ 3) que les études effectuées parallèlement aux rayons X et avec la micro A.T.D., aboutissement aux mêmes conclusions.

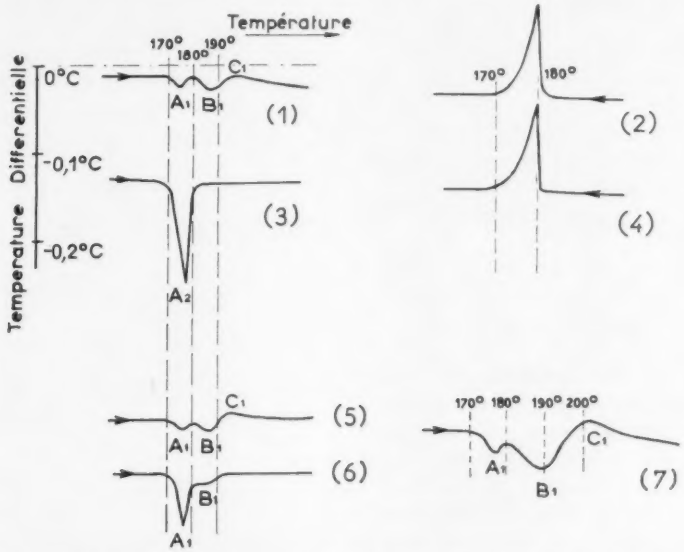

FIG. 2. μA.T.D. d'un fragment (m = 45 μg) de fluorure de lithium irradié (6×10^{18} neutrons/cm^2) (1) premier chauffage, vitesse "standard", (2) refroidissement consécutif, (3) deuxième chauffage, (4) refroidissement consécutif, (5) et (6) chauffage de deux moitiés d'un même échantillon respectivement sans traitement préalable et avec traitement préalable à 160°, (7) chauffage rapide.

Enfin, l'examen des tracés 1, 5, 7, obtenus lors d'un premier chauffage, révèle aussi un effet supplémentaire C_1, exothermique, au-delà de 190°C. Un traitement thermique préalable, à température inférieure à 160°, entre autres conséquences, supprime cet effet; celui-ci est au contraire plus important dans le cas d'un chauffage rapide. Nous pensons qu'il pourrait traduire une recombinaison entre du fluor libre, présent dans des cavités, et du lithium voisin, venant au contact du fait de sa fusion. Le phénomène "neutraliserait" du premier coup la majeure partie du lithium (ou du fluor) susceptible d'une telle rencontre. En tous cas, par la suite, l'effet ne se manifeste plus.

Vol. 18
1961

3. ETUDE PAR RAYONS X ET μA.T.D. DU CHANGEMENT DE PHASE DU LITHIUM PRECIPITE DANS LE FLUORURE DE LITHIUM

On constate, au cours des analyses thermiques, que l'importance relative des effets A_1 et B_1 dépend de la conduite du chauffage (Fig. 2): Les tracés 5 et 6 sont relatifs respectivement aux deux moitiés d'un même échantillon initial. La première moitié, au cours d'un chauffage "standard",* donne le tracé 5; la deuxième est préalablement traitée pendant une heure à 160°C environ, puis refroidie; elle subit alors le même chauffage que la première et donne le tracé 6. On constate enfin que si le premier chauffage est très rapide, sur un autre échantillon, le signal B_1 est accentué (tracé 7). On conclut qu'un traitement thermique favorise la transformation Li c.f.c. → Li c.c., ce qui est en parfait accord avec l'expérience suivante réalisée au moyen des rayons X :

Un premier diagramme (Fig. 3A) est obtenu à température ordinaire et montre au voisinage de la réflexion 111 de fluorure de lithium la tache correspondant à la réflexion 111 de lithium c.f.c.

Le cristal est chauffé lentement jusqu'à une température légèrement inférieure à la température de fusion du lithium métallique ordinaire; un diagramme effectué à cette température (Fig. 3B) fait apparaître trois taches de diffraction supplémentaires (l'une est presque confondue avec la tache 111 de lithium c.f.c.) : elles traduisent la présence de lithium c.c. dans le réseau de fluorure. Lorsqu'on continue à chauffer l'échantillon, le lithium c.c. fond d'abord, et le diagramme correspondant (Fig. 3C) ne montre plus que la tache dûe au lithium c.f.c., qui disparaît elle-même lorsque la température du cristal est encore élevée (Fig. 3D).

On vérifie de plus, qualitativement, que la durée du traitement thermique et une élévation de sa température favorisent la formation de lithium c.c. Toutefois, nous n'avons jamais observé, même après un chauffage de plusieurs heures à 160°C, la transformation complète du lithium c.f.c. en lithium c.c.

Il semble donc que certains domaines de lithium c.f.c. gardent leur structure jusqu'à la fusion. Cette stabilité pourrait être en rapport avec leur taille, leur degré de perfectionnement ou leur situation privilégiée dans un cristal présentant de nombreuses autres imperfections.

* Pour faciliter la comparaison de signaux obtenus au cours d'analyses différentes, on est amené à normaliser les vitesses de chauffage. La vitesse que nous appelons ici "standard" est voisine de 15°C/min.

4. EVOLUTION DES PARTICULES DE LITHIUM c.c. SOUS L'INFLUENCE D'UN TRAITEMENT THERMIQUE ENTRE 200 et 700°C

Cette étude concerne encore des échantillons irradiés à la dose de 6×10^{18} neutrons/cm^2, dans lesquels une fusion préalable du lithium n'a laissé subsister au refroidissement que la phase c.c. Nous avons observé à l'analyse thermique, à

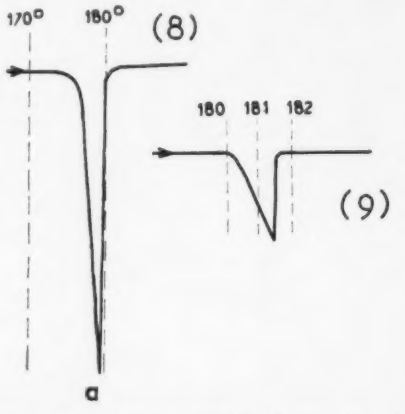

FIG. 4. Fusion d'une de parcelle lithium ($m = 3$ μg): (8) chauffage standard, (9) chauffage lent.

la suite de différents traitements, des modifications importantes et parfaitement reproductibles concernant le profil des signaux de fusion–cristallisation du lithium métallique.

Indiquons d'abord, comme terme de référence, la forme des signaux obtenus à la fusion—en atmosphère inerte—d'échantillons de lithium ordinaire (masse de 1 à quelques μg). Le tracé 8 (Fig. 4) est obtenu à la vitesse de chauffe "standard" utilisée par la suite. On vérifie sur ce type de tracés une bonne proportionnalité entre l'aire du signal et la masse de l'échantillon; cette circonstance nous permettra ultérieurement une évaluation quantitative du lithium métallique précipité dans le fluorure de lithium. Le tracé 9 est obtenu avec un chauffage beaucoup plus lent; pour des raisons expérimentales faciles à analyser, la largeur du signal est alors réduite et sa situation

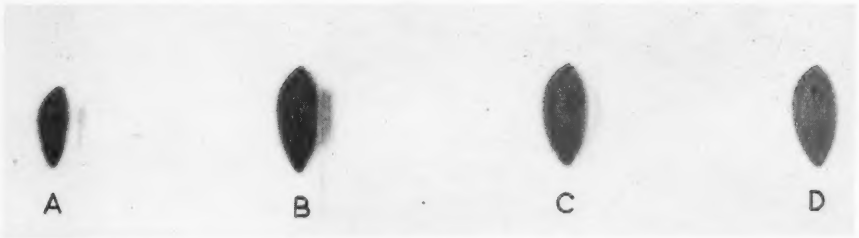

FIG. 3. Diagrammes de rayons X montrant la tâche de réflexion 111 du fluorure de lithium voisinage immédiat :

A—aprés irradiation et avant tout recuit : tache de réflexion 111 du lithium c.f.c.

B—au cours du chauffage à une température légèrement inférieure à la température de fusion du lithium c.c. : les trois taches supplémentaires sont dûes au lithium c.c.

C—la température est légèrement supérieure à la température de fusion du lithium c.c. : la tache dûe au lithium c.f.c. subsiste.

D—à 200°C, toutes les taches autres que celle donnée par le fluorure de lithium ont disparu.

[*facing p.* 134

BLANK
PAGE

Vol
19

dans l'échelle des températures est plus correcte : elle est ici en excellent accord avec les données récentes sur le point de fusion du lithium, $T_f = 180{,}5°C$.[12]

Comparons maintenant le tracé 8 (lithium ordinaire) au tracé 10 (Fig. 5), relatif a un

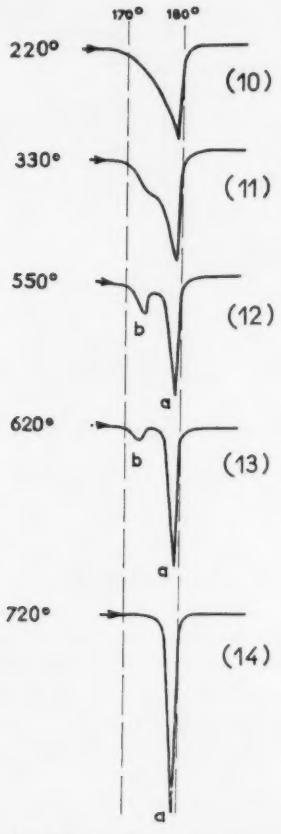

FIG. 5. Influence d'un traitement thermique préalable sur le profil des tracés du fusion : A gauche de chaque courbe, la température maximale atteinte au cours du chauffage précédant la μA.T.D.

échantillon de fluorure de lithium irradié qui a d'abord été porté une fois à 210°C. Les conditions expérimentales sont les mêmes; or, si les deux signaux de fusion se terminent tous deux par un front raide et à la même température (180° de notre repérage), on voit que celui du lithium dans le fluorure de lithium est anormalement large.

On fait alors subir à l'échantillon un cycle de chauffage et refroidisement avec maximum à 330°C. Le nouveau signal de fusion est modifié (tracé 11). Cette modification s'accuse à la suite de cycles thermiques successifs à température maximale de plus en plus élevée (tracés 12 et 13). Enfin, lorsque l'échantillon a été porté à 700°C au moins, et alors seulement, le signal de fusion (tracé 14) coïncide parfaitement avec celui du lithium métallique ordinaire.

La largeur du signal 10, indiquant une fusion débutant 6 à 7° plus bas, doit donc avoir une signification physique. Nous pensons que cette largeur correspond à une répartition continue, en taille et en degrés de perfection cristalline, des grains de lithium.

D'une part, en effet, les surfaces spécifiques de ces particules doivent être considérables; d'autre part, à une organisation cristalline imparfaite doit correspondre un point de fusion mal défini. On est tenté de faire un rapprochement avec les expériences de PATRICK et TEMPER[13] et BATCHELOR et FORSTER[14], qui ont trouvé des abaissements importants du point de fusion pour des substances adsorbées sur du silicagel. Rappelons aussi que CHALMERS[15], puis CHAUDRON *et al.*[16] ont montré sur des échantillons d'étain et d'aluminium que les joints de grains fondaient à une température légèrement inférieure à celle de la fusion des grains eux-mêmes.

De plus, deux diagrammes de rayons X effectués après chauffage de l'échantillon à 250 et 500°C, ne montrent aucune différence de structure, ni d'orientation du lithium c.c., mais une augmentation de la taille moyenne des grains.

Le traitement thermique a sans doute pour effet de perfectionner les amas de lithium et, aussi, d'accroître la taille de certains. Le mécanisme correspondant à cette dernière hypothèse resterait d'ailleurs à éclaircir. Si, en effet, des expériences classiques montrent divers phénomènes où de petites particules viennent nourrir des plus grosses, il y a toujours entre les deux types de particules, un milieu, dont le rôle est essentiel à la compréhension du phénomène. La situation est beaucoup moins claire dans notre cas. Néanmoins, l'apparition du signal fin et long (a) (Fig. 5) correspond certainement à la présence de "bons" cristallites de lithium. Quant au signal plus diffus (b), des amas d'un autre type en sont sans

Vol. 18
1961

doute responsables : on peut les imaginer plus petits, isolés, éloignés des centres de "coalescence" ou bien situés dans le réseau de fluorure de lithium de façon peu favorable à une diffusion.

Les tracés 12 bis de la Fig. 6 (fusion et cristallisation) sont relatifs à un échantillon préalablement porté à 500°, analogue donc à celui du tracé 12, mais de très petite masse (8 μg). On y voit, de ce fait, avec une grande netteté, la distribution du lithium en deux catégories de "grains". Notons que ce tracé peut être reproduit aussi souvent que l'on veut avec l'échantillon considéré; il en est en quelque sorte caractéristique et, pour le modifier

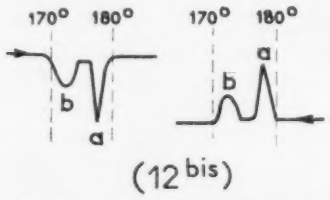

FIG. 6. (12 bis) Tracés de fusion et cristallisation d'un très petit fragment (8 μg) de fluorure de lithium préalablement porté à 550°.

en accroissant le signal (a) aux dépens de (b), il est indispensable de porter l'échantillon à une température supérieure à 500° : Ceci montre que la répartition des amas en deux types est sous la dépendance étroite de la température atteinte.

En définitive, il est certain qu'après chauffage à 700°, on a, dans le cristal de fluorure de lithium, du lithium métallique, dont le signal de fusion est rigoureusement identique à celui d'un échantillon de lithium banal : Ceci autorise une évaluation quantitative grâce à l'aire des signaux; on peut estimer que 5 à 6 *pour cent du lithium ionique initial a été précipité sous forme métallique.* C'est bien l'ordre de grandeur que donnent les rayons X sur des èchantillons de meme origine.

Il est à noter que ce lithium métallique doit être dans un état de très grande pureté et exceptionnellement bien protégé. Citons à cet égard l'expérience suivante : On dispose côte à côte dans le porte-échantillon un fragment de fluorure de lithium traité à 700°C, et un très petit morceau de lithium ordinaire. Dans ces conditions, on obtient (Fig. 7) un signal de fusion unique (tracé 15); par contre, au refroidissement, le signal de cristallisation est dédoublé (tracé 16) et le pic occupant la place correcte (178–180° de notre repérage) correspond au lithium inclus dans le fluorure de lithium : il est fort probable que la lithium ordinaire est souillé d'impuretés, alors qu'il n'en est rien pour le lithium inclus.

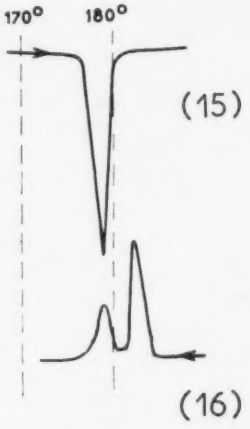

FIG. 7. (15) Fusion et (16) Cristallisation d'un ensemble, fragment de fluorure de lithium irradié et parcelle de lithium métallique.

5. CONCLUSION

L'irradiation des cristaux de fluorure de lithium constitue donc un excellent procédé pour obtenir des particules de lithium métallique d'une exceptionnelle pureté car elles sont parfaitement isolées de l'air atmosphérique tant que la dose de neutrons n'est pas trop grande. Nous devons, du reste, à l'équipe d' ABRAGAM[17] un intéressant renseignement sur la taille des particules de lithium, après traitement à 700° : la forme des signaux de résonance magnétique permet de conclure à des dimensions de l'ordre du micron. Ce résultat confirme notre hypothèse d'un accroissement de la taille des grains par le traitement thermique, accroissement dont le mécanisme reste à préciser.

Il restait à savoir si la précipitation de lithium dans le fluorure de lithium était un effet exceptionnel ou si nous pouvions retrouver cet effet dans d'autres sels de lithium. Nous avons également observé la précipitation de lithium métallique dans des cristaux d'hydrure de lithium, irradiés sous

vide, et ayant reçu 2×10^{18} neutrons par cm^2. On constate par rayons X la précipitation de lithium métallique mais directement sous sa forme normale, l'orientation des grains par rapport au cristal d'hydrure étant sensiblement la même que dans le cas du fluorure. Les tracés de microanalyse thermique différentielle ne font apparaître *également qu'une seule transformation* : fusion ou cristallisation du lithium c.c. Il est à noter que contrairement aux échantillons de fluorure de lithium, les cristaux d'hydrure, altérables à l'air, ont été irradiés sous vide et la température d'irradiation a pu dépasser la température de fusion du lithium, empêchant celui-ci d'apparaître sous la forme c.f.c. L'hydrure de lithium étant c.f.c. mais de paramètre légèrement différent de celui du fluorure, il se peut également que la précipitation de lithium c.f.c. dans le réseau de l'hydrure ne soit pas possible.

Dans les deux cas, fluorure et hydrure, la précipitation de lithium s'accompagne d'un départ de gaz : fluor ou hydrogène; nous avons observé le départ de 1,6 pour cent de l'hydrogène constituant l'hydrure,[18] proportion un peu inférieure à celle du lithium précipité, trouvée par analyse thermique différentielle, mais il est vraisemblable qu'un volume non négligeable d'hydrogène reste inclus dans les cristaux et ne s'échappe que difficilement.

La précipitation de métal dans un sel métallique irradié ne semble pas être un phénomène exceptionnel; elle doit cependant être conditionnée par un grand nombre de facteurs :

(1) Le nombre d'atomes interstitiels et de lacunes produits après une durée d'irradiation raisonnable doit être suffisamment grand; ceci limite sérieusement le nombre des composés où le phénomène puisse être observé.

(2) La taille et le coefficient de diffusion des ions constituants et des atomes neutres correspondants.

Donnons par exemple un ordre de grandeur du rayon des ions Li^+, F^-, H^-

Li^+	0,60 Å
F^-	1,36 Å
H^-	2,08 Å

L'ion Li^+ est de beaucoup le plus petit, par contre les atomes neutres de fluor et d'hydrogène sont beaucoup plus petits que l'atome neutre de lithium :

Li	1,56 Å
F	0,67 Å
H	0,5 Å

Le lithium ne peut donc diffuser que sous la forme d'ions Li^+; les atomes neutres ne sont pas mobiles, ce qui explique la formation des plaquettes de lithium. Par contre, les atomes neutres de fluor ou d'hydrogène peuvent se déplacer facilement dans le réseau et s'associer pour donner du gaz : fluor ou hydrogène qui sort du cristal en s'échappant vers l'extérieur et en remplissant les cavités formées par irradiation.

(3) Le coefficient de recombinaison fluor–lithium ou hydrogène–lithium quelque soit leur forme : atomes neutres ou ions individuels, agrégats d'atomes ou de lacunes, amas et cavités. De toutes façons, la formation des précipités métalliques correspond à la coexistence dans les cristaux étudiés de lithium métallique d'une part, de fluor ou d'hydrogène libre d'autre part. Ceci semblerait invraisemblable en chimie classique mais est lié au mécanisme atomique de précipitation du métal et d'élimination du halogène.

Vol. 18
1961

BIBLIOGRAPHIE

1. Seitz F. et Koehler J. S., *Solid State Physics*. Academic Press, New York (1956).
2. Binder D. et Sturm W. J., *Phys. Rev.* **107,** 106 (1957).
3. Binder D. et Sturm W. J., *Phys. Rev.* **96,** 1519 (1954).
4. Perio P., Tournarie M. et Gance M., *Action des rayonnements de grande énergie sur les solides*, p. 116. Gauthier-Villars, Paris (1956).
5. Smallman R. et Willis B., *Phil. Mag.* **20,** 1018 (1957).
6. Lambert M., Thèse, Paris 1958, Louis Jean, Gap (1959).
7. Lambert M. et Guinier A., *C.R. Acad. Sci., Paris* **245,** 526 (1957).
8. Lambert M. et Guinier A., *C.R. Acad. Sci., Paris* **246,** 1678 (1958).
9. Barrett C. S., *Phase transformations in solids*, p. 351. John Wiley, New York (1951).
10. Cohen M., *Phase transformations in solids*, p. 632. John Wiley, New York (1951).
11. Mazières Ch., *C.R. Acad. Sci., Paris* **248,** 2990 (1959); **249,** 540 (1959).

12. DOUGLAS T. B., EPSTEIN L. F., DEVER J. L. et HOLLAND W. H., *J. Amer. Chem. Soc.* **77,** 2144 (1955).
13. PATRICK W. A. et KEMPER W. A., *J. Phys. Chem.* **42,** 369 (1938).
14. BATCHELOR R. W. et FORSTER A. G., *Trans. Faraday Soc.* **40,** 300 (1944).
15. CHALMERS B., *Proc. Roy. Soc.* **A175,** 100 (1940).
16. CHAUDRON G., LACOMBE P. et YANNAQUIS N., *C.R. Acad. Sci., Paris* **226,** 1372 (1948).
17. RYTER Ch., communication personnelle.
18. LAMBERT M., BERGÉ P., MAZIÈRES Ch. et GUINIER A. *C.R. Acad. Sci., Paris* **249,** 2054 (1959).

J. Phys. Chem. Solids Pergamon Press 1961. Vol. 18, Nos. 2/3, pp. 139–149. Printed in Great Britain.

ELECTRON–HOLE SCATTERING AND MINORITY CARRIER MOBILITY IN GERMANIUM

T. P. McLEAN and E. G. S. PAIGE

Royal Radar Establishment, Malvern, England

(*Received* 1 *August* 1960)

Abstract.—In a previous publication the authors presented a theory of the effects of carrier–carrier scattering on mobility in semiconductors. In this paper we discuss the specific application of the theory to germanium in the temperature and impurity concentration ranges where measurements of the minority carrier mobility have recently been performed. This is a necessary preliminary to the main part of the paper which is a comparison between the theoretically predicted and experimentally observed minority carrier mobility in the region where, previously, discrepancies of the order of a factor of two existed. By the incorporation of electron–hole scattering, theory and experiment are brought into agreement (to within 10 to 20 per cent) for a large range of impurity concentrations, demonstrating the importance of electron–hole scattering on the minority carrier mobility.

Vol. 18
1961

1. INTRODUCTION

RECENTLY, measurements of the minority carrier mobility in germanium have been extended into the temperature range between 20°K and 100°K on several *n*- and *p*-type crystals[1] (hereafter this reference is referred to as I). Within this range, the observed minority carrier mobility was significantly less (by a factor of about two) than the mobility predicted from defect scattering, i.e. scattering by phonons and neutral and ionized impurities, although the observed conductivity could be predicted fairly well. It was suggested that the difference was due to electron–hole scattering, the large magnitude of this scattering arising primarily from the drag effect created by the difference of drift velocities of the two types of carriers.

The authors have presented a theory of the effects of carrier–carrier scattering on mobility in non-degenerate semiconductors[2] (hereafter this reference is referred to as II). It was found that, in general, electron–electron (e–e) and hole–hole (h–h) scattering had only a small effect on the majority carrier mobility while (e–h) scattering had a large effect on the minority carrier mobility. In particular, it was found, using a crude description of defect scattering, that the inclusion of (e–h) scattering in the calculation of the minority carrier mobility lowers it to about the right value and gives it the correct sort of temperature dependence to account for the experimental observations in germanium.

The main purpose of this paper is to demonstrate that by the inclusion of (e–h) scattering the experimental values of minority carrier mobility can be accounted for satisfactorily. To do this we shall make a detailed comparison between theory and the experimental observations. This will be preceded, in Section 2, by a discussion of the application of the theory to germanium in which we shall consider the validity of the assumptions and approximations which are made, while bearing in mind the temperature and concentration ranges of the experimental observations. We shall see that the theory cannot be rigorously applied to germanium, and it becomes a subsidiary objective to demonstrate that, nevertheless, the theory gives an adequate description of mobility in germanium. In Section 3 the terms representing the various scattering processes are evaluated. Section 4 presents the comparison between the theory and the experimental results. We find that all the experimental results can be fitted to within 10 to 20 per cent, and we regard this, together with the values found for certain variable parameters, as a demonstration of the importance of

(e–h) scattering in determining the minority carrier mobility at low temperatures.

We shall assume familiarity with I and II in the subsequent sections of this paper.

2. DISCUSSION OF THE JUSTIFIABILITY OF APPLYING THE THEORY OF CARRIER–CARRIER SCATTERING TO THE ANALYSIS OF THE MINORITY CARRIER MOBILITY IN GERMANIUM

Before making a detailed estimate of the effects of carrier–carrier scattering on mobility in a particular substance it is necessary to consider the assumptions which have been introduced into the theory. In this section we shall discuss such assumptions in the light of the ranges of impurity concentration and temperature over which we wish to apply the theory to germanium. Then we shall state our attitude to those aspects of the physical situation which the theory cannot rigorously describe.

The points in the theory that we wish to discuss are:

(a) it is based on the Boltzmann transport equation,
(b) it employs non-degenerate statistics,
(c) each free carrier is characterized by a single isotropic effective mass and an isotropic relaxation time,
(d) the Rutherford scattering cross-section is used to describe encounters between charged particles, and
(e) scattering by optical phonons is not rigorously included.

These will now be discussed in turn, bearing in mind the ranges of temperature and free carrier concentration used in the experiments, (denoted by lines in Fig. 1) and that the major effects due to (e–h) scattering occur between 20°K to 100°K.

(a) In paper II it was shown that the Boltzmann equation provides a good description of carrier–carrier scattering if the condition

$$\lambda n^{1/3} = 6{\cdot}9\frac{\epsilon^{1/2}T^{1/2}}{n^{1/6}} \lesssim 1 \qquad (1)$$

is fulfilled. Here T is the temperature (°K) and n is the concentration (cm^{-3}) of the free carriers, ϵ is the dielectric constant of the medium and λ is the Debye screening length. Essentially the condition we are trying to establish is that the collisions between free carriers be predominantly binary. This condition cannot be well defined since the distance between free carriers is random and the very use of the word predominate—to require all scattering processes to be binary encounters would be an unnecessarily severe restriction—implies that the condition is to some extent arbitrary. Furthermore, a more relevant condition is that binary encounters should predominate when all scattering processes are taken into account. Therefore the area to the left of the line $\lambda n^{1/3} = 1$, shown in Fig. 1, is intended to be merely an indication of the temperatures and concentrations for which the scattering processes are expected to be predominantly binary. This condition excludes a large portion of the experimental results, but these are in a region where coulomb scattering is unimportant. As a crude criterion to establish the region where coulomb interactions are important we put $\mu_L/\mu_I \geqslant 0{\cdot}1$ where μ_L and μ_I are the lattice and ionized impurity mobility respectively (Section 3). This region is the area to the left of the line $\mu_L/\mu_I = 0{\cdot}1$ shown in Fig. 1; we are encouraged that this region falls within the region where (1) is fulfilled.

(b) The replacement of the Fermi–Dirac distribution function by the Boltzmann distribution function is an excellent approximation for the majority of specimens. Even in the most unfavourable case—the most impure specimen—the difference between the functions is less than 3 per cent.

(c) It is well known that the band structure of germanium is complicated. Electrons populate four equivalent minima in $\boldsymbol{k}$ space, the constant-energy surfaces of which are ellipsoids of revolution. The ratio of the effective masses parallel and perpendicular to the axis of revolution is $m_\parallel/m_\perp = 20$.[3] A consequence of this anisotropy is that the momentum relaxation times, τ, may also be anisotropic. There is evidence to suggest that, while τ for acoustical phonon[4] and neutral impurity scattering is isotropic, the τ for ionized impurity scattering has a pronounced anisotropy[5,6] ($\tau_\parallel/\tau_\perp \sim 12$.) Since this anisotropy arises from the dominant contribution to the scattering probability from small angle scattering, an inherent feature of coulomb interactions, we should expect a similar anisotropy in the scattering of an electron by an electron or hole. The theory is not

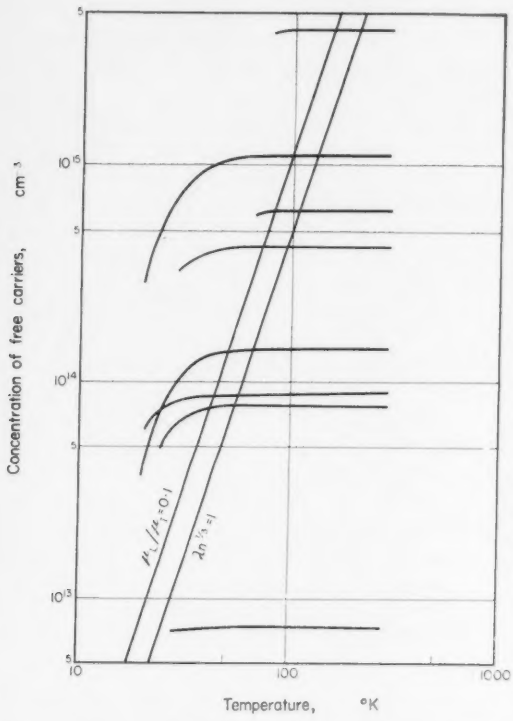

FIG. 1. The ranges of temperature and free carrier concentration of the experimental results presented in I. To the left of the line $\lambda n^{1/3} = 1$ collisions are predominantly binary and to the left of the line $\mu_L/\mu_I = 0{\cdot}1$ ionized impurity scattering is significant.

capable of dealing with this physical situation rigorously.

Holes populate two bands degenerate at the centre of the zone. While the constant energy surfaces of these bands are not spherical, the extent to which they are warped is not large, so that it is usual to characterize the holes in each band by an isotropic effective mass and relaxation time. In effect it is usual to distinguish between two types of hole, the light hole $m_L = 0{\cdot}044\ m_0$ and the heavy hole $m_H = 0{\cdot}31\ m_0$; the theory does not make this distinction.

(d) We have used the Rutherford scattering cross-section to describe encounters between charged particles, and to prevent divergence we have neglected encounters for which the impact parameter is greater than some value d. Our treatment of this cross-section results in a relaxation time for ionized impurity scattering of the CONWELL–WEISSKOPF type[8] and given by equation (6). To estimate the error in the mobility calculated from this relaxation time, μ_R, we have compared it with the mobility calculated from the cross-section determined by the method of partial waves μ_{pw},[9] assuming a scattering potential of the form $(e^2/r)\,e^{-r/\lambda}$ (d is set equal to λ in the comparison). We regard the mobility calculated by the second method as exact.

The general trend is for μ_R to be over-estimated compared with μ_{pw} at low temperatures while at sufficiently high temperatures μ_R is under-estimated; between these extremes there is a large range of temperature where μ_R and μ_{pw} are in good agreement. For example, for an impurity concentration of 10^{15} cm^{-3} μ_R is about 13 per cent greater than μ_{pw} at 50°K while, at 300°K, μ_R is about 10 per cent less than μ_{pw}, of course, when phonon scattering is taken into account the error in the resultant mobility is decreased; it becomes insignificant at 300°K and the difference between μ_R and μ_{pw} is reduced to 2 or 3 per cent at 50°K. At low temperatures the difference between the two mobilities decreases as the impurity concentration is lowered. Thus, as far as majority carriers are concerned, we can describe the mobility to within about 5 per cent over all ranges of temperature and concentration shown in Fig. 1.

A similar calculation of the error introduced by the use of the Rutherford scattering cross-section in the calculation of the minority carrier mobility is not easy to carry out. We have therefore assumed that the error in the cross-section for (e–h) scattering is the same as for ionized impurity scattering and, on this basis, have estimated the error in the minority carrier mobility at 50°K for an impurity concentration of 10^{15} cm^{-3}. If the drag effect lowers the minority carrier mobility by a factor of two—which we shall eventually see is a reasonable estimate for this particular temperature and impurity concentration—then the minority carrier mobility is overestimated by up to 15 per cent. The error decreases rapidly with increasing temperature and is lowered as the impurity concentration is decreased. We regard, therefore, the theory as inapplicable for impurity concentration greater than $1{\cdot}1 \times 10^{15}$ cm^{-3} and consequently we shall not attempt to account for the minority carrier mobility of the specimen

Vol. 18
1961

having an impurity concentration of $4{\cdot}2\times10^{15}$ cm^{-3}. The trend of the calculation below 50°K for the specimen containing $1{\cdot}1\times10^{15}$ cm^{-3} impurities will be indicated. For all other ranges of concentration and temperature the minority carrier mobility can be estimated to within 15 per cent and over most of the ranges the error is considerably less than this value.

(e) If the effective mass of the free carrier is independent of temperature then acoustical phonon scattering is predicted to give a $T^{-1{\cdot}5}$ temperature dependence to the lattice mobility.[10] It has become the vogue to ascribe departures of the lattice mobility from this temperature dependence to optical phonon scattering.[11] For holes, the large departure from a $T^{-1{\cdot}5}$ law would appear to imply a large amount of optical phonon scattering; recently, however, two independent experiments have been performed in this laboratory which indicate that a significant increase in the effective mass of the hole occurs with temperature;[12] as a result it appears that the effect of optical modes on the mobility of holes is small, lowering the mobility by no more than about 5 per cent at 80°K. Optical phonons are calculated to have approximately the same effect on the mobility of electrons at 80°K if their effective mass remains constant. Since the effects of optical phonons are small in the temperature range of interest, the method of describing phonon scattering—by $\tau \propto v^{-1}$, where v is the velocity of the carrier, and taking any departure from the $T^{-1{\cdot}5}$ law outside the averaging integral—leads to very small errors, considerably less than 5 per cent.

We conclude from this discussion that there are ranges of temperature and concentration in which scattering by coulomb forces is expected to be important and where application of the theory to germanium would be permissible but for the implicit assumption of a simple band structure (c). Neither the effective masses nor the anisotropy of the relaxation times for electrons can be treated rigorously. We shall proceed on the assumption that a suitable single value of effective mass for a carrier can be chosen which not only replaces the conductivity mass and the masses appropriate to the various scattering processes but also, to some extent, takes account of the effect of anisotropy on the magnitude of the relaxation time. Accordingly we shall treat the effective mass of the electron and hole as variable parameters to be fixed by a comparison between theory and experiment. Because the impact parameter beyond which coulomb encounters are assumed to be negligible is not a well defined length and to make additional allowances for anisotropy, we also treat d as a parameter which has the same dependence on temperature and impurity concentration as λ but has a variable magnitude, $d = a\lambda$, where a is an adjustable parameter.

In view of the large anisotropy of the effective mass and relaxation times for electrons and the large difference between the effective masses of holes it might appear that this simple description will prove inadequate. To make our approach more plausible we make the following observations:

(i) DEBYE and CONWELL[13] were able to obtain a reasonably good fit to Hall data for n-type germanium using essentially the same assumptions as above, though, of course, (e–h) scattering was absent. (ii) A recent careful study of the ionized impurity scattering mobility of electrons in silicon[14] gave very good agreement for most impurity concentrations with the BROOKS–HERRING[15] formula which assumes a scalar relaxation time (the anisotropy is less pronounced for Si, $\tau_{\parallel}/\tau_{\perp} \sim 4$[6]). (iii) While the mobility of electrons in a particular valley may have a pronounced anisotropy, crystal symmetry ensures the resultant mobility, which we calculate, is isotropic. (iv) During the time it takes to perform the experiment (transit time, defined in I, $\sim 10^{-6}$ sec) a hole makes approximately 10^6 interband transitions and an electron at least 10^3 intervalley transitions. Therefore, the mobility determined is of some "average electron" or some "average hole".

Our attitude, then, is that the difficulty of applying the theory to germanium, which is introduced by the band structure, can be overcome by treating the effective masses and, to a lesser extent, the cut-off to coulomb scattering as variable parameters. This introduces some latitude in the comparison between theory and experiment; it acknowledges that we cannot make a direct comparison between theory and experiment that immediately establishes, unambiguously, the effects of (e–h) scattering. It means we have to attempt to fit the theoretical curves to the experimental results and in so doing to find a set

Vol. 18
1961

of the values of the adjustable parameters which gives the "best fit". There are obviously limits outside which the values of these parameters would be unacceptable. The remarks of the previous paragraph imply that the anisotropy should not have a large effect and, therefore, we should neither expect the values of effective mass to differ appreciably from the conductivity and density of states masses nor expect d to be significantly different from λ.

3. THE THEORY APPLIED TO CONDUCTIVITY AND MINORITY CARRIER MOBILITY IN GERMANIUM

For a mixture of two types of free carriers (electrons and holes) we find in II that the mobilities of the individual types of particle are given by

$$\mu_1^{(N)} = \frac{e_1}{m_1^2} kT a_0^{(N)} \text{ and } \mu_2^{(N)} = \frac{e_2}{m_2^2} kT b_0^{(N)}, \quad (2)$$

where $a_0^{(N)}$ and $b_0^{(N)}$ are given by the solution of the equations

$$\left.\begin{aligned} \sum_{s=0}^{N} [d_{rs}^{(1)} + n_1\beta_{rs}^{(1)} + n_2 y_{rs}^{(12)}] a_s^{(N)} + \frac{e_2 m_1}{e_1 m_2} \sum_{s=0}^{N} n_2 x_{rs}^{(12)} b_s^{(N)} &= 3\delta_{r0} \\ \frac{e_1 m_2}{e_2 m_1} \sum_{s=0}^{N} n_1 x_{rs}^{(21)} a_s^{(N)} + \sum_{s=0}^{N} [d_{rs}^{(2)} + n_2\beta_{rs}^{(2)} + n_1 y_{rs}^{(21)}] b_s^{(N)} &= 3\delta_{r0} \end{aligned}\right\} \quad (3)$$

$r = 0,1,2 \ldots N$, and e_α, m_α and n_α ($\alpha = 1,2$) are the charge, mass and concentration of carriers of type α. The terms $d_{rs}^{(\alpha)}$ represent the interaction of the particle of type α with defects, while the terms $\beta_{rs}^{(\alpha)}$, $x_{rs}^{(\alpha\beta)}$ and $y_{rs}^{(\alpha\beta)}$ relate to the interaction between the free carriers: expressions for these terms will be given below. Although the effects of (e–e) and (h–h) scattering, described by the β_{rs} terms, are small in germanium, these are retained for the sake of completeness. The theory does not yield exact values of μ_α, though the solutions of the equations can be taken to any required order of approximation N, giving values of $\mu_\alpha^{(N)}$ which have been shown to converge as N increases.

The equations (3) can be simplified for comparison with the conductivity and minority carrier mobility. Experimentally the mobility of a group of minority carriers is measured which have concentrations of 1 to 10 per cent of the majority carrier concentration. The values of minority carrier mobility quoted in I were obtained from extrapolating these results to zero minority carrier concentration. Thus, choosing carriers of type 1 as minority carriers, we have $n_1 = 0$. The majority carrier mobility, μ_2, and hence the conductivity is then independent of minority carriers which is physically exact since, of course, no minority carriers were injected when the conductivity was measured.

Both the conductivity and minority carrier mobility will be calculated in the third order approximation.* In II it has been estimated that calculations of minority carrier mobility in this approximation are, in the least favourable region, within 5 per cent of the correct result and calculations of the majority carrier mobility are in error by no more than ~ 3 per cent.

The remainder of this section will be devoted to a consideration of the values of the terms which appear in equations (3). The terms representing defect scattering can be subdivided,

$$d_{rs}^{(\alpha)} = \sum_i d_{rs}^{(\alpha)}(i),$$

where i labels individual defect scattering processes. For any defect scattering mechanism the relaxation time $\tau_\alpha(i)$ is related to $d_{rs}^{(\alpha)}(i)$ by

$$d_{rs}^{(\alpha)}(i) = \frac{1}{(\tau_\alpha(i) v^{\nu(i)})} \frac{2}{\pi^{1/2}} \left(\frac{2kT}{m_\alpha}\right)^{1+\nu(i)/2} \gamma_{rs}(i) \quad (4)$$

where v_α is the velocity of the particle of type α and $v^{-\nu(i)}$ is the velocity dependence of the relaxation time. The required values of the coefficients $\gamma_{rs}^{(i)}$ are given in II. We shall deal with the individual scattering processes under separate

* "Third order approximation" is used here in the same sense as in II.

Table 1. *Values of parameters for electrons and holes in germanium. Fixed parameters obtained from independent experimental observations and calculations, variable parameters found from fitting theoretical curves to the experimentally determined minority carrier mobility.*

Parameter	Type	Electrons	Holes	Units
$p(m/m_0)^{1/2}$	Fixed	47·0	2·14	$cm^{-1}°K^{(1/2-\delta)}$
δ	,,	1·66	2·33	
R	,,	65	43	Å
ϵ	,,	16	16	
m/m_0	Variable	0·12	0·30	
T_c	,,	110	70	°K
T_c'	,,	200	—	°K
δ'	,,	1·9	—	
a	,,	0·8	0·8	

headings but shall group ionized impurity scattering and carrier–carrier scattering together under the general heading of scattering by a coulomb potential.

3.1 *Phonon scattering* ($i = 1$)

Free carriers are scattered by both acoustical and optical phonons, though, as emphasized in Section 2, optical mode scattering is not important at low temperatures. Therefore, to a good approximation, we can write the relaxation time due to phonon scattering of the particle of type α as

$$1/\tau_\alpha(i) = p_\alpha T^{(\delta_\alpha - 1/2)} v_\alpha, \ \nu(i) = 1, \qquad (5)$$

where p_α is a constant measuring the strength of the scattering and $T^{-\delta_\alpha}$ is the temperature dependence of the lattice mobility. The unimportance of optical phonons thus allows us to use the values of γ_{rs}[1] given in II for acoustical phonon scattering. In the region of room temperature the values of δ_α are well known;[15] we therefore regard them as fixed parameters and they are given in Table 1. At lower temperatures δ_α becomes less certain because of ionized impurity scattering while at the lowest temperatures we can anticipate that $\delta_\alpha \to \frac{3}{2}$ if its deviation from this value is due to optical phonon scattering[16] and probably if it is due to a change of effective mass.[12] To allow for this in a simple fashion we have introduced a temperature T_c below which the lattice mobility obeys a $T^{-3/2}$ law; i.e. for

$$T \leqslant T_c, \ 1/\tau_\alpha(i) = p_\alpha T_{c\alpha}{}^{(\delta_\alpha - 1.5)} T v_\alpha.$$

The values of p_α were determined from experimental data at 300°K. Because the effective mass is treated as a variable parameter we are able to find directly only $p_\alpha(m_\alpha/m_0)^{1/2}$. The values shown in Table 1 were obtained from a lattice mobility of holes of 1900 $cm^2\ V^{-1}\ sec^{-1}$ and a lattice mobility of electrons of 3900 $cm^2\ V^{-1}\ sec^{-1}$.[17] The value of 70°K for T_c chosen for holes is acceptable since there is some evidence that there is no change in effective mass between 4°K and this temperature and that a $T^{-3/2}$ law is obeyed.[18] In the fitting of theory to experiment it was realized that an improvement in the fit to electron mobilities could be achieved if the rate of change of mobility was increased above that predicted by a $T^{-1.66}$ law in the region of 150°K. An intermediate region was introduced in which $\mu \propto T^{-\delta'}$; the region extending from T_c, below which $\mu \propto T^{-1.5}$, to T_c', above which $\mu \propto T^{-1.66}$. At the time the fitting was carried out, such a splitting of the lattice mobility into three regions—the intermediate region having the strongest temperature dependence—did not appear unreasonable since HERRING[16] has shown that the combined effects of intraband scattering by acoustical phonons coupled with a discrete energy phonon scattering process (e.g. optical phonons, intervalley phonons) produces just this sort of variation of mobility with temperature. However, the parameters given in Table 1 would imply considerably more optical mode scattering than is now known to be the case[12] and is at variance with our statements concerning optical phonon

scattering in Section 2. We are inclined, therefore, to believe that the introduction of this intermediate region is unrealistic. The relatively small changes in the theoretical curves ($\ll 10$ per cent) which this change of attitude incurs will be discussed when the theoretical curves are presented in Section 4.

3.2 *Scattering by a coulomb potential*

The expression which has been derived for ionized impurity scattering, using the Rutherford scattering cross-section and assuming spherical constant energy surfaces, is

$$1/\tau_\alpha(2) = \frac{2\pi e^4}{\epsilon^2 m_\alpha^2} N^* L' v_\alpha^{-3}, \nu(2) = -3, \quad (6)$$

where N^* is the concentration of ionized impurity atoms and L' is a logarithmic factor the precise form of which depends on how the coulomb potential has been assumed to be modified. Our treatment of the scattering (Section 2) is equivalent to assuming that the coulomb potential is unscreened but cut off at a distance d; this gives

$$L' = \log_e\left[1+\left(\frac{4\epsilon kT}{e^2}\,\mathrm{d}\right)^2\right]. \quad (7)$$

To determine N^* we make the assumption that compensation is negligible, hence $N^* = n_2$, and calculate the concentration of free carriers in exactly the same way as described in I.† (The assumption that compensation is negligible for samples used for the measurement of the minority carrier mobility is discussed in I).

The required expressions for the $\beta_{rs}^{(\alpha)}$, $x_{rs}^{(\alpha\beta)}$ and $y_{rs}^{(\alpha\beta)}$ have been given in the appendix of II. Each of these consists of a factor $\Omega_{\alpha\beta}$ modified by appropriate coefficients, where

$$\Omega_{\alpha\beta} = \frac{e^4}{2\epsilon^2}\left(\frac{\pi}{m_{\alpha\beta}}\right)^{1/2}\frac{L_1}{(2kT)^{3/2}}, \quad (8)$$

$m_{\alpha\beta}$ being the reduced mass, $m_\alpha m_\beta(m_\alpha+m_\beta)^{-1}$. Here again L_1 is a logarithmic term, and, if we choose the cut-off distance of the unscreened coulomb potential of a free carrier to be the same as for an ionized impurity atom, we have $L' = L_1$.‡ The coefficients of $\Omega_{\alpha\beta}$ are also affected by the choice of the cut-off distance through logarithmic factors (L_1, L_2 and L_3).

By choosing the cut-off distance of the coulomb forces to be the same for ionized impurity atoms and for free carriers we have made the effective scattering potentials identical in the two cases. This is reflected in the basic similarity of equations (6) and (8). An important consequence of this is that *no additional variable parameters are introduced by the inclusion of carrier–carrier scattering.*

3.3 *Neutral impurity scattering* ($i = 3$)

ERGINSOY[19] derived the following expression for the relaxation time due to neutral impurity scattering,

$$\frac{1}{\tau_\alpha^{(\beta)}(3)} = \frac{20\hbar}{m_\alpha} R_\beta(N-N^*), \nu(3) = 0, \quad (9)$$

where $N-N^*$ is the concentration of neutral impurity atoms and R_β is the radius of the orbit of the bound carrier of type β to the neutral atom. Values of R_β, from KOHN's theoretical estimates,[20] are given in the table and are regarded as fixed parameters.

4. COMPARISON BETWEEN THE THEORY AND THE EXPERIMENTAL RESULTS

In this section we shall begin by describing the fitting of the theoretical curves to the experimental results and shall present the curves obtained for the final choice of the variable parameters. We shall then comment on how sensitive the theoretical curves are to this choice of parameters. Finally the values of these parameters will be discussed.

We have mentioned in the introduction and have shown elsewhere (II) that the effects of (e–e) or (h–h) scattering on the majority carrier mobility and hence the conductivity, σ, of germanium is small. Fitting the theoretical to the experimentally determined values of σ is, therefore, merely a means of determining the variable parameters to describe defect scattering and is not a test of the

† The effective mass used in this calculation of n_2 is the density of states mass. The calculation of the density of free carriers is regarded as distinct from the calculation of the mobility, and the mass which appears in the calculation of n_2 is not treated as a variable parameter.

‡ We may justify the choice of equal effective screening of mobile and stationary particles on the grounds that the velocity of the mobile particles is low compared with propagation velocity of the space charge.

Vol. 18
1961

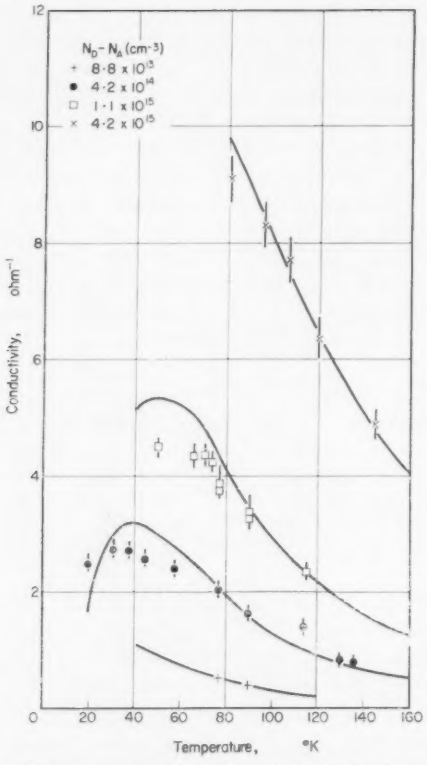

FIG. 2. The conductivity of majority holes in p-type germanium as a function of temperature.

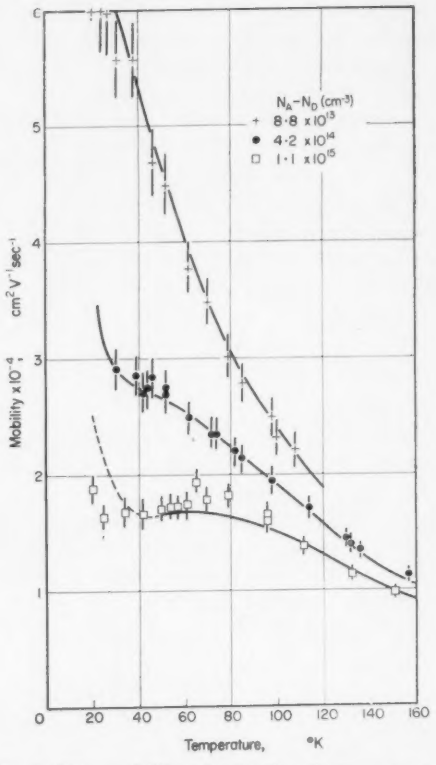

FIG. 3. The mobility of minority electrons in p-type germanium as a function of temperature.

theory of carrier–carrier scattering. As pointed out in Section 3, no additional variable parameters are introduced by the inclusion of carrier–carrier scattering so that, in principle, we can see how well our theory describes (e–h) scattering by comparing the calculated and observed minority carrier mobility μ_1, using the parameters obtained from a fit to the conductivity σ. In practice, however, our procedure has been to choose the parameters from the fit to σ but to allow our choice to be influenced by the degree of agreement achieved between the calculated and observed values of μ_1. This is because the mobility μ_1 is more sensitive than the conductivity to the value of the parameter d.

The calculation of both σ and μ_1 in the third order approximation was performed for the relevant impurity concentrations over a temperature range from 20°K to 160°K on the TREAC digital computor. The results of these calculations using the parameters listed in Table 1 are presented in Figs. 2, 3, 4 and 5 where the experimental values of μ_1 and σ are shown for comparison. The maximum experimental error in the measured values of μ_1 and σ is shown. When making a comparison between the theoretical curves and the experimental points it should be borne in mind that as well as the errors in the theoretical curves which we have discussed there may be errors (not shown in the figures) of several per cent in the experimental points introduced by inhomogeneity of the specimens. In view of these remarks we regard the fit of theory to experiment as reasonable. We observe that for μ_1 the correct sort of temperature dependence is obtained and furthermore, the variation of the temperature dependence with impurity concentration is essentially correct. All the theoretical curves fall within about 10 per cent

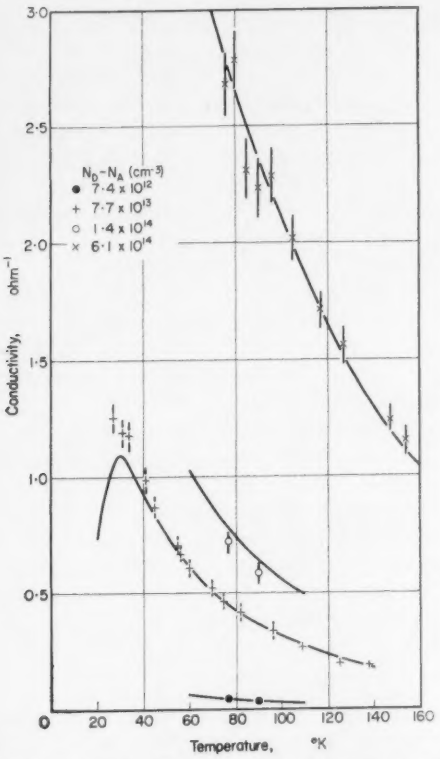

FIG. 4. The conductivity of majority electrons in n-type germanium as a function of temperature.

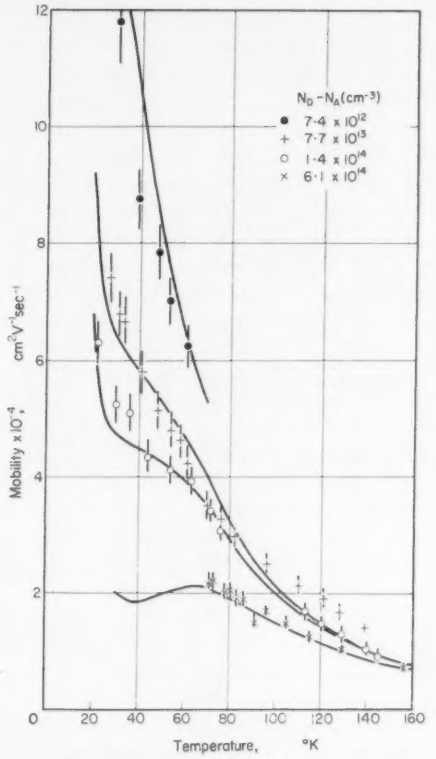

FIG. 5. The mobility of minority holes in n-type germanium as a function of temperature.

of the experimental points, the majority of them being within the experimental error of ~ 6 per cent. It must be emphasized that this degree of agreement is brought about mainly by (e–h) scattering, for, as pointed out in I, there are large discrepancies between theory and experiment if (e–h) scattering is neglected and, as we showed in II, the terms describing (e–h) scattering have a large influence on the mobility. Discrepancies between theory and experiment are to be expected below about 30°K for low resistivity samples because under the conditions of the experiment impact ionization occurs in this region (I). The poorest fit is obtained for the conductivity of holes below 60°K, though nowhere is the discrepancy greater than 18 per cent. The theoretical curves for both the mobility of minority electrons and the conductivity of majority electrons have been deduced on the assumption of an intermediate phonon scattering region where $\mu(1) \propto T^{-\delta'}$ (see Section 3) but which, since completing the computations, we consider to be unrealistic. The exclusion of this region decreases the mobilities by less than 10 per cent even in the most affected cases, i.e. high resistivity specimens. Thus the change brought about by the exclusion of this intermediate phonon scattering region will not significantly detract from the over-all picture of a reasonable fit of the theoretical curves to the experimental points.

The following list of observations on the curve fitting is included to convey an idea of how sensitive the fitting is to the value of the variable parameters; it is made for samples of intermediate impurity concentration.

(i) A 50 per cent increase in m decreases μ_1 and σ by a maximum of about 16 per cent—the maximum change occuring at 40°K.

(ii) A 50 per cent increase in a decreases μ_1 by a maximum of about 14 per cent—the maximum change occuring at 40°K.

(iii) An increase in T_c of 20°K produces a maximum decrease in μ_1 and σ of about 10 per cent, this occuring near T_c.

While we have already made some comments on the chosen values for the variable parameters which enter into the expressions for phonon scattering, we have left until now a discussion of the values chosen for the effective masses and the parameter a. We have pointed out in Section 2 that the extent to which we have established the importance of (e–h) scattering does depend on whether or not these parameters have acceptable values, and we have suggested that d should not differ significantly from $\lambda(a \sim 1)$ and the masses should be close to the conductivity and density of state masses. We note that the value found for the parameter a (0·8) is indeed close to unity, and further that the mass determined for an electron is, in fact, the conductivity mass of the multivalley model. While a conductivity mass cannot be simply defined for holes, since it is dependent on the relaxation processes, the value we have found for the hole mass cannot be very different from it and is close to the density of states effective mass. (If the relaxation times of light and heavy holes are the same the combined conductivity mass is 0·25 m_0. The density of states mass is 0·37 m_0. Both of these are calculated from cyclotron resonance data obtained at 4°K[7].)

5. SUMMARY AND CONCLUSIONS

A consideration of the limitations of the theory as applied to germanium reveals that there are certain ranges of temperature and concentration in which it is valid but for the implicit assumption of isotropic masses and relaxation times. Most of the experimental results of I are included in these ranges. In an attempt to overcome this limitation we have treated the effective mass of each carrier and the cut-off distance to the scattering of a coulomb potential as variable parameters. In addition we have introduced adjustable parameters to describe the phonon scattering.

A good fit of the theoretical curves to the experimental data is achieved using this small number of parameters. There is agreement both with regard to the temperature variation and magnitude of the mobility over a wide range of impurity concentration and a temperature range as large as that for which the theory is valid, and the values assigned to the variable parameters are acceptable. We conclude, therefore, that we have established the importance of the effect of (e–h) scattering on the minority carrier mobility in germanium for, by incorporating it in the calculation of μ_1, we have reduced discrepancies between theory and experiment of the order of a factor of 2 to less than 10 to 20 per cent. Furthermore, we have shown that, although the theory as it is developed at present does not take into account the details of the band structure of germanium, anisotropic effects on the mobility are not sufficiently important to prevent an adequate description of the minority carrier mobility to be given if suitable choices are made for the effective mass and the cut-off to coulomb encounters. We regard the agreement between theory and experiment as empirical justification for our attempt to describe carrier–carrier scattering in germanium using an isotropic mass and relaxation time.

Acknowledgements—The authors would like to thank members of the Mathematics Division, R.R.E., in particular Dr. D. J. HOWARTH for assistance in preparing a programme for the TREAC digital computor. This paper is published by permission of the Controller, H.M. Stationery Office.

REFERENCES

1. PAIGE E. G. S., *J. Phys. Chem. Solids* **16,** 207 (1960). To be referred to as I.
2. McLEAN T. P. and PAIGE E. G. S., *J. Phys. Chem. Solids* **16,** 220 (1960). To be referred to as II.
3. DEXTER R. N., ZEIGER J. H. and LAX B., *Phys. Rev.* **104,** 637 (1956).
4. HERRING C. and VOGT E., *Phys. Rev.* **101,** 944 (1956).
5. LAFF R. A. and FAN H. Y., *Phys. Rev.* **112,** 317 (1958).
6. HAM F. S., *Phys. Rev.* **100,** 1251 (1955).
7. LAX B and MAVROIDES J. G., *Phys. Rev.* **100,** 1650 (1955).
8. CONWELL E. M. and WEISSKOPF V. E., *Phys. Rev.* **77,** 388 (1950).
9. BLATT F. J., *J. Phys. Chem. Solids* **1,** 262 (1957).
10. BLATT F. J., *Solid State Physics*, Vol. IV. Academic Press, New York (1947).
11. See for example STRATTON R., *J. Electronics and Control* **5,** 157 (1958); CONWELL E. M., *J. Phys. Chem. Solids* **8,** 234 (1959).

12. GIBSON A. F., GRANVILLE J. W. and PAIGE E. G. S., *J. Phys. Chem. Solids* (1961); BROWN M. A. C. S., *J. Phys. Chem. Solids* (1961).
13. DEBYE P. P. and CONWELL E. M., *Phys. Rev.* **93,** 693 (1954).
14. LONG D. and MYERS J., *Phys. Rev.* **115,** 1107 (1959).
15. MORIN F. J., *Phys. Rev.* **93,** 62 (1954).
16. HERRING C., *Bell Syst. Tech. J.* **32,** 237 (1955).
17. PRINCE M. B., *Phys. Rev.* **92,** 681 (1953).
18. BAGGULEY D. M. S., POWELL J. A. and TAYLOR D. J., *Proc. Phys. Soc. Lond.* **A 70,** 759 (1957); BROWN D. M. and BRAY R., *Bull. Amer. Phys. Soc.* **5,** 194 (1960).
19. ERGINSOY C., *Phys. Rev.* **79,** 1013 (1950).
20. KOHN W., *Solid State Physics* Vol. V. Academic Press, New York (1957).

Vol. 18
1961

J. Phys. Chem. Solids Pergamon Press 1961. Vol. 18, Nos. 2/3, pp. 150–155. Printed in Great Britain.

VARIATION DU POUVOIR THERMOELECTRIQUE DES ALLIAGES METALLIQUES DU TYPE Cu Znβ EN FONCTION DE L'ORDRE

M. T. BEAL

Faculté des Sciences, Laboratoire de Physique du Solide, Group II—Orsay (S. & O.), France

(*Received* 21 *July* 1960)

Résumé—Nous montrons de façon théorique, en fonction de la température, l'influence du désordre atomique sur le pouvoir thermoélectrique de certains alliages. Nous traitons ici les alliages équivalents au laiton β du point de vue structure cristalline et comportement thermodynamique. On prévoit un abaissement général du pouvoir thermoélectrique et des anomalies plus ou moins marquées au point de transition d'ordre. Ces calculs sont directement transposables sur le plan magnétique.

Abstract—We study theoretically the influence of atomic disorder on the thermoelectric power plotted against temperature, for some alloys. We deal in the present paper with alloys of crystalline structure and thermodynamical behaviour similar to those of β brass. We predict a general lowering of the thermoelectric power and anomalies at the transition point more or less sharply marked. These calculations can be directly transposed to a magnetic study.

1. INTRODUCTION

Nous avons étudié précédemment,[1] en fonction de la température, les variations de résistivité électrique dues au désordre atomique dans les alliages du type CuZnβ: cubiques centrés présentant une transition d'ordre de 2ème espèce. Nous étudions ici les variations de pouvoir thermoélectrique dans les mêmes conditions. Certains paramètres étant inconnus, plusieurs cas sont envisagés, ce qui permet des conclusions assez générales. L'effet global est un abaissement de pouvoir thermoélectrique. L'ordre à longue distance donne l'ordre de grandeur des écarts. L'ordre à courte distance n'y apporte que de légères modifications et seulement au voisinage du point de transition où l'on prévoit un changement de pente. La nature des interactions entre atomes et le nombre d'électrons de conduction interviennent assez peu. Les écarts sont en général petits et leur importance dépend essentiellement du signe du pouvoir thermoélectrique dû aux phonons seuls et de la grandeur relative de la résistivité due aux phonons à celle due au désordre. Dans tous les cas, le pouvoir thermoélectrique total varie linéairement à haute température et ne s'écarte de cette valeur asymptotique qu'au voisinage du point critique d'ordre où les courbes présentent un point anguleux analogue à celui déjà trouvé dans les courbes de résistivité.[1] Notons que les calculs sont valables pour le désordre magnétique.

2. RAPPEL DES FORMULES CLASSIQUES

Le pouvoir thermoélectrique d'un métal pur a pour expression, au-dessus de la température de Debye[2]:

$$p = -\frac{\pi^2}{3}\frac{k^2 T}{e}\left[\frac{\partial \log \rho}{\partial E}\right]_{E=E_F} \qquad (1)$$

où ρ est la résistivité due à la diffusion électrons–phonons, T la température absolue, k la constante de Boltzmann, e la charge de l'électron, E l'énergie électronique et E_F l'énergie de Fermi.

La diffusion par le désordre atomique introduit

une variation relative[3]:

$$\frac{\Delta P}{P} = -\frac{1-\dfrac{\Delta x}{x}}{1+\dfrac{\rho}{\Delta\rho}} \tag{2}$$

avec les notations :

$$x = -E_F\left(\frac{\partial \log \rho}{\partial E}\right)_{E_F},$$

$$\Delta x = -E_F\left(\frac{\partial \log \Delta\rho}{\partial E}\right)_{E_F} \tag{3}$$

où $\Delta\rho$ est la résistivité supplémentaire due au désordre.

3. CONDITIONS DANS LESQUELLES EST FAIT LE PRESENT CALCUL

On a fait ici une étude approximative du cas d'un alliage binaire 50 pour cent, parfaitement ordonné à 0°K, cubique centré à cette température et décomposable en deux sous-réseaux cubiques simples identiques, présentant, d'autre part, une transition d'ordre à longue distance de 2ème espèce.[4]

On ne connaît par le spectre des phonons dans un alliage, mais le paramètre x prenant des valeurs comprises entre -3 et $+2$ dans un métal pur[2], on a envisagé les deux cas où $x = +2$ et $x = -2$.

Nous avons étudié précédemment[1] la variation de résistivité $\Delta\rho$ due aux fluctuations d'ordre à longue et courte distance, en fonction de la température. Nous avions abouti aux formules suivantes, de part et d'autre du point critique d'ordre à la température T_c :

$$\frac{\overline{\Delta\rho}}{\overline{\Delta\rho_0}} = 1+\frac{T_c}{T}A(k_FD) \quad \text{pour } T \geqslant T_c$$

$$\frac{\overline{\Delta\rho}}{\overline{\Delta\rho}} = (1-S^2)\left[1+(1-S^2)\frac{T_c}{T}A(k_FD)\right] \tag{4}$$

$$\text{pour } T \leqslant T_c$$

avec :

$$\log\frac{1+S}{1-S} = 2S\frac{T_c}{T}, \tag{5}$$

où S est l'ordre à grande distance

et

$$A(k_FD) = \frac{1}{(k_FD)^2}\left[\cos 2k_FD - \frac{\sin 2k_FD}{k_FD} + \frac{1-\cos 2k_FD}{2(k_FD)^2}\right] \tag{6}$$

où D est la distance entre atomes proches voisins et k_F la longueur du vecteur d'onde au niveau de Fermi; enfin, $\Delta\rho_0$ est la variation de résistivité due au désordre total, à très haute température.

$\Delta\rho_0$ est constante en température et ne dépend que de k_F par l'intermédiaire, d'une part de la section efficace incohérente par atome, elle-même proportionnelle à[2] $(k_FD)^{-4}$, d'autre part de la vitesse électronique, en k_FD, et enfin de l'inverse du nombre effectif d'électrons par unité de volume, qui est proportionnel à $(k_FD)^3$; $\Delta\rho_0$ est donc de la forme :

$$\Delta\rho_0 \propto (k_FD)^{-6} \tag{7}$$

Il est à noter que la formule en $(k_FD)^{-4}$, pour la section efficace incohérente par atome, n'est pas valable pour les très faibles valeurs des (k_FD); nous n'envisagerons donc que des valeurs de k_FD de l'ordre de 3 ou supérieures.

On a adopté pour ρ la forme de résistivité de haute température

$$\rho = aT$$

où a est une constante; et une courbe de résistivité expérimentale de CuZnβ[5] donne approximativement :

$$T_c \sim \tfrac{1}{2}\Delta\rho_0$$

Nous avons envisagé le cas particulier :

$$\rho \sim \frac{\Delta\rho_0}{2}\frac{T}{T_c} \tag{8}$$

et aussi le cas où :

$$\frac{\rho}{\Delta\rho} \text{ négligeable.} \tag{9}$$

4. CALCULS EFFECTIFS DES VARIATIONS DU POUVOIR THERMOELECTRIQUE

Avec les notations du paragraphe précédent, nous obtenons les formules suivantes :

Vol. 18
1961

(a) $(\rho/\Delta\rho) \sim \frac{1}{2}(T/T_c)$; énergies d'interaction répulsives entre atomes; contribution des ordres à courte et longue distance:

$$\frac{\Delta P}{P} = -\frac{\left(2-\frac{6}{x}\right)\frac{T}{T_c}+\left(2-\frac{6}{x}\right)A+\frac{k_F D}{x}\frac{dA}{d(k_F D)}}{\frac{T^2}{T_c^2}+2\frac{T}{T_c}+2A} \quad \text{pour } T \geqslant T_c \tag{10}$$

$$\frac{\Delta P}{P} = -\frac{\left(2-\frac{6}{x}\right)\frac{T}{T_c}+\left(2-\frac{6}{x}\right)(1-S^2)\,A+\frac{k_F D}{x}(1-S^2)\frac{dA}{d(k_F D)}}{\frac{T^2}{T_c^2}+2(1-S^2)\frac{T}{T_c}+2(1-S^2)^2 A} \quad \text{pour } T \leqslant T_c \tag{11}$$

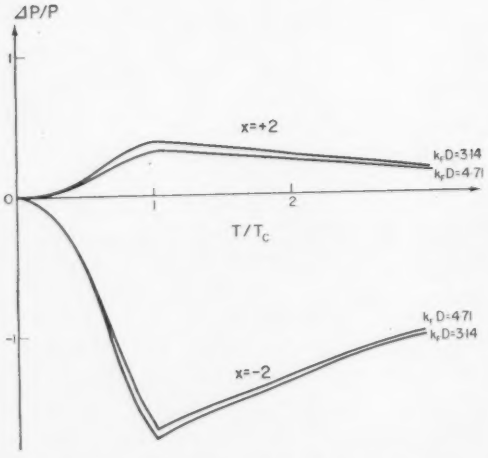

FIG. 1. Courbes de variation relative du pouvoir thermoélectrique pour plusieurs valeurs du paramètre $k_F D$ (k_F vecteur d'onde au niveau de Fermi et D distance entre atomes proches voisins), dans le cas où $\rho/\Delta\rho_0 = \frac{1}{2}\,T/T_c$ (ρ résistivité due aux phonons, et $\Delta\rho_0$ résistivité de désordre total), et où les énergies d'interaction entre atomes sont répulsives.

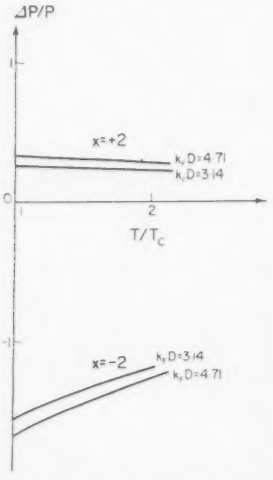

FIG. 2. Courbes analogues à celles de la Fig. 1 mais dans le cas d'énergies d'interaction attractives.

Les courbes de la Fig. 1 illustrent ces formules et sont tracées pour diverses valeurs de $(k_F D)$.

(b) $(\rho/\Delta\rho_0) \sim \frac{1}{2}(T/T_c)$: energies d'interaction attractives entre atomes; contribution des ordres à courte et longue distance :

$$\frac{\Delta P}{P} = -\frac{\left(2-\frac{6}{x}\right)\frac{T}{T_c}-\left(2-\frac{6}{x}\right)A-\frac{k_F D}{x}\frac{dA}{d(k_F D)}}{\frac{T^2}{T_c^2}+2\frac{T}{T_c}-2A} \quad \text{pour } T \geqslant T_c \tag{12}$$

Les courbes correspondant à cette formule sont rassemblées sur la Fig. 2.

Nous ne donnons pas ici de formule correspondant à $T < T_c$; en effet, dans ce cas, l'ordre à longue distance n'existe plus. Il ne subsiste que l'ordre à courte distance qui provoque la formation d'amas, à basse température, et il faudrait d'abord en expliciter la résistivité.

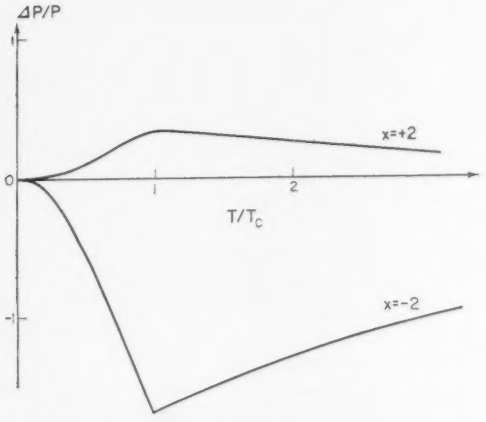

FIG. 3. Courbe analogue à celles de la Fig. 1 mais où on n'a pas tenu compte de l'ordre à courte distance ; la courbe est unique puisque indépendante de k_FD dans ce cas.

(c) $(\rho/\Delta\rho) \sim \frac{1}{2}(T/T_c)$; énergies d'interaction quelconques, contribution de l'ordre à longue distance seul :

$$\frac{\Delta P}{P} = -\frac{\left(2-\frac{6}{x}\right)}{\frac{T}{T_c}+2} \quad \text{pour } T \geqslant T_c \qquad (13)$$

$$\frac{\Delta P}{P} = -\frac{\left(2-\frac{6}{x}\right)(1-S^2)}{\frac{T}{T_c}+2(1-S^2)} \quad \text{pour } T \leqslant T_c \qquad (14)$$

auxquelles correspond la Fig. 3. On remarque que les formules sont indépendantes de k_FD.

(d) $(\rho/\Delta\rho) \sim 0$; énergies d'interaction répulsives entre atomes, contribution des ordres à courte et longue distance.

$$\frac{\Delta P}{P} = -\left(1-\frac{3}{x}\right) - \frac{k_FD}{2x} \times \frac{\overline{\frac{dA}{d(k_FD)}}}{\frac{T}{T_c}+A} \quad \text{pour } T \geqslant T_c \qquad (10')$$

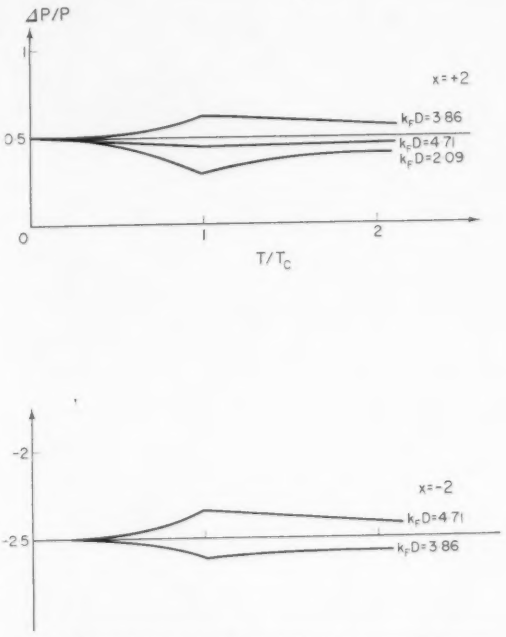

FIG. 4. Courbes de variation relative du pouvoir thermoélectrique pour plusieurs valeurs de k_FD, dans le cas où $\rho/\Delta\rho_0$ est négligeable et où les énergies d'interaction sont répulsives.

$$\frac{\Delta P}{P} = -\left(1-\frac{3}{x}\right) - \frac{k_FD}{2x}(1-S^2)\frac{\overline{\frac{dA}{d(k_FD)}}}{\frac{T}{T_c}+(1-S^2)A} \quad \text{pour } T \leqslant T_c \qquad (11')$$

illustrées sur la Fig. 4.

(e) $(\rho/\Delta\rho) \sim 0$; énergies d'interaction attractives entre atomes, contribution des ordres à courte et longue distance.

$$\frac{\Delta P}{P} = -\left(1-\frac{3}{x}\right) + \frac{k_FD}{2x} \times \frac{\overline{\frac{dA}{d(k_FD)}}}{\frac{T}{T_c}-A} \quad \text{pour } T \geqslant T_c \qquad (12')$$

sur la Fig. 5.

Vol. 18
1961

Nous avons enfin esquissé, sur la Fig. 6, l'allure approximative des courbes de $P+\Delta P$; il faudrait connaître la dépendance exacte en température de P pour plus de précision.

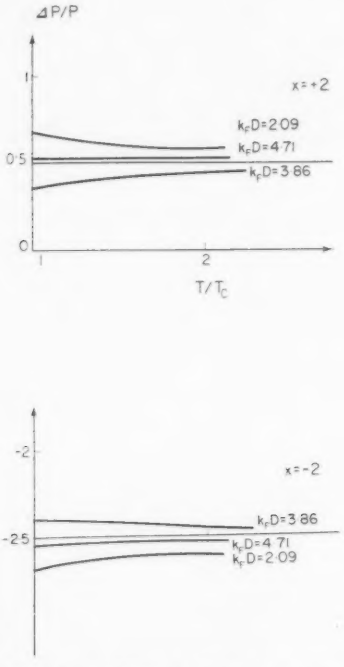

FIG. 5. Courbes analogues à celles de la Fig. 4, mais pour des énergies d'interaction attractives.

5. INTERPRETATION DES RESULTATS ET CONCLUSION

D'après l'ensemble de ces courbes, le désordre produit un abaissement général du pouvoir thermoélectrique. Le pouvoir thermoélectrique total $P+\Delta P$ suit une loi linéaire à très haute température, et s'en écarte surtout au voisinage du point critique où l'on observe un changement de pente dans les courbes. Les déviations par rapport à P sont assez faibles, si P est négatif; et plus fortes si P est positif. En particulier dans le cas où $(\rho/\Delta\rho)\sim 0$, et P positif, on constate que $P+\Delta P$ est toujours négatif; un autre point intéressant sur cet exemple est que les écarts de $P+\Delta P$ à son asymptote de haute température sont positifs ou négatifs suivant les valeurs de k_FD, plus précisément[1] suivant que $(\Delta\rho/\Delta\rho_0) < 1$ ou >1; d'où un changement de pente dans un sens ou dans l'autre à T_c; On a remarqué de tels phénomènes expérimentalement[6] dans des alliages **Pu** Al et il en a été donné une interprétation analogue à celle présentée ici.[7] Dans tous les cas, la contribution de l'ordre à longue distance donne, à elle seule, un bon schéma des courbes, qui ne sont que légèrement modifiées par l'ordre à courte distance et essentiellement au voisinage du point critique.

La nature des interactions entre atomes intervient peu. L'influence de la valeur de k_FD est assez faible dès que celle-ci n'est pas trop petite; mais, comme nous l'avons déjà indiqué, les formules perdent leur validité pour k_FD petit.

Des anomalies de pouvoir thermoélectrique ont été observées expérimentalement dans les métaux de transition et dans AuCu. Celles du fer,[8] correspondant à une transition d'ordre magnétique, semblent en bon accord qualitatif avec notre théorie. Certains résultats obtenus pour le chrome[9] présentent aussi une anomalie peu marquée ; d'autres,[10] au contraire, signalent de grosses déviations au point critique, inexplicables par nos calculs qui seraient à modifier sensiblement pour une structure d'ordre aussi complexe que celle du chrome. Enfin on a trouvé également des anomalies dans AuCu,[11] faibles mais en sens inverse de celles proposées ici. Notons cependant que cet alliage n'entre pas directement dans la catégorie de ceux que nous avons étudiés ; par ailleurs il semble, dès maintenant, que la contribution des termes d'ordre supérieur à $1/T$ dans la résistivité et le pouvoir thermoélectrique puisse modifier le sens des déviations.

En conclusion, notre théorie, dans l'état actuel, ne nous permet pas d'envisager de fortes valeurs de $|P+\Delta P|$ mais il en résulte néanmoins des modifications certaines du pouvoir thermoélectrique dues au désordre surtout au voisinage du point de transition.

Remerciement—Ce travail m'a été suggéré par Monsieur le Professeur J. FRIEDEL, que je tiens à remercier pour ses nombreux conseils.

BIBLIOGRAPHIE

1. BÉAL M. T., *J. Phys. Chem. Solids* **15**, 72 (1960).
2. MOTT N. F. and JONES H., *The Theory of the*

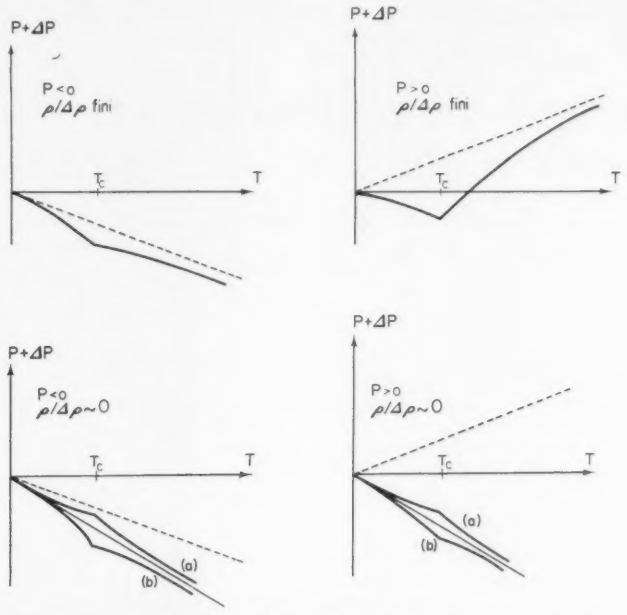

FIG. 6. Courbes donnant l'allure du pouvoir thermoélectrique total $P+\Delta P$ dans les différents cas précisés sur la figure. Les droites en pointillés correspondent au pouvoir thermoélectrique P dû aux phonons. Les courbes (a) correspondent à $\Delta\rho/\Delta\rho_0 < 1$, les courbes (b) à $\Delta\rho/\Delta\rho_0 > 1$.

Vol. 18
1961

Properties of Metals and Alloys. Oxford University Press (1936).
3. FRIEDEL J., *J. Phys. Radium* **14,** 561 (1953).
4. FOWLER R. H. and GUGGENHEIM E. A., *Statistical Thermodynamics*. Cambridge University Press (1939).
5. SEITZ F., *The Modern Theory of Solids*. McGraw Hill, New York (1940).
6. LEE J. A., MEADON G. T., HALL R. O. A. et KING E., mémoire 4, Conf. Int. Pu, Grenoble, 1960.
7. ROCHER Y. A. et FRIEDEL J., à paraitre.
8. LAUBITZ M. J., *Canad. J. Phys.* **38,** 887 (1960).
9. FINE M. E., GREINER E. S. and ELLIS W. C., *J. Metals N.Y.* **56,** 191 (1951).
10. POTTER H. H., *Proc. Phys. Soc. Lond.* **53,** 6095 (1941).
11. BLUE M. D., *Phys. Rev.* **117,** 136 (1960).

J. Phys. Chem. Solids Pergamon Press 1961. Vol. 18, Nos. 2/3, pp. 156–161. Printed in Great Britain.

SUR LA RESISTIVITE ELECTRIQUE DES ALLIAGES DU TYPE Cu_3Au EN FONCTION DE L'ORDRE

M. T. BÉAL

Faculté des Sciences, Laboratoire de Physique du Solide, Groupe II—Orsay (S. & O) France

(*Received* 21 *July* 1960)

Résumé—Nous étudions, théoriquement, l'influence du désordre atomique sur la résistivité électrique des alliages du type Cu_3Au, au-dessous de la température de transition. Au-dessus, nous complétons la courbe obtenue par des calculs effectués précédemment. Nous avons déjà traité le cas des alliages analogues à $CuZn\beta$. Nous utilisons ici les mêmes approximations et concluons aussi à une faible influence de l'ordre à courte distance, complétant celle de l'ordre à longue distance. Le point nouveau est une chute brusque de la résistivité au point critique, conséquence directe de la transition d'ordre de 1ère espèce. Ces résultats se retrouvent sur les courbes obtenues expérimentalement.

Abstract—We study, theoretically the influence of atomic disorder on the electrical resistivity of alloys such as Cu_3Au, below the transition temperature. The effect above that temperature was computed previously. We use the same approximations as in a previous study of $CuZn\beta$ and we conclude here also that there is a slight influence of short range order, in addition to that of long range order. There is a sudden drop of resistivity at the critical point, due to the transition of first order. The same results can be observed on experimental curves.

1. INTRODUCTION

NOUS AVONS étudié précédemment[1] les phénomènes ordre–désordre dans les alliages métalliques, leur variation en température et leur influence sur la résistivité électrique. En dessous de la température critique d'ordre, nous n'avions traité que des alliages du type $CuZn\beta$, à transition d'ordre de 2ème espèce. Nous envisageons ici des transitions de 1ère espèce avec des alliages AB_3 analogues à Cu_3Au. Nous employons les mêmes méthodes : champ moléculaire, interactions entre premiers voisins, électrons libres et approximation de Born dans le calcul des sections efficaces de diffusion. Nous complétons les courbes par les informations trouvées précédemment. Nous constatons encore une petite contribution de l'ordre à courte distance mais, ici, la transition d'ordre à longue distance de 1ère espèce entraine une chute brusque de résistivité à la température critique.

2. PARAMETRES d'ORDRE

L'ordre à longue distance est l'ordre classique S. Les alliages AB_3 considérés ont une structure cubique à faces centrées à l'état parfaitement ordonné $(0°K) - A\,T°K$, on vérifie facilement[2] que :

—le nombre d'atomes A sur des sites occupés par des A à 0° K est

$$\frac{N}{4}\,\frac{1+3S}{4}$$

—le nombre d'atomes A sur des sites B

$$\frac{3N}{4}\,\frac{(1-S)}{4}$$

—le nombre d'atomes B sur des sites A (1)

$$\frac{N}{4}\,\frac{3(1-S)}{4}$$

—le nombre d'atomes B sur des sites B

$$\frac{3N}{4}\,\frac{3+S}{4}$$

si N est le nombre total d'atomes.

Vol. 18
1961

Pour définir l'ordre à courte distance, nous posons, comme pour le cas de CuZnβ,[1] que :

$p_{ij}(\boldsymbol{r})$ est la probabilité de trouver à la distance $\boldsymbol{r}$ d'un atome A_i, un atome j (i et j identiques à n ou e, n et e désignant respectivement des atomes qui occupent les mêmes sites qu'à 0°K ou des sites différents); alors :

$1-p_{ij}(\boldsymbol{r})$ est la probabilité d'y trouver un B_j. De même $q_{ij}(\boldsymbol{r})$ est la probabilité de trouver à $\boldsymbol{r}$ d'un atome B_i, un atome B_j et $1-q_{ij}$ $(\boldsymbol{r})$ celle d'y trouver un A_j. Les valeurs limites pour $\boldsymbol{r}$ très grand, sont les suivantes :

$$\begin{aligned} p_{ij}(\infty) &= \frac{1+3S}{4} \text{ si } j = n \\ p_{ij}(\infty) &= \frac{1-S}{4} \text{ si } j = e \\ q_{ij}(\infty) &= \frac{3+S}{4} \text{ si } j = n \\ q_{ij}(\infty) &= \frac{3(1-S)}{4} \text{ si } j = e. \end{aligned} \tag{2}$$

Et, pour $\boldsymbol{r} = 0$

$$\begin{aligned} &p_{ij}(0) = q_{ij}(0) = 1 \text{ si } i = j \\ &p_{ij}(0) \text{ et } q_{ij}(0) \text{ n'existent pas si } i \neq j. \end{aligned} \tag{3}$$

Le calcul explicite de ces paramètres s'effectue simplement en évaluant l'énergie nécessaire pour échanger deux atomes, l'un à la distance $\boldsymbol{r}$ d'un atome donné, l'autre à une distance infinie. En écrivant la loi d'action de masse, nous aboutissons aux formules suivantes :

$$\frac{p_{in}(\boldsymbol{r})}{1-p_{in}(\boldsymbol{r})} = \frac{1-S}{3+S} \exp -\frac{W}{kT} \times$$

$$\times \left[\sum_{\boldsymbol{r}'} p_{ie}(\boldsymbol{r}') - (3+S)\right]$$

$$\frac{p_{ie}(\boldsymbol{r})}{1-p_{ie}(\boldsymbol{r})} = \frac{1-S}{3+S} \exp -\frac{W}{kT} \times$$

$$\times \left[\sum_{\boldsymbol{r}'_1} p_{in}(\boldsymbol{r}'_1) + \sum_{\boldsymbol{r}'_2} p_{ie}(\boldsymbol{r}'_2) - (3+S)\right] \tag{4}$$

où $W = V_{AA}+V_{BB}-2V_{AB}$; les V représentent les énergies d'interaction entre les atomes considérés, k est la constante de Boltzmann, T la température absolue. Les $\sum$ indiquent des sommations sur les atomes premiers voisins de l'atome situé en $\boldsymbol{r}$: $\sum_{\boldsymbol{r}'}$ s'effectue sur les douze premiers voisins $\sum_{\boldsymbol{r}'_1}$, sur les 4 atomes qui occupent des sites différents du site $\boldsymbol{r}$; $\sum_{\boldsymbol{r}'_2}$ sur les 8 atomes qui occupent des sites identiques au site $\boldsymbol{r}$. A la limite où $\boldsymbol{r}$ devient infini, les formules précédentes donnent la dépendance classique en température de l'ordre à grande distance,[2] dans l'approximation de Bragg-Williams :

$$\frac{(1+3S)(3+S)}{3(1-S)^2} = \exp \frac{4SW}{kT} \tag{5}$$

Des calculs analogues donnent les $q_{ij}(\boldsymbol{r})$—
Nous nous intéressons plus précisément à :

$$\begin{aligned} P_{ij}(\boldsymbol{r}) &= p_{ij}(\boldsymbol{r}) - p_{ij}(\infty) \\ Q_{ij}(\boldsymbol{r}) &= q_{ij}(\boldsymbol{r}) - q_{ij}(\infty) \end{aligned} \tag{6}$$

Il est évident que les nouveaux paramètres ne prennent que des valeurs bien inférieures à l'unité. Nous pouvons donc, comme dans le cas des alliages AB[1], adopter en première approximation les formules approchées suivantes :

$$\begin{aligned} P_{in}(\boldsymbol{r}) &= -\frac{3(1-S)(1+3S)}{16} \frac{W}{kT} \sum_{\boldsymbol{r}'} P_{ie}(\boldsymbol{r}') \\ P_{ie}(\boldsymbol{r}) &= -\frac{(3+S)(1-S)}{16} \frac{W}{kT} \left[\sum_{\boldsymbol{r}'_1} P_{in}(\boldsymbol{r}'_1) + \sum_{\boldsymbol{r}'_2} P_{ie}(\boldsymbol{r}'_2)\right] \\ Q_{in}(\boldsymbol{r}) &= -\frac{(3+S)(1-S)}{16} \frac{W}{kT} \left[\sum_{\boldsymbol{r}'_1} Q_{ie}(\boldsymbol{r}'_1) + \sum_{\boldsymbol{r}'_2} Q_{in}(\boldsymbol{r}'_2)\right] \\ Q_{ie}(\boldsymbol{r}) &= -\frac{3(1-S)(1+3S)}{16} \frac{W}{kT} \sum_{\boldsymbol{r}'} Q_{in}(\boldsymbol{r}'). \end{aligned} \tag{7}$$

3. RESISTIVITE

Soient V_A et V_B les potentiels respectifs d'un atome A et d'un atome B. Comme pour les alliages AB, on vérifie facilement qu'à la distance $\boldsymbol{r}$ d'un atome i, le potentiel diffusant probable sera :

$$(V_A - V_B)\,[P_{in}(\boldsymbol{r}) + P_{ie}(\boldsymbol{r})] \text{ si } i \text{ est un } A$$
$$\text{et} \quad (V_A - V_B)\,[Q_{in}(\boldsymbol{r}) + Q_{ie}(\boldsymbol{r})] \text{ si } i \text{ est un } B. \tag{8}$$

On a vu précédemment[1] que l'expression

$$\times \frac{1}{C(1-C)\,(V_A - V_B)^2}\,\frac{1}{N}\,|\sum_{\boldsymbol{r}} V(\boldsymbol{r}) \exp i\boldsymbol{x}\,.\,\boldsymbol{r}|^2 \tag{9}$$

où $\Delta\rho_0$ est la variation de résistivité constante en température et due au désordre total, $\boldsymbol{x}$ est le vecteur de diffusion, θ l'angle de diffusion, C et $1-C$ les concentrations.

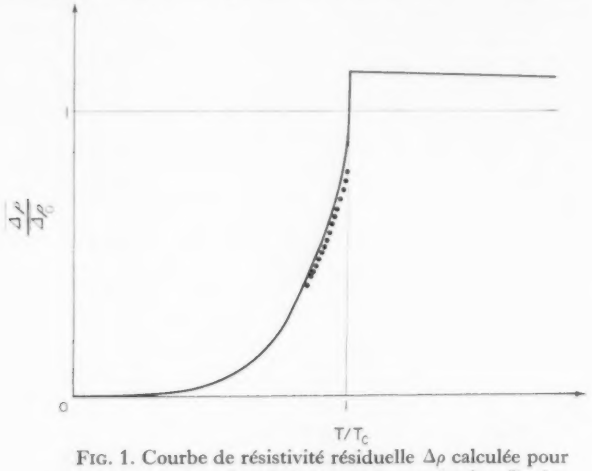

FIG. 1. Courbe de résistivité résiduelle $\Delta\rho$ calculée pour Cu_3Au, en fonction de la température absolue T. $\Delta\rho_0$ est la résistivité de désordre total. En pointillé, la contribution de l'ordre à longue distance seule, en dessous de la température critique T_c.

donnant la variation de résistivité $\Delta\rho$ due au désordre est la suivante :

$$\frac{\overline{\Delta\rho}}{\overline{\Delta\rho_0}} = \tfrac{1}{2}\int_0^{\pi} \sin\theta\, d\theta\,(1-\cos\theta) \times$$

Il reste à évaluer

$$|\sum_{\boldsymbol{r}} V(\boldsymbol{r}) \exp i\boldsymbol{x}\,.\,\boldsymbol{r}|^2,$$

dont l'expression détaillée est donnée par :

$$\frac{|\sum_{\boldsymbol{r}} V(\boldsymbol{r}) \exp i\boldsymbol{x}\,.\,\boldsymbol{r}|^2}{(V_A - V_B)^2} =$$
$$\sum_{A_n} \{[P_{nn}(\mathbf{o}) + P_{ne}(\mathbf{o})] \sum_{\boldsymbol{R}_n} [P_{nn}(\boldsymbol{R}_n) + P_{ne}(\boldsymbol{R}_n)] \exp i\boldsymbol{x}\,.\,\boldsymbol{R}_n\}$$
$$+ \sum_{A_e} \{[P_{ee}(\mathbf{o}) + P_{en}(\mathbf{o})] \sum_{\boldsymbol{R}} [P_{en}(\boldsymbol{R}_e) + P_{ee}(\boldsymbol{R}_e)] \exp i\boldsymbol{x}\,.\,\boldsymbol{R}_e\}$$
$$+ \sum_{B_n} \{[Q_{nn}(\mathbf{o}) + Q_{ne}(\mathbf{o})] \sum_{\boldsymbol{R}_n} [Q_{nn}(\boldsymbol{R}_n) + Q_{ne}(\boldsymbol{R}_n)] \exp i\boldsymbol{x}\,.\,\boldsymbol{R}_n\} \tag{10}$$
$$+ \sum_{B_e} \{[Q_{ee}(\mathbf{o}) + Q_{en}(\mathbf{o})] \sum_{\boldsymbol{R}_e} [Q_{en}(\boldsymbol{R}_e) + Q_{ee}(\boldsymbol{R}_e)] \exp i\boldsymbol{x}\,.\,\boldsymbol{R}_e\}$$

$$\sum_{R_n}, \sum_{R_e}$$

désignent des sommations sur les sites R_n ou R_e autour d'un atome central **o** : n ou e et

$$\sum_{A_n}, \sum_{A_e}, \sum_{B_n}, \sum_{B_e},$$

des sommations sur tous les atomes A ou B, n ou e, du réseau. Dans le même ordre d'approximation qui nous a permis d'écrire les formules (7), nous ne gardons ici qu'une expression approchée. Nous faisons, d'autre part, une moyenne sur les angles comme dans le cas du $CuZn\beta$[1].
Il vient :

$$\frac{\left|\sum_r V(r) \exp ix \,.\, r\right|^2}{(V_A - V_B)^2} =$$

$$\sum_{A_n}\left\{\left[P_{nn}(\mathbf{o})\right]^2\left[1-\frac{(3+S)(1-S)}{4}\frac{W}{kT}\frac{\sin xD}{xD}\right]\right\}$$

$$+\sum_{A_e}\left\{\left[P_{ee}(\mathbf{o})\right]^2\left[1-\frac{(15+29S)(1-S)}{4}\frac{W}{kT}\frac{\sin xD}{xD}\right]\right\} \qquad (11)$$

$$+\sum_{B_n}\left\{\left[Q_{nn}(\mathbf{o})\right]^2\left[1-\frac{(15+29S)(1-S)}{4}\frac{W}{kT}\frac{\sin xD}{xD}\right]\right\}$$

$$+\sum_{B_e}\left\{\left[Q_{ee}(\mathbf{o})\right]^2\left[1-\frac{(3+S)(1-S)}{4}\frac{W}{kT}\frac{\sin xD}{xD}\right]\right\}$$

où D est la distance entre proches voisins et $x = |\boldsymbol{x}| = 2k_F \sin\theta/2$; si k_F est le vecteur d'onde au niveau de Fermi. La résistivité au-dessous du point d'ordre est finalement donnée par :

$$\frac{\overline{\Delta\rho}}{\overline{\Delta\rho_0}} = (1-S^2)\left[1+\frac{(1-S)(3+S)(1+2S)}{1+S}\frac{W}{kT}A(k_FD)\right]$$

avec

$$\frac{(1+3S)(3+S)}{3(1-S)^2} = \exp\frac{4SW}{kT} \qquad (12)$$

et

$$A(k_FD) = \frac{1}{(k_FD)^2}\left[\cos 2k_FD - \frac{\sin 2k_FD}{k_FD} + \frac{1-\cos 2k_FD}{2(k_FD)^2}\right]$$

Cette formule met en évidence une importante contribution de l'ordre à longue distance en $1-S^2$, dans la résistivité, corrigée par un terme faible mais non négligeable, provenant de l'ordre à courte distance.

4. APPLICATION NUMERIQUE ET COMPARAISON AVEC L'EXPERIENCE

Pour Cu_3Au, $k_FD \simeq 3{,}46$, d'où A $(k_FD) \simeq 4/100$ de même pour Au_3Cu on sait[2], d'autre part, que l'ordre à longue distance est stable jusqu'à une température T_c, telle que $W/kT_c = 1{,}22$ et pour laquelle $S_{T_c} = 0{,}463$.

La Fig. 1 donne la courbe de résistivité résiduelle calculée pour Cu_3Au. Elle est nulle avec une pente nulle à 0°K, croît d'abord faiblement et atteint T_c avec une forte pente : +8 ; en ce point

$$\frac{\overline{\Delta\rho}}{\overline{\Delta\rho_0}} = 0{,}89.$$

Vol. 18
1961

Nous avons également tracé sur la Fig. 1, en pointillés, la contribution, à la résistivité, de l'ordre à longue distance seul, qui donne à T_c :

$$\frac{\overline{\Delta\rho}}{\overline{\Delta\rho_0}} = 0{,}79.$$

D'autre part, les calculs faits antérieurement[1] donnent, juste au-dessus de T_c :

$$\frac{\overline{\Delta\rho}}{\overline{\Delta\rho_0}} = 1{,}14$$

avec une pente négative et très faible. On retrouve sur les courbes experimentales une allure générale analogue à celle présentée ici, comme nous allons le montrer plus en détail.

4.1. *Etude à T_c.*

Si nous appelons λ le rapport des valeurs de $(\overline{\Delta\rho}/\overline{\Delta\rho_0})$ juste au-dessous et juste au-dessus de T_c, nous trouvons pour Cu_3Au les chiffres donnés par le tableau ci-dessous :

Tableau 1

λ	d'après :
0,80	nos calculs
0,66	JONES et SYKES[3]
0,75	SIEGEL[4]
0,65	PERIO[5]
0,82	NIX et SHOCKLEY[6]

Nous avons pris soin de retrancher la résistivité due à l'agitation thermique sur les courbes de la littérature. Il est évidemment difficile d'évaluer exactement sur des courbes expérimentales l'écart entre les deux valeurs extrêmes de $\overline{\Delta\rho}/\overline{\Delta\rho_0}$ à T_c. Il est certain néanmoins que cet écart existe et d'un ordre de grandeur comparable dans tous les cas.

4.2. *Etude au-dessus de T_c.*

L'ordre à courte distance contribue à une légère augmentation de la résistivité à T_c par rapport à ses valeurs à très hautes températures, ainsi si T décroît à partir des hautes températures jusqu'à T_c, nous calculons :

$$\frac{\rho T/T_c = 1 - \rho T/T_c = 1{,}4}{\rho T/T_c = 1{,}4} = 0{,}03.$$

KOREVAAR[7] observe la valeur 0,06 pour ce rapport.*

4.3. *Vérification de la loi en $1/T$ pour la résistivité, au-dessus de T_c.*

Nous avons vérifié que les courbes (cf. Fig. 2) de KOREVAAR[7] obéissant, comme nous le prédisions[1], à une loi en $1/T$ pour la résistivité, au-dessus de T_c. Cette comparaison aboutit au résultat ci-dessous :

* Des observations, semble-t-il moins soignées, de WRIGHT et GODDARD[8] donnent 0,12.

Tableau 2

$\frac{\rho T/T_c = 1{,}13 - \rho T/T_c = 1{,}21}{\rho T/T_c = 1{,}21 - \rho T/T_c = 1{,}42}$	d'après :
0,64	KOREVAAR[7] dans AuCu à 14 pour cent de cuivre
0,66	KOREVAAR[7] dans AuCu à 7,5 pour cent de cuivre
0,60	KOREVAAR[7] dans AuCu à 4,6 pour cent de cuivre
0,5	nos calculs relatifs à Cu_3 Au.

4.4. *Dépendance en concentration, pour la résistivité, au-dessus de T_c.*

Nous avions abouti[1], pour un W/kT donné, à une dépendance en $C(1-C)$ pour la résistivité, C étant la concentration en l'un des constituants.

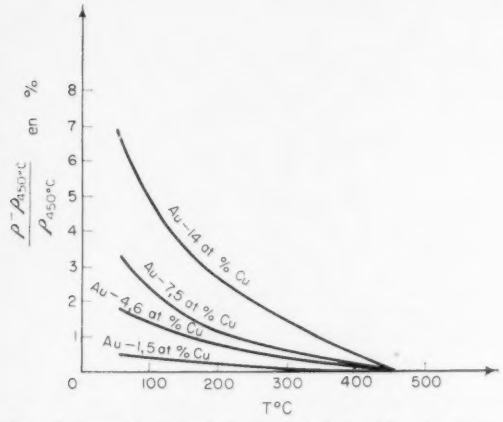

FIG. 2. Reproduction de la Fig. 28 de la thèse de KOREVAAR. Pour différentes concentrations de cuivre en fonction de la température, courbes de résistivités d'alliages or–cuivre : $\rho-\rho 450°C/\rho 450°C$ en %.

Plus précisément, pour une température donnée, nous nous attendons à :

$$\frac{\dfrac{\overline{\Delta\rho}}{\overline{\Delta\rho_0}}-1}{C\,(1-C)} = \text{constante} = m$$

Une comparaison avec les courbes de KOREVAAR[7] (cf. Fig. 2) donne, à peu pres, les valeurs ci-jointes :

Tableau 3

$C = 14$ pour cent	$m = 0{,}14$
$C = 7{,}5$ pour cent	$m = 0{,}12$
$C = 4{,}6$ pour cent	$m = 0{,}12$

qui semblent assez satisfaisantes.

4.5. *Au-dessous de T_c.*

L'allure générale des courbes expérimentales est la même que celle de la nôtre. Par exemple, si nous calculons le rapport de la résistivité pour $T = 0{,}91\ T_c$ à la résistivité lorsque T atteint T_c par valeurs supérieures nous trouvons 0,59 d'après KOREVAAR[7] et 0,47 d'après notre étude. Il est à noter que la courbe de KOREVAAR ne présente pas, à l'approche de T_c, une variation aussi abrupte que la nôtre, mais les conditions dans lesquelles se fait cette approche sont délicates et on ne peut trop s'appesantir sur ce point.

5. CONCLUSION

Nous trouvons pour la résistivité des alliages AB_3, comme pour celle des alliages AB, une forte contribution de l'ordre à longue distance, légèrement modifiée par l'introduction de l'ordre à courte distance, surtout au voisinage du point critique. En ce point, les alliages AB_3 présentent une nette différence par rapport aux alliages AB, avec une chute brusque de résistivité. Ceci n'est qu'une conséquence directe du comportement thermodynamique de l'ordre à longue distance différent dans les deux cas. Enfin, notre étude semble en assez bon accord avec les résultats expérimentaux.

Remerciement—J'ai fait ces calculs sur le conseil de Monsieur le Professeur J. FRIEDEL, que je tiens à remercier ici pour ses encouragements constants.

BIBLIOGRAPHIE

1. BEAL M. T., *J. Phys. Chem. Solids* **15,** 72 (1960).
2. FOWLER R. H. and GUGGENHEIM E. A., *Statistical thermodynamics.* Cambridge University Press (1939).
3. JONES F. W. and SYKES C., *Proc. Roy. Soc.* A**166,** 376 (1938).
4. SIEGEL S., *Phase transformation in solids*, p. 373. Wiley, New York (1951).
5. PERIO P., à paraître.
6. NIX F. C. and SHOCKLEY W., *Rev. Mod. Phys.* **10,** 1 (1938).
7. KOREVAAR B. M., thèse d'ingénieur docteur, Delft (1960).
8. WRIGHT P. and GODDARD K. F., *Acta Met.* **7,** 757 (1959).

Vol. 18
1961

J. Phys. Chem. Solids Pergamon Press 1961. Vol. 18, Nos. 2/3, pp. 162–174. Printed in Great Britain.

DIFFUSION OF SILVER, COBALT AND IRON IN GERMANIUM*

LING Y. WEI†

Electrical Engineering Department, University of Illinois, Urbana, Illinois

(*Received* 2 *March* 1959; *final revision* 17 *December* 1959)

Abstract—Diffusion of Ag, Co and Fe in Ge are investigated by radiotracer techniques. We found that: (1) In most cases, the concentration varies as $\exp(-x/L)$ rather than the Gaussian or the error function as usually expected from Fick's (second) law. (2) The diffusivities of these elements in Ge are in the range of 10^{-6}–10^{-7} cm^2/sec at temperatures around 800°C. The values are higher in low dislocation (less than 10^3 pits/cm^2) than in high dislocation (around 10^5 pits/cm^2) crystals. (3) The solubilities of Ag, Co and Fe in Ge are very low, in the range of 10^{-8}–10^{-9} in atomic fraction. (4) The activation energy of Co diffusion in Ge is about 1 eV, nearly the same as those of Ag, Ni and Fe diffusion as obtained by other workers.

It is suggested that the anomalous diffusion is due to a double stream process which is composed of free species and trapped ones. This trapping mechanism not only leads to a concentration varying approximately as $\exp(-x/L)$ but also offers reasonable explanations for many other experimental facts.

1. INTRODUCTION

FROM STUDIES of diffusion in solids, most of the results can be summarized as follows:

(a) Diffusion follows Fick's law.
(b) Diffusion of substitutional solutes can often be interpreted by a vacancy mechanism.
(c) Diffusion constants for substitutional solutes are usually in the range of 10^{-9}–10^{-14} cm^2/sec.
(d) Diffusion of interstitial solutes, which can hop from one interstice to another, may be much more rapid.

In recent years, work by FULLER[1, 2] VAN DER MAESEN[3] and TWEET[4] on Cu diffusion in Ge gave remarkably different results. They found that:

(a) Cu diffusion in Ge usually does not follow Fick's law.
(b) It cannot be interpreted by a vacancy mechanism alone.
(c) The diffusion constant is about 10^{-5}cm^2/sec (700–900°C) which is a million times higher than those of Group III and V elements in Ge.
(d) Diffusion is structure sensitive.
(e) The activation energy for diffusion is small.

FULLER has speculated[1] that copper may diffuse at high temperatures as Cu^+ or Cu^0, and assume the role of acceptor only at lower temperatures. FULLER and TWEET found, independently, the importance dislocations had for the diffusion. VAN DER MAESEN and BRENKMAN were led to the concept that both substitutional (Cu_s) and interstitial (Cu_i) atoms are present and are in a temperature dependent equilibrium,

$$Cu_i \rightleftarrows Cu_s + Q$$

where the "thermochemically denoted Q" has a positive sign. They proved from their experiments that the Cu diffusion was non-Fickian under most conditions and gave the first analytical treatment of the diffusion.

FRANK and TURNBULL[5] then introduced the

* This paper is based upon a part of thesis submitted to the Graduate College of University of Illinois (1958) in partial fulfilment of the requirement for the degree of Doctor of Philosophy in Electrical Engineering. The work is supported by the United States Air Force through Contract No. AF 18(600)–1310.

† Now at the University of Washington, Seattle 5, Washington.

rôle played by vacancies in the mechanism of Cu diffusion in Ge. In crystals of very high dislocation density, as they conceived, vacancies are supplied and maintained in equilibrium by dislocations in the bulk. For Ge crystals relatively free from dislocations (say less than 100 etch pits/cm^2), they proposed a "dissociative mechanism". This mechanism has been used with some success to interpret the data on Cu diffusion and precipitation in Ge.[4, 6]

Besides the above two limiting cases, there is an intermediate one, corresponding to a medium high dislocation density (10^3–10^5 etch pits/cm^2). Since ordinarily Ge crystals have dislocation densities falling in this range, this intermediate case is the one usually observed. In this case, the concentration of vacancies and their generation rate from dislocations in the bulk may not be sufficient to maintain the equilibrium condition of $Cu_2 \rightleftarrows Cu_i + V$. When this occurs, Cu diffusion will not follow Fick's law. This can be seen easily from VAN DER MAESEN'S equations and is clearly shown in the figures of his paper.[3]

Stimulated by the previous work on Cu diffusion, the present author investigated the diffusion of Ag, Co and Fe in Ge. He found that Fick's law was also not followed in most cases of the diffusion studied. The dissociative mechanism which was considered satisfactory for Cu diffusion seems to be inadequate for interpreting our results. We consider that the diffusion of Ag, Co and Fe in Ge is a double stream process, one stream consisting of free species and another of trapped ones. The free species are probably interstitials. The trapped species include substitutionals and those having either loose or tight association with lattice defects (such as dislocations) and impurities. When a species hops from one trap to another trap, this is considered as the "diffusion of trapped species", and forms the slow stream. A species could switch now and then between the slow and the fast streams. This kind of exchange of species is characteristic of a double stream process.

As we shall show in this paper, the trapping mechanism can explain many experimental facts, particularly the exponential characteristic of concentration versus penetration. The trapping mechanism is more general than the dissociative mechanism in two respects: (a) In the dissociative mechanism, only the role of vacancies is considered. In the trapping mechanism, the effect of all kinds of traps including vacancies on diffusion is implied. (b) In the dissociative mechanism, the equilibrium condition: vacancy + interstitial $\rightleftarrows$ substitutional is assumed. In the trapping mechanism, this equilibrium condition is not necessary but is also not excluded. We suggest that other non-Fickian diffusion might also possibly be explained by the trapping mechanism.

2. EXPERIMENTAL

The Ge crystals used were of three grades: (a) high dislocation, HD $\sim 10^5$ pits/cm^2 (b) low dislocation LD $\sim 10^3$ pits/cm^2 (c) dislocation-free, DF < 100 pits/cm^2, supplied by Dr. A. G. TWEET of the General Electric Research Laboratory. All crystals were single crystals with resistivity around 40 ohm-cm.

Samples cut from HD crystals were about 0·6–1 cm long while those cut from LD and DF crystals were about 3 mm thick. The cross-sectional area was about 1·5 cm^2. All samples were ground to mirror polish on one face with a precision grinding machine.[9] They were first cleaned to remove surface contamination by LOGAN'S method[10] and then treated with Complexion III[3] to prevent diffusion from going around the sides and the back. A solution containing a radioactive isotope of the desired element was brushed over one face of the sample and dried in still air.

A resistance furnace was used for annealing. To facilitate quenching, the sample was not sealed in a Vycor tube but put in a molybdenum basket with the painted side facing down on a thin quartz plate. After annealing, the sample was slid onto an aluminum plate which conducts heat away very rapidly.

The remaining procedures are sectioning, weighing and counting as usually done in radiotracer techniques. Before the first sectioning, the edges or sides were ground off for several diffusion lengths around the sample to minimize the effect on counting of possible side diffusion. β-radiation was counted and the counting efficiency was about 20 per cent.

3. RESULTS

(a) *Silver diffusion*

Figs. 1 and 2 show the penetration curves (log C vs. x) of Ag diffusion in high dislocation and dislocation-free crystals of Ge respectively. We see that curves 2 and 3 of Fig. 1 are very good straight lines, i.e. $C = A(t) \exp(-x/L)$ where C is the concentration of the diffusing species. The surface concentrations are roughly proportional to time. Curve 1 shows a structure effect. In Fig. 2, curves (1, 2, 3) have two distinct parts, a sharply falling initial part and a very flat deeper part. The initial part represents possibly a substitutional diffusion

Vol. 18
1961

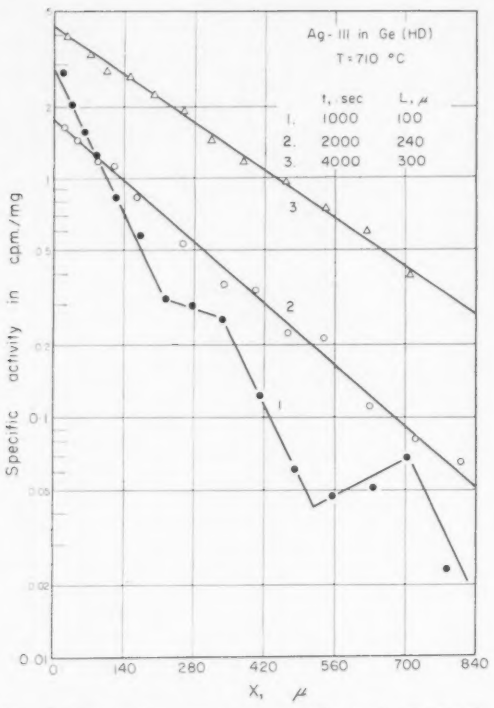

FIG. 1. Penetration curves of Ag diffusion in Ge (high-dislocation, HD).

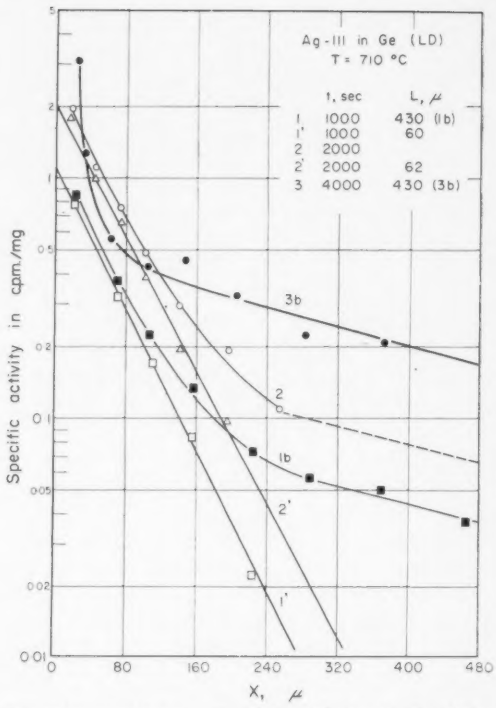

FIG. 2. Penetration curves of Ag diffusion in Ge (dislocation-free, DF).

which is related to the vacancies entering from the surface. However, in the bulk of a dislocation-free crystal, very few vacancies are available and therefore diffusion will be dominated by interstitials. This gives the flat part of the penetration curves.

We shall estimate the "apparent diffusivity" (to be defined in Appendix), which is about what one would obtain if one tried to fit square law penetration. From Fig. 1, for $t = 2000$ sec, $L = 240$ microns,

$$D_a = \frac{2L^2}{t} = \frac{2\times(2{\cdot}4)^2\times10^{-4}}{2000}$$

$$= 5{\cdot}8\times10^{-7}\ \text{cm}^2/\text{cm}.*$$

For $t = 4000$ sec, $L = 300$ microns, we get $D_a = 2\times9\times10^{-4}/4000 = 4{\cdot}5\times10^{-7}$ cm^2/sec. We may take the mean value,

$$D_a = 5\times10^{-7}\ \text{cm}^2/\text{sec}$$

* Curves 1 and 2 have features very similar to case (iv), i.e. $A(t) = ct$ and $L = k\sqrt{t}$, in Appendix, hence formula (A1) is used for D_a.

as the diffusivity of Ag in HD Ge at 710°C. BUGAI has obtained D (computed from erfc function,)[11]

$$D = 4{\cdot}4\times10^{-2}\exp(-23000/RT)$$

At $T = 710$°C, $D = 3\times10^{-7}$ cm^2/sec, which is very close to our value.

In Fig. 2, the lower parts of curves 1 and 3 are very flat with $L = 430$ microns and have features very close to case (i) as described in the Appendix, According to equation (A5), the apparent diffusivity is given by,

$$D_a = \frac{(4{\cdot}3)^2\times10^{-4}}{1000} = 2\times10^{-6}\ \text{cm}^2/\text{sec}.$$

This value may be taken as the interstitial diffusion coefficient of Ag in Ge (at 710°C).

The ordinates in curves 1′ and 2′ of Fig. 2 represent the difference between the concentrations on the initial part of curves 1 and 2 and the straight line extrapolation (not shown) toward the surface from the deeper part of these curves. They (1′ and

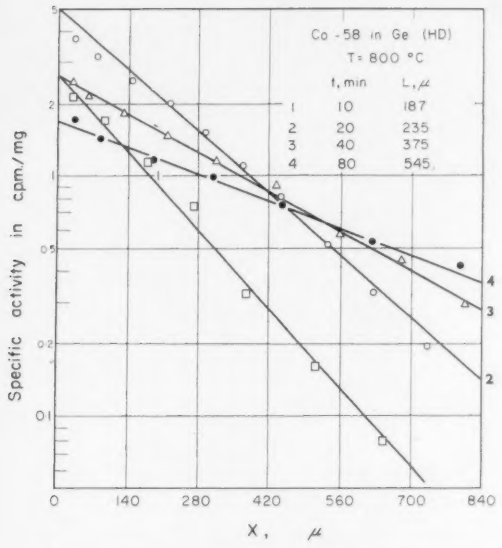

FIG. 3. Penetration curves of Co diffusion in Ge (HD, 800°C), log C vs. x.

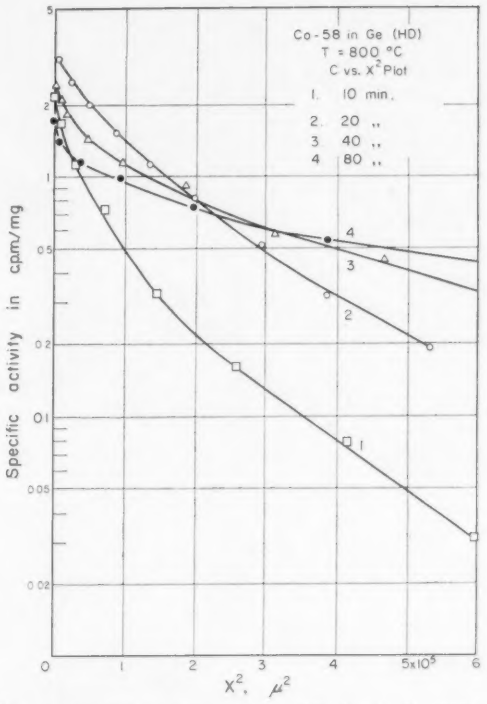

FIG. 4. Penetration curves of Co diffusion in Ge (HD,. 800°C), log C vs. x^2.

2′) may be taken as the concentrations of substitutionals penetrating by vacancy diffusion from the surface. From them, we get,

$$D_a = \frac{36 \times 10^{-6}}{1000} = 3{\cdot}6 \times 10^{-8} \text{ cm}^2/\text{sec}.$$

(Note: Curves 1′ and 2′ of Fig. 2 have the features of case (i) in Appendix. Hence formula (A5) is used here).

(b) *Cobalt diffusion*

Since Co^{58} has a half-life of 72 days and is claimed as "carrier-free", it is better suited for the study of fast diffusion. We have done much work on Co^{58} diffusion in crystals of Ge for different annealing times at three temperatures (750, 800 and 850°C). From Figs. 3–7, we get:

(a) In HD crystals, all penetration curves (log C vs. x) are straight lines (Figs. 3 and 6). The curves in Fig. 4 use the same data as used in Fig. 3 but are plotted as log C vs. x^2. It is very evident that they do not fit either gaussian or erfc function.

(b) In LD (CBS Hytron) crystals at 800°C, the penetration curves (Fig. 5) are straight lines with x^2. At 852°C, the penetration curves in LD crystals are straight lines with x (Fig. 7).

(c) By comparing Fig. 3 with Fig. 5 and comparing Fig. 6 with Fig. 7, we can see that the apparent solubility in HD crystals is much higher than that in LD crystal (the comparison between Figs. 6 and 7 is particularly striking) while the diffusivity in the latter is about 2–3 times that in the former.

From the penetration curves, we calculated the apparent diffusivity, D_a of cobalt in Ge to be 10^{-6}–10^{-7} cm²/sec in the range of 750–850°C. We obtain (Fig. 8),

$$D_a = 4{\cdot}4 \times 10^{-3} \exp(-20000/RT)$$

for Co diffusion in HD crystals of Ge, and

$$D_a = 0{\cdot}16 \exp(-25800/RT)$$

Vol. 18
1961

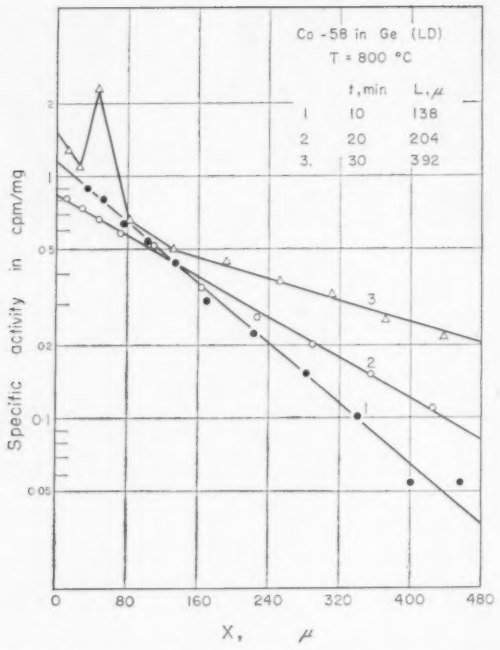

FIG. 5. Penetration curves of Co diffusion in Ge (low-dislocation, LD, 800°C).

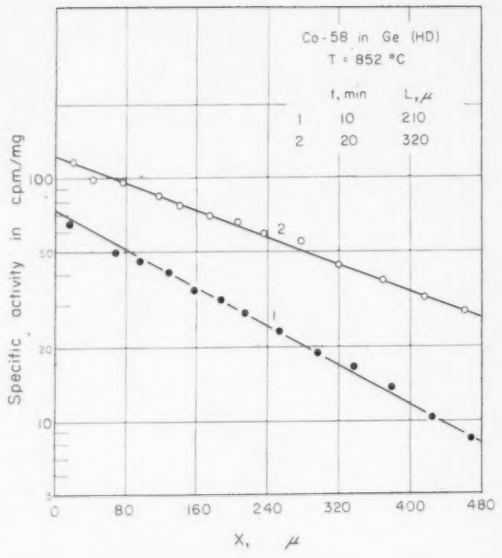

FIG. 6. Penetration curves of Co diffusion in Ge (HD, 852°C).

for Co diffusion in LD crystals of Ge (CBS Hytron). The values of activation energy are very interesting. For Ni diffusion in Ge,[12]

$$D_{Ni} = 0{\cdot}8 \exp(-21000/RT)$$

From BUGAI's measurements on Fe and Ag diffusion in Ge,[11,13]

$$D_{Fe} = 0{\cdot}13 \exp(-25000/RT)$$

$$D_{Ag} = 4{\cdot}4 \times 10^{-2} \exp(-23000/RT)$$

All these activation energies are around 1 eV. This suggests that their diffusion mechanisms may be nearly the same.

(c) *Iron diffusion*

From our data (Figs. 9 and 10), we observed that,

(i) The points are more scattered than those shown in other figures for Ag and Co diffusion in Ge.

(ii) Some of the penetration curves are good straight lines, i.e. C varying as $\exp(-x/L)$. None of the curves has a shape like $\exp(-ax^2)$.

(iii) The maximum concentration is about 2×10^{13} atoms/cm^2 which is the same value as obtained by TYLER[14].

(iv) By comparing Fig. 9 (HD case) with Fig. 10 (LD case), we see no difference in maximum concentration and diffusion lengths. The diffusivity estimated from the diffusion lengths is about $(2{\cdot}3 \pm 0{\cdot}7) \times 10^{-7}$ cm^2/sec at 800°C.

The very low solubility of Fe in Ge and its strong chemical activity impose extreme difficulties in experimentation. Though the tracer measurement appears as one of the best, the results can be widely different in experiments by different workers because of many uncontrolled factors, such as the impurity contents of the tracer and in the crystal. For example, BUGAI obtained the solubility (S) and

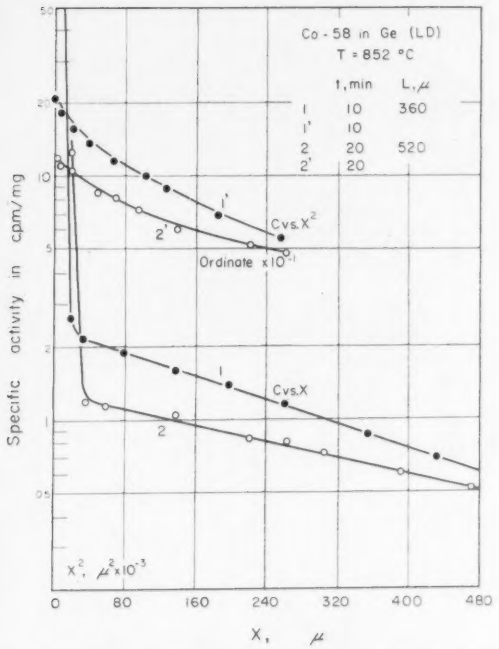

FIG. 7. Penetration curves of Co diffusion in Ge (LD, 852°C).

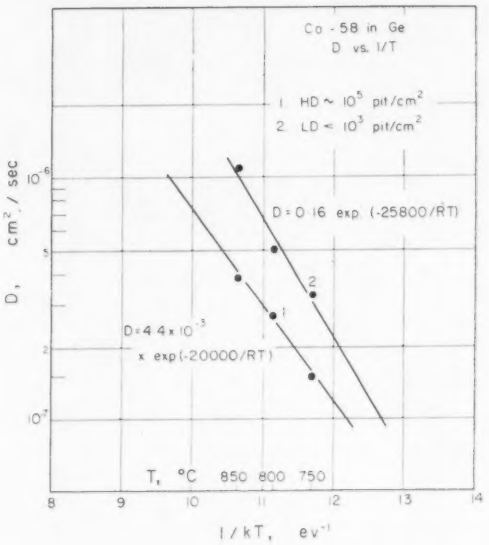

FIG. 8. Diffusivity vs. temperature of Co in Ge (HD).

the diffusivity of Fe in Ge at 800°C as,[13]

$S = 10^{15}$ atoms/cm² = 50 times TYLER's value.[14]

$D = (1{\cdot}6 \pm 0{\cdot}6) \times 10^{-6}$ cm²/sec = 6 times our value.

4. DIFFUSION MECHANISM

If a diffusion process is composed of two streams with different diffusivities and if there is an exchange of flow between them, then by the principle of continuity, we have (for one dimension),

$$\frac{\partial N_1}{\partial t} = D_1 \frac{\partial^2 N_1}{\partial x^2} - K_1 N_1 + K_2 N_2 \qquad (1)$$

$$\frac{\partial N_2}{\partial t} = D_2 \frac{\partial^2 N_2}{\partial x^2} - K_2 N_2 + K_1 N_1 \qquad (2)$$

These equations were first used by VAN DER MAESEN in dealing with Cu diffusion in Ge.[3] Now, we can see that unless $K_1 N_1 = K_2 N_2$, Fick's law will not be followed.

One of the physical interpretations for a double-stream process is a trapping mechanism suggested by Prof. BARDEEN. We may conceive the double stream process as made of a running stream and a trapped stream. The running stream of free species probably interstitials, maintains a quasi-steady flow. During the course of diffusion, some of them may fall into traps. They will be held forever by deep traps but will be released in a short time from shallow traps. As long as the trapping rate is greater than the release rate, the concentration of the trapped species will build up with time. Because of the releasing action, the diffusion length of the running and the trapped streams will increase slowly with time. In the following, we shall give a simple mathematical treatment.

Let N_1, N_2 = concentrations of free and trapped species.

D_1, D_2 = diffusivities of free and trapped species.

K_1 = probability of each free species being trapped per unit time.

Vol. 18
1961

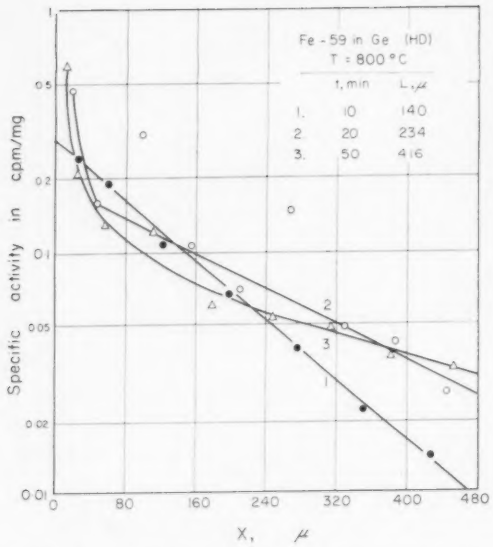

FIG. 9. Penetration curves of Fe diffusion in Ge (HD).

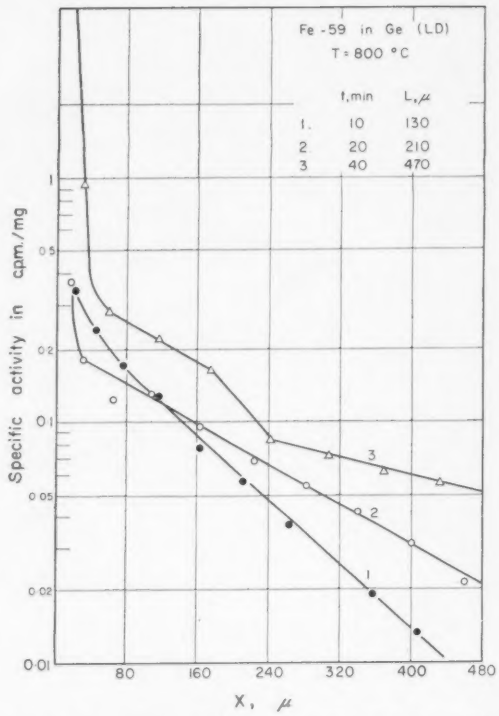

FIG. 10. Penetration curves of Fe diffusion in Ge (LD).

K_2 = probability of each trapped species being released per unit time.

We assume that,

$$K_1 > K_2$$

For simplicity of mathematical treatment, we take

$$D_2 = 0$$

We further assume that the stream of free species maintains a quasi-steady flow,

$$\frac{\partial N_1}{\partial t} = 0$$

The physical significance of $\partial N_1/\partial t = 0$ is as follows. We may consider N_1 to consist mostly of interstitials. As it is generally believed that the interstitials have very low solubility but rather great mobility, N_1 will reach its saturation value within a very short time after diffusion starts. Then, since the concentration is limited by the solubility, N_1 cannot grow with time. Shortly after the start of the diffusion, the process thus consists of the influx of the free species and trapping of them in the bulk at about the same rate.

(a) Dead trapping, $K_2 = 0$

The equations for N_1 and N_2 are:

$$\frac{\partial N_1}{\partial t} = 0 = D_1 \frac{\partial^2 N_1}{\partial x^2} - K_1 N_1 \tag{3}$$

$$\frac{\partial N_2}{\partial t} = K_1 N_1 \tag{4}$$

The solutions are:

$$N_1 = N_0 \exp(-x/L) \tag{5}$$

$$N_2 = K_1 N_0 t \exp(-x/L) \tag{6}$$

where

$$L = \sqrt{(D_1/K_1)} \tag{7}$$

We have to understand that K_1, the trapping probability is proportional to the concentration of the unoccupied traps. When the number of traps,

N_T is great, K_1 may be taken as a constant, and so also is the diffusion length L. If N_T is small, K_1 may decrease with time (because the number of unoccupied traps may decrease) and L will increase accordingly. When all traps are filled, equations (3) and (4) are no longer valid. Instead, we shall have,

$$\frac{\partial N_1}{\partial t} = D_1 \frac{\partial^2 N_1}{\partial x^2}$$

$$N_2 = N_T$$

The total concentration will be,

$$N_t = \frac{N_0}{2\sqrt{(\pi D_1 t)}} \exp(-x^2/4D_1 t) + N_T \qquad (8)$$

The resultant curve (N_t) will thus look like a gaussian when N_T is small (for example, in LD crystals), but will approach the $\exp(-ax)$ shape as N_T becomes greater.

(b) Shallow trapping, $K_2 \neq 0$

The equations for N_1 and N_2 are:

$$\frac{\partial N_1}{\partial t} = 0 = D_1 \frac{\partial^2 N_1}{\partial x^2} - K_1 N_1 + K_2 N_2 \qquad (9)$$

$$\frac{\partial N_2}{\partial t} = K_1 N_1 - K_2 N_2 \qquad (10)$$

The approximate solutions are obtained as follows. Using the assumption $\partial N_1/\partial t = 0$, i.e. N_1 independent of t, we obtain from (10),

$$N_2 = \frac{K_1}{K_2} N_1 [1 - \exp(-K_2 t)] \qquad (11)$$

Substituting this into (9), we get,

$$N_1 = N_0 \exp(-x/L) \qquad (12)$$

where

$$L = (D_1/K_1)^{1/2} \exp(K_2 t/2) \qquad (13)$$

From (11) and (12), we get,

$$N_2 = \frac{K_1}{K_2} N_0 [1 - \exp(-K_2 t)] \exp(-x/L) \qquad (14)$$

A more exact solution for N_2 may be obtained by plugging (12) into (10) but the integration involved is somewhat difficult.

The total concentration is,

$$N_t = N_1 + N_2 = N_0 \times$$

$$\times \exp(-x/L)\left[1 + \frac{K_1}{K_2}[1 - \exp(-K_2 t)]\right] \qquad (15)$$

With two sets of values of L and t, K_1 and K_2 can be calculated from (13). For example, using data from Fig. 1 and $D_1 = 2 \times 10^{-6}$ cm^2/sec, we obtain,

$$K_1 = 5 \times 10^{-3} \text{ sec}^{-1}, \qquad K_2 = 2 \times 10^{-4} \text{ sec}^{-1}$$

Then $K_1/K_2 > 20$ which justifies the trapping mechanism.

Since the solutions for N_1 and N_2 are first-order approximations, they cannot exactly satisfy the original differential equations. Obviously, N_1 given by (12) is not consistent with $\partial N_1/\partial t = 0$. However, if

$$\frac{\partial N_1}{\partial t} \ll D_1 \frac{\partial^2 N_1}{\partial x^2} \qquad (A)$$

our solution may be considered a good approximation. With the substitution of N_1 from (12), the above inequality becomes

$$\frac{x}{L} \cdot \frac{d}{dt}(\ln L) \ll D_1/L^2 \qquad (B)$$

Since the distance of interest is $x \sim 2L$, using (13), we have from (B),

$$K_2 \ll D_1/L^2 \qquad (C)$$

With the above numerical values substituted ($L = 240$ microns from Fig. 1), we see that (C) is satisfied. If one inserts (12) and (14) into (10), one would find the error in per cent to be,

$$\Delta = \frac{x}{2L}\left(\frac{K_1}{D_1} L^2 - 1\right) \qquad (D)$$

At $x = 2L$,

$$\Delta_{2L} = \frac{K_1}{D_1} L^2 - 1 \qquad (E)$$

This is very sensitive with regard to the numerical value of L. For example, when $K_1 = 5 \times 10^{-3}$ sec^{-1}, $D_1 = 2 \times 10^{-6}$ cm^2/sec, and $L = 2{\cdot}4 \times 10^{-2}$ cm,

Vol. 18
1961

one gets

$$\Delta_{2L} = 45 \text{ per cent}$$

However, if $L = 2{\cdot}1 \times 10^{-2}$ cm, $\Delta_{2L} = 10$ per cent. Thus, it would be difficult to judge the approximate solutions simply on the basis of (D). However, the form of the solutions is in qualitative agreement with the general shape of the experimental curves

After a sufficient length of time,

$$N_t = N_0\left(1+\frac{K_1}{K_2}\right)\exp(-x/L) = N_0'\exp(-x/L) \tag{16}$$

where N_0' is the surface concentration. If the source material is exhausted after this time, N_0' will be determined by the following condition,

$$C = \int_0^\infty N_t\,dx = N_0'L$$

$$N_0' = C/L \tag{17}$$

or the surface concentration will decrease with time.

5. DISCUSSION

For diffusion by the "dissociative mechanism", FRANK and TURNBULL obtained,

$$D_s = D_v C_v/(C_v+C_s) \simeq D_{Ge}/C_s', \quad \text{if } C_v \ll C_s$$

where C_v, C_s are the concentrations of vacancies and substitutionals; C_s', the saturation solubility of substitutional Cu atoms, and D_v, D_s and D_{Ge}, the diffusivities of vacancy, substitutional and Ge atoms. An estimate of D_s from this formula is in good agreement with the experimental result by TWEET of Cu diffusion near the surface of a high perfection crystal of Ge.[4] In our experiments, we have used a high perfection crystal supplied by TWEET for Ag diffusion in Ge and obtained data as shown in Fig. 2. In Section 3, we have calculated D_a near the surface of the crystal based on Fig. 2 as

$$D_a = 3{\cdot}6 \times 10^{-8} \text{ cm}^2/\text{sec}$$

Using FRANK and TURNBULL's formula and the values of D_{Ge} and C_s' at $T = 710°C$, for Ag in Ge,

$$D_{Ge} = 6 \times 10^{-15} \text{ cm}^2/\text{sec}$$

$$C_s' = 10^{14}/4{\cdot}5 \times 10^{22} = 2 \times 10^{-9}$$

we would have

$$D_s = 6 \times 10^{-15}/2 \times 10^{-9} = 3 \times 10^{-6} \text{ cm}^2/\text{sec}.$$

This value is higher by two orders of magnitude than the experimental value D_a, $3{\cdot}6 \times 10^{-8}$ (the difference between this D_a and the erfc function extrapolated D is about a factor of 2–3, the latter is usually the smaller one). This would suggest that the diffusion of Ag in Ge is by a mechanism other than the dissociative one. We should realize that the dissociative mechanism occurs if: (1) the interstitial and the vacancy diffuse independently after dissociations and (2) $D_i > D_v$. At very high diffusivities, the interstitials will quickly attain the equilibrium concentration. Under these conditions, the formula for D_s,

$$D_s = D_v C_v/(C_v+C_s)$$

is valid. In the case of Ag diffusion in Ge, we first note that the Ag atoms are much larger than the Ge atoms. Because of the strain interaction between a large interstitial and a vacancy, their diffusion immediately after dissociation would not be entirely "independent". Secondly, D_i of Ag in Ge as obtained above is about 2×10^{-6} cm^2/sec. At 700°C, $D_v = 6 \times 10^{-5}$ cm^2/sec. Hence $D_i < D_v$. At much lower diffusivities, the Ag interstitials may not reach the equilibrium concentration in a short diffusion time. All these conditions do not favor the dissociative mechanism and hence the above formula for D_s is no longer valid for the case of Ag in Ge. Thus a lower value of D_s of the Ag substitutionals in Ge than that calculated from FRANK and TURNBULL's formula is to be expected. When the interstitial and vacancy concentrations do not reach equilibrium and vacancies enter as a third kind of diffusion species having reactions with both substitutionals and interstitials, the situation is difficult to deal with theoretically. This case is worthy of further investigation.

For diffusion of Ag and Co in Ge, we observed that the apparent concentration* is greater in high dislocation than in low dislocation crystals. Most of

* Throughout this paper, the "concentration" usually means the observed concentration which is not necessarily the *equilibrium* concentration.

the data show strikingly the exponential characteristic of concentration vs. penetration distance. All these findings can be interpreted by the trapping mechanism. The concentration measured is the sum of the free species (probably interstitials) and the trapped species. The higher trap density as in the case of HD crystals, would result in (a) a higher concentration of trapped species and (b) a higher trapping rate which will reduce the diffusion length and hence the apparent diffusivity of the composite stream. We have shown in Section 4 that if the trapping rate is greater than the release rate, the concentration will follow a simple $\exp(-x/L)$ law. However, Fick's law will be followed if (a) $K_1N_1 = K_2N_2$ or (b) all traps are filled. This could occur in LD crystals because of low trap density. The case of Fig. 5 may be due to either of these two conditions.

Another interesting conclusion from our study is that in HD crystals, the surface concentration is proportional to time up to a certain time limit. This fact is shown in Fig. 1 (curves 2 and 3), Fig. 3 (curves 1 and 2), and Fig. 6. The rise with time of the surface concentration is predicted by our theory (Section 4). It appears that our theory of trapping mechanism is able to account for many experimental facts and so may be taken as a sound basis in dealing with this type of diffusion.

The limited supply after a certain time as shown by the drop of surface concentration (Figs. 3 and 9) may be due to either or both of the following causes: (a) formation of oxide on the surface. This is quite possible because cobalt and iron are easily oxidized. (b) formation of an alloying layer.

The characteristics of iron diffusion in Ge as described in Section 3 deserve further discussion. To interpret the data, we conceive that "vacancies" may not be a determining factor in Fe diffusion. Instead, some other kind of traps, possibly oxygen may play an important role. If the role of vacancies becomes insignificant, it would be expected that the dislocation density would have little effect on concentration and diffusivity. Furthermore, the concentration of Fe substitutionals (trapped by vacancies) would be small, an important factor contributing to the very low solubility. The impurity traps may have higher concentration than the equilibrium concentration of vacancy and may produce pockets in the crystal. The high rate of trapping, if it can occur, would give the non-Fickian diffusion.

The following table shows us the present status of diffusion of various elements in Ge. It is very interesting to note from Table 1 that most properties of Class B solutes are midway between those of Class A and Class C solutes. The solubilities of

Table 1. *Diffusion in* Ge

Class	A	B	C
Elements	Li Cu Ni*	Ag Co Fe	Au, Zn & Group III IV, V elements
(1) Bond with Ge atoms	very weak	weak	strong
(2) Activation energy for diffusion	$<\frac{1}{2}$ eV	$\sim$1 eV	>2 eV
(3) D† (800°C) in cm²/sec.	10^{-4}–10^{-5}	10^{-6}–10^{-7}	10^{-9}–10^{-13}
(4) Maximum solubility (atomic fraction)	10^{-4}–10^{-7}	10^{-8}–10^{-9}	1–10^{-3}
(5) Diffusion process	interstitial and others	double stream	substitutional
(6) Diffusion mechanism	interstitial, dissociative and others	trapping	vacancy mechanism and others
(7) Fick's law	mostly no	mostly no	yes

* Ni may be considered as an element between class A and B. Its activation energy for diffusion in Ge is 0·9 eV.

† Diffusivity is usually measured in ordinary Ge crystals (10^4–10^6 pits/cm²). D's for Cu, Ni, Ag, Co and Fe are "apparent" rather than "true".

Vol. 18
1961

Class B elements in Ge are the lowest perhaps because they are not good substitutionals due to weak bonding and also not good interstitials due to large atomic size.

6. CONCLUSIONS

From experiments of Ag, Co and Fe diffusion in Ge, we have found:

(a) The concentration often varies approximately as $\exp(-x/L)$, where the diffusion length L increases with time.
(b) In high dislocation crystals, the concentration near the surface increases with time up to a certain time limit.
(c) In some cases, the penetration curves show great irregularities.
(d) The apparent diffusivities of these elements in Ge are very great, in the range of 10^{-6}–10^{-7} cm^2/sec at temperatures around 800°C.
(e) The apparent diffusivities are usually higher in low-dislocation (less than 10^3 pits/cm^2) crystal than in high-dislocation (10^5 pits/cm^2) crystals.
(f) The solubilities are very small in Ge. They are in the range of 10^{-8}–10^{-9} in atomic fraction (700–850°C).
(g) For cobalt diffusion in Ge, the activation energy is about 1 eV which is nearly the same as the value for Ag, and Ni and Fe in Ge obtained by other workers.

In theory, we have shown that a double stream diffusion process would in general not follow Fick's law because of non-equilibrium exchange of streams. The trapping mechanism, a possible interpretation of a double-stream process, not only leads to a concentration varying approximately as $\exp(-x/L)$ but also is able to explain many other experimental facts.

In conclusion, we can say that our experimental results, the theory of double-stream process and its physical interpretations (trapping mechanism) show very good accord. Combining these results with the knowledge of Cu and Ni diffusion in Ge obtained elsewhere, we can further conclude that diffusion of most Group I and transition elements in Ge (700–850°C) has the following characteristics.

(a) Non-Fickian diffusion in many cases.
(b) High diffusion rate.
(c) Very low solubility.
(d) Low activation energy.
(e) Subject to structure and impurity effects.

Acknowledgements—The author wishes to express his gratitude to Professor J. BARDEEN for his guidance and encouragement throughout the course of this study. He is greatly indebted to Dr. VAN DER MAESEN of Philips Research Laboratories (Netherlands) for supplying detailed information on method of surface treatment and to Dr. A. G. TWEET of General Electric Research Laboratory for providing the precious low dislocation Ge crystals. The author wishes also to acknowledge help from Dr. M. F. MILLER in the early stage of experimental work.

APPENDIX

The concept and definition of apparent diffusivity

Throughout this paper, we use "apparent diffusivity" rather than "true diffusivity". This concept may be bewildering and therefore could cause misunderstanding even to those workers who have had long experience in this field. The author should mention that to his knowledge, this concept was originally introduced by VAN DER MAESEN in connection with Cu diffusion in Ge.[3] Later, FULLER, FRANK and TURNBULL used the adjective "apparent" rather liberally for the diffusivity of Cu in Ge.[2, 5] This concept is followed in this paper because none better is available.

The "apparent diffusivity" is defined by the following equation,

$$J(x_1)-J(W) = -D_a\left(\frac{\partial N}{\partial t}\right)_{x_1} - J(W) = \int_{x_1}^{\overline{W}} \frac{\partial N}{\partial t}\,dx \tag{A1}$$

This is just the integration of Fick's second law between x_1 and W (the thickness of the sample). If W is very great in comparison with the diffusion length, which is practically true for most experimental cases, then we can take $J(W) \approx J(\infty) = 0$. Since x_1 can be any point in the sample, there is no need for its subscript. With these simplifications, we get,

$$D_a = -\int_x^{\overline{W}} \frac{\partial N}{\partial t}\,dx \Big/ \left(\frac{\partial N}{\partial x}\right)_x \tag{A2}$$

We now consider (A2) as the "generalized definition" of diffusivity no matter how $N(x,t)$ is obtained and whether or not Fick's law is obeyed. When diffusion follows Fick's law, D from (A2) will be automatically the true diffusivity. However, if Fick's law is not followed, we still can determine D according to (A2) if $N(x,t)$ and only $N(x,t)$ can be found by some means (from experimental or from other theoretical derivation). In this case, D in (A2) is called the "apparent diffusivity".

In our study, we found both from experiment and from theory

$$N(x, t) \cong A(t) \exp(-x/L) \qquad \text{(A3)}$$

where $A(t)$ is the surface concentration, and L the diffusion length. Then based on (A2), the apparent diffusivity, for $W \gg L$, will be given by,

$$D_a = \frac{L}{A}(A'L + AL') + L'x \qquad \text{(A4)}$$

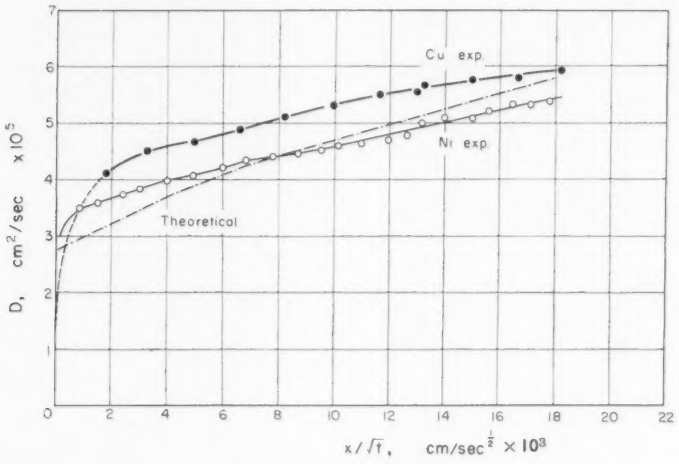

FIG. 11. Diffusivities of Cu and Ni in Ge (After VAN DER MAESEN[3]).

where the prime (′) stands for differentiation with respect to time. Let us consider the following special cases:

(i) $A = ct$, $L = \text{const.}$,

$$D_a = L^2/t \qquad (c = \text{const.}) \qquad \text{(A5)}$$

(ii) $A = \text{const.}$, $L = k\sqrt{t}$,

$$D_a = \frac{L}{2t}(L + x) = \frac{k^2}{2} + \frac{kx}{2\sqrt{t}} = a + b\lambda \qquad \text{(A6)}$$

(iii) $AL = \text{const.}$, $L = k\sqrt{t}$,

$$D_a = \frac{1}{2t}Lx = \frac{kx}{2\sqrt{t}} = \frac{k}{2}\lambda \qquad \text{(A7)}$$

(iv) $A = ct$, $L = kt$,

$$D_a = \frac{3L^2}{2t} + \frac{Lx}{2t} = \frac{3}{2}k^2 + \frac{kx}{2t} = 3a + b \qquad \text{(A8)}$$

From (A5) to (A8), we note that: (a) D_a is not a constant but a function of x and t. (b) In cases (ii)–(iv), D_a is linear with $\lambda (= x/\sqrt{t})$. These two results may surprise some workers in this field. Fig. 11 taken from VAN DER MAESEN's data[3] should serve as a good example to justify our statement.

If we define D_a at $x = L$ as the "nominal Fick diffusivity", D_{an}, then in cases (i) and (ii),

$$D_{an} = L^2/t \qquad \text{(A9)}$$

In case (iii),

$$D_{an} = L^2/2t \qquad \text{(A10)}$$

In case (iv),

$$D_{an} = 2L^2/t \qquad \text{(A11)}$$

Which of formulas (A9)–(A11) should be used depends on which ideal case as set in (A5)–(A8) is nearest to the actual situation. This can be judged without great error simply by examining the penetration curves. This is our basis for obtaining the apparent diffusivity throughout this paper.

Vol. 18
1961

REFERENCES

1. FULLER C. S., STRUTHERS J. D., DITZENBERGER J. A. and WOLFSTIRN K. B., *Phys. Rev.* **93,** 1182 (1954).
2. FULLER C. S. and DITZENBERGER J. A., *J. Appl. Phys.* **28,** 40 (1957).
3. VAN DER MAESEN F. and BRENKMAN J. A., *J. Electrochem. Soc.* **102,** 229 (1955).
4. TWEET A. G., G. E. Report No. 57–RL–1685; *Phys. Rev.* **103,** 828 (1956).
5. FRANK F. C. and TURNBULL D., *Phys. Rev.* **104,** 617 (1956).
6. TWEET A. G., *Phys. Rev.* **105,** 221 (1957).
7. FULLER C. S. and SEVERIENS J. C., *Phys. Rev.* **95,** 21 (1954).
8. DUNLAP W. C., *Phys. Rev.* **97,** 614 (1955).
9. LETAW H., PORTNOY W. M. and SLIFKIN L., *Rev. Sci. Instrum.* **25,** 865 (1954).
10. LOGAN R. A., *Phys. Rev.* **91,** 757 (1953).
11. BUGAI A. A., KOSENKO V. E. and MISELUK E. G., *Zh. tekh. fiz.* **27,** 1671 (1957).
12. VAN DER MAESEN F. and BRENKMAN J. A., *Philips Res Rep.* **9,** 225 (1954).
13. BUGAI A. A., KOSENKO V. E. and MISELUK E. G., *Zh. tekh. fiz.* **27,** 210 (1957).
14. TYLER W. W. and WOODBURY H. H., *Phys. Rev.* **96,** 874 (1954).

J. Phys. Chem. Solids Pergamon Press 1961. Vol. 18, Nos. 2/3 pp. 175–180. Printed in Great Britain.

NEUTRON IRRADIATION OF Cu–Al AT ELEVATED TEMPERATURES

R. H. KERNOHAN and M. S. WECHSLER

Solid State Division, Oak Ridge National Laboratory*
Oak Ridge, Tennessee, U.S.A.

(*Received* 11 *April* 1960; *revised* 11 *May* 1960)

Abstract—The effect of neutron irradiation at elevated temperatures on the electrical resistivity of Cu–Al (15 at. % Al) is described. The results support the idea that at temperatures below 200°C the alloy is in a metastable state. Upon irradiation atomic mobilities are enhanced and the metastability is eliminated, accompanied by a decrease in resistivity. An analysis is made of the temperature dependence of the rate of the atomic rearrangement stimulated by the irradiation. It is found that the activation energy for motion remains constant during the process at about 0·5 eV. A comparison is made with the results of a previous experiment in which the alloy was irradiated at lower temperatures.

Vol. 18
1961

1. INTRODUCTION

THE LATTICE defects produced upon irradiation have two effects in alloys. As in the case of pure metals the presence of the defects themselves alters the properties of the alloys, as is seen most conspicuously in increases in electrical resistivity and hardness. But in alloys the radiation-produced defects may have a second effect. They may stimulate by nucleation or accelerate by enhanced diffusion changes in the relative arrangement of the atoms of different types in the alloy. Since the properties of alloys are often very sensitive to such atomic rearrangements this second effect may predominate.

It is sometimes possible to separate the two effects. It has been shown[1] that when Cu–Al alloys are irradiated by neutrons at about 35°C the resistivity decreases, reaches a minimum and then increases linearly upon further exposure in the reactor. The linear increase in resistivity in the latter stage of the process is believed to be the direct effect of the radiation-produced defects. Earlier in the process, however, this linear increase has superimposed upon it a much larger decrease in resistivity associated with a diffusion-controlled atomic rearrangement. Since the atomic rearrangement reaches a steady state, the two effects may be decomposed by extrapolating to zero time the linear increase observed in the long-time region of the curve. This decomposition of the total effect is further supported by the observation[1] that only a linear increase is observed when the irradiation is carried out at −120°C. The implication is that the diffusion-controlled atomic rearrangement is inhibited because of the lower atomic mobilities at −120°C. Thus, upon neutron irradiation at −120°C a linear increase in resistivity is observed due to the *presence* of the radiation-produced defects but the atomic rearrangement that is the consequence of their *motion* does not take place at −120°C. However, if the temperature of the alloy is subsequently raised above −50°C the defects become mobile and the decrease in resistivity sets in.

The irradiation experiments on Cu–Al indicate that the alloy is initially in a metastable condition and that upon irradiation the atoms rearrange themselves and thereby eliminate the metastability. Recent X-ray diffuse scattering measurements[2] on irradiated Cu–Al indicate that the atomic rearrangement corresponds to short-range ordering, as was postulated earlier as a result of irradiation experiments on alpha-brass.[3–6] The question of

* Oak Ridge National Laboratory is operated by Union Carbide Corporation for the U.S. Atomic Energy Commission.

the mechanism of the atomic rearrangement in these alloys has been discussed recently.[7,8] In terms of short-range order the metastable state is one in which the alloy possesses less short-range order than is characteristic of equilibrium at the irradiation temperature. Upon irradiation, however, the ordering reaction is stimulated and the alloy proceeds to equilibrium at a lower temperature than is normally possible. This point of view implies that the metastable state was

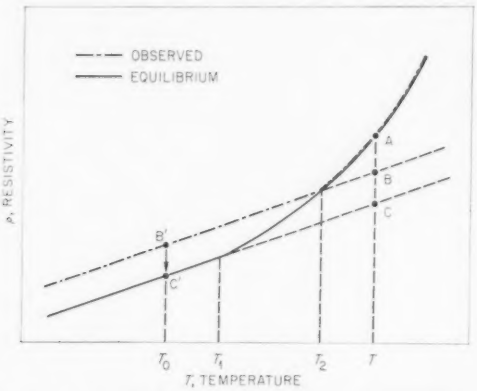

FIG. 1. Schematic plot of resistivity vs. temperature.

frozen in during the cooling from the high temperature used in preparing the alloy initially. In fact, an extension of concepts usually employed in analysing metallurgical reactions suggests that in some cases it may be virtually impossible to cool to room temperature slowly enough to avoid retaining the state of affairs characteristic of a higher temperature. This situation is illustrated schematically in Fig. 1. If it were possible to maintain equilibrium during the cooling, the resistivity would follow the full curve. At temperatures above T_1 the alloy may possess at equilibrium a lesser amount of short-range order,* which has associated with it an additional amount of resistivity indicated by the departure from the line $C'C$. However, under actual circumstances the resistivity upon cooling is thought to follow the equilibrium curve only down to the temperature T_2, at which temperature atomic mobilities become too low to permit further atomic rearrangement. Upon continued cooling the lesser ordered structure characteristic of T_2 is retained and the resistivity follows the line $B'B$. The metastability at room temperature (T_0, Fig. 1) is represented by the distance $B'C'$. Thus, upon irradiation near room temperature, the alloy is able to achieve the equilibrium degree of short-range order and the resistivity decreases from B' to C'. For the 15 at. per cent Al alloy irradiated at 35°C[1] this decrease was observed to be about 0·18 $\mu\Omega$ cm.

Measurements of the electrical resistivity of Cu–Al (15 at. per cent Al) have been made as a function of temperature.[9] It was found for the unirradiated alloy that an additional contribution to the resistivity is made at temperatures above 200°C. Therefore, we may designate T_2 in Fig. 1 as 200°C. It is the purpose of this paper to describe experiments that provide a test of the ideas illustrated in Fig. 1. Since the irradiation is considered to stimulate the rearrangement from the metastable state (dot-dash curve, Fig. 1) to the equilibrium state (full curve) it may be seen that, as the temperature of irradiation is raised above T_1, the magnitude of the decrease should diminish. Finally, since the alloy is already at equilibrium at the temperature T_2, irradiation at 200°C and above should produce little or no change in resistivity. It is seen below that the observed magnitudes of the decreases in resistivity upon irradiation at temperatures between 45°C and 250°C are in general agreement with this description of the phenomenon. Also, the kinetics of the decay curves are studied as a function of irradiation temperature and compared with the previous analysis[1] of similar curves obtained after irradiation at −120°C. Finally, a "step-irradiation" experiment is described in which a sample is irradiated at successively lower temperatures between 250°C and 50°C.

2. EXPERIMENTAL DETAILS

Single crystal samples of Cu–Al (15 at. per cent Al) were used. They were 1/8 in. in diameter and contained short nibs or projections at which the voltage contacts for the resistivity measurements were made. The samples were prepared and heat treated in the same manner as has been described previously.[1,9] In particular, prior to irradiation they were held for several hours at 750°C and

* It may be seen that the argument remains the same if the equilibrium configuration above T_1 involves other types of atomic rearrangement, e.g. the dissolution of GUINIER–PRESTON zones.

cooled at a rate of about 15°C/hr to room temperature.

The resistivity measurements were made at temperature while the samples were in the reactor. The double potentiometer method was used. The sample was mounted inside of a wire-wound heater coil and the heater was placed within an aluminum irradiation capsule. A second auxiliary heater was used to reduce the thermal gradient along the sample. The heaters were powered with direct current. The sleeves used in contacting the voltage nibs and the lead-in wire were made of the same Cu–Al alloy material as the samples. The alloy wire was hard-soldered to copper at a point far removed from the hot zone. The temperatures were measured by two thermocouples spot-welded to the two voltage-contact sleeves. A third thermocouple adjacent to the sample but not in contact with it delivered a control signal to an automatic temperature controller. The temperature was controlled to within $\pm$ 2°C. The resistivity of each sample was measured prior to irradiation as a function of temperature between room temperature and about 160°C. The temperature dependence was linear and the temperature coefficient thus determined was used to correct all resistivity readings to the nominal temperatures given below.

The ORNL Graphite Reactor was used for the irradiations. The fast neutron flux was approximately 3×10^{11} neutrons per cm^2 sec.

3. RESULTS

The in-pile measurements of resistivity upon irradiation at temperatures between 45°C and 250°C are shown in Fig. 2. It is seen that the magnitude of the decrease in resistivity is diminished as the irradiation temperature is raised. At 150°C the decrease in resistivity is about one-half of the decrease at 100°C. Also, at 200°C only a slight decrease in resistivity is observed and at 250°C, only a slight increase. The degree of reproducibility of the data is indicated by a comparision of the two runs conducted at 150°C. In accordance with the above discussion these results indicate that the initial condition of the alloy is characteristic of a temperature between 200°C and 250°C.

It may be seen from Fig. 2 that the rate of approach to the equilibrium resistivity varies with irradiation temperature. The kinetics of the process may be studied by normalizing the decay curves of Fig. 2 to their final values. For the run at 45°C, the resistivity was observed to decrease slowly even after about 2×10^4 min (2 weeks). The final value for this run was estimated from a

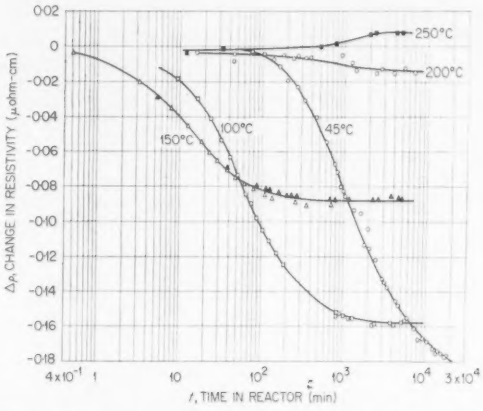

FIG. 2. Changes in resistivity upon irradiation at various temperatures. Cu–Al (15 at. % Al) single crystals. The open and filled triangles refer to separate runs at 150°C.

plot of the curve to a linear time scale as is shown in Fig. 7 of Ref. 1. The normalized decay curves for the 45, 100 and 150°C runs are shown in Fig. 3, where it is seen that the reaction goes on more rapidly at the higher irradiation temperatures.

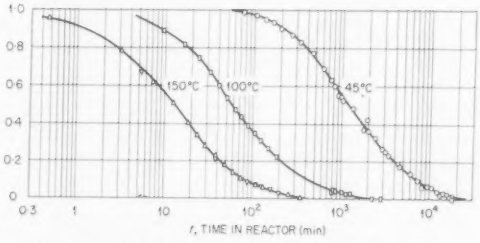

FIG. 3. Normalized decay curves for irradiation temperatures of 45, 100 and 150°C.

The quantity f represents the fraction of the reaction not yet completed at a given time. The time, τ, for various values of f is plotted versus reciprocal irradiation temperature in Fig. 4. The time, τ, is found to obey roughly the relation

$$\tau = \tau_0 \exp\left(\frac{\epsilon_M}{kT}\right)$$

Vol. 18
1961

where ϵ_M is the apparent activation energy for motion. In Fig. 5 ϵ_M is plotted vs. f for the present experiment (triangles) and for the previous experiment[1] (circles) in which the resistivity decrease was measured isothermally at various temperatures following irradiation for three weeks at −120°C. It is interesting that during bombardment the reaction goes on with an activation energy that is approximately constant at about 0·5 eV, whereas the activation energy increases from a low value to about 1·0 eV when the radiation dose is received at a low temperature prior to bringing the sample to the reaction temperature.

In the step-irradiation experiment the effect of varying the irradiation temperature was investigated by irradiating the same Cu–Al (15 at. per cent Al) sample at successively lower temperatures. The initial temperature of irradiation was 250°C and was decreased in 25°C steps. The irradiation period was one-half week for all but the last few irradiations, at which time the period was increased to one week. The results of the step-irradiation experiment are shown in Fig. 6. The resistivity was observed to decrease more slowly and to a lesser extent as the irradiation temperature was reduced. The results shown in Fig. 6 may be analysed with the help of the schematic representation given in Fig. 7. The dot–dash curve, the full curve, and the lines $B'B$ and $C'C$ have the same significance as in Fig. 1. The bracket labelled "$\Delta\rho$" illustrates that the "excess resistivity" plotted in Fig. 6 refers to resistivity in excess of that given by the line $C'C$. The temperature coefficient of the sample was measured before and after the experiment and found to be the same to within 0·1 per cent and, thus, $C'C$ is drawn parallel to $B'B$. After the experiment was completed the measured resistivity values at a given temperature had subtracted from them the values given by the line $C'C$. In this way the temperature-dependent contribution to the resistivity was cancelled out. The validity of the temperature correction is indicated in Fig. 6 by the extent to which the points measured at adjacent temperatures match up. Some discrepancy can be seen, e.g. in the joining of the data taken at 175°C and 150°C; but on the whole the temperature correction seems quite good.

It is suggested in Fig. 7 that the sample is at the outset at equilibrium at 250°C and, therefore,

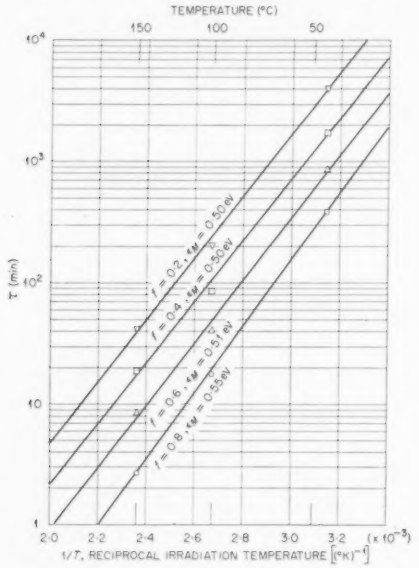

FIG. 4. Times for various fractional amounts of decrease in resistivity vs. reciprocal irradiation temperature.

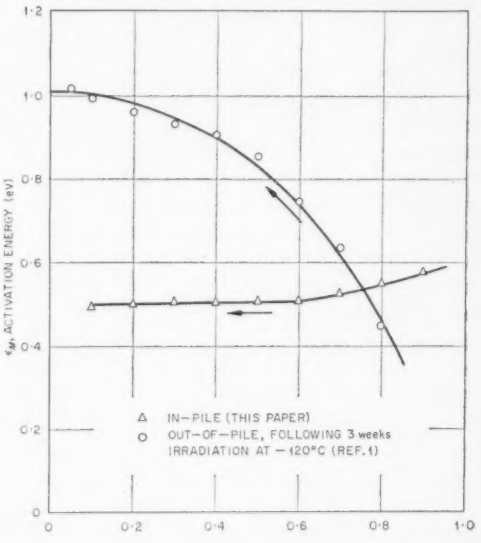

FIG. 5. Activation energy for the motion of the process vs. the fractional decrease in resistivity.

little change in resistivity takes place at this temperature. When the temperature is decreased to 225°C the resistivity is immediately decreased because of the temperature coefficient (short-dashed line labelled "225", Fig. 7). But in addition a decrease in resistivity takes place because of the change in the equilibrium atomic arrangement, e.g. to a more ordered structure (vertical arrow, Fig. 7). This change occurred too rapidly at 225°C for measurement and only the final level is registered in Fig. 6 at this temperature. The vertical arrows in Fig. 7 indicate that the departure from the equilibrium configuration becomes smaller as the temperature is reduced and, thus, the magnitude of the decrease in resistivity becomes progressively smaller, as is the case in Fig. 6. However, at 200°C and below the rate of atomic rearrangement to the equilibrium configuration at each new temperature was sufficiently low to permit measurements to be made as the rearrangement was taking place.

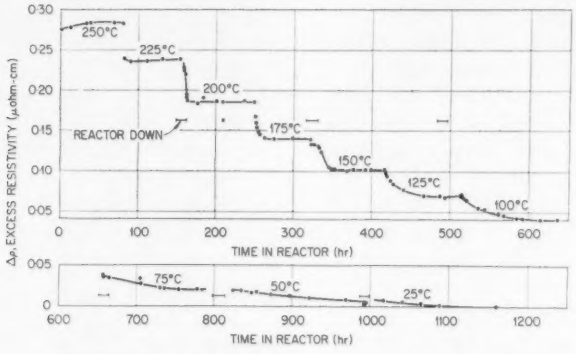

FIG. 6. Step-irradiation experiment. In-pile measurements on Cu–Al (15 at. % Al) at successively lower temperatures.

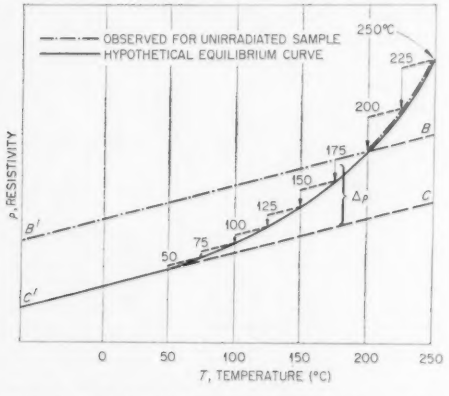

FIG. 7. Step-irradiation experiment (schematic).

4. DISCUSSION

Fig. 2 shows that two main effects are observed when annealed samples of Cu–Al (15 at. per cent Al) are irradiated isothermally at various temperatures. The samples irradiated at higher temperatures undergo a smaller decrease in resistivity and the decrease occurs more rapidly. The smaller magnitude of the change in resistivity at higher temperatures is explained on the assumption that the process stimulated by the radiation corresponds to the transition from a metastable to an equilibrium configuration. The degree of metastability is less at the higher temperatures and, thus, a lesser decrease in resistivity takes place.

As concerns the temperature-dependence of the rate of the reaction, it is of interest to compare the curves shown in Fig. 5. In the previous experiment[1] the decrease in resistivity was observed after the sample had been irradiated, in which case, ϵ_M was found to increase rapidly during the process from low initial values to a value of about 1·0 eV. The energy of 1·0 eV probably corresponds to the motion energy of single vacancies.[10] It would seem that under these circumstances the atomic rearrangement is brought about by virtue of the motion of vacancies in various states of aggregation. Initially the more mobile vacancy

Vol. 18
1961

aggregates make the major contribution, but as they become exhausted the predominant motion shifts to single vacancies. However, in the present experiment the atomic rearrangement takes place while the sample is being irradiated. A dynamic equilibrium is set up in which vacancies are continuously being produced and annihilated; and, therefore, the distribution of vacancies remains rather constant as the process takes place. As a result the activation energy also remains constant at a value (0·5 eV) corresponding to the low end of the activation energy spectrum. This observation is to be compared with that of DIENES and DAMASK[6] on alpha brass. They found that the rate of decrease in resistivity was temperature independent (zero activation energy). Their theoretical analysis[6] predicts that the effective activation energy for radiation-enhanced diffusion is zero for annealing to fixed sinks alone but is one-half of the vacancy motion energy when the annealing involves also bimolecular vacancy-interstitial recombination. On this basis the latter annealing mechanism appears to be more appropriate for Cu–Al.

Important inferences may be drawn concerning the nature of alloys as a result of the investigation described above. It may be true for many alloys that atomic mobilities are too low below a critical freezing-in temperature to permit the equilibrium atomic arrangement to be estabished as a result of thermal treatment alone. In this case physical properties measured at temperatures below the freezing-in temperature will not be characteristic of equilibrium. In particular the phases and solubilities shown on an equilibrium diagram may not be correct. However, diffusion may be sufficiently enhanced as a result of irradiation to allow the rearrangement to the equilibrium configuration to take place at the lower temperatures of interest. Thus, as a result of irradiation the properties of alloys characteristic of thermodynamic equilibrum at low temperatures may be examined. In this way information may be gained concerning the nature of alloys that would be extremely difficult to achieve in the absence of the irradiation treatment. This investigation also indicates the need for caution in the use of practical materials in radiation environments. Since many practical alloys depend upon a metastable configuration for their properties the possibility exists that in a radiation flux the metastable condition will be eliminated with a consequent deterioration of properties.

Acknowledgements—The authors wish to thank D. S. BILLINGTON for many helpful discussions and J. E. THOMAS for assistance in the making of measurements.

REFERENCES

1. WECHSLER M. S. and KERNOHAN R. H., *J. Phys. Chem. Solids* **7,** 307 (1958).
2. HOUSKA C. R. and AVERBACH B. L., *J. Appl. Phys.* **30,** 1525 (1959).
3. ROSENBLATT D. B., SMOLUCHOWSKI R. and DIENES G. J., *J. Appl. Phys.* **26,** 1044 (1955).
4. DAMASK A. C., *J. Appl. Phys.* **27,** 610 (1956).
5. DAMASK A. C., *J. Phys. Chem. Solids* **4,** 177 (1958).
6. DIENES G. J. and DAMASK A. C., *J. Appl. Phys.* **29,** 1713 (1958).
7. DIENES G. J. and DAMASK A. C., *J. Phys. Chem. Solids* **12,** 105 (1959).
8. WECHSLER M. S. and KERNOHAN R. H., *J. Phys. Chem. Solids* **12,** 107 (1959).
9. WECHSLER M. S. and KERNOHAN R. H., *Acta Met.* **7,** 599 (1959).
10. LI C. Y. and NOWICK A.S. , *Phys. Rev.* **103,** 294 (1956).

J. Phys. Chem. Solids Pergamon Press 1961. Vol. 18, Nos. 2/3, pp. 181–195. Printed in Great Britain.

IONISATION PAR CHOC DES IMPURETES DANS LE SILICIUM

JEAN-CLAUDE SOHM

Laboratoire de Physique de l'Ecole Normale Supérieure, Paris, France

(*Received* 14 *March* 1960)

Résumé—Dans un semiconducteur, à température suffisamment basse, les porteurs restent liés aux impuretés dominantes. Celles-ci sont alors en majorité neutres, les impuretés compensatrices étant toutes ionisées. Lorsque l'on fait varier le champ électrique, le nombre de porteurs et leur mobilité varient. On atteint une valeur du champ telle que le phénomène d'ionisation par choc prend une allure d'avalanche. Le phénomène a été mis en évidence sur le germanium,[1] le phosphure d'indium,[2] et récemment sur le silicium[3] où nous l'avons nous-mêmes étudié pour des échantillons de type et de compensation différents.[4]

Abstract—In a semiconductor at low enough temperature, the carriers are bound to the majority impurities. Most of these are then neutral, and the compensating impurities are ionized. The number of carriers and their mobility vary with the electric field. There is a value of the field above which impact ionization multiplies by avalanche. This phenomenon has been observed in germanium,[1] in indium phosphide[2] and recently in silicon,[3] where we have studied it on samples of different types and compensations.[4]

Vol. 18
1961

I. INTRODUCTION

Les deux premiers problèmes qui se posent, lorsqu'on veut observer l'ionisation par choc sur les impuretés, sont :

(a) le choix de la température,
(b) le choix du matériau.

La première condition est déterminée par la valeur de l'énergie d'activation des impuretés. Nous utiliserons les notations chassiques :

N_D = densité de donneurs
N_A = densité d'accepteurs
n = densité électronique
N_c = densité d'états dans la bande de conduction
$\mathscr{E}$ = energie d'activation de l'impureté dominante

Dans le silicium, pour des donneurs et accepteurs classiques, avec des concentrations inférieures à 10^{16} cm^{-3}, nous avons :

$$\mathscr{E}_i \simeq 4\times10^{-2} \text{ à } 5\times10^{-2} \text{ eV}$$

L'ébullition de l'hydrogène liquide sous pression atmosphérique se fait à 20,7°K, ce qui nous donne :

$$kT = 1{,}7\times10^{-3} \text{ eV}$$

donc :

$$kT \ll \mathscr{E}_i$$

Le nombre de porteurs est alors donné (pour le type N par exemple) par la formule :

$$n = \left(\frac{N_D}{N_A} - 1\right) \cdot \frac{N_c}{2} \cdot \exp - \frac{\mathscr{E}_i}{kT} \qquad (1,\text{I})$$

où

$$N_c = 4{,}82\times10^{15} T^{3/2}$$

et à condition que $n \ll N_A$.

Pour une compensation :

$$\frac{N_D}{N_A} = 100$$

la formule (1) nous donne les densités électroniques suivantes :

Tableau 1

$\mathscr{E}_i =$ ↓ \ $T =$	Ebullition de H_2 sous pression atmosp. 20°K	Point triple de H_2 14°K
0,04 eV	$1{,}8\times10^{9}$	5×10^{4}
0,05 eV	$5{,}4\times10^{6}$	12

Ce-ci nous montre que nous pouvons placer les échantillons dans l'hydrogène liquide en étant sûrs d'avoir bloqué les porteurs sur les impuretés dominantes. Ce liquide possède l'avantage d'avoir une forte chaleur de vaporisation (115 cal/g contre 6 pour l'hélium et 48 pour l'azote liquides) assurant un refroidissement énergique.

Le choix des caractéristiques de l'échantillon de silicium se fait en tenant compte des facteurs suivants :

(1) le taux d'impureté dominante doit être inférieur à 10^{18} cm^{-3}, sinon $\mathscr{E}_i = 0$: il y a conduction par bonde d'impureté et il n'est plus question de créer des porteurs par ce mécanisme. L'oubli de cette condition expliquerait certains échecs.

(2) la densité d'impuretés ionisées vaut sensiblement

$$2N_A$$

puisque nous nous sommes placés à une température où

$$n \ll N_A$$

Ces impuretés ionisées peuvent jouer sur deux plans : limitation de la mobilité, ce qui apparaît comme secondaire; et surtout augmentation de la recombinaison. Or c'est elle qui, à l'équilibre, limite le nombre des porteurs. On peut donc prévoir que la création de porteurs sera d'autant plus facile à observer que N_A est plus faible. Nous sommes limités dans cette voie, par les possibilités actuelles de purification, vers $N_A \simeq$ quelques 10^{12} cm^{-3}.

(3) tout en respectant le première condition ($N_D < 10^{18}$ cm^{-3}), nous sommes amenés à prendre

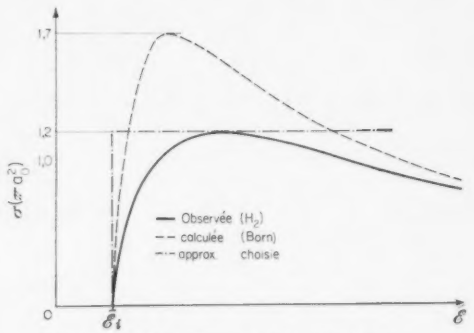

FIG. 1. Section efficace totale d'ionisation.

N_D assez grand. En effet, si nous approximons la section efficace d'ionisation[5] d'une impureté neutre comme le montre la Fig. 1, en tenant compte de la correction :

$$\sigma_{\text{I.N.}} = \sigma_{H_2} \times \epsilon \times \frac{m}{m^*} \qquad (2,\text{I})$$

avec

$$(\sigma_{H_2})_{\max.} = 1{,}2\pi a_0^2$$

$$a_0 = 0{,}53\text{Å}$$

$$\frac{m^*}{m} = 0{,}25$$

$$\epsilon = 13$$

nous pouvons calculer le nombre de chocs ionisants subis par seconde par un électron :

$$\nu = N_n \cdot \sigma \cdot v \qquad (3,\text{I})$$

N_n = nombre d'impuretés neutres par cm^3 en prenant un électron au seuil d'ionisation :

$$v = \left(\frac{2\,\mathscr{E}_i}{m^*}\right)^{1/2}$$

Ceci nous donne pour

$$N_n = N_D = 10^{16}\ \text{cm}^{-3}$$

le nombre de chocs :

$$\nu \simeq 10^{8}\ \text{sec}^{-1}$$

soit

$$\nu \simeq 10^{-7}\, N_D \qquad (4,\text{I})$$

En conclusion, nous sommes amenés à prendre un matériau de compensation aussi faible que possible. Ce résultat avait déjà été signalé par KÖNIG[6]. Avec les limitations qui nous sont imposées cette compensation sera dans le cas le plus favorable :

$$N_D \simeq 10^{17}\ \text{cm}^{-3}$$
$$N_A \simeq 10^{12}\ \text{cm}^{-3} \qquad (5,\text{I})$$
$$\frac{N_D}{N_A} = 10^5$$

Ensuite nous étudierons le comportement d'échantillons de différentes compensations.

II. PARTIE EXPERIMENTALE

Classiquement les mesures de conductivité et d'effet Hall ne présentent aucune difficulté. Cependant le fait que les porteurs soient bloqués thermiquement entraîne quelques précautions expérimentales.

(1) Les échantillons peuvent être très résistants. Pour une géométrie standard :

$$L = 20\ \text{mm}$$
$$l = 3\ \text{mm} \qquad (1,\text{II})$$
$$d = 1\ \text{mm}$$

et une énergie d'activation :

$$\mathscr{E}_i = 0{,}04\ \text{eV}$$

nous obtenons à 20°K :

$$R = 2{,}3\ \text{M}\Omega \text{ pour } N_D/N_A = 10^3$$
$$R = 230\ \text{M}\Omega \text{ pour } N_D/N_A = 10.$$

Nous sommes donc amenés à prévoir un appareillage adéquat pour les fortes résistances et en particulier à utiliser un voltmètre à forte impédance d'entrée (Multimesureur E.R.I.C. Lemouzy impédance d'entrée $> 10^{12}\Omega$). Celui-ci travaillant obligatoirement avec un pôle à la masse nous obtenons le schéma de mesure de la Fig. 2.

Pour éviter de refermer des courants de fuite par le secteur la source de tension est obtenue à partir de piles ou d'une batterie d'accumulateurs et d'une commutatrice. Les appareils et les connexions sont blindés à la masse commune. L'isolement général du montage (de fil à fil ou entre fil et masse) est de $5 \times 10^{12}\Omega$ (essais sous haute tension).

(2) Plus basse est la température moins l'effet des contacts est négligeable. Nous avons utilisé le procédé de nickelage Electroless qui est assez

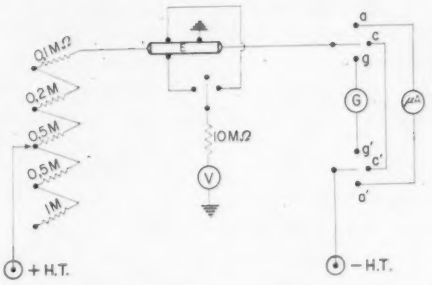

FIG. 2. Schéma de mesure. V = Voltmètre G = Galvanomètre, μA = micro-ampèremètre, E = Echantillon.

capricieux. On ne peut éviter qu'il y ait une mince couche de silice entre le nickel et le silicium. Nous avons vérifié expérimentalement que les mesures de conductivité sont entachées d'erreur lorsque l'on omet de mettre des sondes. La phrase rituelle "Contacts ohmiques et non injectants à toute

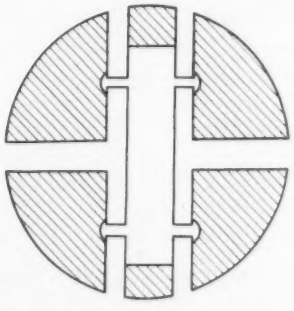

FIG. 3. Dessin schématique d'un échantillon. Parties nickelées et soudées en hachures.

température" est à l'origine de bien de déconvenues. Si un bon contact se voit peu, un mauvais contact peut, à basse température, tenir 1.000 V en inverse sans "claquer".

Afin d'éviter les résistances de contact élevées, nous avons réalisé des échantillons suivant le dessin de la Fig. 3. Nous les obtenons en découpant

Vol. 18
1961

une rondelle de silicium avec un jet de sable, la buse de la sableuse étant montée sur un chariot de tour dont l'un des mouvements est entraîné par un moteur à vitesse variable et muni d'un vernier. Ce-ci nous a permis de réaliser une géométrie bien parallélépipédique et des sondes d'effet Hall bien face à face.

Ces deux points sont importants : lorsque la loi d'Ohm n'est pas suivie, et que la géométrie n'est pas de translation parallèlement au courant, les lignes de courant se déplacent quand le champ électrique varie. Il s'ensuit qu'une mauvaise géométrie nuit non seulement aux mesures absolues (incertitude sur les dimensions) mais aussi aux mesures relatives.

Pour mesurer l'effet Hall, les montages classiques ne conviennent pas (Fig. 4) : l'un parce qu'il

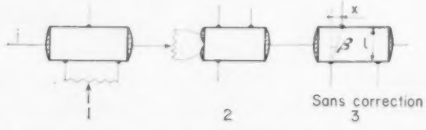

FIG. 4. Montages de mesure de l'effet Hall.

déforme les équipotentielles, l'autre parce qu'il nécessite la mise en parallèle sur l'échantillon d'un potentiomètre de résistance nettement plus grande. Ce qui entraîne quelques complications quand le circuit de sonde peut atteindre $10^9\Omega$. Il reste alors à aligner les sondes de telle sorte que

$$\beta \ll \theta \qquad (2,II)$$

où θ est l'angle de Hall. Or nous savons que la mobilité de Hall varie avec le champ magnétique, mais que cette variation est faible si :

$$\operatorname{tg}\theta = 10^{-8}\mu_H \times H \simeq \text{quelques pour cent.}$$

Il faut donc :

$$\beta \leqslant \tfrac{1}{2} \text{ degré.}$$

(3) Le nombre de porteurs est très sensible à la température, comme le montre la formule (1,I). En effet :

$$\frac{\Delta n}{n} = \log e \cdot \frac{\epsilon_i}{kT}\frac{\Delta T}{T} \qquad (3,II)$$

et, pour l'hydrogène à 20°K :

$$T = 4{,}4 \times 10^{-3} \times \Delta p(\text{mm Hg})$$

soit

$$\frac{\Delta n}{n} = 1 \text{ pour cent pour } \Delta p = 5 \text{ mm Hg.}$$

Cette condition est plus contraignante au point triple, où nous avons :

$$\frac{\Delta n}{n} = 15 \text{ pour cent pour } \Delta p = 5 \text{ mm Hg.}$$

Ceci donne une idée de la précision avec laquelle doit être réglée la pression lorsque l'on désire faire varier la température du bain cryogénique.

Le formule (3,II) nous donne aussi :

$$\frac{\Delta n}{n} = 10\frac{\Delta T}{T} \text{ à } 20°\text{K} \qquad (4,II)$$

Or une certaine puissance électrique est dissipée dans l'échantillon. Si nous voulons que la variation du nombre de porteurs qui en résulte soit inférieur à 5 pour cent il faut que l'élévation de température ne dépasse pas le $1/10^6$ de degré. Nous avons étudié le problème de l'échauffement dans les deux cas limites suivants :

(a) la température est uniforme dans l'échantillon, mais supérieure à celle du bain

(b) la surface de l'échantillon est à la température du bain, mais il existe un gradient à l'intérieur.

Dans l'étude de ces deux cas, nous avons revu les résultats assez intuitifs suivants :

— si la longueur L est supérieure nettement aux dimensions transversales, elle n'intervient pas.

— la section $l\ d$ doit être aussi faible que possible.

— pour une section donnée, il faut une géométrie aussi plate que possible : $d \ll l$.

Nous en avons déduit une puissance maxima admissible de l'ordre du Watt pour la première condition, et de $1/10^6$ de Watt pour la seconde (pour la géométrie de l'échantillon et le liquide réfrigérant indiqués). Si cet ordre de grandeur paraît énorme par rapport à certaines expériences préalables, nous nous permettons de signaler que, entre une réfrigération à courant gazeux et le contact direct avec un liquide à forte chaleur

Vol. 18
1961

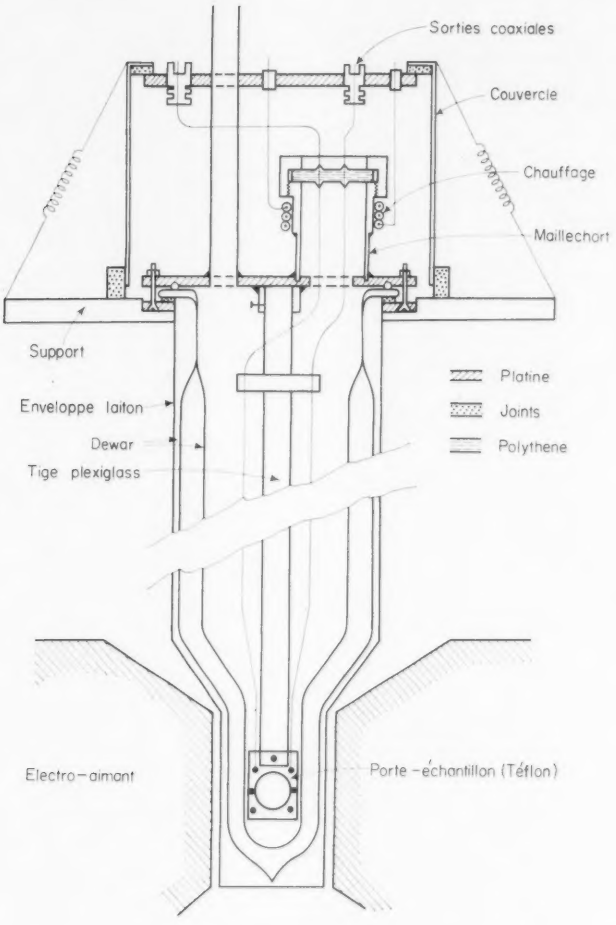

FIG. 5. Appareillage cryogénique.

Tableau 2

Gaz	He	H_2	Ne	N_2
Température d'ebullition ($p = 1$ atm.) (°K)	4,3	20,4	27,3	77,7
Chaleur de vaporisation (cal/g)	6	115	16	48

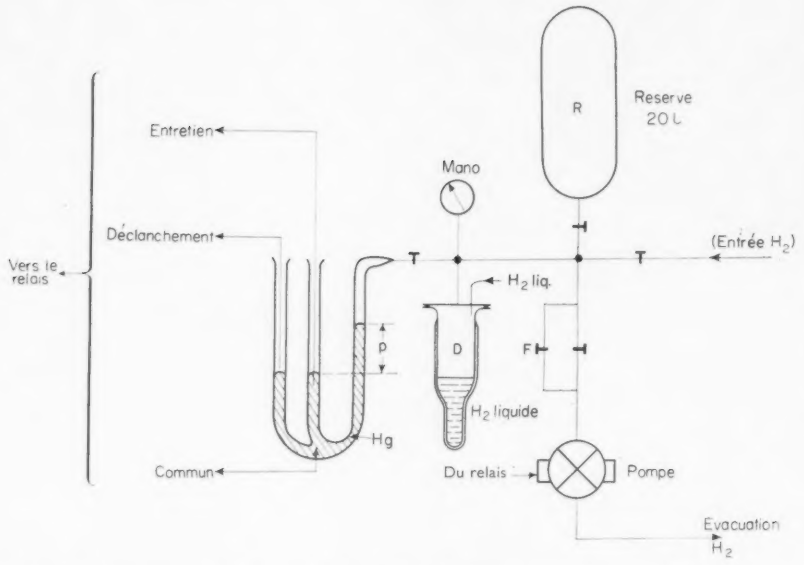

FIG. 6. Régulation de la température par la pression. D = Dewar R = Réserve F = Fuite réglable.

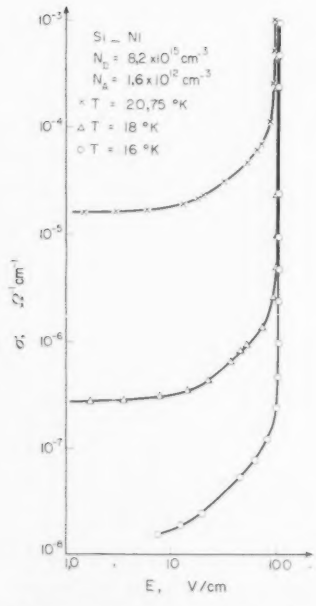

FIG. 7. Conductivité électrique en fonction du champ électrique. Echantillon N1.

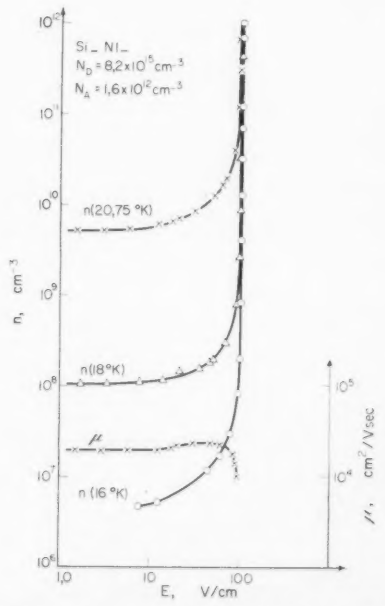

FIG. 8. Densité de porteurs et mobilité de Hall en fonction du champ électrique. Enchantillon N1.

de vaporisation, il y une différence énorme. La comparaison entre les différents gaz (Tableau 2) montre la position privilégiée de l'hydrogène à ce point de vue. Ajoutons que :

(a) pour la mise en évidence de l'avalanche, la puissance dissipée dans l'échantillon était inférieure à 10^{-3} W.

(b) dans la zône d'avalanche, des mesures en continu et en impulsions se sont révelées concordantes jusqu'à plusieurs Watts, car, dans cette zône, la création due au champ électrique est si intense qu'elle masque facilement une légère création thermique.

(4) Il reste une dernière précaution : éviter de recréer par la lumière les porteurs bloqués thermiquement. Une enceinte maintient le Dewar dans l'obscurité (Fig. 5). Nous avons aussi placé nos échantillons dans une enceinte métallique à la température de l'hydrogène liquide afin d'éliminer aussi l'infra-rouge lointain. Nous n'avons constaté aucune différence dans nos mesures.

Nous ajouterons que l'état de la surface ne semble pas jouer de rôle décelable à la précision de nos mesures. On voit sur la photographie que la partie utile de l'un des échantillons—le plus résistant—a été polie chimiquement. Les autres échantillons ont une surface sablée.

La Fig. 6 montre le principe de la régulation de température.

Vol. 18
1961

III. RESULTATS

Nous avons tracé les courbes (conductivité, mobilité et nombre de porteurs) relatives à trois échantillons N et un échantillon P, dont les caractéristiques sont rassemblées dans le tableau suivant :

Nous pouvons dégager de ces expériences les traits suivants :

(1) Comme il était prévisible, le champ d'avalanche croît lorsque N_D/N_A décroît. La comparaison est particulièrement frappante pour N1 et N2 qui ont à peu près le même nombre de donneurs, mais diffèrent fortement par le nombre d'accepteurs (Tableau 4).

(2) Nous pourrons diviser les courbes $\sigma(E)$ en trois régions :

— une région ohmique, pour $E < 10$ V/cm.

— une région de création modérée :

$$10 \text{ V/cm} < E < E_a$$

— une zône d'avalanche pour $E = E_a$.

La zône de création modérée présente un maximum secondaire pour N3, qui correspond à un palier de la courbe $n(E)$, avec :

$$E \simeq 100 \text{ V/cm}$$

$$n = 3n_0.$$

Nous en donnons l'explication suivante : pour un échantillon compensé comme N3, le champ d'avalanche est repoussé vers des valeurs élevées de E (1.400 V/cm). Vers 100 V/cm, la création par choc sur les impuretés neutres est très faible. L'équation du nombre de porteurs est approximativement :

$$n = \frac{C_t(N_D - N_A)}{R(E) \times N_A} = \frac{C_t}{R(E)} \times \left(\frac{N_D}{N_A} - 1\right)$$

ou

$$\frac{n}{n_0} = \frac{R(0)}{R(E)} \qquad (1,\text{III})$$

Tableau 3

Echantillon	Figure n°	Impureté dominante	Compensation	Mobilité à 20°K à bas champ électrique (cm^2/V sec)	Champ à l'avalanche (V/cm)
N1	7–8	Phosphore	$N_D/N_A = 5{,}000$	19.3000	100
N2	9–10	Antimoine	$N_D/N_A = 20$	5.000	800
N3	11–12	Antimoine	$N_D/N_A = 10$	4.300	1.400
P	13–14	Bore	$N_A/N_D = 300$	16.000	260

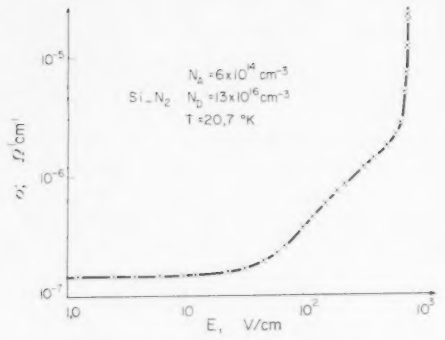

FIG. 9. Conductivité électrique en fonction du champ électrique. Echantillon N2.

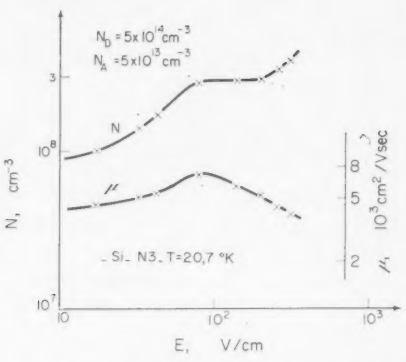

FIG. 12. Densité de porteurs et mobilité de Hall en fonction du champ électrique. Echantillon N3.

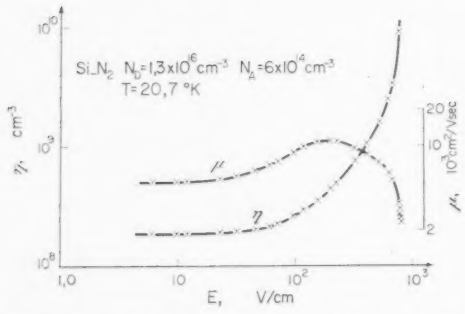

FIG. 10. Densité de porteurs et mobilité de Hall en fonction du champ électrique. Echantillon N2.

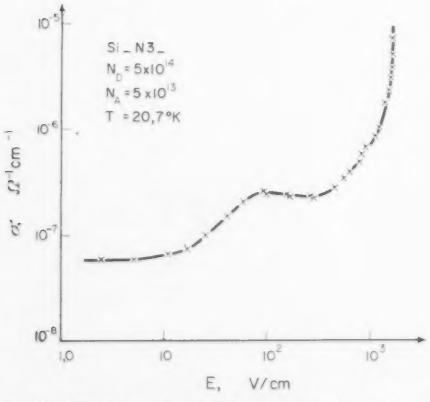

FIG. 11. Conductivité électrique en fonction du champ électrique. Echantillon N3.

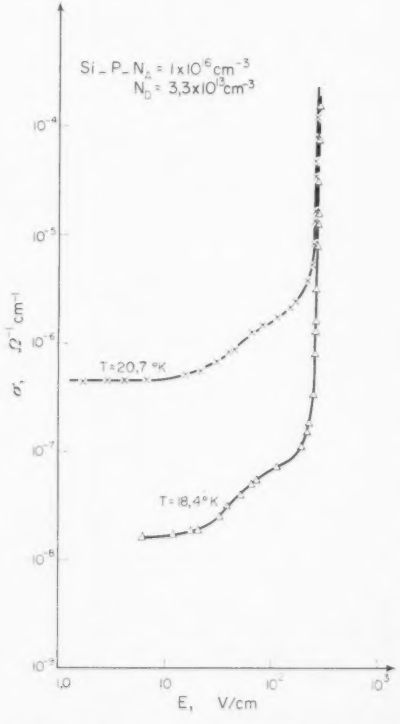

FIG. 13. Conductivité electrique en fonction du champ électrique. Echantillon de type P.

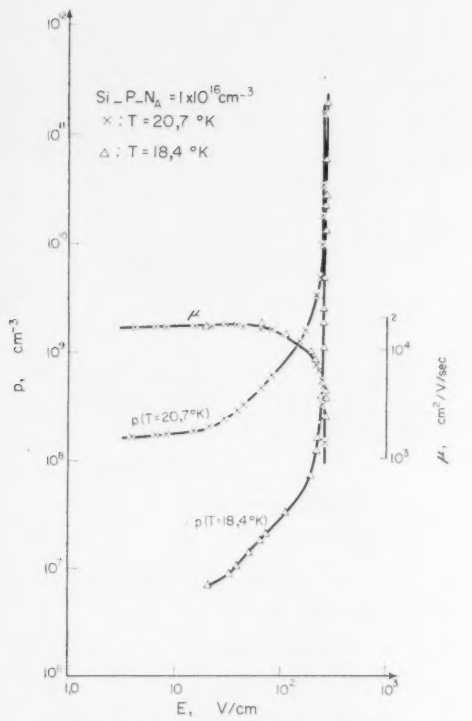

FIG. 14. Densité de trous et mobilité de Hall en fonction du champ électrique. Echantillon P.

n_0 = nombre de porteurs pour $E = 0$
$R(0)$ = taux de recombinaison directe pour $E = 0$
$R(E)$ = taux de recombinaison directe pour $E \neq 0$
C_t = taux de création thermique

Quand le champ électrique croît, le taux de recombinaison décroît, et il est très probable qu'il tende vers une limite R_m. D'où le palier dans le nombre de porteurs. La fin du palier, pour

$$E \simeq 200 \text{ V/cm}$$

est due au fait que le phénomène de création par choc prend alors une importance non négligeable, et se traduit par une augmentation plus rapide de n. Si cette interprétation est exacte, le phénomène sera encore plus marqué pour des échantillons plus compensés.

(3) Les courbes de mobilité ont toutes la même allure : croissantes avec E, elles passent par un maximum vers 100 V/cm et décroissent fortement au moment de l'avalanche. La croissance initiale avec le champ électrique semble indiquer que la diffusion par les impuretés ionisées domine. Ce résultat n'est établi en toute rigueur que dans l'approximation des électrons chauds[8]; néanmoins, la section efficace étant proportionnelle à $1/v^3$, le temps de relaxation croît lorsque la vitesse moyenne (ou l'énergie moyenne $\langle \mathscr{E} \rangle$) de la distribution croît. On sait que, dans les mêmes conditions, la mobilité resterait constante avec le champ électrique si elle était dûe à la diffusion par les impuretés neutres.

La concordance entre les valeurs de μ mesurées à bas champ électrique et les formules correspondantes, est mauvaise, comme le montre le Tableau 4 pour les échantillons de type N.

Les formules utilisées sont :
—pour les impuretés ionisées

$$\mu = \frac{8\sqrt{(2)}}{\pi\sqrt{(\pi)}} \frac{K^2(kT)^{3/2}}{m^{*1/2}N_i e^3}$$
$$\mu = \frac{4{,}94 \times 10^{19}}{N_i} \text{ à } 20°\text{K} \qquad (2,\text{III})$$

avec une correction : celle de CONWELL et WEISSKOPF[9] :

$$[\log(1+X^2)]^{-1}$$
$$X = \frac{7 \times 10^5}{(N_i)^{1/3}} \text{ à } 20°\text{K} \qquad (3,\text{III})$$

ou celle de BROOKS–HERRING[10] :

$$\left[\log(1+b) - \frac{b}{1+b}\right]^{-1}$$
$$b = \frac{2 \times 10^{17}}{n_0} \text{ à } 20°\text{K.}^* \qquad (4,\text{III})$$

* Cette expression suppose que les porteurs, de densité n_0, sont responsables de l'effet d'écran. Or nous savons (pour le type N par exemple) que, à la température où nous sommes placés :

$$n_0 \ll N_A^- \qquad N_A^- \neq N_D^+$$

et que ce sont les centres fixes d'un signe qui sont, en fait, écrantés par les centres fixes de l'autre signe. Il faut alors remplacer n_0 par N_A.

Vol. 18
1961

Tableau 4

Données				Mobilité mesurée	Mobilité calculée (cm^2/V sec)			
					Impuretés ionisées			Impuretés
Echantillon	$N_D(cm^{-3})$	$N_D(cm^{-3})$	$n_0(cm^{-3})$	(cm^2/V sec) μ_H	sans correction	correction C.W.	correction B.H.	neutres
N1	$8{,}2\times10^{15}$	$1{,}6\times10^{12}$	5×10^{9}	19.300	$1{,}5\times10^{7}$	$5{,}1\times10^{6}$	$2{,}3\times10^{6}$	34.000
N2	$1{,}3\times10^{16}$	$6{,}5\times10^{14}$	$1{,}9\times10^{8}$	5.000	$3{,}8\times10^{4}$	37.500	4.700	20.000
N3	5×10^{14}	5×10^{13}	10^{8}	4.300	$4{,}9\times10^{5}$	250.000	55.000	560.000

— pour les impuretés neutres, la formule d'ERGINSOY[11] :

$$\mu = \frac{2{,}8\times10^{20}}{N_n} \qquad (5,III)$$

où

N_i = densité d'impuretés ionisées
N_n = densité d'impuretés neutres
n_0 = densité électronique

Nous voyons sur le Tableau 4 que la concordance n'est bonne que pour N2. L'échantillon N3 posséde une mobilité anormalement basse, peut-être due à des impuretés formant des niveaux profonds, ne modifiant donc pas le nombre de porteurs, mais en nombre suffisant pour diminuer la mobilité. Pour l'échantillon N1, c'est la mobilité calculée à partir des impuretés neutres qui se rapproche le plus de la mobilité mesurée.

Nous savons que, si nous disposons d'un champ magnétique assez intense pour réaliser la condition :

$$\mathrm{tg}\,\theta = \omega_c \times \tau \geqslant 1 \qquad (6,III)$$

nous obtenons :

$$\frac{\mu_H}{\mu} \to 1$$

Mais que, par contre, si H est assez faible, de telle sorte que

$$\mathrm{tg}\,\theta \ll 1$$

le rapport

$$f = \frac{\mu_H}{\mu}$$

est caractéristique du type de collision: soit :

$f = 1$ impuretés neutres

$f = 1{,}18$ phonons

$f = 1{,}93$ impuretes ionisées.

En faisant croître H, nous avons obtenu, dans la région ohmique, pour N2 :

$\mu_H = 5.000$ cm^2/V sec pour $H = 1.000$ G

$\mu_H = 3.300$ cm^2/V sec pour $H = 15.000$ G.

Pour N1, la variation de μ_H avec H dans la région ohmique est représentée Fig. 15. Le champ

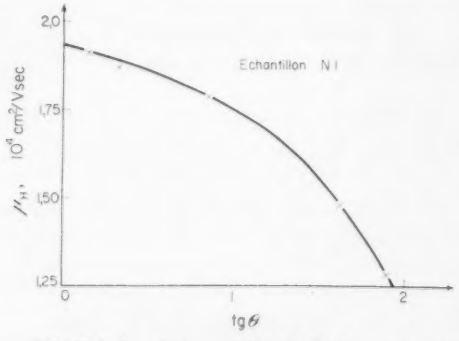

FIG. 15. Variation de la mobilité de Hall avec le champ magnétique. Echantillon N1.

magnétique n'est pas suffisant pour conclure de façon formelle. Il semble cependant que seules les impuretés ionisées permettent une telle décroissance de μ_H avec H.

SHOCKLEY[12] a exposé pourquoi la formule de Conwell–Weisskopf est fausse à basse température.

Soit a, la distance moyenne entre impuretés ionisées :

$$a = (N_i)^{-1/3}$$

qui vaut :

$$a = 10^3 \text{ Å si } N_i = 10^{15} \text{ cm}^{-3}$$
$$a = 10^4 \text{ Å si } N_i = 10^{12} \text{ cm}^{-3}.$$

L'énergie d'interaction électrostatique vaut :

$$\begin{aligned} \mathscr{E} &= 0{,}06\, kT \text{ à } T = 300^\circ\text{K} \\ \mathscr{E} &\neq kT \qquad \text{à } T = 20^\circ\text{K} \end{aligned} \qquad (7,\text{III})$$

Si, à température ordinaire, l'électron doit s'approcher de $a/16$ du centre diffuseur pour subir une déviation appréciable, il n'en est plus de même à basse température. D'autre part, le temps passé par l'électron dans la cellule d'arête a, est en première approximation :

$$\sqrt{\left(\frac{300}{20}\right)} = 4 \text{ fois plus grand.}$$

Donc, si pendant ce temps l'électron perd une fraction de son énergie (par émission d'un phonon), il peut se piéger sur un état excité du centre chargé (quand celui-ci est positif, doneur ionisé). On rejoint ainsi la notion de "piège géant" introduit par LAX[13]. Le rayon de la première orbite de Bohr dans le silicium est de 25 Å et par conséquent :

$a = 10^3$ Å correspond l'état excité $n = 6$

$a = 10^4$ Å correspond l'état excité $n = 20$.

Enfin, l'importance d'un tel mode le recombinaison doit croîte avec l'energie moyenne de la distribution.

(4) Pour des champs magnétiques de l'ordre de 10.000 Gauss, nous avons observé un phénomène de magnéto-résistance négative pour les échantillons les plus conpensés (N2 et N3). Cet effet ne se produit que si $\boldsymbol{B}$ posséde une composante perpendiculaire à $\vec{E}$. Il intervient dans la zône où l'ionisation est très faible (et correspond au palier du nombre de porteurs dans N3). Dans cette zône, le nombre de porteurs varie comme $R^{-1}(E)$; l'effet du champ H serait donc de modifier la recombinaison. Nous signalons à l'appui de cette hypothèse que le rapport de la force magnétique à la force électrique :

$$\frac{F_m}{F_e} \nearrow \text{ si } n \nearrow$$

où n représente la $n^{\text{ième}}$ orbite de Bohr.

Ce rapport est égal à l'unité dans le silicium, pour :

$$\left|\begin{array}{ll} \text{l'état excité} & n = 10 \\ \text{le champ magnétique} & H = 10^4 \text{ G} \end{array}\right. \qquad (8,\text{III})$$

Expérimentalement, nous avons tracé la conductivité en fonction du champ électrique

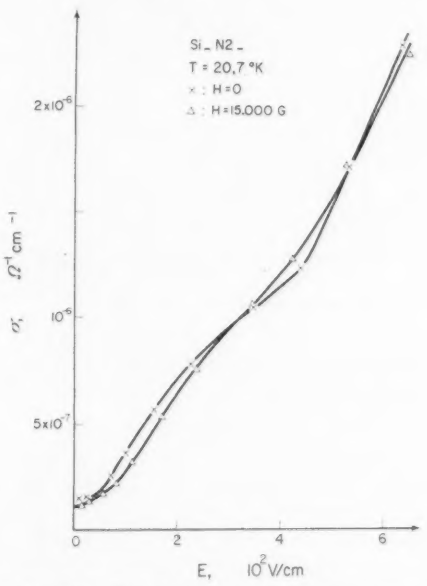

FIG. 16. Effet d'un champ magnétique transverse sur la variation de la conductivité en fonction du champ électrique longitudinal. Echantillon N2.

longitudinal, en présence du champ magnétique indiqué Figs. 16 et 17, perpendiculaire au champ électrique.

On peut objecter que le champ total régnant dans l'échantillon est

$$\vec{E} = \vec{E}_x + \vec{E}_y$$

avec

$$E_x \simeq E_y$$

Vol. 18
1961

pour les champs magnétiques utilisés. Ceci revient à corriger E_x d'un facteur $\sqrt{2}$ au plus, pour obtenir σ en fonction du champ électrique total. Le phénomène disparaît alors pour N2, mais se maintient pour N3. Nous voyons donc que ce sont les échantillons les plus compensés (N_D/N_A faible) qui présentent les propriétés les plus curieuses.

(5) Nous noterons enfin un effet comparable à celui observé par SASAKI[14] et ses collaborateurs. Lorsque la loi d'Ohm

$$j = \sigma \vec{E}$$

n'est plus vérifiée scalairement (σ varie), elle ne l'est plus vectoriellement : les vecteurs $\vec{j}$ (densité de courant) et $\vec{E}$ (champ électrique) ne sont plus colinéaires. Nous remarquerons que c'est la projection de l'angle $(\vec{E}, j)$ sur le plan de l'échantillon que nous mesurons ainsi. Les résultats sont portés Figs. 19 et 20. Il nous est difficile d'en tirer des résultats, les échantillons n'ayant pas été préalablement orientés. Il semble cependant que l'on puisse atteindre ainsi le scattering inter-valleé, qui fut un moment présenté comme un obstacle au phénomène d'ionisation par choc des impuretés dans le silicium[15].

Expérimentalement, nous avons procédé de la manière suivante :

— dans la région ohmique, nous mesurons la tension E_y qui apparaît entre les deux sondes d'effet Hall en l'absence de tout champ magnétique. Nous en déduisons l'angle β que fait la droite joignant ces sondes avec la perpendiculaire au courant. Nous trouvons :

$$\beta = \frac{E_y}{E_x} = \text{constante} \simeq 10^{-2}$$

Comme $E_x < 10$ V/cm pour que l'échantillon soit ohmique, E_y varie de 10–100 mV/cm. Lorsque la loi d'Ohm n'est plus suivie, nous mesurons, suivant le sens relatif de β et α :

$$\alpha \pm \beta = E_y/E_x \qquad (9,\text{III})$$

L'angle α étant obtenu par différence, sa mesure

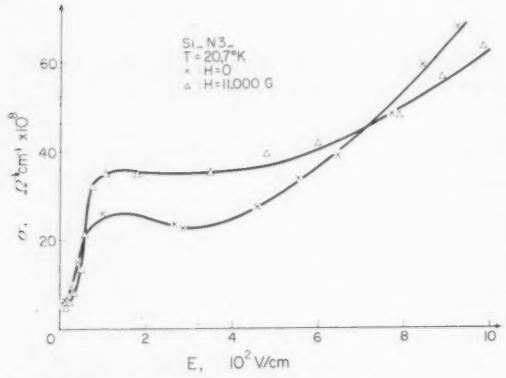

FIG. 17. Effet d'un champ magnétique transverse sur la variation de la conductivité en fonction du champ électrique longitudinal. Echantillon N3.

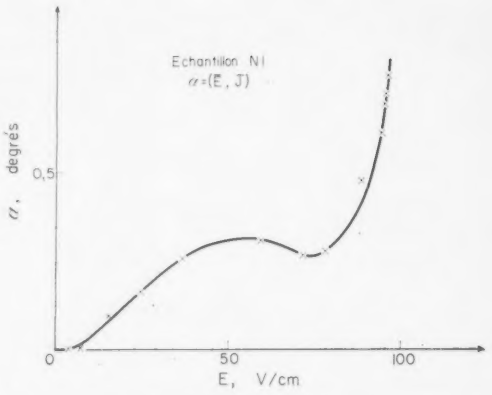

FIG. 19. Projection sur le plan de l'échantillon de l'angle entre le champ électrique E et la densité de courant J. Echantillon N1.

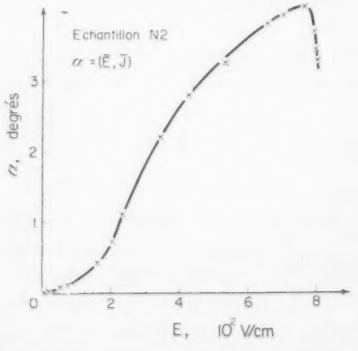

FIG. 20. Projection sur le plan de l'échantillon de l'angle entre le champ électrique E et la densité de courant J. Echantillon N2.

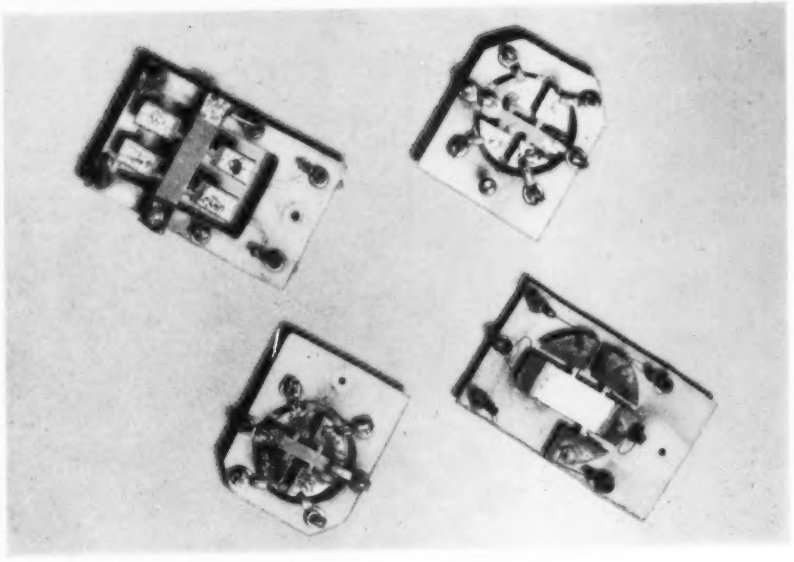

FIG. 18. Photo des quatre échantillons.

[*facing p.* 192

BLANK
PAGE

Vol.
19

n'a de sens que si

$$\alpha \gg \beta \qquad \alpha = (\bar{E}, j).$$

Mais nous avons vu que, pour l'effet Hall, nous avons (2,11) :

$$\theta \gg \beta$$

et par conséquent α et θ peuvent être du même ordre de grandeur. En fait, quand E croît, l'angle

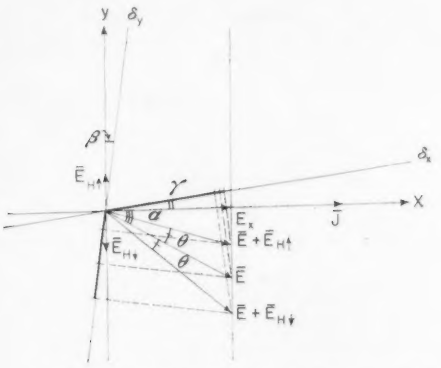

FIG. 21. Défauts de géométrie des échantillons. Définition des angles α, β et θ.

α l'emporte sur l'angle θ et la précision sur l'effet Hall diminue d'autant. Ces angles sont représentés Fig. 21, moins l'effet de magnéto-résistance négligeable à bas champ magnétique.

IV. DISCUSSION

Malgré sa simplicité de principe (chocs ionisants), le phénomène d'ionisation des impuretés neutres par les porteurs n'a pas donné lieu à une théorie satisfaisante. Il nous faut signaler en particulier qu'il n'existe pas de formule valable reliant le champ d'avalanche aux caractéristiques du matériau et à la température. Des considérations de "bilan détaillé" ont conduit KÖNIG[16] à écrire l'équation :

dn/dt = nombre porteurs créés − nombre porteurs recombinés = 0 ce qui introduit un certain nombre de facteurs inconnus, mais permet cependant de prévoir que

$$E_a \nearrow \text{ quand} \left(\frac{N_D}{N_A} - 1\right) \searrow \qquad (1,\text{IV})$$

sans donner la dépendance $E_a(N_D, N_A, T)$, ce qui était prévisible.

Nous savons que l'étude des phénomènes de transport à haut champ électrique est résolue dans le cas où les échanges d'énergie par chocs inter-électroniques sont dominants.[17] Nous pouvons alors définir une température électronique T_e différente de la température T du réseau, et écrire la fonction de distribution :

$$f(\bar{p}) = \exp - \frac{(\bar{p}-\bar{p}_0)^2}{2mkT_e} \qquad (2,\text{IV})$$

avec l'hypothèse complémentaire :

$$\frac{p_0^2}{2mkT_e} \ll 1$$

qui traduit le fait que l'énergie cédée à la population électronique sert principalement à élever sa température. A basse température, lorsque la densité électronique est faible, et les collisions inter-électroniques rares, cette méthode risque de n'être qu'une mauvaise approximation. On peut s'en persuader d'après les calculs d'ADAWI[18] où il est démontré qu'un taux d'impuretés ionisées assez faible pour ne pas modifier la mobilité (2 pour cent), donne à haut champ électrique des écarts de 30 pour cent. Les conditions sont encore plus graves à basse température, car les chocs contre les impuretés sont nettement plus fréquents que les chocs sur les phonons acoustiques.

Nous pouvons évoluer grossièrement la fréquence de ces chocs, dont le rôle est le suivant :

(a) sur les impuretés ionisées, distribution angulaire des porteurs (ν_i).
(b) sur les phonons, limitation de l'énergie de la distribution (ν_{ph}).
(c) inélastiques sur les impuretés neutres : création de porteurs (ν_c).

Pour un électron *thermique*, la mobilité mesurée ($\simeq 10^4$ par exemple) ou calculée ($\simeq 10^6$, pour les phonons) donne une idée de la fréquence de chocs :

$$\begin{aligned} \nu_i &= 10^{12}\ \text{sec}^{-1} \\ \nu_{ph} &= 10^{10}\ \text{sec}^{-1} \\ \nu_c &= 0 \end{aligned} \qquad (3,\text{IV})$$

Un électron, *au seuil d'ionisation*, d'energie :

$$E_i \simeq 25\ kT \text{ à } T = 20°\text{K},$$

Vol. 18
1961

a une vitesse 5 fois plus grande. Connaissant la variation de τ avec v, nous en déduisons :

$$\nu_i = 8\times 10^9 \text{ sec}^{-1}$$

$$\nu_{ph} = 5\times 10^{10} \text{ sec}^{-1}$$

$$\nu_e = 10^8 \text{ sec}^{-1}, \text{ pour } N_D = 10^{15}, \text{ d'après (4,I).} \qquad (4,IV)$$

En conclusion :

(a) si nous négligeons le phénomène d'ionisation, nous voyons que les transitions électroniques sont commandées à faible vitesse par les impuretés ionisées, à grande vitesse par les phonons. Il faut, de toutes façons, tenir compte de ces derniers dans la recherche d'une solution au-delà du premier ordre (qui donne la loi d'Ohm), puisqu'ils limitent l'énergie de la distribution.

(b) Nous voyons par contre que les chocs ionisants sont moins fréquents que les précédents, et qu'ils pourraient donc être négligés dans l'opérateur de collision. Nous pouvons supposer qu'ils modifient très peu la forme de la fonction de distribution $f(\bar{k}, E)$.* Il existe une objection à cette façon de voir : la décroissance brutale de la mobilité au moment de l'avalanche, vérifiée pour tous les échantillons.

Nous ferons une dernière remarque. L'expression (4,I) donne une idée du temps de mise en équilibre du nombre de porteurs (largement plus grand que le temps de mise en équilibre de la distribution); si nous admettons qu'il faut une dizaine de chocs pour que cet équilibre soit réalisé, (ce qui est trés arbitraire), nous trouvons un ordre de grandeur :

$$t = \frac{10^8}{N_d} \text{ sec}$$

soit

$$t = 10 \text{ m}\mu\text{ sec pour } N_D = 10^{16} \text{ cm}^{-3}$$
$$t = 10\,\mu\text{ sec} \quad \text{pour } N_D = 10^{13} \text{ cm}^{-3} \qquad (5,IV)$$

soit donc un ordre de grandeur facilement observable pour un échantillon de 400 Ω cm à température ordinaire. On peut expliquer ainsi les mesures de KÖNIG[16] : pour le germanium, la correction ϵ m/m* est environ 3 fois plus grande que pour le silicium. Donc, pour $N_D = 2\times 10^{13}$ cm^{-3}, $t \simeq$ quelques μ sec.

En fait, un calcul de bilan détaillé montre que t passe par un maximum, qui vaut approximativement :

$$t_m = 2\left(\frac{n}{n_i}\right)^{1/2} \times (n_0 R_0)^{1/2} \times \nu^{-1/2} \qquad (6,IV)$$

où

- n = densité de porteurs à l'équilibre
- n_0 = densité de porteurs à bas champ électrique
- ni = densité de porteurs d'énergie supérieure à $\mathscr{E}_i$
- R_0 = taux de recombinaison à bas champ électrique
- ν = fréquence des chocs ionisants par un porteur

et le temps de réponse est maintenant :

t proportionnel à $\nu^{-1/2}$, au lieu de ν^{-1} précédemment.

Cette formule est obtenue grâce à des approximations assez grossières. De toutes façons, il est évident que la mise en évidence de t doit se faire sur des échantillons assez purs, puisque :

$$t \uparrow \text{ si } N_D \downarrow .$$

La formule (6,IV) permettrait d'atteindre ni/n, soit la fraction de la distribution responsable de l'ionisation. Ce nombre doit être faible, on peut s'en persuader de la manière suivante : nous savons que la condition de validité de la loi d'Ohm s'écrit :

$$v_D \ll v,$$

où

- v_D = vitesse moyenne dans le sens du champ électrique = μE
- v = vitesse moyenne d'agitation thermique.

A cette condition, la fonction de distribution pour un champ E donné, est celle pour $E = 0$ décalée de $\bar{p}_0$:

$$f(\bar{p}, E) = \exp - \frac{(\bar{p}-\bar{p}_0)^2}{2mkT}$$

et l'énergie moyenne des porteurs est :

$$\langle \mathscr{E} \rangle = \tfrac{3}{2}kT + \tfrac{1}{2}m^* v_D^2.$$

Prenons les différents échantillons au début de

* Le calcul de WOLFF[19], sur l'ionisation bande à bande, a été fait dans l'hypothèse inverse. La fonction de distribution est alors fortement perturbée au-delà du seuil d'ionisation.

l'avalanche : si nous leur appliquons $v_D = \mu E$, nous trouvons :

$$\begin{aligned} &N1 : v_D = 2\times 10^6 \text{ cm/sec} \\ &N2 : v_D = 2\times 10^6 \text{ cm/sec} \qquad (6,IV) \\ &N3 : v_D = 8\times 10^6 \text{ cm/sec} \end{aligned}$$

alors que la vitesse moyenne d'agitation thermique vaut sensiblement :

$$v = 6\times 10^6 \text{ cm/sec à } 20^\circ\text{K}.$$

Bien qu'utilisé en dehors de ses limites de validité, ce modèle nous montre que l'energie moyenne de la distribution a au plus doublé, et que par conséquent le nombre de porteurs n_t d'energie supérieure à $\mathscr{E}_t$ est faible, puisque :

$$\mathscr{E}_t \simeq 20 \text{ à } 25\ kT.$$

C'est donc bien la "queue de la distribution" qui est responsable de l'avalanche.

CONCLUSION

L'étude des phénomènes de conduction en fonction du champ électrique, dans le silicium (de type *n* ou *p*) à basse température, met en évidence l'effet d'ionisation par choc des impuretés neutres par les porteurs présents. Les courbes de la densité des porteurs et de leur mobilité en fonction du champ électrique ont éte tracées pour divers échantillons, montrant l'effet important de la compensation sur l'allure des phénomènes, et en particular sur le champ d'avalanche; les deux valeurs extrêmes observées pour ce dernier sont : 100 V/cm et 1.400 V/cm. Pour tous les échantillons de type *n*, un effet analogue à celui observé par SASAKI[14] a été mis en évidence. Enfin, ce sont les échantillons les plus compensés (de même que pour le germanium) qui montrent les propriétés les plus curieuses : palier dans la courbe du nombre des porteurs, effet de magnétorésistance négative dans la même région.

Parmi les divers développements possibles de ces expériences, l'étude d'échantillons très compensés et la mise en évidence de la fin de l'ionisation sont actuellement poursuivies par ZYLBERTSEJN.

Remerciements—Je tiens à remercier ici M. le Professeur P. AIGRAIN et M. J. BOK qui sont à l'origine de cette étude et m'ont guidé durant son développement.

BILBIOGRAPHIE

1. DARNELL F. J. et FRIEDBERG S. A., *C.I.T., Techn. Rep.* No. 1, pp. 58–69 et 127–132; SCLAR N. et BURSTEIN E., *J. Phys. Chem. Solids* **2,** 1 (1957); KÖNIG S. H., *Phys. Rev.* **110,** 986, 988 (1958).
2. STEELE M. C., *Bull. Amer. Phys. Soc.* (ser. 2) **3,** 112 (1958).
3. KAISER W. et WEATHLEY G. H., *Phys. Rev. Letters* **3,** 334 (1959).
4. SOHM J. C., *C.R. Acad. Sci., Paris* **25,** 2737 (1959).
5. MOTT N. F. et MASSEY H. S. W., *Theory of Atomic Collisions*, p. 245. Oxford University Press (1949).
6. KÖNIG S. H., *Proc.* 1958 *Intern. Conf. Semiconductors*, pp. 227–234.
7. MCWHORTER A. L. et REDIKER R. H., *Proc. Inst. Radio Engrs., N.Y.* **47,** 1207 (1959).
8. BOK J., Thèse, Paris (1959).
9. CONWELL E. et WEISSKOPF V. F., *Phys. Rev.* **77,** 388, 390 (1959).
10. Voir: CONNELL E. M. et DEBYE P. P., *Phys. Rev.* **93,** 693 (1954).
11. ERGINSOY C., *Phys. Rev.* **79,** 1013 (1950).
12. SHOCKLEY W., *Electrons and Holes in Semiconductors*, p. 260. Van Nostrand, New York (1950).
13. LAX M., *Proc.* 1958 *Intern. Conf. Semiconductors*, pp. 66–73.
14. SASAKI W., SHIBUYA M., MIZUGUCHI K. et HATOYAMA G. M., *Proc.* 1958 *Intern. Conf. Semiconductors*, pp. 250–6.
15. LAMPERT M. A., HERMAN F. et STEELE M. C., *Phys. Rev. Letters* **2,** 394 (1959).
16. KÖNIG S. H., voir (1).
17. FRÖHLICH H. et PARANJAPE B. V., *Proc. Phys. Soc. Lond.* **B.69,** 21, 866 (1956); BOK J., Thèse, Paris (1959).
18. ADAWI I., *Phys. Rev.* **112,** 1567 (1958).
19. WOLFF P. A., *Phys. Rev.* **95,** 1415 (1954).

Vol. 18
1961

J. Phys. Chem. Solids Pergamon Press 1961. Vol. 18, Nos. 2/3, pp. 196–202. Printed in Great Britain.

ASPECT PHENOMENOLOGIQUE DE QUELQUES PROPRIETES PHYSIQUES DU PLUTONIUM ET DES SOLUTIONS SOLIDES PLUTONIUM–ALUMINIUM δ

Y. A. ROCHER et J. FRIEDEL

Service de Physique des Solides B.P. No. 11, Orsay (S. et O.) France.

(*Received* 27 *June* 1960)

Résumé—Les anomalies de résistivité et de pouvoir thermoélectrique observées à basse température dans le Plutonium et les Plutonium–Aluminium δ sont interprétées comme dues à une transformation ordre–désordre. De l'évolution de l'ordre local au-dessus de la température critique, on déduit le nombre d'électrons de conductibilité : ce nombre décroît de 1 à 0,8 par atome, lorsque la teneur d'Aluminium passe de 0 à 10 pour cent, dans les solutions solides δ. La nature possible de l'ordre à basse température est discutée.

L'anomalie d'expansion observée en phase δ et dans les solutions solides δ est liée à un mécanisme thermiquement activé. L'énergie d'activation correspondante croît linéairement de 0,17 à 0,27 eV/at., lorsque la teneur d'Aluminium passe de 0 à 5 pour cent.

Abstract—The low temperature anomalies of electrical resistivity and thermoelectric power observed in Plutonium and δ Plutonium–Aluminium solid solutions are interpreted in terms of an order–disorder change. A study of short-range order above the critical temperature indicates a decrease in the number of conduction electrons from 1 to 0·8 per atom as one goes from pure δ Plutonium to the 10 at. pour cent Aluminium δ solid solution. The possible nature of the low temperature order is discussed.

The anomalous expansion observed in δ Plutonium and δ Plutonium–Aluminium solid solutions is related to a thermally activated process. The corresponding activation energy increases linearly from 0·17 to 0·27 eV/at. as the Aluminium atomic concentration goes from 0 to 5 per cent.

1. INTRODUCTION

Les proprietes physiques du Plutonium et de certains alliages riches en Plutonium présentent des anomalies tout à fait remarquables, généralement communes à toutes les phases, aussi bien les phases α, β, γ, de basse et moyenne températures que des phases δ, δ', ϵ, de haute température.

Deux propriétés indiquent dans toutes les phases une forte densité électronique au niveau de Fermi : la chaleur spécifique électronique[1] et la susceptibilité magnétique.[2] Elles sont élevées et varient peu avec la température. En particulier, la variation de la susceptibilité magnétique avec la témperature ne laisse pas apparaître d'anomalie associable à une transition ordre–désordre magnétique.[3] Par contre, la chaleur spécifique du Plutonium α présente un double pic vers 50°K et un pic simple vers 125°K.[4]

La résistivité électrique est forte et, à température assez élevée, varie peu avec la température.[5,6] Dans le Plutonium α, on observe de 0° K à 100°K une croissance très rapide suivie d'un maximum vers 105°K, auquel succède une décroissance continue jusqu'à la transformation $\alpha\beta$. L'anomalie de résistivité est analysable en T^{-1}. Le phénomène a même allure dans le Plutonium δ, stabilisé jusqu'à basse température par des additions d'aluminium, la décroissance qui suit le maximum est cependant un peu plus rapide et est suivie d'un minimum au-delà duquel la résistivité croît faiblement. Les positions du minimum et du maximum varient avec la concentration d'Aluminium (Fig. 1).

Le comportement de la résistivité électrique du Plutonium est analogue à celui que l'on observe dans certaines substances présentant à basse température un ordre magnétique ou atomique.

Ainsi le maximum de résistivité correspondrait-il à une transition ordre–désordre qui pourrait être, comme l'a suggéré Friedel (*loc. cit.*) une transition ordre–désordre atomique, analogue à cellesque l'on observe dans les substances ferroélectriques

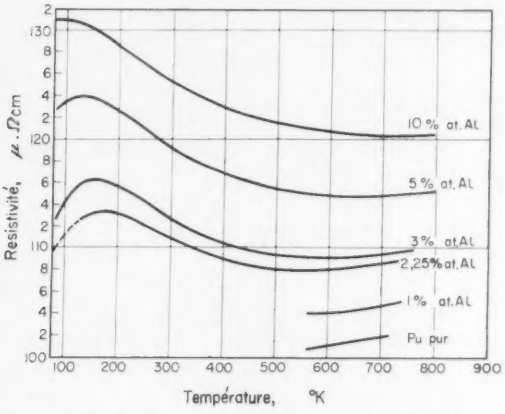

FIG. 1. Resistivites des solutions solides Plutonium–Aluminium δ.

pour le Plutonium α de structure très complexe, ou bien une transition de l'état antiferromagnétique à l'état paramagnétique pour les Plutonium–Aluminium δ, dont la symétrie cristalline

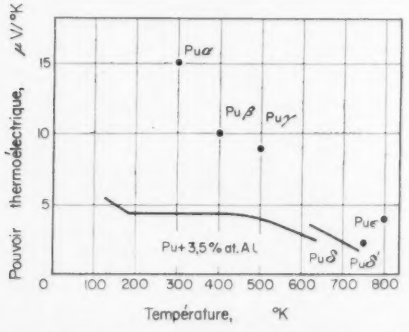

FIG. 2. Pouvoir thermoelectrique absolu du Plutonium et d'une solution solide Plutonium–Aluminium δ à 3,5 pour cent at. Al.

est trop élevée pour permettre un comportement ferroélectrique. On note un tel comportement dans les alliages MnCu[7] et CrFe,[8] où le maximum de résistivité correspond à la température de Néel déterminée par diffraction de neutrons.

Le pouvoir thermoélectrique est toujours positif.[6] Il prend des valeurs élevées dans les phases α, β, et γ, et plus faibles dans les phases δ, δ′ et ε. Le pouvoir thermoélectrique d'un Plutonium δ stabilisé par 3,5 at. pour cent d'aluminium laisse apparaître une cassure avec changement de pente positif à une température très voisine de celle pour laquelle on observe un maximum de résistivité (Fig. 2).

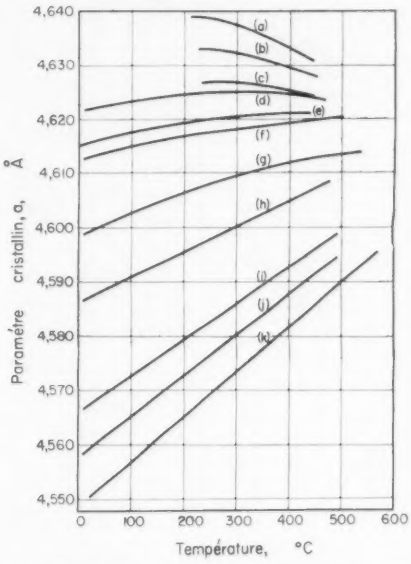

FIG. 3. Variation du paramètre cristallin avec la température pour les solutions solides Plutonium–Aluminium δ.

Enfin les phases δ et δ′ présentent un coefficient de dilatation négatif.[5] Le phénomène est aussi observé dans les Plutonium–Aluminium δ, mais il disparaît progressivement lorsque la teneur en Aluminium croît ou si la température décroit (Fig. 3).

Nous nous proposons d'étudier l'aspect phénoménologique de ces propriétés et d'en tirer les conclusions qui éventuellement s'en dégageront.

2. ETUDE DU COMPORTEMENT DE LA RESISTIVITE ELECTRIQUE ET DU POUVOIR THERMOELECTRIQUE AU VOISINAGE D'UNE TRANSFORMATION ORDRE–DESORDRE

2.1 *Résistivité électrique*

DE GENNES et FRIEDEL[10] et BEAL[11] ont étudié

Vol. 18
1961

théoriquement la variation de la résistivité au voisinage d'une transition ordre–désordre. Dans le cas d'une transition magnétique, la résistivité peut s'analyser en plusieurs termes—un terme dû aux vibrations du réseau, proportionnel à T, pour les hautes températures : $\rho_p T$

—un terme dû aux diffusions désordonnées des électrons par les moments magnétiques localisés à chaque atome. Ce terme est lié aux degrés d'ordre à longue distance et d'ordre local présents dans la substance. Il s'écrit :

$$\rho_m = (1-\phi^2)\left[1+(1-\phi^2)\frac{T_c}{T}f(k_F D)\right]\rho_{m_0} \quad (2.1)$$

où ρ_{m_0} représente la résistivité due au désordre total. ϕ est le paramètre d'ordre à longue distance.

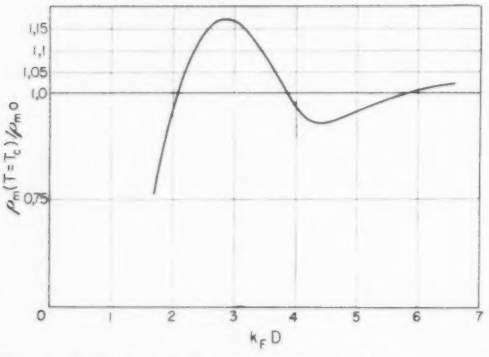

FIG. 4. Variation du rapport $\rho_m(T = T_c)/\rho_{m_0}$ avec le paramètre $k_F D$.

Le crochet représente la contribution due à l'ordre local. T_c est la température de transition, k_F le vecteur d'onde au niveau de Fermi, D la distance entre atomes magnétiques voisins.

$$f(k_F D) = \frac{3}{2(k_F D)^2}\left[\cos 2k_F D - \frac{\sin 2k_F D}{k_F D} + \frac{1-\cos 2k_F D}{2(k_F D)^2}\right] \quad (2.2)$$

Cette analyse est valable pour un système ordonné de structure c.f.c., dans lequel la tendance à l'ordre local est isotrope.[15]

A T_c en particulier on a

$$\rho_m(T_c) = [1+f(k_F D)]\rho_{m_0} \quad (2.3)$$

Les variations du quotient $\rho_m(Tc)/\rho_{m_0}$ en fonction du paramètre $k_F D$ sont représentées Fig. 4.

2.2 *Pouvoir thermoélectrique*

Le pouvoir thermoélectrique est donné, au dessus de la température de Debye, par la formule[12]

$$S = \frac{\pi^2 k^2}{3|e|} T \frac{\partial \log \rho}{\partial E_F} \quad (2.4)$$

où E_F est l'énergie de Fermi, et ρ la résistivité totale.

Nous allons étudier la variation du pouvoir thermoélectrique d'une solution solide diluée, riche en atomes magnétiques et présentant un point de transition antiferromagnétique. Nous supposerons le terme de résistivité dû aux diffusions par les atomes magnétiques et par les atomes étrangers très supérieur au terme dû aux vibrations du réseau. Dans ces conditions :

$$\rho = \rho_p T + \rho_A + \rho_{m_0}(1-\phi^2)\left[1+(1-\phi^2)\frac{T_c}{T}f(k_F D)\right]$$

$$= (\rho_A+\rho_{m_0})\left[1+\frac{\rho_p T}{\rho_A+\rho_{m_0}} - \phi^2\frac{\rho_{m_0}}{\rho_A+\rho_{m_0}} + (1-\phi^2)^2\frac{T_c}{T}\frac{\rho_{m_0}}{\rho_A+\rho_{m_0}}f(k_F D)\right] \quad (2.5)$$

Au voisinage de la température de transition, ϕ est petit ou nul; $f(k_F D)$ est petit, de l'ordre de 0,15 au plus. Donc S peut s'écrire

$$S \simeq \frac{\pi^2 k^2}{3|e|} T\left[\frac{\partial}{\partial E_F}\log(\rho_A+\rho_{m_0}) + T\frac{\partial}{\partial E_F}\left(\frac{\rho_p}{\rho_A+\rho_{m_0}}\right) - \phi^2\frac{\partial}{\partial E_F}\left(\frac{\rho_{m0}}{\rho_A+\rho_{m_0}}\right) + (1-\phi^2)^2\frac{T_c}{T}\frac{\partial}{\partial E_F}\left(\frac{\rho_{m_0}}{\rho_A+\rho_{m_0}}f(k_F D)\right)\right] \quad (2.6)$$

Près de la température de transition ϕ^2 peut s'écrire :

$$T < T_c : \phi^2 \simeq 3\left(\frac{T_c - T}{T}\right)$$

$$T > T_c : \phi^2 = 0$$

Finalement on obtient pour S

—au-dessous du point de transition :

$$S \simeq \frac{\pi^2 k^2}{3|e|}\left\{T\frac{\partial}{\partial E_F}\log(\rho_A+\rho_{m_0})+T^2\frac{\partial}{\partial E_F}\left(\frac{\rho_p}{\rho_A+\rho_{m_0}}\right)+3(T-T_c)\frac{\partial}{\partial E_F}\left(\frac{\rho_{m_0}}{\rho_A+\rho_{m_0}}\right)+\right.$$
$$\left.+T_c\left(1+3\frac{(T-T_c)}{T}\right)^2\frac{\partial}{\partial E_F}\left[\frac{\rho_{m_0}}{\rho_A+\rho_{m_0}}f(k_FD)\right]\right\} \qquad (2.7)$$

—au-dessus du point de transition :

$$S \simeq \frac{\pi^2 k^2}{3|e|}\left\{T\frac{\partial}{\partial E_F}\log(\rho_A+\rho_{m_0})+T^2\frac{\partial}{\partial E_F}\left(\frac{\rho_p}{\rho_A+\rho_{m_0}}\right)+T_c\frac{\partial}{\partial E_F}\left[\frac{\rho_{m_0}}{\rho_A+\rho_{m_0}}f(k_FD)\right]\right\} \qquad (2.8)$$

Calculons le changement de pente au point de transition :

$$\left(\frac{dS}{dT}\right)_{T>T_c}=\frac{\pi^2k^2}{3|e|}\left\{\frac{\partial}{\partial E_F}\log(\rho_A+\rho_{m_0})+2T\frac{\partial}{\partial E_F}\left(\frac{\rho_p}{\rho_A+\rho_{m_0}}\right)\right\} \qquad (2.9)$$

$$\left(\frac{dS}{dT}\right)_{T<T_c}=\frac{\pi^2k^2}{3|e|}\left\{\frac{\partial}{\partial E_F}\log(\rho_A+\rho_{m_0})+2T\frac{\partial}{\partial E_F}\left(\frac{\rho_p}{\rho_A+\rho_{m_0}}\right)+\right.$$
$$+6\frac{T_c^2}{T^2}\left(4-\frac{3T_c}{T}\right)\frac{\partial}{\partial E_F}\left(\left(\frac{\rho_{m_0}}{\rho_A+\rho_{m_0}}f(k_FD)\right)\right)+$$
$$\left.+3\frac{\partial}{\partial E_F}\left(\frac{\rho_{m_0}}{\rho_A+\rho_{m_0}}\right)\right\} \qquad (2.10)$$

On doit donc observer à T_c un changement de pente égal à :

$$\Delta\left(\frac{dS}{dT}\right)=-\frac{\pi^2k^2}{|e|}\frac{\partial}{\partial E_F}\left\{\frac{\rho_{m_0}}{\rho_A+\rho_{m_0}}[1+2f(k_FD)]\right\} \qquad (2.11)$$

3. APPLICATION AU PLUTONIUM α ET AU PLUTONIUM, ALUMINIUM δ

3.1 *Résistivité électrique*

La détermination du quotient $\rho_m(T_c)/\rho_{m_0}$ permet de calculer le terme (k_FD) si l'on relie le pic de résistivité à la présence d'ordre local k_FD, dans un métal compact est directement lié au nombre n d'électrons de conductibilité par atome par : $k_FD \simeq 3{,}5n^{1/3}$.

Dans le Plutonium α, l'anomalie décroît comme T^{-1}, on peut en déduire le rapport $\rho_m(T_c)/\rho_{m_0}$: 1, 137.

Dans les Plutonium–Aluminium δ, il faut d'abord corriger les variations de ρ avec la température pour compenser les termes dus aux vibrations du réseau et aux atomes d'Aluminium. La dépendance du niveau de Fermi vis à vis de la température introduit une petite variation de la résistivité, que l'on peut estimer à 0,3 $\mu\Omega$ cm au plus dans le Plutonium δ.

En extrapolant depuis les hautes températures jusqu'à 0°K pour déterminer ces termes, on obtient alors les valeurs rassemblées dans le Tableau 1 :

Tableau 1

% Al	2,25	3	5	10
ρ_A	10,5	12,2	20,6	37,5
ρm_0	94	93,3	91,4	82
$\rho_m\ (T = T_c)$	101,5	103,3	103,4	93,5
$\rho_m\ (T = T_c)/\rho_{m_0}$	1,080	1,107	1,131	1,140
k_FD (1)	2,30	2,37	2,47	2,52
n (1)	0,29	0,32	0,36	0,38
k_FD (2)	3,5	3,36	3,25	3,20
n (2)	1,02	0,90	0,82	0,87

Vol. 18
1961

Les valeurs de $\rho_m(T = T_c)/\rho_{m_0}$ peuvent se situer d'un côté ou de l'autre du maximum de la courbe représentant les variations de $f(k_FD)$. Deux sens de variations pour k_FD et n sont donc à envisager, lorsque la concentration d'Aluminium passe de 0 à 10 pour cent (la valeur pour le Plutonium δ pur est obtenue par extrapolation). En particulier :

—ou bien le nombre n d'électrons de conductibilité croît de : 0,3 à 0,4 (n_1) ;
—ou bien ce nombre n décroît de : 1 à 0,8 (n_2).

La variation du pouvoir thermoélectrique va nous permettre de choisir entre les deux hypothèses.

3.2 *Pouvoir thermoélectrique*

On observe sur un Plutonium–Aluminium δ à 3,5 pour cent at. d'Aluminium, un changement de pente positif, égal à $1,4 \times 10^{-8}$ volt/°K², au point de transition. La comparaison des termes de résistivité introduits par les atomes d'Aluminium et le désordre magnétique montre que les perturbations créées sont du même ordre, et par conséquent, les sections efficaces de diffusion des atomes d'Aluminium et des atomes magnétiques auront des dépendances analogues vis-à-vis de l'énergie. On déduit de l'équation (2.11) :

$$-2\frac{\pi^2k^2}{|e|}\frac{\rho_{m_0}}{\rho_A+\rho_{m_0}}\frac{\partial f(k_FD)}{\partial E_F} = 1,4\times10^{-8}$$

ou

$$\frac{df(k_FD)}{d(k_FD)} \times \alpha\frac{k_FD}{E_F} = -0,11/\text{eV}$$

$\dfrac{df(k_FD)}{d(k_FD)}$ est donc négatif. Avec une valeur raisonnable de α, (α est lié à la pente de la densité d'états au niveau de Fermi); on trouve une valeur de k_FD légèrement supérieure à 3.

BÉAL[13] a développé une autre méthode qui conduit au même résultat.

Lorsqu'on passe du Plutonium δ pur au Plutonium allié à 3,5 pour cent at. d'Aluminium, on observe une diminution du pouvoir thermoélectrique de 24 pour cent à 600°K. La variation ΔS du pouvoir thermoélectrique accompagnant une variation $\Delta\rho$ de résistivité est donnée par FRIEDEL[14] :

$$\frac{\Delta S}{S} = -\frac{1-\dfrac{\Delta x}{x}}{1+\dfrac{\rho}{\Delta\rho}} \qquad (3.1)$$

avec

$$\Delta x = -E_F\frac{\partial \log \Delta\rho}{\partial E_F}$$

$$x = -E_F\frac{\partial \log \rho}{\partial E_F}$$

connaissant S, ΔS, x, Δx, on en déduit

$$\frac{\partial \log \Delta\rho}{\partial E_F} = -\frac{\Delta x}{E_F} = 0,17/\text{eV}$$

Or, lorsque la concentration d'Aluminium croît, on observe une variation de la résistivité additionnelle moins rapide que ne le prévoit la règle de Nordheim en C $(1–C)$. On peut en déduire une diminution de E_F.

4. EXPANSION THERMIQUE DES PLUTONIUM–ALUMINIUM δ

Il est possible de décrire l'expansion thermique des Plutonium–Aluminium δ par la somme de deux termes, l'un linéaire, l'autre exponentiel ;

Tableau 2

% Al	0	1	2,25	2,6	3	5	7	10	12
a_0(Å)	4,636	4,626	4,616	4,607	4,605	4,588	4,573	4,548	4,526
$\alpha\times10^6$	3,4	4,1	5,2	5,5	6,3	7,5	9,8	14,5	18,
Δa(Å)	0,28	0,28	0,28	0,28	0,28	0,28	—	—	—
ΔE (eV/at.)	0,175	0,198	0,215	0,227	0,235	0,27	—	—	—

si α est le paramètre à la température T :

$$a = a_0(c)[1+\alpha(c)T]-\Delta a(1-c)\frac{1}{1+\exp[\Delta E(c)/kT]} \quad (4.1)$$

a_0 apparaît comme le paramètre à 0°K, α comme le coefficient de dilatation à 0°K,

Δa comme un terme de contraction constant et ΔE comme une énergie d'activation pour le mécanisme à la base du phénomène observé. a_0, α et ΔE sont des fonctions de la concentration d'Aluminium. On obtient les valeurs réunies dans le Tableau 2.

Dans le domaine 0–5 pour cent at. d'Aluminium, ΔE apparaît comme une fonction linéaire de la concentration d'Aluminium.

Si l'on reprend les valeurs données par ELLIOT *et al.*[9] pour les alliages Pu Ce, on peut analyser de la même manière la variation du paramètre avec la température. Pour les trois alliages à 3,4 ; 4 et 8 pour cent de Cerium, on peut déterminer ΔE on trouve 0,163, 0,19 et 0,48 eV/at. respectivement. Il semblerait que l'énergie d'activation diminue à partir de la valeur pour le Plutonium pur, passe par un minimum, puis augmente de nouveau ; davantage de teneurs seraient nécessaires pour préciser le phénomène.

L'aspect phénomènologique de l'expansion thermique suggère la présence de défauts thermiquement activés, qui pourraient consister en excitations d'électrons d'un niveau à un autre. ΔE apparaîtrait comme la séparation des deux niveaux.

Des mesures de paramètre au-dessous de la température ambiante seraient utiles pour préciser l'analyse de ce phénomène.

5. DISCUSSION

On s'attendrait à voir le nombre d'électrons de conductibilité augmenter avec la concentration d'Aluminium, puisqu'en principe ce métal apporte trois électrons de conductibilité, soit davantage que n'en compte le Plutonium. Or, la variation du pouvoir thermoélectrique indique le choix de la seconde des hypothèses envisagées à la suite de l'étude de la résistivité : le nombre d'électrons de conductibilité passe de 1 à 0,8 lorsque la concentration d'Aluminium passe de 0 à 10 pour cent. Dans les mêmes conditions E_F diminue.

Il faut maintenant préciser l'action de la température et des additions d'éléments tels que l'Aluminium sur la structure électronique du Plutonium.

Il apparaît que le Plutonium δ pur compte près d'un électron de conductibilité par atome et la valeur positive du pouvoir thermoélectrique indique une pente positive de la densité électronique au niveau de Fermi. Cette densité est élevée, de l'ordre de 6 à 7 électrons par atome et par électron-volt, et

$$\left(\frac{1}{n}\frac{dn}{dE}\right)_{E_F}$$

est de l'ordre de 0,5 par électron-volt.

Si l'on se rappelle, par exemple, que le Cerium se présente sous deux variétés cubiques à faces centrées, dont l'une, la plus dense, correspond à la structure électronique $5d^26s^2$, et l'autre à la structure $4f^15d^16s^2$, on est tenté d'envisager des excitations thermiquement activées d'électrons $5f$ vers la bande de conduction, pour expliquer le coefficient de dilatation négatif.

Ces excitations ne vont pas modifier beaucoup la densité électronique et créer sans doute un léger terme de résistivité dû à une modification locale de la section efficace de diffusion. Si l'on introduit une valeur raisonnable de ce terme, on peut recalculer le rapport ρ_m/ρ_{m_0} $(T = T_c)$, et on voit que sa variation est très peu modifiée.

On ne s'attend donc pas à un accroissement notable de la densité d'états au niveau de Fermi. Le faible accroissement du terme de Pauli dans la susceptibilité paramagnétique compensera la diminution du terme dû au magnétisme des couches internes.

La présence de défauts thermiquement activés avec une énergie ΔE entraine un terme de chaleur spécifique

$$\Delta Cv = \frac{(\Delta E)^2}{kT^2}\frac{\exp\left(\frac{\Delta E}{kT}\right)}{\left[1+\exp\left(\frac{\Delta E}{kT}\right)\right]^2}$$

Pour le Plutonium δ pur ($\Delta E = 0{,}175$ eV/at.) on trouve:

T (°C)	350°	400	450
ΔCv (cal/mol)	0,75	0,80	0,85

Vol. 18
1961

Expérimentalement, en effet, on n'observe pas la croissance exponentielle de la chaleur spécifique généralement associée à la création de défauts.

L'addition d'aluminium est accompagnée des effets suivants :

— la température du pic de résistivité diminue ;
— l'énergie de Fermi et le nombre d'électrons de conductibilité diminuent
— l'énergie d'activation associée au mécanisme à la base du coefficient de dilatation négatif augmente.

Pour mieux comprendre ces résultats, il serait nécessaire de connaître les perturbations liées à la présence de quelques atomes non magnétiques au milieu d'un réseau d'ions magnétiques. Ainsi la variation de la température ordre–désordre et les fortes résistivités résiduelles à 0°K, en particulier, pourraient-elles être expliquées. On peut envisager un mécanisme de superéchange couplant antiferromagnétiquement deux atomes de Plutonium par l'intermédiaire d'un atome d'Aluminium. L'évolution de la structure électronique avec la teneur en Aluminium est certainement accompagnée d'une évolution des propriétés magnétiques. Des mesures de susceptibilité magnétique pour diverses teneurs d'Aluminium permettraient sans doute une meilleure compréhension des phénomènes étudiés ici.

REFERENCES

1. Dean D. J., Kay A. E. et Loasby R. G., *J. Inst. Met.* **86,** 464 (1958).
2. Coffinberry A. S. et Waldron M. B., *Progr. Nucl. Energy* V, I, 354 (1956).
3. Cohen J., à paraître. Institut Fourier Grenoble.
4. Sandenaw T. A., Olsen C. E. et Gibney R. B., mémoire 42, Conf. Int. Pu, Grenoble (1960).
5. Sandenaw T. A. et Olsen C. E., mémoire 41, Conf. Int. Pu, Grenoble (1960).
6. Lee J. A., Meadon G. T., Hall R. O. A. et King E., mémoire 4, Conf. Int. Pu, Grenoble (1960).
7. Bacon G. E., Dunmur I. W., Smith J. H. et Street R., *Proc. Roy. Soc.* A **241,** 223 (1957).
8. Rajan N. S., Waterstrat R. M. et Beck P. A., U.S. Air Force, WADC, Contract n°33 (616) 3789.
9. Elliot R. O., Gschneidner K. A. et Kempter C. P. mémoire 34, Conf. Int. Pu, Grenoble (1960).
10. de Gennes P. G. et Friedel J., *J. Phys. Chem. Solids* **4,** 71 (1958).
11. Beal M. T., *J. Phys. Chem. Solids*, a paraître.
12. Mott N. F. et Jones H., *Theory of the Properties of Metals and Alloys.* Cambridge University Press (1936).
13. Beal M. T., *J. Phys. Chem. Solids*, a paraître.
14. Friedel J., *Canad. J. Phys.* **34,** 1190 (1956).
15. Rocher Y. A., *J. Phys. Chem. Solids*, a paraître.

Vol. 19

J. Phys. Chem. Solids Pergamon Press 1961. Vol. 18, Nos. 2/3, pp. 203–206. Printed in Great Britain.

IONIC CONDUCTIVITY OF THALLIUM CHLORIDE

R. J. FRIAUF

University of Kansas, Lawrence, Kansas

(*Received* 6 *June* 1960)

Abstract—The conductivity of single crystals of thallium chloride has been measured with an a.c. impedance bridge. The results can be represented by the empirical formula $\sigma = \sigma_0 \exp(-W/kT)$, with $W = 0{\cdot}82$ eV and $\sigma_0 = 5{\cdot}3 \times 10^3$ (ohm-cm)$^{-1}$ for 370–420°C, and $W = 0{\cdot}72$ eV and $\sigma_0 = 8{\cdot}9 \times 10^2$ (ohm-cm)$^{-1}$ for 160–370°C.

The conductivity is compared to earlier work, and several reasons are advanced for considering it to be predominantly ionic. Self-diffusion coefficients for thallium obtained by use of radioactive tracers are much smaller than might be expected from the conductivity on the basis of the Einstein relation. Several tentative explanations for this apparent discrepancy are proposed, and further work is discussed.

THE MECHANISMS of ionic conductivity and diffusion have been studied extensively in alkali halide and silver halide (AgCl and AgBr) crystals.[1, 2] Since all of these substances (except for CsCl, CsBr, and CsI) have the sodium chloride type structure (f.c.c.), it has seemed desirable to investigate transport properties in crystals having other structures. This has been done for the cesium halides by other workers[3–7] and is presently being done for TlCl and TlBr, which also have the cesium chloride type structure (s.c.), in this laboratory.[8] In connection with diffusion measurements in thallium chloride, which will be discussed briefly below, the ionic conductivity has been measured rather carefully and is presented here as a report on these investigations.

Conductivity measurements have been made on four samples, two each cut from two different single crystals. One sample had evaporated platinum electrodes backed with platinum foil; otherwise the electrodes were formed by painting alcohol-dag (colloidal graphite in isopropyl alcohol) directly onto the ends of the samples. The samples were mounted inside a loosely fitting Pyrex cylinder in a small stainless steel sample holder with a stainless steel spring holding platinum discs in contact with the electrodes on the samples. The sample holder was evacuated, filled to about half an atmosphere of argon, and sealed before heating.[9] A.C. electrical measurements were

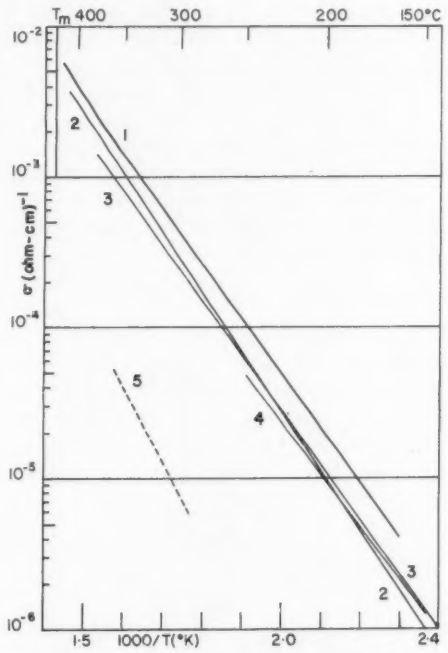

FIG. 1. Ionic conductivity of thallium chloride. The length of the lines indicates the range of the temperature measurements by the various authors. (1) This work. (2) LEHFELDT, Ref. (13.) (3) PHIPPS and PARTRIDGE, Ref. (14.) (4) HAUFFE and GRIESSBACH-VIERK, Ref. (15.) (5) Calculated from the self-diffusion of thallium as described in the text.

made at frequencies from 1 to 100 kc/sec with a General Radio Type 716–C capacitance bridge with an auxiliary resistance box in parallel with the standard capacitor of the bridge.[10]

A composite conductivity curve is shown in Fig. 1. The measurements on different samples and with different kinds of electrodes are consistent and reproducible within 2 to 3 per cent, most of this random error being introduced by the measurements of the sample dimensions. The absolute value of the conductivity may be in error by a slightly larger amount because standard thermocouple tables were used with the chromel–alumel thermocouple, but a calibration run on a AgCl sample led to over-all errors no larger than 5 to 10 per cent when compared with other authors.[11] Because the vapor pressure of TlCl approaches 1 mm near the melting point,[12] it was feared that contamination or decomposition of the sample might occur at the higher temperatures, but in a period of 74 hr of slowly increasing the temperature from 360 to 420°C (melting point at 427°C) no change in conductivity at a given temperature could be observed. After prolonged heating near the melting point some change in conductivity was observed at temperatures more than 60°C below the highest temperature, and the sample did show some signs of contamination on removal.

The conductivity shown in Fig. 1 can be represented by the empirical formula

$$\sigma = \sigma_0 \exp(-W/kT). \qquad (1)$$

With the parameters shown in Table 1 the observed values are fitted to within 2 per cent in the high temperature region, within 5 per cent down to 210°, and within 10 per cent at lower temperatures. The break at 370°C is not really as abrupt as indicated; there is rather a gradual increase of activation energy W as the temperature approaches the melting point.

The results of previous investigations are shown in the figure and the table. Although the agreement of activation energies is reasonably good, the magnitude of the conductivity is in most cases lower than the results of this work by 40–50 per cent. The reason for this discrepancy is not immediately clear, but it is probably related to the methods of preparing the samples and attaching the electrodes. LEHFELDT used single crystals, but melted platinum electrodes onto the samples.[13] PHIPPS and PARTRIDGE used polycrystalline samples solidified in an iron mold and applied electrodes with a graphite pencil or by sputtering platinum.[14] HAUFFE and GRIESSBACH-VIERK used pressed powder samples with melted-on platinum electrodes.[15]

For several reasons it is believed, in agreement with all other authors, that the conductivity is predominantly ionic rather than electronic. Large polarization effects have been observed in connection with the a.c. measurements of resistance, both in this and earlier work,[14] and the effects are qualitatively similar to those observed in other ionic conductors[10]; electronic conductivity would not lead to such large polarization effects. The high temperature results described above do not show any changes which might be ascribed to a partial decomposition leading to electronic conductivity as in stoichiometric excess or deficit semiconductors; on the other hand the anomalous rise in conductivity at high temperatures is similar to that observed in the silver halides.[11, 16] Furthermore HAUFFE and GRIESSBACH-VIERK have obtained approximate verification of Faraday's laws of electrolysis, with chlorine ions apparently dominating.[15]

Table 1. *Parameters for the ionic conductivity of thallium chloride*

Temperature range	$\sigma(T_m)$ (ohm-cm)$^{-1}$	σ_0 (ohm-cm)$^{-1}$	W (eV)	Author
370–420°C	$6{\cdot}8 \times 10^{-3}$	$5{\cdot}3 \times 10^{3}$	0·82	This work.
160–370°C	—	$8{\cdot}9 \times 10^{2}$	0·72	This work.
50–410°C	$5{\cdot}2 \times 10^{-3}$	$2{\cdot}5 \times 10^{3}$	0·79	LEHFELDT[13]
130–390°C	$3{\cdot}4 \times 10^{-3}$	$4{\cdot}7 \times 10^{2}$	0·72	PHIPPS and PARTRIDGE[14]
150–250°C	—	$2{\cdot}1 \times 10^{2}$	0·69	HAUFFE and GRIESSBACH-VIERK[15]

Continued work on the self-diffusion of thallium by using radioactive tracers is in general agreement with preliminary results reported earlier.[8] The present diffusion results have been converted to conductivity values for presentation in Fig. 1 by means of the Einstein relation

$$f\sigma_{Tl^+} = (Ne^2/kT)D_{Tl}^*, \qquad (2)$$

where N is the number of positive ions per unit volume and D_{Tl}^* is the measured diffusion coefficient for Tl^{204}. The correction factor f for correlation or displacement effects has been taken as unity for this comparison because the actual mechanism for the transport of thallium ions in the crystal is not yet known.

There are two possible kinds of explanations for the surprisingly small value of the conductivity which is apparently associated with the thallium ions. One possibility is that Schottky defects are present and that chlorine ions carry the major part of the current; this situation is indeed suggested by HAUFFE and GRIESSBACH-VIERK on the basis of their attempted transport measurements and also on some observations of a decrease in conductivity for TlCl containing small amounts of $PbCl_2$.[15] In this case the correction factor f in equation (2) should have the value 0·655 to correct for correlation effects associated with the motion of vacancies on a simple cubic lattice,[17] and the results will then amount to a determination of the transport number of Tl^+ ions.

The other possibility is that Frenkel defects occur, with interstitial thallium ions carrying the bulk of the current by an interstitialcy mechanism. This situation is conceivable because of the relatively small size and large polarizability of the Tl^+ ion and is perhaps indicated by the rather small activation energy; the value of 0·72 eV for TlCl is much more comparable to the 0·97 eV for AgBr and 1·03 eV for AgCl, where silver Frenkel defects and interstitialcy motion are known to occur,[18–22] than to the 1·70 to 2·10 eV for the sodium, potassium, and rubidium halides, where Schottky defects are prevalent.[1, 2] Interstitial thallium ions could conceivably occur at the center of a face (A) or of an edge (B) of the unit cell shown in Fig. 2(a); position A is favored by repulsive energy, position B by Coulomb energy. For interstitialcy motion from position B the minimum value for the correlation factor is $\frac{1}{3}$ when the knocked-out ion moves in line with the incident ion (to the opposite edge of the cube in Fig. 2(a));[23] this value is not small enough to begin to explain the experimental results. But for a thallium ion in position A, consideration of Fig. 2(b) shows that in the predominant form of interstitialcy motion the interstitial ion will be confined to move along the line in space determined by its two nearest thallium neighbors. For this particular case, where the interstitialcy motion is not only linear but also one-dimension the correlation factor f in equation 2 is zero![23, 24] In an actual crystal there would be some chance for an interstitial ion to escape from its line of motion by moving through the center of a cube edge, but this would be a much less probable occurrence. Hence it appears that this mechanism might account for the very small observed values of f.

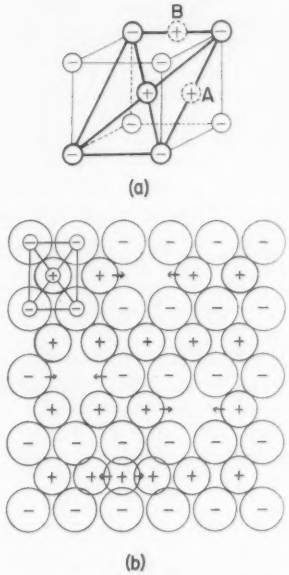

FIG. 2. (a) A unit cell for the CsCl type structure (simple cubic) of TlCl. The two possible interstitial positions for thallium ions are shown at A and B. (b) A (110) plane of TlCl, with the ionic radii drawn to scale. This is the plane which is emphasized by heavy lines in (a). The plane contains two positive ion vacancies (upper and right), a negative ion vacancy (left), and an interstitial positive ion in a Type A position (lower).

It is evident that measurements of the diffusion of chlorine will help to distinguish between these two possibilities, and such measurements are to be carried out in the near future, along with an extension of the thallium diffusion measurements to higher temperatures. A more complete report on the methods of sample preparation and diffusion measurements will be given when these results are available.

Acknowledgements—It is a pleasure to thank Mr. GLENN CONKLIN and Mr. DONALD FOSTER for assistance in constructing the equipment and making some of the measurements.

REFERENCES

1. LIDIARD A. B., *Handbuch der Physik* (Springer-Verlag, Berlin 1956), Vol. XX, gives a thorough discussion.
2. Collected tables for ionic conductivity may be found in FRIAUF R. J., *American Institute of Physics Handbook* pp. 5–185. McGraw-Hill, New York, (1957), and in JOST W., WAGNER H. G. and WEISS K., *Landolt-Bornstein Zahlenwerte und Funktionen* (6th Ed.) Vol. II, Part 6, p. 223. Springer-Verlag, Berlin (1959).
3. HARPUR W. W., MOSS R. L. and UBBELOHDE A. R., *Proc. Roy. Soc.* A**232,** 196 (1955).
4. HARPUR W. W. and UBBELOHDE A. R., *Proc. Roy. Soc.* A**232,** 310 (1955).
5. LAURENT J. F. and BENARD J., *J. Phys. Chem. Solids* **3,** 7 (1957).
6. LYNCH D. W., *Phys. Rev.* **118,** 468 (1960).
7. LAURENCE N., *Phys. Rev.* **118,** 988 (1960).
8. FRIAUF R. J., *Bull. Amer. Phys. Soc.* **3,** 127 (1958).
9. Details of the construction of the sample holder are described by FRIAUF R. J., *Rev. Sci. Instrum.* **31,** 1161 (1960).
10. FRIAUF R. J., *J. Chem. Phys.* **22,** 1329 (1954).
11. EBERT I. and TELTOW J., *Ann. Phys.* **15,** 268 (1955).
12. *Gmelins Handbuch der Anorganischen Chemie* (8th Ed.) Vol. XXXVIII, p. 261. Verlag Chemie, GmbH, Berlin (1953).
13. LEHFELDT W., *Z. Phys.* **85,** 717 (1933).
14. PHIPPS T. E. and PARTRIDGE E. G., *J. Amer. Chem. Soc.* **51,** 1331 (1929).
15. HAUFFE K. and GRIESSBACH-VIERK A. L., *Z. Elektrochem.* **57,** 248 (1953).
16. TELTOW J., *Ann. Phys.* **5,** 63, 71 (1949).
17. COMPAAN K. and HAVAN Y., *Trans. Faraday Soc.* **52,** 786 (1956).
18. COMPTON W. D., *Phys. Rev.* **101,** 1209 (1956).
19. MCCOMBIE C. W. and LIDIARD A. B., *Phys. Rev.* **101,** 1210 (1956).
20. COMPTON W. D. and MAURER R. J., *J. Phys. Chem. Solids* **1,** 191 (1956).
21. FRIAUF R. J., *Phys. Rev.* **105,** 843 (1957).
22. MILLER A. S. and MAURER R. J., *J. Phys. Chem. Solids* **4,** 196 (1958).
23. COMPAAN K. and HAVEN Y., *Trans. Faraday Soc.* **54,** 1498 (1958).
24. BARDEEN J. and HERRING C., *Imperfections in Nearly Perfect Crystals*, p. 261. (edited by SHOCKLEY W.). John Wiley, New York (1952).

J. Phys. Chem. Solids Pergamon Press 1961. Vol. 18 Nos. 2/3, pp. 207–209. Printed in Great Britain.

MANGANESE RARE EARTH COMPOUNDS WITH THE $MgZn_2$ STRUCTURE

J. H. WERNICK and S. E. HASZKO

Bell Telephone Laboratories, Incorporated, Murray Hill, New Jersey

(*Received* 3 *June* 1960)

Abstract—Two new AB_2 compounds, $ErMn_2$ and $TmMn_2$ having the $MgZn_2$ structure are reported. The transition from the cubic Mn rare earth compounds to the hexagonal compounds is discussed. Crystallographic data for these two compounds and for $HfMn_2$ having the same structure are reported.

INTRODUCTION

THE PURPOSE of this paper is to report on the crystallographic investigation of two new Mn rare earth compounds (Table 1) with the $MgZn_2$ structure (a hexagonal Laves phase).* It is part of a continuing study of the magnetic properties and structures of binary systems involving the rare earths. In previous papers, some magnetic properties[1] and crystallographic data[2,3] of such systems were reported.

EXPERIMENTAL

The compounds were prepared in an argon atmosphere by induction melting, in fused silica crucibles, mixtures of the stoichiometric amounts of the constituent elements.† X-ray powder photographs were taken with CrKα radiation and the use of Straumanis type Norelco cameras of 114·6mm diameter.

The structures of $ErMn_2$ and $TmMn_2$ were determined from powder data only. These two compounds, AB_2, ($MgZn_2$ structure) belong to space group $P6_3/mmc$-D^4_{6h}, with

4A in (f): 1/3, 2/3, z; 2/3, 1/3, $\bar{z}$; 2/3, 1/3, 1/2+z; 1/3, 2/3, 1/2−z

2B_I in (a): 000; 001/2

6B_{II} in (h): $x, 2x, 1/4; 2\bar{x}, \bar{x}, 1/4; x, \bar{x}, 1/4; \bar{x}, 2\bar{x}, 3/4; 2x, x, 3/4; \bar{x}, x, 3/4$.

Because the intensities of the reflections on the powder photographs are similar, relative intensities were computed only for $ErMn_2$ for CrKα radiation

* There are three AB_2 phases called the Laves phases. One has the cubic $MgCu_2$ structure, and the other two have the hexagonal $MgZn_2$ and $MgNi_2$ structures. The hexagonal phases differ from the cubic phase in the stacking of the close packed layers.

† The rare earth elements were more than 99 per cent pure; Mn and Hf 99·9 per cent.

Table 1. *Lattice constants and interatomic distances for* AB_2 *compounds*

AB_2	a*(Å)	c(Å)	c/a	$d^6_{B_I-B_{II}}$ $d^2_{B_{II}-B_I}$	$d^3_{A-B_I}$ $d^6_{B_I-A}$	$d^3_{A-B_{II}}$ $d^2_{B_{II}-A}$	$d^6_{A-B_{II}}$ $d^4_{B_{II}-A}$	$d^4_{B_{II}-B_{II}}$	d^3_{A-A}	d^1_{A-A}
$ErMn_2$	5·281	8·621	1·63	2·64	3·10	3·10	3·10	2·64	3·24	3·23
$TmMn_2$	5·241	8·565	1·63	2·62	3·07	3·08	3·07	2·62	3·22	3·21
$HfMn_2$	4·995	8·213	1·64	2·51	2·93	2·94	2·93	2·50	3·06	3·08

* Lattice constants are within ± 0·005 Å.

(Table 2). No attempt was made to refine the parameters $z = 1/16$ and $x = -1/6$. In the calculation of intensities, the THOMAS and UMEDA[4] atomic scattering factors corrected for dispersion[5] were used. Corrections for absorption were not made. The good agreement between observed and calculated interplanar spacings and intensities supports the correctness of the proposed structure. Powder intensities, measured with a Norelco diffractometer using unfiltered CuKα radiation, gave additional verification to the choice of structure.

The X-ray density of $ErMn_2$ is 8·83g/cm^3, and it is 2·5 per cent higher than the density, 8·61g/cm^3, measured by the liquid displacement method. This small discrepancy is undoubtedly due to the nature of the bulk sample—the material is very brittle and contains microcracks.

Powder patterns of samples of $ErMn_2$ sealed in evacuated quartz ampules and quenched in water

Table 2. Observed and calculated spacings and intensities for $ErMn_2$. CrKα *radiation*

$hk{\cdot}l$	$d_{obs.}$	$d_{calc.}$	$I_{obs.}$[+]	$I_{calc.}$
10·0	4·552	4·574	*w*	53
00·2	4·308	4·311	*w*	35
10·1	4·022	4·040	*w*	45
10·2	3·124	3·137	*w*	51
11·0	2·632	2·641	*m–s*	215
10·3	2·427	2·433	*s*	299
20·0	2·283	2·287	*w*	47
11·2	2·246	2·252	*s*	283
20·1	2·204	2·210	*m–s*	143
00·4	2·155	2·155	*vw*	16
20·2	N.O.*	2·020	—	1
10·4	1·949	1·950	*vw*	10
20·3	1·788	1·789	*vw*	20
21·0	1·726	1·729	*vw*	8
21·1	1·694	1·695	*vw*	9
10·5	1·6132	1·6134	*w*	46
21·2	1·6035	1·6044	*vw*	16
20·4	N.O.*	1·5684	—	1
30·0	1·5245	1·5245	*w*	48
21·3	1·4801	1·4813	*m–s*	165
30·2	1·4366	1·4373	*m–s*	96
00·6		1·4368		16
20·5	1·3765	1·3767	*m–s*	137
10·6		1·3708		18
21·4	1·3491	1·3485	*vw*	10
22·0†	1·3202	1·3203	*m–s*	133
31·0	1·2684	1·2685	*vw*	9
22·2	1·2626	1·2624	*w*	20
11·6		1·2621		20
31·1	1·2555	1·2549	*vw*	10
21·5	1·2208	1·2208	*m–s*	132
31·2	1·2166	1·2169	*m*	23
20·6		1·2166		79
10·7	1·1896	1·1892	*w*	40
31·3	1·1604	1·1604	*vs*	559

[+] *s* = strong, *m* = medium, *w* = weak, *v* = very

*N.O. = not observed

† Beginning here, *d* values for α_1 and α_2 averaged.

from 1140°C and samples annealed for four days at 500°C did not show any indication of change in structure. It therefore appears that the hexagonal form is the stable modification below 1140°C.

We have also prepared $HfMn_2$, which has been reported by ELLIOT[6,7] to have the $MgNi_2$ structure ($a = 4{\cdot}996$ Å, $c = 16{\cdot}300$ Å) but which tends to form the $MgZn_2$ structure at lower temperatures. (No lattice constants were reported.) The powder pattern of a sample of our ingot is similar (except for changes in interplanar spacings) to $ErMn_2$ and $TmMn_2$. For $HfMn_2$, having the $MgZn_2$ structure, $a = 4{\cdot}995$ Å and $c = 8{\cdot}213$ Å (Table 1). The relative intensities computed on the basis of the $MgNi_2$ structure for all of the above compounds were not in agreement with the observed intensity data.

DISCUSSION

In other papers,[3,8] it was shown that the room temperature form of the AB_2 phase, where A = Gd, Tb, Dy, Ho, Er and Tm and B = Al, Fe, Co and Ni, has the $MgCu_2$ structure. On the other hand, this structure is present only for the Mn compounds of Gd, Tb, Dy and Ho. It was also shown[3] that the rate of decrease of the lattice constants for the cubic Mn compounds (and hence the interatomic distances) is more rapid with increasing atomic number of the rare earth (or with decreasing size of the rare earth atom), indicating stronger electronic interactions or election overlap. One is tempted to assume that the valence electron to atom ratio is constant and the Fermi energy remains essentially the same in the Mn compounds because the 4*f* states are presumed to be localized. However, it appears that the Fermi energy is increasing rapidly with increasing atomic number of the rare earth, and at Er, a change in structure occurs so as to yield a Brillouin zone which can accommodate extra electrons. The electronic interaction through which this can occur is an open question, and more data are obviously needed. Indeed, the complex nature of Mn (as indicated by the number of solid state transitions occuring in Mn) may be an important factor here. The magnetic data[9] presently being obtained should shed more light on the electronic structure of these compounds.

Acknowledgements—Discussions with P. W. ANDERSON, J. R. KLAUDER and M. TANENBAUM are appreciated. The authors also wish to thank R. G. TREUTING and W. J. ROMANOW for discussions concerning the IBM 704 intensity program, D. DORSI for preparing the compounds, and V. B. COMPTON for the diffractometer trace.

REFERENCES

1. NESBITT E. A., WERNICK J. H. and CORENZWIT E., *J. Appl. Phys.* **30,** 365 (1959).
2. WERNICK J. H. and GELLER S., *Acta. Cryst., Camb.* **12,** 662 (1959).
3. WERNICK J. H. and GELLER S., *Trans. Amer. Inst. Min. (Metall.) Engrs.* **218,** 866 (1960).
4. THOMAS L. H. and UMEDA K., *J. Chem. Phys.* **26,** 293 (1957).
5. DAUBEN C. H. and TEMPLETON D. H., *Acta. Cryst., Camb.* **8,** 841 (1955).
6. ELLIOT R. P., Armour Research Foundation, Chicago, Illinois, Technical Report 1, OSR-TN-247, August, 1954.
7. HANSEN M., *Constitution of Binary Alloys* (2nd Ed.) McGraw-Hill, New York (1958).
8. HASZKO S. E., *Trans. Amer. Inst. Min. (Metall.) Engrs.* **218,** 958 (1960).
9. WILLIAMS H. J., WERNICK J. H. and SHERWOOD R. C., to be published.

Vol. 18
1961

J. Phys. Chem. Solids Pergamon Press 1961. Vol. 18, Nos. 2/3, pp. 210–214. Printed in Great Britain.

POLARISATION DYNAMIQUE EN BAS CHAMP DES PROTONS DU PARADICHLOROBENZENE

A. LANDESMAN

Centre d'Etudes Nucléaires, Saclay, France

(*Received* 12 *August* 1960)

Résumé—Nous étudions la polarisation dynamique des protons par "effet solide" dans des champs magnétiques statiques de 10 à 40 G, dans le paradichlorobenzène, en mettant à profit la forte interaction quadrupolaire du chlore. En soumettant le cristal à un champ magnétique de radiofréquence intense, nous avons obtenu l'augmentation théorique de l'aimantation des protons. Les probabilités de transition ont été calculées et mesurées pour différentes valeurs du champ statique et du champ de radiofréquence.

Abstract—In d.c. magnetic fields from 10 to 40 G we study dynamic polarization of protons by the "solid state effect" in paradichlorobenzene. We take advantage of the large quadrupole splitting of the chlorines. We obtain the expected enhancement of the magnetization of protons, when irradiated by r.f. magnetic field at the right frequency. Transition probabilities are calculated and measured as a function of r.f. power and d.c. field.

1. INTRODUCTION

NOUS ÉTUDIONS la polarisation dynamique des protons du paradichlorobenzène par "effet solide".[1–4] Le système comprend deux espèces de spins en interaction :

— les spins I des protons qui ont un temps de relaxation T_I long,

— les spins S des chlores qui ont un temps de relaxation T_S court par rapport à T_I :

$$T_I \gg T_S \tag{1}$$

Leur facteur de Boltzmann qui est accru par interaction quadrupolaire est supérieur à celui des spins I[1] dans les bas champs magnétiques où nous opérons (10 à 40 G).

Soient ω_I la fréquence de Larmor des spins I et Ω_S une des fréquences de résonance du chlore, dans un champ magnétique H_0. Si par un champ de radiofréquence $2H_1 \cos \omega t$ perpendiculaire au champ statique H_0, à la fréquence $\omega = \Omega_S \pm \omega_I$, on induit une transition de probabilité W telle que

$$W \ll T_S^{-1},$$

on augmente la polarisation des protons dans le rapport

$$\mp [WT_I/(WT_I+1)](\Omega_S/\omega_I).$$

Par suite de l'interaction dipolaire entre les protons et les chlores, cette transition W n'est pas complètement interdite.

Pour que les fréquences $\Omega_S+\omega_I$ et $\Omega_S-\omega_I$ soient bien séparées et que l'on n'ait pas d'effet différentiel[3] il faut que l'on ait

$$\omega_I \gg \Delta\omega \tag{2}$$

où $\Delta\omega$ est la largeur de raie résultante des deux systèmes de spins.

En bas champ les fréquences de résonance Ω_S du chlore sont de l'ordre de la fréquence quadrupolaire pure qui est pour ^{35}Cl à température ordinaire $\Omega = 34{,}28$ Mc. Si la probabilité de transition est assez grande ($W \gg T_I^{-1}$) l'aimantation M_0 des protons polarisés est égale à leur aimantation à l'équilibre thermique dans un champ magnétique $\Omega_S/\gamma_I \approx \Omega/\gamma_I = 8000$ G. A partir de l'instant où la transition W est induite l'aimantation des protons croît exponentiellement et tend vers la valeur limite

$$[WT_I/(WT_I+1)]M_0$$

avec une constante de temps $W+T_I^{-1}$.

Le temps de relaxation T_S du chlore-35 dans le paradichlorobenzène à température ordinaire

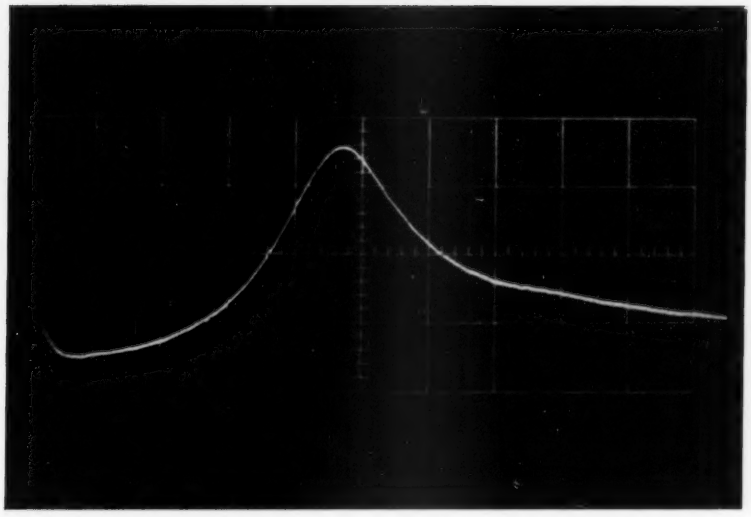

FIG. 1. Signal de proton dans le paradichlorobenzène observé par passage rapide à 400 kc après polarisation dynamique dans un champ $H_0 = 10$ G. Le champ tournant h_1 à 400 kc est égal à 0,25 G et la vitesse du balayage du champ magnétique $\dot{H}_0$ est telle que $h_1/\dot{H}_0 = 3{,}6$ ms. La trace représente un balayage de 17 G.

[*facing p.* 210

BLANK
PAGE

Vol.
19

est $2{,}2 \times 10^{-2}$ sec.[5] Le temps de relaxation T_I des protons dans notre échantillon a été mesuré pour différentes valeurs du champ magnétique (Tableau 1). La condition (1) est remplie, le rapport T_I/T_S étant au moins égal à 400 dans nos expériences.

La largeur de la raie quadrupolaire pure de ^{35}Cl dans un monocristal de paradichlorobenzène a été mesurée par divers auteurs; elle est d'une fraction de kilocycle par seconde. La largeur de raie des protons, qui est d'environ 6 kc,[6] est, comme prévu, plus grande que celle du chlore. La condition (2), où $\Delta\omega$ est donc la largeur de raie des protons, est satisfaite si $H_0 \gg \Delta\omega/\gamma_I = 1{,}4$ G.

2. MESURE DE L'AIMANTATION OBTENUE PAR POLARISATION DYNAMIQUE

Nous mesurons l'aimantation des protons à la fréquence de 400 kc, par passage adiabatique rapide, dans un système de bobines croisées à compensation extérieure[3] (Fig. 1). Les expériences sont faites à température ordinaire avec un monocristal d'environ 2 cm^3. La principale difficulté réside dans l'échauffement du cristal par le champ de radiofréquence, car la fréquence quadrupolaire de ^{35}Cl varie de 3,14 kc par °C.[7] Nous mesurons le champ tournant de radiofréquence H_1 grâce à un petit enroulement aux bornes duquel est induite une tension proportionnelle à H_1.

Tableau 1. *Temps de relaxation des protons en fonction du champ magnétique*

H_0 (G)	T_I
10	10 sec
15	25 sec
40	2 min 30 sec
60	4 min
4500	$\approx$ 1 hr

Le signal des protons à l'équilibre thermique dans les bas champs où nous opérons est inobservable. Pour déterminer l'aimantation M_0, nous comparons le signal obtenu après polarisation dynamique, proportionnel à M_0, avec le signal obtenu dans l'échantillon polarisé[8] dans un champ $H_0 = 5500$ G, puis transporté dans les bobines de Helmholtz. Pour éviter la dépolarisation des protons dans le champ terrestre, l'échantillon est transporté dans l'entrefer d'un petit aimant permanent. Cette comparaison nous permet de vérifier que l'aimantation M_0 obtenue par polarisation dynamique a bien la valeur prévue plus haut, aux erreurs expérimentales près (20 pour cent). La même vérification a été faite, en utilisant l'isotope ^{37}Cl du chlore.

3. CALCUL DES PROBABILITES DE TRANSITION

Dans le paradichlorobenzène Cl⟨⬡⟩Cl, il existe une température de spin au sein du système des protons, par suite du couplage dipolaire entre les protons, qui est beaucoup plus fort que le couplage entre un proton et le chlore premier voisin, situé sur la même molécule que le proton, en position ortho par rapport à celui-ci, à une distance $r = 2{,}81$ Å.[9-10] L'abondance isotopique naturelle de ^{35}Cl est $n = 0{,}754$. Dans un monocristal il y a deux orientations A_1 et A_2 pour les axes quadrupolaires, c'est-à-dire pour les axes Cl–Cl des différentes molécules; l'angle (A_1, A_2) est égal à 75 degrés.

Le champ statique H_0 est parallèle à A_1 et le champ de radio-fréquence H_1 est perpendiculaire à H_0 dans le plan (A_1, A_2). Le champ H_1, qui fait avec A_2 un angle de 15 degrés, a peu d'action sur les chlores correspondant à l'orientation A_2.

Nous calculons d'abord une probabilité de transition W_0 pour une paire de noyaux : un proton et le chlore premier voisin. Par suite du fort couplage dipolaire entre les protons, la probabilité de transition effective est $W = (n/2)W_0$ où $n/2$ est la probabilité pour un proton d'être premier voisin d'un chlore ^{35}Cl, et d'être dans une molécule orientée suivant A_1. Nous négligeons les interactions entre toutes les paires chlore–proton qui ne sont pas formées de premiers voisins.

En champ bas l'énergie Zeeman des chlores est toujours petite par rapport à leur énergie quadrupolaire. Les niveaux d'énergie d'une paire chlore–proton sont donnés Fig. 2. Par suite de l'interaction chlore–proton $\mathcal{H}_{IS}$, on peut induire

une "transition d'effet solide" telle que

$$3/2+\leftrightarrow 1/2-,$$

l'état $|3/2+\rangle$, par exemple, étant en réalité

$$|3/2+\rangle+|3/2-\rangle\langle 3/2-|\mathscr{H}_{IS}|3/2+\rangle/\omega_I.$$

Deux cas peuvent se présenter :

1. Un champ magnétique statique tel que

$$\gamma_S H_0 = \omega_S \gg \Delta\omega$$

ce qui donne, pour ^{35}Cl, $H_0 \gg \Delta\omega/\gamma_S = 14$ G; les huit niveaux de la Fig. 2 sont complètement séparés les uns des autres.

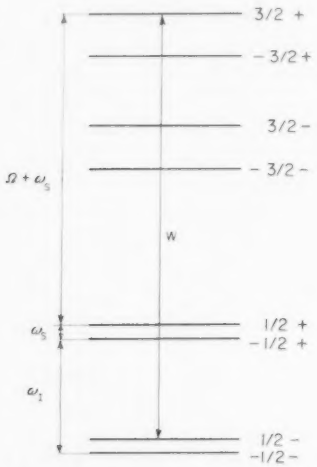

FIG. 2. Niveaux d'énergie et états propres d'une paire chlore–proton. Les signes $\pm$ 3/2, $\pm$ 1/2 se rapportent au chlore et les signes $\pm$ se rapportent au proton.

2. Un champ magnétique tel que

$$\omega_I > \Delta\omega > \omega_S$$

ce qui permet de négliger l'énergie Zeeman des chlores.

Dans le cas 1, pour les différentes transitions $|\Delta I_z+\Delta S_z| = \Delta m = 0$ ou 2; 1; 3 on trouve des probabilités de transition de la forme

$$W(\Delta m) = n/2\, f(\Delta m)(H_1/H_0)^2(\hbar\gamma_S^2/r^3)^2\Delta\omega^{-1}$$

le Tableau 2 donnant les facteurs angulaires $f(\Delta m)$.

Dans le cas 2 il est facile de voir que les différentes fréquences de transition données par le Tableau 2 se réduisent à deux, $\omega = \Omega \pm \omega_I$, pour lesquelles la probabilité de transition est

$$W_t = 2W(^0_2)+W(1)+W(3).$$

Le Tableau 2 donne également les valeurs calculées pour les probabilités de transition réduites.

$$w(\Delta m) = W(\Delta m)(H_0/H_1)^2.$$

4. MESURES DES PROBABILITES DE TRANSITION

Nous avons vérifié, dans un champ $H_0 = 15$ G, que l'amplitude du signal augmente exponentiellement avec le temps de polarisation. De l'ensemble de ces exponentielles, pour différentes valeurs de H_1, nous déduisons W et T_I. Nous vérifions que la probabilité de transition W est proportionnelle à H_1^2 (Fig. 3). L'accord est satisfaisant entre cette détermination du temps de relaxation T_I (qui donne $T_I = 30$ sec) et la mesure directe de T_I (voir Tableau 1).

Tableau 2

$\Delta m = \lvert\Delta I_z+\Delta S_z\rvert$	ω	$f(\Delta m)$	$w(\Delta m)(\text{sec}^{-1})$
0 ou 2	$\Omega\pm(\omega_I\pm\omega_S)$	$(27/16)(\pi/2)^{1/2}\cos^2\theta\sin^2\theta(5-3\cos 2\phi)$	2,00
1	$\Omega\pm(\omega_I-2\omega_S)$	$(3/8)(\pi/2)^{1/2}(3\cos^2\theta-1)^2$	0,03
3	$\Omega\pm(\omega_I+2\omega_S)$	$(27/8)(\pi/2)^{1/2}\sin^4\theta$	1,55

Les facteurs angulaires $f(\Delta m)$ et les probabilités réduites $w(\Delta m)$ sont définis pour les différentes transitions par

$$w(\Delta m) = W(\Delta m)(H_0/H_1)^2 = (n/2)f(\Delta m)(\hbar\gamma_S^2/r^3)^2\Delta\omega^{-1}.$$

Les angles polaires $\theta \approx 50$ degrés et $\phi \approx 32$ degrés définissent la direction de l'axe chlore–proton par rapport au champ magnétique statique H_0 et au champ de radiofréquence H_1.

Dans une seconde étape, nous mesurons pour une même transition ($|\Delta m| = 0$), en fonction du champ H_0, la variation de la probabilité de transition réduite $W(H_0/H_1)^2$, indépendante du champ de radio-fréquence (Fig. 4, courbe en pointillé). Cette variation concorde avec celle déduite des calculs précédents (Fig. 4, courbes en trait plein). Le désaccord des valeurs absolues peut s'expliquer pour les raisons suivantes :

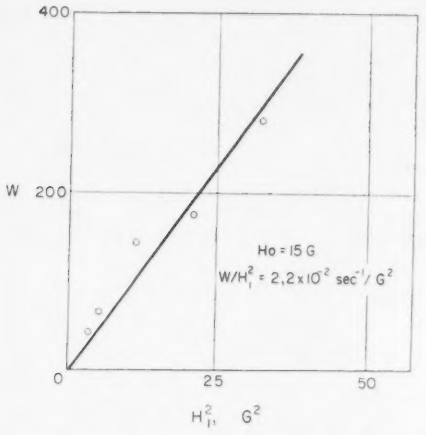

FIG. 3. Probabilité de transition, en unités arbitraires, en fonction du carré du champ tournant de radio-fréquence.

— l'axe quadrupolaire peut faire un angle non nul avec le champ H_0.

— les valeurs des angles polaires qui définissent l'orientation de l'axe chlore–proton par rapport au champ H_0 et au champ de radiofréquence ne sont pas connues avec une grande précision.

— les interactions entre toutes les paires chlore–proton qui ne sont pas formées de premiers voisins peuvent ne pas être négligeables.

5. CONCLUSION

Nous avons appliqué la méthode de polarisation dynamique dans un cas où le grand facteur de Boltzmann des spins S fortement couplés au réseau n'est pas d'origine magnétique. Bien que les deux spins I et S soient en quantités comparables dans le paradichlorobenzène, la raie des protons n'est pas élargie par interaction avec les chlores, par suite du petit moment magnétique

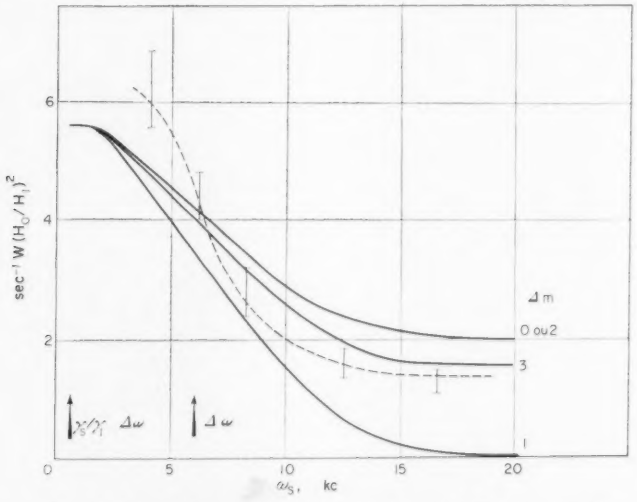

FIG. 4. La courbe en pointillé donne la probabilité de transition réduite $W(H_0/H_1)^2$ mesurée en fonction de la fréquence de Lamor ω_s de ^{35}Cl. Les courbes en trait plein sont données par

$$w(\Delta m)+[w_t-w(\Delta m)]\exp[-\tfrac{1}{2}(\omega_s/\Delta\omega)^2]$$
$$w_t = 2w(^0_2)+w(1)+\omega(3) = 5{,}58\ \text{sec}^{-1}.$$

de ces derniers, ce qui a permis de faire des expériences en bas champ. Il serait possible d'obtenir un effet de polarisation dynamique plus important en utilisant le brome ou l'iode qui ont des séparations quadrupolaires plus grandes que le chlore ($\Omega/\gamma_I \approx 50$ kG ou 200 kG). Il serait également possible d'utiliser une séparation électronique en champ nul mais dans ce cas, par suite de la largeur de raie électronique $\Delta\omega$ (au moins égale à quelques mégacycles par seconde) on ne pourrait pas opérer en bas champ.

Remerciements—Ce travail a été fait sous la direction de Monsieur le Professeur A. ABRAGAM et de Monsieur I. SOLOMON, et je tiens particulièrement à les remercier.

BIBLIOGRAPHIE

1. ABRAGAM A. et PROCTOR W. G., *C.R. Acad. Sci. Paris* **246,** 2253 (1958).
2. ERB E., MOTCHANE J. L. et UEBERSFELD J., *C.R. Acad. Sci., Paris* **246,** 3050 (1958).
3. COMBRISSON J. et SOLOMON I., *J. Phys. Radium* **20,** 683 (1959).
4. BORGHINI M. et ABRAGAM A., *C.R. Acad. Sci., Paris* **248,** 1803 (1959).
5. WOESSNER D. E. et GUTOWSKY H. S., *J. Chem. Phys.* **27,** 1072 (1957).
6. SOLOMON I., communication privée.
7. TIEN-CHUAN WANG, *Phys. Rev.* **99,** 566 (1955).
8. GOLDMAN M., *C.R. Acad. Sci., Paris* **246,** 1038 (1958).
9. CROATTO U., BEZZI S. et BUA E., *Acta Cryst., Camb.* **5,** 825 (1952).
10. BUYLE-BODIN M., Thèse, Université de Paris (1954).

J. Phys. Chem. Solids Pergamon Press 1961. Vol. 18, Nos. 2/3, pp. 215–217. Printed in Great Britain.

ENERGY GAPS IN BISMUTH TRIOXIDE*

D. M. MATTOX and L. GILDART

University of Kentucky, Lexington, Kentucky

(*Received* 1 *August* 1960)

Abstract—A unique method of preparing polycrystalline films of Bi_2O_3 having thicknesses in the range 10 to 100μ is presented. Using these films temperature vs. resistance measurements give a thermal energy gap of $2{\cdot}07 \pm 0{\cdot}07$ eV in the temperature range 400 to 550°K. Optical transmission studies at room temperature and liquid nitrogen temperature give optical energy gaps of 3·1 eV at 77°K and 2·85 eV at 300°K. This gives an apparent temperature dependence of $-1{\cdot}1 \times 10^{-3}$ eV/°K in this temperature range assuming a linear variation.

INTRODUCTION

A REVIEW of the literature on semiconducting compounds of the Group Vb–Group VIb elements of the form A_2B_3 reveals comparatively little published work on bismuth trioxide, Bi_2O_3. The reason for this is not hard to find: Molten bismuth trixode cannot be contained in crucibles of commonly available materials. That this is so has already been observed,[1] and SILLEN[2] states that molten bismuth trioxide attacks glass.

The authors found that molten bismuth trioxide dissolves its way through a Vycor test tube (96 per cent silica) in about fifteen minutes' time; and that crucibles of alumina, magnesia, zirconia, platinum and stainless steel are likewise unsatisfactory. Graphite crucibles have a reducing action on molten bismuth trioxide, and rapidly reduce it to metallic bismuth. Surface melting of sintered samples of the trioxide would therefore seem to be a better approach to the problem.[3]

PREPARATION OF Bi_2O_3 FILMS

Despite the inherent difficulties a method has been developed by the authors for preparing polycrystalline films of bismuth trioxide using a graphite crucible, and is described below. Films formed in this manner are quite fragile but can be mounted in sample holders if carefully handled.

The method takes advantage of the large difference between the melting points of bismuth metal, 271°C, and the trioxide, 828°C.[4] When bismuth metal is melted in a graphite crucible, open to the air and the temperature is raised toward the melting point of the trioxide, the metal begins to oxidize. If the temperature is then raised slightly above the melting point of the trioxide, the graphite of the crucible reduces the trioxide back to bismuth and a molten pool of pure bismuth fills the crucible. If the temperature is then lowered slightly below the melting point of the trioxide a uniform film of Bi_2O_3 forms rapidly and covers the surface of the melt. This film may be lifted from the surface using a nichrome wire loop. Films formed in this way are pale yellow in appearance, microcrystalline and have fairly uniform thicknesses. Since the thickness of the film depends mainly on the temperature of the melt, and only slightly on the time, films of desired thickness can be prepared by adjusting the temperature. Satisfactory films can be obtained in thicknesses ranging from 10 to 100μ.

It should be noted that if the melt is not heated initially above the melting point of the trioxide, the resulting films turn out to be too granular, and contain inclusions of slag.

There may be scattered inclusions of bismuth metal but these can be avoided by visual inspection and uniform sections of film as large as four square centimeters in area can easily be selected from the main pieces. For temperature studies, films are carefully mounted on glass slides, and fine nichrome

* This work was supported in part by the United States Air Force through the Air Research and Development Command.

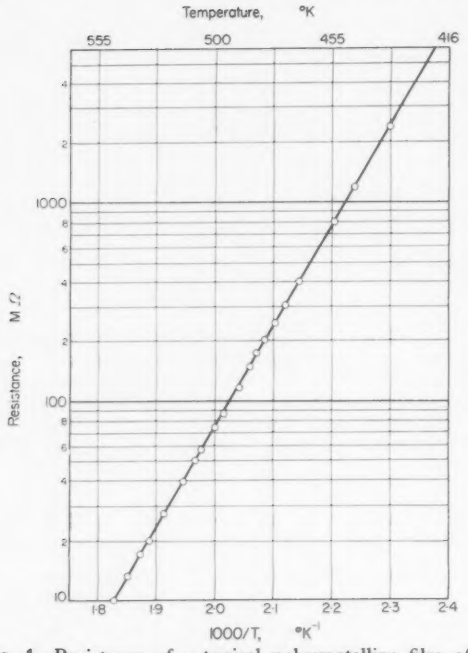

FIG. 1. Resistance of a typical polycrystalline film of Bi_2O_3 as a function of temperature.

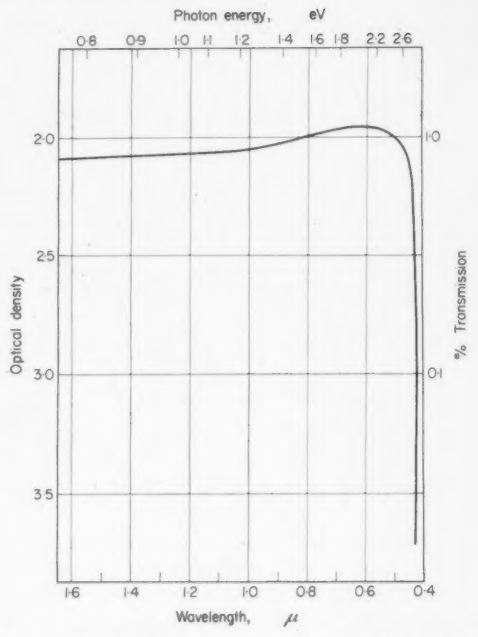

FIG. 2. Optical transmission of a polycrystalline Bi_2O_3 film 30μ thick.

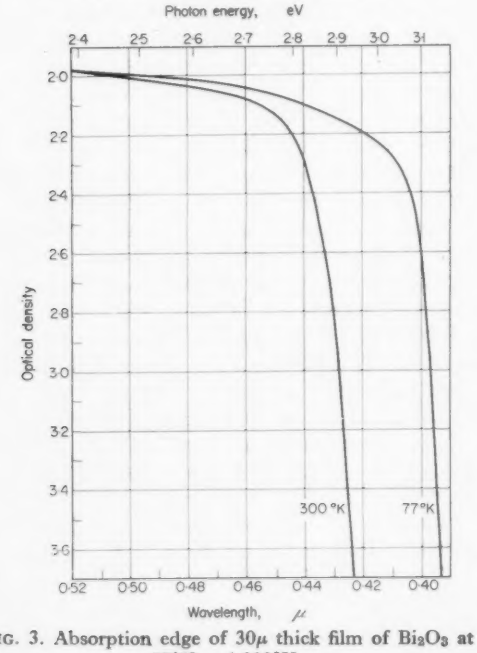

FIG. 3. Absorption edge of 30μ thick film of Bi_2O_3 at 77°K and 300°K.

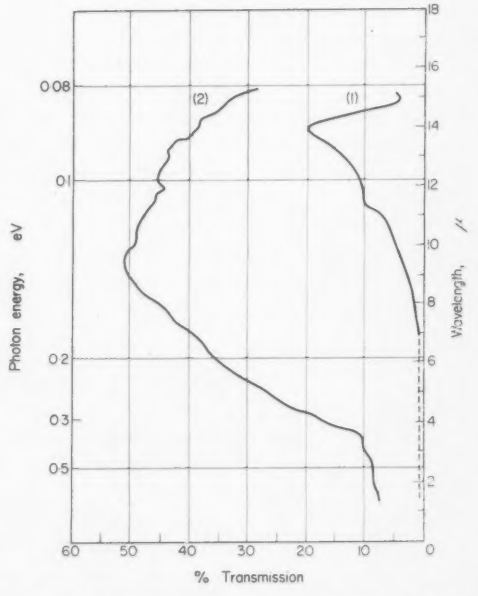

FIG. 4. Infrared transmission of two 30μ thick films of Bi_2O_3 at 300°K.

wires are attached as electrodes by means of silver paste. For optical transmission studies, the films are mounted on suitable frames.

Portions of various Bi_2O_3 films were powdered and an X-ray powder diffraction study was made. Without exception the patterns were those of the normal orthorhombic form of Bi_2O_3, with no indication that other phases or large proportions of impurity were present.

THERMAL AND OPTICAL MEASUREMENTS

For thermal measurements a film, mounted as described, is put into an electric oven and a voltage applied to it. The temperature is slowly raised at a rate of about 5°C/min. The small current through the sample is fed into the Y-axis input of an Autograf X–Y recorder. The temperature of the oven is monitored by a thermocouple and its output fed into the X-axis input.

Table 1 gives the thermal energy gap for a series of Bi_2O_3 films in the region of 400–550°K as determined from the plots of the X–Y recorder.

Table 1. Thermal energy gaps for polycrystalline films of Bi_2O_3 *in the temperature range* 400–550°K

Sample	$E_{g_{th}}$
1	1·99
2	2·05
3	2·20
4	2·07
5	1·99
6	2·12
	Average $E_{g_{th}} = 2{\cdot}07 \pm 0{\cdot}07$ eV

Figure 1 shows the resistance of a typical sample as a function of temperature. From this graph and crude measurements on the width and thickness of the sample, we have made an order of magnitude measurement for the resistivity of 10^4 ohm-cm at 500°K. This agrees with the results given by MANSFIELD[5] on sintered samples of Bi_2O_3 powder at this temperature.

Figure 2 shows the optical transmission at 300°K of a typical film of Bi_2O_3 through the visible range as measured on a Cary model 14R spectrophotometer.

Figure 3 shows the absorption edge for this film at two temperatures, 300°K and 77°K. The optical energy gap for these films is found to be 3·1 eV at 77°K and 2·85 eV at 300°K giving an apparent temperature dependence of $-1{\cdot}1 \times 10^{-3}$ eV/°K, on the assumption that a linear variation holds over this temperature range. This is to be compared with the activation energy of 3·2 eV, as obtained by DOYLE[6], on films 300 Å thick, who prepared his films by oxidizing metallic bismuth layers deposited on glass substrates. The authors prepared films by the method of DOYLE, but found that as the bismuth oxidized, the film broke up into a granular structure resembling a smoke deposit.

Figure 4 shows the infrared transmission for two samples as determined by Perkin–Elmer model 21 infrared spectrophotometer. Curve 1 is for the sample used for the above optical transmission studies and curve 2 is for a sample which showed maximum transmission. Other samples lay between these two extremes. All the samples show a maximum infrared transmission in the 10–12μ region.

Acknowledgements—The authors are indebted to Dr. C. NELSON and the Solid State Division of the Oak Ridge National Laboratory for the use of their Cary spectrophotometer.

REFERENCES

1. MELLOR J. W., *A Comprehensive Treatise on Inorganic and Theoretical Chemistry* Vol. IX, Chapter 53, p. 646. Longmans, Green and Co., New York (1922).
2. SILLEN L. G. *Ark., Kemi* 12A, **18,** 1 (1937).
3. RAYMOND R. J. and STERLING H. F., described by WILSON J. M., *Birmingham Symposium on the Metallurgical Aspects of Semiconductors,* Feb. 25 (1958).
4. VAN ARKEL A. E., FLOOD E. A. and BRIGHT N. F. H., *Canad. J. Phys.* **31,** 1009 (1953).
5. MANSFIELD P., *Proc. Phys. Soc. Lond.* **62**B, 476 (1949).
6. DOYLE W. P., *J. Phys. Chem. Solids* **4,** 144 (1958).

Vol. 18
1961

J. Phys. Chem. Solids Pergamon Press 1961. Vol. 18, Nos. 2/3, pp. 218–237. Printed in Great Britain.

IMPURITY STATES IN SOLID NEON*†

ALBERT GOLD‡

Department of Physics and Institute of Optics, University of Rochester, Rochester, New York§

(*Received* 11 *July* 1960)

Abstract—A formalism for the treatment of optical absorption by an isolated substitutional impurity center is given. The tight-binding approximation is used and the method of constructing one-electron trial functions for the system is outlined. The first-order absorption energies, oscillator strengths and integrated absorption coefficients are computed in an approximation which includes spin–orbit interaction and the overlapping of heterocentric atomic wave functions through terms of order S^2. The first-order energies are corrected for van der Waals interactions using a variational formalism. A phenomenological method for computing the emission energies of the system is given. The specific example of an argon impurity atom in solid neon is treated numerically. The computation predicts absorption lines at 11·7 and 11·6 eV due, respectively to the $^1P_1$ and $^3P_1$ states of the argon impurity, with an uncertainty of 1·3 eV. The oscillator strengths for these transitions are calculated to be 0·164 and 0·017 respectively, giving rise to integrated absorption coefficients of $0{\cdot}84 \times 10^6\, N_0$ and $0{\cdot}09 \times 10^6\, N_0$ eV cm^{-1} for the two states, where N_0 is the (small) fractional concentration of impurities in the host lattice.

1. INTRODUCTION

THE COMPUTATION of the optical properties of an isolated substitutional impurity in an otherwise undisturbed infinite crystal lattice has been an object of extensive theoretical interest for some twenty years. The goal of this work has been the achievement of a quantitative understanding of the influence of the atoms of the crystal and of lattice vibration on the absorption and emission spectra of a foreign atom introduced into a solid in small concentration. These studies attempt to explain the shifting of the absorption energies from their atomic positions, the transfer of energy to lattice vibrations resulting in the Stokes shift, the broadening of sharp atomic lines into bands, and the quantum efficiency of the luminescence process. The pressure and temperature dependence of all of these phenomena have been investigated. A large literature has accumulated in the field.[1]

Atoms in a dilute gas may be treated as independent, non-interacting systems to a very good first-approximation, whereas in a solid or liquid the interactions are known to be large. Indeed, one of the most successful approaches in the theory of impurities in solids is the effective mass approximation in which the center's electronic wave functions are computed using an effective mass and a dielectric constant κ appropriate to the non-metallic crystal. In this extreme the impurity itself is treated as a point charge Ze/κ, where Z is the difference of the valences of the impurity and the host atoms. Thus the details of the impurity center are completely ignored.

We shall adopt the viewpoint of the opposite extreme according to which the electronic properties are predominantly determined by the impurity atom itself, the interactions with the lattice being treated as relatively weak. A modified form of the Heitler–London scheme, accordingly, seems appropriate, in contrast to the generalization of the Bloch approach mentioned above. We deal briefly in the following paragraphs with the historical development of the "tight-binding" approximation as applied to impurities in solids.

* Based in part on a thesis submitted to the University of Rochester, Rochester, New York, in partial fulfillment of the requirements for the degree Doctor of Philosophy.

† Research supported in part by the U.S. Air Force through the Air Force Office of Scientific Research of the Air Research and Development Command.

‡ Eastman-Kodak Predoctoral Fellow in Physics (1958–59).

§ Present address: Department of Physics, University of Illinois, Urbana, Ill.

Most of the workers in the field have concentrated their efforts on the experimentally convenient case of heavy metal impurities in alkali-halides. The classic model of such a center was proposed by SEITZ[2] in 1938 for the system KCl : Tl. The first attempt at a detailed numerical computation for such a system was made by WILLIAMS on a semi-classical basis for KCl : Tl using the Seitz model.[3] In this case and in a later computation by POTENKHINA for NaCl : Ag[4] reasonable agreement with experiment has been obtained. However, certain quite serious questions have arisen in connection with the methods of computation used.[5]

LAX and others[6,7] have made studies on the interactions of such centers with the local lattice modes to which they give rise and have discussed the temperature dependence of the spectra. Recently KRISTOFFEL has made a significant contribution to the understanding of the electronic–vibrational coupling.[8]

During the past few years considerable interest has developed in both pure crystalline rare-gases and in solid rare-gases containing impurities, and several optical studies of their properties have been undertaken.[9,10,11] Magnetic resonance studies of impurity centers in these materials have also been performed.[12,13]

LÖWDIN has reviewed the advances which have been made in treating the ground-states of pure alkali-halide crystals from first principles.[14] Recently KNOX[15,16,17] has performed the first detailed quantum-mechanical and numerical computation on the optically preparable states of a pure insulating crystal, specifically the lowest-lying exciton bands in solid argon using the Heitler–London model. Thus far, however, no attempt has been made to predict the optical properties of an impurity center from first-quantum-mechanical principles.*

We here undertake the computation of the wave functions and absorption energies of the system composed of an isolated argon impurity in solid neon in the Heitler–London approximation using the symmetrical orthogonalization method[18] of LÖWDIN as developed by KNOX[15,16]. The overlapping of heterocentric atomic wave functions is explicitly taken into account through terms of second order in S (an overlap parameter to be defined). An exact diagonalization is made in the first order of perturbation theory, taking into account the effects of spin–orbit interaction and the crystal field for absorptions involving transitions to the ^1P and ^3P terms of the $3p^54s$ configuration of the argon impurity.

The absorption energies so obtained are then corrected for the dipole–dipole (van der Waals) interactions between the center and its neighbors using the variational method of BUCKINGHAM[19] for computing the van der Waals constants appropriate to the excited-states.

The oscillator strengths for the transitions are computed to first-order, and the method of DEXTER is used to obtain the integrated absorption coefficients.[20]

The emission energies of the system are calculated on a phenomenological, classical basis. As is customary, we (crudely) represent neighboring lattice distortion by a single "breathing mode" and the equilibrium configuration for the ground-state is estimated from empirical data using a Lennard-Jones (12,6) potential. The equilibria for the excited-states, and subsequently the emission energies, are calculated by fitting (12,6) potentials using the computed van der Waals and excitation energies.

Sections 1 through 7 treat the formalism of the problem, discussing successively he model and Hamiltonian, the symmetrically orthogonalized wave functions of LÖWDIN, the first-order energy matrix, the dipole–dipole interaction, the oscillator strengths, and the construction of the configuration coordinates. Section 8 is a general review of the method of numerical computation and Sections 9 through 11 present, respectively, numerical results for the first-order energy parameters, the van der Waals computation and emission energies, and the oscillator strengths and related quantities. The results of the calculation are discussed in Section 12 and comparison with available, related experimental data is made.

* Since the preparation of this manuscript, the paper by N. N. KRISTOFFEL, *Opt. i Spectrosk.* **7**, 45 (1959) (translation) has been brought to the author's attention. In this paper, configuration coordinate curves are constructed for the $^1S_0$ and $^3P_1$ states of the system KCl : Tl, and absorption and emission spectra associated with transitions between these states are computed quantum mechanically, using approximations outlined in Ref. (8). No detailed account of the calculation is given.

2. THE MODEL AND THE HAMILTONIAN

The model which we choose to represent an impurity center in a rare-gas crystal consists of an impurity atom of atomic number Z_A surrounded by a lattice of $N-1$ (identical) atoms of the host material having atomic number Z_I. The host atoms contained in the first shell of the impurity's neighbors are allowed to relax radially so as to minimize the energy of the system in its ground-state. These assumptions correspond to a concentration of impurities so low that interactions among impurity atoms may be neglected, and to the commonly made approximation that only the "breathing mode"[21] (the synchronous radial motion of all of the center's nearest neighbors) has an appreciable effect on the energy of the system. The Heitler–London or tight-binding approximation[22] is assumed valid; that is, the wave functions which serve as trial solutions are taken as orthonormalized, antisymmetrized products of one-electron functions of the free atomic constituents. In particular, the excited-states of the system to be considered are those wherein the impurity is in a state of localized excitation corresponding to one of its low-lying atomic levels. These levels are taken to be of sufficiently low energy that excitations of the host crystal will not be significantly coupled to them and that the resulting absorption bands will not be lost under the fundamental absorption of the host lattice.

For convenience we shall adopt a double subscript notation for electronic coordinates; this will consist of a pair of indices Jj where J runs over nuclear sites and j runs from 1 to Z_J.[23] In some instances it will be expedient to denote the impurity's electronic coordinates explicitly; in that event the indices Aa will be reserved for the center and the convention will be adopted that all running sums and products on J exclude A. In this notation the Hamiltonian for the system of $Z_J(N-1)$ host electrons and Z_A electrons centered on the impurity in a static equilibrium lattice may be written as:

$$H = -\frac{\hbar^2}{2m}\sum_I\sum_i \nabla_{Ii}^2 + \tfrac{1}{2}\sum_{I\neq J}\sum_J \frac{Z_I Z_J e^2}{|\boldsymbol{R}_I - \boldsymbol{R}_J|} +$$

$$+\tfrac{1}{2}\sum_I\sum_i\sum_{\substack{J\\ Ii\neq Jj}}\sum_j \frac{e^2}{|\boldsymbol{r}_{Ii}-\boldsymbol{r}_{Jj}|} -$$

$$-\sum_I\sum_i\sum_J \frac{Z_J e^2}{|\boldsymbol{r}_{Ii}-\boldsymbol{R}_J|} +$$

$$+\frac{i\hbar}{2m^2c^2}\sum_I\sum_i \boldsymbol{S}_{Ii}\cdot\nabla_{Ii}V(\boldsymbol{r}_{Ii})\times\nabla_{Ii}. \tag{2.1}$$

The five terms are, respectively, the kinetic energy of the electrons, the potential energy of the nuclei, the potential energy of the system of electrons, the potential energy of the electrons interacting with the nuclei, and finally the spin–orbit interaction. In equation (2.1) the symbols e, $\hbar$, c, and m have their usual meanings and ∇_{Ii} is the gradient operator for the coordinate $\boldsymbol{r}_{Ii}$. The notation $Ii \neq Jj$ means that every term for which $I = J$ and $i = j$ is excluded from the summation over I and i. The positions of the nuclei are denoted by $\boldsymbol{R}_I$. $V(\boldsymbol{r}_{Ii})$ is the potential due to all electrons and nuclei except electron Ii. $\boldsymbol{S}_{Ii}$ is the spin operator for electron Ii. We shall assume that the lattice maintains cubic point symmetry about the impurity A.* Nuclear kinetic energies are missing from (2.1). We assume the lattice to be static at its equilibrium configuration.

3. TRIAL WAVE FUNCTIONS

In treating the first-order problem we wish to find the eigenvalues and eigenfunctions of the Schrödinger equation

$$H\Psi_\alpha = E_\alpha\Psi_\alpha, \tag{3.1}$$

where H is given by (2.1). The method is straightforward. It consists of finding the eigenvalues and eigenvectors of the matrix H whose elements are formed using a suitable complete set of trial functions chosen for convenience, and with the Heitler–London model in mind.

(a) *Ground-state*

An unnormalized zero-order ground-state crystal wave function may be written

$$\chi_0(\boldsymbol{r},\boldsymbol{\sigma}) = \mathscr{A}_M \prod_a \phi_{Aa}(\boldsymbol{r}_{Aa},\boldsymbol{\sigma}_{Aa}) \prod_I \prod_i \phi_{Ii}(\boldsymbol{r}_{Ii},\boldsymbol{\sigma}_{Ii}). \tag{3.2}$$

* In particular we shall concern ourselves with a substitutional impurity in a face-centered cubic lattice.

Here $\mathscr{A}_M$ is the usual antisymmetrization operator operating on all M electrons of the system and is defined as

$$\mathscr{A}_M = (M!)^{-1/2} \sum_{\nu} (-1)^{p_\nu} P_\nu, \tag{3.3}$$

where P_ν is one of the $M!$ permutations of M objects, $(-1)^{p_\nu}$ is the parity of P_ν, and the sum runs over all $M!$ permutations of electronic coordinates. The ϕ_{Jj} are taken to be the normalized one-electron functions of an atom in its ground-state centered at nucleus J, and j denotes the set of central field quantum numbers, nlm_lm_s, describing each function. The vector $(\boldsymbol{r}, \boldsymbol{\sigma})$ stands for the entire set of electron space and spin coordinates and will often be omitted for brevity. The products over I and i run from 1 to $(N-1)$ and 1 to Z_I respectively and the product over a runs from 1 to Z_A.

In order to normalize χ_0 we adopt the well-known symmetrical orthogonalization technique introduced by LÖWDIN[14,18]. In computing $\int|\chi_0|^2\,d\tau$ the following overlap integrals are encountered:

$$S_{Ii,Jj} = \int \phi_{Ii}(\boldsymbol{r}, \boldsymbol{\sigma})^* \phi_{Jj}(\boldsymbol{r}, \boldsymbol{\sigma})\,d\tau - \delta_{IJ}\delta_{ij} \tag{3.4}$$

The deltas are the usual Kronecker symbols. LÖWDIN showed that an appropriate normalization constant compensating for the non-orthogonality of ϕ_{Ii} centered on different nuclei is automatically introduced into χ_0 if one replaces each function ϕ_{Ii} by the following linear combination of functions:

$$\varphi_{Jj}(\boldsymbol{r}, \boldsymbol{\sigma}) = \sum_{K=1}^{N} \sum_{k=1}^{Z_K} (\mathbf{I}+\mathbf{S})^{-1/2}{}_{Jj,Kk} \phi_{Kk}(\boldsymbol{r}, \boldsymbol{\sigma}) \tag{3.5}$$

Here $\mathbf{I}$ and $\mathbf{S}$ are the unit and overlap matrices respectively. Conditions for convergence and divergence of a power series expansion of the matrix elements encountered in (3.4) are discussed in detail in LÖWDIN's review.[14] We shall assume such an expansion converges and write φ_{Jj} explicitly to second-order in S as

$$\varphi_{Jj} = \phi_{Jj} - \tfrac{1}{2} \sum_K \sum_k S_{Kk,Jj}\phi_{Kk} + \\ + \sum_K \sum_k \sum_L \sum_l S_{Kk,Ll} S_{Ll,Jj} \phi_{Kk}. \tag{3.6}$$

Retention of higher order terms would lead to formidable formal complications and an impractically large quantity of numerical work.

The following function is a simple multiple of χ_0 and is normalized:

$$\Psi_0(\boldsymbol{r}, \boldsymbol{\sigma}) = \mathscr{A}_M \prod_a \varphi_{Aa}(\boldsymbol{r}_{Aa}, \boldsymbol{\sigma}_{Aa}) \prod_I \prod_i \varphi_{Ii}(\boldsymbol{r}_{Ii}, \boldsymbol{\sigma}_{Ii}). \tag{3.7}$$

The ground-state energy of the system is then given by

$$E_0 = \int \Psi_0^* H \Psi_0\,d\tau \tag{3.8}$$

We shall consider its evaluation in detail later.

(b) *States of localized excitation*

A normalized state in which the impurity atom has been raised to an excited-state λ is built in a manner completely analogous to that used in constructing the ground-state. It is given by

$$f_A(\lambda; \boldsymbol{r}, \boldsymbol{\sigma}) = \mathscr{A}_M \prod_a \varphi^\lambda_{Aa}(\boldsymbol{r}_{Aa}, \boldsymbol{\sigma}_{Aa}) \times \\ \times \prod_I \prod_i \varphi_{Ii(A\lambda)}(\boldsymbol{r}_{Ii}, \boldsymbol{\sigma}_{Ii}). \tag{3.9}$$

The symmetrically orthogonalized functions φ^λ_{Aa} and $\varphi_{Ii(A\lambda)}$ are defined exactly as in (3.6) with the exception that wherever an atomic function ϕ_{Aa} at site A appears, a function ϕ^λ_{Aa} belonging to the atomic excited state λ is to be used. The notation $\varphi_{Ii(A\lambda)}$ is used only for $I \neq A$.

Although we have built the state $f_A(\lambda)$ from single determinants of one-electron functions it is feasible and desirable to use linear combinations of the zero-order functions which will diagonalize all or part of the atomic Hamiltonian. Thus, the localized excitation states actually used in the computation may be of the form

$$\Phi_A(\mu) = \sum_\lambda (\mu|\lambda) f_A(\lambda), \tag{3.10}$$

where the coefficients $(\mu|\lambda)$ are exactly those obtained from constructing linear combinations of zero-order determinants in the related atomic problem.[24] The states λ and coefficients most convenient to use in treating the p^5s configuration at sites of cubic symmetry use the Cartesian form

Vol. 18
1961

of the p function as given by KNOX[25] and will be used throughout the present paper.

We shall assume that excited states of the host crystal atoms are sufficiently energetically separated from those of the p^5s configuration of the impurity that they need not be mixed with the localized excitation here. If, for example, we consider an argon impurity in solid neon we have excitation energies of the order of 11·6 eV for the impurity compared with 16·7 eV for the host.[26,27] Host crystal absorption as treated in the work of DEXTER[20] will not be considered in the present calculation.

4. MATRIX ELEMENTS

Since the Franck-Condon principle states that excitations will take place between Born-Oppenheimer states having the same nuclear configuration, we may proceed to compute the first-order absorption energy using a static array of nuclei in positions corresponding to those giving a minimum total energy for the ground-state of the system, E_0. Using this ground-state energy as a reference we shall calculate

$$E_1(\mu,\mu') = (\mu|H|\mu') - E_0\delta_{\mu\mu'}, \tag{4.1}$$

where

$$(\mu|H|\mu') = \int \Psi_A^*(\mu) H \Psi_A(\mu')\, d\tau \tag{4.2}$$

We shall explicitly treat the case of an excited impurity in a p^5s configuration. Its normal configuration is taken to be p^6 and it is assumed to rest substitutionally in an otherwise perfect monatomic lattice whose constituents are in p^6 normal states. It will be further assumed that the spin–orbit term of H [equation (2.1)] is "atomic" in nature, i.e. that the expectation value of $\nabla V \times \nabla$ contributes to $(\mu|H|\mu')$ only in the vicinity of the nucleus of excited atom A. This assumption removes the necessity of considering spin-induced splitting by the crystal field, and is quite reasonable, since the atomic spin–orbit interaction is associated with the tightly bound p^5 hole rather than with the spatially extended s electron. These assumptions are discussed by KNOX in Ref. (15). As KNOX has pointed out, great care must be taken in applying them to excited states where the atomic p function involved in the spin–orbit interaction is *not* tightly bound to its lattice site.[16,28] Thus, we replace the last term of (2.1) by

$$H_s = \sum_I \sum_i \xi_I(\mathbf{r}_{Ii}) \boldsymbol{L}_{Ii} \cdot \boldsymbol{S}_{Ii}, \tag{4.3}$$

where $\boldsymbol{L}_{Ii}$ is the orbital angular momentum operator $i\hbar \mathbf{r}_{Ii} \times \nabla_{Ii}$ and ξ_I is defined by

$$\xi_I(r) = (2m^2c^2r_I)^{-1} \partial V(r_I)/\partial r_I, \tag{4.4}$$

in which $r_I = |\mathbf{r} - \mathbf{R}_I|$.

The matrix $\mathbf{E}_1(\mu,\mu')$ connecting the twelve p^5s states discussed in Section 3 and in Ref. (16) is found to have the following form:

$$\mathbf{E}_1 = \begin{bmatrix} \mathbf{A}_1 & \mathbf{O} & \mathbf{O} \\ \mathbf{O} & \mathbf{A}_2 & \mathbf{O} \\ \mathbf{O} & \mathbf{O} & \mathbf{A}_3 \end{bmatrix}, \tag{4.5}$$

where

$$\mathbf{A}_1 = \begin{array}{c} \\ X \\ Y \\ Z \\ X' \\ Y' \\ Z' \end{array} \begin{array}{c} \begin{array}{cccccc} X & Y & Z & X' & Y' & Z' \end{array} \\ \begin{bmatrix} {}^1E & 0 & 0 & -\lambda\zeta/\sqrt{(2)} & 0 & 0 \\ 0 & {}^1E & 0 & 0 & -\lambda\zeta/\sqrt{(2)} & 0 \\ 0 & 0 & {}^1E & 0 & 0 & -\lambda\zeta/\sqrt{(2)} \\ -\lambda\zeta/\sqrt{(2)} & 0 & 0 & {}^3E+\frac{1}{2}\zeta & 0 & 0 \\ 0 & -\lambda\zeta/\sqrt{(2)} & 0 & 0 & {}^3E+\frac{1}{2}\zeta & 0 \\ 0 & 0 & -\lambda\zeta/\sqrt{(2)} & 0 & 0 & {}^3E+\frac{1}{2}\zeta \end{bmatrix} \end{array}, \tag{4.6}$$

$$\mathbf{A}_2 = \begin{array}{c} \\ XY \\ YZ \\ ZX \\ ZR \\ YY \end{array} \begin{array}{c} \begin{array}{ccccc} XY & YZ & ZX & ZR & YY \end{array} \\ \left[\begin{array}{ccccc} {}^3E-\frac{1}{2}\zeta & 0 & 0 & 0 & 0 \\ 0 & {}^3E-\frac{1}{2}\zeta & 0 & 0 & 0 \\ 0 & 0 & {}^3E-\frac{1}{2}\zeta & 0 & 0 \\ 0 & 0 & 0 & {}^3E-\frac{1}{2}\zeta & 0 \\ 0 & 0 & 0 & 0 & {}^3E-\frac{1}{2}\zeta \end{array}\right] \end{array}, \tag{4.7}$$

$$\mathbf{A}_3 = \begin{array}{c} \\ R \end{array} \begin{array}{c} \begin{array}{c} R \end{array} \\ \left[\begin{array}{c} {}^3E+\zeta \end{array}\right] \end{array} \tag{4.8}$$

The submatrices **O** denote appropriate blocks of zeros and the abbreviations "XR" $= 3X^2-R^2$ and "YY" $= Y^2-Z^2$ have been used in labeling the rows and columns of $\mathbf{A}_2$. The various quantities appearing in the matrix elements are defined as follows

$$^1E = \int \Psi_A(X)^*(H-H_s)\Psi_A(X)\,d\tau - E_0, \tag{4.9}$$

$$^3E = \int \Psi_A(X')^*(H-H_s)\Psi_A(X')\,d\tau - E_0, \tag{4.10}$$

$$\zeta = 2\int \Psi_A(X')^* H_s \Psi_A(X')\,d\tau, \tag{4.11}$$

$$\lambda\zeta = -\sqrt{(2)}\int \Psi_A(X)^* H_s \Psi_A(X')\,d\tau \tag{4.12}$$

Although the non-zero matrix elements themselves are considerably more complicated, $\mathbf{E}_1$ is seen to have exactly the same form as the corresponding atomic p^5s matrix.[24] BETHE has shown that terms of different J will not mix regardless of the nature of the interactions in H, so long as H has cubic symmetry.[29] This accounts for the null submatrices in (4.5). One further expects the states X, Y, Z to be degenerate and uncoupled from one another; the same statement applies to X', Y', Z'. Thus we need concern ourselves only with optically preparable $J = 1$ states. We further notice that (4.6) is diagonal with respect to the Cartesian components of the P states reducing the secular problem to a two-by-two diagonalization involving, say, Y and Y' states. This is completely analogous to the secular problem encountered in work on phosphors like KCl : Tl.[5]

The quantities (4.9) through (4.12) have been computed in the S^2 approximation. This means that any quantity which involves more than two products of orthogonal or heterocentric wave functions is dropped. In the case of ^1E and ^3E one first writes the total energy of the crystal in the form introduced by LÖWDIN[18] with the exception that the Z_A wave functions associated with atom A belong to appropriate zero-order excited-states of the atom. Then the original expression for E_0 is subtracted analytically from $(\mu|H|\mu)$ of the excited-state μ. A straightforward but extremely lengthy algebraic computation produces the result

$$^3E = \epsilon_A+\epsilon_C+\epsilon_X+\epsilon_L+\epsilon_T, \tag{4.13}$$

where ϵ_A is the difference between the energies of the pure-triplet and ground-states of the free atom, and the "Coulomb", "exchanges", "LÖWDIN", and "three-center" terms are defined, respectively, as

$$\begin{aligned}
\epsilon_C = &\sum_a [1+\sum_K \sum_k (\bar{S}_{Kk,Aa})^2] \int |\phi_{Aa}|^2 C^A\,d\tau \\
&- \sum_a [1+\sum_K \sum_k (S_{Kk,Aa})^2] \int |\phi_{Aa}|^2 C^A\,d\tau \\
&+ \sum_a \sum_K \sum_k [(\bar{S}_{Kk,Aa})^2 \int |\phi_{Kk}|^2 (C^{AK}+\bar{C}_A)\,d\tau \\
&-(S_{Kk,Aa})^2 \int |\phi_{Kk}|^2 (C^{AK}+C_A)\,d\tau] \\
&+ \sum_K \sum_k \sum_{J\neq K} \sum_j (S_{Kk,Jj})^2 \int |\phi_{Kk}|^2 (\bar{C}_A - C_A)\,d\tau,
\end{aligned} \tag{4.14}$$

Vol. 18
1961

$$\epsilon_X = -\sum_a \sum_K \sum_k [(Kk, \overline{Aa}|g|\overline{Aa}, Kk) - (Kk, Aa|g|Aa, Kk)], \quad (4.15)$$

$$\epsilon_L = -\sum_a \sum_K \sum_k [(\bar{S}_{Kk,Aa})^2(Kk, \overline{Aa}|g|Kk, \overline{Aa}) - (S_{Kk,Aa})^2(Kk, Aa|g|Kk, Aa)], \quad (4.16)$$

^1E differs from ^3E only in that appropriate (singlet) radial wave functions are used in the computation and ϵ_A is to be taken as the energy difference between the pure-singlet and ground-state energies of the free atom.

It should be pointed out that the last terms of both (4.14) and (4.17) were omitted by KNOX in each of his corresponding equations.[15,16] However

$$\epsilon_T = -\sum_a \sum_K \sum_k [\bar{S}_{Kk,Aa} \int \bar{\phi}_{Aa}(2C^{KA} + C_K^k + \bar{C}_A^a)\phi_{Kk}\, d\tau - S_{Kk,Aa} \int \phi_{Aa}(2C^{KA} + C_K^k + C_A^a)\phi_{Kk}\, d\tau] - 2\sum_K \sum_k \sum_{J \neq K} \sum_j S_{Kk,Jj} \int \phi_{Kk}(\bar{C}_A - C_A)\phi_{Jj}\, d\tau \quad (4.17)$$

In equations (4.14) through (4.17) a bar over any symbol means that wave functions from the excited (triplet) configuration are to be used when atom A is involved. Elsewhere, ground-state functions are used. The following additional abbreviations have been made

$$C_L(\boldsymbol{r}) = \sum_l \int |\phi_{Ll}(\boldsymbol{r}', \boldsymbol{\sigma}')|^2 e^2 |\boldsymbol{r}' - \boldsymbol{r}|^{-1}\, d\tau' - Z_L e^2 |\boldsymbol{R}_L - \boldsymbol{r}|^{-1}, \quad (4.18)$$

$$C^{L,M,\ldots,T} = \sum_{K \neq L,M,\ldots,T} C_K(\boldsymbol{r}), \quad (4.19)$$

$$(Ii, Jj|g|Kk, Ll) = \int \phi_{Ii}(1)^* \phi_{Jj}(2)^* \frac{e^2}{r_{12}} \phi_{Kk}(1)\phi_{Ll}(2)\, d\tau_1 d\tau_2 \quad (4.20)$$

Thus, C_L is the classical Coulomb potential due to the entire atom L when its electrons are in states labeled $l = 1, 2, \ldots, Z_L$, and $C^{L,M,\ldots,T}$ is the combined potential due to all atoms in the lattice except $L, M, \ldots T$. When the k-th electron is to be excluded from the sum in $C_L(\boldsymbol{r})$, we write $C_L^k(\boldsymbol{r})$.

The summations over a in (4.14) through (4.17) run over the configuration $1s^2 \ldots np^6$ in the ground-state and over $1s^2 \ldots np^5 n's$ when the center is excited. In the latter case the np functions may be chosen as $npx+$, $npx-$, $npy+$, $npy-$, $npz+$. It has been shown[15] that in the S^2 approximation they are both small in magnitude and probably give rise to no serious numerical errors in his work.

The atomic wave functions used in computations from (4.14) through (4.17) must be solutions of the atomic Hartree–Fock equations. If they are not, additional exchange corrections as given by LÖWDIN[14] are necessary.

KNOX has given many helpful formulae for the evaluation of ϵ_C, ϵ_L, ϵ_X, and ϵ_T[15] and we have developed others which are particularly convenient for performing sums in a distorted lattice. All of these terms are of importance when computed numerically for the case of an argon impurity in solid neon. The first three give rise to appreciable depressions of the excitation energy. The three-center term provides a very large positive contribution.

After a tedious derivation, we find the spin–orbit parameters λ and ζ are given to order S^2 by the relationships

$$\zeta = [1 + \tfrac{3}{4}\sum_K \sum_k (\bar{S}_{Kk,npz+})^2]\zeta_p + \tfrac{1}{4}\sum_K \sum_k \sum_{k' \neq k} \bar{S}_{Kk,npz+}\bar{S}_{Kk',npz+} \times \int \phi_{Kk} H_s \phi_{Kk'}\, d\tau - \sum_K \sum_k (\bar{S}_{Kk,npz+} \int \phi_{Kk} H_s \bar{\phi}_{npz+}\, d\tau), \quad (4.21)$$

$$\lambda\zeta = \{1+\tfrac{3}{8}\sum_K\sum_k[(\bar{S}_{Kk,npz+})^2+(\bar{S}_{Kk,npz+})^2]\}\lambda_p\zeta_p+$$

$$+\tfrac{1}{4}\sum_K\sum_k\sum_{k'}(\bar{S}'_{Kk,npz+}\bar{S}_{Kknpz+}\int\phi_{Kk}H_s\phi_{Kk'}\,d\tau)-$$

$$-\tfrac{1}{2}\sum_K\sum_k(\bar{S}'_{Kk,npz+}\int\phi_{Kk}H_s\phi_{npz+}\,d\tau+$$

$$+\bar{S}_{Kk,npz+}\int\phi'_{npz+}H_s\phi_{Kk}\,d\tau) \tag{4.22}$$

Here ζ_p and λ_p are the atomic spin–orbit parameters and primed quantities with a bar over them are to be evaluated using functions belonging to the atomic pure-singlet. Equation (4.22) is identical with the similar expression given in the appendix of Ref. (28). Equation (4.21) is derived in an entirely analogous manner. In the argon-in-neon computation only those terms containing ζ_p and $\lambda_p\zeta_p$ contribute appreciably to the spin–orbit parameters of the system. The remainder are listed here for the sake of completeness.

It must be pointed out that the simplicity of the first-order expressions for the excitation energy presented above is a result of taking energy *differences* with the nuclear positions held fixed. If one wished to perform a complete calculation for a configuration coordinate model this analytic procedure could not be used because of the presence of many terms dependent parametrically on nuclear positions. However, if one were able to construct a suitable ground-state configuration coordinate in some appropriate and simple manner (perhaps semi-empirically) the first-order excited state curve could be constructed, in principle, by repeated point by point application of the results of the present section.

5. VAN DER WAALS INTERACTIONS

Since the bonding of a molecular crystal is entirely due to van der Waals forces it seems necessary to take them into account in a computation of excitation energies. In the usual treatment of such problems it is customary to expand the electrostatic inaction between pairs of atoms in a multipole series and then to treat the dipole–dipole (and perhaps the dipole–quadrupole) interactions explicitly. These are written in the form $-(c_1R_{12}^{-6}+$ $+c_2R_{12}^{-8}+\ldots)$ where R_{12} is the internuclear separation and c_1 and c_2 are constants. The validity of such a procedure in cases where the charge distributions involved are overlapping has been discussed in detail by BROOKS[30]. He concludes that though the procedure is, of course, not rigorously justified, it nonetheless may be expected to give reasonable results if only the lower order terms of the expansion are considered at small internuclear separations.

In solids it is usually assumed that only two-body interactions are of importance and the van der Waals energy is evaluated using the simple lattice sums given by LENNARD-JONES and INGHAM[31]. Three-body interactions in solid argon have been examined by AXILROD and have been shown to be negligibly small.[32]

Theoretical study of dipole–dipole interactions has been conducted along two principal lines. The first is the use of second-order perturbation theory. A rigorous pursuit of the treatment would require the knowledge of *all* of the excited-state wave functions of the constituents of the system and is therefore so difficult as to be out-of-the-question. EISENSCHITZ and LONDON introduced certain simplifying assumptions into the theory which permit the computation of van der Waals constants to be made from an empirical knowledge of the polarizabilities and first ionization potentials of the atoms involved.[33] MARGENAU has given a thorough review of progress made in its application.[34] The second approach is the use of the Ritz-Rydberg variational principle. Earliest work with this method was carried out by SLATER[35] and KIRKWOOD[36] and it was further developed by BUCKINGHAM[19]. Here knowledge of the wave functions of the constituent atoms in the state of immediate interest is sufficient to perform the computation.

There are two objections to the use of the Eisenschitz–London method in the present computations. First, the polarizabilities of rare-gas atoms in excited-states are not experimentally known. Second, the use of such a procedure would seem contrary to the spirit of computing the excitation energies from first principles. Thus, we adopt the method of BUCKINGHAM to compute van der Waals constants for the ground- and excited-states of our system. The energy differences thus encountered will be added to the first-order excitation energies derived from the results of

Vol. 18
1961

Section 4. A calculation of van der Waals interactions formally similar to ours has been made by POTEKHINA in considering the system NaCl : Ag.[4]

BUCKINGHAM computes the dipole–dipole interaction between two atoms assuming that the wave function for the system is represented by a simple product of the two (antisymmetrized) atomic wave functions. The details of the computation will not be repeated here.* The result for the dipole–dipole interaction is as follows

$$E_{d-d} = -C(1,2)/R^6, \tag{5.1}$$

$$C(1,2) = \tfrac{4}{9} \sum_{1i} \sum_{2j} (R^2)_{1i}^2 (R^2)_{2j}^2 / [(R^2)_{1i} + (R^2)_{2j}], \tag{5.2}$$

where

$$(R^2)_{Kk} = (Kk|r^2|Kk) - \sum_{k' \neq k} [(Kk|x|Kk')^2 + (Kk|y|Kk')^2 + (Kk|z|Kk')^2]. \tag{5.3}$$

In the matrix elements of (5.3) the symbols r, x, y, z retain their usual meaning as coordinates measured from the nucleus of atom K. The summations on i and j in (5.2) run only over quantum numbers occupied by electrons in the atomic state considered. We include this last statement to emphasize the fact that electronic wave functions belonging to higher excited states are unnecessary in BUCKINGHAM's formalism.

Only the dipole–dipole interaction will be taken into account in the present computation. DOBBS and JONES have discussed the validity of neglecting higher order terms for the ground-state of rare-gases and conclude that satisfactory fits to elastic and thermodynamic data may be made using a simple LENNARD-JONES (12, 6) potential.[37] It would seem inconsistent to include higher multipole effects for the excited-states without also including second-order exchange interactions between pairs of atoms; the use of a simple product of atomic wave functions as encountered in BUCKINGHAM's work excludes these.

* Though we have verified BUCKINGHAM's final results we note that several of the evaluation theorems concerning integrals containing products of minors of SLATER determinants are incorrect. However, the errors made seem to be compensatory.

6. OSCILLATOR STRENGTHS AND INTEGRATED ABSORPTION COEFFICIENTS

Using the customary procedure[24] for the exact diagonalization of the two-by-two matrix connecting the $J = 1$ singlet and triplet states of the same m the following expressions are obtained for the dipole matrix elements for electric dipole transitions to the optically preparable first-order states of the p^5s configuration

$$^1\boldsymbol{M} = \int \Psi(^1S_0)^* \sum_i e\boldsymbol{r}_i \Psi(^1P_1)\, d\tau = (1+\zeta^2\mathscr{F}^{-2})^{-1/2}\, \boldsymbol{d}_0, \tag{6.1}$$

$$^3\boldsymbol{M} = \int \Psi(^1S_0)^* \sum_i e\boldsymbol{r}_i \Psi(^3P_1)\, d\tau = (1+\mathscr{F}^2\zeta^{-2})^{-1/2}\, \boldsymbol{d}_0. \tag{6.2}$$

Here $\boldsymbol{d}_0$ is the dipole matrix element obtained evaluating the integral

$$\int \Psi(^1S_0)^* \sum_i e\boldsymbol{r}_i \Psi(^1P)\, d\tau$$

using wave functions belonging to the pure singlet state of the system. The spin–orbit parameters ζ and λ are defined in Section 4,

$$\frac{1}{\sqrt{(2)}}\mathscr{F} \equiv \tfrac{1}{2}\Delta - \tfrac{1}{4}\zeta + [(\tfrac{1}{2}\Delta - \tfrac{1}{4}\zeta)^2 + \tfrac{1}{2}\lambda^2\zeta^2]^{1/2}, \tag{6.3}$$

and $\Delta \equiv {}^1E - {}^3E$. Corrected to second-order in overlap $\boldsymbol{d}_0$ is given by

$$\boldsymbol{d}_0 = \boldsymbol{M}_0 + \boldsymbol{\rho}, \tag{6.4}$$

where

$$\boldsymbol{M}_0 = e \int \phi_{A4s}(\boldsymbol{r})\boldsymbol{r}\phi_{A3px_\alpha}(\boldsymbol{r})\, d\boldsymbol{r}, \tag{6.5}$$

and

$$\boldsymbol{\rho} = \{\delta + \tfrac{1}{2}\sum_I \sum_i [(S_{Ii,3px_\alpha})^2 + (\bar{S}_{Ii,4s})^2]\}\boldsymbol{M}_0 - \sum_I \sum_i S_{Ii,3px_\alpha} \int \phi_{4s} e\boldsymbol{r}\phi_{Ii}\, d\boldsymbol{r} - \sum_I \sum_i \bar{S}_{Ii,4s} \int \phi_{3px_\alpha} e\boldsymbol{r}\phi_{Ii}\, d\boldsymbol{r} + \sum_I \sum_i S_{Ii,3px_\alpha}\bar{S}_{Ii,4s} \int e\boldsymbol{r}|\phi_{Ii}|^2\, d\boldsymbol{r}. \tag{6.6}$$

The quantity δ is a correction term which accounts for the fact that the expressions

$$\int \phi_\mu(\mathbf{r})\phi_\nu(\mathbf{r})\, d\tau - \delta_{\mu\nu}$$

do not in general vanish. It is defined and computed in Appendix A of Ref. (15).

In complete analogy to the free atomic case[27,28] the oscillator strengths for the singlet and triplet transitions are given, respectively, by

$$^1f = \frac{8\pi^2\nu(^1P_1, {}^1S_0)}{he^2} \frac{(|d_0|^2 - |\rho|^2)}{(1+\zeta^2\mathscr{F}^{-2})}, \qquad (6.7)$$

$$^3f = \frac{8\pi^2\nu(^3P_1, {}^1S_0)}{he^2} \frac{(|d_0|^2 - |\rho|^2)}{(1+\mathscr{F}^2\zeta^{-2})} \qquad (6.8)$$

where the quantities $\nu(\lambda, {}^1S_0)$ are the first order transition frequencies. The quantity $|d_0|^2 - |\rho|^2$ instead of $|d_0|^2$ is used in the numerators of (6.7) and (6.8) in order to eliminate terms of fourth-order in overlap.

Following DEXTER[20] we write the integrated adsorption coefficient as

$$\int \mu_\lambda(E)\, dE = \frac{1}{n}\left(\frac{2\pi e^2\hbar}{mc}\right)\left(\frac{n^2+2}{3}\right)^2 N_0{}^\lambda f, \qquad (6.9)$$

where ${}^\lambda f$ is the oscillator strength for the transition as given above, N_0 is the concentration of impurities, and n is the index of refraction of the host crystal at the energy of the transition. The errors, uncertainties and implications of equation (6.9) are discussed in Ref. (20).

7. CONSTRUCTION OF CONFIGURATION COORDINATES

In order to compute the energies at which impurity-induced absorptions and emissions will occur it is necessary to have a knowledge of the energy of the system as a function of all nuclear coordinates. Since this is obviously an impractical task using all 10^{23} nuclear coordinates involved, it has become customary to reduce the number which are taken into account to a tractable few, in particular, one. The coordinate customarily retained is the so called "breathing mode" which involves only the synchronous radial motion of the impurity's nearest neighbors.[1,3,4] In addition to being the local mode which intuitively seems most effective in determining the energy of the system, it possesses, in a cubic lattice, the further virtue of preserving the simple symmetry properties of the system. We shall adopt its use without further ado, noting only that a justification can be given for the formal procedure of treating only one mode, even when many modes of oscillation are known to be important.[6,7a]

The ground-state configuration for a dilute rare-gas alloy could, in principle, be computed by repeated application of LÖWDIN's method for the determination of binding energies. However, in the absence of ionic (Madelung) contributions encountered in computations involving, for example, alkali-halides, this task becomes exceedingly difficult, involving poorly known small differences between large numbers and the inaccuracies attendant to strong dependence on the tails of Hartree–Fock atomic wave functions. For excited-states involving highly overlapping wave functions the situation is even worse and the labor involved multiplied. Thus, in the present paper, we resort to a semi-empirical treatment. The ground-state configuration coordinate is constructed using a Lennard–Jones (12,6) potential and the data on rare-gas crystals compiled by DOBBS and JONES[37]. The excited-state configuration coordinates are constructed from a (12,6) potential using a van der Waals constant computed by the method of Section 5 and a repulsive coefficient determined by the energy difference between the ground-state minimum and the excited state calculated using the formalisms of Sections 4 and 5, at the ground-state equilibrium lattice distance. Thus, emission energies may be computed on a classical, phenomenological basis, in analogy to the method which has been used in heavy-metal sensitized alkali-halide phosphors.[3,4] These results should not be taken to represent a theoretical determination of luminesence spectra from first principles. At best the emission predictions are of a semi-quantitative or qualitative nature.

(a) *Ground-state equilibrium*

The interaction energy of a pair of rare-gas atoms may be written empirically as

$$E(R_{AB}) = 4\epsilon_{AB}[(\sigma_{AB}/R_{AB})^{12} - (\sigma_{AB}/R_{AB})^6], \qquad (7.1)$$

Vol. 18
1961

where R_{AB} is the internuclear distance between atoms A and B, ϵ_{AB} is the depth of the potential well between them and σ_{AB} is the intercept of the potential on the R_{AB} axis. Using the results of LENNARD-JONES and INGHAM[31] we may write the interaction of a single atom of type A with the rest of an undistorted face-centered cubic lattice composed of atoms of type B as

$$E(a_{AB}) = 4\epsilon_{AB}[12{\cdot}13(\sigma_{AB}/a_{AB})^{12} - -14{\cdot}45(\sigma_{AB}/a_{AB})^{6}], \quad (7.2)$$

where a_{AB} is the nearest neighbor distance for the host lattice. To account for the relaxation of the nearest neighbors of the center in determining the ground-state equilibrium position we correct (7.2) to read

$$E(a_{AB}+q) = E(a_{AB})+\Delta E_1(q)+\Delta E_2(q), \quad (7.3)$$

where in a face centered cubic lattice

$$\Delta E_1(q) = 48\epsilon_{AB}[(\sigma_{AB}/a_{AB})^{12}-(\sigma_{AB}/a_{AB})^{6}- -(\sigma_{AB}/[a_{AB}+q])^{12}+(\sigma_{AB}/[a_{AB}+q])^{6}], \quad (7.4)$$

$$\Delta E_2(q) = 96\epsilon_{BB}[(\sigma_{BB}/a_{AB})^{12}-(\sigma_{BB}/a_{AB})^{6}- -(\sigma_{BB}/[a_{AB}+q])^{12}+(\sigma_{BB}/[a_{AB}+q])^{6}]. \quad (7.5)$$

Here q is the deviation from the host crystal nearest neighbor distance in the separation of the atoms in the breathing shell from the center. $\Delta E_1(q)$ represents the change of the interaction between the impurity and its neighbors; $\Delta E_2(q)$ is the change in energy among the host atoms. The equilibrium distance for the ground-state is found simply by inserting the empirically determined nearest neighbor distance for the host as a_{AB} and differentiating (7.3) with respect to q.

In deriving the equilibrium position from the data given by DOBBS and JONES[37] it is necessary to use the following well-known semi-empirical "combining relationships" for the constants ϵ_{AB} and σ_{AB}.[38] Given that ϵ_{AA}, ϵ_{BB}, σ_{AA}, σ_{BB} are the constants appropriate to pairs of atoms of the same species we have

$$\epsilon_{AB}\sigma_{AB}^{6} = \sigma_{AA}^{3}\sigma_{BB}^{3}(\epsilon_{AA}\epsilon_{BB})^{1/2}, \quad (7.6)$$

$$\epsilon_{AB} = (\epsilon_{AA}\epsilon_{BB})^{1/2} \quad (7.7)$$

(b) *Luminescence spectra*

It is convenient for our present purposes to rewrite (7.1) in the form

$$E(R_{AB}) = \frac{A_{AB}}{R_{AB}^{12}} - \frac{C(AB)}{R_{AB}^{6}} \quad (7.8)$$

Here $C(AB)$ is the same as the van der Waals constant encountered in Section 5 and A_{AB} is the appropriate constant for the repulsion. Then for the system as a whole in an excited state we write, (neglecting small changes in host–host interactions)

$${}^{\mu}E_{\text{abs}} - {}^{\mu}E_{\text{atomic}} = \sum_{B}\left\{\frac{({}^{\mu}A_{AB}-{}^{0}A_{AB})}{{}^{0}R_{AB}^{12}} - - \frac{[{}^{\mu}C(AB)-{}^{0}C(AB)]}{{}^{0}R_{AB}^{6}}\right\}, \quad (7.9)$$

$${}^{\mu}E_{\text{lum}} - {}^{\mu}E_{\text{atomic}} = \sum_{B}\left\{\frac{({}^{\mu}A_{AB}-{}^{0}A_{AB})}{{}^{\mu}R_{AB}^{12}} - - \frac{[{}^{\mu}C(AB)-{}^{0}C(AB)]}{{}^{\mu}R_{AB}^{6}}\right\}. \quad (7.10)$$

In (7.9) and (7.10) the prescript zero refers to the ground-state, the prescript μ on the various symbols indicates the excited-state to which absorption and from which emission takes place, ${}^{\mu}E_{\text{abs}}$ is the absorption energy at the ground-state equilibrium as computed from Sections 4 and 5, ${}^{\mu}E_{\text{atomic}}$ is the excitation energy of the corresponding atomic state, and the ${}^{\mu}R_{AB}$ are the equilibrium separations for the states in question; ${}^{\mu}E_{\text{lum}}$ is the energy of the emission from the minimum of the excited state curve. Knowing ${}^{\mu}E_{\text{abs}}$, ${}^{\mu}E_{\text{atomic}}$, ${}^{0}R_{AB}$, ${}^{0}A_{AB}$ and the various van der Waals constants we may proceed to calculate ${}^{\mu}A_{AB}$, ${}^{\mu}R_{AB}$, and hence ${}^{\mu}E_{\text{lum}}$. Again we emphasize that such a procedure is no better than semi-quantitative.

8. GENERAL REMARKS ON THE COMPUTATION FOR THE SYSTEM Ne : A

Though several computations of a semi-quantitative nature have been carried out for impurity states in ionic crystals, no detailed quantitative account of them has been made in the tight-binding approximation. KNOX has carried out the first complete numerical calculation of optical

absorption by a pure crystal based on the present first-order formalism.[15,16,17] The most ambitious attempts at treating the impurity problem have been made by WILLIAMS[3] and POTEKHINA[4] who did not explicitly account for overlap. This is wholly understandable in terms of the amount of labor encountered in the numerical evaluation of energies through terms of order S^2.*

We have chosen to consider the system Ne : A in detail for several reasons. The lattice, in its ground-state, is a cubic array of neutral atoms in closed-shell configurations and the absence of strong ionic or covalent bonds leads to relatively large interatomic spacings. Thus, we would expect the tight-binding approximation to hold best in such a simple molecular crystal. Neon is the rare-gas of lowest atomic number which crystalizes in a cubic lattice, and argon is the lightest rare-gas which has a lower absorption than this host and will thus be expected to lead to minimum lattice distortion; finally, necessary Hartree–Fock atomic wave functions are available for both species in the states to be considered.[26,39,40]

Vol. 18
1961

Only states built from the $3p^5 4s$ configuration of the argon impurity will be considered. Hartree–Fock functions for the higher excited-states of the argon atom are not known and, in any event, their inclusion would force explicit consideration of configuration interactions both between the atomic argon states and with the excited states of the host lattice, vastly increasing the complexity of the problem.

The two- and three-center integrals involving atomic wave functions are evaluated using the alpha-function method of LÖWDIN[14] which was used in a somewhat different notation by KUNIMUNE[41]. As the lattice constant representative of a real neon crystal we choose $5{\cdot}9\ a_0$ (nearest neighbor distance) in accordance with the recent measurements of HENSHAW[42]. Using the method of Section 7 the equilibrium separation of the impurity from its nearest neighbors is found to be $6{\cdot}3\ a_0$. Ground-state and excited-state argon functions were interpolated and tabulated at constant intervals of $0{\cdot}05\ a_0$ for use in computing the necessary alpha-functions. Ground-state neon functions were similarly treated. The interval $0{\cdot}05\ a_0$ was chosen because it was small enough to yield a reasonable picture of the wave functions as they varied rapidly near the nuclei, but large enough to restrict the functions to a reasonable number of tabular entries. (It was also small enough to ensure the accuracy of the necessary "Simpson's rule" integrations.) Because of the large spatial extent of the singlet and triplet $4s$ functions it was necessary in many instances to extend the computations through third neighbors and through $1s$ functions on the neighbors.

The numerical work described herein was carried out at the University of Rochester Computing Center, using an IBM type-650 Magnetic Drum Data Processing Machine. Three machine-language programs by Rimmer and Knox were used for the major tasks of evaluating alpha-functions and double and single integrals.[43] The computation required about one-hundred and thirty hours of machine running time. Analytic reduction of the integrals to explicit form for machine evaluation, organization of the material and preparations for machine operation consumed something over twice this amount of time and about one-hundred and twenty thousand punched cards.

9. COMPUTATION OF FIRST-ORDER ENERGY PARAMETERS

Our first task will be the computation of the "electrostatic" energy change, ${}^{2S+1}E$, of (4.13), giving the first-order energy change of the system when the impurity is raised from its normal configuration to a state of definite multiplicity $2S+1$ in the $3p^5 4s$ configuration. Equations (4.14) through (4.17) are used in obtaining ${}^{2S+1}E$ from Hartree–Fock functions. The quantities λ and ζ are computed from equations (4.21) and (4.22). The lattice sums encountered in these computations are straightforward and most have been treated in Ref. (15). Only the essential features of the numerical work will be presented here.

Table 1 summarizes the first-order electrostatic contributions as listed in equation (4.13) for the

* *Note added in proof:* Since the completion of the present work the paper of POTEKHINA N. D., *Opt. i Spectrosk.* **8,** 437 (1960) has appeared. In it absorption and emission energies are calculated in a configuration coordinate model for the ${}^3D$ term of the $4d^9 5p$ configuration of the silver ion impurity in NaCl : Ag. Overlap is taken into account to second-order but spin–orbit interaction is neglected. There seems to be some question about the convergence of the overlap expansion in the calculation which is not discussed.

Table 1. Contributions to ^1E and ^3E, the first-order electrostatic energy of the pure-singlet and triplet crystal states relative to the ground-state. A discussion of the calculation is given in the text. All energies are measured in electron volts

	Singlet		Triplet	
Interaction	Contribution	Running total	Contribution	Running total
ϵ_C	− 2·876	− 2·876	− 2·169	− 2·169
ϵ_L	− 0·555	− 3·431	− 0·495	− 3·114
ϵ_X	− 3·899	− 7·330	− 3·725	− 6·839
ϵ_T	+ 8·083	+ 0·753	+ 7·666	+ 0·827
ϵ_A	+11·357	+12·110	+11·188	+12·015

singlet and triplet terms. The quantities ϵ_A are the pure-singlet and pure-triplet energies computed for the free atom in Ref. (26), with a probable error of $\pm 0{\cdot}5$ eV given there for both quantities.

The various difficulties and errors encountered in the evaluation of ϵ_L, ϵ_X, and all but the last terms of ϵ_C and ϵ_T have been discussed previously.[17]

The principal source of error in ϵ_C is the necessity for computing the small differences between the large electron–electron and electron–nucleus interactions. The exchange interactions, ϵ_X, present an entirely different problem. The alpha-function expansions encountered converge so slowly that extrapolation methods must be used to sum them in many instances. The three-center term, ϵ_T, combines, to some extent, the problems encountered in computing both ϵ_C and ϵ_X. ϵ_L presents no particular difficulties and has a high numerical accuracy.

The last term in ϵ_C is found to be negligibly small, depending as it does on the squares of overlaps of ground-state neon functions and yields a contribution smaller than the numerical accuracy to which it can be computed. In any event, ϵ_C is completely dominated by the terms involving the excited 4*s* electron.

The last term of ϵ_T, which was omitted by Knox[16], may be written as a sum over terms of the form

$$e^2 S_{Il,I'l'} \int_{\substack{I,I' \neq A \\ I' \neq I}} \phi_{Il}\phi_{I'l'} \sum_{a=1}^{Z_A} \left(\frac{|\phi_{Aa}|^2}{r_{12}} - \frac{1}{|\boldsymbol{R}_A - \boldsymbol{r}|} \right) d\tau. \tag{9.1}$$

We may think of $\phi_{Il}\phi_{I'l'}$ as a fictitious "overlap charge distribution" of magnitude $S_{Il,I'l'}$. For $a \neq 4s$ we find that the contributions to the nuclear and electronic parts of (9.1) are nearly cancelling and give rise to contributions of the order of $e^2(S_{Il,I'l'})^2/R$ where R is the distance of the "center of gravity" of the fictitious overlap charge distribution from the nucleus of the impurity and is in general no less than the smaller of R_I and $R_{I'}$. In the case $a = 4s$ we find that the deviation from $e^2(S_{Il,I'l'})^2/R$ for the electronic part of the coulomb interactions is of the order of 6 to 7 per cent. The largest overlap integrals encountered among ground-state neon functions are as follows: (all are for first neighbors)

$$S(2px, 2px)_{6.3a_0} = -0{\cdot}00609;$$

$$S(2px, 2s)_{6.3a_0} = -0{\cdot}00203;$$

$$S(2s, 2s)_{6.3a_0} = 0{\cdot}00023.$$

Of these only the last will fail to suffer large cancellations during the performance of the lattice sums over I and I'. Because $\phi_{Il}\phi_{I'l'}$ does not overlap appreciably with nucleus A, we find that the 4*s* term is a sum of terms of the order of

$$(1{\cdot}07)e^2(S_{Il,I'l'})^2/R - e^2(S_{Il,I'l'})^2/R.$$

The resulting contributions of order

$$(0{\cdot}07)e^2(S_{Il,I'l'})^2/R,$$

where $R \gtrsim 6{\cdot}3\ a_0$, (the largest single contribution is of the order of $4 \times 10^{-6}\ e^2/a_0$) are well below the limit of our computational error in computing the individual integrals of the form (9.1), not to speak of the over-all computational error in ϵ_T. Thus,

these terms will be neglected in the present calculation.

It should be noted at this point that the so-called "three-on-one" terms give the largest contribution to ϵ_T. These are the terms formally included in (4.17) which involve only two centers. In the case of the singlet they amount to 6·960 eV and for the triplet to 6·526 eV. Again, as in all of the other parts of (4.13), the excited 4*s* electron terms are vastly dominant.

of its exciton absorption spectrum.[17] These last results are not surprising in light of the fact that the spin–orbit interaction involves the tightly bound 3*p* hole which is not strongly influenced by the crystal field.

Diagonalizing the two-by-two matrix

$$\begin{pmatrix} {}^1E & -\lambda\zeta/\sqrt{(2)} \\ -\lambda\zeta/\sqrt{(2)} & {}^3E+\tfrac{1}{2}\zeta \end{pmatrix} \tag{9.4}$$

we arrive at the following values for the first-order

Table 2. Van der Waals constants computed for various pairs of rare-gas atoms from wave functions using Buckingham's variational method compared to various experimental determination. The values in the second column represent the range found by Buckingham using various experimental data. Those in the third column are computed from the work of Dobbs and Jones fitting the constants for a (12,6) *potential with data on pure solid rare-gases. Symbols are defined in the text. All constants are in units of* 10^{-60} *erg cm*^{6}

Constant	Present calc.	Buckingham (expt.)	Dobbs and Jones (expt.)
^{0}C(Ne, Ne)	6·77	4·69–7·48	8·51
^{0}C(A, A)	129·02	55·5–107	104·78
^{0}C(A, Ne)	27·85	—	29·88
^{1}C(A, Ne)	101·66	—	—
^{3}C(A, Ne)	92·81	—	—

Using an over-all estimate of ten per cent for the computational error resulting from the computational difficulties previously discussed we write,

$$\begin{aligned} {}^1E &= 12{\cdot}1 \pm 1{\cdot}2 \text{ eV} \\ {}^3E &= 12{\cdot}0 \pm 1{\cdot}2 \text{ eV} \end{aligned} \tag{9.2}$$

The spin–orbit parameters ζ and λ have been computed using equations (4.21) and (4.22). It is found that the only appreciable contributions in each case come from the leading terms (the coefficients of ζ_p and $\lambda_p\zeta_p$). We obtain the results

$$\begin{aligned} \zeta &= 0{\cdot}1159 \text{ eV} \\ \lambda &= 1{\cdot}001. \end{aligned} \tag{9.3}$$

The value of ζ_p is 0·1157 eV for the free atom, and λ is identical with its atomic counterpart λ_p. We note the interesting fact that the values (9.3) are precisely the same as those obtained for a pure argon lattice in connection with the computation

excitation energies of the $3p^54s$ configuration:

$$\begin{aligned} {}^1W &= 12{\cdot}18 \pm 1{\cdot}2 \text{ eV} \\ {}^3W &= 12{\cdot}01 \pm 1{\cdot}2 \text{ eV} \end{aligned} \tag{9.5}$$

Here ^1E and ^3E are the pure-singlet and triplet excitation energies computed above, and ^1W and ^3W are the eigenvalues of (9.4).

10. COMPUTATION OF VAN DER WAALS ENERGIES

In an attempt to ascertain the accuracy of Buckingham's method[19] for the evaluation of van der Waals constants we have calculated the coefficient of the R^{-6} interaction for pairs of argon and neon atoms in their ground-states as well as for argon–neon with the argon atom in various states. These results are presented in the first column of Table 2. The second column represents values computed by Buckingham using various experimental data (e.g. atomic polarizabilities, second

Vol. 18
1961

virial coefficients, and scattering cross-sections). The values in the third column are derived from the (12,6) potential constants computed from experimental data on pure neon and argon lattices by DOBBS and JONES. The entry for ${}^0C$(A, Ne) in that column is derived using the semi-empirical "combining relationships" of Section 5, i.e. by demanding that $C(A, B) = [C(A, A)C(B, B)]^{1/2}$. Rather than enter into a detailed (and probably fruitless) argument of the merits of the various numbers encountered we shall content ourselves with noting that the computed constants are at least semi-quantitatively correct, and are, in any event, the best one can do for the excited-states without a great deal more labor, which will be shown to be unjustified. However, one should be cautioned not to take them in too literal a fashion.

We have used calculated values for the pure-singlet and pure-triplet van der Waals constants and values derived from the empirical data of DOBBS and JONES for the ground-state van der Waals constants to compute a correction to the first-order excitation energies. Writing ${}^\mu E_{\text{abs}} = {}^\mu W + {}^\mu E_{vdW}$ where ${}^\mu E_{vdW} = E_{d\text{-}d}(\mu) - E_{d\text{-}d}({}^1S_0)$ we have

$$\begin{aligned} {}^1E_{\text{abs}} &= 11{\cdot}69 \text{ eV} \\ {}^3E_{\text{abs}} &= 11{\cdot}58 \text{ eV} \end{aligned} \tag{10.1}$$

Taking the accuracy of the dipole–dipole energies to be ± 25 per cent, the estimated errors in (10·1) are $\pm 1{\cdot}3$ eV.

Using the same values of the van der Waals constants as in the computation of the correction to the absorption energy and the value ${}^0A_{\text{ANe}} = 2{\cdot}653 \times 10^{-104}$ erg cm^{12} derived from the empirical potential for the ground-state in equations (7·9) and (7.10) we obtain the following phenomenological predictions for the emission energies: ${}^1A_{\text{ANe}} = 22{\cdot}139 \times 10^{-104}$ erg cm^{12}; ${}^3A_{\text{ANe}} = 23{\cdot}211 \times 10^{-104}$ erg cm^{12}; and ${}^1R_{\text{ANe}} = 7{\cdot}41\ a_0$; ${}^3R_{\text{ANe}} = 7{\cdot}59\ a_0$

$$\begin{aligned} {}^1E_{\text{lum}} &= 11{\cdot}26 \text{ eV} \\ {}^3E_{\text{lum}} &= 11{\cdot}11 \text{ eV} \end{aligned} \tag{10.2}$$

In obtaining (10.2) we have used the values ${}^1E_{\text{atomic}} = 11{\cdot}36$ eV; ${}^3E_{\text{atomic}} = 11{\cdot}19$ and the absorption energies (10.1). These results are to be considered no more than semi-quantitative and are included because they are simple to obtain while still being of some interest.

The values of ${}^\mu R$ obtained are a clear indication of the uncertainty of the computation. They indicate that the predicted emissions will take place at a breathing-shell separation which is greater than the normal lattice constant (7·1 a_0) of a pure *argon* crystal. They also state that ${}^3R > {}^1R$, a result contrary to what one would expect considering the relative extent of the singlet and triplet charge distributions.

11. OSCILLATOR STRENGTHS AND INTEGRATED ABSORPTION COEFFICIENTS

Using the formalism of Section 6 and the computed values $\delta = 0{\cdot}20$ (this value is taken from Ref. 26) and $\Delta \equiv {}^1E - {}^3E = 0{\cdot}095$ in addition to the computed first-order energies and spin–orbit parameters we obtain the following values for the dipole matrix elements encountered:

$$M_0 = 0{\cdot}379ea_0;\ \rho = 0{\cdot}078ea_0;$$
$$|d_0|^2 - |\rho|^2 = 0{\cdot}202e^2a_0^2.$$

These values give oscillator strengths

$$\begin{aligned} {}^1f &= 0{\cdot}164 \\ {}^3f &= 0{\cdot}017. \end{aligned} \tag{11.1}$$

These may be compared with calculated values of the free argon atom of ${}^1f = 0{\cdot}185$ and ${}^3f = 0{\cdot}052$.[26] Since the computed oscillator strengths have a very strong dependence on Δ, a quantity which is a poorly known small difference of large numbers, we assign a probable error of ± 20 per cent to the singlet value and ± 40 per cent to the triplet. These represent the same range of uncertainty encountered in the atomic calculation, wherein the problems encountered are much the same.

The integrated absorption coefficients obtained using the oscillator strengths (11.1) are

$$\begin{aligned} \int \mu_1(E)\, dE &= 0{\cdot}84 \times 10^6 N_0 \text{ eV cm}^{-1} \\ \int \mu_3(E)\, dE &= 0{\cdot}09 \times 10^6 N_0 \text{ eV cm}^{-1} \end{aligned} \tag{11.2}$$

where N_0 is the fractional concentration of the impurity. Since we have no knowledge, experimentally, of the index of refraction of the argon

host crystal at the energies of the absorptions, and since a calculation of these indices is beyond the scope of the present work, we have arbitrarily adopted a value of $n = 1$ in (6.9). Thus, the results (11.2) should be taken as being of an order-of-magnitude quality.

12. DISCUSSION

We have presented a generalization of the Heitler–London approximation for the ground- and excited-states of a substitutional impurity in a solid rare-gas crystal. Explicit consideration has been given to the overlapping of heterocentric atomic wave functions and spin–orbit interaction in determining the first-order excitation energies and oscillator strengths. The equilibrium ground-state lattice configuration has been calculated from an empirically obtained (12,6) potential, but the remainder of the first-order absorption calculation has proceeded from first principles. Van der Waals corrections to the excitation energies have been computed using a variational procedure. Predictions of the emission energies have been made on a phenomenological basis using computed excitation energies and excited-state van der Waals constants and the empirical interatomic potential for the ground-state.

In calculating the first-order excitation energies three basic assumptions have been made. They are: (1) the assumed validity and accuracy of the atomic Hartree–Fock functions involved, (2) the neglect of perturbations on pure $3p^54s$ states by higher excited-states of the impurity and by host crystal excited-states, (3) the assumed convergence of the LÖWDIN orthonormalization series at terms of order S^2.

The use of Hartree–Fock functions for the excited state of the impurity probably places a lower limit of 5 per cent on the attainable accuracy of the first-order calculation. The dipole matrix elements derived from these functions, depending as they do on the tails for their accuracy, are probably given to not much better than 20–30 per cent.[26,27]

Ref. (16) discusses the neglect of configuration interactions in connection with the exciton problem in solid rare-gases. The conclusions drawn therein may be taken over bodily to the consideration of higher excited-states of the impurity itself and do, indeed, justify their neglect. The difference of almost five volts between the predicted absorption energies of the present work and the atomic absorption to the $2p^53s$ state of neon suggest that host crystal coupling may be neglected. Although KNOX has predicted a depression of the order of two-and-a-half volts in going from the free atom to the first exciton bands of solid argon[17] giving rise to absorptions in the neighborhood of 1380 Å (9 eV) in the crystal, his conclusions seem to be in disagreement with the experimental work of SCHNEPP and DRESSLER[9] wherein no absorption is observed in solid argon at wavelengths greater than 1200 Å (10·3 eV). In addition, SCHNEPP and DRESSLER observed absorptions in solid xenon and solid krypton which were within 0·1 eV of their atomic positions. Thus, we conclude that there are unlikely to be any states of the neon host lattice which are appreciably coupled to the argon $3p^54s$ transitions.

The third assumption above is without doubt the worst made in the present computation. Table 3, consisting of overlap integrals between an excited argon atom and a neon atom in its normal configuration, calculated for various interatomic separations, is presented for general reference. It will be noted that, in point of fact, LÖWDIN's[14] condition for the *divergence* of the sum

$$\sum_{Kk} S_{Jj,\,Kk} > 1$$

(for any Jj), is met at the computed equilibrium breathing shell position of $6{\cdot}3\ a_0$ from the center. This is to say that

$$\sum_{I} S_{4s,\,I2s} = 1{\cdot}117 > 1.$$

However, the situation may not be as dire as first appearances indicate. We note two points (other than the very weak support of present experimental evidence which indicates that absorption lines are little shifted from their atomic positions for various other impurities in solid rare-gases). First, we have computed the relevant overlap integrals at various interatomic distances and find that the series do meet LÖWDIN's criterion for convergence,

$$\sum_{Ii} |S_{Aa,Ii}| < 1 \text{ (all } Ii),$$

at breathing shell distances of $6{\cdot}7$ and $6{\cdot}9\ a_0$ for the

Vol. 18
1961

Table 3. Several representative overlap integrals (computed with the wave functions of Refs. 26 and 40). All 4s functions belong to the singlet term of the argon atom except those which are primed and taken from its triplet term. The second term of each argument belongs to the normal configuration of the neon atom. These quantities are dimensionless and are functions of the interatomic separation R which heads the columns with values corresponding to the equilibrium distances for the system in its ground-state. Standard nomenclature for p functions in a diatomic configuration is used

	$R = 6{\cdot}3\ a_0$	$R = 8{\cdot}3\ a_0$	$R = 10{\cdot}2\ a_0$
$S(4s, 2p\sigma)$	0·03985	0·02691	0·01461
$S(4s', 2p\sigma)$	0·04202	0·02682	0·01399
$S(4s, 2s)$	0·09514	0·04883	0·02361
$S(4s', 2s)$	0·09305	0·04557	0·02106
$S(4s, 1s)$	−0·00834	−0·00441	−0·00209
$S(4s', 1s)$	−0·00871	−0·00409	−0·00186
$S(3p\sigma, 2p\sigma)$	0·01385	0·00171	0·00020
$S(3p\pi, 2p\pi)$	−0·00210	−0·00018	−0·00001

pure-triplet and singlet states respectively, and also that the principal overlap integrals (in the sense of those most important in determining the energy parameters of the problem) suffer a change of $\lesssim 10$ per cent in going from $6{\cdot}3\ a_0$ to their "radii of convergence". Further, the configuration coordinate curves, especially that for the ground-state, are quite flat, having a total energy change of about 0·1 eV above the minima in a range $5{\cdot}9\ a_0$ to $7{\cdot}6\ a_0$. Since the phenomenologically predicted minima of the excited-state curves lie well beyond the minimum of the ground-state, small changes in the assumed point of excitation will have a rather small effect on the predicted absorptions. Thus we may expect the results computed at $6{\cdot}3\ a_0$ to be physically reasonable.

The computed van der Waals constants contribute a correction of the order of 7 per cent to the predicted absorption energies, and thus, great accuracy in their value is not essential to the present work. Those for which comparison may be made to the DOBBS and JONES values for pure solids are seen to agree with a range of 6 to 25 per cent. This is certainly adequate for our present purposes. The use of van der Waals constants for states of pure multiplicity and with the neglect of overlap corrections is an expedient adopted in the light of the fact that additional corrections would be no more plausible than the results of the simple calculation, and the labor involved would be fruitlessly multiplied. Further, it would seem inconsistent to consider overlap explicitly in the van der Waals calculation while neglecting, as one does in the Buckingham variational formalism, interatomic exchange terms which are of order S^2.

The use of a phenomenological potential in computing the emission energies is, as previously noted, no more than a semi-quantitative calculation. Experimental credence for this sort of procedure is gained from the work of MCCARTY and ROBINSON[11]. They have succeeded in determining empirical potential constants (in particular, excited-state polarizabilities and repulsive constants) for various molecular impurity species introduced into a rare-gas matrix from optical measurements. They then find that these quantities give good agreement with experiment when the impurity is introduced into a different rare-gas matrix. They use the equivalent of the so-called "combining relations" of Section 5 in making these fits. We must note, however, that we have made no attempt to take into account such potentially important considerations as the JAHN–TELLER[44] effect in the luminescence calculation. Throughout the computation we work in the static approximation. This is to say that we invoke the Franck–Condon principle for the excitation and compute the integrated absorption coefficient on the

assumption that Born–Oppenheimer wave functions are applicable to the vibrating crystal and that the CONDON[45] approximation is valid. We have made no attempt to compute the temperature dependence of the spectra, or to compute the first, or higher-order moments using, say, the formalism of LAX[6].

There exists, at present, no experimental data with which direct comparison of the results of the present calculation may be made. However, there are some results which at least serve to verify the "spirit" of our predictions. SCHNEPP and DRESSLER's previously quoted experimental work on pure solid rare-gases[9] finds absorption energy shifts of the order of tenths of volts from the free atomic values. SCHNEPP has also investigated the optical absorption spectra of magnesium and manganese atoms in rare-gas matrices and finds energy shifts of the same order of magnitude.[10] These are positive or negative depending on the particular impurity and matrix involved. In all cases he finds splittings of the lines corresponding to the removal of the degeneracy of the P states. These are ascribed to the impurities finding themselves in sites of lower than cubic symmetry, e.g. in interstitial positions or surface sites.

McCARTY and ROBINSON[11] have examined the absorption spectra of Hg, NH, Na, and C_2 in argon, krypton and xenon lattices. Their results are of the same general tenor as SCHNEPP's. Shifts, either red or blue, of the order of tenths of volts from the corresponding atomic lines are observed. Line splitting presumably caused by a multitude of trapping sites, including surface positions, are also noted, especially in the case of the sodium impurity where extremely complex spectra are observed. Unfortunately, no measurements have yet been made of the luminescence, if any, from these centers. We present Table 4 for quick reference to calculated (blue) absorption line shifts of the present work. They seem to agree in order of magnitude with those discussed above. It is hoped that the experiments for the system Ne : A will be performed despite their technical difficulty. Such work would serve not only to test the present specific case, but would serve as an important guide in determining the validity of the Heitler–London model for impurity centers, with the S^2 approximation, however, serving as an important qualification.*

It seems both unfortunate and apparent that both the present calculation and KNOX's work[17] share a common failing. The powerful tool of symmetrical orthogonalization has indeed produced a formally correct procedure for performing the computation; however, the large amount of numerical work involves Hartree–Fock functions, and in particular small differences between large numbers computed with them, so that our extensive labors are rewarded with no better than ten per cent computational accuracy.

The difficulty is that the Hartree–Fock functions are unavoidably not very accurate on the tails, and it is the tails that are responsible for the difference between electronic and nuclear electrostatic interactions between neighbors. Further, we have considered only terms up to second-order in overlap

Table 4. Comparison of calculated absorption and emission energies with those computed for the free argon atom

State	E_{atomic}(eV)	E_{abs}(eV)	E_{lum}(eV)	Absorption blue shift (eV)
$^1P_1$	11·36	11·69	11·26	0·33
$^3P_1$	11·19	11·58	11·11	0·37

* *Note added in proof:* In a recent private communication K. DRESSLER has given the following experimental results for shifts of the 1469 Å resonance line of the free Xe atom when it is placed in various solid matrices. In pure solid Xe : −0·09 eV; in solid Kr : +0·58 eV; in solid A : +0·82 eV. The last two measurements represent the systems most closely resembling that of the present calculation yet observed experimentally. The "agreement-in-spirit" with present predictions is encouraging.

Vol. 18
1961

and have entirely neglected the possibility of large contributions from the quartic and higher terms. Finally, in the computation of exchange and three-center energies we have been forced to terminate alpha-function expansions of the integrals after a small number of terms and use extrapolation methods to sum the series.

Carrying out a computation to higher order in overlap, say, S^4, would be a task of huge proportions. It is clear that just doing the lattice sums for the many, complex multi-center terms that would arise would require years of algebraic manipulation. The necessary numerical work would be increased by at least an order of magnitude. With all this, however, the use of Hartree–Fock functions would lead to results no more numerically precise or plausible than those of this work.

At first it would seem that the use of a crude method for estimating the electrostatic forces which bind the crystal together is inconsistent with the use of an extension of KNOX's elaborate formalism for the localized excitation energy. However, the large numerical uncertainties incurred in the first-order calculation do, indeed, make the use of the simple van der Waals formalism as good as the remainder of the calculation. It seems clear that an approach outside of the simple Heitler–London approximation will be necessary to gain a deeper quantitative insight into processes involving the excitation of atoms to spatially extended states in even the most "tightly-bound" of solid-state systems. A fundamental limitation is placed on computations of the present type by the use of the best available (Hartree–Fock) atomic wave functions. It would seem that the course of future research must be directed to the development of more satisfactory zero-order wave functions to represent the excited-states of the system. Generalizations of the method of linear combinations of atomic orbitals or the adaptation of the Bloch scheme may be of value in this pursuit.

Acknowledgements—The author wishes to express his sincere thanks to Professor D. L. DEXTER for suggesting this calculation and for his continuing advice, guidance and encouragement throughout the course of the work. Stimulating and helpful discussions with Professors R. S. KNOX and I. D. FOX are gratefully acknowledged. He wishes to thank Dr. O. SCHNEPP for furnishing him with his experimental results prior to their publication, and Mr. M. P. RIMMER for his assistance with parts of the numerical computations.

REFERENCES

1. For a review see DEXTER, D. L. in *Solid State Physics*, Vol. VI (Edited by SEITZ F. and TURNBULL D.) Academic Press, New York (1958).
2. SEITZ F., *J. Chem. Phys.* **6,** 150 (1938).
3. WILLIAMS F. E., *J. Chem. Phys.* **19,** 457 (1951) and subsequent publications.
4. POTEKHINA N. D., *Opt. i Spectrosk.* **2,** 388 (1957).
5. See, for example, KNOX R. S. and DEXTER D. L., *Phys. Rev.* **104,** 1245 (1956).
6. An extensive review is given by LAX M., *Proceedings of the Photoconductivity Conference* (Edited by BRECKENRIDGE R. G. *et al.*). John Wiley, New York (1956).
7. a. LAX M., *J. Chem. Phys.* **20,** 1752 (1952);
   b. PEKAR S. I., *Usp. Fiz. Nauk* **50,** 193 (1953) and earlier publications;
   c. LUBCHENKO A. F., *Opt. i Spectrosk.* **2,** 1439 (1957);
   d. RASHBA E. I., *Opt. i Spectrosk.* **2,** 75, 88 (1957);
   e. KLICK C. C., *Phys. Rev.* **85,** 154 (1952) and subsequent publications.
8. KRISTOFFEL N. N., *Trudy Inst. Fiz. i Astron. Akad. Nauk. Eston. S.S.S.R.*, No. 7, 85 (1958).
9. SCHNEPP O. and DRESSLER K., *J. Chem. Phys.* **33,** 49 (1960).
10. SCHNEPP O., *J. Phys. Chem. Solids* **17,** 188 (1960).
11. MCCARTY M. and ROBINSON G. W., *Mol. Phys.* **2,** 415 (1959).
12. FONER S. N., COCHRAN E. L., BOWERS V. A. and JEN C. K., *J. Chem. Phys.* **32,** 963 (1960).
13. ADRIAN F. J., *J. Chem. Phys.* **32,** 972 (1960).
14. LÖWDIN P. O., *Advanc. Phys.* **5,** 1 (1956).
15. KNOX R. S., thesis (unpublished), University of Rochester (1958).
16. KNOX R. S., *J. Phys. Chem. Solids* **9,** 238 (1959).
17. KNOX R. S., *J. Phys. Chem. Solids* **9,** 265 (1959).
18. LÖWDIN P. O., thesis, Uppsala, Sweden (1948); *Ark. Mat. Astr. Fys.* **35A,** Nos. 9 and 30 (1948).
19. BUCKINGHAM R. A., *Proc. Roy. Soc.* **A160,** 94, 113 (1937).
20. DEXTER D. L., *Phys. Rev.* **101,** 48 (1956).
21. See, for example, Ref. (1) for a discussion of the validity of this procedure.
22. See SEITZ F., *Modern Theory of Solids*. McGraw-Hill, New York (1940).
23. For the most part we shall attempt to conform to the notation of Ref. (16).
24. CONDON E. U. and SHORTLEY G. H., *The Theory of Atomic Spectra*. Cambridge University Press (1935).
25. See Appendix A of Ref. (15).
26. KNOX R. S., *Phys. Rev.* **110,** 375 (1958).
27. GOLD A. and KNOX R. S., *Phys. Rev.* **113,** 834 (1959).
28. KNOX R. S., *Phys. Rev.* **115,** 1095 (1959).
29. BETHE H. A., *Ann. Phys., Lpz.* **3,** 133 (1929).
30. BROOKS F. C., *Phys. Rev.* **86,** 92 (1952).
31. LENNARD-JONES J. E. and INGHAM A. E., *Proc. Roy. Soc.* **A107,** 636 (1925).

32. AXILROD B. M., *J. Chem. Phys.* **19,** 719 (1951).
33. EISENSCHITZ R. and LONDON F., *Z. Phys.* **60,** 491 (1930).
34. MARGENAU H., *Rev. Mod. Phys.* **11,** 1 (1939).
35. SLATER J. C., *Phys. Rev.* **36,** 57 (1930).
36. KIRKWOOD J. G., *Phys. Z.* **33,** 57 (1932).
37. DOBBS E. R. and JONES G. O., *Reports on the Progress of Physics*, Vol. XX, p. 516. Physical Society, London (1957).
38. See, for example, HIRSCHFELDER J. O., CURTISS C. F. and BIRD R. B., *Molecular Theory of Gases and Liquids*. John Wiley, New York (1954).
39. HARTREE D. R. and HARTREE W., *Proc. Roy. Soc.* **A166,** 450 (1938).
40. WORSLEY B. H., *Canad. J. Phys.* **36,** 289 (1958).
41. KUNIMUNE M., *Progr. Theor. Phys.* **5,** 412 (1950).
42. HENSHAW D. G., *Phys. Rev.* **111,** 1470 (1958).
43. RIMMER M. P. and KNOX R. S., unpublished report, University of Rochester (1958).
44. JAHN H. A. and TELLER E., *Proc. Roy. Soc.* **A161,** 220 (1937); JAHN H. A., *Proc. Roy. Soc.* **A164,** 117 (1938).
45. For a thorough discussion of these approximations and their validity see Ref. (1).

Vol. 18
1961

J. Phys. Chem. Solids Pergamon Press 1961. Vol. 18, Nos. 2/3, pp. 238–252. Printed in Great Britain.

THERMOLUMINESCENCE IN ANHYDRITE

W. L. MEDLIN

Socony Mobil Oil Company, Inc., Field Research Laboratory, Dallas, Texas

(*Received* 9 *August* 1960)

Abstract—The thermoluminescent properties of anhydrite have been investigated by duplicating the features observed in natural samples with synthetic preparations. The inclusion of all impurities which are likely to serve as activators and which are commonly found in natural samples was studied by coprecipitating various concentrations of each impurity with high purity $CaSO_4$. It was found that Mn^{++}, Zn^{++}, Sb^{+++}, Pb^{++}, and Cd^{++} produce characteristic peaks in the glow curves. However, Pb^{++} and Cd^{++} do not have appreciable effects except at high concentrations and Sb^{+++} rarely occurs in natural anhydrite. Therefore, only Mn^{++} and Zn^{++} are of importance in interpreting the glow curves of most natural samples.

The intensity of thermoluminescence as a function of activator concentration was determined for Mn^{++} and Sb^{+++} but could not be measured over a suitable range for Zn^{++} because it was impossible to coprecipitate sufficient amounts of this ion. The impurity concentrations were measured by colorimetric procedures.

Three of the low temperature glow peaks observed in natural samples were shown to be associated with anion omissions. It was also demonstrated that all three of the peaks are due to trapping states which belong to a single center.

The suppression of thermoluminescence by such impurities as Fe, Co, Ni, etc., was also investigated. The only case where quenching occurred was for Fe in the presence of Zn^{++}. This partly accounts for the relatively low emission intensities in natural samples but in general the low intensities are due to the effective exclusion of Mn^{++}, Zn^{++}, and Sb^{+++} from the natural crystals.

1. INTRODUCTION

THIS IS the second in a series of investigations of thermoluminescence in the common rock minerals. A previous publication[1] described the thermoluminescent properties of calcite. The results of the calcite study demonstrated that most of the thermoluminescent characteristics in naturally occurring samples are due to trace amounts of a few impurities. Electronic levels of the impurity ions provide the trapping sites and luminescent centers necessary for thermoluminescence to occur and therefore serve as activators. The presence of other impurities results in quenching the luminescence due to the activator ions. The problem in explaining the thermoluminescent characteristics of naturally occurring samples is simply to determine which ions can function as activators or quenchers when present in the crystal lattice. The technique used here consists of coprecipitating each impurity of interest with an otherwise pure sample of anhydrite crystals. The glow curves of these synthetic samples are then compared with the important features of the glow curves of natural samples.

2. EXPERIMENTAL APPARATUS

The glow curve apparatus is illustrated in Fig. 1. The unit is similar to one described previously.[1] It is designed to heat a powdered sample from 77 to 750°K at a linear rate which can be varied from 0·1°K/min to 10°K/min (a heating rate of 0·5°K/min was used for the present work). The linear heating rate was maintained by a control system which increased the power input to the induction heater according to a predetermined program. The control system also provided a means of holding the temperature of the sample constant which allowed for the measurement of isothermal decay curves.

The intensity of emission from the sample is measured by a 5819 photomultiplier tube and plotted as a function of the sample temperature by a two-pen Leeds and Northrup recorder. The temperature is measured by an iron–constantan

thermocouple placed directly under the sample as shown in Fig. 1. Provision has been made for converting the photomultiplier signal into units of luminous intensity by arranging a calibrating source of known intensity[2] with the same geometry and the same surface area as the sample (3·87 cm²) to provide the proper conversion factor.

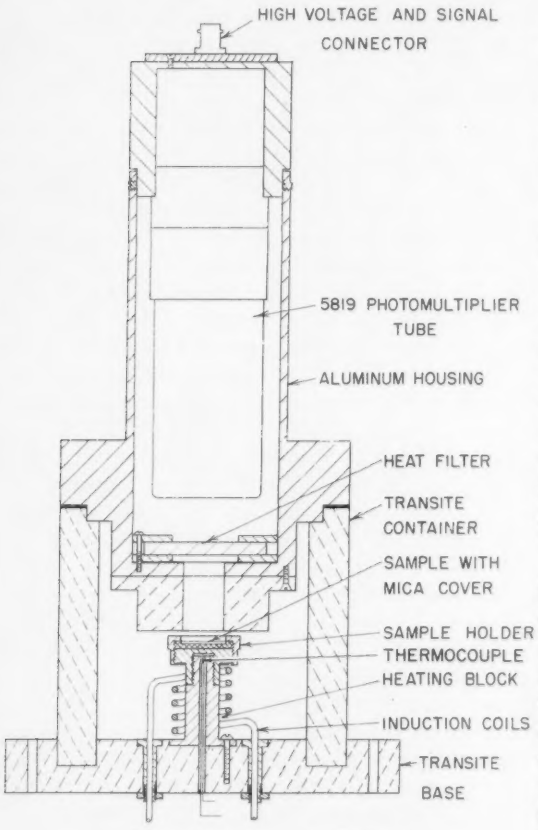

FIG. 1. Glow curve apparatus.

All of the samples studied here were activated by X-rays. For the glow curve experiments, the samples were activated for 5 min at liquid nitrogen temperature by a Mo tube operated at 15 mA and 35 KVP.

3. EXPERIMENTAL PROCEDURE

In order to investigate the effects of a particular impurity on the thermoluminescent properties of anhydrite, it is necessary to add controlled amounts of the impurity to an otherwise pure sample. A method often used in the preparation of phosphors consists of firing a mixture of the pure sample and the impurity at temperatures high enough to result in diffusion of the impurity into the lattice of the matrix material. This technique has been used by at least four investigators to prepare $CaSO_4$ phosphors containing Mn[3], Sm[4] and Pb[5] as activators.

For the present application where it is desirable to know the molar concentration of the added impurity (in the crystal lattice), the firing technique has been found unsatisfactory. The results obtained for a large number of samples containing Mn or Pb as the activator were not reproducible in terms of luminescent efficiency as a function of activator concentration. These samples were prepared by mixing the impurities (as sulfates) with high purity gypsum ($CaSO_4 \cdot 2H_2O$) and firing for two hours at 1050°C. The gypsum was obtained by precipitation from a solution of high purity $CaCl_2$[6] and $(NH_4)_2\,CO_3$. It should be mentioned that the direct precipitation of anhydrite is not possible and the only method available for preparing synthetic samples is by the dehydration of gypsum which occurs at temperatures well below 1050°C.[7]

The failure of this method to provide reproducible results can evidently be attributed to two factors: (1) the small dimensions of the individual anhydrite crystals and (2) the inaccuracy in determining the activator ion concentrations. The first of these is inherent in the method of preparation. It is to be expected that the removal of the water molecules from the gypsum lattice would prevent the formation of very large anhydrite crystals unless the process occurs quite slowly. The second factor is due to the formation of insoluble oxides of the impurity ions at the high temperatures required for firing. Since these oxides cannot be separated from the anhydrite matrix they are included in the determination of the impurity concentration but do not contribute to the thermoluminescence.

A method which eliminates the concentration problem is one in which the impurity ion is coprecipitated with gypsum. The excess impurity is then removed by washing before the sample is fired. However, this does not eliminate the problem of crystal size and it was found that the results of this method were still not reproducible.

Vol. 18
1961

A satisfactory procedure was devised by making use of the dehydrating properties of H_2SO_4 at elevated temperatures. In this case, the impurity ion is coprecipitated with gypsum by adding concentrated H_2SO_4 to a dilute solution of $CaCl_2$ and evaporating at 90–95°C until all of the water has been removed. The remaining slurry is then heated to 300–350°C to remove the excess H_2SO_4. During the early part of this cycle all of the gypsum is converted to anhydrite and as the heating continues, relatively large crystallites of anhydrite (100–1000 microns) are formed. Excess impurity ions are removable by washing and the method was found to give reproducible results in all cases.

Two criteria were used in selecting the impurity ions whose effects would be investigated. Only those ions which are commonly found as impurities in naturally occurring anhydrite and which are likely to serve as activators were considered. On this basis, the following impurities were investigated: Mn^{++}, Zn^{++}, Sb^{3+}, Pb^{++}, Cd^{++}, Fe^{++}, Fe^{3+}, Co^{++}, Ni^{++}, Cu^{++}, Ag^{+}, Bi^{3+}, Al^{3+}, Ti^{3+}, V^{++}, Cr^{3+}, Sn^{++}, As^{3+} and As^{5+}. Of these, Mn^{++}, Zn^{++}, Sb^{3+}, Pb^{++} and Cd^{++} were found to be activators and the remaining impurities had no observable effects. The rare earths were not considered here because of their rare occurrence in natural samples and, with the exception of Cl^{-} and NO_3^{-}, the effects of anion impurities were not investigated either.

It is clear that many of the impurity ions mentioned above will not be readily included in the anhydrite lattice. Ions such as Pb^{++} and Cd^{++} should be included in a simple substitutional manner without much difficulty because they have about the same ionic size and coordination tendencies as Ca^{++} in the sulfate lattice. On the other hand, ions like Mn^{++} and Zn^{++} which have the wrong coordination numbers (6 and 4 respectively as opposed to 8 for Ca^{++}) and Sb^{+++} and Bi^{+++} which have the wrong charge are not likely to be included without distorting the lattice appreciably. Also, it is questionable whether such ions as Fe^{+++} and Ag^{+}, which can be converted to the divalent states rather easily, will be included in the trivalent or monovalent state at all. This follows from the general tendency for the impurity ion to assume the valence of the lattice. In addition to this, the presence of hot, concentrated H_2SO_4 during the last cycle of the sample preparation provides an oxidizing medium which also influences the valence of the impurity ion.

The quenching effects of the well known poisons, Fe^{++}, Fe^{+++}, Co^{++}, and Ni^{++} were investigated by coprecipitating various concentrations of each of them with constant amounts of the activator ions. The effects of the less versatile poisons, Cu^{++}, Al^{+++}, and Be^{++} were also investigated.

In order to obtain quantitative results for the efficiency of luminescence as a function of concentration for the various activator and quencher ions it was necessary to develop procedures for measuring impurity concentrations as low as a few p.p.m. Colorimetric methods were found to be satisfactory for this purpose. Suitable procedures for the determination of Mn^{++}, Fe^{++}, Fe^{+++}, Co^{++}, Ni^{++}, and Pb^{++} have already been developed for calcite[1] and were readily adapted to the anhydrite samples. However, the determinations are less sensitive in anhydrite because of its lower solubility in aqueous solutions (the solubility in 7–10 per cent HCl is about 0·02 g/ml).

For the determination of Sb^{+++}, the standard Rhodamine-B extraction method[8] was used. A procedure developed by Moss and Mellon[9] was used for the determination of Cu^{++} and procedures reported by Medlin[10] were used for determining the Zn^{++} and Cd^{++} concentrations.

4. RESULTS

The presence of Mn^{++} in the anhydrite lattice produces a prominent glow peak at 390°K and a minor peak at 120°K. These are illustrated in Fig. 2 for a sample containing 380 p.p.m. Mn^{++}. The small peak at 200°K is a non-impurity defect which will be discussed later. The badly obscured peak at about 460°K is probably due to Mn^{++} but the presence of the more intense peak at 390°K prevents conclusive identification in this case.

The sample illustrated in Fig. 2 was annealed at 800°C for 2 hr. At low concentrations, the heating had no observable effect on the Mn^{++} glow peaks but at concentrations greater than optimum, the effect was to decrease the glow peak intensity. This is illustrated in Fig. 3 which shows the variation in glow peak intensity (plotted as a normalized relative efficiency) for the 390°K peak as a function of Mn^{++} concentration. The points

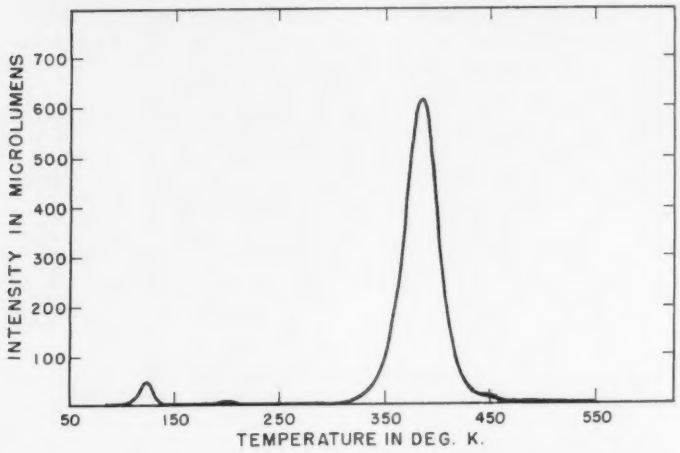

FIG. 2. Glow curve for a synthetic anhydrite sample containing Mn^{++} as an added impurity.

corresponding to the annealed samples are distinguished from those for unheated samples. An efficiency curve for the 120°K glow peak is not shown because the data in this case were erratic and did not fit a smooth curve except at low concentrations. This indicated that while the peak is clearly due to Mn^{++}, its intensity is influenced by other crystal properties (such as crystal dimensions, etc.) which could not be adequately controlled here.

The theoretical curve drawn in Fig. 3 was computed from a relation derived by JOHNSON and

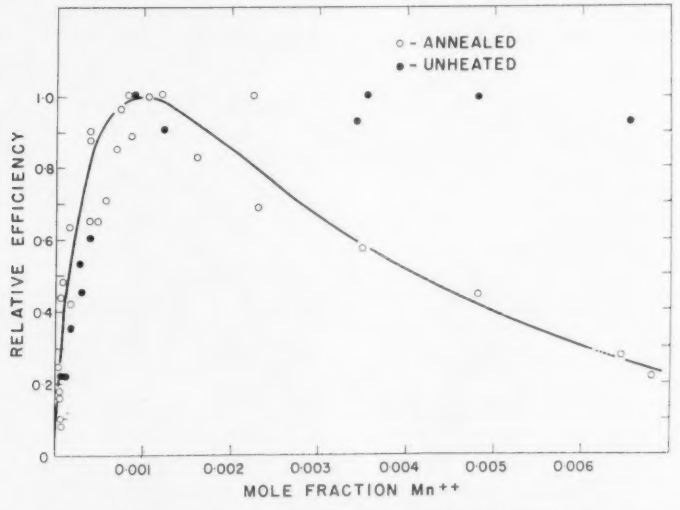

FIG. 3. Efficiency of luminescence as a function of impurity concentration for the 390°K glow peak due to Mn^{++} showing the effects of annealing.

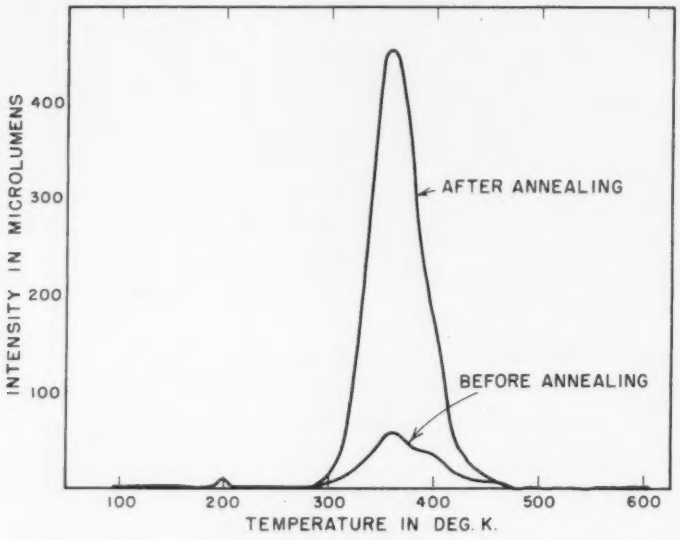

FIG. 4. Glow curve for a synthetic anhydrite sample containing Sb^{+++} as an added impurity.

WILLIAMS[11] for concentration quenching,

$$\eta = \frac{C(1-C)^z}{C+\gamma(1-C)}$$

where η is the efficiency of luminescence, C is the mole fraction of the activator ion and z and γ are parameters whose values are chosen to give the best fit to the experimental points.

The inclusion of Sb^{+++} in the anhydrite lattice resulted in a prominent glow peak at 355°K and a minor peak at 200°K. The glow curve for a

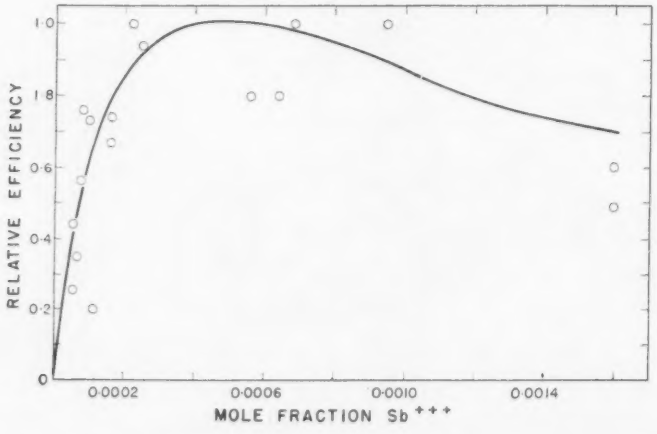

FIG. 5. Efficiency of luminescence as a function of impurity concentration for the 355°K glow peak due to Sb^{+++}.

sample containing 680 p.p.m. Sb^{+++} is shown in Fig. 4. In this case the effect of annealing is pronounced. Both of the Sb^{+++} glow peaks are intensified by approximately an order of magnitude. Incidentally, it is the effect due to annealing which excludes the possibility that the 200°K peak results from the non-impurity defect mentioned above because the defect glow peak is unaffected by annealing.

particular foreign anion or such monovalent cations as Na^{+}, K^{+} or Ag^{+}. It was also observed that the presence of either Fe^{++}, Fe^{+++} or Cu^{++} markedly decreased the concentration of Sb^{+++} in the solid.

The addition of Zn^{++} to the anhydrite lattice results in four principal glow peaks at 180°K, 200°K, 230°K and 330°K as illustrated in Fig. 7. The results of luminescent efficiency vs. activator

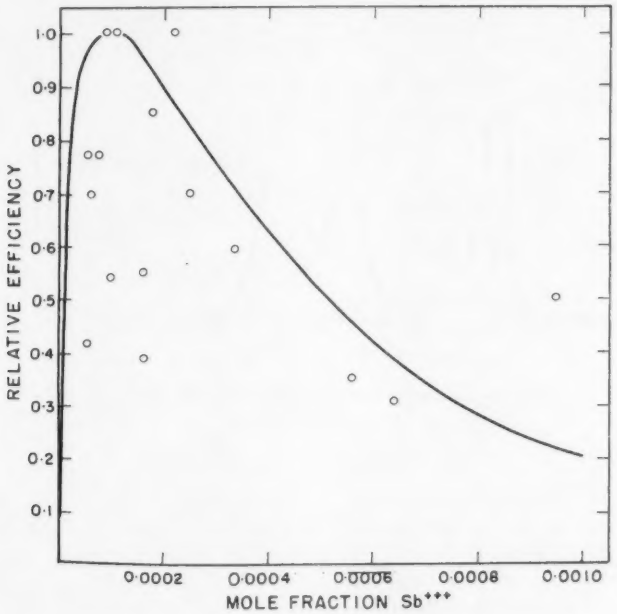

FIG. 6. Efficiency of luminescence as a function of impurity concentration for the 200°K glow peak due to Sb^{+++}.

The 390°K and 460°K glow peaks shown for the unheated sample in Fig. 4 are undoubtedly due to trace amounts of Mn^{++}, and are almost completely obscured in the annealed sample. Figs. 5 and 6 show the efficiency of luminescence for the Sb^{3+} glow peaks as a function of concentration. It was found that the Sb^{3+} ion was not readily included in the anhydrite lattice which is not surprising in view of the earlier discussion.

No effort was made to account for the charge compensation necessary for the inclusion of Sb^{+++} in the anhydrite lattice. It was found that the mechanism appeared to be independent of any concentration are incomplete in this case because of the limited quantities of Zn^{++} which could be included in the anhydrite lattice. This is presumably due to the distortions produced by the zinc ion which is considerably smaller and has a different coordination number than the calcium ion in anhydrite. The greatest concentration obtained here was 770 p.p.m. in a sample prepared from a solution 80 per cent saturated in $ZnCl_2$. The effect of annealing is also pronounced for the Zn^{++} activator, resulting in an increase of about three in the intensities of all glow peaks. It is evidently significant that the impurities whose

Vol. 18
1961

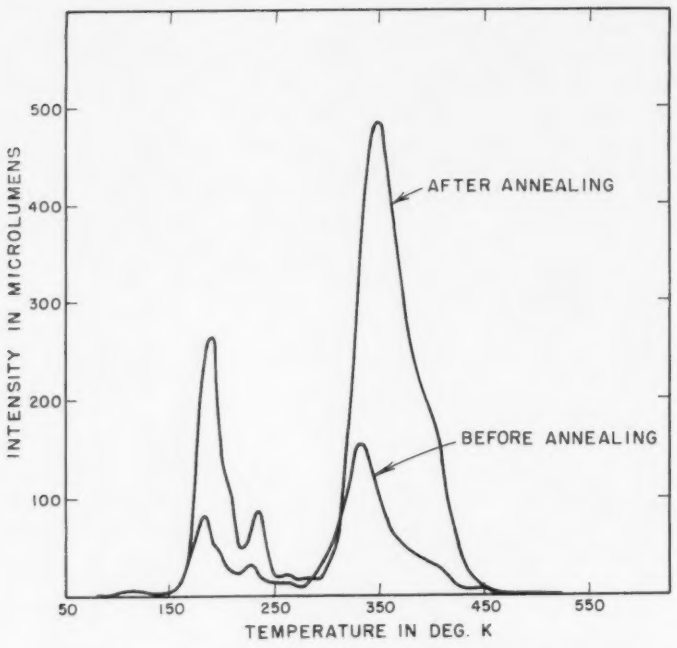

FIG. 7. Glow curve for a synthetic anhydrite sample containing Zn^{++} as an added impurity.

thermoluminescence is most affected by annealing are those which are least readily included in the anhydrite lattice, viz. Sb^{+++} and Zn^{++}.

The use of concentrated solutions of zinc and antimony salts in coprecipitating Zn^{++} and Sb^{3+} with anhydrite required that trace impurities in all of the salts be accounted for. Only three such impurities, Fe, Pb, and As were present in concentrations large enough to be considered and it was shown that none of them affected the thermoluminescence of anhydrite.

An interesting phenomenon has been observed for the zinc activator which apparently involves transitions between different zinc trapping levels. If a sample activated at liquid nitrogen temperature (77°K) is heated to 280–300°K, all of the traps represented by the low temperature peaks at 180°K, 200°K, and 230°K are emptied but most of the traps corresponding to the 330°K peak remain filled. If the sample is then cooled to 77°K and again heated, it is found that the peaks at 180°K, 200°K, and 230°K are still present (with reduced

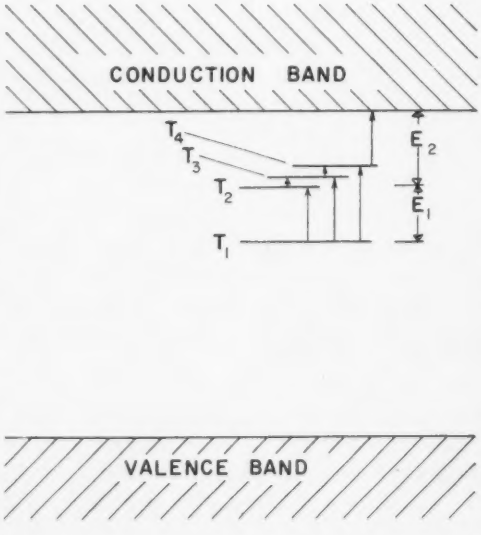

Fig. 8. Proposed energy level scheme for zinc trapping states.

intensities). However, when the sample is originally heated to 380°K to empty all of the traps associated with the 330°K peak, none of the glow peaks reappear after cooling.

An explanation of this behavior is illlustrated in Fig. 8. The electron traps corresponding to the 330°K, 230°K, 200°K, and 180°K glow peaks are represented by T_1, T_2, T_3 and T_4, respectively. It is clear that over a small range of temperatures below 180°K, electrons in T_1 have enough thermal energy to be transferred to T_2, T_3 and T_4, either by direct or cascade transitions. Some of these electrons are then raised to the conduction band but if this occurs at a slower rate than the transitions from T_1, an appreciable number of the traps at the T_2, T_3 and T_4 levels will remain filled.

This interpretation was confirmed by initially cooling a sample to 160°K and maintaining this temperature for several minutes before cooling to 77°K. The glow curve obtained in this case exhibited peaks at 180°K, 200°K, and 230°K of considerably greater intensities.

Clearly, this mechanism requires that the energy difference between the deep and shallow traps be slightly less than the energy difference between the shallow traps and the conduction band (assuming that the frequency factor, ν is the same in all cases). Since T_2, T_3 and T_4 are evidently closely spaced in this case (as indicated by the overlapping of their glow peaks), the T_3 and T_4 traps can be filled by thermal transitions from T_2. If this is true, it is only required that "E", in Fig. 8 be slightly less than E_2.

The activator properties of Pb^{++} and Cd^{++} are significantly different from those of Mn^{++}, Sb^{+++}, and Zn^{++} in that their effects are limited to relatively large concentrations. Neither impurity has an appreciable effect at the concentrations normally found in natural samples.

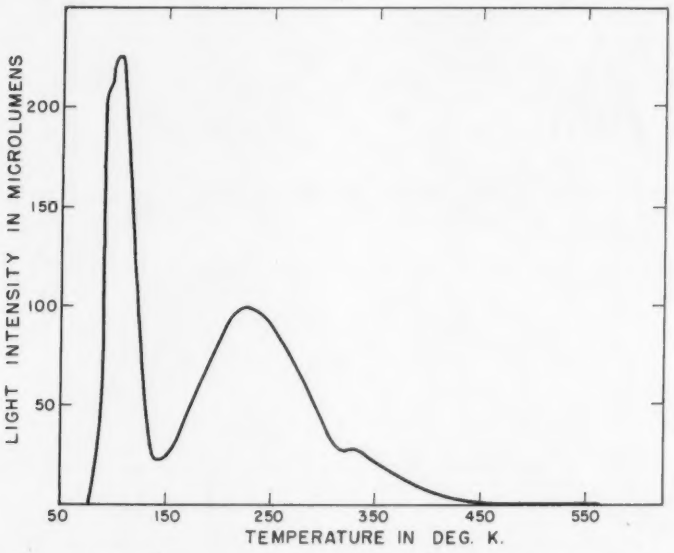

FIG. 9. Glow curve for a synthetic anhydrite sample containing Pb^{++} as an added impurity.

Figure 9 is the glow curve for an anhydrite sample containing 15 mole per cent Pb^{++} which was found to be about the optimum concentration for all of the glow peaks. Two very sharp peaks occur at 95°K and 105°K and a much broader peak at 225°K. The partially obscured peak at about 340°K is evidently due to trace amounts of Mn^{--}

In Fig. 10, glow curves are shown for several concentrations of Cd^{++} ion. The results are complicated by the fact that there are a number of glow peaks whose relative intensities vary

Vol. 18
1961

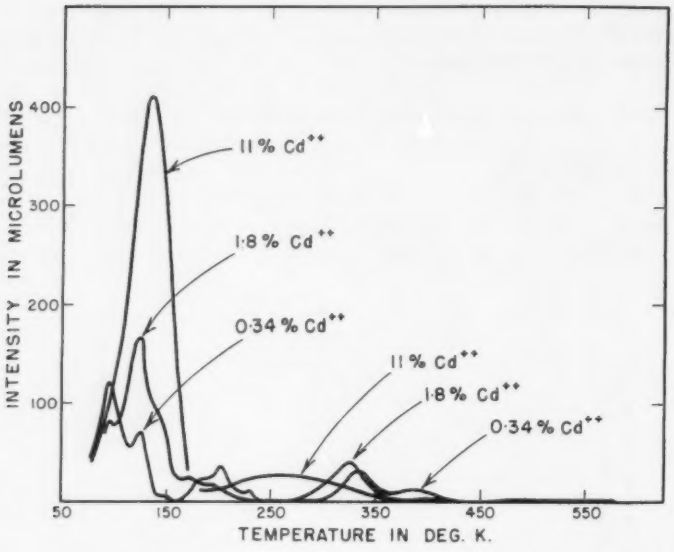

FIG. 10. Glow curve for synthetic anhydrite samples containing various concentrations of Cd^{++} as an added impurity.

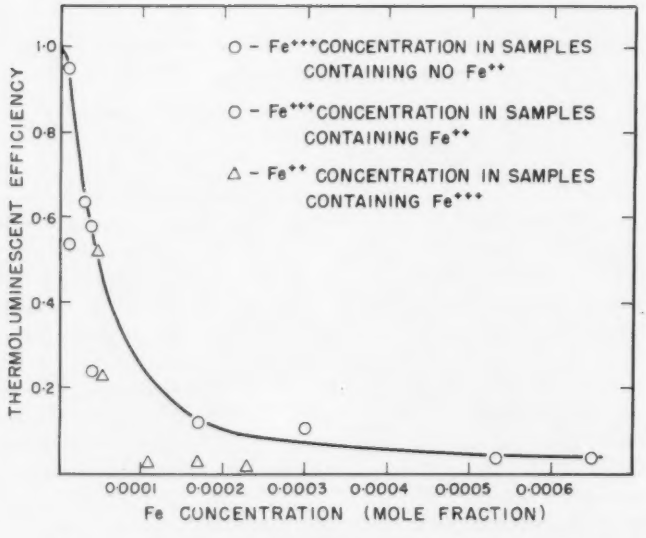

FIG. 11. Quenching effect of Fe^{++} and Fe^{+++} in the presence of Zn^{++} in anhydrite.

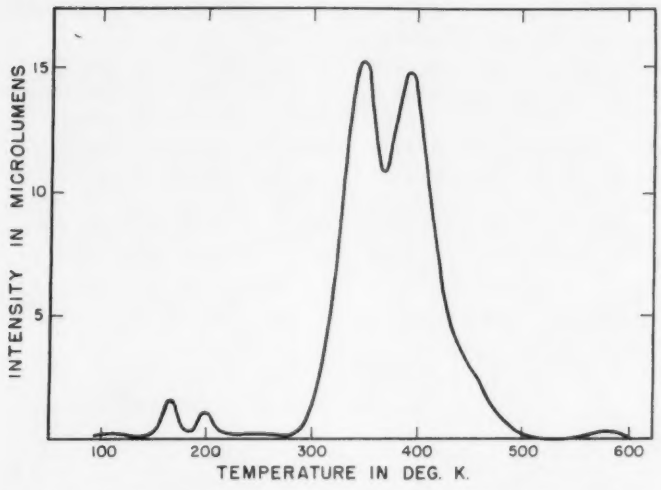

FIG. 12. Glow curve for a synthetic anhydrite sample containing less than 10 p.p.m. of any impurity.

considerably at the lower concentrations. Also, there is a shift in temperature of some of the glow peaks with variations in the Cd^{++} concentration. At least seven glow peaks due to Cd^{++} can be identified at the lowest concentration shown (3400 p.p.m.). These occur at temperatures of 95°K, 125°K, 150°K, 180°K, 200°K, 230°K, and 330°K. The peak at 390°K in Fig. 10 is apparently due to Mn^{++}. At higher concentrations the glow curve is reduced to two peaks at 140°K and 260°K.

The only quenching effects observed for any of the activators in anhydrite were those involving Fe^{++} and Fe^{+++} in the presence of Zn^{++}. Fig. 11 shows the results of Fe concentration for the 350°K glow peak. The results for the other Zn^{++} glow peaks are similar to Fig. 11 except that the effect is not as pronounced and at Fe concentrations greater than about 500 p.p.m. the intensities of these peaks are greater than the 350°K peak.

It was found that the oxidizing medium of hot, concentrated H_2SO_4 used in preparing the samples made it impossible to add Fe^{++} to the lattice without including appreciable quantities of Fe^{+++}. Therefore, the results for the ferrous iron are somewhat difficult to interpret. To illustrate the results as clearly as possible, three sets of points have been plotted in Fig. 11: (1) the ferric content in samples which contained no Fe^{++}, (2) the ferrous content in samples which also contained Fe^{3+} and (3) the ferric content in samples which also contained Fe^{++}. A smooth curve has been drawn through the points for case (1) and the result that the points for cases (2) and (3) are consistently on or below this curve is interpreted to mean that Fe^{++} quenches the Zn^{++} luminescence at least as effectively as Fe^{3+}. More detailed conclusions are not justified in view of the fact that the most significant data involve iron concentrations less than 50 p.p.m. where the precision of the colorimetric determinations becomes poor (± 25 per cent). In addition, it was found, as mentioned earlier, that the concentration of Zn^{++} ion in samples containing Fe did not remain constant for different Fe concentrations. In order to account for this effect it was assumed that the luminescent efficiency is a linear function of zinc concentration in the range involved here (130–460 p.p.m.). This is in agreement with the measurements obtained earlier for zinc concentrations up to 770 p.p.m.

The glow curve for a synthetic sample containing less than 10 p.p.m. of any impurity is shown in Fig. 12. At least six glow peaks can be distinguished at 160°K, 200°K, 350°K, 390°K, 460°K, and 580°K. The peaks at 390°K and 460°K coincide with the glow peaks due to Mn^{++} (cf. Fig. 2) and the sample shown here contains enough Mn^{++} (5 p.p.m.) to account for the

observed intensities. There is also evidence of the other Mn^{++} peak at 120°K and the results for Mn^{++} activation show a smooth enhancement of these peaks as the concentration is increased.

The glow peaks at 200°K and 350°K coincide with peaks due to Sb^{+++} and Zn^{++} (cf. Figs. 4 and 7). However, since neither of these peaks is affected by the addition of Fe^{++} or by annealing and since a smooth increase in intensity with increasing Zn^{++} or Sb^{+++} content is not observed, of the 180°K glow peak was not appreciably affected.

As in the case of the Zn^{++} activator, it was found that localized transitions occurred between the traps corresponding to the 160°K, 200°K, and 350°K glow peaks. Therefore all three of these trapping levels are identified with the same center.

The decomposition of anhydrite to CaO at temperatures above 1200°C provides a means of determining the effect of replacing a SO_4 ion in the

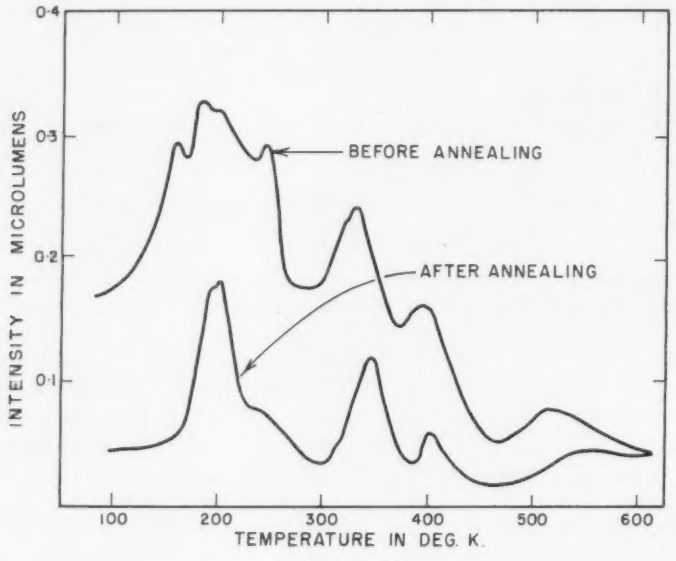

FIG. 13(a)

both of these impurities are eliminated as possible causes. It appears that the most reasonable explanation of these peaks and of those at 160°K and 580°K are non-impurity defects such as missing ions, dislocations, etc. It is quite possible that some or all of these defects may be introduced during the X-ray bombardment but it was impossible to verify this since ordinary ultraviolet radiation is not energetic enough to activate the samples.

The addition of Sn^{4+} to introduce cation vacancies in the anhydrite lattice produced no significant changes in the glow curve. But the addition of $P_2O_7^{4-}$ ions resulted in increased intensities in the 200°K and 350°K glow peaks indicating that they are associated with anion vacancies. The intensity anhydrite lattice by an $0^=$ ion. Samples were heated for periods long enough to provide concentrations as high as 5000 p.p.m. of this defect (as determined with a thermal gravimetric balance) without observing any important changes in the glow curve.

The "freezing in" of lattice distortions produced at high temperatures was also investigated. Several samples were heated to 1100°C and suddenly cooled by immersion in water but there were no observed changes in the glow curve.

The glow curves for some representative samples of natural anhydrite are illustrated in Fig. 13. These were selected from some twenty-five samples including outcrop specimens and samples taken from well cores of various depths. X-ray

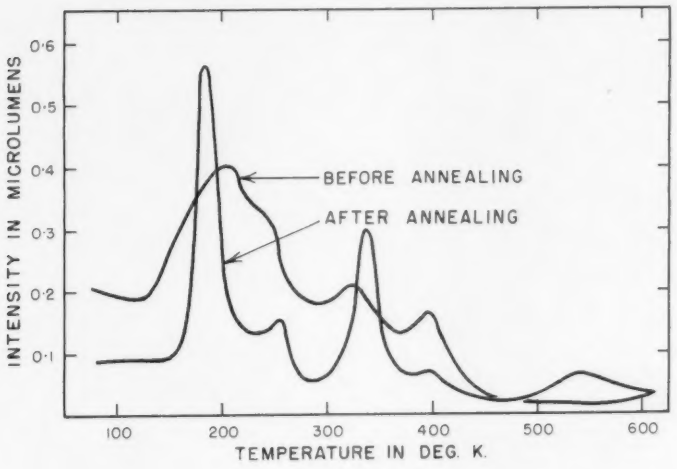

FIG. 13(b)

powder patterns were obtained for all of the samples to insure against the presence of other mineral impurities.

All of the important features of the glow curves in Fig. 13 can be explained by the presence of zinc, manganese, and iron and by the lattice defects discussed above. The effects of annealing (2 hr at 800°C) are also illustrated. Curve (a) is perhaps the most typical result. Glow peaks can be distinguished in the unheated sample at 160°K, 180°K, 200°K, 240°K, 330°K, 390°K, and 520°K. The peak at 160°K which disappears in the annealed

Vol. 18
1961

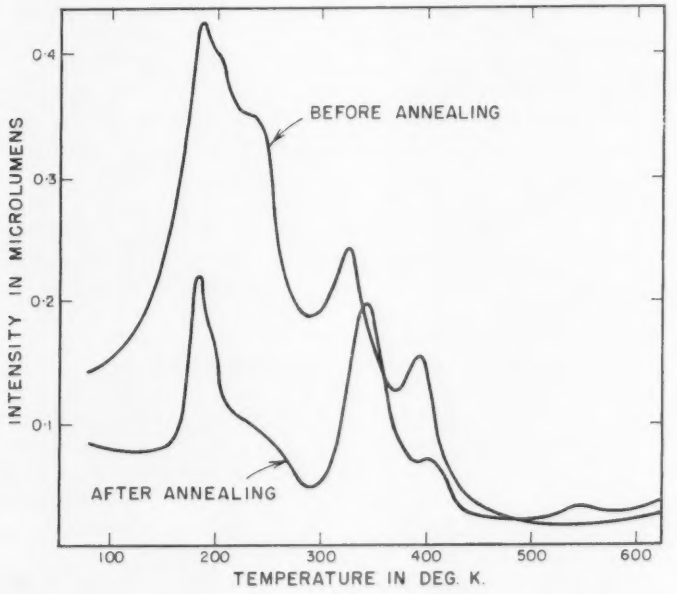

FIG. 13(c)

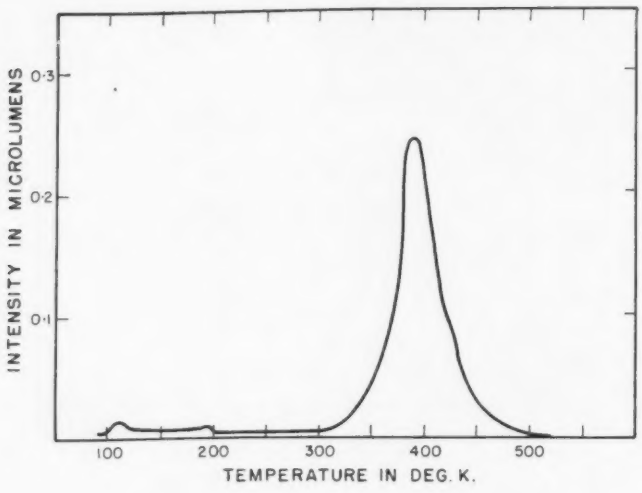

FIG. 13(d). Glow curves for samples of natural anhydrite.

curve is evidently due to the anion omission defect discussed above. The four peaks at 180°K, 200°K, 240°K, and 330°K are due to Zn^{++}. The shifting of the 330°K peak to 350°K in the annealed curve removes any ambiguity in associating this peak with an anion omission level. The greater intensities of the 180°K and 200°K peaks (compared with the 330–350°K peak) are interpreted as being due to the presence of iron which selectively quenches the high-temperature Zn^{++} peak more effectively than the others. The glow peak at 390°K is clearly due to manganese, whereas the peak at 520°K, which shifts to 550°K in the annealed sample, has not been identified but is apparently due to a non-impurity defect.

The enhancement of the Zn^{++} peaks with annealing is more clearly illustrated in (b) of Fig. 13. In (c) the glow curve does not exhibit the peak at 160°K due to cation vacancies, even in the unheated sample. Without exception it was found that this peak, which existed in about two-thirds of the natural samples before annealing, was removed by heating at 800°C for two hours.

A sample containing more Mn^{++} than usual is illustrated in (d) of Fig. 13. In this case the Zn^{++} peaks are insignificant and the effect of annealing is negligible. The low temperature peak due to Mn^{++} at 120°K is also apparent.

The most significant feature of all the glow curves in Fig. 13 is their relatively low level of light emission compared with the synthetic samples. For example, the intensity of the 390°K peak in synthetic samples containing the optimum manganese concentration is greater by two orders of magnitude than the corresponding peak in (d) of Fig. 13. The peak intensity in this natural sample corresponds to a Mn^{++} concentration of about the same level as the pure synthetic samples (cf. Fig. 12) and the manganese content must be considerably lower in the other natural samples in Fig. 13. Unfortunately, this could not be verified by analytical determinations since the concentration levels involved here are just at or below the limit of detectability by colorimetric or spectrographic methods. It was possible to show by spectrographic analysis that none of the natural samples contained more manganese than the pure synthetic samples (about 5 p.p.m.).

It can be shown[12] that during the early part of the glow peak due to a particular trapping level, the increase in intensity is approximately proportional to $\nu \exp(-E/kT)$ where E is the activation energy associated with the trap, k is Boltzmann's constant, T is the temperature and ν is the frequency factor for emptying the trap. This provides what is probably the best means of

Table 1. Activation energies and frequency factors in anhydrite

Defect	T_g in °K	E in eV	ν in sec^{-1}
Mn^{++} ion	390	1·0	10^{12}
Mn^{++} ion	520	1·1	10^{9}
Zn^{++} ion	190	0·52	10^{12}
Zn^{++} ion	350	1·0	10^{12}
Sb^{+++} ion	200	0·50	10^{11}
Sb^{+++} ion	360	0·95	10^{12}
anion omission	180	0·45	10^{11}
anion omission	220	0·54	10^{12}

determining E. However, it is required that the glow peak be fairly isolated, at least on the low temperature side, to avoid interference from neighboring glow peaks. Most of the lower temperature interference can be removed by annealing at a temperature near the glow peak but in anhydrite, this method was found to be ineffective for some of the peaks due to Zn^{++} and vacancy defects because of the inter-trap transitions discussed earlier.

Once E has been determined it is possible to compute a value for the frequency factor, ν from the relation,[12]

$$\nu = \frac{\beta E}{kT_g^2} \exp\left(\frac{E}{kT_g}\right)$$

where T_g is the temperature of the glow peak and β is the heating rate. Values of E and ν for some of the glow peaks due to Mn^{++}, Zn^{++}, Sb^{+++} and omission defects in anhydrite are listed in Table 1. In general, the values of ν are somewhat higher than those reported for trapping levels in other crystals[13] which range from 10^6 to 10^{10} $sec.^{-1}$

The isothermal decay of emission associated with each of the glow peaks in anhydrite has been studied here. In all cases the decay obeys the relation,

$$I = I_0 \left(\frac{b}{b+t}\right)^n$$

which is the form predicted for a second order process[14] involving transitions through the conduction band. This means that the values of E in Table 1 represent the energy difference between the trapping levels and the conduction band which is in agreement with the conductivity experiments of LEPPER[15] for the $CaSO_4$:Mn system. The behavior of the parameters b and n with variations

Table 2. Isothermal decay parameters in anhydrite

Impurity	T_g in °K	Activation time in sec	Temperature in °K	b	n
680 p.p.m. Mn^{++}	390	45	300	30	0·92
680 p.p.m. Mn^{++}	390	300	300	60	0·78
680 p.p.m. Mn^{++}	390	45	335	150	1·74
680 p.p.m. Mn^{++}	390	305	335	200	1·59
680 p.p.m. Mn^{++}	390	45	360	40	1·57
680 p.p.m. Mn^{++}	390	300	360	50	1·34
680 p.p.m. Mn^{++}	390	45	390	20	1·54
680 p.p.m. Mn^{++}	390	300	390	25	1·35
680 p.p.m. Mn^{++}	390	45	420	5	1·36
680 p.p.m. Mn^{++}	390	300	420	10	1·07
680 p.p.m. Mn^{++}	390	45	455	5	1·12
680 p.p.m. Mn^{++}	390	300	455	10	1·06

Vol. 18
1961

in temperature and activation time have been investigated for the 390°K Mn^{++} peak and the results are given in Table 2. It is significant that the values of b increase with activation time since the second order decay model predicts that b should decrease as the fraction of filled traps is increased.[16]

The spectral distributions of the thermoluminescence have not been measured for any of the samples prepared here. However, the principal glow peaks for Mn^{++}, Sb^{+++} and Zn^{++} are intense enough at the optimum concentrations to be observed visually. It was found by this method that the emission from the 390°K Mn^{++} peak was in the green region (5000 Å) whereas all of the principal peaks for Zn^{++} and Sb^{+++} were in the blue region (4500 Å).

5. CONCLUSIONS

Thermoluminescence in anhydrite results from the presence of any one of five impurity ions: Mn^{++}, Zn^{++}, Sb^{+++}, Pb^{++} and Cd^{++}. Of these, only Mn^{++}, Zn^{++} and Sb^{+++} result in appreciable luminescent emission at very low impurity concentrations and only Mn^{++} and Zn^{++} appear to be important in interpreting the glow curves of most natural samples. The presence of an omission defect which is associated with an anion vacancy accounts for other thermoluminescent features which are often observed in natural samples. Annealing the natural samples at 800°C removes these features and has considerable effect on the glow curve due to Zn^{++}. Similar effects are observed for the Zn^{++} and Sb^{+++} glow peaks in synthetic samples.

A significant feature of the traps associated with the zinc and omission defect levels is the thermal transfer of electrons from deeper to shallower traps at temperatures where the transition rate from the deep traps to the conduction band is negligible. These transfer processes allow the deeper traps to be emptied at appreciable rates at temperatures well below the corresponding glow peak.

The emission intensities in natural anhydrite are much lower than those found in the carbonate minerals such as calcite and dolomite. This is partly due to the presence of Fe which suppresses the thermoluminescence due to Zn^{++} but mostly it reflects the low concentrations of Mn^{++}, Zn^{++}, and Sb^{++} in natural samples. These impurities are effectively excluded from the anhydrite lattice because of differences in ionic radii, coordination tendencies, and valence.

Acknowledgements—The author wishes to thank J. J. McALPIN, H. G. BUFFORD and W. R. HORNBUCKLE for their assistance, and Socony Mobil Oil Company, Inc. for permission to publish this paper.

REFERENCES

1. MEDLIN W. L., *J. Chem. Phys.* **30,** 451 (1959).
2. Supplied by United States Radium Corporation, New York.
3. WATANABE K., *Phys. Rev.* **77,** 748 (1949); NOSENKO B. M., REVZIN L. S. and YASKOLKO V. A., *Opt. i Spektrosk.* **3,** 345 (1957).
4. RIEHL N. and KEPPEL H., *Naturwissenschaften* **42,** 624 (1955).
5. AOKI Y., patent number 978, Japan, 1953.
6. Supplied by Johnson Mathey Company, London.
7. KELLEY K. K., SOUTHARD J. C. and ANDERSON C. T., Bureau of Mines Tech. Paper 625 (1941).
8. SANDELL E. B., *Colorimetric Determinations of Traces of Metals*, p.165. Interscience, New York (1950).
9. MOSS W. L. and MELLON M. G., *Indstr. Engng. Chem.*, Anal. Ed. **15,** 116 (1943).
10. MEDLIN W. L., *Anal Chem.* **32,** 632 (1960).
11. JOHNSON P. D. and WILLIAMS F. E., *J. Chem. Phys.* **18,** 1477 (1950).
12. RANDALL J. T. and WILKINS M. H. F., *Proc. Roy. Soc.* **184**A, 366 (1945).
13. LEVERENZ H. W., *Luminescence of Solids*, p. 177. John Wiley, New York (1950).
14. ADIROVITCH E. I., *J. Phys. Radium* **17,** 705 (1956); LEHOVEC K., *J. Opt. Soc. Amer.* **45,** 219 (1955).
15. LEPPER J., *Z. Naturf.* **10**a, 47 (1955).
16. ADIROVITCH E. I., *J. Phys. Radium* **17,** 705 (1956).

J. Phys. Chem. Solids Pergamon Press 1961. Vol. 18, Nos. 2/3, pp. 253–255. Printed in Great Britain.

THE TEMPERATURE DEPENDENCE OF DIELECTRIC CONSTANTS

E. E. HAVINGA

Philips Research Laboratories, N.V. Philips' Gloeilampenfabrieken, Eindhoven, Netherlands

(*Received* 17 *August* 1960)

Abstract—It is shown that for isotropic and for cubic materials there are three factors contributing to the temperature dependence of a dielectric constant: a direct volume expansion effect and the influences of volume expansion and of temperature on polarizability. A simple method is given to determine the values of the separate contributions from measurements. For some alkali halides and $BaTiO_3$ the magnitudes of the three effects are calculated and discussed.

IN THIS paper we shall show, for isotropic and for cubic materials, that the temperature dependence of a dielectric constant is due to three effects which can be distinguished by experiments. The starting point is the macroscopic Clausius–Mosotti equation, which is exact for any isotropic dielectric[1]:

$$\frac{\epsilon-1}{\epsilon+2}=\frac{4\pi\alpha_m}{3V} \tag{1}$$

Here ϵ is the dielectric constant and α_m is the polarizability of a macroscopic small sphere with a volume V, which sphere is large in comparison with the lattice dimensions. This polarizability α_m is proportional to the number of unit cells in the sphere, but it may further be a complicated function of the polarizability of the ions, the force constants and the geometry of the lattice of the dielectric.

Differentiation of equation (1) with respect to temperature gives:

$$\frac{1}{(\epsilon-1)(\epsilon+2)}\left(\frac{\partial\epsilon}{\partial T}\right)_p=-\frac{1}{3V}\left(\frac{\partial V}{\partial T}\right)_p+$$
$$+\frac{1}{3\alpha_m}\left(\frac{\partial\alpha_m}{\partial V}\right)_T\left(\frac{\partial V}{\partial T}\right)_p+\frac{1}{3\alpha_m}\left(\frac{\partial\alpha_m}{\partial T}\right)_V \tag{2}$$

or

$$\frac{1}{(\epsilon-1)(\epsilon+2)}\left(\frac{\partial\epsilon}{\partial T}\right)_p=A+B+C \tag{2a}$$

Hence we can distinguish three factors contributing to the temperature dependence of a dielectric constant:

A: The decrease in the number of polarizable particles per unit volume as the temperature increases, a direct result of volume expansion.

B: The increase in the polarizability of a constant number of polarizable particles with the increase in the available volume as the temperature increases.

C: The dependence of polarizability on temperature, the volume remaining constant.

Especially the temperature dependence of the dielectric constant of cubic $BaTiO_3$, which can be expressed in the form of a Curie–Weiss law, has attracted much attention. JONKER and VAN SANTEN[2] for example have pointed out the importance of the direct volume effect (factor *A*), which in this case appeared already to be sufficient to describe the whole phenomena. On the other hand DEVONSHIRE[3], SLATER[4] and TRIEBWASSER[5] proposed and worked out a model to explain the dependence of polarizability on temperature, the volume remaining constant (factor *C*). Furthermore DEVONSHIRE[3] derived an expression for the combined influence of the factors *A* and *B*, which expression involves elastic and electrostrictive constants, together with the coefficient of expansion. This expression was also used by TRIEBWASSER[5].

Table 1. *The three effects contributing to the temperature dependence of a dielectric constant. In parentheses values calculated with the use of the correction term in equation* (25) *of the paper of* TRIEBWASSER[5]; *they are good in agreement with the values calculated with equation* (3*a*)

Compound	ϵ	$\frac{10^5}{(\epsilon-1)(\epsilon+2)}\left(\frac{\partial\epsilon}{\partial T}\right)$	$A\times10^5$	$B\times10^5$	$C\times10^5$
LiF	9·29	+3·7	−3·5	+5·7	+1·5
KCl	4·69	+5·8	−3·2	+6·6	+2·4
NaCl	5·63	+5·4	−4·0	+8·4	+1·1
$BaTiO_3$ (cubic)	>1000	−0·6	−1·3	+1·5(+1·6)	−0·8(−0·9)

There is, however, a more direct and simple method to arrive at an experimental discrimination between the three effects, as we shall show below. In view of the existence of an equation of state of the form $f(p,V,T) = 0$ for isotropic and cubic materials, we have for the dependence of the dielectric constant on compression the relation

$$(\partial\epsilon/\partial_p)_T = (\partial\epsilon/\partial V)_T(\partial V/\partial p)_T$$

So the differentiation of equation (1) with respect to pressure gives:

$$\frac{1}{(\epsilon-1)(\epsilon+2)}\left(\frac{\partial\epsilon}{\partial p}\right)_T = -\frac{1}{3V}\left(\frac{\partial V}{\partial p}\right)_T + \\ +\frac{1}{3\alpha_m}\left(\frac{\partial\alpha_m}{\partial V}\right)_T\left(\frac{\partial V}{\partial p}\right)_T \qquad (3)$$

or

$$\frac{1}{(\epsilon-1)(\epsilon+2)}\left(\frac{\partial\epsilon}{\partial p}\right)_T = (A+B)\frac{(\partial V/\partial p)_T}{(\partial V/\partial T)_p} \qquad (3a)$$

Hence, to calculate the magnitudes of the three effects A, B and C separately, it will suffice to determine

$$\epsilon,\ (\partial\epsilon/\partial T)_p,\ (\partial\epsilon/\partial p)_T,\ (1/V)(\partial V/\partial T)_p$$

and

$$(1/V)(\partial V/\partial p)_T$$

by experiment.

For some compounds the necessary data are available[6,7,8,9]; the results of calculations based thereon are given in Table 1.

For the listed compounds the three factors are of the same order of magnitude. It will be seen that in all cases the volume-dependence of polarizability overcompensates the direct volume-expansion effect. The only respect in which $BaTiO_3$ differs greatly from the alkali halides is that the sign of the term

$$C = (1/3\alpha_m)(\partial\alpha_m/\partial T)_V$$

is reversed. Now it has been shown by VAN VLECK[10] that this term C should be equal to zero if only linear restoring forces were limiting the value of the polarization. Both in the alkali halides and in $BaTiO_3$, then, the potential energy of a unit cell at a constant volume cannot be expressed in terms of the squares of the displacements of the charges (of electrons and of nuclei) only; but further terms in the power series expansion of this even function must be added. However, in contrast to the situation for the alkali halides, the sign of the extra terms for $BaTiO_3$ is such that the restoring force constants are larger at displaced positions than at the potential minimum. The motion of an ion in such a potential field in fact is the basis of the theory of DEVONSHIRE[3] and SLATER[4].

It would be worthwhile to extend the measurements of the quantities needed for this analysis to a large number of compounds with a broad range of dielectric constant values in order to verify whether the behaviour of $BaTiO_3$ is normal for materials with a high dielectric constant or whether it is a special property of ferroelectrics and anti-ferroelectrics only. The fact that a large negative temperature coefficient has been found for

a number of other materials with a high dielectric constant[11] is an indication that it is perhaps a normal property of high-ϵ materials to have higher order terms which increase the restoring forces.

REFERENCES

1. FRÖLICH H., *Theory of Dielectrics*, (2nd. Ed). Clarendon Press, Oxford (1958).
2. JONKER G. H. and VAN SANTEN J. H., *Science* **109**, 632 (1949).
3. DEVONSHIRE A. F., *Phil. Mag.* (7) **40**, 1040 (1949).
4. SLATER J. C., *Phys. Rev.* **78**, 748 (1950).
5. TRIEBWASSER S., *J. Phys. Chem. Solids* **3**, 53 (1957).
6. LANDOLT–BÖRNSTEIN, *Phys. Chem. Tabellen*, (5 Auflage). Julius Springer, Berlin (1293).
7. MAYBURG S., *Phys. Rev.* **79**, 375 (1950).
8. MERZ W. J., *Phys. Rev.* **78**, 52 (1950).
9. KÄNZIG W., *Solid State Physics* **4**, 1 (1957).
10. VAN VLECK J. H., *J. Chem. Phys.* **5**, 556 (1937).
11. JONKER G. H., *De Ingenieur* **65**, E.154 (1953).

Vol. 18
1961

LETTERS TO THE EDITOR

Concerning the Fermi surface topology of metals and open orbits from magnetoresistance and Hall effect data

(*Received* 29 *June* 1960)

ALEKSEEVSKII and GAIDUKOV (A & G) have recently reported[1] a Fermi surface topology for copper that has "arms" (extensions of the Fermi surface that touch the Brillouin zone boundary) in the ⟨100⟩, ⟨110⟩ and ⟨111⟩ directions, and is thus in disagreement with the topology of PIPPARD[2] which has "arms" in only the ⟨111⟩ directions. The A & G model was determined from their magnetoresistance data using the theory of LIFSHITZ and PESCHANSKII (L & P),[3] who have also derived the same model for copper.[4] Interpretation of similar data, obtained from an extensive study by ourselves,[5] has led us to a topological model possessing "arms" in only the ⟨111⟩ directions. This model is further substantiated by newly observed "fine structure" in the magnetoresistance, and is confirmed by the detailed anisotropic behavior of the Hall constant.

The purpose of this letter is to point out that (i) while the topology of the Fermi surface determines the magnetoresistance behavior, magnetoresistance data *alone* does not generally define a unique Fermi surface topology, and that (ii) the model for copper with only ⟨111⟩ "arms", has been derived using an important concept: under certain conditions (such as exist in copper), open orbits occur along major crystalline directions other than those of the "arms", i.e. *not* along the "undulating cylinders".* This relationship between the directions of the "arms" of the Fermi surface and the possible directions of open orbits is clearly a feature that applies to metals in general. It seems likely that a reinterpretation of magnetoresistance data for gold[6] making use of this idea of "higher order" open orbits will lead to a simpler topology, possibly that of copper.†

According to the theory, a magnetoresistance anisotropy which has an H^2 dependence on magnetic field is generally indicative of an open Fermi surface, one which touches the Brillouin zone boundary. For each field direction giving a high magnetoresistance, there exists a band of open orbits whose direction is perpendicular to the field. A band of such open orbits, all having the same net direction, leads to a magnetoresistance "ridge" (magnetoresistance vs. magnetic field direction) that follows a great circle on the unit sphere perpendicular to the direction of the open orbits. The "ridge" is absent near those field directions for which the number of open orbits becomes vanishingly small, such as certain symmetry directions.

The essential consideration in deriving a Fermi surface topology from a set of open orbit directions is that each of the appropriate topological shapes must support a band of open orbits on its surface in each of the pertinent directions, and only in those directions. In general, this "boundary condition" does not define a unique topology. The most obvious topology is one in which there are "arms" along the direction of each "principal" band (i.e. a band which exists for nearly all magnetic field directions perpendicular to it) of open orbits as was proposed by A & G[1] and by L & P[4]. However, when the shape of the Fermi surface is appropriate, it can support orbits in directions other than those of the "arms". In copper, for example, we find that the ⟨111⟩ "arms" can support the necessary bands of orbits in the ⟨100⟩ and ⟨110⟩ directions. In fact, there are also other directions, namely the ⟨113⟩ and ⟨133⟩ directions, for which the surface supports much smaller bands of orbits and gives rise to a

* Although other configurations such as "corrugated planes" can support open orbits, only Fermi surfaces generated by intersecting "undulating cylinders" are discussed in this Letter. This simple representation is adequate for copper and probably for many other metals.

† Since this report was completed, an article by PRIESTLEY [*Phil. Mag.* **5**, 111 (1960)] has appeared in which he reanalyzed the gold data of A & G[1]. He concluded that the gross features of the magnetoresistance of gold follow from a Fermi surface topology similar to that of copper. PRIESTLEY's approach involves the determination of the orientations of the magnetic field for which holes exist, and in so doing has made implicit use of the existence of secondary open orbits.

Vol. 18
1961

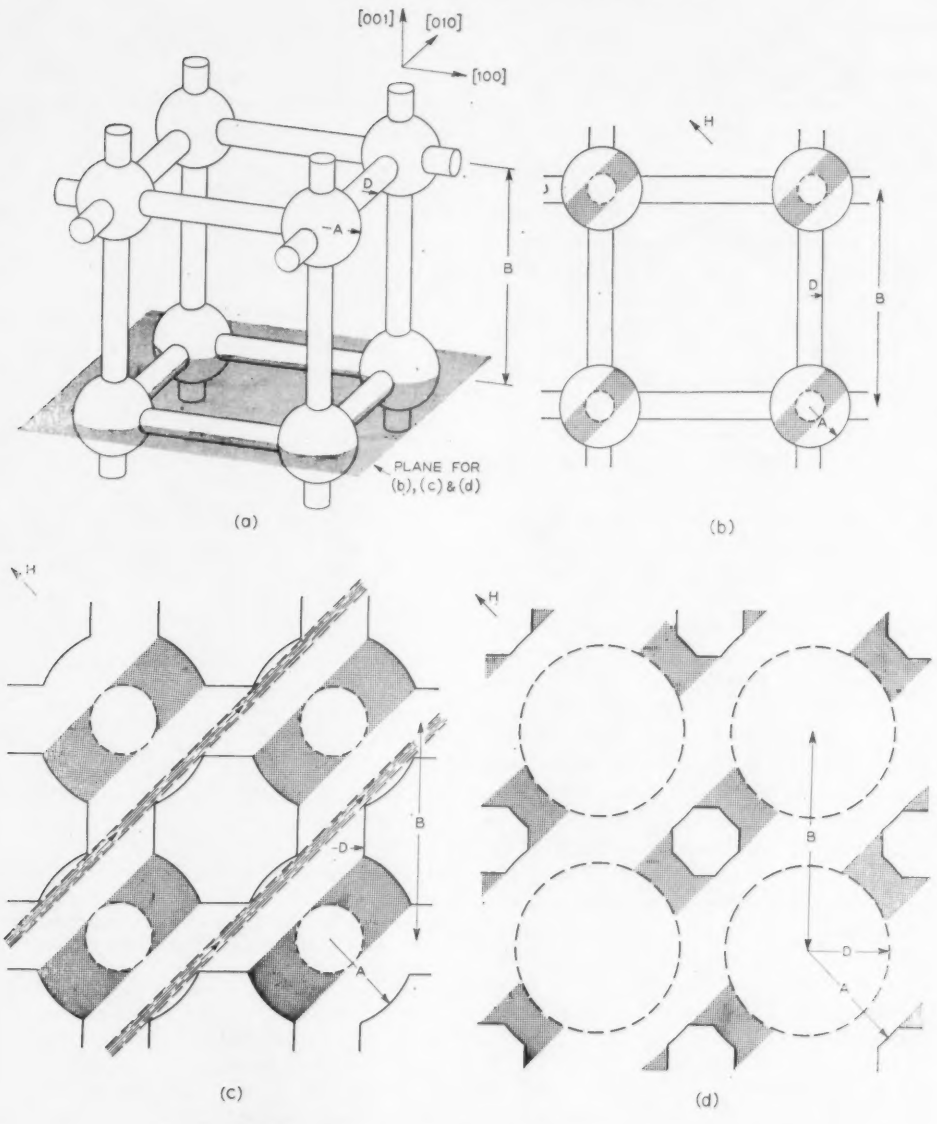

FIG. 1. Illustration showing how the existence of secondary open orbits is dependent on the shape of the Fermi surface. The schematic representation of a portion of a simple hypothetical Fermi surface model is shown in (a). The model is composed of spheres, of radius A, connected by cylinders, of radius D, to form a simple cubic network of unit length B. Relative values of A and D are varied for each of (b), (c) and (d) for which the plane of the cross-section is that indicated in (a). Primary open orbits are possible for a net [001] direction, perpendicular to the plane of the paper, and thus, perpendicular to the magnetic field. A projection of these primary open orbits onto the plane of the cross-section is shown by the cross-hatched regions of each subfigure. Secondary open orbits lie in the plane of the cross-section and are perpendicular to the magnetic field; they exist in (c), but not in (b) or (d).

series of small magnetoresistance "ridges" that have actually been observed. Further accounting for these small magnetoresistance "ridges" suggests the possible existence of even smaller bands of open orbits along ⟨012⟩, ⟨112⟩ and ⟨122⟩ directions.

Since "arms" in only one of the ⟨111⟩ directions are needed to support a ⟨111⟩-directed open orbit, these orbits are called *primary* open orbits; each of the ⟨100⟩- and ⟨110⟩-directed open orbits require just two differently directed ⟨111⟩ "arms" alternately repeated, and these orbits are called *secondary* open orbits. Similarly, the ⟨113⟩- and ⟨133⟩-directed open orbits involve three ⟨111⟩ "arms" and are thus *ternary* open orbits, and the open orbits along ⟨012⟩, ⟨112⟩ and ⟨112⟩ directions become *quaternary* open orbits.

The fact that secondary open orbits occur in the general case and that their existence depends on the shape of the Fermi surface is illustrated for a simple hypothetical model shown in Fig. 1. When the magnetic field is chosen along a [$\bar{1}$10] direction, for example, Figs. 1(b), 1(c) and 1(d) show a primary band of open orbits that is present which extends to infinity in the [001] direction, perpendicular to the plane of the paper. However, only in Fig. 1(c) is the shape of the Fermi surface such as to permit an additional band of orbits—secondary open orbits—which lead off in the [110] direction. In the example of Fig. 1(b) the spheres are too small to support similar [110]-directed open orbits, while in the example of Fig. 1(d) the cylinders are too large. When H is along the [$\bar{1}$10] axis, a geometrical study shows that a band of secondary open orbits is present which leads off in the [110] direction when the following inequalities hold:

$$(8)^{1/2}D < B < (8)^{1/2}A$$

and

$$B < 2D+2(A^2-D^2)^{1/2}.$$

Since in most cases it is difficult by means of magnetoresistance data alone to distinguish among a number of possible Fermi surface topologies, an independent means to obtain additional information is required, such as can be obtained from the Hall constant. We have measured the Hall constant for a number of orientations in copper and find that these data strongly support the Pippard topology. Further details concerning our experimental work and its interpretation in terms of the ideas proposed here will be published at a later date.

Bell Telephone Laboratories J. R. KLAUDER
Murray Hill J. E. KUNZLER
New Jersey

References

1. ALEKSEEVSKII N. and GAIDUKOV YU, *Zh. exsp. teor. fiz.* **36,** 447 (1959); *Soviet Physics JETP* **9,** 311 (1959).
2. PIPPARD A., *Phil. Trans.* **A250,** 325 (1957); MORSE R. and GAVENDA J., *Bull. Amer. Phys. Soc.* **4,** 463 (1959); **5,** 151 (1960) (post deadline paper); SHOENBERG D., *Nature, Lond.* **183,** 171 (1959); *Phil. Mag.* **5,** 105 (1960); LANGENBERG D. N. and MOORE T. W., *Phys. Rev. Letters* **3,** 328 (1959).
3. LIFSHITZ I. and PESCHANSKII V., *Zh. exsp. teor. fiz.* **35,** 1251 (1958); *Soviet Physics JETP* **8,** 875 (1959).
4. LIFSHITZ I. and PESCHANSKII V., *Zh. exsp. teor. fiz.* **38,** 188 (1960).
5. KUNZLER J. and KLAUDER J., *Bull. Amer. Phys. Soc.* **5,** 150 (1960).
6. GAIDUKOV YU., *Zh. exsp. teor. fiz.* **37,** 1281 (1959); *Soviet Physics JETP* **10,** 913 (1960). The touching of the Fermi surface for gold has also been inferred from ultrasonic attenuation measurements, MORSE R., MAYERS A. and WALKER C., *Phys. Rev. Letters* **4,** 605 (1960).

The existence of Kramers-Kronig relations for the magneto-conductivity tensor

(*Received* 14 *December* 1959; *revised* 8 *August* 1960)

McCLURE[1, 2] has derived Kramers-Kronig relations between the σ_{xx} and σ_{xy} components of the conductivity tensor using the assumption that the relaxation time is a function of energy and k_z and not of position on the orbit. The orbits are restricted to circular orbits only and the magnetic field is in the z direction where the z direction is an axis of symmetry of the energy surfaces. McCLURE then proceeds to show that such dispersion relations provide a powerful means of obtaining information concerning the number of carriers, their mobilities, etc., from experimental data. It is therefore of great interest to discover

whether the dispersion relations for σ_{xx} and σ_{xy} can hold for a more general relaxation time and more general orbits.

The Kramers-Kronig relations relate the real and imaginary parts of a complex function if the function is analytic in the upper half plane. By using the periodicity of the relaxation time on the orbit we discovered that the function $\sigma = \sigma_{xx} + i\sigma_{xy}$ is no longer analytic in the upper half plane when the relaxation time is not constant on the orbit. We therefore can conclude that the constancy of the relaxation time on the orbit is not merely a sufficient condition for the existence of Kramers-Kronig relations but is also a necessary one.

We have been unable to find dispersion relations for arbitrarily shaped orbits. However, McCLURE's derivation of the Kramers-Kronig relations for the components of the magneto-conductivity tensor with constant relaxation time on the orbit can be extended from the case of circular orbits to the case of elliptical orbits. The method is to transform an ellipsoid into a sphere. The transformation can be done for the magnetic field oriented at arbitrary angles to the principal axes of the ellipsoid. Dispersion relations can be obtained for various combinations of components of the conductivity tensor, the effective masses, and the angles at which the magnetic field is oriented to the principal axes by solving a series of linear equations. For the case where the magnetic field is along a principal axis, the expressions simplify and we have the following dispersion relations

$$\sigma_{xx}(H) = \frac{p}{\pi}\int_{-\infty}^{+\infty} \frac{dH'}{H-H'}\left(\frac{m_x}{m_y}\right)^{1/2}\sigma_{xy}(H')$$

$$\sigma_{xy}(H) = \frac{p}{\pi}\int_{-\infty}^{+\infty} \frac{dH'}{H-H'}\left(\frac{m_y}{m_x}\right)^{1/2}\sigma_{xx}(H')$$

We therefore conclude that relations similar to those derived by McCLURE for circular orbits can be derived for elliptical orbits. However, the simple form of the Kramers-Kronig relations that held for circular orbits no longer hold even for the simple extention to elliptical orbits. For the case of a single ellipsoid, we can determine the ratio of the effective masses in the two directions perpendicular to the magnetic field, when the magnetic field is in the direction of a principal axis, by finding what factor must multiply σ_{xy} for the dispersion relations to hold. For the more complicated case of several ellipsoids, the more general relations can be used to separate the contributions from each type of carrier if the effective masses and the orientation of the field to the principal axes is known.

Acknowledgement—The author wishes to acknowledge many helpful discussions with Professor M. H. COHEN.

Institute for the Study of Metals H. N. SPECTOR
University of Chicago
Chicago 37
Illinois, U.S.A.

References

1. McCLURE J., *Phys. Rev.* **101,** 1642 (1956).
2. McCLURE J., *Phys. Rev.* **112,** 715 (1958).

The electrolysis of thorium oxide crystals

(*Received* 1 *May* 1958; *revised* 29 *July* 1960)

AN EXPONENTIAL rate law for the electrolytic liberation of oxygen from thorium oxide has been observed. It is of interest that the empirical value of the exponent is always of the order of eV/kT, where e and k take their usual meaning as universal constants, T is the temperature of the oxide crystal, and V the applied voltage.

Measurements of the electrolytic evolution of oxygen from a thorium oxide crystal were made at this laboratory some time ago. A recent re-examination of the data shows that the voltage dependence of the rate of oxygen liberation r may be expressed as

$$r = A\exp(zeV/kT)$$

where z is a number between 1 and 2 (z being constant for a given specimen at a given point in its history).

Experimental details have been presented elsewhere.[1] Briefly, a thorium oxide crystal with evaporated platinum electrodes was heated *in vacuo* in a resistance furnace. When current (0–300 μA) was passed through the crystal,

oxygen was liberated: a portion of the liberated oxygen could escape through a slit in the furnace heat shield. Some of this oxygen could collect on a tungsten filament, and be detected by the poisoning of the thermionic emission therefrom. A calculated calibration was made based on what is known of the thermionic behaviour of oxygen-contaminated tungsten,[2] and on the geometry of the experiment. This calibration is believed to be valid within a factor of two. Application of

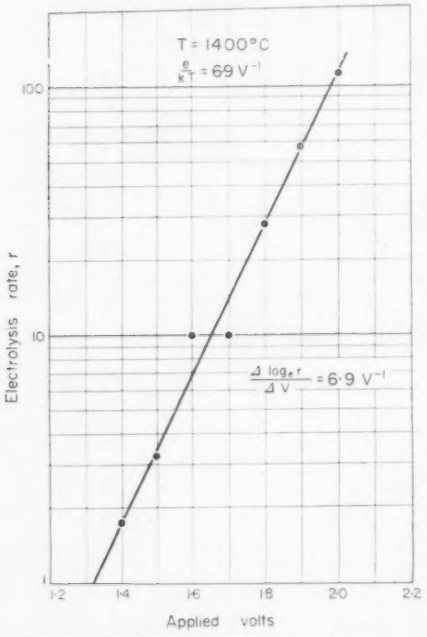

FIG. 1. Rate of electrolytic liberation of oxygen from a thorium oxide crystal as a function of applied voltage.

the calibration suggested that one oxygen atom is liberated for every two electrons measured in the external circuit. Proportionality between current and evolution rate is good except at very low currents. Previous work[3] also leads one to suppose that the conduction is virtually 100 per cent ionic.

Values of oxygen evolution rate for one experimental run are given in Fig. 1. The exponential increase with voltage is seen. The slope for the run shown is 6·9 V^{-1}; the calculated value of e/kT for the temperature of 1673°K is also 6·9 V^{-1}.

During the history of a specimen, there was a tendency for the data to shift to the right (i.e. more voltage required for a given rate) and for the slope of the line to increase somewhat. The exponential character however, was maintained over a wide variety of conditions, and the slope in all cases lay in the range between e/kT and $2e/kT$.

The problem of the carrier concentration as a function of position in an ionic conductor with blocked electrodes and applied voltage has been treated by JAFFE[4] and others[5, 6]. By applying the Einstein diffusion equation to one of JAFFE's results, and also invoking symmetry conditions developed by JAFFE, the not unexpected relationship is obtained:

$$N_b = N_0 \exp(qV/2kT)$$

where V is the applied voltage. N_0 is the carrier concentration when the material is in thermal equilibrium with no applied potential; N_b is the carrier concentration at the electrode; q is the charge of the carrier which may be e, $2e$, or possibly higher.

To bridge the gap between JAFFE's treatment and experimental results, one must consider (a) the effect of unblocking the electrodes, (b) the nature of the rate-limiting process, (c) the charge of the carrier. The formal similarity between the theoretical expression for blocked electrodes and the empirical expression leads to the hope that an understanding of this solid ionic conductor may be possible in terms of JAFFE's model.

Bartol Research Foundation of the Franklin Institute
Swathmore
Pennsylvania
U.S.A.

D. L. GOLDWATER

References

1. GOLDWATER D. L. and DANFORTH W. E., *Proceedings of the Third National Conference on Tube techniques*. New York University Press, N.Y. (1958).
2. DEBOER J. H., *Electron Emission and Adsorption Phenomena*, p.145 ff. Cambridge University Press (1935).
3. DANFORTH W. E. and BODINE J. H., *J. Franklin Inst.* **260,** 467 (1955).
4. JAFFE G., *Ann. Phys., Lpz.* **16,** 217 (1933).
5. MACDONALD J. R., *Phys. Rev.* **92,** 4 (1953).
6. FRIAUF R. J., *J. Chem. Phys.* **22,** 1329 (1954).

Über den Einfluss von Temperatur und äusserer Umgebung auf den Photo-Magneto-Elektrischen (PEM-) Effekt bei CdS.

(*Received* 25 *July* 1960)

BEI KÜRZLICH durchgeführten Untersuchungen über den PEM-Effekt bei CdS-Einkristallen zeigte es sich, dass das den Kristall umgebende Medium den beobachteten PEM-Strom stark beeinflusst. Wir beobachteten, wenn sich der Kristall im Hochvakuum befand, bisweilen PEM-Ströme, die um den Faktor 100 die an Luft gefundenen Werte übertrafen. Wir nehmen an, dass bei den Messungen in Luft die Oberflächenrekombinationsgeschwindigkeit für die Löcher $v_{s,p}^{\text{Luft}}$ durch adsorbierte Schichten stark erhöht wird ; sie lässt sich in diesem Fall wie folgt abschätzen : $v_{s,p}^{\text{Luft}} \approx 3 \times 10^5$ cm/s. Aus den im Hochvakuum gefundenen Ergebnissen lässt sich vermuten, dass hier die Oberflächenrekombination nur geringen Einfluss hat, so dass man annehmen muss, $v_{s,p}^{\text{Vac}} < 2500$ cm/s. Um gut reproduzierbare Ergebnisse zu erhalten, muss man die Untersuchungen im Hochvakuum durchführen.

Die beobachteten PEM-Ströme waren bei annähernd spektralreinen CdS-Kristallen am grössten und führten bei Zimmertemperatur auf Löcherdiffusionslängen L_p bis zu 3×10^{-4}cm (unter der Annahme $\mu_n + \mu_p \approx 100$ cm^2/Vs). In stärker verunreinigten Kristallen unbekannten Reinheitsgrades wurden L_p-Werte bis hinab zu $1{,}5 \times 10^{-6}$ cm beobachtet. In diesem Fall ($L_p \ll 1/\kappa$, κ = Absorptionskoeffizient für das verwendete Licht) muss man bei der Berechnung von L_p beachten, dass an die Stelle von L_p in der üblichen Formel für den PEM-Strom das Produkt κL_p^2 tritt.

Bei fast allen Kristallen beobachtet man nach tieferen Temperaturen hin eine Abnahme des PEM-Stromes (Bild 1, Kurve 1). Diese lässt sich mit einer Abnahme der Löcherlebensdauer τ_p nach tiefen Temperaturen hin in Zusammenhang bringen.[1] Eine genaue Analyse zeigt, dass hierfür eine in etwa 0,1 bis 0,2 eV Abstand vom oberen Rand des Valenzbandes befindliche Termgruppe die Ursache sein muss.

Bei einer Reihe von Kristallen verringerte sich durch eine thermische Behandlung bei 120 bis 170°C der PEM-Strom in offenbar irreversibler Weise (Bild 1, Kurve 2). Diese irreversiblen Veränderungen der Kristalle in Bezug auf den PEM-Effekt, die wahrscheinlich auf ziemlich komplexen Vorgängen beruhen, führten bei einigen Kristallen sogar zu einer Umkehr des Vorzeichens des PEM-Stromes, was zunächst ausserordentlich überraschte, da diese Erscheinung ja bedeutet, dass ein Diffusionsstrom von Elektronen oder Löchern aus dem Kristallinnern nach aussen fliesst. Dass diese Erscheinung auf eine starke, unsymmetrische Oberflächenrekombination zurückzuführen ist,

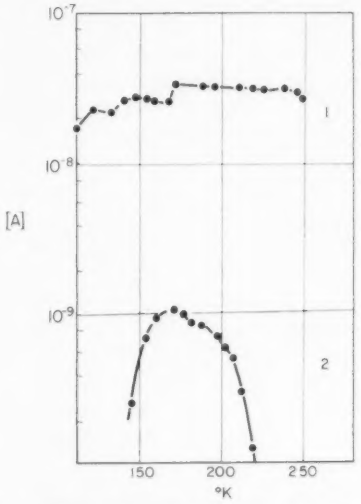

ABB. 1. Temperaturabhängigkeit des PEM-Stromes. Kurve 1: Kristall unvorbehandelt ; Kurve 2 : Kristall etwa 20 min bei 120°C in Luft (Druck etwa 0,1 Torr) ausgeheizt.

konnte durch besondere Versuche ausgeschlossen werden. Ebenso liefert der Nernst-Effekt mit dem bei der Belichtung entstehenden Temperaturgradienten einen um den Faktor 10 zu kleinen Wert gegenüber dem beobachteten. Am wahrscheinlichsten erscheint uns folgende Erklärung[2] für diesen "anomalen" PEM-Effekt : Die durch das Licht in einer dünnen Oberflächenschicht erzeugten inneren Photoelektronen haben zunächst eine grössere Energie, als sie dem thermischen Gleichgewicht mit dem Gitter entspricht. Sie diffundieren als "heisse" Elektronen in das Kristallinnere hinein. Ein entsprechender Diffusionsstrom thermischer Elektronen muss dann

aus Neutralitätsgründen zur Oberfläche fliessen. Dieser Strom thermischer Elektronen wird jedoch wegen der Energieabhängigkeit der Streuung am akustischen Zweig (solange nicht Conwell–Weisskopf-Streuung überwiegt) stärker durch das Magnetfeld abgelenkt als der Strom "heisser" Elektronen. Eine quantitative Abschätzung nach einem einfachen Modell, das mit zwei Trägersorten ("heissen" und thermischen) und entsprechenden Diffusionskoeffizienten und Beweglichkeiten arbeitet, gestattet aus dem anomalen PEM-Effekt die Zeit τ_h abzuschätzen, die ein Elektron braucht, um sich mit dem Gitter ins thermische Gleichgewicht zu setzen. Wir erhalten $\tau_h \approx 4 \times 10^{-13}$s. Vergleicht man diesen Wert mit der freien Flugzeit τ_0 der thermischen Leitfähigkeitselektronen in CdS ($\tau_0 \approx 0{,}5 \times 10^{-13}$s), so erkennt man, dass offenbar wenige "Stösse mit dem Gitter" zur Herstellung des Gleichgewichtes genügen. Wahrscheinlich spielt bei diesem Prozess die spontane Emission von Schallquanten des optischen Zweiges eine entscheidende Rolle. Den "anomalen" PEM-Effekt muss man offenbar immer dann beobachten können, wenn es gelingt durch eine hinreichend starke Verringerung der Minoritätsträgerdiffusionslänge, den normalen PEM-Effekt zum verschwinden zu bringen.

Eine ausführliche Veröffentlichung ist in der Zeitschrift für Physikalische Chemie beabsichtigt.

Anerkennungen — Der Verfasser möchte den Herrn Dr. BROSER und Dr. HILDISCH für die Überlassung der Kristalle und Herrn Dr. E. A. NIEKISCH für viele fruchtbare Diskussionen und Anregungen danken.

II. Physikalisches Institut J. AUTH
der Humboldt-Universität
Berlin

Literatur

1. BROSER I. und BROSER-WARMINSKY R., *J. Phys. Chem. Solids* **6**, 386 (1958).
2. AUTH J., *Phys. Verh. Mosbach* **10**, 130 (1959).

Polarization of low temperature luminescence from thallium-containing sodium nitrite single crystals

(*Received* 13 *July* 1960)

IN THE previous paper[1] by some of the present authors it was reported that pure silver nitrite and silver-containing sodium nitrite crystals show yellow luminescence associated with a fine structure at liquid air temperature. In the continuation of this work it was found that pure sodium nitrite crystal emits blue luminescence with a fine structure at liquid air temperature, and further that thallium or lead-containing sodium nitrite crystal show red luminescence similar to that from silver-containing salt. The result of pure $NaNO_2$ is just the same as observed by SIDMAN[2,3] but was obtained independently of him.

In this letter the results of a study on the polarization of the luminescence from Tl^+-containing $NaNO_2$ single crystals are reported. Single crystals were prepared by means of the Bridgman method. Thallium salt was added to molten $NaNO_2$ with content of 0·1 mol. per cent. Single crystals containing more than this content could not be made by this method.

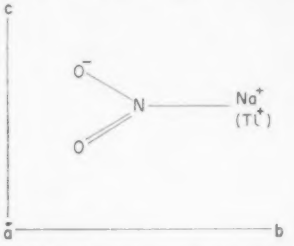

FIG. 1. Pictorially shown crystal structure of $NaNO_2$ containing Tl^+.

Luminescent properties were measured at liquid nitrogen temperature by the excitation of 3650 Å mercury line. $NaNO_2$ has an absorption band due to NO_2^- ion with maximum around 3500 Å which is polarized in the *a*-direction of the crystal, i.e. perpendicular to the plane of NO_2^- ion (see Fig. 1). This absorption has been assigned to a transition in which one of the unshared electrons on N atom is raised to an antibonding π orbital of NO_2^- ion ($n_N \rightarrow \pi^*$).[3,4] By the 3650 Å excitation Tl^+-containing $NaNO_2$ shows the luminescence with blue and red bands as shown in Fig. 2, the former with a sharp fine structure being due to NO_2^- and the latter with maximum around 6300 Å due to Tl^+. When Tl^+ salt is added a new but very weak absorption band appears around 4600 Å. This band was so weak that neither the observation of Tl^+ luminescence by the direct excitation due to this absorption, nor even the

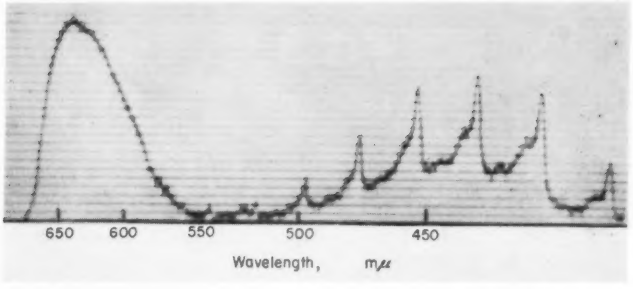

FIG. 2. Microphotometer trace of emission spectrum from Tl^+-containing $NaNO_2$ at 77°K by the excitation of 3650 Å line.

[*facing p.* 262

BLANK
PAGE

Vol.
19

measurement of the polarization of this absorption, was successful.

The polarization characteristics of blue and red luminescence at 77°K are shown in Fig. 3. Degree of polarization P is given by

$$P(\theta) = [(I_{\parallel} - I_{\perp})/(I_{\parallel} + I_{\perp})]_{\theta},$$

where $I_{\parallel}$ and $I_{\perp}$ are luminescent intensities, each corresponding to the case where polarizer and analyzer are either parallel or perpendicular to each other, and θ is an angle between the electric vector of exciting light and crystal axis shown as the horizontal line in the figure for each case. Marks beside each curve like $\overset{b}{+}\!-\!a$ mean that the exciting light was irradiated perpendicularly to the crystal plane indicated, and luminescence was observed in the same direction.

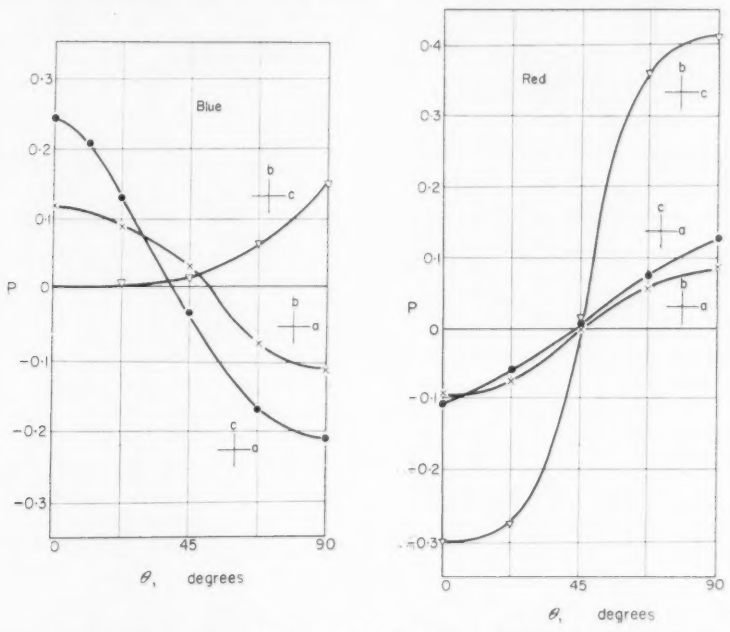

FIG. 3. Degree of polarization P of the blue and red luminescence from Tl^+-containing $NaNO_2$ single crystal at 77°K. θ is an angle between the electric vector of exciting light and crystal axis which is shown by horizontal line of the marks beside each curve like $\overset{b}{+}\!a$.

The blue luminescence is polarized in the a-direction, i.e. the same direction as that of 3500 Å absorption, which is a quite reasonable result. The red luminescence is polarized in the b-direction, which is the direction connecting Tl^+ and N if Tl^+ in the crystal is assumed to replace Na^+. It is suggested that a weak coordination bond is formed between Tl^+ and N because of the unshared electrons of the latter. Then the red luminescence may be assigned to a transition between the excited and ground level of this bond. This seems to explain reasonably the results of polarization. Instead of this the following explanation might be also possible. An assumption may be made that the red luminescence is assigned to the reverse of a transition in which one of the unshared electrons on the N atom is raised to the empty $6p$ orbital of Tl^+. Then the experimental results seem understood by this assumption. If these considerations are correct, then it is suggested that since the 3650 Å excitation line here used causes $n_N \rightarrow \pi^*$ transition within NO_2^-, some kind of intermolecular transfer of excitation energy should take place to produce the red luminescence.

Vol. 18
1961

A detailed paper of this study will appear in the near future.

Institute for Solid State Physics SHOJI MAKISHIMA
University of Tokyo TAKESHI TOMOTSU
Minato-Ku MASAO HIRATA
Tokyo RYOZO KAMBE
Japan SHIGEO SHIONOYA

References

1. MAKISHIMA S. and TOMOTSU T., *Bull. Chem. Soc. Japan* **27,** 476 (1954).
2. SIDMAN J. W., *J. Amer. Chem. Soc.* **78,** 2911 (1956).
3. SIDMAN J. W., *J. Amer. Chem. Soc.* **79,** 2669 (1957).
4. TRAWICK W. G. and EBERHARDT W. H., *J. Chem. Phys.* **22,** 1462 (1954).

To the structure and oxygen content of copper and copper–manganese ferrite

(*Received* 11 *July* 1960)

VARIOUS authors[1, 2] reported Cu ferrite to be tetragonal beneath and cubic above a certain temperature, for which values between 480 to 760°C were published. The cubic structure could be preserved down to room temperature only by quenching the samples. Further it is reported,[3] that an addition of 1·5–55 per cent of Mn_3O_4 to $CuFe_2O_4$ would cause the structure of the mixed spinel, heated in air at 1000°C, to be cubic at room temperature even after cooling at a very low rate.

During a previous investigation[4] there arose some questions, concerning the interpretation of differential thermal analysis curves of mixtures of CuO and Fe_2O_3 (1 : 1) and of some mixtures of $CuFe_2O_4$ and MnO_x. We studied therefore the changes, occurring during the heating of two homogenous oxide mixtures of the compositions $CuOFe_2O_3$ and 0·42 CuO_x, 0·43 Fe_2O_3, 0·15 MnO_y respectively. The mixtures were preheated in air for 3 hr at temperatures between 600–1100°C, reground, pressed and heated finally for 10 hr at temperatures between 600–1100°C, the furnace atmosphere being air for one part and oxygen for the remaining part of samples. The medium cooling rate was 9°C/min. With one series of samples preheating was omitted.

X-ray analysis of the cooled samples, differential thermal analysis (DTA) in air and chemical determination of the oxygen content were used for the investigation.

The DTA curve of copper ferrite showed only a single reversible endothermic minimum beginning at ~970°C, with its peak at ~1015°C (Fig. 1, curve 1). The position of the minimum was independent of the preceding heat treatment of the samples. According to chemical analysis, a steep loss of oxygen (0·6–0·7 wt. per cent) occurred simultaneously between 900–1000°C. The structure of the ferrite below this loss, that is up to 900°C, was tetragonal, after heating at 1000°C both a cubic and a tetragonal spinel phase were present simultaneously. No precipitated oxides of copper or iron were found. After heating at 1100°C still more oxygen was lost and, besides the cubic spinel phase, a phase of the type of $CuFeO_2$ appeared on the debyegram.

The DTA curve of the copper–manganese-ferrite (Fig. 1, curve 2) showed two endothermic minima. The first of them, beginning at ~960°C and with its peak at ~1005°C, was accompanied by a change of the structure of the spinel from tetragonal to cubic, but by no (or by no appreciable) change in the oxygen content of the samples. Due to the experimental conditions and the slow rate of the reverse process no corresponding exothermic peak appeared on the cooling curve of the DTA. The second minimum, beginning at ~1010°C, with its peak at ~1060°C, resembled in shape and reversibility the only minimum of pure copper ferrite. It was also in correspondence with a steep loss in oxygen content (0·6–0·7 wt. per cent) and with the occurrence of a phase of the $CuFeO_2$ type in addition to a cubic spinel phase.

The reported results, especially those of the DTA, lead us to the assumption, that in pure copper ferrite the tetragonal–cubic crystallographic transition takes place at the same time as the change in oxygen content, that is when there is an appreciable increase of the concentration of Cu^+ ions, or it is proceeding too slowly and within too wide a temperature range, to be registered by our methods. In copper–manganese-ferrite with cation compositions suitable for spinel formation there is a clear tetragonal to cubic crystallographic transition without any accompanying chemical change.

The dependence of the structural and chemical changes in the system CuO–MnO–FeO on atmo-

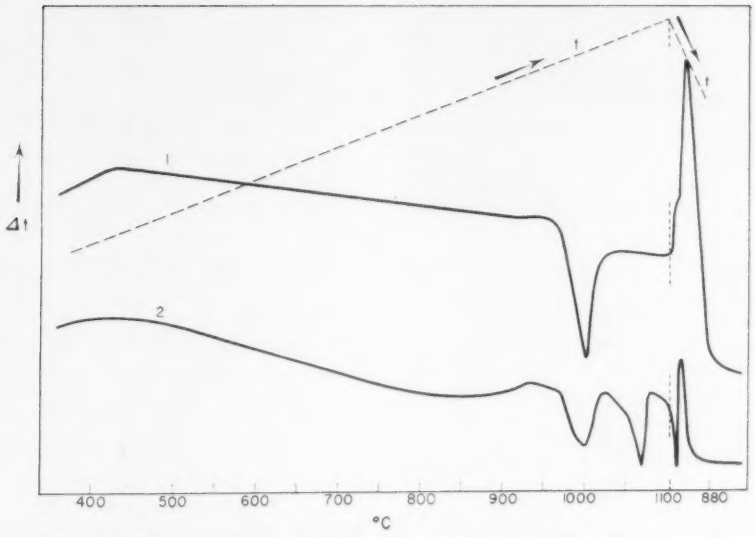

FIG. 1. Differential thermal analysis (1) of copper-ferrite; (2) of copper–manganese-ferrite (composition see text); Δt difference of temperature between measured sample and reference sample; dotted line t heating and cooling curve of the furnace.

Vol. 18
1961

sphere, temperature and preceding heat treatment will be dealt with in detail in a future paper.

Institute of Technical Physics
of the Czechoslovak Academy
of Sciences
Prague
Czechoslovakia

A. BERGSTEIN
L. ČERVINKA

References

1. TOROPOV N. A. and BORISENKO A. N., *Ž. prikl. Chim.* **11,** 1165 (1950).
2. WEIL L., BERTAUT F. and BOCHIROL L., *J. Phys. Radium* **11,** 208 (1950).
3. DELORME C., *Bull. Soc. franç. Minér.* **81,** 79 (1958).
4. BERGSTEIN A., *Coll. Cz. Chem. Commun.*, to be published.

Room temperature luminescence in pure alkali halides*

(*Received* 3 *October* 1960)

LUMINESCENCE in pure alkali halides has been observed by several investigators.[1] At liquid nitrogen temperature light absorbed in the fundamental absorption band can excite luminescence with nearly unit efficiency. The emission is in the visible. Alkali halides are also known to luminesce during coloring with X-rays at room temperature.[2] Irradiation with γ-rays also gives rise to visible emission.[3]

We have observed a weak luminescence in NaCl, KCl, KBr and KI associated with coloring by ultraviolet light at room temperature. The irradiation for coloring and excitation was obtained from a vacuum monochromator with a hydrogen discharge lamp. The luminescence was detected with a 5819 photomultiplier having response from 3600 A to 6300 A. Single crystals from the Harshaw Chemical Company were used. The KI showed the well-known thallium emission which however was independent of coloring by u.v. and could be neglected. One crystal of NaCl grown at this laboratory with no detectable OH absorption behaved in all respects like the Harshaw material known to contain OH.

All pure crystals showed luminescence at room temperature building up to maximum intensity

* This work is supported in part by the Office of Naval Research.

with a few seconds irradiation. We associate this delay with the formation of a color center by the light. It is known that light absorbed in the fundamental absorption band produces high densities of F-centers.[4] We found the centers responsible for the luminescence stable at room temperature but bleaching with visible light (for KI light above a wavelength of 6850 A suffices) reduces the emission.

The measured excitation spectra are shown in Fig. 1. The total luminescence seen by the photomultiplier is plotted against the energy of the exciting photons. The minima occur at energies corresponding to "exciton peaks" in the absorption spectra.[5] This effect has also been observed by TEEGARDEN at low temperature. He suggests the high optical absorption in the region of the absorption peak confines the excitation to the surface layers favoring radiationless recombination at the surface.

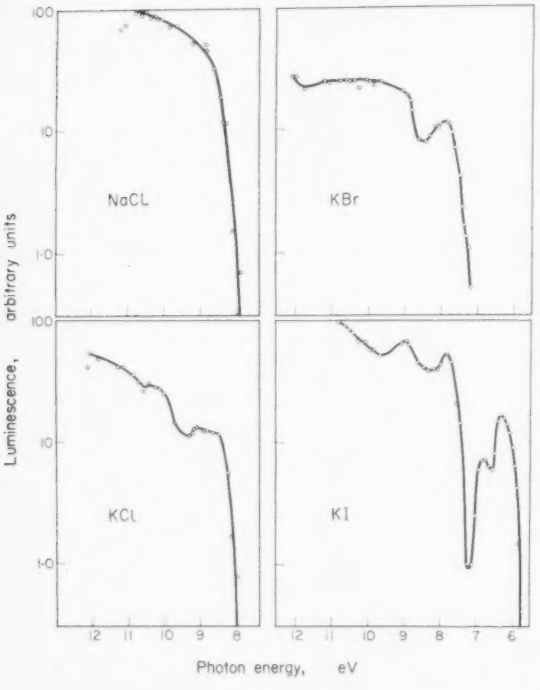

FIG. 1. Excitation spectra measured after extended u.v. irradiation. We associate the sharp threshold at low energy with the onset of band-to-band transitions.

Following TAFT and PHILIPP[6] in their treatment of external photoemission we have taken for the threshold of luminescence the point where the yield is two orders of magnitude below the high energy saturation value. Table 1 summarizes these results. The onset of band-to-band transitions has been ascribed to a shoulder in the optical absorption spectra commonly appearing on the high energy side of the first exciton peak(s).[6] The yield of the 300°K luminescence rises rapidly at this shoulder. If we assume this identification of the position of the absorption shoulder with the energy of the band gap, we are led to conclude that the 300°K luminescence results from a process such as the successive recombination of free electrons and holes at color centers. The sum of the luminescence threshold and the electron affinity then should give the threshold for external photoemission. From Table 1 it will be seen that the electron affinities obtained in this manner are of the right order of magnitude.

Table 1. *Thresholds for luminescence at room temperature compared to the thresholds for external photoemission. The electron affinity is the difference between the two thresholds.*

Salt	Threshold for luminescence, eV	Threshold for photoemission, eV	Electron affinity, eV
NaCl	7·9	8·5 (a)	0·6
KCl	8·0	8·7 (b)	0·7
KBr	7·1	8·1 (b)	1·0
KI	5·8	7·3 (b)	1·5

(a) after Ref. (7)

(b) after Ref. (6)

We hope a study of the temperature dependence of the 300°K luminescence, which we will undertake next, will clarify the relation between the effect observed by us and the other types of luminescence found in pure alkali halides.

Acknowledgements—The author wishes to thank Dr. F. FUMI and Dr. H. S. SACK for helpful discussions and

particularly Dr. P. L. HARTMAN for assistance and encouragement.

Department of Physics and T. TIMUSK
Laboratory of Atomic and Solid
State Physics
Cornell University
Ithaca
New York

References

1. TEEGARDEN K. J., *Phys. Rev.* **105,** 1222 (1957); VAN SCIVER W. and HOFSTADTER R., *Phys. Rev.* **97,** 1181 (1956); MARTIENSSEN W., *Z. Phys.* **133,** 153 (1952).
2. PERRINE J. O., *Phys. Rev.* **22,** 48 (1923); CHATTERJEE A., *Indian J. Phys.* **23,** 265 (1950); SPICER W. E., *Phys. Rev.* **106,** 726 (1957).
3. MORGENSHTERN Z. L., *Optik i Spektrosk.* **8,** 672 (1960).
4. SMAKULA A., *Z. Phys.* **63,** 762 (1930); APKER L. and TAFT E., *Phys. Rev.* **79,** 964 (1950).
5. EBY J. E., TEEGARDEN K. J. and DUTTON D. B., *Phys. Rev.* **116,** 1099 (1959). These authors give an extensive set of absorption spectra that we have made much use of.
6. TAFT E. A. and PHILIPP H. R., *J. Phys. Chem. Solids* **3,** 1 (1957).
7. TAYLOR J. W. and HARTMAN P. L., *Phys. Rev.* **113,** 1421 (1959).

Vol. 18
1961

On the thermodynamics of the Au–Pt system

(*Received* 19 *September* 1960)

THE GOLD–PLATINUM system shows a distinctly asymmetric miscibility gap in the solid (f.c.c.) state. Such a gap may in principle be brought about by an infinity of excess free-energy functions. For instance the mixing entropy may be taken to be Gibbsian, the excess free energy then being a function of concentration only. More generally, it can be taken to depend on temperature[1,2,3]; but only a non-linear dependence on T corresponds with specific-heat effects: deviations from Kopp's law. Therefore, it is not surprising that among the parameters chosen for defining the miscibility-gap boundary, specific heats play generally no rôle, or only a minor and implicit one.

On the other hand, WEISS and TAUER[4] recently made an interesting attempt to understand the asymmetry of the Au–Pt miscibility gap from specific-heat effects alone. It is the purpose of this letter to point out that, although the mentioned authors have clearly brought to light that electronic specific heats may have an important influence on the asymmetry of the miscibility gap, there is a real danger that the calculated gap shows additional, undesirable features if the energy at zero temperature is taken to be symmetric.

WEISS and TAUER used the free-energy equation

$$\begin{aligned} G(\text{in cal.}) = {} & Bc(1-c)+ \\ & +RT\{c\ln c+(1-c)\ln(1-c)\}- \\ & -5{\cdot}11T/(0{\cdot}221+\theta/T)- \\ & -\tfrac{1}{2}\gamma T^2-0{\cdot}0002\theta^2, \end{aligned} \qquad (1)$$

where c is the atomic fraction of Pt and the Debye temperature $\theta = 164+69c$. Some other terms which are linear with concentration occurring in Ref. (4) have been omitted here. The first two terms at the right-hand side are those of a regular solution. The last term is a very small correction. The third term is an approximation for the contribution of the Debye specific heats. Its influence on the asymmetry is slight.

The asymmetry of the gap is brought about mainly by the fourth term, arising from the electronic specific heat γT. The change of γ with c due to the filling of the d-band was taken to be analogous to that measured in Cu–Ni alloys. For c between 1 and 0·4 it was assumed to remain $16{\cdot}2\times10^{-4}$ cal/mole deg^2 (the value for Pt), falling off for $c < 0{\cdot}4$ towards $1{\cdot}67\times10^{-4}$ cal/mole deg^2 (the value for Au) as in Fig. 1.

The authors used the experimental critical point ($T = 1535$°K, $c = 0{\cdot}615$) to fix the parameter B at 6087 cal, by putting d^2G/dc^2 zero, which is a necessary—though not sufficient—condition for a critical point. In addition, they used an experimental tie-line at 1000°K, with $c_1 = 0{\cdot}26$ and $c_2 = 0{\cdot}97$, in constructing their γ,c-curve. It gives γ and $d\gamma/dc$ at $c = 0{\cdot}26$. Although 97 at. per cent Pt checks with the determinations by TIEDEMA *et al.*,[5] the Pt-rich tangent-point at the 1000°G, c-curve in Fig. 2 of WEISS and TAUER corresponds rather to $c_2 = 0{\cdot}93$. Indeed, a c_2 value of 0·94 or more would necessitate γ at $c = 0{\cdot}26$ to be *greater* than $16{\cdot}2\times10^{-4}$. In copying their γ curve in the present Fig. 1 we found good agreement with $c_2 = 0{\cdot}93$.

The tie-lines computed by WEISS and TAUER at 800° and 1400°K are quite asymmetric, but it is clear that the miscibility gap following from

equation (1) should become virtually symmetric at low temperatures, because the γ term is quadratic in T. This must also be the case at the top, when both concentrations exceed 0·4; then the γ term plays no rôle, as was remarked already by VAN DER TOORN and TIEDEMA[3]. Indeed, by putting both d^2G/dc^2 and d^3G/dc^3 zero we calculated the critical point at $T = 1626°K$, $c = 0{\cdot}497$. This is well above the experimental *solidus* curve. A number of tie-lines were then calculated from equation (1) and the resulting tie-line above 1350°K was calculated, as at about this temperature the experimental solidus curve is attained.

GRUBE *et al.*[6] found complications in gold-rich alloys that had been cold worked and annealed at about 900°C. But TIEDEMA *et al.*[5] could not confirm these results, and state that the 90/10 Au–Pt alloy is homogeneous everywhere below the solidus.

Equation (1) could formally be made to conform more satisfactorily to the experimental miscibility

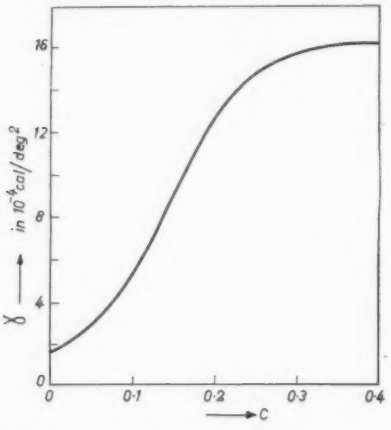

FIG. 1. Electronic specific-heat coefficient γ of Au with 0 to 40 at. per cent Pt, as used by WEISS and TAUER[4].

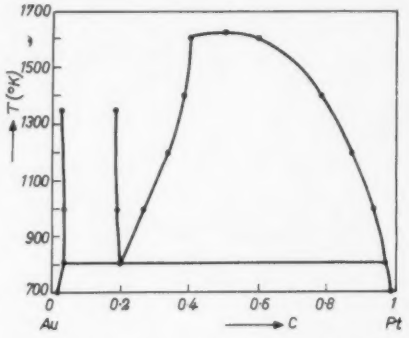

FIG. 2. Au–Pt phase diagram computed from WEISS and TAUER's free-energy equation.

phase-diagram is shown in Fig. 2. Naturally it would vary somewhat with the detailed course of the γ curve taken. The kink at 40 at. per cent Pt could be avoided if in Fig. 1 at $c = 0{\cdot}4$ not only $d\gamma/dc$ but also $d^2\gamma/dc^2$ were zero. But anyhow the curvature necessary to pass through $c = 0{\cdot}380$ at 1400°K (in good accord with WEISS and TAUER's tangent in their Fig. 2) would be anomalous.

An even more serious drawback of WEISS and TAUER's equation is the resultant additional miscibility gap at low Pt concentrations. Apparently the authors failed to observe that above about 800°K the G,c-curves have *two* stable double tangents. The gap at the gold-rich side does not close in a critical point. If one would use equation (1) formally at very high T, the γT^2 term would dominate and yield a gap between $c = 0$ and $c = 0{\cdot}2$, defined by the tangent to the γ curve from its starting point at $c = 0$. No gold-rich gap by altering the γ,c-curve. Presumably this curve should then begin to fall off already at low Au concentrations, and show no pronounced kink or concave part. It is a separate question, whether or not it is likely that the filling of the d-band would influence the specific heat but not the energy at zero temperature.

Philips Research Laboratories J. L. MEIJERING
N.V. Philip's Gloeilampenfabrieken
Eindhoven
Netherlands

References

1. LUMSDEN J., *Thermodynamics of Alloys*. Institute of Metals, London (1952).
2. HARDY H. K., *Acta. Met.* **1**, 202 (1953).
3. VAN DER TOORN L. J. and TIEDEMA T. J., *Acta Met.* **8**, 711 (1960).
4. WEISS R. J. and TAUER K. J., *J. Phys. Chem. Solids* **7**, 249 (1958).
5. TIEDEMA T. J., BOUMAN J. and BURGERS W. G., *Acta Met.* **5**, 310 (1957).
6. GRUBE G., SCHNEIDER A. and ESCH U., *Heraeus Festschrift* p. 20 (1951).

Magnetocrystalline anisotropy of cobalt-substituted manganese ferrite

(*Received* 18 *July* 1960; *revised* 1 *September* 1960)

SEAVEY and TANNENWALD[1] have observed the change in magnetocrystalline anisotropy caused by a partial substitution of cobalt for manganese in manganese ferrite ($MnFe_2O_4$). The measurements were made at microwave frequencies. More recently PEARSON[2] measured the anisotropy of these compounds using the static torque method. In both of these investigations it was found that the anisotropy contribution of cobalt was much smaller than in cobalt-substituted magnetite ($Co_xFe_{3-x}O_4$).[3] A crystal-field model which accounted for the anisotropy in the latter compound has been given.[4] The purpose of this note is to show how the picture in magnetite may be modified in order to account for the effect of cobalt substitution in manganese ferrite.

According to the crystal field model,[4] the spin $S(=3/2)$ of Co^{2+} is acted upon by both the molecular exchange field $\boldsymbol{H}$ and spin-orbit energy of the form $\pm\alpha\lambda\boldsymbol{k}\cdot\boldsymbol{S}$. Here $\alpha\hbar$ is the orbital angular momentum, λ is the spin–orbit constant, $\boldsymbol{k}$ is a unit vector parallel to the three-fold axis of the octahedral site occupied by the ion, and β is the Bohr magneton. The fact that the spin–orbit energy may be represented to first order by the indicated term is a consequence of the assumption that the ground state is an orbital doublet. The choices in sign of the spin–orbit energy correspond to the orientations of the orbital angular momentum in the two orbital states. These effects give rise to eight energy levels

$$\epsilon = M|2\beta\boldsymbol{H} \pm \alpha\lambda\boldsymbol{k}|, \quad (M = \pm 1/2, \pm 3/2) \tag{1}$$

where M is the spin quantum number.

If the concentration of cobalt is small, the orientation of the spontaneous magnetization $(\alpha_1\alpha_2\alpha_3)$ may be taken parallel to $\boldsymbol{H}$. Then the free energy $\mathscr{F}(\alpha_1\alpha_2\alpha_3)$ of substituted cobalt may be calculated in the usual way using the energy levels of equation (1). The cobalt contributions to the conventional anisotropy constants K_1 and K_2 are given by

$$\Delta K_1 = 4\mathscr{F}(110) - 4\mathscr{F}(100) \tag{2}$$

and a similar equation for ΔK_2 if terms beyond second order in the phenomenological expansion are neglected.

In the case of $Co_xFe_{3-x}O_4$ the values $H = \infty$ and $\alpha\lambda = -132\ \text{cm}^{-1}$ were found to be consistent with experimental data for ΔK_1 and ΔK_2 over a wide range of temperatures.[4] An analysis of the magnetic annealing effect yielded the estimate $\beta H = 320\ \text{cm}^{-1}$. The calculated values of ΔK_1 and ΔK_2 are not very sensitive to the choice between these two values of H.

SEAVEY and TANNENWALD[1] and PEARSON[2] found that ΔK_1 in $Co_xMn_{1-x}Fe_2O_4$ is smaller and its percentage variation with temperature is greater than in $Co_xFe_{3-x}O_4$. This suggests that the energy levels in the manganese case must be spaced more closely. PEARSON found that for $H = \infty$ adjustment of $\alpha\lambda$ could not bring about agreement over the whole temperature range. Moreover, the similarity in crystal field environment suggests that $\alpha\lambda$ should not differ greatly.

It seems natural, therefore, to leave $\alpha\lambda$ fixed and vary H because H is sensitive to the nature of the cations participating in the exchange interaction. We have calculated ΔK_1 vs. temperature as outlined, using the value of $\alpha\lambda$ obtained from magnetite and adjusting H to obtain a fit of PEARSON's torque results.[2] The calculated curve is shown with the experimental points in Fig. 1. The similar results of SEAVEY and TANNENWALD were not plotted because of uncertainty in composition. The fit shown in Fig. 1 should not be regarded as highly quantitative because the dependence of H on temperature is neglected.

It is interesting to observe that the value $\beta H = 87\ \text{cm}^{-1}$, about one-fourth of that in magnetite, is required to produce agreement. One could object that it is out of proportion with the Curie temperature T_c (858°K for magnetite and 573°K for manganese ferrite). However, this result is not necessarily contradictory since H and T_c do not involve precisely the same exchange interactions. The value of H is determined only by those interactions involving Co^{2+} explicitly while T_c is influenced by all exchange interactions.

PEARSON[2] considered the alternative suggestion[5] that the substituted cobalt ion in manganese ferrite might occupy a singlet orbital ground state rather than a doublet. This would be the case if the sign of the trigonal splitting were reversed or if a non-trigonal crystal field

component were present. Such a component might be present because of the mixture of Mn and Fe cations on octahedral sites in the 20 per cent inverse[6] spinel structure of $MnFe_2O_4$. However, it would seem that a singlet orbital state would necessarily produce the wrong qualitative behavior. The anisotropy would be

It should be noted that the straightforward application of the orbital-doublet model to the anisotropy of the cobalt ion is not likely to succeed in all spinel ferrite hosts. The results for volume dependence of anisotropy in cobalt-substituted nickel ferrite[8] and the temperature dependence of anisotropy in $CoFe_2O_4$[9] indicate that in each

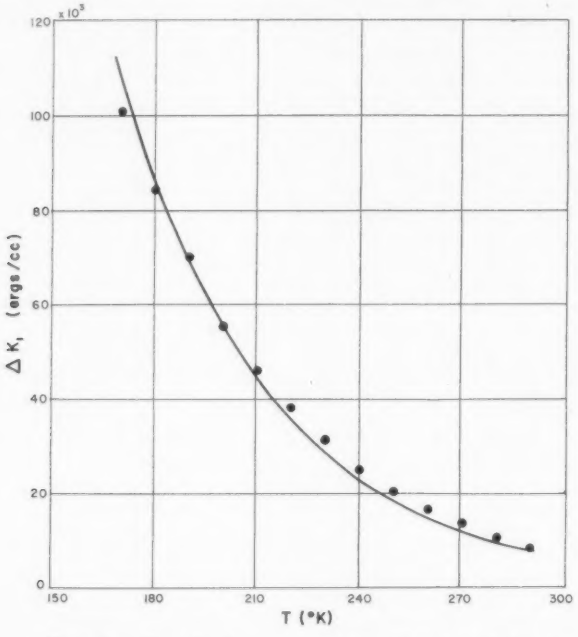

FIG. 1. Contribution to anisotropy of cobalt in $Co_{0.01}Mn_{0.99}Fe_2O_4$ as a function of temperature. Experimental points are due to PEARSON. The calculated curve is based on the values $\alpha\lambda = -132$ cm^{-1} and $\beta H = 87$ cm^{-1}.

smaller, to be sure, because it would appear in a higher order approximation to the spin–orbit energy.[7] However, the percentage variation of anisotropy with temperature would be *smaller* because of the smaller opportunity for thermal excitation of orbital states. The M^{10} law gives about half the required slope with respect to temperature. It is particularly the requirement that the percentage variation of anisotropy with temperature be *greater* in the manganese ferrite case which leads to our suggestion. Although the evidence is not conclusive our proposal seems to be in closest accord with experiment.

of these inverse spinels the effect of non-axial crystal fields is important.[8,10] *A priori* estimates of the doublet splitting due to the non-axial field in an inverse ferrite are comparable to spin–orbit energy[10,11] and tend to support these conclusions.[10]

Since the non-axial crystal fields are generally expected in an inverse spinel, existing evidence suggests that Fe_3O_4 and $MnFe_2O_4$ may be exceptional in this respect. The reason for the axial symmetry in the case of Fe_3O_4 may be a rapid transfer of electrons leading to frequent interchange between Fe^{2+} and Fe^{3+} on octahedral sites.

The reason in the case of $MnFe_2O_4$ may be that this ferrite is near enough to normal that the non-axial field for most sites is negligible.

Acknowledgements—It is a pleasure to acknowledge the benefit of discussions with Dr. PEARSON and the assistance of Dr. R. H. RAMEY, who programmed machine computations.

International Business Machines Corporation
Research Center
Yorktown Heights, New York

J. C. SLONCZEWSKI

References

1. SEAVEY M. M. and TANNENWALD P. E., *Proc. Inst. Radio Engrs., N.Y.* **44,** 1343 (1956).
2. PEARSON R. F., *Proc. Phys. Soc. Lond.* **74,** 505 (1959).
3. BICKFORD L. R., JR., BROWNLOW J. M. and PENOYER R. F., *Proc. Inst. Elect. Engrs.* **104B,** Suppl. No. 5, 238 (1957); PENOYER R. F. and BICKFORD L. R., JR., *Phys. Rev.* **108,** 271 (1957).
4. SLONCZEWSKI J. C., *J. Appl. Phys.* **29,** 448 (1958); *Phys. Rev.* **110,** 1341 (1958).
5. SMIT J. and WOLF W. in private communications to PEARSON.
6. HASTINGS J. M. and CORLISS L. M., *Phys. Rev.* **104,** 328 (1956).
7. YOSIDA K. and TACHIKI M., *Progr. Theor. Phys. Osaka* **17,** 331 (1957); WOLF W. P., *Phys. Rev.* **108,** 1152 (1957).
8. KAMINOV I. P., *J. Appl. Phys.* **31,** 220S (1960).
9. SHENKER H., *Phys. Rev.* **107,** 1246 (1957).
10. TACHIKI M., *Progr. Theor. Phys. Osaka* **23,** 1055 (1960).
11. TSUYA N., *Sci. Rep. Inst. Tôhoku Univ.* **B8,** 161 (1957).

Vol. 18
1961

BOOK REVIEW

K. MENDELSSOHN: **Cryophysics.** Volume 7 of Interscience Tracts on Physics and Astronomy, edited by R. E. MARSHAK. Interscience Publishers, Inc., New York, 1960. 183 pp., Cloth $4.50, Paper $2.50.

THE last ten years have seen a tremendous expansion and progress in physics at low temperatures. The well-known introductory books on this field, namely, VON LAMMEREN's *Technik der tiefen Temperaturen* (1941), L. C. JACKSON's *Low Temperatures Physics* (1948) and SIMON's *Low Temperature Physics—Four Lectures* (1952) do not suffice any longer to give an adequate idea of the present state of this field.

Although there are several recent specialized reviews and books on low temperature physics, a short introductory text is most welcome. This book, *Cryophysics* by Dr. K. MENDELSSOHN, one of the well-known workers in this field, is aimed for advanced students or "for those interested but not necessarily engaged" in this field. As such it is very useful, is well written and contains at the end of every chapter many references to specialized treatises for those interested in a more quantitative and advanced study of low temperature phenomena.

The first chapter "Cryogenics" covers the techniques of gas liquefaction, the storage of refrigerants and the techniques for reaching temperatures below 1°K by means of adiabatic demagnetization and nuclear cooling.

Chapters 2 and 3 fall under the heading of, respectively, "Thermometry" and "Specific Heats". Description of gas thermometers, magnetic thermometry for the region below 1°K and secondary thermometers, like platinum and germanium thermometers are included. Different kinds of specific heat, due to lattice vibrations, order–disorder transformation, conduction electrons as well as Schottky anomalies are discussed.

Chapter 4, on "Magnetism," treats paramagnetism and antiferromagnetism, and describes the different ways of orienting nuclei at low temperatures. A simple description and explanation of the de Haas–Van Alphen effect is also given. Chapter 5 covers the transport phenomena in dielectrics and metals. "Superconductivity" and "The Helium Problem" covered in Chapters 6 and 7 are treated especially in detail and give a very good idea of the problems involved and the progress achieved in the last few years. Some of the properties of liquid and solid helium 3, an element now easily obtainable, are briefly discussed. Chapter 8 treats miscellaneous interesting problems not fitting into any of the subjects previously discussed. It treats the melting curve for gases, thermal expansion and mechanical properties of solids, trapped free radicals, bubble chambers and masers. An appendix gives the vapor pressure of condensed hydrogen, liquid He^4 and He^3.

HORST MEYER

ERRATUM

A. MANY, N. B. GROVER, Y. GOLDSTEIN and E. HARNIK, Discussion of the paper by R. F. GREENE, *J. Phys. Chem. Solids* **14,** JD5 (1960).

Page JD5, right hand column, third line from bottom; read λ_n/L_D for $\lambda_n L_D$.

J. Phys. Chem. Solids Pergamon Press 1961. Vol. 18, No. 4, pp. 273–285. Printed in Great Britain.

LOW TEMPERATURE PARAMAGNETIC RESONANCE OF TRAPPED O_2

S. FONER

Lincoln Laboratory, Massachusetts Institute of Technology, Lexington 73, Massachusetts

H. MEYER*

Gordon McKay Laboratory, Harvard University, Cambridge, Massachusetts

and

W. H. KLEINER

Lincoln Laboratory,† Massachusetts Institute of Technology, Lexington 73, Massachusetts

(*Received* 6 *July* 1960)

Abstract—Low temperature paramagnetic resonance experiments of oxygen molecules trapped in single-crystal β-quinol clathrate are described. The large zero-field splitting of the trapped O_2 dictated use of high fields and high frequencies. Measurements with d.c. and pulsed magnetic fields, and 4 mm and 8 mm wavelength radiation were therefore employed for the experiments with various fractions p of the β-quinol cages occupied by molecules. The results are interpreted in terms of the hindered rotation theory applied by MEYER *et al.* to magnetic susceptibility measurements. The trigonal axis was identified as the axis of minimum energy, and the zero-field splitting was measured to be about 4·4°K, in reasonable agreement with the value derived from magnetic susceptibility measurements. The paramagnetic resonance on samples with $p \lesssim 0{\cdot}2$ showed a complex structure composed of several lines which extended over a range of 2 kg, and could be resolved at 1·5°K. Experiments with dilute systems of O_2 in N_2 clathrate crystals ($p_{O_2} < 0{\cdot}05$) showed three well resolved component lines corresponding to zero-field splittings D' D_0', D_2' with $D_0'/k = 4{\cdot}36 \pm 0{\cdot}05$°K, $(D_1' - D_0')/k = 0{\cdot}127 \pm 0{\cdot}01$°K, and $(D' - D')/k = 0{\cdot}094 \pm 0{\cdot}01$°K. The relative intensities of the components can be interpreted quantitatively as a function of p by associating the three zero-field splittings with occupation of the two cages nearest to a resonating molecule by zero, one, or two molecules, respectively. The change in hindrance potential due to van der Waals forces between the O_2 and its nearest N_2 neighbors is calculated, and the resulting zero-field splitting changes are compared with those derived from the resonance spectrum. An upper limit for the paramagnetic spin–lattice relaxation time of O_2 in β-quinol, $T_1 \leqslant 50$ μsec at 1·5°K, was estimated from the pulsed field resonance data.

1. INTRODUCTION

THE CRYSTALLOGRAPHIC properties of β-quinol clathrate have been studied extensively by several authors,[1] and recently measurements of the paramagnetic susceptibility of O_2 trapped in this compound have been reported.[2, 3, 4] These latter measurements suggested the paramagnetic resonance experiments described in this paper. The β-quinol clathrate crystal is an ideal container for several types of gas molecules, allowing 2×10^{21} molecules/cm^3 to be stored at room temperature. This concentration is equivalent to an ideal gas pressure of 80 atm. The crystal structure contains regularly spaced, almost spherical cages, each of which can trap at most one gas molecule. The O_2 molecule is constrained by the cage so that the gas cannot condense, and apparently no chemical bond is formed between the O_2 and the cage atoms. The β-quinol crystal has trigonal symmetry (space group $R\bar{3}$) and all the cages are equivalent. The

* Now at the Department of Physics, Duke University, Durham, North Carolina.

† Operated with support from the U.S. Army, Navy, and Air Force.

Vol. 18
1961

cage centers form a trigonal lattice which may be regarded as a body centered cubic lattice compressed along the cube diagonal, so that in terms of its hexagonal lattice constants $a = 16{\cdot}6$ Å and $c = 5{\cdot}5$ Å; $c/a = 0{\cdot}33$, considerably smaller than the b.c.c. value of 0·61. If the cage did not interact with the trapped O_2, the behavior of the free paramagnetic O_2 molecule in its lowest rotational states could be studied at low temperatures. Actually, the cage influences the molecular motion and these interactions are reflected in the paramagnetic properties. For temperatures above 4°K, the magnetic susceptibility[3, 4] of O_2 in the clathrate is that expected of the free gas without interaction. The deviations from the free gas susceptibility below 4°K were interpreted by O'BRIEN and VAN VLECK[4] as follows. At low enough temperatures, the oxygen molecules carry out a hindered rotation in the cages, with a hindrance potential V which to first approximation can be written

$$V = V_0(1-\cos 2\theta) \tag{1}$$

where θ is the angle between the molecular axis and the direction of minimum energy. The spin motion is described in terms of a spin Hamiltonian with a zero-field splitting term due to the coupling of the spin ($S = 1$) to the molecular axis. If the molecular axis is fixed ($V_0 = \infty$), the zero-field splitting is $D/k = 5{\cdot}66$°K;[4] if the rotation is not completely hindered the effect is to reduce the splitting to

$$D' = D(\tfrac{3}{2}\langle\cos^2\theta\rangle_{\text{av.}} - \tfrac{1}{2}) \cong D[1-\tfrac{3}{2}\langle\theta^2\rangle_{\text{av.}}] \tag{2}$$

where $\langle\cos^2\theta\rangle_{\text{av}}$ is the expectation value of $\cos^2\theta$. The spin Hamiltonian of the lowest 3 levels of the oxygen molecule in a magnetic field can then be written as

$$\mathscr{H} = g\beta\boldsymbol{H}\cdot\boldsymbol{S} + D'[S_z^2 - \tfrac{1}{3}S(S+1)] \tag{3}$$

where z is the axis of minimum potential energy of the molecule, $g = 2{\cdot}00$ and β is the Bohr magneton.

From susceptibility measurements between 4·2°K and 0·2°K on an O_2 clathrate powder[3, 4] D'/k was found to be 4·15°K. Since only the lowest hindered rotational state is populated at these temperatures, only the zero point motion need be considered. For small enough amplitudes,

$$E = h\nu = 4\pi^2\nu^2 I\langle\theta^2\rangle_{\text{av}} \tag{4}$$

where ν is the frequency of rotation and I is the momentum of inertia (for O_2, $I = 1{\cdot}95\times10^{-39}$ cgs). The dependence of ν on the hindrance potential V_0 is given by the relation

$$\nu = \frac{1}{\pi}\left(\frac{V_0}{I}\right)^{1/2} \tag{5}$$

Using equations (2) and (4), one finds

$$\nu \sim 0{\cdot}49\times10^{12}\ \text{sec}^{-1}.$$

The large quantity of clathrate required for the susceptibility measurements precluded use of a single crystal in order to determine the equilibrium orientation of the O_2 molecules with respect to the trigonal symmetry axis (c-axis) of the β-quinol crystal. It was suggested,[4] however, that the O_2 molecule would be aligned with its large dimension along the c-axis. Paramagnetic resonance experiments of O_2 in single crystal clathrates would, of course, permit a more detailed examination of the hindered rotation model, but the large value of D' necessitates the use of r.f. frequencies and applied magnetic fields well above those generally available. Such experiments with 4 mm and 8 mm wavelength radiation and pulsed or d.c. magnetic fields are described in this paper. Both dilute and concentrated O_2 samples were studied, but only the dilute O_2 results were amenable to detailed interpretation.

2. EXPERIMENTAL TECHNIQUES

An extremely simple form of a reflection spectrometer was used for both the 4 mm and 8 mm wavelength measurements. Microwave power was supplied by a low power klystron to a waveguide circuit. The suitably oriented clathrate crystal was held by Apiezon grease to a thin shorting end-wall of a long, thin-walled, silver-plated section of stainless steel waveguide. Resonant absorption was observed as a change in microwave power reflected from the end-wall assembly when the magnetic field was swept through the resonance. The waveguide was immersed in liquid helium for measurements from 1·5°K to 4·2°K, liquid helium being excluded from the waveguide. The gain in sensitivity attained with the combination of high frequencies and large waveguide filling factor permitted measurements without the use of cavity techniques even for the pulsed field experiments with relatively dilute paramagnets.

Vol. 18
1961

Low field measurements were made with a d.c. magnet which could be rotated in a horizontal plane perpendicular to the waveguide axis. The large value of D' and limited d.c. fields (less than 18 kG) permitted the angular variation of only one resonance line ($M_s = 0 \leftrightarrow M_s = -1$) to be observed with 4 mm radiation.

Pulsed fields were essential for measurements at high fields for 8 mm or 4 mm radiation. These fields were produced by an oscillatory capacitor discharge through suitably constructed solenoids, which operated at room temperature. The details of the capacitor bank and coil designs are published elsewhere.[6] The microwave waveguide and surrounding Dewar assembly were inserted in a 1 in. i.d. pulsed field coil for these measurements. Peak fields of 180 kG could be obtained over about 10 cm^3 with discharge of the 2000 μf, 3000 V capacitor bank. The fields were calibrated at fixed points by paramagnetic resonance of MnF_2. The field variation with time was observed as the integrated output voltage of a search coil positioned in the working volume. The absolute accuracy of the pulsed field measurements was well within 5 per cent. This technique has been employed for various other resonance experiments for which a large applied field is required in order to "tune" the resonance to relatively low frequencies.[7]

The clathrate crystals were grown from a saturated solution of quinol in *n*-propyl alcohol as described by EVANS and RICHARDS[2]. The O_2 pressure under which the crystallization took place varied between 200 and 1500 lb/in.^{2} The crystals showed distinctly the symmetry axis and were somewhat red in color, possibly because of a slight oxidation of the quinol by O_2 during crystallization. Nitrogen clathrates with small O_2 concentrations, grown under pressures up to 2000 lb/in.^{2} of N_2 did not have this coloring.

3. EXPERIMENTAL RESULTS

A. *High concentration of* O_2

The first resonance experiments on concentrated O_2 β-quinol crystals were performed at 4·2°K with pulsed fields. Resonance lines of about 2 kG width were observed with the field parallel and perpendicular to the *c*-axis. The resonance spectrum could be interpreted in terms of the spin Hamiltonian, equation (3), with the quantization axis along the *c*-axis of the crystal. One concludes that the hindrance potential V is minimum along the *c*-axis. The same conclusion was reached for N_2 molecules trapped in β-quinol.[8]

The energy level diagrams for measurements with the applied field H parallel or perpendicular to the *c*-axis are shown in Fig. 1. The observed spectra are compared with the resonance conditions obtained from the eigenvalues of equation (3):

$$h\nu = |D' \pm g\beta H| \quad \text{for } H \parallel z$$
$$h\nu = \tfrac{1}{2}[D' \pm (D'^2 + 4g^2\beta^2H^2)^{1/2}] \text{ for } H \perp z \qquad (6)$$

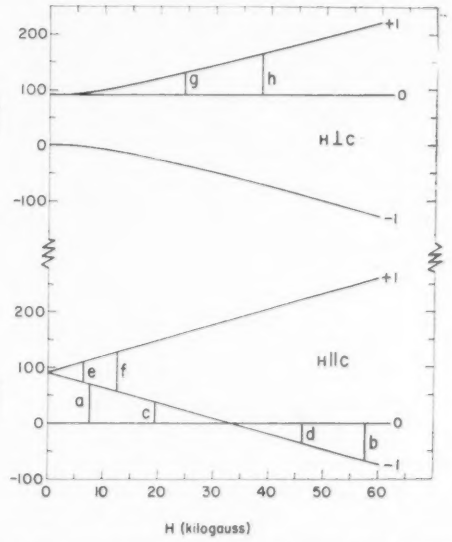

FIG. 1. Energy level diagrams for the spin Hamiltonian of equation (3) with $S = 1$ and $D' = 33$ kG. Possible transitions at 36 kMc/s (c,d,e,g) and 71 kMc/s (a,b,f,h) are indicated. The high field limit values of M_s are shown on the right.

The measured pulsed field values are indicated in Fig. 1 for both the 4 mm and 8 mm data with O_2 clathrate grown under a pressure of 1500 lb/in.^{2} Although it was difficult to align the *c*-axis exactly parallel to the pulsed magnetic field, the additional resonance after "cross-over" at higher fields permitted a correction to be made. For instance, if the *c*-axis were parallel to H, and the relaxation time were sufficiently short, the field interval between the low field and high field resonances (a and b, or c and d in Fig. 1) would be given by $\Delta H_1 = 2h\nu/g\beta$. Misorientation of H with

respect to z would result in a smaller interval, ΔH. The resonance field of the $|\Delta M_s| = 2$ transition (e or f) for $H \parallel z$ is $H_2 = h\nu/2g\beta$, but the transition is not allowed. When H is not aligned along z the corresponding transition is allowed, but then H_2 will occur at a field value greater than $h\nu/2g\beta$. Thus misalignment of H with respect to the c-axis can be estimated from the measured values of ΔH and $h\nu$. The value of $|D'|$ can be determined from the "cross-over field" H_c and $D' = g\beta H_c$ where $H_c \simeq \frac{1}{2}(H_a + H_b) \simeq \frac{1}{2}(H_c + H_d)$ for slight misorientations. The energy differences for H making a small angle $\eta = \arcsin \delta$ with respect to the c-axis are approximately

$$|\Delta M_s| = 1: h\nu = D' \mp g\beta H + \frac{\delta^2}{2} D' g\beta H \left[\frac{\pm D' + 3g\beta H}{D'^2 - (g\beta H)^2}\right] + \frac{\delta^4 27 D'^2 (g\beta H)^3}{8}\{\ \} + \ \ldots \qquad (7)$$

$$\{\ \} = \frac{2D' g\beta H \pm [D'^2 - 3(g\beta H)^2]}{[D'^2 - (g\beta H)^2][D'^2 + 3(g\beta H)^2]^2}$$

$$|\Delta M_s| = 2: h\nu = 2g\beta H - \delta^2\left[\frac{D'^2 g\beta H}{D'^2 - (g\beta H)^2}\right] - \delta^4 \frac{27 D'^2 (g\beta H)^3}{4}\left\{\frac{D'^2 - 3(g\beta H)^2}{[D'^2 - (g\beta H)^2][D'^2 + 3(g\beta H)^2]^2}\right\} + \ \ldots$$

under the conditions that $D'^2 \ll (g\beta H)^2$ or $D'^2 \gg (g\beta H)^2$, i.e. far from the "cross-over" point. The high field quantum numbers are used here. These conditions are certainly met by the 4 mm experiments. The sign of D' may be determined from intensity measurements as a function of temperature, or from magnetic susceptibility measurements.

An additional rhombic term $E(S_x^2 - S^2)$ in equation (3) would lead to $|\Delta M_s| = 1$ transitions

$$h\nu = D' \pm (g^2\beta^2 H^2 + E^2)^{1/2} \qquad \text{for } H \parallel z$$

$$h\nu = \tfrac{1}{2}(D' - 3E) \pm [g^2\beta^2 H^2 + \tfrac{1}{4}(D' + E)^2]^{1/2} \qquad \text{for } H \perp z \qquad (8)$$

Assuming that $E^2 \ll D^2$ and $0 < |E| < h\nu/2$, we would have the following results for $H \parallel z$: (a) ΔH_1 would be greater than $2h\nu/g\beta$, (b) H_2 would be less than $h\nu/2g\beta$, and (c) the $|\Delta M_s| = 2$ transition would be allowed. None of these effects have been observed, and we conclude that $|E|$ is small.

The hindered rotation model indicates that the D' values associated with higher rotational levels of the O_2 molecule should be smaller, since $\langle\theta_2\rangle_{av}$ increases. Attempts to observe paramagnetic resonance for these higher levels with pulsed fields have been unsuccessful with either 4 mm or 8 mm radiation. In both cases the field for resonance did not change for temperatures to about 12·5°K and the line width increased so rapidly that it was not possible to detect the resonance at higher temperatures.

The observed line width of about 2 kG at 4·2°K was surprisingly large, and could not be explained in a simple way. Measurements were therefore extended to lower temperatures in order to examine the line broadening mechanism in more detail. Since the transition $M_s = 0 \leftrightarrow M_s = -1$, observed with 70·7 kMc/s radiation occurred at relatively low H, d.c. measurements could be made. A complex structure containing at least six lines could be resolved at 1·5°K. The angular variation of each line could be followed for $\pm 20°$ from the c-axis; the lines varied uniformly as δ^2. (Similar data for dilute O_2 are shown in Fig. 4.) Further resolution was attempted by decreasing the O_2 concentration in the clathrate crystal. Typical results are shown in Fig. 2. The magnetic fields for the data are not indicated because orientation with respect to the magnetic field is not identical. The general characteristics of these experiments were: (1) As the O_2 concentration was decreased, the peak intensity shifted from high to low field. (2) For the lowest O_2 concentration (grown at 200 lb/in.^{2}) three resolved main peaks were observed. In this case, the highest intensity occurred at lowest H, and additional low intensity peaks were superimposed [see Fig. 2(d)]. (3) Annealing various crystals at 60°C affected the relative intensities of the lines somewhat, but the

results did not seem to show a systematic trend. The high field part of the spectrum was usually enhanced by annealing. The positions of the various lines for all samples seemed to occur at approximately the same field, but the intensities varied. The lowest O_2 concentration (200 lb/in.^{2}) samples. Most of the remainder of this paper will be concerned with the analysis and interpretation of these data.

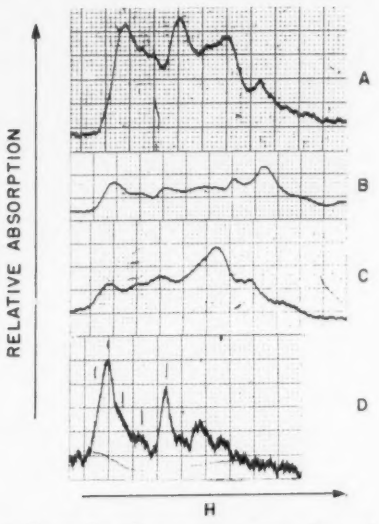

FIG. 2. Examples of resonance spectra for various concentrated O_2 clathrates taken with 70·7 kMc/s radiation and at 1·6°K. Samples A, B, and C were grown with 1500 lb/in.^{2} O_2 pressure and subsequently were annealed at 60°C in O_2 at pressures of 1000 lb/in.^{2}, 1000 lb/in.^{2}, and 14·7 lb/in.^{2}, respectively. Sample D was grown with 200 lb/in.^{2} O_2 pressure and not annealed. The percentages of filled cages, obtained from gas analysis, were A–39, B–39, C–31 and D–18.

crystal showed a spacing of 800 ± 100 G between major peaks. Samples with 18 to 40 per cent of the cages filled with O_2 were studied as a function of anneal. The average value of D', estimated as the center of the broad resonance line, was $33{\cdot}0 \pm 0{\cdot}6$ kG (4·43°K).

The 18 per cent O_2 data (Fig. 2d) suggested that even further resolution would be observed with increased dilution. It was not possible to grow sufficiently large single crystals of more dilute O_2 clathrates. Instead, crystals with a large concentration of N_2 and a small concentration of O_2 ($p_{O_2} < 0{\cdot}05$) were used. To a large extent the significant information from the resonance data was obtained using these "dilute O_2 in N_2"

B. *Dilute* O_2 *in* N_2 *clathrates*

Spin resonance was observed using two concentrations of O_2 in N_2 clathrate. These were grown with 40 lb/in.^{2} O_2 and either 750 lb/in.^{2} N_2 or 2000 lb/in.^{2} N_2. The results of d.c. measurements at 4 mm and 1·6°K are shown in Figs. 3(a) and 3(b). In each case, three well resolved lines are obtained, but the relative intensities are quite different. The spacing between lines is about 900 G for either material. Consistent results were obtained with resonance measurements on several crystals grown in the same batch. Accurate comparison of the D' values of the three lines was possible with d.c. measurements for these two dilute clathrates. In order to estimate errors due to crystallographic mis-orientation, the fine structure was examined as a function of angle. The results for these two crystals are superimposed in Fig. 4. The angular orientation of the c-axis is

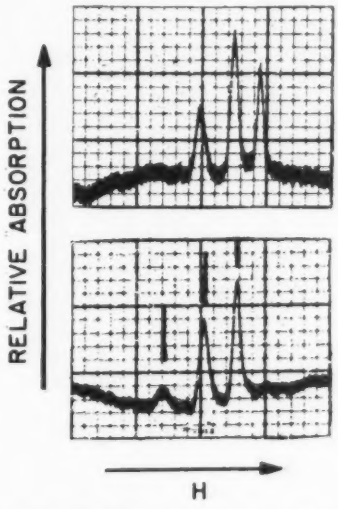

FIG. 3. Absorption spectra for dilute O_2 in N_2 clathrates at 1·6°K and with 70·0 kMc/s radiation. Top figure (a): $p = 0{\cdot}55$ corresponding to $\theta = +7{\cdot}5°$ in Fig. 4. Bottom figure (b): $p = 0{\cdot}75$ corresponding to $\theta = -10°$ in Fig. 4. The corresponding field values for resonance are given in Fig. 4.

Vol. 18
1961

estimated to be within 5° of the plane of the applied H. The value of D' and spacing between lines agree within the experimental error for the two crystals. The average values of the D''s for these lines in kilogauss are $D'_0 = 32{\cdot}4 \pm 0{\cdot}4$, $D'_1 = 33{\cdot}4 \pm 0{\cdot}4$ and $D'_2 = 34{\cdot}15 \pm 0{\cdot}4$, respectively 4·36, 4·48 and 4·58°K.

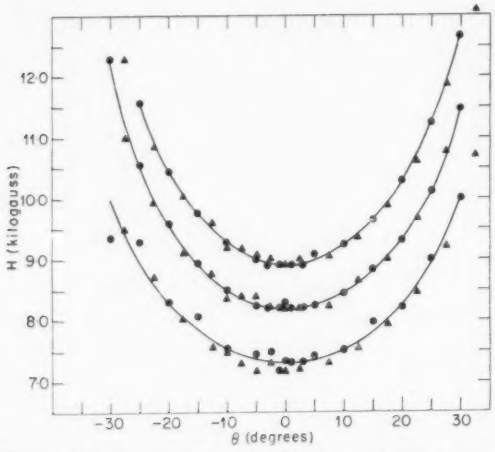

FIG. 4. Angular variation of the three fine structure resonance peaks for dilute O_2 in N_2 β-quinol crystals. All data were taken at 1·6°K and with 70·0 kMc/s radiation. The triangles correspond to Fig. 3(a), $p = 0{\cdot}55$; the circles correspond to Fig. 3(b), $p = 0{\cdot}75$.

Pulsed field measurements at 4·2°K and 1·5°K were made in order to examine the fine structure in more detail. If, for instance, the additional lines were due to population of higher rotational states, (a situation which seems quite unlikely) then the field dependence of the paramagnetic resonance for some of these states would be quite different from the ground state, and the spacings between the fine structure lines would reflect this effect. The $|\Delta M_s| = 1$ transition with 4 mm radiation permits measurements to be made with the resonance lines separated by about 50 kG. Some typical results of these experiments, shown in Fig. 5, illustrate the type of information obtained with the pulsed field techniques.

The pulsed magnetic field executes a few oscillations of a damped sinusoidal character and each time the magnetic field passes through a resonance, a change in absorption is recorded. By "tuning" the peak amplitude of the first half cycle of pulsed field so that it is slightly above the resonance field value, (i.e. by carefully adjusting the charging voltage of the capacitor bank) it is possible to resolve the high field $|\Delta M_s| = 1$ resonance. Resolution of the low field transition is then attained on succeeding oscillations of the field, since the time interval spent at a given lower field continues to increase as energy is dissipated by the oscillatory circuit. The horizontal scale in Fig. 5 is linear in time, but quite nonlinear in H. For this reason, each of the resonances are labelled *a*, *b*, *c*, *d*, *e*, or *f* according to Fig. 1, and a subscript *i* is added to indicate the *i'th* time that the particular resonance is observed in a given trace. The same notation is used for the selected portions of time expanded traces also shown in Fig. 5.

Two additional results were obtained with the low temperature pulsed field measurements. First, the spacing between the fine structure components was about 900 G (within 10 per cent) for both the *a* and *b* lines, and the relative intensities of components were the same. Second, a broad resonant absorption at $H \approx 15$ kG was also observed, but it was difficult to resolve any fine structure. Since H was greater than $h\nu/2g\beta$, and $\Delta H = 46$ kG between the *a* and *b* transition, this line has been identified as a $|\Delta M_s| = 2$ transition (type *f* in Fig. 1). The results are consistent with H making about a 20° angle with respect to the *c*-axis. Further remarks concerning this additional resonance will be presented in the discussion of spin–lattice relaxation.

4. DISCUSSION

All the low temperature paramagnetic resonance data on O_2 molecules trapped in β-quinol are consistent with the spin Hamiltonian equation (3), as far as the over-all positions of the resonances are concerned, with $D' = 4{\cdot}4$°K and the z-axis along the *c*-axis of the crystal. No evidence for a possible orthorhombic contribution $E(S^2 - S^2)$ has been found, but it is difficult to estimate a lower limit for $|E|$. The contribution of any orthorhombic term is presumed to be negligible.

The low temperature magnetic susceptibility data[4] with $p = 0{\cdot}40$ was fitted earlier with the same spin Hamiltonian with $D' = 4{\cdot}15$°K. The difference between the D' values from the resonance and the susceptibility experiments is not quite within the experimental error, but the disagreement is not believed to be significant. The maximum errors of the susceptibility are estimated to be 3 to 4 per cent. More accurate values

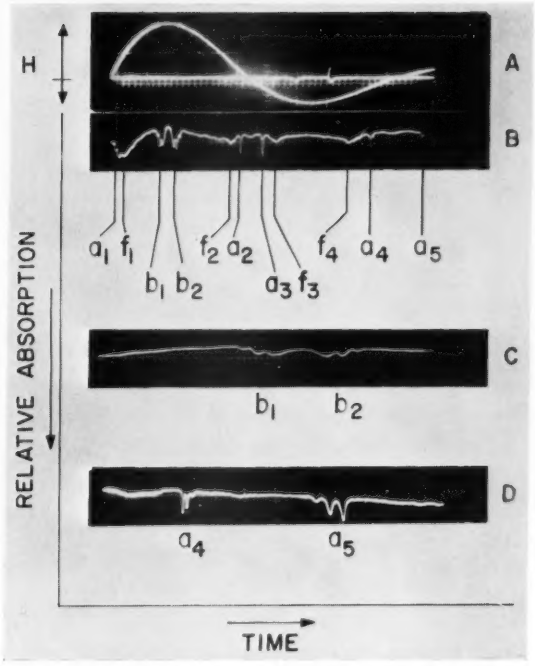

FIG. 5. Pulsed field resonance spectra taken at 1·5°K with 4 mm radiation. A: Pulsed field vs. time (100 μsec/large division). B: Relative absorption vs. time (100 μsec/large division). C: High field resonances expanded (20 μsec/large division). D: Low field resonances expanded (20 μsec/large division).

[*facing p.* 278

BLANK
PAGE

Vol.
19

of D' are expected from the resonance data, since the distribution of paramagnetic ions in a given crystallite is observed directly rather than by a random average over many crystals. The values of D_0', D_1', and D_2' are more accurate, but the proper weighting of each line is difficult to determine for the high concentration O_2 samples because of additional line broadening effects and apparently limited uniformity of the O_2 distribution in the crystal.

As mentioned in the introduction, the spin Hamiltonian equation (3) follows naturally from a simple hindered rotator model, and the value of D' determines the value of the hindering potential coefficient V_0.

A. *Fine structure*

With the data available we have been able to give a detailed interpretation of the fine structure of the resonance lines only for the dilute O_2 in N_2 samples.

We first rule out the possibility that a more complicated single-cage Hamiltonian in place of equation (3) can alone account for the observed fine structure. The relative intensities of the fine structure components would be independent of concentration for any single-cage Hamiltonian. Further, the components might be expected to have different temperature and field dependencies; the data show no evidence for this.* In fact the fine structure is well described as a function of both field orientation and temperature by a superposition of three resonances, each given by the spin Hamiltonian equation (3), but each with its own D' value. This leaves crystal interactions among the trapped molecules and crystal imperfections to account for the fine structure.

We account quantitatively for the observed concentration dependence of the relative intensities of the component resonances in terms of interaction among the trapped molecules in the following way. The spin Hamiltonian of a resonating molecule has the value D_0', D_1', or D_2', according to whether the two nearest neighbor cages are occupied by 0, 1, or 2 molecules. Effects of occupancy of more distant cages are neglected to a first approximation since they are considerably farther away: the two nearest neighbors are at a distance of 5·5 Å along the c-axis, while the six second nearest neighbors are 9·8 Å away and the six third nearest neighbors are 10·3 Å away. Assuming the molecules occupy the cages at random, the two cages nearest to a resonating molecule are occupied by 0, 1, or 2 molecules with probabilities q^2, $2pq$, and p^2, where p as before is the fraction of cages occupied and $q = 1-p$ is the fraction empty. The peak intensities I_0, I_1 and I_2 of the fine structure lines should be proportional to these probabilities for similar lines, and consequently they should satisfy a consistency relation which is independent of the value of p, e.g. $(4I_0I_2/I_1^2)^{1/2} = 1$. Best comparisons can be made when the I's are about equal—when one line has a very low intensity, background noise can lead to relatively large deviations from 1. Alternatively, the value p_1 calculated from the intensity ratio

$$r_1 = I_0/I_1 = \frac{p_1}{2(1-p_1)}$$

and the value p_2 calculated from

$$r_2 = I_2/I_1 = \frac{1-p_2}{2p_2}$$

can be compared for consistency. The two consistency criteria are not independent and are related approximately by $(4r_1r_2)^{1/2} \equiv (4I_0I_2/I_1^2)^{1/2} = 1-(p_1-p_2)/2\bar{p}(1-\bar{p})$, where $\bar{p} = (p_1+p_2)/2$. Some care must be used when interpreting such comparisons because the values of p will be most sensitive to the ratios of intensities when these are most nearly equal. Finally, if the spin–lattice relaxation time is short, the intensities will vary appreciably if the magnetic field interval between fine structure lines is large, simply because the equilibrium population differences will vary with field. In the present case, this last effect is neglected, but it can account for almost a 5 per cent change in intensity at 1·5°K even for the low field a transitions. Further discussions of such effects will be considered when the relaxation time estimates are examined. To test the model, one can use either of the above consistency criteria or one can compare the values of p with those obtained from volumetric analysis of the N_2 gas evolved by the β-quinol when

* More detailed arguments of this type have been used[9] to rule out explanations based only on a single-cage model for the fine structure observed in the nuclear electric quadrupole spectrum[8] of N_2 molecules trapped in β-quinol.

Vol. 18
1961

Table 1. Consistency tests of random occupancy and comparison of resonance and gas analysis values of p for dilute O_2 in N_2 β-quinol

Sample	$(4I_0I_2/I_1^2)^{1/2}$	p_1	p_2	$\bar{p}$(resonance)	p(gas analysis)
750 lb/in.^{2} N_2; 40 lb/in.^{2} O_2	1·1 ± 0·1	0·58 ± 0·01	0·55 ± 0·01	0·565 ± 0·02	0·55 ± 0·02
2000 lb/in.^{2} N_2; 40 lb/in.^{2} O_2	1·1 ± 0·1	0·745 ± 0·005	0·72 ± 0·04	0·73 ± 0·04	0·85 ± 0·04

melted. The results of these tests for several intensity measurements on two particular crystals are given in Table 1, where the errors correspond to an estimated maximum range of the intensity data.

The errors indicated for the gas analysis are for similar samples taken from the same batch of crystals used for the resonance experiments, but the gas analysis was made about 1½ years before the final intensity data were obtained. The general agreement of p_1 and p_2 for a given crystal, the value of $(4I_0I_2/I_1^2)^{1/2}$, and the reasonably close correspondence to the measured gas content of the crystals all indicate that the three lines are associated with the three possible configurations of N_2 occupancy of the two equivalent nearest neighbor cages, and hence with three values of D'.

Since the present model rests on the above analysis, some further comments may be in order. If the assumption of similar line shapes is justified, the deviations of the data from consistency provide some evidence for slight clustering of gas molecules. This appears to be the case for the $\bar{p} = 0{\cdot}56$ sample in particular, but more detailed measurements of the line intensities will be necessary before such conclusions can be justified. Even though the scatter of p_2 is large because I_0 is small, the value of p can be determined with a precision comparable to that of the gas analysis techniques. Finally, the apparent discrepancy between $\bar{p} \approx 0{\cdot}73$ and the gas analysis is not thought to be significant.

The data also show that the value of D' increases as the number of occupied nearest neighbor cages goes from zero to two.

B. *Calculation of fine structure intervals*

We now apply a simplified model for the interaction among the trapped molecules to calculate $D_1'-D_0'$ and $D_2'-D_1'$. The direct part of the interaction is represented as a sum of pair potentials. The indirect part of the interaction, the part which involves n-body forces, $n>2$, and which involves the β-quinol structure as an intermediary, is neglected. A sufficiently accurate calculation of the indirect part appears to be difficult. An important simplification arises with this model because the caged molecules are not in contact. This allows us to avoid dealing with the difficult problem of direct repulsive interactions which ordinarily plagues van der Waals calculations. Changes of the lattice parameters with changing trapped molecule concentration are neglected.*

The pair potential is approximated by the attractive inverse sixth power contribution to the dispersion or London interaction.† The dependence on orientation of the interacting molecules is included, as given by LONDON[11]. London's pair potential depends on spherical polar coordinates of the molecular axes with respect to the intermolecular axis. For the β-quinol crystal it is more natural to deal with spherical polar coordinates θ, ϕ and θ', ϕ' of the two molecular axes relative to the trigonal axis of the crystal and with the angle

* Recent X-ray diffraction measurements[10] at room temperature show that the average lattice parameters do not change by more than 0·1 per cent for trapped O_2 and N_2 concentrations between $p = 0{\cdot}2$ and $p = 0{\cdot}8$.

† Quadrupole–quadrupole interaction in first order of perturbation theory also contributes to the pair potential. The uncertainty in the known values of the quadrupole moments of O_2 and N_2 makes the contribution difficult to estimate accurately. Note that this interaction is absent when the trapped neighbor is a rare gas. We hope to consider the quadrupole–quadrupole contributions in more detail at a later time when O_2 spin resonance data with rare gas neighbors is available.

ψ between the intermolecular axis and the trigonal axis. We neglect deviations from cylindrical symmetry in the orientational motion of the molecule, although the cage potential is actually trigonal; we accomplish this by averaging London's expression uniformly with respect to ϕ and ϕ'.

We describe the effect of the interaction on the rotational motion of the resonating molecule, and hence on D', as a change in the orientational potential of the hindered rotator. The orientational potential is approximated as earlier by equation (1) and the effect of the interaction is represented entirely as a change δV_0 in the strength V_0 of the orientational potential. The change δV_0 is then the coefficient of $-2\cos^2\theta$ in London's potential averaged with respect to ϕ and ϕ' and summed over all occupied neighboring cages with the appropriate A, B, B', C parameters defined below and an appropriate θ' value for each molecular pair in the sum. The expression for δV_0 is conveniently written in the form

$$\begin{aligned}\delta V_0 = &\sum[\tfrac{1}{4}(-A+7B+B'-7C)+\\ &+\tfrac{9}{4}(A-B-B'+C)\cos^2\theta']R^{-6}+\\ &+\sum[\tfrac{3}{4}(4A-7B-4B'+7C)-\\ &-\tfrac{45}{4}(A-B-B'+C)\cos^2\theta']R^{-6}\sin^2\psi+\\ &+\sum[\tfrac{27}{8}(A-B-B'+C)(3\cos^2\theta'-1)]\times\\ &\times R^{-6}\sin^4\psi \qquad (9)\end{aligned}$$

where

$$A=\tfrac{1}{4}h\alpha_{\parallel}\alpha'_{\parallel}\frac{\nu_{\parallel}\nu'_{\parallel}}{\nu_{\parallel}+\nu'_{\parallel}} \qquad C=\tfrac{1}{4}h\alpha_{\perp}\alpha'_{\perp}\frac{\nu_{\perp}\nu'_{\perp}}{\nu_{\perp}+\nu'_{\perp}}$$

$$B=\tfrac{1}{4}h\alpha_{\parallel}\alpha'_{\perp}\frac{\nu_{\parallel}\nu'_{\perp}}{\nu_{\parallel}+\nu'_{\perp}} \qquad B'=\tfrac{1}{4}h\alpha_{\perp}\alpha'_{\parallel}\frac{\nu_{\perp}\nu'_{\parallel}}{\nu_{\perp}+\nu'_{\parallel}} \qquad (10)$$

are the parameters defined by London which involve anisotropic polarizability and effective frequency parameters α and ν of the two interacting molecules (h is Planck's constant). The remaining terms of London's potential formula not represented in equation (9) are assumed not to affect the orientational motion of the resonating molecule; their presence would only shift the zero of rotational energy in this approximation.

The contribution to δV_0 from a neighboring N_2 molecule trapped at various distances from the resonating molecule is given in Table 2. The contribution of a nearest neighbor far outweighs the rest on account of the inverse sixth power dependence on distance. Also, cancellations are important in decreasing the average effect from more distant neighbors. Thus, assuming for the moment that the neighboring cages are all occupied by N_2 molecules, the negative contribution $-0{\cdot}252$°K to δV_0 from the twelve second and third nearest neighbors is half cancelled by the contribution $+0{\cdot}128$°K from the fourth nearest neighbors. The effect from more distant neighbors is quite negligible. Thus, the non-nearest neighbor part of δV_0 is on the average less than $-0{\cdot}124/4{\cdot}10 = -0{\cdot}03$ of a nearest neighbor

Table 2. Contributions to δV_0 from the neighboring N_2 molecules. Contributions to δV_0 from a nitrogen molecule trapped in a $\langle n_1 n_2 n_3\rangle$ type site is given for all sites neighboring the resonating molecule within a radius of 16·6 Å. *The position of the n_1 n_2 n_3 site with respect to the site of the resonating molecule is given by $\boldsymbol{R}_n = n_1\boldsymbol{a}_1+n_2\boldsymbol{a}_2+n_3\boldsymbol{a}_3$, where $\boldsymbol{a}_1$, $\boldsymbol{a}_2$ and $\boldsymbol{a}_3$ are primitive cell vectors of the trigonal lattice. The second and third columns give the number of equivalent sites of type $\langle n_1\, n_2\, n_3\rangle$ and their distance from the resonating molecule.*

$\langle n_1 n_2 n_3\rangle$	M_n	R_n (Å)	δV_0(°K)
111	2	5·50	4·10
100	6	9·76	−0·024
110	6	10·26	−0·018
220	2	11·00	+0·064
211	6	12·04	−0·002
221	6	13·27	+0·0003
322	6	16·03	+0·0015
333	2	16·50	+0·0056
∞	6	16·6	−0·0009

part. Whereas the nearest neighbors produce a resolved spectrum of three lines, the remaining neighbors only broaden these lines by a negligible fraction of the observed line width. In the remainder of this section we consider only nearest neighbor contributions to δV_0. Deviations from the values in Table 2, due to nearest neighbor O_2 molecules in place of N_2 molecules, are ignored on account of the smallness of the O_2 concentration.

The contribution of a nearest neighbor to δV_0

Vol. 18
1961

Table 3. Contribution to δV_0 from various nearest neighbor molecules. The rows refer to resonating molecules and the columns to neighboring molecules. δV_0 is in units of °K. The polarizabilities quoted by LONDON[11] *and the isotropic effective frequences quoted by* LONDON[12] *were used in computing δV_0. The effective values of θ' were taken to be $\theta' = 23{\cdot}1°$ for O_2, corresponding to $D_0' = 4{\cdot}36$°K, and $\theta' = 15{\cdot}7°$ for N_2, derived from the nuclear electric quadrupole resonance data.*[8]

		Neighbor molecule					
		O_2	N_2	Ne	A	Kr	Xe
Resonating molecule	N_2	3·19	3·58	0·63	2·22	3·07	4·49
	O_2	3·66	4·10	0·71	2·53	3·53	5·20

is given in Table 3 for various types of neighboring molecules. Values for N_2 as the resonating molecule are included for possible use in connection with nuclear electric quadrupole experiments. It is interesting to observe that the δV_0's for O_2 resonance and for N_2 and O_2 neighbors are larger by factors 1·52 and 1·59 than they would be if these neighbors were able to rotate freely.

The parameter D' is related via $\langle\cos^2\theta\rangle_{\text{av.}}$ to V_0 by equation (2). We simplify this by using the relation

$$\langle 1-\cos 2\theta\rangle = 2\left(\frac{\hbar^2}{16\pi^2 I V_0}\right)^{1/2}, \tag{11}$$

valid in the harmonic oscillator approximation for the ground level of the hindered rotator, and obtain

$$D' = D[1-(\gamma/V_0)^{1/2}] \tag{12}$$

$$= D_0' + D(\gamma/V_{00})^{1/2}\left[\frac{1}{2}\frac{\delta V_0}{V_{00}} - \frac{3}{8}\left(\frac{\delta V_0}{V_{00}}\right)^2 + \right.$$

$$\left. + \frac{5}{16}\left(\frac{\delta V_0}{V_{00}}\right)^3 - \ldots\right] \tag{12'}$$

where $\gamma = (3/4)^2(\hbar^2/I)$ and $D_0 = D[1-(\gamma/V_{00})^{1/2}]$; $\gamma/k = 2{\cdot}32$°K for O_2 and $\gamma/k = 3{\cdot}18$°K for N_2. Use of the harmonic oscillator approximation for the ground level is justified by MEYER *et al.*[4]

The contribution to δV_0 is the same from each nearest neighbor, so that the fine structure intervals $D_1'-D_0'$ and $D_2'-D_1'$ would be equal if D' were linearly related to V_0. Values of $D_1'-D_0'$, $D_2'-D_1'$, and their ratio, computed using equation (12) are given in Table 4 for several types of nearest neighbors of the resonating O_2 molecule. The values in the N_2 column may be compared with the resonance experiment values $D_1'-D_0' = 0{\cdot}127\pm0{\cdot}01$°K, $D_2'-D_1' = 0{\cdot}094\pm0{\cdot}01$°K and $(D_2'-D_1')/(D_1'-D_0') = 0{\cdot}74$. Although the calculated and experimental values are given to two significant figures for convenience in presentation, the precision warrants only one. The ratios are seen to be in good agreement, and the intervals agree in sign, but the magnitudes of the calculated intervals are small by a factor of 2.

We are inclined to regard the discrepancy between the calculated and experimental fine structure intervals as arising from the approximations of the London theory rather than as evidence against our model. Discrepancies of this order are common for applications of the London theory.[13] Although errors in the theoretical values due to inaccuracies in the dispersion theory parameters may be appreciable, they probably do not account entirely for the discrepancy. The indirect part of the interaction, which we have neglected, probably makes a significant contribution. An estimate of the magnitude of the third order perturbation theory contributions to the indirect part of the interaction, made by using equation (1.12) of KIHARA[14], gives a (repulsive) contribution of the same order of magnitude as the contribution of the direct part of the interaction, although somewhat smaller. This suggests that fourth and higher order perturbation theory contributions may be important, and that an alternative approach is needed if more accurate calculation of the molecular interaction is desired.

If the direct part of the interaction among molecules is assumed to contribute the same fraction

Table 4. Calculated fine structure intervals for trapped O_2 spin resonance. The fine structure intervals are given in °K *as computed using equation* (12) *with* $V_{00} = 44{\cdot}0$°K *corresponding to* $D_0' = 4{\cdot}36$°K, $V_{01} = V_{00} + \delta V_0$, and $V_{02} = V_{00} + 2\delta V_0$. *The* δV_0 *values are taken from Table* 3.

	Neighbor molecule					
	N_2	O_2	Ne	A	Kr	Xe
$D_1' - D_0'$	0·057	0·051	0·011	0·036	0·049	0·071
$D_2' - D_1'$	0·050	0·046	0·010	0·033	0·044	0·061
$\frac{D_2' - D_1'}{D_1' - D_0'}$	0·88	0·89	0·95	0·92	0·90	0·85

to the whole interaction and any errors in the dispersion theory parameters are in the same direction when different neighbor molecules are substituted, the model can be further tested by other spin resonance experiments. Dilute O_2 in A and dilute O_2 in Xe β-quinol are favorable cases. The fine structure intervals should be resolved in both cases, according to Table 4, and the expected intervals bracket the N_2 intervals. Because A and Xe are spherically symmetric, we do not require orientation data such as was required for the N_2 molecules (see equation 9). Paramagnetic resonance experiments with these rare gas clathrates are planned.

The success of resonance experiments with dilute O_2 trapped in β-quinol clathrate suggests that similar experiments with dilute O_2 trapped in other types of clathrates, such as gas hydrates,[5] may be of interest.

C. *Spin–lattice relaxation time*

In principle the pulsed field measurements can be employed for measurements of the spin–lattice relaxation time T_1. If, for instance, T_1 is long compared to the half-period of the pulsed field, T_p, the zero-field population difference would be maintained unless cross-relaxation[15] or mixing at the cross-over point occurred. If H could be oriented exactly along the c-axis, intensity measurements of the transitions between the $M_s = 0$ and $M_s = -1$ levels would permit estimates of T_1 at high field to be made. Attempts to carry out such experiments with the O_2 clathrates were not successful.

As mentioned in Section III B, a transition was observed at about 15 kG which was identified as a $|\Delta M_s| = 2$ transition (f in Fig. 1). This identification was based on the following results: (a) the transition has not been observed for H parallel to the c-axis in dilute or concentrated O_2 clathrates, as would be predicted by a spin Hamiltonian with only a D' term; (b) the orientation of the crystal can be estimated from the $|\Delta M_s| = 1$ transitions and again it is apparent that H is not aligned along the c-axis; (c) the intensity of the $|\Delta M_s| = 2$ transition is appreciable, but it decreases with decreasing temperature. Although absolute intensity measurements were not feasible with the pulsed field techniques employed here, comparisons of the ratios of intensities with the $|\Delta M_s| = 1$ transitions could be obtained during the same pulsed field sweep, so that numerous experimental errors could be minimized. Rather large changes of intensities could be seen when the temperature was varied from 4·2°K to 1·5°K because D' was slightly greater than 4°K. Based on the identification of the $|\Delta M_s| = 2$ transition, an upper limit of T_1 has been estimated. A summary of this approach is given below.

First we consider the extreme case of $T_1 \gg T_p$. In this case, at $H = 0$ the population difference between the $M_s = +1$ and -1 levels will be very small if $|E| \ll D$ and will be zero if $E = 0$; thus transitions such as e or f in Fig. 1 would not be observable for any orientation. The other extreme case, $T_1 \ll T_p$, of course does permit such transitions to be observed under proper circumstances. Calculations of population differences for $T_1 = 0$ have been made as a function of H and temperature to examine the expected intensity variations when

Vol. 18
1961

H is parallel to the c-axis. For all transitions the population differences change very rapidly when $D'/2 < g\beta H < 3D'/2$.

Two comparisons with experiment are shown in Table 5. $R_1(T)$ is the ratio at temperature T of the peak intensity of the a transition to that of the f transition, and $R_2(T)$ is the ratio of the peak intensity of the a to that of the b transition at temperature T. The calculated ratios of population differences at the given temperatures and resonance fields are also indicated for the case $T_1 = 0$, H parallel to the c-axis, and $D' = 33$ kG. The agreement is within the experimental error.

Table 5. *Comparison of measured and calculated intensity ratios,* $R_1(T)$ *and* $R_2(T)$, *assuming* $T_1 = 0$ *and* $D' = 33$ kG. *The calculated ratio* $R_1(4{\cdot}2°\text{K})/R_1(1{\cdot}5°\text{K})$ *assumes that the transition probabilities are independent of* T, *and the calculated ratios* $R_2(T)$ *assume that the transition probabilities are independent of* H *and* T.

Ratio	Measured	Calculated
$R_1(4{\cdot}2°\text{K})/R_1(1{\cdot}5°\text{K})$	$0{\cdot}52 \pm 0{\cdot}2$	0·42
$R_2(4{\cdot}2°\text{K})$	$1{\cdot}0 \pm 0{\cdot}2$	0·8
$R_2(1{\cdot}5°\text{K})$	$1{\cdot}0 \pm 0{\cdot}2$	1·0

In principle T_1 could be estimated from such data if T_p could be varied over a wide range. This was not convenient. Instead, the shortest time interval between the $|\Delta M_s| = 1$ and that identified as a $|\Delta M_s| = 2$ transition was examined, in this case the time interval between a_2 and f_2 in Fig. 5. From this time interval and the relative intensities a limit of $T_1 \leqslant 50\mu$ sec at 1·5°K was estimated.

At first glance it might appear that the spin–lattice relaxation time should be long because the spins are not directly coupled to the lattice; the molecule is only weakly bound to the cage by van der Waals forces. The coupling of the spin to the lattice probably comes about via coupling of the spin to the molecule which in turn is coupled to the lattice by the surrounding cage which hinders free molecular rotation. The rotational motion of the O_2 molecule may be compared to the orbital motion of an electron of a paramagnetic ion for purposes of discussion of T_1. In the clathrate the rotational motion is not nearly so well quenched as is the orbital electronic motion of a typical $3d$ group transition metal ion, i.e. the cage potential acting on the O_2 molecule is much smaller than the corresponding crystalline potential acting on the paramagnetic ion. This suggests that the coupling of the O_2 spin to the lattice may be strong, and T_1 may be correspondingly short.

One puzzling feature of the $|\Delta M_s| = 2$ transition is the great broadness of the line, whereas it would appear that a sharp line should be seen because $d(h\nu)/dH$ (where $h\nu$ is the separation between energy levels) is larger for the $|\Delta M_s| = 2$ transition than for the $\Delta M_s = 1$ line. The resolution may be partially degraded by the rapidly increasing population differences which occur during the field sweep for this transition. The $|\Delta M_s| = 1$ (a and b) transitions at 70 kMc/s are not expected to show appreciable intensity changes due to population changes, but the intensity of the $|\Delta M_s| = 2$ (f) transition is sensitive to small field changes because these populations are changing rapidly. In general, analysis of relative intensities of widely spaced lines requires that population differences as a function of magnetic field be considered, particularly when $D' \geqslant kT$. If the field sweep rate is comparable to $1/T_1$, estimates of T_1 can be made. This has not been attempted here.

E. *Status of concentrated clathrate data*

The intensity measurements were decisive for analysis of the dilute O_2 clathrate results. In contrast, the limited resolution of the concentrated O_2 resonance data, and the non-reproducibility of the intensity patterns for crystals from the same batch, did not permit detailed analysis of the complex spectra. Many mechanisms may contribute to the line broadening and fine structure. These include dipolar and exchange interactions between O_2 molecules, and coupling of translational and rotational motion of a molecule in a given cage to the lattice and to other molecules. To examine any of these mechanisms, intensity measurements as a function of temperature and concentration are essential. The most reasonable approach appears to be resonance experiments with increasing concentrations of O_2 in the clathrate, but with sufficiently dilute O_2 so that only neighbor pairs and triples are present with appreciable probability. In this way, if a resolved spectrum is found,

it may be possible to determine which mechanisms are important.

The nuclear electric quadrupole resonance experiments of MEYER and SCOTT[8], made with concentrated N_2 clathrates, showed a complex structure which might be compared with the O_2 data. At present we are not able to correlate this data with the dilute O_2 data. In particular, the intensity variation of the NQR data with N_2 concentration is not understood. Experiments with dilute N_2 samples may be required before a detailed comparison can be made.

SUMMARY

The paramagnetic resonance of O_2 in β-quinol clathrate is consistent with the hindered rotation model developed earlier by MEYER *et al.*[4] to explain the static susceptibility. The resolved spectrum for O_2 in N_2 β-quinol clathrate demonstrated that the value of D' for each O_2 was directly related to occupancy of the nearest neighbor cages, and that three types of cages were present. A major contribution to the different D' values can be attributed to direct van der Waals interaction between neighboring trapped molecules. The results of these resonance experiments suggests related experiments for study of trapped molecules in their lowest hindered rotation states.

Acknowledgements—We wish to acknowledge the interest of Professor J. H. VAN VLECK in these experiments. We are grateful for the computational assistance provided by JANE COE, VIRGINIA JOHNSON, and ANN SHERMAN. Valuable assistance with the experiments was given by B. FELDMAN and in the early stages by E. D. THOMPSON. We would like also to thank FRED QUELLE for many useful discussions.

One of us (Dr. HORST MEYER) was supported by a joint contract of the Office of Naval Research and the Atomic Energy Commission Nonr 1866(19) and by joint contract of the Office of Naval Research and the National Security Agency Nonr 1866(33).

REFERENCES

1. PALIN D. E. and POWELL H. M., *J. Chem. Soc.* 208 (1947); POWELL H. M., *ibid.* 61 (1948); PALIN D. E. and POWELL H. M., *ibid.* 571 (1948); POWELL H. M., *ibid.* 298, 300, 468 (1950).
2. EVANS D. F. and RICHARDS R. E., *J. Chem. Soc.* 3295 (1952); COOKE A. H. and DUFFUS H. J., *Proc. Phys. Soc. Lond.* A**64,** 124 (1954).
3. COOKE A. H., MEYER H., WOLF W. P., EVANS D. F. and RICHARDS R. E., *Proc. Roy. Soc.* **225**A, 112 (1954).
4. MEYER H., O'BRIEN M. C. M. and VAN VLECK J. H., *Proc. Roy. Soc.* **243**A, 414 (1957).
5. VAN DER WAALS J. H. and PLATTEEUW J. C., *Advanc. Chem. Phys.* **2,** 1–57 (1959).
6. FONER S. and KOLM H. H., *Rev. Sci. Instrum.* **28,** 799 (1957); **27,** 547 (1956).
7. FONER S., *J. Phys. Radium* **20,** 336 (1959).
8. MEYER H. and SCOTT T. A., *J. Phys. Chem. Solids* **11,** 215 (1959).
9. KLEINER W. H., QUELLE F. and FONER S., Lincoln Laboratory Solid State Research Quarterly Progress Report, October 15, 1959, p. 64. (unpublished).
10. WAREKOIS E. P., private communication.
11. LONDON F., *J. Phys. Chem.* **46,** 305 (1942).
12. LONDON F., *Trans. Faraday Soc.* **33,** 8 (1937).
13. HIRSCHFELDER J. O., CURTISS C. F. and BIRD R. B., *Molecular Theory of Gases and Liquids* p. 966. John Wiley, New York (1954); PITZER K. S., *Advanc. Chem. Phys.* **2,** 59 (1959).
14. KIHARA T., *Advanc. Chem. Phys.* **1,** 271 (1958).
15. BLOEMBERGEN N., SHAPIRO S., PERSHAN P. S. and ARTMAN J. O., *Phys. Rev.* **114,** 445 (1959).

Vol. 18
1961

J. Phys. Chem. Solids Pergamon Press 1961. Vol. 18, No. 4, pp. 286–289. Printed in Great Britain.

SOME SEMICONDUCTING PROPERTIES OF BISMUTH TRISULFIDE*

L. GILDART,† J. M. KLINE‡ and D. M. MATTOX

University of Kentucky, Lexington, Kentucky

(*Received* 25 *August* 1960)

Abstract—Single crystals, dendrites, and crystalline films of bismuth trisulfide, Bi_2S_3, have been prepared and studied. From the films a thermal energy gap of 0·72 eV is found, in the range 300–400°K. From the single crystals, optical energy gaps of 1·4 eV at 77°K, and 1·2 eV at 300°K, are found; and resistivity, carrier concentration and mobility at 300°K are 0·85 ohm cm, 3×10^{17} cm^{-3} and 50 cm^2/volt sec, respectively. Thermal conductivity and Seebeck coefficient are found to be 0·0206 W/cm°C, and 550μV/°C, for single crystal samples in a direction parallel to the principal cleavage planes at 300°K. Preparation techniques, and the apparatus used in the thermal conductivity and Seebeck coefficient measurements, are described.

INTRODUCTION

THE PRODUCTION of single crystals of bismuth trisulfide Bi_2S_3, is made difficult by the high vapor pressure of sulfur above the melting point of bismuth trisulfide and the fact that this compound disassociates upon being melted at atmospheric pressure. Nevertheless, it has been possible to develop techniques for producing single crystals and whiskers, and they are described in detail.

It may be noted that various authors disagree in their published results on the semiconducting properties of Bi_2S_3.[1–4]

EXPERIMENTAL

Sample preparation:

The constituents are weighed out in stoichiometric proportions and put into a Vycor (96 per cent silica) tube, which is then evacuated and sealed. The constituents are reacted and the compound is melted in a special furnace, constructed so that the sample tube rotates continuously during melting to aid in mixing, and to insure a uniform temperature. The furnace can be tilted about a horizontal axis; single crystals are produced by tilting the furnace 90° while the sample is molten, and letting the sample, still in the Vycor tube, be dropped from the melting zone at a rate of about 6 in. day by clockwork. The space above the melt fills with sulfur vapor leaving behind a corresponding excess of bismuth, but this causes no difficulty; the large difference between the melting point of bismuth trisulfide (850°C[1]) and bismuth (271°C) insures that excess bismuth will freeze out as a separate phase at the top of the melt as the sample crystallizes.

It is found that if the temperature is symmetric about the sample tube, and the temperature gradient is parallel to the axis of the tube as it is lowered from the melting zone, the crystal grows with its principal cleavage planes parallel to the axis of the tube; if the temperature distribution is asymmetric about the tube or if the gradient is skewed the crystal grows with its cleavage planes inclined to the axis of the tube. Using the procedure outlined, Bi_2S_3 single crystals a centimeter or more in diameter, and several centimeters long can be grown. They are brittle and tend to shatter when machine cut, but may be easily cleaved.

For a certain limited range of values of the temperature gradient within the furnace, whiskers or dendrites of Bi_2S_3 grow from the vapor phase as the sample is lowered from the melting zone.

* Supported by the Air Force Office of Scientific Research.

† Now at the Bandung Institute of Technology, Bandung, Indonesia.

‡ On leave from the University of Mississippi, University, Mississippi.

These dendrites are ribbon-shaped, approximately 0·1 mm × 0·01 mm, and as much as 40 mm long. They are very regular, flexible, may be easily cleaved parallel to their long axis, and are probably single crystals. That these crystals are exactly of stoichiometric proportion cannot be assumed.

Because the crystalline samples have a resistivity too low for satisfactory resistance vs. temperature studies, polycrystalline films of Bi_2S_3 were prepared as follows: Films of metallic bismuth were deposited on glass substrates and heated in a sulfur atmosphere for about 24 hours. The resulting films apparently contain no free bismuth and have a high resistivity.

MEASUREMENTS

(a) *Thermal energy gap from films*:

The films are prepared for study using silver paste electrodes and nichrome lead-wires, they are put into a controlled furnace and a heating–cooling cycle is run, the temperature changing at about 5°C/min. The resulting change of resistance with temperature is plotted by an Autograf x–y recorder. It is found that after a few heating–cooling cycles the curves become quite reproducible. Fig. 1 shows a typical curve obtained in this manner.

Measurements on a series of these curves gives a thermal energy gap $E_{g_{th}}$, of $0{\cdot}72 \pm 0{\cdot}05$ eV in the range 300–400°K. This value agrees well with that obtained by KONOROV[2] on sintered samples from resistance vs. temperature measurements in this range.

(b) *Hall constants for single crystals*:

Samples having dimensions of about 0·1 cm × 0·1 cm × 1 cm are cleaved from the larger crystals for Hall and resistivity measurements. Electrical contact is made by melting a small lead bead in the V of a current carrying nichrome wire until the oxide layer has disappeared, and then touching the lead droplet to the surface of the sample. The resulting contact is ohmic, physically strong, and small wires may be soldered to it.

Resistivity and Hall measurements are made using apparatus built after the ideas of DAUPHINEE and MOOSER[5]. The average resistivity from a series of these samples is $0{\cdot}85 \pm 0{\cdot}05$ ohm cm at 300°K. This value is somewhat higher than that given by BLACK[1] but in agreement with the predictions of MOOSER and PEARSON[6]. Resistivities are found to be a factor of five to ten higher on polycrystalline samples prepared after the method of BLACK, and seem to be dependent on the degree of crystallization.

Results from the Hall measurement are not very consistent due to noise difficulties. The mean

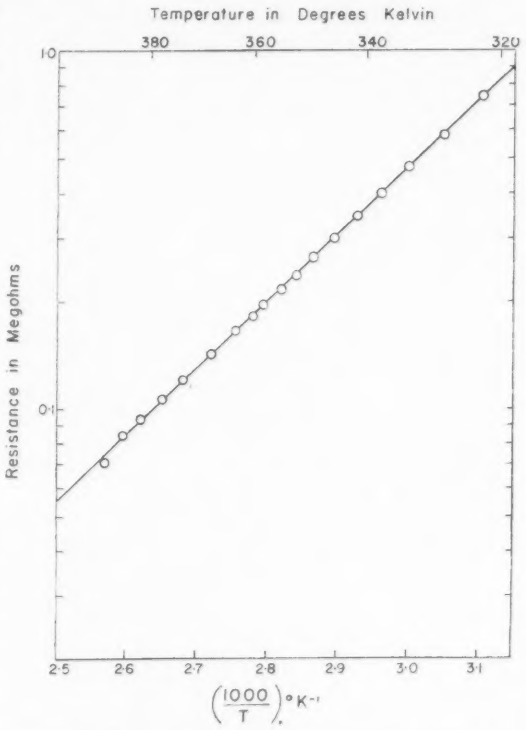

FIG. 1. Resistance as a function of temperature for a polycrystalline film of Bi_2S_3.

carrier concentration turns out to be about 3×10^{17} cm^{-3}. Mobility is 50 cm^2/V sec at 300°K. These values agree with what would be expected when the resistivity difference between the present samples and those of BLACK is taken into account; his samples had higher carrier concentrations and mobilities and a correspondingly lower resistivity.

(c) *Optical transmission*:

For optical transmission measurements samples of Bi_2S_3 having thicknesses from 0·1 to 0·5 mm are cleaved from large single crystals. Fig. 2 shows the optical transmission at 300°K for a typical sample,

Vol. 18
1961

0·3 mm thick, perpendicular to the cleavage planes, as measured on a Cary model 14 spectrophotometer. Fig. 3 shows the absorption edge for this sample at 77°K and at 300°K giving an optical energy gap of 1·4 eV at 77°K and 1·2 eV at 300°K. This is an apparent temperature dependence of -8×10^{-4} eV/C° over this temperature range, assuming a linear variation. Samples 0·1 mm thick show no measurable infrared transmission in the range 2·0–15 microns on a Perkin–Elmer spectrophotometer.

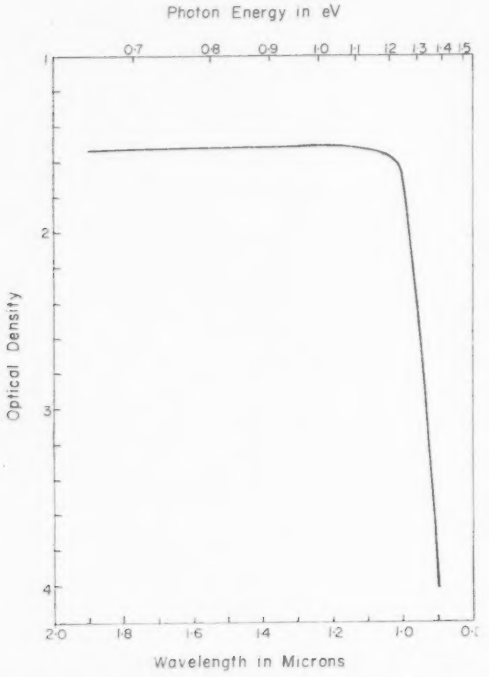

FIG. 2. Optical transmission for single crystal Bi_2S_3 at 300°K.

(d) *Thermal conductivity and Seebeck coefficients*:

The thermal conductivity K, and Seebeck coefficient S, of small cylindrical samples of single crystal bismuth trisulfide are measured with the apparatus shown in Fig. 4 which is designed for use with samples that are limited in size (small solid cylinders) and which at the same time have a very low thermal conductivity. A comparison method, in which the conductivity of the unknown is compared to the conductivity of a standard material is employed.[7,8] The unknown sample is in series with a standard sample and the two are put between a heat source and a heat sink. Sample faces are machined and lapped. A thin layer of vacuum grease heavily impregnated with copper powder insures low thermal resistance at the three interfaces.

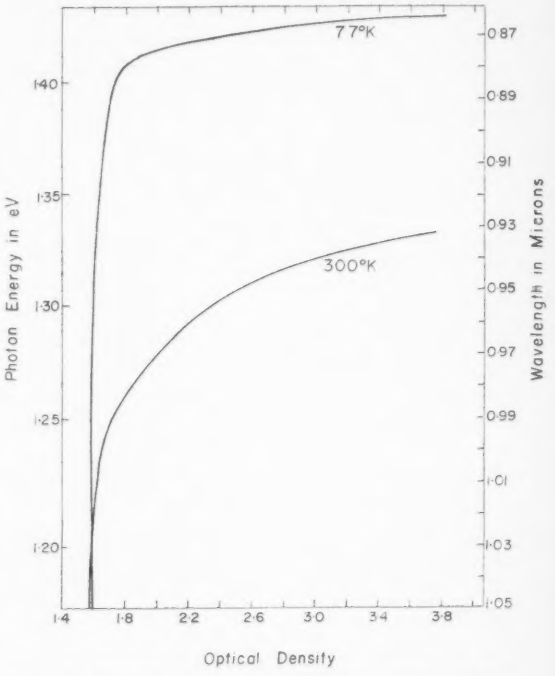

FIG. 3. Optical absorption edge for single crystal Bi_2S_3, at 77°K and 300°K.

Temperature differences T_1-T_2 and T_2-T_3 are determined at thermal equilibrium by means of thermocouples placed at the three interfaces. The thermal conductivity K_u of the unknown sample is then given by

$$K_u = K_s L_u A_s (T_1-T_2)/L_s A_u (T_2-T_3)$$

Here the subscript s refers to the standard, and u to the unknown sample with T being the temperature, L the length, and A the cross sectional area.

Since it is better to use a standard having a thermal conductivity comparable to that of the

unknown, bismuth metal was chosen. This has a thermal conductivity of 0·09426 W/cm °C for single crystals in the direction parallel to the cleavage planes, according to NISHOIKA[9]. Test runs on polycrystalline bismuth, polycrystalline antimony and nearly stoichiometric *n*- and *p*-type bismuth telluride in the place of the unknown sample, gave results which agree with those reported for these compounds.[9,10,11]

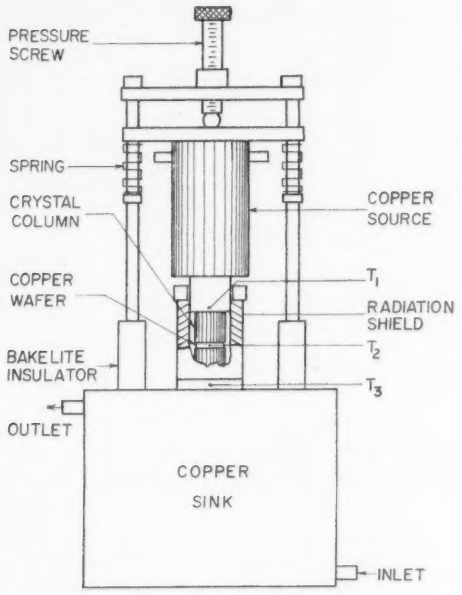

FIG. 4. Apparatus used for measuring the thermal conductivity and Seebeck coefficient of Bi_2S_3.

The mean value of thermal conductivity for seven bismuth trisulfide samples, is 0·0206 ± 0·0005 W/cm C°. These measurements were made at 300°K with the thermal gradient parallel to the cleavage planes.

Seebeck coefficient studies are made on single crystals of Bi_2S_3 using the apparatus shown in Fig. 4, with the copper wafer containing thermocouple T_2 and the standard removed. The Seebeck coefficient S, measured at the average temperature T_A is given by

$$S = E_s/\Delta T$$

and

$$T_A = (T_1 + T_3)/2$$

where E_s is the Seebeck voltage established by the temperature difference ΔT between the source and sink. The Seebeck voltage and temperature difference are obtained simultaneously.

HORNE[12] has given a criterion for the reliability of Seebeck coefficient measuring apparatus; a plot of Seebeck voltage vs. temperature difference giving a straight line through the origin, identifies a properly functioning device. The apparatus meets this requirement.

The Seebeck coefficient for single crystal Bi_2S_3 samples, measured at 300°K has an average value of 550 μV/°C ± 50 μV/°C when the thermal gradient is parallel to the cleavage planes. Preliminary investigations indicate that the Seebeck coefficient is not appreciably different in a direction perpendicular to the cleavage planes. Polycrystalline samples have a Seebeck coefficient ranging from 700–850 μV/°C depending on the degree of crystallization. These results on the polycrystalline samples agree with those given by BLACK *et al.*[1] on polycrystalline samples but are lower than the findings of KONOROV[2] for sintered samples.

Acknowledgements—The authors are indebted to T. E. JOHNSON of this laboratory and C. M. NELSON of the Solid State Division of the Oak Ridge National Laboratories for their help.

REFERENCES

1. BLACK J., CONWELL E. M., SEIGLE L. and SPENCER C. W., *J. Phys. Chem. Solids* **2,** 240 (1957).
2. KONOROV P. P., *Zh. tekh. fiz.* **26,** 1126 (1956).
3. GORIUNOVA L., *Soviet Phys.—Tech. Phys.* **1,** 1583 (1957).
4. KOLOMIETS B. T., *Zh. tekh. fiz.* **19,** 126 (1949).
5. DAUPHINEE T. M. and MOOSER E., *Rev. Sci. Instrum.* **26,** 660 (1955).
6. MOOSER E. and PEARSON W. B., *J. Phys. Chem. Solids* **7,** 65 (1958).
7. BALLARD S. S., MCCARTHY K. A. and DAVIS W. C., *Rev. Sci. Instrum.* **21,** 905 (1950).
8. STUCKES A. D., *Phys. Rev.* **107,** 427 (1951).
9. NISHIOKA S., *Memoirs of College of Science, University of Kyoto* **A25,** 147 (1954).
10. *Bulletin, American Smelting and Refining Co.*, New York (1959).
11. SATTERTHWAITE C. B. and URE R. W., Jr., *Phys. Rev.* **108,** 1164 (1957).
12. HORNE R. A., *Rev. Sci. Instrum.* **31,** 459 (1960).

Vol. 18
1961

J. Phys. Chem. Solids Pergamon Press 1961. Vol. 18, No. 4, pp. 290–296. Printed in Great Britain.

THEORETICAL CALCULATIONS OF THE ENTHALPIES AND ENTROPIES OF DIFFUSION AND VACANCY FORMATION IN SEMICONDUCTORS*

R. A. SWALIN

Department of Metallurgy, University of Minnesota, Minneapolis

(*Received* 22 *August* 1960)

Abstract—Enthalpies and entropies of vacancy formation and diffusion have been calculated for elements having the diamond structure. In the calculations, the potential between nearest neighbor atoms is assumed to have the form of the Morse function. In this fashion kinetic parameters of crystals are calculated by the use of properties determined from equilibrium properties. One of the factors facilitating calculation results from the open nature of the diamond lattice. Because of this, an atom, moving from its equilibrium position into a vacancy, does not pass through a geometric barrier as is the case for more close-packed structures.

Calculations yield values for the enthalpies of formation of vacancies of 2·07 eV, 2·32 eV and 4·16 eV for germanium, silicon and diamond respectively. Experimental results available for germanium yield 2·01 eV.

Calculations of the activation enthalpies of self diffusion, assuming a vacancy mechanism, are 3·02, 3·38 and 6·18 eV for germanium, silicon and diamond. Experimental information for germanium indicates a value of 2·98 eV.

A. INTRODUCTION

ELEMENTAL semiconductors, (gray tin, germanium, silicon and diamond) fall into a class of materials known as covalent crystals. The hybrid sp^3 bond orbitals for an atom in these materials can be thought of as overlapping with orbitals of neighboring atoms forming a classical two-electron bond. As a result these crystals can be fruitfully considered as consisting of a regular array of atoms held together by classical covalent bonds. This picture implies that as far as the energetics of the lattice is concerned, an atom is influenced primarily by its nearest neighbors. As is well known, the covalent bond approach has had considerable success in organic chemistry research but has not been used extensively in solid state research. The purpose of the present paper is to use the covalent bond approach for obtaining kinetic parameters.

In order to perform the calculations, it is necessary to have an expression for the energy as a function of separation of atoms in a crystal. Several semi-empirical expressions have been used in calculations for crystals. For example, GIRIFALCO and STREETMAN[1] and FURTH[2] have used a 5–7 potential for vacancy calculations in body-centered cubic materials. DIENES[3] has calculated the activation energy for diffusion in graphite by use of a Born–Mayer potential for the repulsive term and a van der Waals interaction for the attractive term. KANZAKI[4] has used a 6–10 potential for face-centered cubic materials. One form which has had considerable success is the Morse function.[5,6] According to this expression the enthalpy, ΔH, expended in increasing the distance between two nearest neighbors from the equilibrium value d_0 to d is

$$\Delta H = D\{1+\exp[-2\alpha(d-d_0)]-$$
$$-2\exp[-\alpha(d-d_0)]\} \qquad (1)$$

where D represents the energy of dissociation of a covalent bond (obtainable from the heat of sublimation) and α is related to the second derivative of the enthalpy vs. distance curve. Values of α

* Research sponsored by the Office of Naval Research.

for most elements can be obtained from force constant data of WASER and PAULING[7]. The relation as derived by SWALIN[8] is

$$\alpha = \left(\frac{k}{2D}\right)^{1/2} \tag{2}$$

where k is the force constant of the bond derived from compressibility data.

B. THE ENTHALPY OF VACANCY FORMATION

The enthalpy of formation of a vacancy in a perfect lattice can be thought of as consisting of two parts (a) the enthalpy expended in removing an atom from the interior of a crystal and depositing it on the surface and (b) the enthalpy gained by the relaxation of neighbors surrounding the vacancy. The contribution to the enthalpy of vacancy formation from (a) consists of the dissociation of Z bonds (where Z is the coordination number) in order to remove the atom from the interior of the crystal to a distance of infinity and the formation of $Z/2$ bonds upon transferring the atom from infinity to the surface of the crystal. Thus the net cost is equal to $\frac{1}{2}ZD$.

In Fig. 1(a) is shown a segment of the diamond structure and Fig. 1(b) shows schematically a lattice site after removal of an atom. It is seen that four unshared valence electrons are left as a result of the removal. According to chemical theory, one would expect a considerable reduction of energy if these four electrons arrange themselves so as to form two covalent bonds satisfying the requirement that each atom in the crystal has no more than four bonds. To accomplish this, bonds will have to form between atoms in next-nearest neighbor positions. Thus, not considering any relaxations, upon formation of a vacancy, we have broken $\frac{1}{2}Z$ or 2 bonds having an energy of D and formed two high energy bonds with a length of $1{\cdot}64\ d_0$.

More energy could possibly be gained by allowing these two new bonds to shorten. To do this, however, will result in an increased separation between atoms in next nearest positions from the vacancy. Therefore, an optimum relaxation can be obtained. Let us consider for the purpose of illustration that the two covalent bonds form between d and g and between e and f respectively in Fig. 1(b). (Since these atoms are all in equivalent

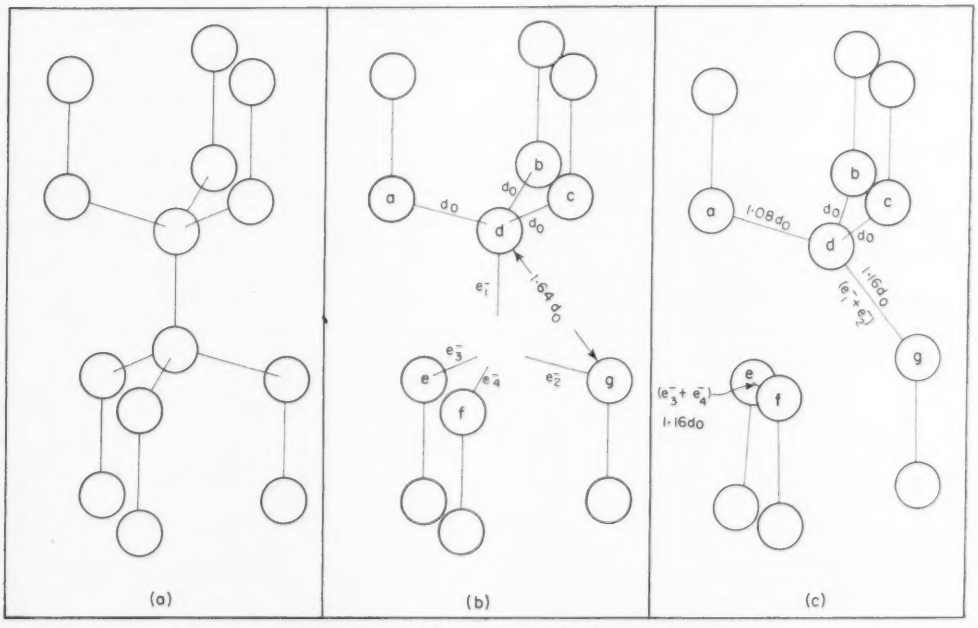

FIG. 1. (*a*) Arrangement of atoms in the diamond lattice.
(*b*) Unrelaxed vacancy. (*c*) Vacancy after relaxation has occurred.

positions with respect to the vacancy, the two bonds can be distributed in several equivalent positions.) In order to lower the energy of the vacancy, atoms d and g will relax toward one another. The same will be true of e and f. As a result of this relaxation second nearest neighbor bonds will be elongated. Calculations as well as examination of the diamond lattice indicate that the lattice bonds will be least disrupted if d rotates about b and c, keeping the interatomic distance constant. In like fashion g will move toward d by rotating about two of its neighbors not shown on the diagram. The same will be true of e and f. Thus the relaxation will result in the elongation of four second nearest neighbor bonds instead of twelve. Instead of forcing all the distortion to occur in the second nearest neighbor bonds, it should be distributed throughout several shells. Since each of the four second nearest neighbor bonds is connected with three third nearest neighbor bonds, a total of 12 third nearest neighbor bonds will be affected. Similar reasoning yields 36 fourth nearest neighbor bonds, 108 fifth nearest neighbor, etc. yielding the relationship $4\times 3^{(n-2)}$ atoms affected where n is the number of the shell.

In order to facilitate calculations, it will be assumed that the strain persists out to the seventh nearest neighbor and further that the strain follows a geometric pattern. That is to say, the strain, ϵ, of the second nearest neighbor will be considered to be twice that of third nearest neighbor bond, the strain of the third nearest neighbor is twice that of the fourth nearest neighbor, etc. Thus, four bonds are strained an amount ϵ_2, twelve third nearest neighbor bonds are strained $\epsilon_2/2$, etc. Using a Morse function coupled with the previous statements, we obtain the following equation for the strain energy due to relaxation of the nearest neighbors around the vacancy

$$\Delta H_2=\sum_{n=2}^{n=6} 4\times 3^{(n-2)}D\left\{1+\exp\left[-2\alpha\left(\frac{\epsilon_2}{2^{(n-2)}}\right)\right]-\right.$$
$$\left.-2\exp\left[-\alpha\left(\frac{\epsilon_2}{2^{(n-2)}}\right)\right]\right\} \qquad (3)$$

The quantity ϵ_2 is related to the inward relaxation X of nearest neighbors in the following fashion: the elongation of the second nearest neighbors ϵ_2 reduces the strain from X to $(X-\epsilon_2)$ which has to be taken care of by the third, fourth, fifth, and sixth neighbor bonds. These bonds, however, by virtue of their geometric relation to one another will increase the relaxation in proportion to about twice their change of dimension. Thus, a strain $\epsilon_2/2$ in the third neighbor shell will be effective to the extent of ϵ_2 etc., yielding

$$X=\epsilon_2+2\sum_{3}^{6}\epsilon_n=\epsilon_2+2\sum_{3}^{6}\frac{\epsilon_2}{2^{(n-2)}}=2{\cdot}88\,\epsilon_2 \qquad (4)$$

Therefore

$$\Delta H_2=\sum_{n=2}^{n=6} 4\times 3^{(n-2)}D\left\{1+\right.$$
$$+\exp\left[-2\alpha\left(\frac{X}{(2{\cdot}88)2^{(n-2)}}\right)\right]$$
$$\left.-2\exp\left[-\alpha\left(\frac{X}{(2{\cdot}88)2^{(n-2)}}\right)\right]\right\} \qquad (5)$$

Equation (5) yields a positive ΔH_2. The negative enthalpy due to relaxation of the two nearest neighbor bonds from $1{\cdot}64\ d_0$ to $(1{\cdot}64\ d_0-2x)$ is

$$\Delta H_3=2D\{\exp[-2\alpha(0{\cdot}64\ d_0-2X)]-$$
$$-2\exp[-\alpha(0{\cdot}64\,d_0-2X)]\} \qquad (6)$$

The variable X will be the value which will cause the sum of ΔH_2 and ΔH_3 to be a minimum. Using values of α and d_0 for germanium, silicon and diamond, it is found graphically that the sum ΔH_2 and ΔH_3 reaches a minimum when X has values such as to make the distance between d and g and between e and f diminish from $1{\cdot}64\ d_0$ to $1{\cdot}16\ d_0$. This results in the second nearest neighbor bonds such as a–d having a length of $1{\cdot}08\ d_0$. This situation is shown in Fig. 1(c).

The enthalpy for formation of a vacancy, ΔH_v is given by

$$\Delta H_v=\Delta H_1+(\Delta H_2+\Delta H_3) \qquad (7)$$

ΔH_1 represents the enthalpy expended in moving the atom from the interior to the surface and $(\Delta H_2+\Delta H_3)$ represents the enthalpy gained by relaxation and new bond formation around the vacancy.

In Table 1 are shown the values of ΔH_1, $(\Delta H_2+\Delta H_3)$, and ΔH_v for germanium, silicon and

Table 1. Calculations of the enthalpy of formation of a vacancy for germanium, silicon and diamond

Element	α(Å^{-1})	d_0(Å)	D(eV)	ΔH_1(eV)	$(\Delta H_2+\Delta H_3)$ (eV)	ΔH_f(eV)
Ge	1·50	2·44	1·63	3·26	−1·19	2·07
Si	1·56	2·34	1·83	3·66	−1·34	2·32
Diamond	2·30	1·54	3·61	7·22	−3·06	4·16

diamond along with values of α, d_0, and D used in the calculations. Values of D, the single bond energy, and d_0 were taken from Ref. (8) and α was computed from equation (2), using the k values of Ref. (6).

Thus using the approach presented in this paper, enthalpies of vacancy formation of 2·07 eV, 2·32 and 4·16 eV are obtained for germanium, silicon and diamond respectively. No experimental values of this quantity are available for silicon and diamond but measurements have been made for germanium. Quenching experiments performed by MAYBURG[10] yield $\Delta H_v = 2{\cdot}01$ eV and those of LOGAN[11] yield 2 eV. The value obtained from the theory is quite close.

Vol. 18
1961

C. THE ENTROPY OF VACANCY FORMATION

The entropy of vacancy formation will consist of the following two parts: (a) an increase of vibrational amplitude of atoms surrounding the vacancy due to the relaxation and (b) a configurational entropy due to the freedom of position of the new bonds. The contribution due to (b) can be readily evaluated as shown below.

In Fig. 1(c) it is seen that there is an uncertainty in position of the covalent bonds. The bond d–g could be between d and f or d and e with the bond e–f shifting to e–g and g–f respectively. This we will call ΔS_1. Independent of this the bond a–d could be between b–d or c–d. This we will call ΔS_2.

Using the standard relation the configurational entropy ΔS_c is given by

$$\Delta S_c = \sum k \ln W \qquad (8)$$

With regard to ΔS; there are two bonds of the same type distributed in three configurations. Therefore

$$W = \frac{3!}{2!1!} = 3 \text{ and } \Delta S_1 = k \ln 3$$

In the second case, two bonds of length d_0 and one of length $1{\cdot}08\ d_0$ are distributed amongst three positions or

$$W = \frac{3!}{2!\,1!} = 3 \text{ and } \Delta S_2 = k \ln 3$$

Therefore

$$\Delta S_c = 2k \ln 3 = 4{\cdot}4 \text{ entropy units} \qquad (9)$$

ΔS_c is the same for germanium, silicon and diamond. In addition to this term, as mentioned, will be another term which has a magnitude dependent upon the elastic properties of the material. This second term is more difficult to calculate than ΔS_c.

Comparing the calculated ΔS_c with experimental data for germanium we find that measurements from quenching experiments yield $\Delta S_v = 3{\cdot}8$ entropy units[10] and estimates of ΔS_v from the temperature derivative of moduli yield 6·7 entropy units.[11] It would appear therefore that the principal term in ΔS_v is ΔS_c. Assuming therefore that $\Delta S_v \sim \Delta S_c$, one can estimate the equilibrium vacancy concentration as a function of temperature for germanium, silicon, and diamond to be in terms of C_v, the number of vacancies per cm^3.

$$\text{Ge} \quad : C_v \cong 4{\cdot}2 \times 10^{23} \exp\left[-\frac{2{\cdot}07}{kT}\right] \text{cm}^{-3}$$

$$\text{Si} \quad : C_v \cong 4{\cdot}6 \times 10^{23} \exp\left[-\frac{2{\cdot}32}{kT}\right] \text{cm}^{-3}$$

$$\text{Diamond} \quad : C_v \cong 1{\cdot}5 \times 10^{24} \exp\left[-\frac{4{\cdot}16}{kT}\right] \text{cm}^{-3}$$

D. THE ENTHALPY OF VACANCY DIFFUSION

One of the striking features of the diamond structure compared with metallic structures with

regard to the diffusion process is the openness of the diamond lattice. Upon observing a lattice model it is clear that when an atom and a nearest neighbor vacancy exchange places no dilation of the lattice for elements having the diamond structure need occur. This should be contrasted with the close-packed metallic lattices in which the diffusing atom in moving to a vacancy must pass through a lattice constriction. This point makes accurate calculation of energetics difficult for metallic structures because of the inability to make detailed calculations of the strain energy at the saddle point.

In contrast we will consider the process of diffusion in semiconductors in a fashion analogous to the enthalpy calculations of Section B.

The jump process is shown in Fig. 2. In Fig. 2(a) is shown the vacancy with nearest neighbors at distances calculated in Section B. Atom d which will be considered as the one moving into the vacancy has four bonds, two with a length of d_0, one with a length of $1{\cdot}08\ d_0$ and one with a length of $1{\cdot}16\ d_0$. Fig. 2(b) shows the atom halfway in its jump from the initial position 1 to the final position 3. It is seen that the two bonds which originally had a length of d_0 are increased to $1{\cdot}25\ d_0$, the one which had a length of $1{\cdot}08\ d_0$ is increased to $1{\cdot}10\ d_0$ and the one of length $1{\cdot}16\ d_0$ is decreased to $1{\cdot}04\ d_0$. The enthalpies associated with these changes can therefore be considered to represent the enthalpy of vacancy motion, ΔH_m. Fig. 2(c) shows the completed jump where the vacancy and atom have changed places.

ΔH_m therefore consists of the following three terms; ΔH_4, the enthalpy expended in increasing one bond from $1{\cdot}08\ d_0$ to $1{\cdot}10\ d_0$, ΔH_5 the enthalpy expended in increasing two bonds from d_0 to $1{\cdot}25\ d_0$ and ΔH_6 the enthalpy expended in decreasing one bond from $1{\cdot}16\ d_0$ to $1{\cdot}04\ d_0$. Using the Morse function

$$\Delta H_4 = D\{\exp[-2\alpha\, d_0(0{\cdot}10)] - 2\exp[-\alpha\, d_0(0{\cdot}10)] - \\ -\exp[-2\alpha\, d_0(0{\cdot}08)] + 2\exp[-\alpha\, d_0(0{\cdot}08)]\}$$

$$\Delta H_5 = 2D\{1+\exp[-2\alpha\, d_0(0{\cdot}25)] - \\ -2\exp[-\alpha\, d_0(0{\cdot}25)]\}$$

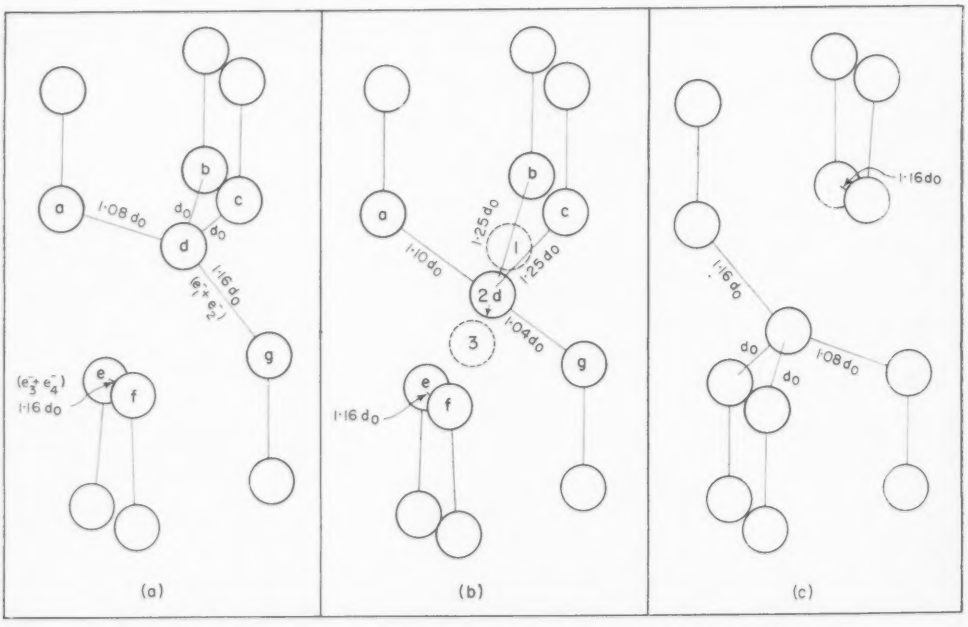

FIG. 2. (*a*) Arrangement of vacancy and nearest neighbors in the diamond lattice. (*b*) Diffusing atom in saddlepoint position. (*c*) Crystal after exchange of atom with a vacancy.

$$\Delta H_6 = D\{\exp[-2\alpha\, d_0(0{\cdot}04)] - 2\exp[-\alpha\, d_0(0{\cdot}04)] - \exp[-2\alpha\, d_0(0{\cdot}16)] + 2\exp[-\alpha\, d_0(0{\cdot}16)]\}.$$

Using the values of α and d_0 cited in Section B we find the following values of ΔH_m

Ge : $\Delta H_m = 0{\cdot}95$ eV

Si : $\Delta H_m = 1{\cdot}06$ eV

Diamond : $\Delta H_m = 2{\cdot}02$ eV

Experimentally, diffusion data have only been obtained for germanium. Using the activation enthalpy for self diffusion in germanium of 2·98 eV measured by LETAW *et al.*[12] and subtracting the enthalpy of formation determined by MAYBURG[10] yields a value for ΔH_m of 0·97 eV compared with the theoretical value of 0·95 eV.

In the case of silicon, annealing of electron bombardment damaged crystals was associated with an activation enthalpy of about 1·3 eV.[13] This process is presumably concerned with vacancy migration.

Vol. 18
1961

E. THE ENTROPY OF VACANCY DIFFUSION

As discussed in Section C for the case of the entropy associated with vacancy formation, the entropy for migration ΔS_m will consist of a configurational term and a vibrational term. Proceeding as in the preceding case, we will calculate the configurational part and assume that most of the total is associated with this term.

From Fig. 2(b), it is seen that the configuration has five bonds associated with it, four between the diffusing atom and its nearest neighbors and one between *e* and *f*. Since we have the restriction that only four bonds can be associated with a given atom, the position of the fifth bond will be determined by the placement of the other four. We will assume that each of the six bond sites is equivalent with regard to each of the four bonds. In this fashion

$$W = \frac{6!}{2!1!1!2!} = 180$$

and

$$\Delta S_c = k \ln 180 = 10{\cdot}3 \text{ entropy units.}$$

In order to calculate the entropy of activation, from this quantity must be subtracted the entropy of the atom in its equilibrium position prior to jumping. This is equal to the entropy of vacancy formation and therefore the configuration entropy associated with the jump process is

$$\Delta S_m = 10{\cdot}3 - 4{\cdot}4 = 5{\cdot}9 \text{ entropy units} \qquad (10)$$

This is to be compared with the value of $\Delta S_m = 12$ for germanium calculated in Ref. (11) using experimental self-diffusion data and equilibrium vacancy concentration determined by MAYBURG[10]. It appears that the vibrational contribution to ΔS_m is important.

F. ACTIVATION ENTHALPIES AND ENTROPIES FOR SELF-DIFFUSION

Assuming a vacancy mechanism for self-diffusion, the activation energy for self-diffusion is given by the well known expression

$$Q = \Delta H_v + \Delta H_m \qquad (11)$$

and ΔS_D, the entropy of activation

$$\Delta S_D = \Delta S_v + \Delta S_m \qquad (12)$$

As seen in the last sections the change in configurational entropy associated with the rearrangement of bonds after creation of a vacancy counts for virtually the entire term ΔS_v, suggesting a rather small vibrational contribution. On the other hand, the configurational contribution to ΔS_m accounts for only half of the experimental value for germanium. Since it may be of some interest to have approximate values of the self-diffusion constant for silicon and diamond in which cases experimental values do not exist, we will assume $\Delta S_m = 2\Delta S_c$ as calculated from equation (10) based on results for germanium. Therefore, applying equation (12) we find that $\Delta S_D = 16{\cdot}4$ entropy units.

The self-diffusion coefficient D is found experimentally to be given by

$$D = D_0 \exp[-Q/kT] \qquad (13)$$

where D_0 is the frequency factor. Assuming diffusion to be a random walk process it is found for the diamond lattice that

$$D_0 = \tfrac{1}{8} f a^2 \nu \exp[\Delta S_D/k] \qquad (14)$$

where a is the lattice parameter, ν is the Debye

Table 2. Calculated values of D_0 and Q for self-diffusion

Element	a(Å)	$\nu \times 10^{-12}$(sec^{-1})	D_0(cm^2/sec)	Q(eV)
Germanium	5·66	7·65	5·4	3·02
Silicon	5·43	13·8	8·9	3·38
Diamond	3·57	41·8	11·6	6·18

frequency and f is the correlation factor equal to $\frac{1}{2}$ for the present case.[13] In Table 2 are listed calculated values of D_0 and Q for the elements of interest. Standard values of a and ν given in Refs. (14) and (15).

As discussed earlier no direct experimental self-diffusion results are available for silicon. Several measurements have been made of impurity diffusion, however. The activation enthalpies obtained for substitutional impurities vary between about 3·47 eV and 4·65 eV and D_0 has been found to vary between 0·32 and 1031 cm^2/sec. Our calculated value of 3·38 eV for the activation enthalpy of self-diffusion is consistent with these experiments although on the lower side.

G. CONCLUSIONS

The calculations presented in the previous section using the Morse function, indicate that this approach can yield rather good results for the case of covalent crystals. These calculations suggest that considerations involving elemental concepts of chemical structure which have been so fruitfully applied to equilibrium properties of crystals can also be successfully used for calculation of kinetic properties.

In principle, therefore, one should be able to extend this approach so as to obtain enthalpies of formation of higher order defects such as divacancies and also their enthalpies of motion. Such calculations will be performed in the future.

REFERENCES

1. Girifalco L. A. and Streetman J. R., *J. Phys. Chem. Solids* **4,** 182 (1958).
2. Furth R., *Proc. Roy. Soc.* A**183,** 87 (1944).
3. Dienes G. J., *J. Appl. Phys.* **23,** 1194 (1952).
4. Kanzaki H., *J. Phys. Chem. Solids* **2,** 24 (1957).
5. Morse P. M., *Phys. Rev.* **34,** 57 (1929).
6. Slater J. C., *Introduction to Chemical Physics.* McGraw Hill, New York (1939).
7. Waser J. and Pauling L., *J. Chem. Phys.* **18,** 747 (1950).
8. Swalin R. A., *Acta Met.* **7,** 736 (1959).
9. Pauling L., *Nature of the Chemical Bond* (3rd Ed.) Cornell University Press, Ithaca, New York (1960).
10. Mayburg S., *Phys. Rev.* **95,** 38 (1954).
11. Logan R. A., *Phys. Rev.* **101,** 1455 (1956).
12. Letaw H., Portnoy W. M. and Slifkin L., *Phys. Rev.* **102,** 636 (1956).
13. Bemski G. and Augustyniak W. M., *Phys. Rev.* **108,** 645 (1957).
14. Compaan K. and Haven Y., *Trans. Faraday Soc.* **54,** 1498 (1958).
15. *American Institute of Physics Handbook* (edited by Gray D. E.) American Institute of Physics, New York, N.Y. (1957).
16. Kittel C., *Introduction to Solid State Physics* (2nd Ed.) John Wiley, New York (1956).

J. Phys. Chem. Solids Pergamon Press 1961. Vol. 18, No. 4, pp. 297–306. Printed in Great Britain.

SOME OPTICAL AND ELECTRICAL PROPERTIES OF SEMICONDUCTING DIAMONDS

A. HALPERIN and J. NAHUM*

Department of Physics, The Hebrew University, Jerusalem, Israel

(*Received* 3 *October* 1960)

Abstract—Two semiconducting (Type IIb) diamonds were examined for some of their optical and electrical properties. The energies of the extra absorption bands in the infrared typical to Type IIb specimens were found to fit very well the thermal activation energies obtained both from the dark conductivity and the thermoluminescence. The experiments indicate discrete levels of 0·21, 0·30, 0·37, 0·52 and about 0·7 eV above the valence band.

Nearly the same spectral distribution was found for the u.v. excited luminescence, the electroluminescence, and the thermoluminescence, all having their main maximum at about 0·48 μ.

Excitation spectra for the thermoluminescence and the photoconductivity were also measured. Some other experiments describe the conductivity and voltaic glow curves of the same specimens.

Vol. 18
1961

INTRODUCTION

SINCE the discovery of semiconducting—Type IIb—diamonds by CUSTERS[1], these diamonds have been investigated by several workers. A short review of this work was given recently by MITCHELL[2].

In the present work two Type IIb diamonds were examined for some of their optical and electrical properties, The results obtained with the two specimens were almost identical, and as far as results of other investigations were available for comparison, the agreement was very good. This indicates that the properties of the examined specimens are typical for Type IIb diamonds.

The optical measurements in the present work included the absorption in the u.v. and infrared, the luminescence, and the thermoluminescence. The latter has not been investigated at all (for Type IIb diamonds) by earlier workers, and was, therefore, examined now in more detail.

Other measurements included the dark conductivity as function of temperature, the photoconductivity, and current glow curves.

Of interest in the results is the good correlation between the energy levels obtained from the absorption measurements, and those obtained from the conductivity and thermoluminescence. Optical and thermal activation energies differ usually from each other, so that the agreement between the two in the present work is of special interest.

EXPERIMENTAL

A Beckman DK Spectrophotometer was used for absorption measurements between 0·2 and 3 μ. In these, the crystal was mounted in a vacuum cryostat similar in construction to the one described previously.[3] Absorption at longer wavelengths (up to about 10 μ) was measured at room temperature with the diamond fitted in a suitable holder just in front of the entrance slit of a Beckman IR-2 spectrophotometer equipped with NaCl optics.

Glow curves were taken with the diamond mounted in another vacuum cryostat, which served also for the conductivity measurements. A 13 stage, E.M.I. 6256B photomultiplier was used as detector. Amplification, recording devices, temperature measurements etc. were similar to those in previous work.[3]

Thermoluminescence was excited with monochromatic light of about 20 Å spectral width, obtained from a Hanovia type 507 C, 800 W xenon compact arc lamp in conjunction with a Beckman DU monochromator.

The rate of warming for obtaining the glow

* Detached from the Israel Atomic Energy Commission.

curves was about 15°/min throughout the present work.

Thermoluminescence excitation spectra were obtained point by point. The constant excitation at all wavelengths necessary in these measurements[4] was assured by changing the monochromator slit widths which were calibrated for this purpose.

Spectral distribution of the light emitted during the glow was measured with a liquid-air cooled photomultiplier as described elsewhere.[5,6]

RESULTS

(a) *Absorption spectra*

The u.v. absorption spectrum was found to be identical with that reported by CLARK[7] for Type IIb diamonds. In short—at 80°K it showed a sharp edge at 2250 Å (5·5 eV) and no absorption at longer wavelengths near the edge. At higher temperatures some structure appeared in the region 2250–2400 Å, which grew stronger on increasing the temperature.

In the visible there was no absorption except for a tail of a broad band in the infrared which extended as a weak continuum into the visible.

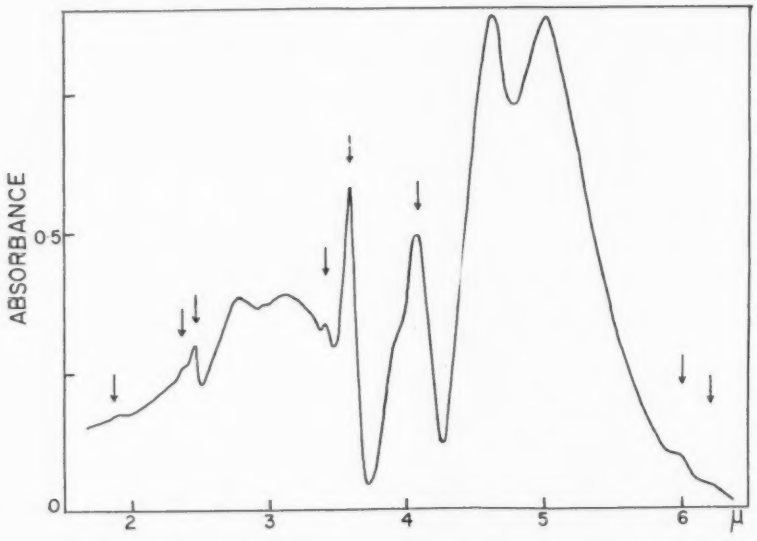

FIG. 1. Infrared absorption spectrum of a Type IIb diamond at room temperature. Arrows indicate extra absorption bands typical to Type IIb.

Conducting silver paint made the contacts to the diamond. Currents were measured with a Keithley model 410 micro-microammeter and recorded on a 20 mV Speedomax recorder. This arrangement enabled currents of 3×10^{-15} A to be read.

Weak electric fields of about 25 V/cm (with 3–4 mm between the electrodes) were applied in the current glow curves and in the dark conductivity measurements. Up to about 1000 V/cm, however, had to be used for measuring the photoconductivity at liquid-air temperature.

Of interest is the spectrum in the infrared shown in Fig. 1. The bands near 3, 4, 4·6, and 5 μ are present in all diamonds including Type I and Type IIa specimens, and seem to be characteristic of the diamond lattice absorption.[8] Additional bands, however, appear in the absorption spectrum of Type IIb diamonds, These are indicated by arrows in Fig. 1. They fit well the bands reported by earlier investigators[9,10] except for the weak absorption at 6 μ which has been omitted by the

Table 1. *Wavelengths* (*in* μ) *and energies* (*in* eV) *of the extra infrared absorption bands in Type IIb diamonds.*

Wavelength (μ)	1·85	2·35	2·43	3·40	3·58	4·05	6·0	6·2
Energy (eV)	0·67	0·53	0·51	0·364	0·345	0·305	0·206	0·20

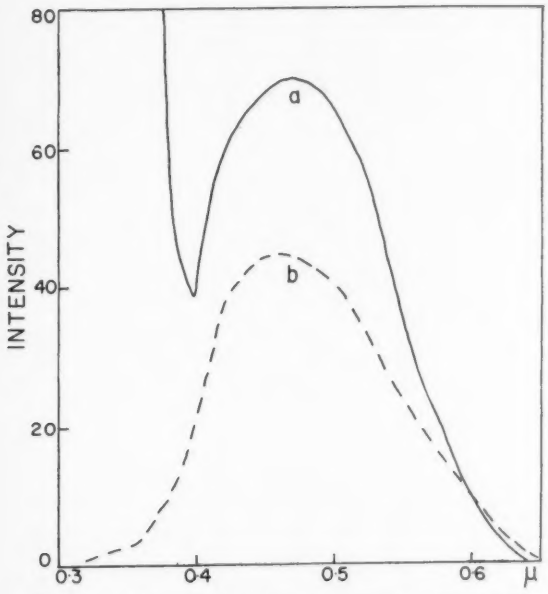

FIG. 2. (a) Luminescence spectrum of a Type IIb diamond at 80°K on excitation with 0·36 μ.
(b) electroluminescence spectrum at room temperature.

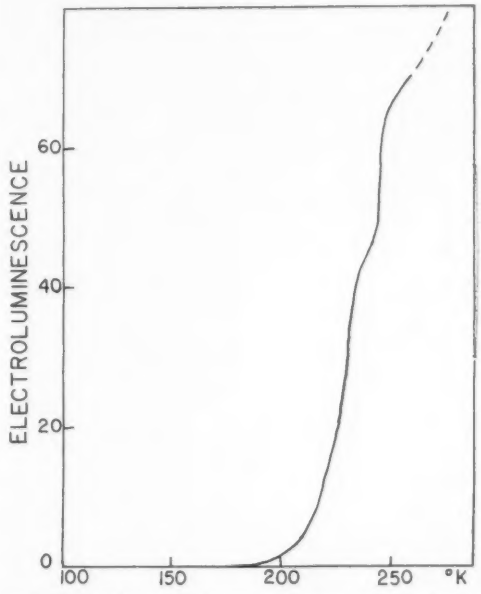

FIG. 3. Dependence of electroluminescence intensity of a Type IIb diamond on temperature.

earlier workers. A list of the extra bands is given in Table 1.

(*b*) *Luminescence and electroluminescence spectra*

Type IIb diamonds exhibit very weak luminescence, and DYER and MATTHEWS[11] have not been able to indicate the existence of fluorescence at all in these diamonds, Nevertheless, using high sensitivity of the detector, and good filtration of a narrow band of exciting light we succeeded in recording the luminescence spectrum. The 0·36 μ exciting light was obtained from a xenon 507C lamp with a Hilger 246D quartz monochromator and a Wratten 18A filter which reduced the stray light. The spectrum at 80°K is shown in Fig. 2(a). It shows a broad band at 0·47 μ. No correction has been made for the change in sensitivity of the photomultiplier with wavelength. Exciting light of somewhat shorter wavelengths gave similar results. The low intensity of the radiation from the xenon lamp at shorter wavelengths, however, did not enable such measurements on excitation further in the u.v. The results at room temperature were similar to those at 80°K.

The electroluminescence spectrum of the same specimens at room temperature is shown in Fig. 2(b). This was obtained with a.c. of about 100 V peak at 50 cycles (with about 4 mm between the electrodes). The spectrum is the same as obtained on excitation with u.v., with the advantage that

disturbances by the exciting light [see to the left of Fig. 2(a)] do not appear now.

The crystal did not show an even distribution of the electroluminescence intensity, but rather bright spots appeared at several points. The electroluminescence reduces at lower temperatures and nothing could be detected at 80°K. The dependance of the electroluminescence intensity on temperature is given in Fig. 3.

Our results differ from those of WOLFE and WOODS[12] who photographed the electroluminescence spectrum which was found to peak at

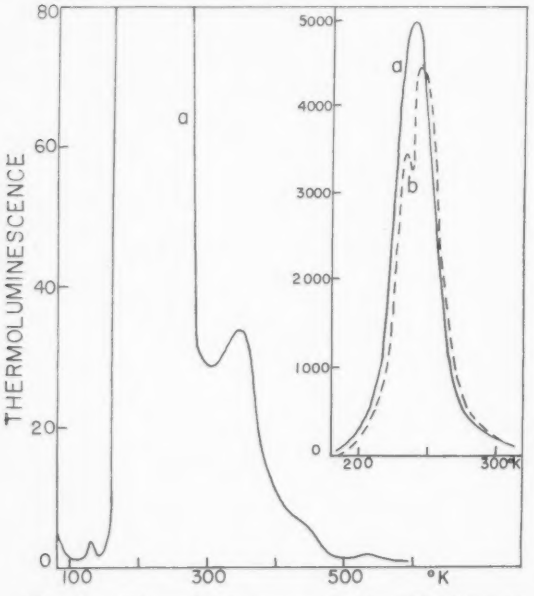

FIG. 4. a: Thermoluminescence of a Type IIb diamond excited with 2250 Å. Given on a reduced scale in the enclosure. b: (in the enclosure) the same as a but after partial bleaching. Two peaks at 230 and 245°K are now resolved.

0·44 μ. We noticed visually a blue electroluminescence just on applying the electric field, but this turned to greenish-yellow after a short time when the spectrum was recorded. It seems that the photographed spectrum obtained by WOLFE and WOODS included the blue component.

(c) *Thermoluminescence*

The two Type IIb diamonds examined in the present work gave practically identical glow curves with only minor differences in the relative intensities of the various peaks from one specimen to the other. The glow differed, however, entirely from that reported[13] for Type I diamonds. Fig. 4 shows the glow curve of the Type IIb diamonds after excitation with 2250 Å. A weak peak appears at 140°K, a very intense one at 240°K, and another at 350°K with a shoulder near 420°K. The glow

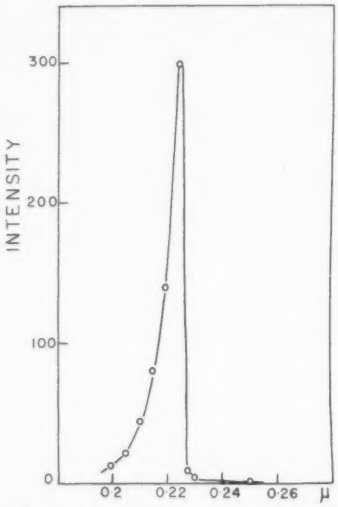

FIG. 5. Thermoluminescence excitation spectrum for the 240°K peak.

at 240°K is given on a reduced scale in the enclosure to the right of Fig. 4 (curve a). On excitation followed by partial bleaching, holding the crystal for some time at 200°K, the glow at 240°K can be resolved into two peaks—at 230 and 245°K —as shown in Fig. 4b (in the enclosure). On excitation at room temperature there appears also a peak at 500–550°K, which is the region where the main peak of Type I diamonds appears.[13]

The excitation spectrum for the glow peaks of the examined diamonds is given in Fig. 5. It shows a sharp maximum at 2250 Å with an abrupt fall towards longer wavelengths, and a somewhat slower fall at shorter wavelengths, The latter indicates that the glow is a bulk effect. The fall totowards longer wavelengths seems to go in parallel with the fall in the absorption in this region, and

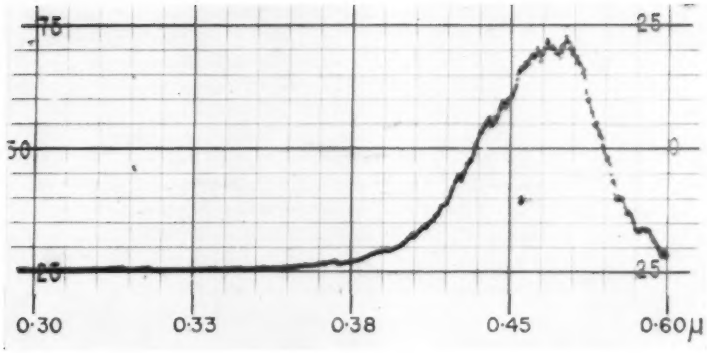

FIG. 6. Thermoluminescence spectrum of the 240°K peak.

[*facing p.* 300

BLANK
PAGE

Vol.
19

with it also a fall in the fraction of the incident light which is absorbed in the crystal.

The spectral distribution of the light emitted during the glow at 240°K is shown in Fig. 6. The spectrum is essentially the same as that of the luminescence and electroluminescence (Fig. 2). It has a maximum at about 0·48 μ with shoulders towards shorter wavelengths, which seem to be present also in the luminescence.

The relative intensities of the different peaks in the glow curve depended on the conditions of excitation. On excitation at 80°K, the peak at 140°K got saturated at exposures of only a few minutes, while the 240°K glow did not fully saturate even with exposures of 2 hr. The peaks at higher temperatures saturate still slower, and their intensities relative to that of the 240°K peak grow continuously with the exposure time.

(d) *Thermal activation energies*

Computation of the activation energies from the glow peaks was carried out by the methods fully described previously.[14,15] The method of initial rise was used repeatedly on the same glow just as in Ref. (15). From "cleaned" peaks, activation energies were calculated also from the formulas:[15]

$$E_1 = (1{\cdot}72/\tau)\, kT_g^2\,(1-2{\cdot}58\Delta), \qquad (1)$$

$$E_2 = (2/\tau)\, kT_g^2\,(1-3\Delta). \qquad (2)$$

Here E_1 was obtained for first order kinetics, and E_2 for second order, k is Boltzmann's constant, T_g is the peak temperature, $\tau = T_g - T_1$, where T_1 is the half intensity temperature at the lower temperature side of the peak, and $\Delta = 2kT_g/E$ is a correction factor small compared to one. Formulas (1) and (2) assume excitation into either the conduction or the valence band and not to an excited level within the forbidden gap. The good agreement with the initial rise values (E_i) supports this view, which follows also from other arguments to be discussed below.

Some examples of the calculated activation energies are given in Table 2.

Two typical examples are for the peak at 140°K, and two for that at 240°K (one for each specimen). The latter gave a T_g value above 250°K. This was caused by the effective cleaning of the peak by series of initial rise measurements which bleached away more than 95 per cent of the 240°K glow, leaving only a comparatively weak component above 250°K. The symmetry factor* μ_g for the peak at 250°K is about 0·5 which indicates[14] a nearly second order process. This follows also from the comparison of E_1 and E_2 to E_i.

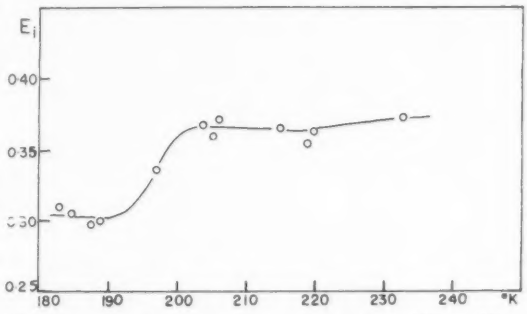

FIG. 7. Activation energies from the glow of Type IIb diamonds in the temperature range 180–240°K as obtained from initial rise curves.

As already mentioned, the 240°K glow is composed of more than one peak. The activation energies of its components were obtained from initial rise measurements which covered the whole

* $\mu_g = (w-\tau)/w$, where w is the half intensity width of the glow peak; see Refs. (14) and (15).

Table 2. Typical examples of activation energies computed by the method of initial rise (E_i), and from formulas (1) *and* (2), *E_1 and E_2 respectively. For the meaning of the other parameters see text.*

T_g°K	μ_g	τ°K	Δ	E_1(eV)	E_2(eV)	E_i(eV)	Specimen
140	—	11·6	0·115	0·175	0·192	0·21	I
139	—	10·3	0·12	0·19	0·21	0·20	I
252	0·51	18·6	0·115	0·358	0·388	0·372	I
253	0·50	18·4	0·115	0·36	0·39	0·375	II

Vol. 18
1961

temperature range 180–250°K. Results from such a series of measurements are given in Fig. 7. Below 200°K the initial rise curves give an activation energy of about 0·30 eV. At about 200°K there is a rise in the curve to about 0·37 eV. The exact values depended to some extent on amount of excitation, showing a tendency of the activation energies to increase (up to 0·40 eV in the extreme case) at prolonged excitations.

100°K which yielded interesting new results. Prior to each set of dark conductivity measurements the diamond was kept for some 15 min at 600°K to remove any possible effects of former excitations. Fig. 9 shows a log-currrent vs. $1/T$ plot of the conductivity, which was obtained with only 4·5 V across the diamond. To avoid the current at the higher temperatures being limited by the resistance in series with the diamond, the

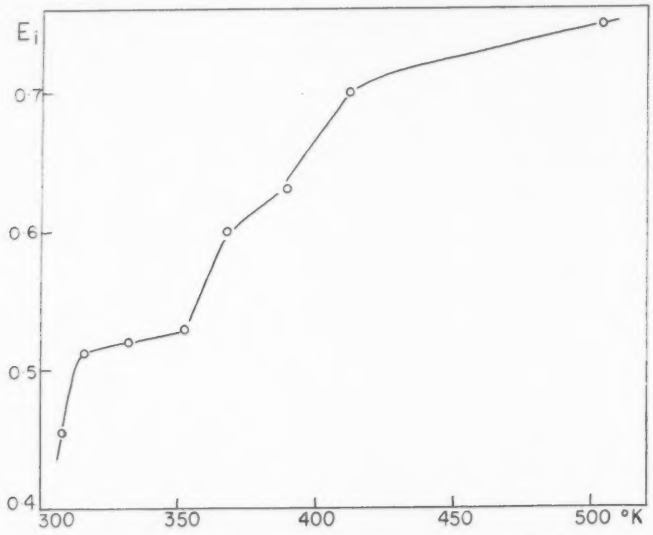

FIG. 8. As Fig. 7 for the temperature range 300–500°K.

Similar results were obtained above room temperature. In this case, however, the results are somewhat less accurate because of the lower glow intensities. Fig. 8 shows the activation energy distribution in this region. It indicates a level of about 0·52 eV at 350°K and at higher temperatures values of up to above 0·7 eV are obtained.

(e) *Dark conductivity*

The basic property of Type IIb diamonds is its semiconductivity. It has been investigated by several workers.[1,10,16,17] Hall effect measurements by these authors have shown the current carriers to be holes. The dark conductivity was also measured by these authors, but unfortunately neither of them took measurements below 180°K. We have repeated these measurements down to about

latter was reduced to 10^3 ohms. Only the part of the plot from 125 to 420°K is shown in Fig. 9. At higher temperatures the slope of the curve decreases until a maximum (minimum of resistivity) is reached.[18]

While the earlier workers obtained an activation energy of 0·35–0·38 eV from their measurements, our plots (Fig. 9) give three portions, each forming a straight line, but with different slopes. The portion between 125 and 220°K corresponded to an energy of 0·22 eV. The next (220–260°K) gave 0·30 eV, and the third (280–420°K) gave 0·38 eV.

Similar measurements with the second specimen gave 0·20 and 0·29 eV for the first and second portions respectively. At higher temperatures (above 240°K) the slope started to decrease, apparently because of bad contacts, and the higher

energy could not be obtained. Nevertheless, the agreement between the two specimens is very good, and the energies obviously fit well the infrared absorption bands and the thermal activation energies computed from the glow curves.

The diamonds showed some rectification even with good silver-point contacts. Of interest is that the direction of rectification changed at about

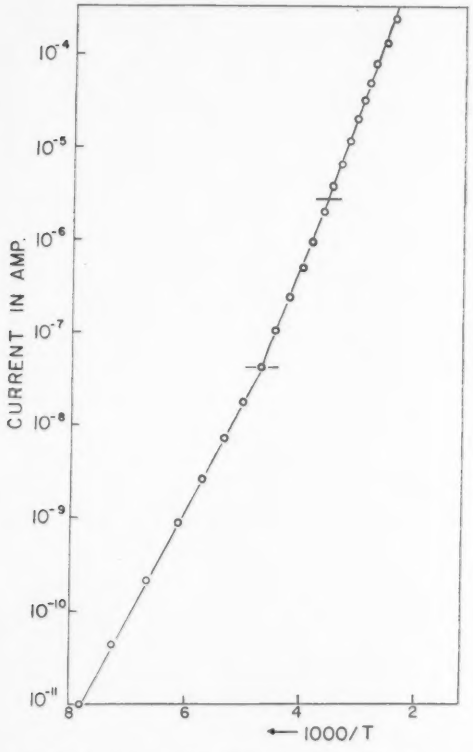

FIG. 9. Dark conductivity plots of a Type IIb diamond with log-current in the ordinate vs. $1000/T$ in the abcissa.

130°K. This seems to be in agreement with the results of AUSTIN and WOLFE[17], who noticed that their Type IIb diamonds lost the *p*-type character on cooling to −150°C.

(f) *Photoconductivity*

The high dark conductivity masked completely the photoconductivity at room-temperature.[18] Measurements were, therefore, carried out only at liquid-air temperature. Illumination with wavelengths longer than 2200 Å gave a photo-conductivity build-up curve rising continuously to the steady state value. Light of shorter wavelengths, however, showed rise-curves which reached a maximum soon after exposure, from which the photoconductivity decreased to a lower steady value.

The excitation spectrum for the photoconductivity is shown in Fig. 10. Adjustment of the calibrated slits of the monochromator secured constant energy of the exciting light at all wavelengths. All the points for the curve were taken

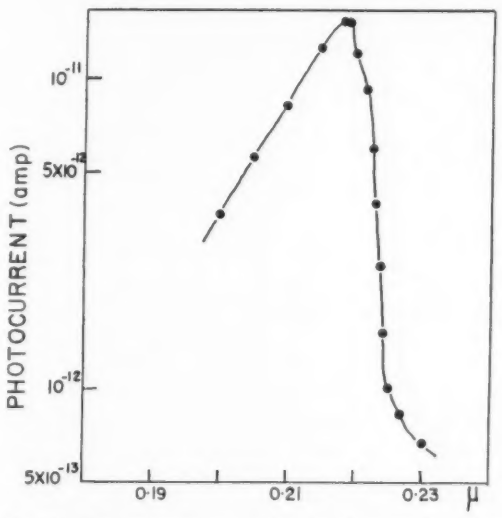

FIG. 10. Excitation spectrum for the photoconductivity of a Type IIb diamond at 80°K.

after the steady state has been reached. The excitation spectrum (Fig. 10) exhibits a maximum slightly below 2200 Å, and some structure is indicated towards longer wavelengths. With the other specimen, this structure was more pronounced and the main maximum appeared above 2200 Å.

Photoconductivity was observed also on illumination with longer wavelengths in the u.v. and visible. This, however, was much weaker compared to that obtained with light near the edge, and equilibrium could not be reached even after very long illuminations.

Vol. 18
1961

Infrared light (1–4 μ) showed considerable photoconductivity. The exact excitation spectrum in this region has not been measured as yet because of experimental difficulties.

(g) *Current glow curves*

We shall distinguish between *conductivity glow curves* describing the current as function of temperature on applying a constant potential difference from an external source to the excited crystal, and *voltaic glow curves* obtained with no external voltage supply during the measurement.

The high dark conductivity of Type IIb diamonds makes it difficult to obtain conductivity glow curves with these crystals. However, using only 1·5 V across the crystal and prolonged excitation with 2250 Å, a glow peak at about 125°K was obtained as shown in Fig. 11(a).

The voltaic glow curves show complicated effects depending on the circuit during excitation, on the wavelength of the exciting light, and on the polarity of the voltage applied to the crystal during excitation. These effects need a detailed investigation, and only examples of some preliminary experiments will be given now.

Figure 11(b) describes the voltaic glow curve obtained on excitation with 2250 Å and with only the crystal and the input resistance of the Keithley micro-microammeter in the circuit during the excitation and during the recording of the glow. Only one peak appears which fits well the thermoluminescence at 140°K, and nothing is seen at 240°K, where the main thermoluminescence was recorded.

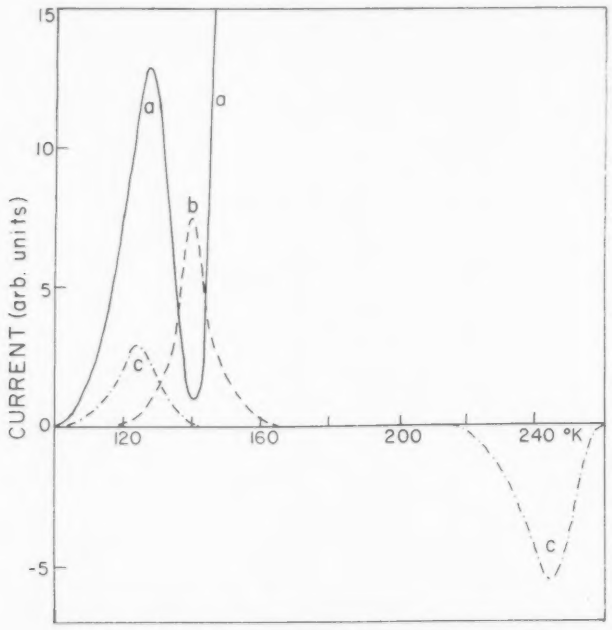

FIG. 11. (a) Conductivity glow curve of a Type IIb diamond excited with 2250 Å at 80°K, with 1·5 V across the diamond. (b) Voltaic glow excited at 80°K with 2250 Å. Specimen in a closed circuit with no external voltage supply during excitation and measurement. (c) As (b), but with specimen in an open circuit during excitation.

Figure 11(c) was obtained with the crystal in an open circuit (with the battery terminal disconnected) during excitation, and short-circuited, as before, during the recording of the glow. There

appears now one peak at 125°K and another at 240°K, the latter showing a reversed polarity.

DISCUSSION

The energies of the extra absorption bands of Type IIb diamonds in the infrared were found to fit well the thermal activation energies obtained, both from the dark conductivity, and from the thermoluminescence. A comparison of the computed energies is given in Table 3.

Table 3. Comparison of activation energies for Type IIb diamonds obtained from the extra infrared absorption bands, from the dark conductivity, and from the thermoluminescence peaks.

	Activation energies in eV				
Optical (infrared)	0·20 0·206	0·305	0·345 0·364	0·51 0·53	0·67
Dark conductivity	0·21	0·30	0·38	—	—
Thermoluminescence	0·21	0·30	0·37	0·52	~0·7

The higher energies (0·52, 0·67 eV) could not be obtained from the slopes in the dark conductivity curve, because it saturates and even reaches a maximum at higher temperatures.[17]

Because of the comparatively low concentration of the shallower traps (0·21 eV), the contribution of the carriers at the 0·30 eV levels became dominant at temperatures as low as 220°K. This is why the change in slope from 0·2 to 0·3 eV could clearly be observed. An indication of the relative concentrations of the 0·2 and 0·30–0·37 eV traps has been obtained from the relative intensities of the glow at 140° and 240°K. The intensity of the latter at prolonged excitations was found at least 1000 times that of the 140°K glow peak, which fits the dark conductivity measurements.

Correlation between the infrared and dark conductivity measurements has already been reported by earlier investigators for the 0·35–0·38 eV level. This was shown in the present work to hold also for the 0·2 and 0·3 eV levels. For the thermoluminescence, however, the correlation found in the present work is completely new. It is of special importance in light of the fact that thermal activation energies obtained from glow curves do not fit generally the optical activation energies. The good agreement obtained in the present work serves, therefore, also as a justification of the methods used for the computation of the activation energies from the glow curves.

The Hall measurements[10, 16, 17] have shown the *p*-type character of Type IIb diamonds above 130°K. From this it was concluded that the discrete levels (at 0·2, 0·3, 0·37 eV etc.) are located near the valence band, and on raising the temperature, holes are released into the valence band. The spectral measurements of the luminescence, electroluminescence and thermoluminescence show that the centers at which the holes recombine with electrons are located at 2·6–2·8 eV above the valence band; or at about the middle of the forbidden gap.

The excitation spectrum for the thermoluminescence (Fig. 5) indicates the following process: light of about 2250 Å raises electrons to the conduction band (or to levels near it) and leaves free holes in the valence band. The latter become trapped in the discrete levels near the valence band, while the former may occupy the luminescence centers. Thermal activation then releases the trapped holes, which emit the thermoluminescence on recombination with electrons in the centers. This view is further supported by the photoconductivity excitation spectrum (Fig. 10). The band structure in this spectrum near the edge indicates the existence of discrete levels, possibly near the conduction band.

The voltaic effects seem quite complicated, and no attempt will be made now to explain them.

Acknowledgement—We acknowledge with thanks the help of Dr. J. F. H. Custers of the Diamond Research

Vol. 18
1961

Laboratory, Johannesburg, who provided the diamonds used in the present work.

REFERENCES

1. CUSTERS J. F. H., *Physica* **18,** 489 (1952).
2. MITCHELL E. W. J., *J. Phys. Chem. Solids* **8,** 444 (1959).
3. BRANER A. A. and HALPERIN A., *Phys. Rev.* **108,** 932 (1957).
4. ARBELL H. and HALPERIN A., *Phys. Rev.* **117,** 45 (1960).
5. HALPERIN A. and KRISTIANPOLLER N., *J. Opt. Soc. Amer.* **48,** 996 (1958).
6. HALPERIN A., KRISTIANPOLLER N. and BEN-ZVI A., *Phys. Rev.* **116,** 1081 (1959).
7. CLARK C. D., *J. Phys. Chem. Solids* **8,** 481 (1958).
8. LAX M. and BURSTEIN E., *Phys. Rev.* **97,** 39 (1955).
9. CLARK C. D., DITCHBURN R. W. and DYER H. B., *Proc. Roy. Soc.* A**237,** 75 (1956).
10. WEDEPOHL P. T., *Proc. Phys. Soc. Lond.* B**70,** 177 (1957).
11. DYER H. B. and MATTHEWS I. G., *Proc. Roy. Soc.* **A243,** 320 (1957).
12. WOLFE R. and WOODS J., *Phys. Rev.* **105,** 921 (1957).
13. BULL C. and GARLICK G. F. J., *Proc. Roy. Soc.* **63,** 1283 (1950).
14. HALPERIN A. and BRANER A. A., *Phys. Rev.* **117,** 408 (1960).
15. HALPERIN A., BRANER A. A., BEN-ZVI A. and KRISTIANPOLLER N., *Phys. Rev.* **117,** 416 (1960).
16. BROPHY J. J., *Phys. Rev.* **99,** 1336 (1955).
17. AUSTIN I. G. and WOLFE R., *Proc. Phys. Soc. Lond.* B**69,** 329 (1956).
18. BELL M. D. and LEIVO W. J., *Phys. Rev.* **111,** 1227 (1958), measurement of the photoconductivity of Type IIb diamonds at room temperature by using a light chopping technique.

J. Phys. Chem. Solids Pergamon Press 1961. Vol. 18, No. 4, pp. 307–315. Printed in Great Britain.

LONG-RANGE ORDER IN Fe–Al ALLOYS—II THERMOELECTRIC POWER*

G. EREZ and P. S. RUDMAN

Department of Physics, Israel Institute of Technology, Haifa, Israel

(*Received* 24 *May* 1960; *revised* 4 *August* 1960)

Abstract—The thermoelectric power, TEP, relative to copper has been measured in Fe–Al alloys: (a) for the alloy 25·05 at. per cent Al over the temperature range 100–950°C; (b) at room temperature over the composition range 17·0–28·5 at. per cent Al as a function of quenching temperature. The critical temperature for the Fe_3Al structure was marked by a sharp change in slope of the TEP vs. temperature plot and the phase boundary was accordingly determined; for stoichiometric Fe_3Al, $T_c = 560 \pm 5$°C. The critical temperature of the FeAl structure was not marked by a similar change in slope; however, a change in slope of the TEP vs. composition plot defines this transformation. Fe_3Al order acts to increase while FeAl order acts to decrease the TEP. The results are interpreted in terms of distortion of the density of states curve of the 4*s* band due to the formation of new Brillouin zones accompanying ordering. The results are discussed in terms of the change on ordering of the kinetic energy of the 4*s* electrons as being the origin of the ordering energy for the Fe_3Al.

Vol. 18
1961

INTRODUCTION

THE order–disorder transformations in Fe rich Fe–Al alloys may be defined by specifying the respective compositions of the three interpenetrating cubic lattices, α, β, and γ, as illustrated in Fig. 1.

In Fe_3Al type order, Fe atoms preferentially occupy the α and β lattices and Al atoms the γ lattice. In FeAl type order, Fe atoms preferentially occupy the α lattice but the β and γ lattices are identically occupied. In the disordered phase all of the lattices are identically occupied. The FeAl type order can be accounted for by the usual quasi-chemical, nearest neighbor bond, order–disorder theory. It can, however, be seen from Fig. 1 that for Fe_3Al type order, wherein the β lattice is differentiated from the γ lattice, at least second neighbor bonding must be required for the quasi-chemical approach, since the nearest neighbors of the β and γ lattices are identical. The quasi-chemical calculation, using higher order interactions, has been made for the Fe–Al system by several authors[1–4] in essential agreement with the available experimental data.

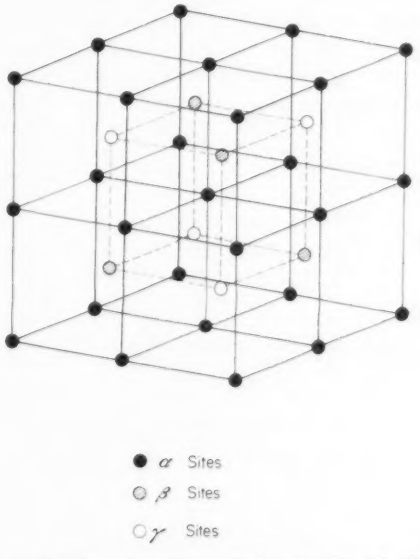

FIG. 1. Lattice sites for ordering in Fe–Al alloys.

* The research reported in this document has been sponsored in part by the Wright Air Development Center of the Air Research and Development Command, U.S. Air Force, through its European Office, Contract No. AF 61 (052)—122 and represents a portion of the Sc.D. thesis of G. EREZ.

However, the quasi-chemical model is not the only possible approach to the ordering energy. On ordering, new Brillouin zones are formed corresponding to the superlattice Bragg reflections and it has been shown by SLATER[5] and by NICHOLAS[6] that this may lower the energy of the free electrons and thus account for the ordering energy. LIPSON[7] has, however, discounted this view with respect to ordering in the Fe–Al system in favor of strain energy relief as the primary source of the ordering energy. Nevertheless, it seems probable that the Brillouin zone effect is significant in Fe–Al ordering and in this paper are presented the results of measurements of thermoelectric power as a function of temperature, long-range order, and composition in the neighbourhood of the composition Fe_3Al in an effort to estimate the Brillouin zone effect.

Very few measurements of TEP in alloys undergoing order–disorder transformations have been reported. Presumably this is because the interpretation of the results in terms of electronic structure is difficult, and that as potential alloys for thermocouple material such alloys have been avoided because the order–disorder transformation introduces undesirable time dependent effects. Nevertheless, SATO[8] employed such measurements in a study of long-range order in Cu_3Au, though he did not obtain an unambiguous interpretation of his data in terms of electron band structure; and COOPER *et al.*[9] and BLUE[10] have observed the variation of the thermoelectric power during ordering of CuAu.

Table 1. *Chemical analysis of alloys*

17·0 ± 0·6 at. per cent Al
(22·8 ± 0·2 at. per cent Al)[a]
23·6 ± 0·6 at. per cent Al
24·3 ± 0·8 at. per cent Al
(25·1 ± 0·1 at. per cent Al)[a]
26·5 ± 0·8 at. per cent Al
(28·5 ± 0·2 at. per cent Al)[a]

[a] These alloys were supplied with chemical analyses by the U.S. Naval Ordnance Laboratory, White Oak, Maryland.

ALLOY PREPARATION

The alloys were made by mixing iron (Fisher Scientific Co., Cat. No. 1–61) and aluminum (British Drug Houses Ltd., fine powder) powders, pressing into briquettes, melting the briquettes in alumina crucibles in a molybdenum resistance furnace, and then chill casting into a copper mold. The furnace was evacuated to a pressure of 10^{-3}mm Hg until the temperature rose to 1000°C, at this point dry hydrogen or argon to a pressure of 1 cm Hg was introduced to reduce the evaporation rate. The ingots, 1 cm dia. × 8 cm long, were homogenized by hot rolling at 1000°C into 1 mm thick strip. The test samples were cut from the strip and then annealed under a 1 cm Hg pressure of hydrogen at 1300°C for about 2 hr. The results of the chemical analyses are summarized in Table 1.

Alloys of higher Al contents were too brittle to roll and hence set the upper limit on the composition range.

MEASUREMENTS OF THERMOELECTRIC POWER

The TEP of a thermocouple is given as

$$\frac{dV}{dT} = -\frac{1}{e}(G_2 - G_1) \tag{1}$$

where

V = voltage
T = temperature (on absolute scale)
e = electron charge
G_i = absolute thermoelectric power of material i.

The absolute TEP at not too low temperatures can be given in terms of fundamental electronic properties of the material by MOTT's theory in the form[11]

$$G = \tfrac{1}{3}\pi^2 k^2 T \left\{ \frac{\partial}{\partial E} \ln \tau v^2 n \right\}_{E_F} \tag{2}$$

where

k = Boltzman's constant
E_F = Fermi energy
τ = relaxation time
v = electron speed
n = density of states

it having been assumed that τ and v are functions of the electron energy, E, only; and that only one band contributes significantly. Making the reasonable assumption that the relaxation time varies with temperature as[11] $\tau = \tau_0 T^{-r}$, then G/T will be independent of temperature as is approximately found in pure metals that do not undergo phase transformations. If in ordering there is a significant

effect on the free electrons, then it may be expected that G/T will depend on temperature through the variation of long-range order with temperature. Conversely, it may be hoped to interpret such TEP data in terms of the effect of long-range order on the electron band structure.

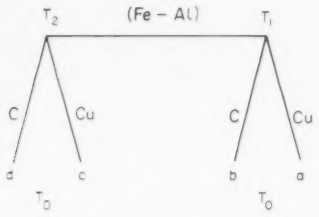

FIG. 2. Thermocouple connections.
(Fe–Al)—Sample, Cu—Copper, C—Constantan.

To find the thermoelectric power as a function of long-range order, the measurement may be made either at temperature in the range of the order–disorder transformation, or at some convenient fixed base temperature on samples that have been quenched sufficiently rapidly from the transformation range to retain the equilibrium degree of order. The results of both methods are reported here. The thermocouple connections are illustrated in Fig. 2.

The measurements at temperature were made by placing the alloy sample (dimensions $1\times4\times70$ mm), with the copper and constantan leads fixed with clamps, in a resistance tube furnace with a gradient such that $\Delta T = T_2 - T_1 \simeq 20°C$. The temperature was varied by a program controller at a rate of 10°C per hour. The furnace was automatically controlled to $\pm 1°$ and was filled with an atmosphere of hydrogen. Referring to Fig. 2, the voltages measured were V_{ac}, V_{bd}, V_{ab}, V_{cd} and using standard copper–constantan thermocouple tables, $V_{ab} \rightarrow T_1$, $V_{cd} \rightarrow T_2$ and $V_{ac} - V_{bd} \rightarrow \Delta T$. The voltages were measured with a potentiometer. In Fig. 3 is plotted $1/T \cdot dV/dT$ for the alloy 25·05 at. per cent Al (relative to copper, i.e. V_{ac}).

It is seen that for $T > 560°C$, $1/T \cdot dV/dT$ is appreciably constant. This temperature corresponds to the critical temperature[1] for the transformation Fe_3Al type order → FeAl type order and according to the previous discussion of equation (2), for $T > T_c$ this plateau is to be expected. Although the experimental points in Fig. 3 are extended only to 800°C, the measurements have been extended to 950°C, and the plateau continues

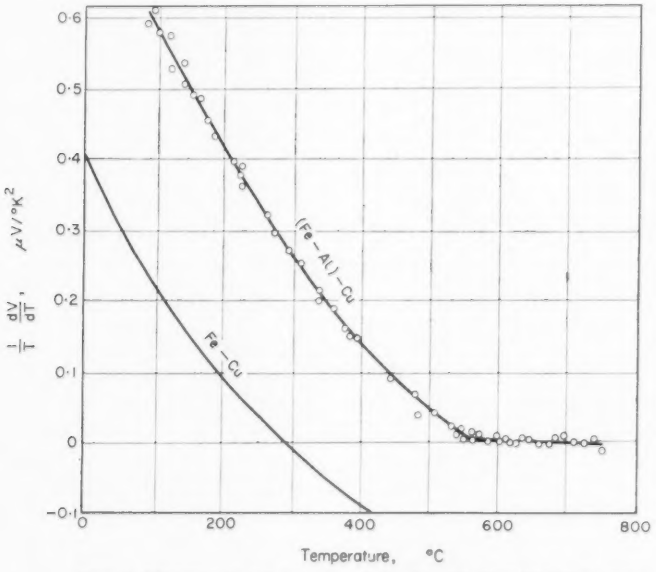

FIG. 3. Thermoelectric power of the Fe–Al alloy 25·05 at. per cent Al relative to Cu as a function of temperature.

Vol. 18
1961

without a break to the highest measured temperature. This is of interest because TAYLOR and JONES[12] have given 850°C as the temperature of the transformation FeAl type order → disorder for this composition. For low temperatures, the long-range order must approach a constant value, either the thermodynamic equilibrium value or a frozen-in value due to negligible diffusion. In either case a plateau at lower temperatures is to be expected but is not found in Fig. 3. This may be explained by the fact that this alloy is ferromagnetic and so the samples. The samples for this work were U shaped. To each leg was clamped a copper wire; one leg was held in a constant temperature bath at 20°C and the other leg in a bath whose temperature was varied between 20 and 50°C at a rate of about 1°C per min. The baths were of kerosene and the temperatures were measured by a mercury in glass thermometer. The results for the several compositions are illustrated in Fig. 4.

Here both the upper and lower plateaus are observed as expected. In the region 250–350°C there

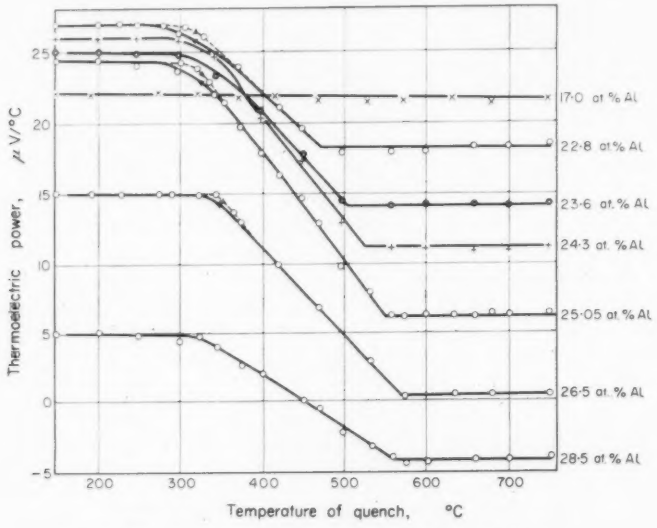

FIG. 4. Thermoelectric power of Fe–Al alloys relative to Cu as a function of quenching temperature; measured in the range 20–50°C.

density of states is dependent on temperature for temperatures less than the Curie point. In Fig. 3 is also plotted the TEP for an Fe–Cu couple (values taken from standard tables) and the similar behaviour seems to support this view. TEP measurements at temperature, in addition to being less convenient, have the disadvantage that what is obtained is the effect of long-range order smeared out over the temperature range ΔT.

Having established that nothing of interest occurs for $T > 600$°C and that below this temperature rapid quenching essentially preserved the equilibrium long-range order, the remaining measurements were made on rapidly quenched was a small hysteresis whose smallness shows that thermal equilibrium was well approached. For the sake of clarity in Fig. 4, the hysteresis has not been drawn for all the samples. The annealing times for the temperatures below 300°C were of the order of 100 hr at each temperature so that the cumulative time below the critical temperature for any alloy approached 1000 hr. The temperature of the upper break is plotted in Fig. 5 superimposed on the relevant section of the phase diagram according to RUDMAN[1]. It is seen that the results coincide with the previously given α_1/α_2 boundary between Fe_3Al type order and FeAl type order. The accuracy of the determination is ± 5°C, taking into account the

accuracy of temperature measurement and the ability to define the point of the change of slope.

The fact that dV/dT does not exhibit a discontinuity at the transformation temperature, only a change in slope, indicates that the order–disorder transformation, Fe_3Al type order → FeAl type order, is of second order, or first order but with a very small jump at the critical temperature.

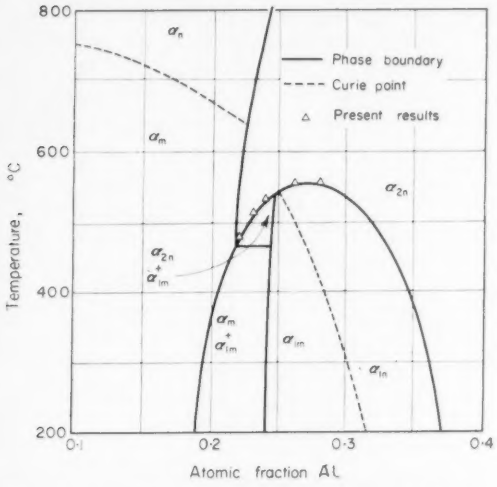

FIG. 5. Section of the Fe–Al phase diagram with the results of the present thermoelectric measurements superimposed.

In Fig. 6 is plotted the high temperature plateau and low temperature plateau TEP values from Fig. 4 as a function of composition. Actually the absolute TEP is plotted, the correction from the value relative to copper of Fig. 4 has been made taking $G_{Cu}(20°C) = 1{\cdot}73\mu V/°C$ from CUSAK and KENDALL[13]. We note that the high temperature plot exhibits a sharp break at about 21·5 at. per cent Al which on reference to Fig. 5 is seen to correspond to the FeAl type order → disorder boundary. Presumably this transition is not felt on the TEP vs. temperature plots because the boundary is nearly vertical.

From Fig. 6 it is seen that the addition of Al to Fe in the disordered terminal solid solution acts to increase the TEP. Increasing FeAl type order, which corresponds to increasing Al content, can be seen from the high temperature plateau plot to decrease the TEP. From Fig. 4 it is clearly seen that Fe_3Al type order acts to increase the TEP. The low temperature plateau plot of Fig. 6 is thus seen to exhibit the superposition of the opposing effects of the FeAl and Fe_3Al type ordering processes: FeAl type order monotonically decreases the TEP with increasing Al content; Fe_3Al type order increases the TEP with maximum effect at the stoichiometric composition. The low temperature

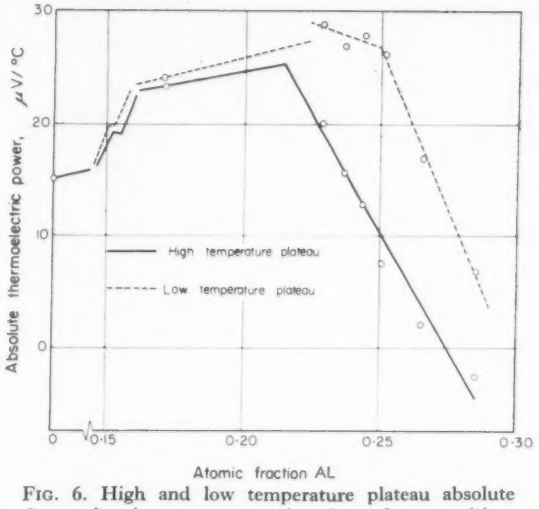

FIG. 6. High and low temperature plateau absolute thermoelectric power as a function of composition.

plateau is seen to exhibit somewhat erratic behavior for Al contents less than 25 at. per cent. This is consistent with the two phase region of Fig. 5 since the precipitation would make equilibrium conditions difficult to obtain.

DISCUSSION OF RESULTS

We assume that only the 4*s* electrons contribute to the TEP of these alloys. The 4*s* density of states curve is rather flat so that a small change in shape or in the electron to atom ratio would result in a large shift in the Fermi level, E_F. However, the Fermi level also cuts the much denser 3*d* levels (the material is ferromagnetic so that the 3*d* levels are not full) and this has a stabilizing effect on the Fermi level. Thus we assume that to a first approximation the Fermi level is independent of degree of order and of composition. We also assume that

$$n(E_F) \gg \left(\frac{dn}{dS}\right)_{E_F} \Delta S + \left(\frac{dn}{dE}\right)_{E_F} \frac{d(E_F)}{dX} \Delta X$$

Vol. 18
1961

where

X = composition
S = long-range order parameter

and hence approximate $n(E_F)$ by a constant for all compositions and states of order.

Equation (2) for the absolute TEP may be written as

$$G = \frac{\pi^2 k^2 T}{3}\left(\frac{1}{n}\cdot\frac{dn}{dE} + \frac{1}{\tau v^2}\cdot\frac{d\tau v^2}{dE}\right)_{E_F} \qquad (3)$$

A priori the TEP behavior could be attributed either to the density of states term, $1/n \cdot dn/dE$, or to the scattering term, $1/\tau v^2 \cdot d(\tau v^2)/dE$, or to the combination. Thus, without additional information or assumptions the TEP data cannot be interpreted in terms of fundamental behavior.

Let us first consider the scattering term. We can expect negligible variation in the electron speed, v. The relaxation time, τ we can resolve into two components: τ_S, the relaxation due to atomic disorder scattering (as perfect order is approached:

$$\tau_S \xrightarrow[S\to 1]{} \infty$$

and as complete disorder is approached:

$$\tau_S \xrightarrow[S\to 0]{} \tau_0,$$

and τ_T, the relaxation time due to thermal scattering, such that

$$1/\tau = 1/\tau_S + 1/\tau_T \qquad (4)$$

We can estimate the relative importance of the two scattering mechanisms from resistivity measurements since

$$\rho_{ord} \propto 1/\tau_T, \quad \rho_{dis} \propto 1/\tau_T + 1/\tau_0,$$

so that

$$(\rho_{dis} - \rho_{ord})/\rho_{ord} = \tau_T/\tau_0.$$

Using the data of SYKES and EVANS[14] for Fe_3Al we obtain that $\tau_T/\tau_0 \simeq \frac{1}{2}$ at room temperature. Thus thermal scattering is the dominant mechanism in these alloys. The relaxation time can thus be expanded in a series as

$$\tau = \tau_T[1 - \tau_T/\tau_S + (\tau_T/\tau_S)^2 - \ldots] \qquad (5)$$

According to WILSON[11], we can write $\tau_T \propto E^s$ and $\tau_S \propto E^t$. Introducing these relations into equation (5) we obtain

$$\frac{1}{\tau}\frac{d\tau}{dE} = \frac{s}{E_F} + \frac{(s-t)}{E_F}\left[-\frac{\tau_T}{\tau_S} + \left(\frac{\tau_T}{\tau_S}\right)^2 - \ldots\right] \qquad (6)$$

Thus for the present case with $\tau_T/\tau_S \lesssim \frac{1}{2}$, the TEP would be expected to vary only weakly with the scattering term.* As noted previously, Fe_3Al type order acts to increase the TEP while FeAl type order acts to decrease the TEP, however, both types of order would act to increase τ_S and hence the scattering term does not appear to be capable of accounting for the TEP behavior of these alloys.† Concomitantly with changes in order occur changes in the magnetic state, in the elastic constants and in the volume and hence it is possible that on taking these effects into account, the scattering term could account for the TEP data. However, in lieu of adequate data and theory concerning these effects, we will assume that the variation in the scattering term can be neglected. And now consider the density of states term.

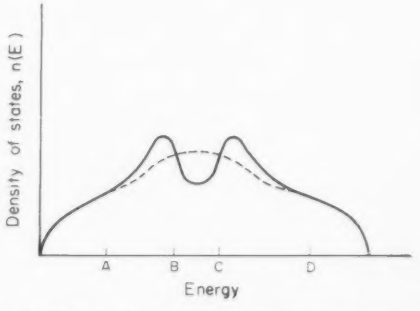

FIG. 7. Effect of long-range order on energy band structure.

– – – – – disorder ——— long-range order.

* The referee has pointed out that in the case of many partially filled bands $s = t = -\frac{1}{2}$ and hence the argument against the scattering mechanism is stronger. In the present case there are two partially filled bands and hence we can probably expect $s - t < 2$ (the free electron case) but we shall not need to rely on this point.

† BLUE[10] has interpreted his TEP data in CuAu primarily as a scattering problem. In CuAu:

$$(\rho_{dis} - \rho_{ord})/\rho_{ord} = \tau_T/\tau_0 \simeq 2.$$

Thus for CuAu the scattering term depends strongly on the degree of order.

We assume that only the 4*s* band is significantly distorted by the new Brillouin zones formed on ordering. The effect of a new zone on the density of states is schematically illustrated in Fig. 7. Thus depending on the position of the Fermi level, dn/dE may either be increased or decreased on ordering. After SLATER[5], we assume that the density of states at an arbitrary state of order, S, is given as

$$n(S) = n(0)+\Delta nS \tag{7}$$

where

$$\Delta n = n(1)-n(0)$$

$n(0)$ = density of states for complete disorder
$n(1)$ = density of states for perfect order
S = long-range order parameter.

For an alloy of X atomic fraction A and $(1-X)$ atomic fraction B, with perfect order only at the equiatomic composition, AB, the long-range order parameter takes the form[1]

$$\begin{aligned} S &= 2Xf(X, T), && X < \tfrac{1}{2} \\ &= 2(1-X)f(1-X, T), && X > \tfrac{1}{2} \end{aligned}$$

where

$$\begin{aligned} f(X, T) &= 0, && T > T_c \\ &\to 1 && T \to 0 \end{aligned}$$

The Fe rich Fe–Al alloys present a more complex behavior because there are two overlapping ordering processes. It is convenient to define two order parameters:[1] S_{11} to describe the FeAl type, and S_{31} to describe the Fe_3Al type. Taking X as the atomic fraction Al we then obtain:

$$\begin{aligned} S_{11} &= 2Xf(X, T) && X < \tfrac{1}{2} \\ S_{31} &= 2(2X)f(2X, T) && X < \tfrac{1}{4} \\ &= 2(1-2X)f(1-2X, T) && \tfrac{1}{4} < X < \tfrac{1}{2} \end{aligned} \tag{8}$$

so that:

$$S_{11} \to 1 \text{ as } X \to \tfrac{1}{2},\ T \to 0;$$

$$S_{31} \to 1 \text{ as } X \to \tfrac{1}{4},\ T \to 0.$$

We now assume that under superposed ordering the density of states is given as:

$$n(S_{11}, S_{31}) = n(0)+\Delta n_{11}S_{11}+\Delta n_{31}S_{31} \tag{9}$$

and

$$\frac{dn}{dE} = \frac{dn(0)}{dE} + \frac{d\Delta n_{11}}{dE}S_{11} + \frac{d\Delta n_{11}}{dE}S_{31} \tag{10}$$

If we attribute the variation in the TEP to the change in dn/dE with the state of order, and if we assume that $d\Delta n_{11}/dE = \text{const.} > 0$, and $d\Delta n_{31}/dE = \text{const.} < 0$, we can see that the TEP behavior of Figs. 4 and 6 is well described. For $X > 22$ at. per cent Al, the high temperature plateaus correspond to $S_{31} = 0$ and $S_{11} = 2X$ (because of the nearly vertical nature of the FeAl → disorder boundary, for $X > 22$ at. per cent Al, $S_{11} \to (S_{11})_{max} = 2X$) and the linear decrease in the TEP with increasing Al content beyond 22 at. per cent Al is thus accountable for by the assumption of $d\Delta n_{11}/dE > 0$. The TEP increase with decreasing temperature is consistent with the increase in S_{31} with decreasing temperature provided that $d\Delta n_{31}/dE < 0$.

The variation of the low temperature plateau TEP with composition is similarly explained as the superposed variation of $(S_{11})_{max}$ and $(S_{31})_{max}$, as given by equations (8), with composition.

It now must be shown that $d\Delta n_{11}/dE > 0$ and $d\Delta n_{31}/dE < 0$ follow from the effect of ordering on the density of states. Under the superposed FeAl and Fe_3Al ordering the 4*s* band will be distorted by three new Brillouin zones: letting a be the lattice parameter of the body-centered disordered unit cell, then, referring to Fig. 1, it is seen that the volumes of the primitive unit cells in the respective structures are $V_{dis} = a^3/2$, $V_{FeAl} = a^3$, $V_{Fe_3Al} = (2a)^3/4 = 2a^3$. Accordingly, the volumes of the Brillouin zones will be in the ratio $V^*_{dis}/V^*_{FeAl}/V^*_{Fe_3Al} = 1/\frac{1}{2}/\frac{1}{4}$ and hence the original disordered zone capable of holding 2 electrons will be cut by three new zones, an FeAl type holding 1 electron and two Fe_3Al types holding $\frac{1}{2}$ and $1\frac{1}{2}$ electrons respectively.

Let us consider that the Fermi level falls just to the low energy side of the first Fe_3Al zone. This would correspond to the neighborhood of point B of Fig. 7, so that $d\Delta n_{31}/dE < 0$. A Fermi level at this energy would then be on the low energy tail of the distortion by the FeAl zone. This would correspond to just on the high energy side of point A of Fig. 7 and would yield $d\Delta n_{11}/dE > 0$. The inequalities $d\Delta n_{11}/dE > 0$ and $d\Delta n_{31}/dE < 0$ by no means uniquely fix the placement of the Fermi

Vol. 18
1961

level (though if an accurate calculation of the band shape were available they might) but the above choice of somewhat less than $\frac{1}{2}$ electron per lattice site in the 4*s* band appears to be the most probable.

It is of interest to compare this choice with an independent estimate of the number of 4*s* electrons. The number of electrons in the 4*s* band can be estimated from the magnetic moment data of PARSONS *et al.*[15] for ordered Fe_3Al who give the moment per Fe atom as 1·8 Bohr magnetons. Considering the number of electrons per lattice site, and letting n_{d+} and n_{d-} be the respective number of 3*d* electrons of spin up and of spin down, n_s be the number of 4*s* electrons, and assuming that $n_{d+} = 5$, and that each Al atom contributes 3 electrons to the 3*d* and 4*s* bands, then we have

$$\tfrac{3}{4}(n_{d+}+n_{d-})+n_s = \tfrac{1}{4}\times 3+\tfrac{3}{4}\times 9$$

but

$$n_{d+}-n_{d-} = 1{\cdot}8,\ n_{d+} = 5$$

so that

$$n_s = 0{\cdot}6.$$

This is slightly on the high energy side of the first new Fe_3Al zone but the effective contribution of the Al in this calculation has probably been overestimated, since it is also observed from magnetic measurements[15] that for dilute alloys the effect of Al additions to Fe is essentially as a diluent, that is, valence effectively zero.

As noted previously, the motivation for this investigation was to check the hypothesis that Brillouin zone effects accompanying ordering may contribute to the ordering driving force. From the conclusion that the 4*s* band is distorted to significantly affect the TEP it does not necessarily follow that there is also a significant contribution to the ordering energy. The change in the electron energy between the ordered and disordered states is given as

$$U = U_{\text{ord}}-U_{\text{dis}} = \int_{E_0}^{E_F} E\times f\times$$

$$\times\,[\Delta n_{11}(S_{11})_{\max}+\Delta n_{31}(S_{31})_{\max}]\,dE \quad (11)$$

where f = Fermi–Dirac distribution function.

Thus to calculate this energy difference the quantities Δn_{11} and Δn_{31} are required, whereas we have seen that the TEP data can only yield $d\Delta n_{11}/dE$ and $d\Delta n_{31}/dE$.* Thus although we are not able from the present data to obtain any numerical estimate of this integral we can make the following observation: after NICHOLAS[6], provided that the Fermi level falls in the region $\Delta n \neq 0$, the energy of the ordered state will be lower than that of the disordered state, i.e. $\Delta U < 0$. This difference will rise to a maximum somewhere near the middle of the band. We have seen that the probable Fermi level for Fe_3Al occurs at the beginning of the rise in the ΔU curve and we are thus led to the prediction that a higher electron/atom ratio for this structure would perhaps lead to a larger energy gain. The isomorphous ordering in Fe_3Si does in fact exhibit a much more stable long-range order. According to GLASER and IVANIC[16], it disorders at about 1120°C as compared to 560°C for Fe_3Al.

SUMMARY OF RESULTS

The thermoelectric power TEP relative to copper of an Fe–Al alloy, 25·05 at. per cent Al, has been measured over the temperature range 100–950°C. A sharp change in slope at 560°C marks the transformation Fe_3Al type order → FeAl type order. No indication was obtained of the FeAl type order → disorder transformation that according to TAYLOR and JONES[12] should occur at about 850°C. This is presumably due to the nearly vertical nature of this boundary so that it is not crossed sharply.

The TEP at room temperature of Fe–Al alloys relative to copper has been measured as a function of the degree of long-range order, in the composition range 17·0–28·5 at. per cent Al by rapidly quenching samples from different temperatures. The curves of TEP as a function of quenching temperature are characterized by plateaus in both the high and low temperature regions. The departure from the upper plateau is interpreted as the critical temperature of the Fe_3Al type order and confirms RUDMAN's[1] version of the phase diagram.

A plot of the high temperature and low temperature plateau TEP values as a function of composition shows that while Fe_3Al type order acts to increase the TEP, FeAl type order acts to decrease

* A change in the ground level, E_0, would also be an important part of the ordering energy. However, this energy is the *mean* potential energy of the electrons and hence would presumably not depend strongly on the degree of order.

the TEP. The TEP data plotted in this manner does reveal the FeAl → disorder transformation as between 21 and 22 at. per cent Al at 600°C in essential agreement with TAYLOR and JONES[12].

The TEP data has been interpreted by applying MOTT's formulation to the 4*s* electrons. It is shown that due to the large thermal scattering in these alloys the effect of the change in the relaxation time, τ, on ordering has a minor effect on the TEP and the data has been interpreted in terms of the distortion to the density of states from the new Brillouin zones formed on ordering.

It is shown that this model, with a Fermi level corresponding to somewhat less than $\frac{1}{2}$ electron per lattice site in the 4*s* band is capable of explaining the inverse effects on the TEP of FeAl and Fe_3Al type order. It is pointed out that assuming that the lowering of the kinetic energy of the free electrons is the origin of the ordering energy, the thermoelectric data for Fe–Al alloys indicate that a somewhat higher electron to atom ratio would result in an even more stable structure and it has been noted that this is in fact borne out by Fe_3Si.

Vol. 18
1961

REFERENCES

1. RUDMAN P. S., *Acta Met.* **8,** 321 (1960).
2. SATO H., Research Institute for Iron and Steel and Other Metals (Japan), Report No. 614 (1951).
3. MATSUDA S., *J. Phys. Soc. Japan* **6,** 131 (1951).
4. ADACHI K., *Sci. Rep. Tohoku Univ.* **35,** 30 (1951).
5. SLATER J. C., *Phys. Rev.* **84,** 179 (1951).
6. NICHOLAS J. F., *Proc. Phys. Soc. Lond.* **66A,** 201 (1953).
7. LIPSON H., *Progress in Metal Physics* Vol. 2, pp. 47–50. Butterworths, London (1950).
8. SATO T., *J. Phys. Soc. Japan* **5,** 268 (1950).
9. COOPER H., SCHWED P. and WEBELER R. W., *J. Appl. Phys.* **27,** 516 (1956).
10. BLUE M. D., *Phys. Rev.* **117,** 134 (1960).
11. WILSON A. H., *Theory of Metals.* Cambridge University Press, New York (1953).
12. TAYLOR A. and JONES R. M., *J. Phys. Chem. Solids* **6,** 16 (1958).
13. CUSAK N. and KENDALL P., *Proc. Phys. Soc. Lond.* **72,** 898 (1958).
14. SYKES C. and EVANS H., *J. Iron St. Inst.* **131,** 225 (1935).
15. PARSONS D., SUCKSMITH W. and THOMPSON J. E., *Phil. Mag.* **3,** 1174 (1958).
16. GLASER F. W. and IVANICK W., *J. Metals, N.Y.* 1290 (1956).

J. Phys. Chem. Solids Pergamon Press 1961. Vol. 18, No. 4, pp. 316–319. Printed in Great Britain.

ELECTRON SPIN RESONANCE SPECTRUM OF STRETCHED POLYETHYLENE

D. LIBBY and M. G. ORMEROD

Physics Branch, Royal Military College of Science, Shrivenham, Swindon, Wilts.

(*Received* 13 *May* 1960)

Abstract—The ESR spectrum of stretched polyethylene, irradiated at 77°K, has been observed at various orientations of the applied magnetic field with respect to the axis of stretch. The different spectra resulting have been explained in terms of the anisotropy of the α-hydrogen atom which has been resolved due to the orientation of the molecule chains on stretching. Values obtained for the α-hydrogen hyperfine component separation are in good agreement with those found by other workers for irradiated single crystals.

INTRODUCTION

IT HAS previously been reported by the authors[1] that the ESR spectrum of stretched polyethylene when irradiated and observed at 77°K is different from unstretched. In this paper this difference is investigated further.

EXPERIMENTAL

The material studied was a low density polyethylene, Alkathene 7. It was stretched at a rate of 15 per cent increase per minute using a tensile testing machine to give a natural elongation of about 500 per cent after which it broke. Immediately after breaking there was a partial recovery giving a permanent natural elongation of 450 per cent. Two strips were cut perpendicular and parallel to the axis of stretch.

The samples were irradiated *in vacuo* at liquid nitrogen temperature 77°K using a Co^{60} source (2400 curies) for four hours to a nominal dose of 2 megarads. While the specimens were kept at a low temperature the spectra were recorded as derivative traces using a high frequency magnetic field modulation X-band spectrometer. Signals were recorded at 77°K and 195°K. Basically the same spectra were obtained at both temperatures but in some cases at the lower temperature the lines were broader in the wings and therefore less well resolved. In general the better resolved spectra at the higher temperature were used for interpretation

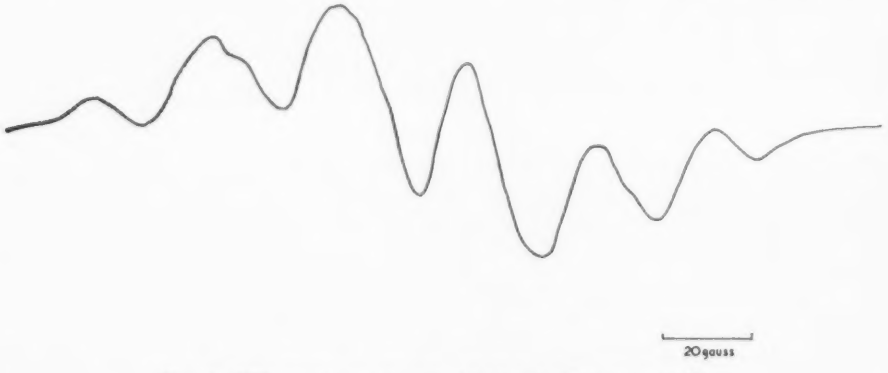

FIG. 1. ESR spectrum of unstretched polyethylene at 77°K.

purposes. Where theoretical curves were constructed a Gaussian line shape was assumed.

RESULTS

The spectra displayed in Figs. 1–5 were obtained at various orientations of the applied magnetic field with respect to the direction of stretch.

FIG. 2. ESR spectrum of stretched polyethylene at 77°K with the applied magnetic field perpendicular to the direction of stretch.

All the spectra are interpreted as being due to the radical

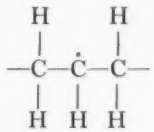

where the β-hydrogen atoms give rise to one hyperfine component separation and the α-hydrogen atom to another.

The theoretical curve shown in Fig. 3 was constructed assuming an absorption peak intensity ratio of 1:4:6:4:1 for the five main components and using the following values

β hyperfine component separation	= 30 G
α hyperfine component separation	= 14 G
line width	= 11.5 G

and that in Fig. 4 using

β hyperfine component separation	= 30 G
α hyperfine component separation	= 32·5 G
line width	= 8·5 G

In Figs. 1 and 5 for unstretched polyethylene and stretched polyethylene with the applied magnetic field at 45° to the direction of stretch, the α and β hyperfine component separations are approximately equal and are about 26 G and the line width about 18 G.

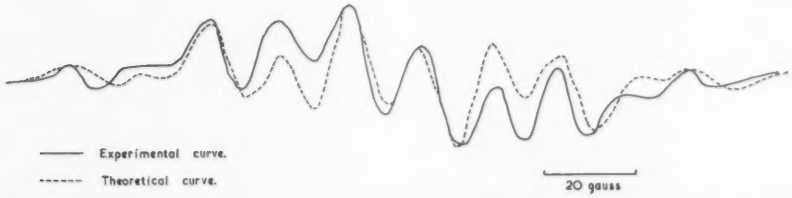

FIG. 3. ESR spectrum of stretched polyethylene at 195°K with the applied magnetic field perpendicular to the direction of stretch.

DISCUSSION

The proton hyperfine component separation arises from the interaction between the magnetic moment of the unpaired electron and that of the neighbouring nuclei. This separation can be divided into an isotropic and an anisotropic component. In general the anisotropic component is smeared out owing to the random orientations.

Several authors[2–4] have studied this anisotropy in single crystals. In particular MCCONNELL *et al.* have studied the α-hydrogen atom in the radical $\cdot CH(COOH)_2$ produced by the X-irradiation of a single crystal of malonic acid. They find that the

Vol. 18
1961

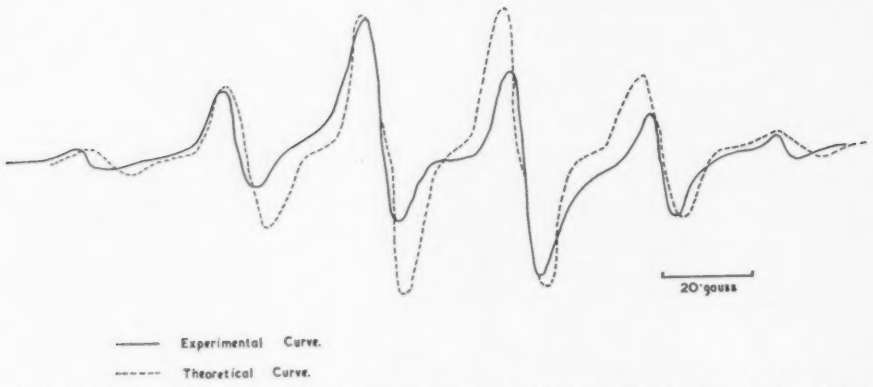

FIG. 4. ESR spectrum of stretched polyethylene at 195°K with the applied magnetic field parallel to the direction of stretch.

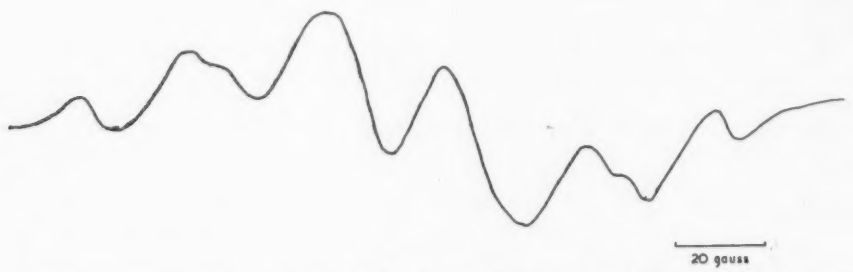

FIG. 5. ESR spectrum of stretched polyethylene at 77°K with the applied magnetic field at 45° to the direction of stretch.

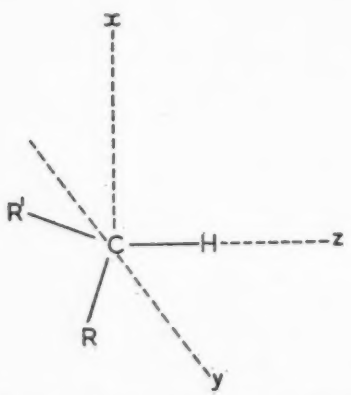

FIG. 6. The Cartesian axis system in the radical

$$\begin{array}{l} R'—\dot{C}—R \\ \quad\quad | \\ \quad\quad H \end{array}$$

In the case of stretched polyethylene the direction of stretch is along the y-axis.

z, x, y components of the diagonal (electron-spin)–(nuclear-spin) coupling dyadic for the α-hydrogen atom are of the same relative sign and of magnitudes 11, 22, and 32·5 G respectively. These axes are related to the molecule as shown in Fig. 6.

It is assumed that the α-hydrogen atom adopts a position such that the CH bond bisects the HCH angle of the undamaged parent molecule.

When polyethylene is stretched the molecule chains are orientated along the direction of stretch. X-ray photographs of the specimens (Figs. 7 and 8), taken using a Philips X-ray diffraction unit, provide an indication of the extent of this orientation.

We would expect at radiation damage centres that the α-hydrogen atom would be at right angles to the molecule chain and hence at right angles to the axis of stretch which is along the y axis in Fig. 6. It will therefore show anisotropy.

When the applied magnetic field is perpendicular

Vol. 18
1961

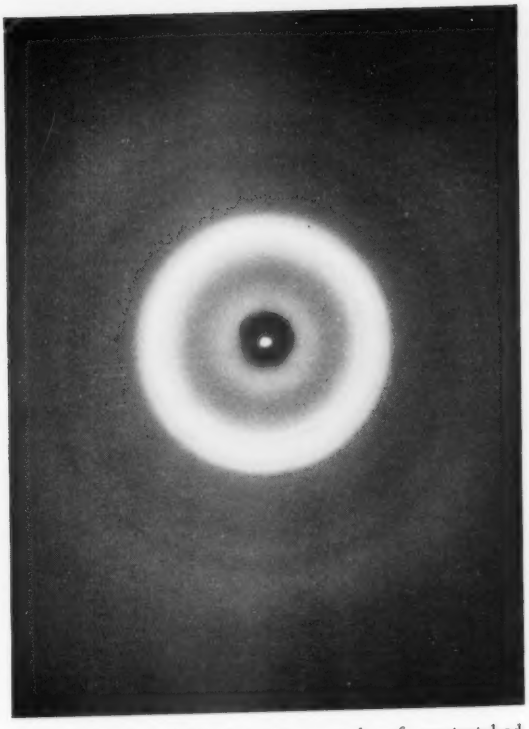

FIG. 7. X-ray diffraction photograph of unstretched polyethylene.

[*facing p.* 318

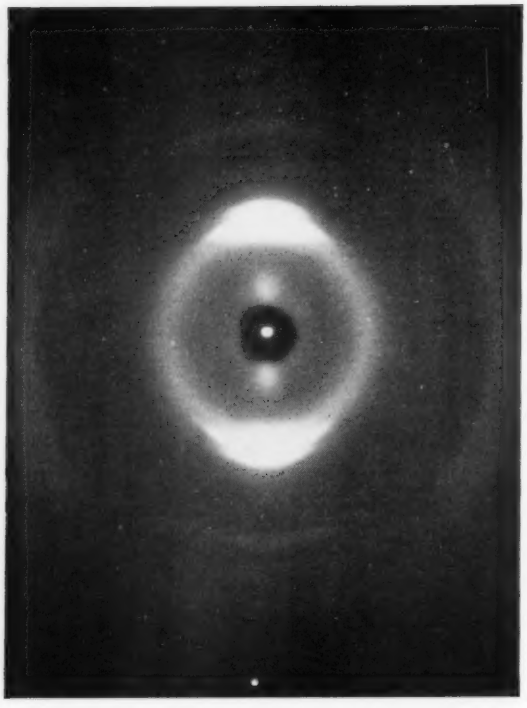

FIG. 8. X-ray diffraction photograph of stretched polyethylene.

to the direction of stretch it is randomly orientated in the *xz* quadrant. The experimental value of 14 G (Fig. 3) for the α hyperfine component separation is in rough agreement with McConnell's values, from which one would expect a value of about 16 G.

When the applied magnetic field is parallel to the direction of stretch (*y* axis), the experimental value of 32·5 G (Fig. 4) for the α hyperfine component separation is in exact agreement with McConnell's value. The narrower line width in this case is also as expected.

When the applied magnetic field is at 45° to the direction of stretch the α hyperfine component separation is composed of contributions from each of the canonical orientations. This approximates to the randomly orientated case as is experienced in unstretched polyethylene. The spectrum in this case (Fig. 5) is identical with that of unstretched polyethylene (Fig. 1).

Acknowledgements—The authors wish to thank Mr. L. G. Stoodley for his invaluable assistance in the design and construction of the spectrometer, Mr. F. J. Spooner for taking the X-ray photographs, Dr. D. H. Whiffen for helpful comments and Professor A. Charlesby for his suggestions and encouragement.

REFERENCES

1. Libby D., Ormerod M. G. and Charlesby A., *Polymer* **1**, 212 (1960).
2. McConnell H. M., Heller C., Cole T. and Fessenden R. W., *J. Amer. Chem. Soc.* **82**, 766 (1960).
3. Ghosh D. K. and Whiffen D. H., *Mol. Phys.* **2**, 285 (1959).
4. Miyagawa I. and Gordy W., *J. Chem. Phys.* **32**, 255 (1960).

Vol. 18
1961

J. Phys. Chem. Solids Pergamon Press 1961. Vol. 18, No. 4, pp. 320–328. Printed in Great Britain.

THE FERMI SURFACE AREAS OF MAGNESIUM, ZINC AND CADMIUM

E. FAWCETT

Physics Department, Royal Radar Establishment, Malvern, England

(*Received* 26 *August* 1960)

Abstract—The surface conductance under anomalous skin effect conditions of polycrystalline samples of the hexagonal divalent metals magnesium, zinc and cadmium is measured and used to determine their Fermi surface areas. The results for zinc and cadmium are in good agreement with the theoretical values, which are estimated in the nearly-free electron approximation for recently proposed models of their Fermi surfaces. For magnesium the Fermi energy is regarded as a variable parameter, and the experimental value for the area provides a sensitive measure of its position relative to the calculated energy levels at points of high symmetry in the Brillouin zone. The area for each metal when combined with the d.c. conductivity and the electronic specific heat also yields average values of the mean free path and Fermi velocity.

1. INTRODUCTION

A RELATIONSHIP between the area of the Fermi surface of a metal and its surface conductance under anomalous skin effect conditions was pointed out by CHAMBERS[1]. The theorem was stated in a more exact form by PIPPARD[2] as follows: the average of the cubes of the principal values of the surface conductance Σ for all orientations of the crystal axes with respect to the metal surface is related to the free area S of the Fermi surface in wave-vector space by the expression,

$$\langle \Sigma^3 \rangle = \frac{e^2 S}{6\sqrt{3}\pi^3 \omega^2 h}, \qquad (1)$$

ω being the angular frequency.

The free area S does not include the regions of the Fermi surface in contact with the Brillouin zone boundaries, which do not contribute to the current, so that for a polyvalent metal one expects S to be less than the free electron value S_0 for a spherical Fermi surface containing the same number of conduction electrons. The deviation of S from S_0 is difficult to interpret directly and unambiguously in terms of the shape of the Fermi surface and its distribution among the several occupied Brillouin zones, but may be of value in conjunction with other more detailed experimental or theoretical methods of investigating the Fermi surface.[3]

This method of estimating the area of the Fermi surface was used to study the hexagonal divalent metals magnesium, zinc and cadmium. No band-structure calculations are available for zinc or cadmium, and the results of the present work are interpreted in terms of the nearly-free electron approximation based on models of their Fermi surfaces proposed by HARRISON[4]. The results for magnesium are related to FALICOV'S[5] band-structure calculations, and provide a sensitive measure of the position of the Fermi level with respect to the energy levels calculated at points of high symmetry in the Brillouin zone.

The area S of the Fermi surface may also be combined with the d.c. conductivity σ and the electronic specific heat γT to obtain average values of the electron mean free path l and the velocity v at the Fermi surface. The expressions relating these quantities are[6]:

$$\sigma = \frac{e^2 S}{6\pi^2 h} \langle l \rangle, \qquad (2)$$

and

$$\gamma = \frac{k^2 S}{6h} \left\langle \frac{1}{v} \right\rangle. \qquad (3)$$

Evidently measurements of the surface conductance of a large number of single crystals of different orientations would provide the required average, but very much less labour is involved in measuring one or two fine-grain random polycrystalline samples of the metal. The latter approach was adopted and is thought to have yielded accurate results within the limitations imposed by the following sources of error inherent in the method:

(a) It is difficult to prepare a completely random polycrystalline sample:

(b) Even for such a sample the quantity measured is the average surface resistance $\langle 1/\Sigma \rangle$, and the substitution of $\langle 1/\Sigma \rangle^{-3}$ for $\langle \Sigma^3 \rangle$ in equation (1) will result in an underestimate of S if Σ is anisotropic.

(c) The method depends upon the measurement of a surface property to deduce a characteristic of the bulk metal.

2. THEORY

The principal values of the surface conductance of a plane single crystal of a metal under anomalous skin effect conditions are given by the expressions,

$$\sum_{\binom{x}{y}} = \left\{ \frac{2e^2}{3^{3/2}\pi^3\omega^2 h} \int_0^{2\pi} \frac{\left[\binom{\cos}{\sin}\psi\right]^2 d\psi}{K\left(\frac{\pi}{2}, \psi\right)} \right\}^{1/3}, \quad (4)$$

the origin of ψ being chosen so that

$$\int_0^{2\pi} \frac{\sin\psi\cos\psi}{K\left(\frac{\pi}{2}, \psi\right)} d\psi = 0;$$

here the polar coordinates (χ,ψ) of the electron velocity directed along the normal at a point on the Fermi surface are referred to the normal to the plane of the metal as z-axis, so that the integral of the Gaussian curvature $K(\chi,\psi)$ is taken over the locus of points $(\pi/2, \psi)$ where the velocity lies in the plane. These expressions were first derived in a slightly different form by PIPPARD[2], who used the heuristic method known as the "ineffectiveness concept" to extend to a Fermi surface of quite general shape the rigorous theory for an ellipsoidal Fermi surface given by SONDHEIMER[7]; the formal analysis for a general Fermi surface was given by KAGANOV and AZBEL[8].

From equations (4) we obtain a mean value,

$$\sum^3 = \tfrac{1}{2}\left(\sum_x^3 + \sum_y^3\right) = \frac{e^2}{3^{3/2}\pi^3\omega^2 h} \int_0^{2\pi} \frac{d\psi}{K\left(\frac{\pi}{2}, \psi\right)}.$$

The average value of Σ^3 over all orientations (θ, ϕ) of the crystal axes with respect to the normal to the plane of the metal is,

$$\left\langle \sum^3 \right\rangle = \frac{e^2}{3^{3/2}\pi^3\omega^2 h} \times \int_0^{2\pi} d\phi \int_0^{\pi} \sin\theta\, d\theta \int_0^{2\pi} \frac{d\psi}{K\left(\frac{\pi}{2}, \psi\right)} \times \frac{1}{\int_0^{2\pi} d\phi \int_0^{\pi} \sin\theta\, d\theta}.$$

The integral in the numerator may be proved equal to $2\pi S$ (when equation (1) follows at once) by means of a theorem which states that the ratio of the areas of corresponding elements of a surface and its spherical image is equal to the reciprocal of the Gaussian curvature.[9]

Equations (4) are strictly correct only in the "extreme anomalous limit" when the electron mean free path is very much greater than the microwave skin depth, and when relaxation effects are neglected. DINGLE[10] has made a detailed evaluation of the theory for a free electron model, tabulating the surface conductance in the transition from conditions of the "normal skin effect" through "anomalous skin effect without relaxation" to "extreme anomalous limit with relaxation". The observed surface conductance for each metal is corrected by means of DINGLE's tables to obtain the value corresponding to the "extreme anomalous limit without relaxation".

Table 1. Surface conductance of brass calibration plate

Alloy	a $\rho \times 10^6$ Ω cm	b Σ_a Ω^{-1}	c $\frac{\Sigma_c}{\Sigma_a}$	Σ_c Ω^{-1}	d Average
Monel	29·1	4·95	2·95	14·6	
Brass	4·00	13·4	1·06	14·8	14·53
Manganin	7·83	9·55	1·49	14·2	

a. d.c. resistivity ρ measured at 4·2°K.
b. Conductance Σ_a of alloy, $1/\Sigma_a = 2\pi\sqrt{(\upsilon\rho.)}$
c. Measured ratio of conductance Σ_c of brass plate to Σ_a.
d. r.m.s. standard deviation of Σ_c^3 is 5·2 per cent.

3. EXPERIMENTAL

(a) *Method*

The surface conductance of each metal sample was measured in an apparatus similar to one described previously.[11] The sample forms one wall of a cavity resonant at about 36 Gc/s, which is contained in an evacuated enclosure immersed in liquid helium at 4·2°K. The support for the sample, which constitutes its only thermal link to the helium bath, is of fairly high thermal resistance. The rise in temperature when microwave power is coupled into the cavity is indicated by the unbalance of a Wheatstone's bridge, one arm of which contains a resistance thermometer attached to the sample. The microwave power absorbed is measured by substituting, in a heater attached to the sample, joule heating sufficient to produce the same unbalance. A simultaneous measurement of the power absorbed by the brass calibration plate forming the opposite wall of the cavity enables its conductance to be compared directly with that of the sample.

To calibrate absolutely its conductance Σ_c, the brass calibration plate is compared with samples of three alloys, monel, brass and manganin. These were mechanically polished, finishing with alumina powder, and annealed. A rectangular block for d.c. resistivity measurement was prepared from the same batch of material. Comparisons with the monel and manganin samples before, after, and in the course of the experiments, showed no significant change of the conductance ratio Σ_c/Σ_a, the average value for each alloy being given in Table 1. The value of Σ_c/Σ_a for the brass sample differs from unity presumably because the brass calibration plate was made from a different batch of material. The d.c. resistivity ρ is in all cases so high as to justify the use of the normal skin effect equation, $1/\Sigma_a = 2\pi\sqrt{(\upsilon\rho)}$, to calculate the conductance Σ_a of the alloy. The frequency υ was measured in each microwave experiment and never varied by more than about 0·3 per cent from its average value 35·5 Gc/s.

(b) *Samples*

The zinc and cadmium, each of spectrographic purity 99·9997 per cent, were supplied by the Consolidated Mining and Smelting Co., the magnesium of purity 99·99 per cent by Magnesium-Elektron, in the form of rolled strip about 0·1 in. thick and 1·0 in. wide. Two samples of each metal were prepared, one from the strip without further mechanical treatment, the other cross-rolled perpendicular to the length of the strip. The cross-rolling was carried out in two stages, each of approximately 10 per cent reduction, with annealing for one minute at 100°C after each stage. This procedure was intended to reduce the grain size by permitting recovery and some primary recrystallization after cold work. It was found that, for the zinc and cadmium, annealing at a higher temperature or for longer periods induced coarsening of the grain structure, presumably due to secondary recrystallization or continuous growth, and for this reason a low temperature solder (Sn/In eutectic) was used to attach the heater and resistance thermometer to the sample. A reduction of average grain size from about 0·13 mm to 0·10 mm was achieved in zinc and cadmium, while the grain size in magnesium remained unchanged at about 0·03 mm after cross-rolling and annealing. The cross-sectional area of the microwave cavity is about 10 mm^2 so that the measured conductance is an average over about 500–1000 grains for the zinc and cadmium samples and about 10,000 for the magnesium.

The three metals were electropolished in solutions of orthophosphoric acid with water or ethanol.[12] Horizontal electrodes were used and the solution stirred to avoid the formation of bubbles at the anode. On removal from the solution the surface was washed in hot distilled water, rinsed in alcohol, dried, and inspected microscopically. The electropolish was repeated as necessary until the optimum degree of smoothness was achieved.

The degree of preferred orientation of some of the samples was measured by means of an oscillating crystal X-ray camera. The pole figures for an untreated

magnesium sample (Fig. 1) show that the basal plane lies predominantly within about 45° from the sample plane. The distribution for a cross-rolled sample was rather similar. The zinc and cadmium showed a much less pronounced preferred orientation, with still some tendency for parallelism of the basal plane and the sample plane in the untreated samples but an almost random distribution in the cross-rolled samples.

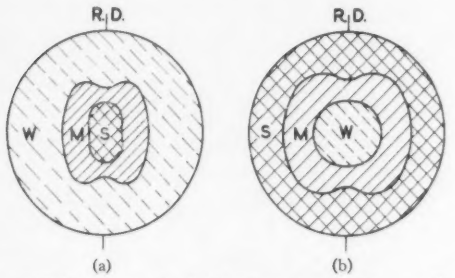

FIG. 1. Pole figures of rolled magnesium; R.D. ≡ rolling direction, S ≡ strong, M ≡ medium, W ≡ weak.
(a) basal plane (0001) (b) hexagonal prism plane ($10\bar{1}0$).

The d.c. resistivity ratio between room temperature and 4·2°K of each metal was also measured, a wire of suitable dimensions being prepared by cutting a rectangular block from the strip and reducing with an etchant.

4. RESULTS

The measured surface conductance Σ for the various samples of magnesium, zinc and cadmium is given in Table 2. The scatter of the four values of Σ for each metal may be attributed to variation of the degree of preferred orientation, to variation of the quality of the polished surface, or to random errors of measurement. Since there appears to be no systematic difference between the values for current parallel and perpendicular to the rolling direction or for samples cross-rolled and measured as supplied, the deviations are in fact treated as random errors. Accordingly the average $\langle\Sigma\rangle$ is unweighted, and the percentage standard deviation of Σ^3 is used to obtain an estimate of the accuracy of the final result.

The conductance is corrected for relaxation and effects due to finite mean free path, using estimates of the mean free path and Fermi velocity obtained from the present work (Table 3) to calculate the appropriate parameters for substitution in DINGLE's tables.[10] The corrected value Σ_∞ is used to evaluate the area S of the Fermi surface by substituting Σ_∞^3 for $\langle\Sigma^3\rangle$ in equation (1). This is conveniently expressed as in Table 2 by

Table 2. Surface conductance and Fermi surface area of magnesium, zinc and cadmium

	a	b			c	d	e	f	g	
	I	$\Sigma\ \Omega^{-1}$		$\langle\Sigma\rangle$ Ω^{-1}	Σ_∞ Ω^{-1}	r.m.s. dev. per cent	S a.u.	$\frac{S}{S_0}$	$r\frac{S}{S_0}$	prob. error
		cross roll	as supplied							
Mg	X	64·6	65·5	66·0	66·0	12	3·4	0·51	0·60	0·07
	Y	64·1	69·9							
Zn	X	65·3	68·9	66·6	64·4	11	3·1	0·35	0·41	0·05
	Y	69·2	63·1							
Cd	X	62·6	63·0	61·1	58·6	11	2·3	0·33	0·39	0·04
	Y	57·3	61·6							

a. Microwave current direction parallel and perpendicular to the *original* rolling direction of the metal strip as supplied is denoted by X and Y respectively.
b. Measured ratio Σ/Σ_c converted to absolute conductance Σ using the calibration constant $\Sigma_c = 14{\cdot}53\ \Omega^{-1}$ from Table 1.
c. Σ_∞ is the conductance in the extreme anomalous limit after correcting for relaxation and finite mean free path effects.
d. r.m.s. standard deviation of Σ^3.
e. Fermi surface area expressed in atomic units, in which the unit of length in wave-vector space is the reciprocal of the Bohr radius.
f. Free election area $S_0 = 16\pi^3(\sqrt{3}/\pi a^2 c)^{2/3}$ for the lattice spacings c and a at 4°K.[13]
g. Factor $r = 1{\cdot}18$ to correct for the anisotropy of Σ (see text).

Vol. 18
1961

its ratio S/S_0 to the free electron value S_0 for a spherical Fermi surface containing two electrons per atom. However this represents the lower limit of the true value, since as was remarked in §1 any anisotropy of Σ will result in the inequality $\langle\Sigma^3\rangle > \langle 1/\Sigma\rangle^{-3}$. For the two metals tin[11] and copper[14] for which a detailed study of the anisotropy of Σ has been made the ratio $r = \langle\Sigma^3\rangle/\langle 1/\Sigma\rangle^{-3}$ of the two averages was estimated to be 1·25 and 1·11 respectively. The low value of r for copper reflects the fact that its Fermi surface is accommodated in the first Brillouin zone of the f.c.c. lattice and is not distorted too severely from a sphere, for which of course $r = 1$. The shape of the Fermi surface of tin is not known, but it must consist of several sheets in different Brillouin zones since tin is quadrivalent and has two atoms per unit cell, and the consequent distortion of the surface accounts for the high value of r. It would seem reasonable to adopt for the hexagonal metals under consideration a value of r between these two extremes, say the mean $r = 1{\cdot}18$ with an accuracy of about 6 per cent. S/S_0 is accordingly multiplied by this factor to correct for the anisotropy of the conductance.

An estimate of the probable error may be obtained by combining as random errors the 5 per cent standard deviation of the cube of the calibration constant (Table 1) and the standard deviation of Σ^3 (Table 2, column d), the resultant being given in the last column of Table 2. The systematic errors mentioned in § 1 have not been included explicitly in this estimate: the correction by the factor r has an accuracy of about 6 per cent, rather smaller than the above estimate of the probable error; defective polishing of the sample surfaces is thought not to have introduced a significant error; and the zinc and cadmium samples have little preferred orientation. For magnesium the preferred orientation is such that crystal directions within about 45° of the hexagonal axis are represented only to a small extent in the average, so that the estimate of the area will accordingly be high or low if these directions have conductances lower or higher than the true average. The value $S/S_0 = 0{\cdot}33$ for cadmium is in reasonably good agreement with the value 0·35 obtained by CHAMBERS[1] using an extruded cylindrical sample at 1·2 Gc/s and 3·6 Gc/s, though he considered his estimate to be probably low since the sample did not have a good surface finish.

The electron mean free path at 4·2°K for the particular samples used and the Fermi velocity were calculated from the experimental values of the Fermi surface area by means of equations (2) and (3), and are given in Table 3. These values represent averages over the whole Fermi surface, and also v is in fact the average $\langle 1/v\rangle^{-1}$, but this value of the Fermi velocity is still of rather more physical significance than that obtained in the

Table 3. Electron mean free path and Fermi velocity of magnesium, zinc and cadmium

	a	b		c	d	e	f	g	h
	σ_{HE}/σ_{RT}	σ_{RT} Ω^{-1}cm^{-1} $\times 10^{-5}$	σ_{HE} Ω^{-1}cm^{-1} $\times 10^{-8}$	rS a.u.	l cm $\times 10^{4}$	γ j/m/d $\times 10^{3}$	v cm/sec $\times 10^{-7}$	v_0 cm/sec $\times 10^{-7}$	τ sec $\times 10^{11}$
Mg	195	2·30	0·45	4·0	5	1·34	7·1	15·9	0·7
Zn	1640	1·74	2·85	3·7	33	0·66	9·0	18·3	3·7
Cd	2830	1·33	3·75	2·7	58	0·71	8·7	16·3	6·7

a. Measured ratio between the d.c. conductivities at 4·2°K, σ_{He}, and at room temperature, σ_{RT}.
b. σ_{RT} for polycrystalline sample.[15]
c. Fermi surface area from Table 2 column e corrected by the factor $r = 1{\cdot}18$.
d. Mean free path l at 4·2°K from equation (2).
e. Coefficient γ of electronic specific heat.[16]
f. Fermi velocity v from equation (3).
g. Fermi velocity v_0 for free electron model with two electrons per atom.
h. Relaxation time $\tau = l/v$ at 4·2°K.

usual approximation of a quasi-free electron model with an isotropic effective mass.

5. DISCUSSION

The spherical free electron Fermi surface corresponding to two electrons per atom is shown in relation to the first and second Brillouin zones of a hexagonal close-packed lattice in Fig. 2(a).

An interpretation of the available experimental data for the de Haas–van Alphen effect in zinc and cadmium by means of the free electron approximation was suggested by HARRISON[4]. In zinc the observed de Haas–van Alphen oscillations[18] have periods and symmetry with respect to the crystal orientation appropriate to the needle-shaped pockets of electrons at K in the 3–4 zone of Fig. 2(c)

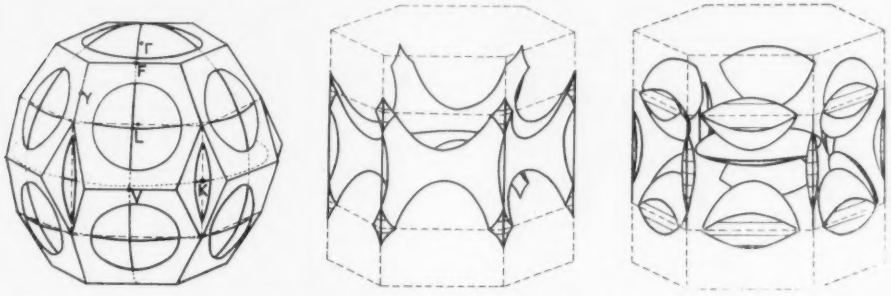

FIG. 2. Fermi surface for free electrons in relation to the Brillouin zones for a h.c.p. metal with $c/a = \sqrt{8/3} = 1{\cdot}633$ (cf. $c/a = 1{\cdot}623$ for magnesium at 4°K).

(a) extended zone scheme showing overlap into the 3–4 zone at Γ L and K.
(b) Holes in the 1–2 zone after remapping with Γ at the centre of the zone (after HARRISON[4]).
(c) electrons in the 3–4 zone after remapping in the 1–2 zone according to the reduced zone scheme (after HARRISON[4]).

Overlap into the third and fourth zones occurs at at Γ, L and K. Because of the symmetry properties of the space group there is no energy discontinuity between the first and second zones along the edges and diagonals of the hexagonal face separating them.[17] They may therefore be remapped to form what we shall call the 1–2 zone, shown in Fig. 2(b), within which the energy is a continuous function of the wave-vector to a first order approximation. Fig. 2(b) illustrates the crown-shaped Fermi surface containing holes in the 1–2 zone, and the free electron Fermi surface in the 3–4 zone is remapped in a similar way in Fig. 2(c).

The c/a ratio for zinc at low temperatures is 1·8246[13] and the Brillouin zones are contracted in the direction of the hexagonal axis, resulting in an increased overlap at Γ and decreased overlap at L and K compared with Fig. 2(a). In Fig. 3 showing the first and second zones and the free electron sphere for cadmium the c/a ratio is just greater than the critical value of 1·8607 at which overlap ceases at the zone edge K.[4]

and also the horizontal and diagonal arms of the crown-shaped pocket of holes in the 1–2 zone of Fig. 2(b). The experimental value of the cross-sectional area of the horizontal arm is a factor ten

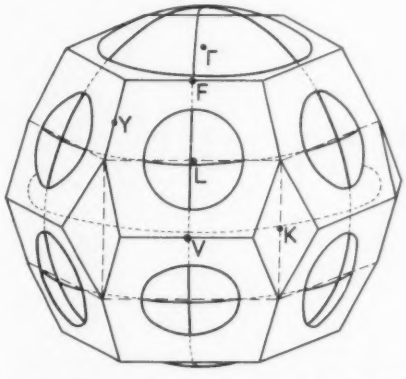

FIG. 3. Fermi surface for free electrons in relation to the extended Brillouin zone scheme of cadmium with $c/a = 1{\cdot}862$ at 4°K.[13]

Vol. 18
1961

smaller than the free electron value, which is attributed by Harrison to the effect of the crystal potential in depressing the energy in the 1–2 zone near the zone edge at F.

In cadmium only de Haas–van Alphen oscillations due to the diagonal arms are observed.[19] The absence of needles at K in the 3–4 zone in the free electron case (Fig. 3) is consistent with this result, and Harrison deduces from the absence of oscillations corresponding to the horizontal arm that the energy at the zone edge F is so far depressed by the crystal potential as to pinch the arm off. No de Haas–van Alphen oscillations due to the electrons at Γ and L in the 3–4 zone have been observed for either zinc or cadmium, presumably because of the relatively large cross sectional areas and correspondingly short periods.

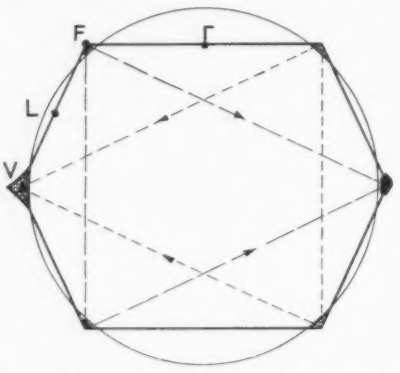

FIG. 4. Section through the extended Brillouin zone scheme of cadmium to show schematically how the Fermi surface near F is perturbed by the crystal potential and how the holes near points equivalent to F are remapped to form a horizontal arm of the "crown".

- - - - indicates wave-vectors connecting the segments of a sphere (cross-hatched regions) corresponding to the free electron Fermi surface;

— — indicates wave vectors connecting the holes corresponding to the perturbed Fermi surface (shaded regions), which vanish completely when the arm is pinched off.

An estimate of the free areas of the Fermi surfaces of zinc and cadmium may be obtained in the approximation of nearly-free electrons[17] if the horizontal arm at F (Figs. 3 and 4) is assumed to be just pinched off in both metals, the energy at F being depressed by the crystal potential to the Fermi level. The secular equation for a point with wave-vector $\boldsymbol{k}$ at F is,

$$\begin{vmatrix} \frac{1}{2}\boldsymbol{k}^2-E & V_{101} & V_{002} \\ V_{101} & \frac{1}{2}\boldsymbol{k}^2-E & V_{101} \\ V_{002} & V_{101} & \frac{1}{2}\boldsymbol{k}^2-E \end{vmatrix} = 0, \quad (5)$$

where V_{101} and V_{002} are the Fourier components of the crystal potential corresponding to the plane waves (101) and (002) which connect F with the equivalent points as shown in Fig. 4; the units here are $4\pi/\sqrt{3}a$ a.u. for the x- and y-coordinates and $2\pi/c$ a.u. for the z-coordinate. Solution of equation (5) gives the eigenvalues,

$$E = \tfrac{1}{2}\boldsymbol{k}^2 - V_{002}$$

and (6)

$$E = \tfrac{1}{2}\boldsymbol{k}^2 + \tfrac{1}{2}[V_{002} \pm \sqrt{(V_{002}^2 + 8V_{001}^2)}].$$

For the point L the solution of a similar secular equation gives the eigenvalues (each doubly degenerate),

$$E = \tfrac{1}{2}\boldsymbol{k}^2 \pm V_{101}, \quad (7)$$

and for a point Y along the diagonal arm (Fig. 3), the equivalent points to which are connected by the plane wave (100), the eigenvalues are,

$$E = \tfrac{1}{2}\boldsymbol{k}^2 - V_{100}$$

and (8)

$$E = \tfrac{1}{2}\boldsymbol{k}^2 + \tfrac{1}{2}[V_{100} \pm \sqrt{(V_{100}^2 + 8V_{101}^2)}].$$

The energy gap $2|V_{101}|$ at L is provisionally assumed to be large enough to prevent overlap there into the 3–4 zone, so that one obtains from equation (7),

$$|V_{101}| \geqslant E_0 - E_L, \quad (9)$$

where E_L and E_0 are the free electron energies at L and at the Fermi surface. The depression ΔE_F of the lowest eigenvalue below the free electron energy E_F at F is seen from equation (6) to be,

if $$\Delta E_F = V_{002}, \quad (10a)$$

$$|V_{101}| < |V_{002}| \quad \text{and} \quad V_{002} > 0,$$

$$\Delta E_F = \tfrac{1}{2}[\sqrt{(V_{002}^2 + 8V_{101}^2)} - V_{002}] \geqslant |V_{101}|,$$

if (10b)

$$|V_{101}| \geqslant |V_{002}| \quad \text{and} \quad V_{002} > 0,$$

$$\Delta E_F = \tfrac{1}{2}[\sqrt{(V_{002}^2+8V_{101}^2)}+|V_{002}|] \geqslant \sqrt{2}|V_{101}|,$$

if

$$V_{002} \leqslant 0. \tag{10c}$$

The condition that the horizontal arm at F should be just pinched off may be written,

$$\Delta E_F = E_F - E_0, \tag{11}$$

and the value of $|V_{101}|$ obtained from equation (9) when substituted in equation (10c) is found to be inconsistent with equation (11), thereby ruling out the possibility $V_{002} \leqslant 0$.

If it is now assumed that $|V_{101}| < |V_{002}|$, equations (10a) and (11) give an estimate for V_{002}. The equation of energy surfaces near Γ in the nearly-free electron approximation may then be written,

$$\begin{vmatrix} \tfrac{1}{2}(\boldsymbol{K}_\Gamma+\boldsymbol{\varkappa})^2-E & V_{002} \\ V_{002} & \tfrac{1}{2}(\boldsymbol{K}_\Gamma-\boldsymbol{\varkappa})^2-E \end{vmatrix} = 0,$$

or

$$E = \tfrac{1}{2}(K_\Gamma^2+\varkappa^2) \pm V_{002}\left\{1+\frac{(\boldsymbol{K}_\Gamma \cdot \boldsymbol{\varkappa})^2}{V_{002}^2}\right\}^{1/2} \tag{12}$$

where $\boldsymbol{\varkappa}$ is measured from the point Γ with wave-vector $\boldsymbol{K}_\Gamma$ equal to half the reciprocal lattice vector. By equating the higher energy solution of equation (12) to the Fermi energy E_0 and retaining only the first term in the expansion of the square root, the equation of the Fermi surface in the 3–4 zone near Γ is obtained:

$$\begin{aligned} E_0-(\tfrac{1}{2}K_\Gamma^2+V_{002}) &= \tfrac{1}{2}(\alpha\kappa_\parallel^2+\kappa_\perp^2), \\ \alpha = 1+\frac{K_\Gamma^2}{V_{002}} &= 1+\frac{2E_\Gamma}{V_{002}}, \end{aligned} \tag{13}$$

where $\kappa_\parallel$ and $\kappa_\perp$ denote the components of $\boldsymbol{\varkappa}$ parallel and perpendicular to $\boldsymbol{K}_\Gamma$. The area of the ellipsoid of revolution described by equation (13) is then the required contribution of the electrons to the total area, since the area of the needle-shaped pockets of electrons at K estimated from the de Haas–van Alphen effect data is negligibly small. The number of electrons in the 3–4 zone, and therefore of holes in the 1–2 zone, is also given by equation (13), and the contribution of the holes to the area is obtained by scaling down the free electron area by the two-thirds power of the ratio of the number of holes.

The assumption of the inequality, $|V_{101}|<|V_{002}|$, was necessary for the above analysis since otherwise it is not possible to estimate a value for V_{002}. But for the opposite sign of the inequality the equation of the Fermi surface near Γ will not differ to any great extent from equation (13) so long as $|V_{101}| \geqslant |V_{002}|$. In fact $|V_{101}|$ cannot be too large or the lowest eigenvalue at Y,

$$E = \tfrac{1}{2}k^2-\tfrac{1}{2}[\sqrt{(V_{100}^2+8V_{101}^2)}-V_{100}], \tag{14}$$

Table 4. Theoretical estimates of Fermi surface area of magnesium, zinc and cadmium

Metal	Ratio of area to free electron value						Energy gap Ry		
	electrons				holes	total area	Γ	L	
	Γ	L	K	sum			$2V_{002}$	$2V_{101}$	
Zn	0·184	0·286	0·000	0·470	0·530	1·00			free electron
	0·130	0·000	0·000	0·130	0·314	0·44	0·154	0·13+	no overlap at L
	0·130	0·147	0·000	0·277	0·347	0·62	0·154	0·090	overlap at L
						0·41			experimental
Cd	0·194	0·269	0·000	0·463	0·537	1·00			free electron
	0·142	0·000	0·000	0·142	0·332	0·47	0·122	0·10+	no overlap at L
						0·39			experimental
Mg	0·117	0·372	0·010	0·499	0·501	1·00			free electron
	0·087	0·048	0·040	0·175	0·177	0·35	0·103	0·119	$E_0 = 0·66$
	0·108	0·185	0·055	0·348	0·296	0·64	0·103	0·119	$E_0 = 0·68$
						0·60			experimental

Vol. 18
1961

will be so low as to pinch off the diagonal arm here; for the same reason V_{100} is assumed positive in deriving equation (14) from equation (8), and the zero value of the energy gap between the first and second zones at K and L[17] justifies the further assumption that $|V_{101}| \geqslant |V_{100}|$. In the most favourable case, $|V_{101}| = |V_{100}|$, with $|V_{101}|$ estimated from equation (9) with the equality sign, the area of the diagonal arm at the narrowest point is reduced to about 50 per cent of the free electron value in both zinc and cadmium, while for $V_{100} = 0$ the reduction is to about 25 per cent. The former result is reasonably consistent with the experimental values for this area, which is about 80 per cent in zinc and about equal to the free electron area in cadmium.[14]

The results of the calculation are given in Table 4, and the total areas are seen to be in reasonably good agreement with the experimental values. The assumption that in zinc and cadmium there is no appreciable overlap of electrons into the 3–4 zone at L appears to be justified. If the absorption edge at about 0·090 Ry indicated by the infra-red reflection data for zinc[20] is tentatively associated with the energy gap at L, the resultant overlap increases the total area to a value much greater than the upper limit of the experimental value. The theoretical estimate for cadmium is already, with no overlap at L, rather higher than the experimental value of the area. The approximations made in the calculations, especially in estimating the area of the hole surface, are rather crude, and further analysis without the aid of other experimental or theoretical data is unprofitable.

For magnesium the results of a band structure calculation by the orthogonalized plane wave method are available.[5] There is overlap at Γ and L, and also at K where the energy in the 3–4 zone is further below the Fermi energy than in the free electron case. The areas of these regions and of the hole surface were estimated by the methods described above, but using the calculated energy values, and the results are given in Table 4. The size of the region of overlap at L is rather sensitive to the value chosen for the Fermi energy E_0, and better agreement of the total area with the experimental value is obtained if a value for E_0 is adopted about 0·02 Ry higher than the first provisional estimate of 0·66 Ry.[21]

Acknowledgements—The author is indebted to Dr. D. H. PARKINSON for his encouragement, to Mr. D. HUNTLEY and Mr. P. E. HARTWRIGHT for assistance in the experiments, and to Dr. L. M. FALICOV and Dr. W. A. HARRISON for making their results available before publication. This paper is published by permission of the Controller, H.M.S.O.

REFERENCES

1. CHAMBERS R. G., *Proc. Roy. Soc.* **A215,** 481 (1952).
2. PIPPARD A. B., *Proc. Roy. Soc.* **A224,** 273 (1954).
3. See for example HEINE V., *Proc. Roy. Soc.* **A240,** 340, 354, 361 (1957).
4. HARRISON W. A., *Phys. Rev.* **118,** 1190 (1960), and private communication.
5. FALICOV L. M., to be published.
6. See for example PIPPARD A. B., *Reports on Progress of Physics*, Vol. XXIII, p. 176. Physical Society, London (1960).
7. SONDHEIMER E. H., *Proc. Roy. Soc.* **A224,** 260 (1954).
8. KAGANOV M. I. and AZBEL' M YA., *Dokl. Akad. Nauk SSSR* **102,** 49 (1955).
9. WEATHERBURN C. E., *Differential Geometry of Three Dimensions*, Vol. 1, § 87. Cambridge University Press, London (1927).
10. DINGLE R. B., *Physica* **19,** 311 (1953); see also CHAMBERS R. G., *Physica* **19,** 365 (1953).
11. FAWCETT E., *Proc. Roy. Soc.* **A232,** 519 (1955).
12. MCG. TEGART W. J., *The Electrolytic and Chemical Polishing of Metals*. Pergamon Press, London (1956).
13. GRÜNEISEN E. and GOENS E., *Z. Phys.* **29,** 141 (1924), cited by HARRISON W. A., Ref. (4).
14. PIPPARD A. B., *Phil. Trans.* **A250,** 325 (1957).
15. *American Institute of Physics Handbook*. McGraw-Hill, New York (1957).
16. PARKINSON D. H., *Reports on Progress in Physics*, Vol. XXI, p. 226. Physical Society, London (1958).
17. See for example JONES H., *The Theory of Brillouin Zones and Electronic States in Crystals*. North-Holland Publishing Co., Amsterdam (1960).
18. VERKIN B. I. and DMITRENKO I. M., *Isv. Akad. Nauk* **19,** 409 (1955).
19. BERLINCOURT T. G., *Phys. Rev.* **94,** 1172 (1954).
20. GIVENS M. P., *Solid State Physics* (edited by SEITZ F. and TURNBULL D.) Vol. VI, p. 313. Academic Press, New York (1958).
21. FALICOV L. M., private communication.

J. Phys. Chem. Solids Pergamon Press 1961. Vol. 18, No. 4, pp. 329–344. Printed in Great Britain.

AN EXPERIMENTAL EQUATION OF STATE FOR SODIUM*

R. I. BEECROFT† and C. A. SEWNSON

Institute for Atomic Research and Department of Physics, Iowa State University, Ames, Iowa

(*Received* 1 *August* 1960)

Abstract—An experimental equation of state for sodium has been obtained for pressures to 20,000 atm and for temperatures from 20°K to the melting point. Various experimental details are given of an apparatus with which it is possible to obtain pressure–volume data which are reliable to $\pm 0{\cdot}002$ in $\Delta V/V_0$ over this range of temperature and pressure. The equation of state can be represented to within the above accuracy by an expression which is derived from the assumption that the isothermal compressibility is linear with volume and has no explicit temperature dependence. A discussion is given of the effect of these assumptions on the validity of calculations of the variation with volume of the temperature dependent contribution to the thermodynamic functions. Grueneisen constants as obtained from various definitions are calculated as functions of temperature and volume, and the validity of the Mie–Grueneisen equation of state as it applies to sodium appears open to question below room temperature. Recent high pressure ultrasonic experiments on sodium are interpreted as being in agreement with this conclusion.

Vol. 18
1961

1. INTRODUCTION

AN EXPERIMENTAL investigation of the thermodynamic properties of the simpler substances over a wide range of temperature and pressure is of considerable interest, since in these cases one can hope for an understanding of their behavior from basic principles. Recent theoretical work on the equation of state at absolute zero of the alkali metals[1] and the solidified rare gases[2] gives results which are in fair agreement with experiment.[2,3] The separate problems of calculating and measuring changes in volume with pressure over a fairly wide temperature range are much more difficult, with neither explicit theoretical calculations nor experimental measurements (except for solid helium[4,5]) of the temperature-dependent part of the equation of state existing for any solid. A simplifying generalization which has been useful follows from the assumption that the entropy of a substance depends on its volume only through a characteristic temperature. This leads to the Mie–Grueneisen equation of state,[6] which will be discussed later. The validity of this assumption can be tested only by experiments in which thermodynamic functions are altered significantly by the variation of both temperature and pressure.

Sodium was chosen as the subject of an initial investigation of the equation of state over wide variations of temperature and pressure because it is convenient to work with experimentally, and because it approaches an ideal metal in the behavior of many of its properties. The objectives of these experiments were two-fold; first, to extend previous measurements at very low temperatures to higher pressure, and second, to investigate the effects of both pressure and temperature on the thermodynamic functions for sodium and to ascertain the extent to which their behavior could be expressed by the Mie–Grueneisen equation of state. The rather large sodium compressions which could be produced by the available pressure ($-\Delta V/V_0 = 0{\cdot}2$ in 20,000 atm) were sufficient to cause substantial changes in the temperature-dependent contributions to the thermodynamic functions.

* Contribution No. 873. This work was performed in the Ames Laboratory of the Atomic Energy Commission.

† Present address: Naval Ordnance Laboratory, Corona, California.

Previous work on the equation of state of sodium includes several measurements of the volume compression at pressures up to 100,000 atm by BRIDGMAN, as well as a determination by him of the variation with pressure (to 20,000 atm) of the mean linear thermal expansion coefficient between 0° and 95°C.[7–11] SIEGAL and QUIMBY have measured the thermal expansion of sodium at zero room temperature.[3,7,9,14] The sample (with length approximately equal to diameter) was placed in a heavy-walled Carboloy cylinder (see Fig. 1b), the ends of which were closed by Carboloy pistons. This assembly was placed in a hydraulic press with long tension and compression members (Fig. 1a) which was used to apply force to the pistons. To a first approximation, the variations in

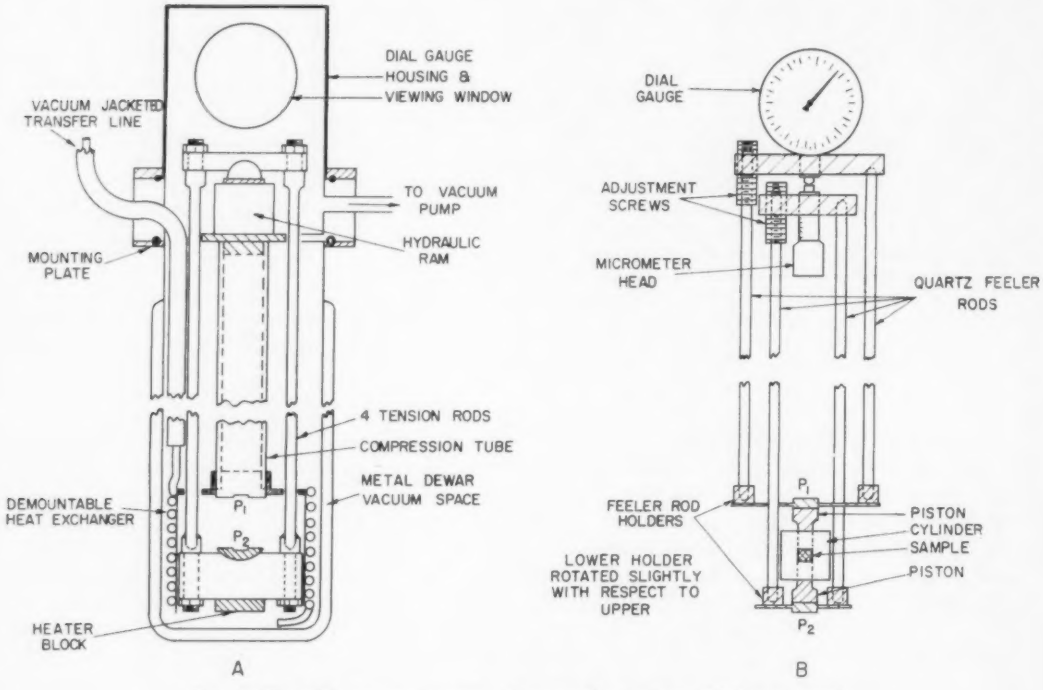

FIG. 1. The high pressure press and measuring system which was used in these experiments.

pressure as a function of temperature,[12] while DANIELS has used ultrasonic techniques at room temperature[13] to obtain the elastic constants and their variation with pressure for single crystal sodium. Pressure–volume data to 10,000 atm have also been published for temperatures of 4°K and 77°K.[3]

2. EXPERIMENTAL DETAILS

The general method which was used in this work resembles closely the techniques developed by BRIDGMAN to obtain rough compressions near the length of the sample with temperature and with applied force are directly related to the changes in volume if the shear strength of the sample is small, as is the case for the alkali metals.[15] The high pressure apparatus and the method of obtaining various sample holder temperatures between 100°C and 20°K, as well as the various corrections which must be applied, are discussed in detail below. Essentially, the approximate nature of the techniques which were used limited the experimental accuracy to one or two per cent, the magnitude of the uncertainty being difficult to evaluate.

Vol. 18
1961

The sodium used for these measurements was Dupont Reactor Grade,* with the only major impurity listed in a typical analysis being 80–100 p.p.m. potassium (the concentrations of all other impurities were less than this by two orders of magnitude). The samples were loaded into the holders in a dry box, with some contamination of the surfaces likely. No extraordinary precautions were taken to prevent this contamination, since it was felt not to be serious for these relatively crude measurements.

The apparatus which was used in these experiments has been represented by the two separate sketches in Fig. 1. Fig. 1(a) shows the hydraulic press, Dewar vessel, dial gauge housing, and cooling system. Fig. 1(b) shows the sample holder, feeler rod holders and dial gauge sensing arrangements. This separation into a force-producing apparatus and a compression-measuring apparatus has been made since the design of the press is relatively arbitrary, while the measuring system evolved only after many difficulties had been encountered. These will not be enumerated, since the design which is given should have been obvious from the beginning.

The hydraulic ram (Fig. 1a) was a commercial 10 ton unit (Blackhawk) which was modified by the substitution of an "O" ring for the usual chevron packing. The oil pressure to drive the ram (up to 10,000 p.s.i.) was supplied directly by a dead-weight gauge so that the force could be changed monotonically in equal increments.[3,14] The tension and compression members were made from stainless steel and in order to reduce heat conduction losses, their dimensions were chosen so as to give a safety factor of less than two with respect to yielding. The two ball and socket joints assisted in the elimination of difficulties due to misalignment.

The part of the press below the ram was enclosed in a continuously pumped metal dewar which was sealed to the mounting plate by an "O" ring. The top of the press was enclosed by the vacuum-tight dial gauge housing so that the entire volume surrounding the press could be evacuated. Temperatures above room temperature were obtained by means of the heater, and in this case the temperature was regulated by means of a thermocouple (not shown) which used a switch on the pen drive of a recording potentiometer to activate an "on-off" relay in the heater current supply line. For work below room temperature, a cryogenic fluid from an external container (in this case either liquid nitrogen or liquid hydrogen) was drawn into the Dewar by pumping a partial vacuum in the space around the press. The bottom of the press (and, hence, the sample holder) was surrounded by a boiling liquid when working from 63°K to 77°K or at 20°K, while a principle which has been described previously[16] was used to maintain intermediate temperatures. The earlier apparatus used manual control of the gas pressure in the space surrounding the press to vary the rate at which the cryogenic fluid was drawn into the heat exchanger. The temperature of the press was regulated at any desired level by adjusting the flow of liquid so that the heat leak into the sample holder area was exactly compensated by the refrigeration contained in the fluid (both latent heat and enthalpy of the vapor). In the current apparatus, automatic control was obtained by using a copper resistance thermometer (of about 60 Ω resistance) wound on the heat exchanger as a sensing element on a bridge circuit. The off-balance of this bridge was used to drive a commercial servo-amplifier-motor unit which operated a needle valve located in the rough vacuum pumping line. Thus, when the heat exchanger temperature rose, the valve opened and more fluid was drawn in to cool the exchanger, and vice versa. The large volume of the space surrounding the press caused considerable time lag and, hence, hunting in the heat exchanger temperature, but this was offset by the large heat capacity of the base of the press and a rather inadequate thermal connection between it and the heat exchanger. Thus, relatively large fluctuations in the heat exchanger temperature (of the order of several degrees) resulted in very small (0·5 degrees or less) fluctuations in the sample holder temperature.

The problem of measuring accurately small changes in the length of the sample led to the measuring apparatus which is shown in Fig. 1(b). The dial indicator (Starrett, model 655–611, 0·2 in. travel, 10^{-4} in. divisions) was calibrated against a precision micrometer screw (linear to 10^{-5} in.), and only the most linear part of the range was used. The indicator body was mounted directly on two

* We are indebted to Mr. D. A. SWALHEIM of the Sodium Products Sales Test Laboratory, E. I. du Pont de Nemours and Co., Niagara Falls, New York, for furnishing us with this sodium.

6 mm quartz rods which rested in sockets on the upper feeler rod holder. The bottom feeler rod holder was in loose contact with the pin of the dial indicator as is shown in Fig. 1(b). Great care was necessary to insure that equal weight was supported by the individual rods in each pair, and the effects of friction were minimized as much as possible by keeping the rods strictly vertical. The great length of the rods (48 in.) complicated these problems. Nevertheless, when all the adjustments had been made, changes in length of as little as $0{\cdot}5\,\mu$ could be detected (although not always believed). The ends of the pistons and the matching sides of the feeler rod holders were ground flat in order to prevent curvature from appearing in the initial portions of a P–V measurement.

The sample holder cylinders (55B Carboloy, 0·250 or 0·353 in. i.d., 0·81 in. o.d., 1·0 in. long) were jacketed with a sleeve of hardened beryllium copper (Berylco 25), 0·125 in. thick.* The sleeve was used because after many cycles (over 100) to 20,000 atm, the Carboloy in the smaller cylinder appeared to fatigue and fracture with radial cracks. The jacket prevented flying fragments which on one occasion broke the quartz feeler rods and damaged a dial indicator. The pistons were made from 779 Carboloy and were roughly of the shape shown in Fig. 1(b). In general, the maximum sample pressure was restricted to 20,000 atm in order to prevent yielding of the sample holder in the course of a series of runs. Extrusion of the sample through the narrow gap between the pistons and the cylinder wall was prevented through the use of small ($0{\cdot}030 \times 0{\cdot}030$ in) triangular extrusion rings which were made from drill rod.[3]

Sample temperatures were measured with a copper–constantan thermocouple which was clamped to the side of the sample holder cylinder. The wire from which this thermocouple was made had been calibrated previously in this laboratory, and the temperatures are believed to be accurate to better than 0·5°C. The thermocouple voltages were measured using a Rubicon type B potentiometer with a permanent record of the temperature as a function of time being obtained from a 0–100 microvolt recording potentiometer which was used in place of a galvanometer. This recorder also was used to control the heater current for runs above room temperature, the switch which was attached to the recorder indicator having a hysteresis of about one microvolt or 0·03°C.

The procedures which were used for taking and analyzing the data have been discussed in detail elsewhere, and will be mentioned here only briefly.[14,3] Indicator readings were taken at monotonically increasing and then decreasing pressures in increments of as little as 200 atm sample pressure in order to evaluate the effects of friction. Data for a typical run are shown in Fig. 2. The data almost always were smooth to 5×10^{-5} inches (about 1μ), and, after a seasoning cycle to full pressure, were generally reproducible to this order of magnitude when successive cycles were made at the same temperature.

The apparent pressures on the sample were calculated from the oil pressure in the ram (as given by the deadweight gauge) and the ratio of the areas of the ram and the sample holder piston. Any variation of these areas with pressure was ignored as being of second order in this calculation. The "true" pressure for a given sample length was obtained as the mean of the increasing and decreasing pressures for this displacement, with the assumption that the friction was independent of the direction of compression. The two ends of the experimental hysteresis curves (see the inset in Fig. 2) show the effect of the change in direction of the friction force as the direction of compression was reversed. Finally, the compression of the sample was separated from the compression of the pistons and feeler rod pads and the expansion of the cylinder with pressure by subtracting a "press correction" which was obtained from a similar run in the same sample holder using a sample of known compression (indium in this case). The increase in the area of the cylinder with pressure makes it essential that the known and unknown samples have the same length. The data which were used for the compression of indium[14] can be represented by,

$$(V-V_0)/V_0 = -(\Delta V/V_0)$$
$$= -2{\cdot}66 \times 10^{-6}p + 1{\cdot}82 \times 10^{-11}p^2 \qquad (1)$$

* A convenient method for making the sleeve a shrink-fit to the cylinder was to machine the sleeve to be a slight press fit in the untreated condition and then to harden it *in situ* on the cylinder. The change in the density of the beryllium copper on hardening (of the order of one-half per cent) resulted in the application of considerable stress to the Carboloy after the end of the hardening treatment (2 hr at 325°C).

where p is measured in atm. It always was found that the press corrections which were obtained through the use of these data were linear functions of the pressure. The magnitude of the press correction was of the same order of magnitude as the indium compression in the calibration runs, and is indicated in Fig. 2. Carboloy was assumed to

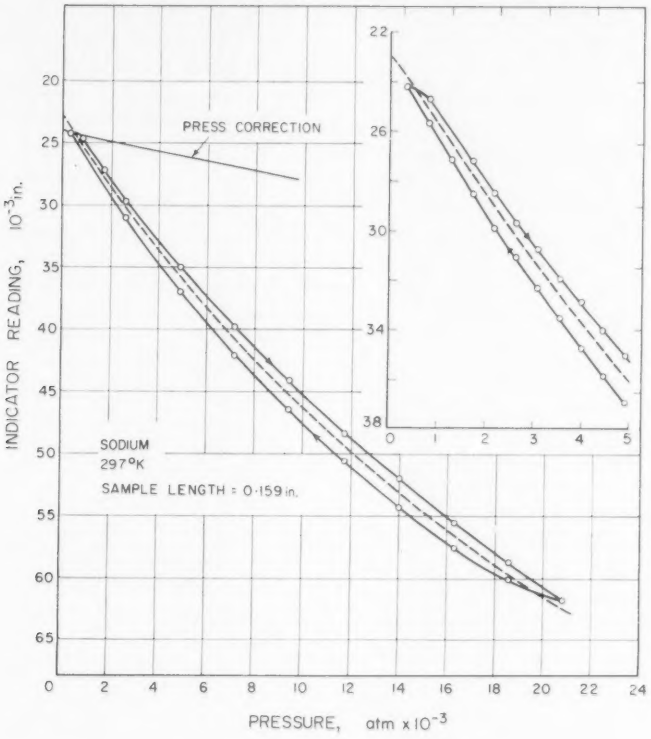

FIG. 2. Atypical isotherm, showing the raw data in terms of the apparent change in length of the sample vs. sample pressure.

have a negligible (within a few per cent) variation of its elastic constants with temperature, so the press correction was evaluated only at room temperature. This seemed to be the only reasonable course available, since no reliable data exist for the compression of indium at lower temperatures.

The temperature variation of the extrapolation of the experimental data to zero pressure can be used to estimate the volume thermal expansion of the sample material. The sample holder corrections necessary for this purpose are temperature dependent and quite large, and include a contribution due to the differential contraction of the beryllium copper jacket on the cylinder. An empirical temperature-dependent correction was obtained by using an indium sample, and this was checked by a calculation which used the thermal expansions and elastic moduli of the two types of Carboloy[17] and the beryllium copper.[18] Although the agreement was satisfactory, there is some reason to suspect that the thermal expansion data which we obtained for sodium are not as accurate as we had hoped. These difficulties will be discussed in the next section.

3. THE EXPERIMENTAL DATA AND RELATED CALCULATIONS

The experimental points for each isothermal run were plotted on a large-scale graph (as in Fig. 2)

Vol. 18
1961

and the friction correction applied by determining the mean pressure for each displacement. These corrected dial indicator readings were smoothed graphically and tabulated for equal increments of sample pressure (2000 atm for the small sample holder, 1000 atm for the large sample holder), with the lowest pressure being taken as 2000 atm and 1000 atm, respectively, for the two sample holder sizes. The initial portions of the curves were uncertain due to a rapidly changing friction and this procedure seemed to be more valid than to extrapolate the curves graphically to zero pressure. An IBM 650 computer was used to obtain a least-squares fit of these tabulated data to various power series. Except in one or two cases (which required a quartic equation), the data could be fitted by a cubic expression to within our measuring accuracy (roughly 10^{-4} in.), and this cubic expression was used consistently. Thus, the data as corrected for friction were reduced to a series of equations of the form;

$$l = l_0 + b_1' P + b_2 P^2 + b_3 P^3. \qquad (2)$$

The machine-determined extrapolated length at zero pressure (l_0) was used with the tabulated data to obtain the apparent changes with pressure of the length of the sample, $l - l_0$, from which were subtracted the changes in indicator reading due to the press correction. Finally, these changes in length were divided by the zero pressure length of the sample ($L_0(T)$) (as obtained from thermal expansion data) to give:

$$\Delta l/L_0 = (V - V_0)/V_0 = -\Delta V/V_0. \qquad (3)$$

This expression was considered to be valid to a first approximation since the press correction was evaluated in an identical manner. The values of $\Delta V/V_0$ as obtained in this manner are given in Table 1 for runs which were made with the two sample holders.

The coefficients of the power series of equation (2) can be used to give an analytic expression for $\Delta V/V_0$, since the linear press correction affects only the coefficient b_1'. If b_1 represents the corrected value of this coefficient, then,

$$\begin{aligned} -\Delta V/V_0 &= \Delta l/L_0 \\ &= (b_1 P + b_2 P^2 + b_3 P^3)/L_0 \\ &= a_1 P + a_2 P^2 + a_3 P^3. \end{aligned} \qquad (4)$$

The coefficients a_1, a_2 and a_3, which were determined, essentially, by a least-squares fit, also are given in Table 1.

The agreement between the $\Delta V/V_0$ data as obtained with the two sample holders is satisfactory, and is perhaps better than could be expected. The room temperature sample lengths were 0·1622 in. for the small diameter holder and 0·2983 in. for the large diameter holder. The two runs at 297°K with the small holder were separated by a considerable interval of time, during which runs at lower and higher temperatures were made. The run with the large sample holder at 359°K gave inconsistent values of the zero pressure length, and, hence, the data were normalized to fit onto a smooth isobar through the other data at 10,000 atm. An attempt was made to obtain high pressure data above the zero pressure melting point (371°K) but these runs always ended with extrusion of the sample even though the sample pressure was kept considerably above the melting pressure for the given temperature.

An attempt was made to fit the $\Delta V/V_0$ data of Table 1 by an equation given by BIRCH and derived from Murnaghan's theory of finite strain.[19,3] Least squares fits of the data to this two constant equation were obtained through the use of the IBM 650. These fits always were found to have systematic deviations from the experimental data which seemed outside experimental accuracy. In particular, the initial compressibilities so derived appeared to be excessively high. It is not known whether the fault lies in the data or in the applicability of the equation.

The data of Table 1 can be used to calculate the thermodynamic functions for sodium as a function of temperature and pressure only if the change in volume with temperature at zero pressure is known. In principle, the observed changes with temperature of the extrapolated sample length (Δl_0) at zero pressure (obtained from the least squares fit of equation 2) could be used to calculate this quantity. These were small ($7{\cdot}6 \times 10^{-3}$ in. when the small sample holder was cooled from room temperature to 20°K), and the correction for the sample holder contraction large ($1{\cdot}3 \times 10^{-3}$ in. over the same temperature interval). The situation was more favorable for the larger sample (the correction being less and the change in length greater), but our data were not as extensive. The

Table 1. Experimental values of $\Delta V/V_0$ and the coefficients of the least squares fit of these data to the polynomial, $(-\Delta V/V_0) = a_1p+a_2p^2+a_3p^3$

Pressure (atm)		Temperature, °K														
		20°K	51°K	77°K	77°K*	115°K	138·6°K	171°K	201°K	204°K	246°K	297°K	297°K	297°K*	349°K	359°K*,†
0	$\Delta V/V_0$, per cent	0	0	0	0	0	0	0	0	0	0	0	0	0	0	0
1000		1·3	1·3	1·4	1·4	1·4	1·4	1·4	1·5	1·4	1·5	1·5	1·5	1·6	1·6	1·7
2000		2·6	2·6	2·6	2·7	2·7	2·8	2·8	2·9	2·8	3·0	3·0	3·0	3·1	3·1	3·3
4000		4·9	4·9	5·0	5·1	5·1	5·2	5·3	5·5	5·4	5·6	5·7	5·7	5·8	5·9	6·2
6000		7·0	7·0	7·2	7·2	7·3	7·4	7·5	7·8	7·7	8·0	8·1	8·0	8·2	8·4	8·6
8000		8·9	8·9	9·1	9·1	9·2	9·4	9·5	9·9	9·7	10·1	10·2	10·2	10·3	10·5	10·8
10,000		*Obs.* 10·6 *Calc.* (10·8)	10·6 (10·8)	10·8 (10·9)	10·8 (10·9)	11·0 (11·0)	11·1 (11·2)	11·3 (11·4)	11·7 (11·6)	11·5 (11·6)	11·9 (11·9)	12·1 (12·1)	12·1 (12·1)	12·1 (12·1)	12·5 (12·4)	12·6 (12·5)
12,000		12·1	12·2	12·4	12·2	12·6	12·7	12·9	13·3	13·2	13·6	13·8	13·8	13·7	14·2	14·3
14,000		13·5	13·6	13·8	—	14·0	14·2	14·4	14·8	14·7	15·1	15·4	15·4	—	15·8	—
16,000		14·8	14·9	15·1	—	15·3	15·5	15·7	16·1	16·1	16·5	16·8	16·8	—	17·3	—
18,000		16·0	16·1	16·3	—	16·5	16·7	17·0	17·4	17·4	17·8	18·1	18·1	—	18·6	—
20,000		*Obs.* 17·0 *Calc.* (17·3)	17·1 (17·3)	17·4 (17·5)	—	17·6 (17·7)	17·8 (17·9)	18·1 (18·2)	18·5 (18·5)	18·4 (18·5)	18·9 (18·9)	19·3 (19·3)	19·2 (19·3)	—	19·8 (19·7)	—
$-a_1\times10^5$ (atm^{-1})		1·335	1·327	1·382	1·464	1·401	1·429	1·447	1·549	1·484	1·556	1·581	1·572	1·642	1·633	1·766
$+a_2\times10^{10}$ (atm^{-2})		3·18	2·97	3·46	5·08	3·46	3·67	3·59	4·51	3·76	4·25	4·32	4·16	5·19	4·44	6·21
$-a_3\times10^{15}$ (atm^{-3})		3·8	3·0	4·5	11·9	4·3	4·9	4·4	7·1	4·8	6·0	6·2	5·5	8·7	6·1	12·0
V_0(cm^3/mol)		22·68	22·70	22·75	22·75	22·86	22·95	23·09	23·22	23·23	23·43	23·68	23·68	23·68	23·93	24·00(†)

* Large sample holder.

† Normalized at 10,000 atm.

results of these calculations of the volume changes at zero pressure are given in Fig. 3, where a comparison is made with values of $\Delta V/V_0$ calculated from direct linear expansion measurements due to SIEGAL and QUIMBY[12]. The deviations of their data from the small sample holder determinations seem outside our expected experimental error, but the agreement with the more precise large holder reasonable as a probable uncertainty. These data are identical to this accuracy with previous measurements to 10,000 atm at 4·2°K,[3] while the room temperature results agree similarly with precise hydrostatic pressure linear compression measurements by BRIDGMAN[11]. The slight differences found in making this last comparison are much smaller than would be expected from pressure

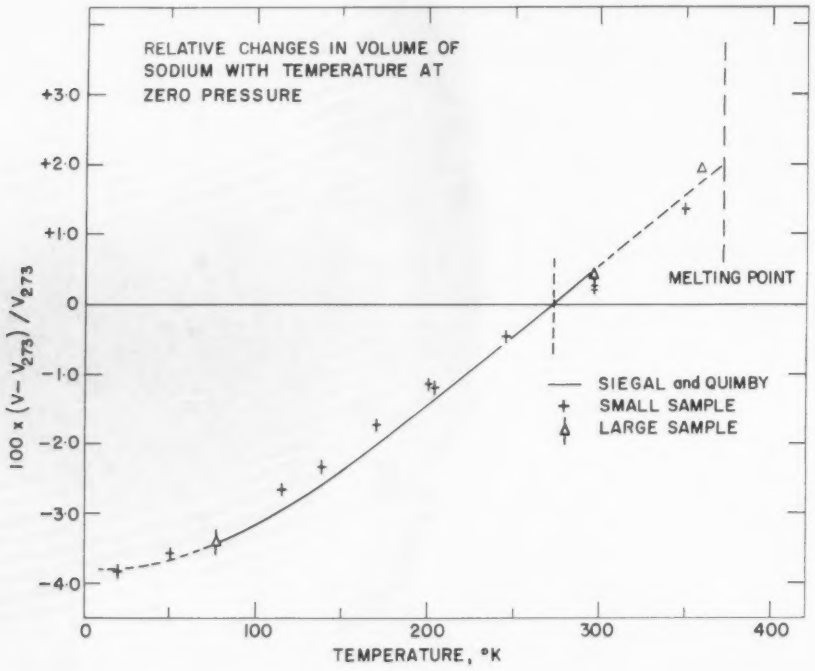

FIG. 3. The volume change in sodium with temperature at atmospheric pressure.

data is sufficiently good so that we felt justified in assuming SIEGAL and QUIMBY's data rather than our own. The resulting molar volumes at zero pressure (assuming a value of 23·68 cm³ at room-temperature) also are given in Table 1 for each of the temperatures at which a run was made.

The evaluation of the accuracy of data such as these is difficult in view of the approximate nature of the pressure transmission and the empirical nature of the determination of corrections. An estimate of about one per cent of the total compression (or $\pm 0{\cdot}002$ in $\Delta V/V_0$) would seem to be scale errors, for instance, or errors due to our friction corrections. The agreement with BRIDGMAN's higher pressure data to 40,000 kg/cm² (which were obtained by a method which is the same as that described here) is not good, and the reason is not known.[7,9] These data of BRIDGMAN's are open to some question since he found it necessary to sheath his samples with aluminum or copper to prevent the alkali metals from attacking the Carboloy under pressure. We found this precaution to be unnecessary for sodium, at least. Finally, our values for $(-a_1)$ at room temperature should give

the zero pressure isothermal compressibility, and they are in reasonable agreement with the room temperature value of $1{\cdot}64\times10^{-5}$ atm^{-1} which can be deduced from the ultrasonic data of DANIELS[13] (using $(k_T/k_s) = 1{\cdot}069$ as discussed below).

The temperature dependence of the a_n (equation (4) and Table 1) shows considerable scatter. This is not surprising, since the precise values must depend strongly on the graphical smoothing of the individual isotherms which accompanied the application of the friction correction. Various empirical correlations were attempted in order to reduce the significance of this effect. The most successful involved the plotting of the isothermal compressibilities ($k_T = -V^{-1}(\partial V/\partial P)_T$, using equation 4) as a function of the volume for six pressures (0,2000, 5000, 10,000, 15,000 and 20,000 atm) for each of the isotherms in Table 1. The results of this plot are shown in Fig. 4. The degree of overlap between low pressure–high temperature data, and high pressure–low temperature data is shown by the triangles which represent the 20°K isotherm and the open circles which represent the room temperature isotherms. There seems to be no explicit temperature dependence of the compressibility, and, to a first approximation, a linear dependence of this compressibility on the volume. A least-squares fit of these 82 points to a linear function gives,

$$k_T = -V^{-1}(\partial V/\partial P)_T = A[1-(V/\nu)]$$
$$= -3{\cdot}09\times10^{-5}[1-(V/15{\cdot}61)]\ \text{atm}^{-1}, \qquad (5)$$

where the coefficients are as stated.

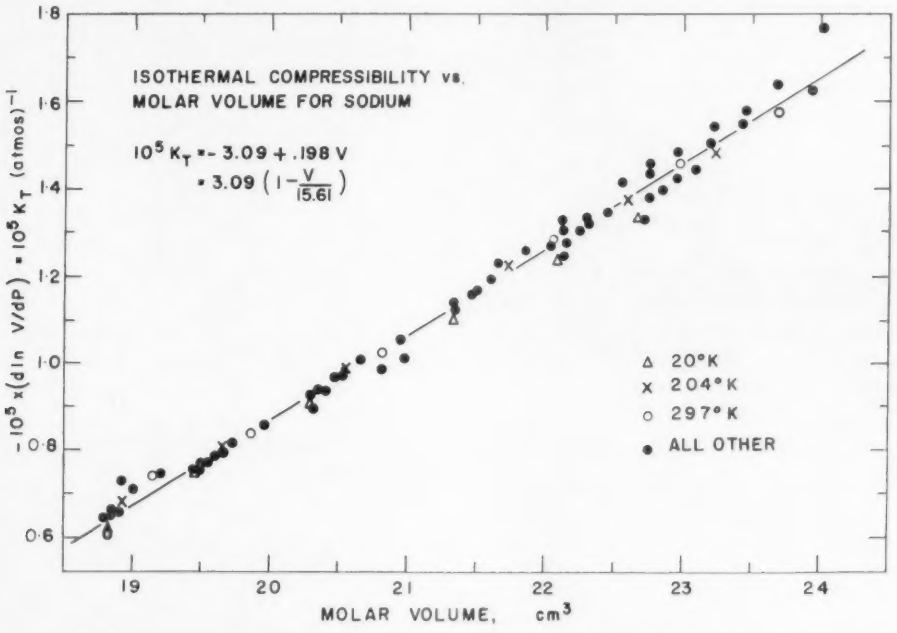

FIG. 4. The isothermal compressibility of sodium as a function of molar volume. The solid line represents a least squares fit of the points shown to a straight line.

The adequacy of this expression can be tested by verifying that in integrated form it represents the actual experimental data in Table 1. The temperature dependence of the compressibility at zero pressure is due solely to the normal volume expansion at zero pressure ($V_0(T)$), and this is included as an integration constant. Thus, one can write,

$$\Delta V/V_0 = \frac{1-\exp(AP)}{\exp(AP)-[1-\nu/V_0(T)]^{-1}} \qquad (6)$$

Vol. 18
1961

where $A = -3{\cdot}09\times10^{-5}$ atm^{-1}, $\nu = 15{\cdot}61$ cm^3/mol and $V_0(T)$ is the molar volume at zero pressure for a given temperature. Typical values of $\Delta V/V_0$ as obtained from this expression are given in Table 1 for 10,000 atm and 20,000 atm. The agreement is well within the expected experimental uncertainties. This is gratifying, since only two adjustable constants plus the molar volume as a function of temperature have been used to represent these data which were obtained in fifteen different runs at thirteen different temperatures. Equation (5) plus the zero pressure volume expansion data have been used as the basis for the calculations which will be discussed in the next section.

Equation (6) represents both the earlier linear compression data of BRIDGMAN[11] and the low temperature data[3] to within experimental accuracy. The constants A and ν which best fit these data give a zero pressure isothermal compressibility at 300°K of $1{\cdot}60\times10^{-5}$ atm^{-1}, in good agreement with the value of $k_T = 1{\cdot}64\times10^{-5}$ atm^{-1} which can be calculated from DANIELS' ultrasonic data if the ratio $k_T/k_s = 1{\cdot}069$ is used. Similarly, the pressure dependence of the bulk modulus can be calculated from;

$$dB_T/dP = [1-(\nu/V)]^{-1}. \tag{7}$$

At room temperature this varies from 2·94 at zero pressure to 3·12 at 2000 atm, with an average value of 3·03. In order to compare this with DANIELS' average value of $(\partial B_s/\partial P)_T = 3{\cdot}6$[13] which was obtained over the same pressure range, a correction must be applied both for the difference between the two moduli ($B_s/B_T = 1{\cdot}069$) and the variation of this ratio with pressure (about three per cent). The net result is a calculated average value of dB_s/dP in 2000 atm of 3·14 which is not in agreement with the ultrasonic data.[13]

Sodium at zero pressure exhibits a low temperature martensitic transformation from its normally b.c.c. structure to a h.c.p. structure, and this transition can be induced by deformation at temperatures as high as 50°K.[20] The volume change (0·2 per cent) is so small that we could not have detected it in these experiments. However, there is the possibility that the relatively poorer agreement between the calculated and experimental $\Delta V/V_0$'s for the two lowest temperatures (20°K and 50°K, Table 1) is due to a slightly smaller compression for the h.c.p. phase than for the b.c.c. phase.

4. DISCUSSION

The thermodynamic functions for a one-component, single phase system can be calculated explicitly if the Helmholtz free energy, $F(V, T) = U-TS$, is known as a function of volume and temperature.[6] It is convenient to use the following relationships and definitions:

$$\begin{aligned} F(V, T) &= U_0(V)+F^*(V, T) \\ &= U_0(V)+U^*(V, T)-TS(V, T)\cdot \end{aligned} \tag{8}$$

$$\begin{aligned} P &= -(\partial F/\partial V)_T = -dU_0/dV- \\ &(\partial F^*/\partial V)_T = P_0(V)+P^*(V, T) \end{aligned} \tag{9}$$

$$\begin{aligned} V^{-1}B_T &= (Vk_T)^{-1} = -(\partial P/\partial V)_T \\ &= d^2U_0/dV^2+(\partial^2F^*/\partial V^2)_T \\ &= V^{-1}[B_0(V)+B_T^*(V, T)]. \end{aligned} \tag{10}$$

Here, the subscripts $(_0)$ refer to temperature-independent quantities, and the asterisks (*) refer to quantities which are temperature and volume dependent and which approach zero at absolute zero. These latter terms are, presumably, contributions due to the lattice vibrations.

If the bulk modulus, B (or the compressibility), is to be a function of the volume only, then $B_T^* = 0$, P^* is a function of the temperature only, and the volume dependence of F^* must contain only terms which are linear in V. The entropy and the internal energy are related to the equation of state ($P(V, T)$) by the thermodynamic relationships,

$$\begin{aligned} (\partial S/\partial V)_T &= (\partial P/\partial T)_V \\ &= -(\partial V/\partial T)_P/(\partial V/\partial P)_T = \beta/k_T \end{aligned} \tag{11}$$

$$(\partial U/\partial V)_T = T(\partial P/\partial T)_V-P. \tag{12}$$

Since the temperature dependent part of the pressure, P^*, is independent of the volume, one can write immediately that $\beta/k_T =$ constant $= \beta_0/k_{T0}$, where the subscripts $(_0)$ here refer to zero pressure. [No confusion should arise due to the different meaning of this subscript in equations

(8)–(10).] These equations can be written to give

$$(\partial S/\partial V)_T = \beta_0/k_{T0};\ S(V, T) - S(V_0, T) = \beta_0/k_{T0}(V - V_0) \quad (13)$$

$$(\partial U^*/\partial V) = T\beta_0/k_{T0} - P^* \quad (14)$$

where equation (14) has been written in terms of the temperature-dependent internal energy only.

The linear volume dependence of F^*, U^* and S is a direct consequence of the assumption that k_T does not contain an explicit temperature dependence. The temperature dependence of P^* will depend on the constant which must be evaluated when equation (10) is integrated to obtain the equation of state. This is most conveniently introduced as the volume, $V_0(T)$, at which the pressure is zero for a given temperature (as in equation 6). Hence, using the linear dependence of k_T on volume (equation 5), the pressure for a given temperature and volume can be written as,

$$P(T, V) = A^{-1}\ln(1-\nu/V)/(1-\nu/V_0(0)) - A^{-1}\ln(1-\nu/V_0(T))/(1-\nu/V_0(0)) + P_0(V) + P^*(T). \quad (15)$$

$P^*(T)$ and the data which were used in its calculation are given in Table 2.

The volume dependence of the internal energy can be calculated from equation (12) as,

$$U(V, T) = U(V_0, T) + T\beta_0/k_{T0}(V - V_0(T)) - (\nu/A)\ln(V_0(T)/V) - P(V-\nu), \quad (16)$$

where use has been made of the constancy of β/k_T for this model. At absolute zero,

$$U_0(V) = U_0(V_0) - (\nu/A)\ln(V_0(0)/V) - P(V-\nu). \quad (17)$$

$U_0(V)$ and $P_0(V)$ as calculated from equations (15) and (17) are given in Table 3 along with the experimental values of $P_0(V)$.

Equation (16) gives the variation of the total internal energy with volume for a given temperature above absolute zero. In general, it is useful to separate this into two contributions, one being due to the volume dependence of the lattice energy at absolute zero (equation (17) above), and the other involving only the lattice vibration or phonon contributions ($U^*(T, V)$). Calorimetric data for the specific heat at constant pressure (C_p)[21] can be integrated from $T = 0$ to give the enthalpy as a function of temperature at zero pressure, with the

Table 2. The various quantities which were used to calculate the volume variation of the thermodynamic functions for sodium

T, °K	$V_0(T)$[a], cm³/mol	$\beta_0 \times 10^4$[a], °K⁻¹	$k_{T0} \times 10^5$[b], atm⁻¹	$S(V_0, T)$[c], cal/mol deg	$U_{cal}(T)$[d], cal/mol	$P^*(T)$[e], atm
0	22·68	0	1·400	0	0	0
50	22·70	(0·3)	1·405	3·70	78	—
100	22·81	(0·41)	1·445	5·63	314	418
150	22·99	1·78	1·459	7·92	597	927
200	23·21	1·99	1·512	9·66	900	1610
250	23·45	2·03	1·551	11·08	1220	2300
300	23·70	2·03	1·600	12·28	1546	2970
350	(23·95)	(2·03)	1·649	—	(1900)	3660

(a) calculated from Ref. (12)

(b) calculated from equation (5)

(c) from Ref. (21)

(d) calculated from Ref. (21)

(e) calculated from equation (15)

Vol. 18
1961

Table 3. The variation of the internal energy and pressure of sodium with volume at absolute zero. The experimental data for 20°K also are given for comparison

V, cm³/mol	$U_0(V)$, cal/mol	$P_0(V)$, atm × 10^{-3}	$P_0(V)$, atm × 10^{-3} (exp)
19·0	680	18·03	18·3
19·5	489	14·40	14·7
20·0	311	11·31	11·6
20·5	209	8·64	8·9
21·0	120·5	6·28	6·4[5]
21·5	55·7	4·18	4·3
22·0	18·2	2·28	2·3
22·5	5·3	0·55	0·6
23·08	0	0	0
23·0	4·3	−0·97	—
23·5	24·1	−2·40	—
24·0	66·3	−3·70	—

zero of energy being arbitrarily chosen as the energy at zero pressure and zero temperature. Thus, the absolute value of the enthalpy as calculated in this manner contains a contribution due to the work done in expanding the lattice as well as a contribution from the purely thermal vibrations of the lattice (or U^*). Equation (17) can be used to correct for this difference between the enthalpy and the internal energy, with P in this expression now becoming $P_0(V)$ (the pressure which would produce the volume, V, at absolute zero, a negative quantity at low external pressures and high temperatures). Then,

$$U^*(V, T) = H_{\text{cal}}(P = 0, T) - (v/A)\ln(V_0(T)/V_0(0)) + T(\beta_0/k_{T0})(V - V_0(T)) - P^*(T)(V - v). \quad (18)$$

The linear dependence of U^* on volume is found, and the data necessary for the evaluation of U^* are given in Table 2.

The foregoing outlines the expressions which according to the results of these experiments, can be used to calculate the thermodynamic functions of sodium as a function of volume for various temperatures. The calculation of the same quantities from first principles is quite difficult, and often the simplifying assumption is made that the entropy (or specific heat at constant volume) can be represented by a law of corresponding states, $S = S(\theta/T)$, where the total volume dependence of the entropy is contained in the characteristic temperature, θ.[6,22] A special example is given by the Debye model,[6] although no model need be assumed for the following discussion. If, and only if, $S = S(\theta(V)/T)$, then one can write:

$$P^*(V, T) = \Gamma(V)(U^*(V, T)/V) \quad (19a)$$

where

$$-(d\ln\theta/d\ln V) = \Gamma(V) = (\beta V/C_v k_T). \quad (19b)$$

This is the Mie–Grueneisen equation of state, with Γ, the Grueneisen constant, being a dimensionless number which is of the order of unity for many substances.[23] A generalization is possible to the case where the entropy is made up of the sum of several terms, each of which can be written in the form $S_i = S_i(\theta_i(V)/T)$. Then, a Γ_i exists for each θ_i, and one can speak of the contribution to the thermal pressure or the thermal expansion of each of the terms as follows:

$$P^*(V, T) = \sum P_i^*(V, T) = V^{-1}\sum \Gamma_i(V)U_i^*(V, T) \quad (20a)$$

and

$$-(d\ln\theta_i/d\ln V) = \Gamma_i(V) = \beta_i V/C_{vi}k_T. \quad (20b)$$

An example of this is given by the independent contributions of the free electrons and the lattice to the heat capacity of a metal. The effects of these electronic terms have been ignored in the following discussion, which is concerned with temperatures at which the free electrons make a very small direct contribution to the thermodynamic properties.

All of the experimental quantities in equations (19a) and (19b) are known, or can be evaluated, so it is possible to calculate Γ as a function of both T and V. $\Gamma(V)$ can be calculated from equation (19a) using equation (15) for P^*, equation (18) for U^*, and the data in Table 2. In general, since P^* is dependent on the temperature only, and U^* is of the form $(C(T)+D(T)V)$, Γ is given by the expression,

$$\Gamma(V, T) = (P^*V/(C+DV)). \quad (21)$$

The results of this calculation are given for three temperatures (100°K, 200°K, 300°K) in Fig. 5. Γ also can be calculated from the right-hand-side of equation (19b), and the results of these calculations for zero pressure are given as the open circles in Fig. 5 for the same temperatures. It can be seen that the two calculations are not in agreement below room temperature. This is not surprising, since the equations (19) are self-consistent only if Γ is a function of volume only, and Fig. 5 shows that this is not true at or below 200°K.

(DUGDALE and MACDONALD)

$$\Gamma_{DM} = -(V/2)(\partial^2 PV^{2/3}/\partial V^2)/(\partial PV^{2/3}/\partial V)-(1/3)$$
$$= (1/2)[(B/3)+(2P/9)-$$
$$-(B\partial B/\partial P)/((2P/3)-B)]-(1/3) \qquad (23)$$

These have been calculated for room temperature, and are shown also in Fig. 5. The very small change in shape of the isotherms with temperature

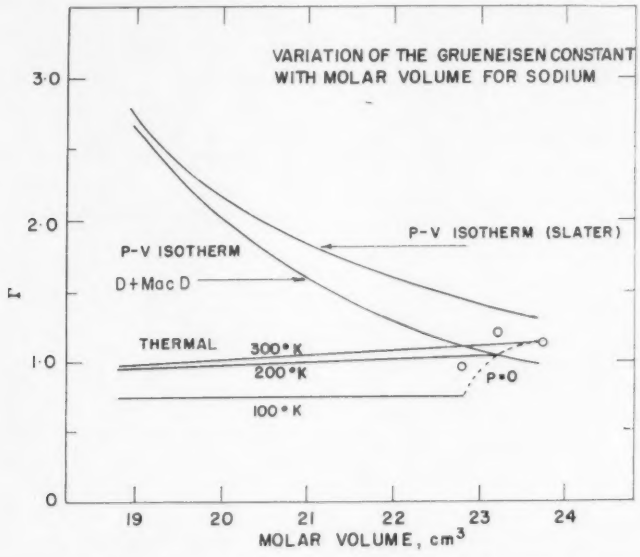

FIG. 5. The volume variation of the Grueneisen constant as given by various definitions.

Other comparisons are possible. Since Γ is related to the volume dependence of the characteristic temperature which, in turn, is related to the force constants of the lattice, one would expect a relationship between the equation for a pressure–volume isotherm and Γ. Two such relationships have been proposed in the literature for isotropic solids, one by SLATER[24] and the other by DUGDALE and MACDONALD[25] (which does not seem to have a really firm theoretical basis).[22] These expressions are given by,

(SLATER)

$$\Gamma_{Slater} = -(V/2)(\partial^2 P/\partial V^2)/(\partial P/\partial V)-(2/3)$$
$$= (1/2)(\partial B/\partial P)_T-(1/6) \qquad (22)$$

results in only very small temperature dependences of these Γ's, in contrast with those derived from equations (19).

The statement has been made that the derivatives in equations (22) and (23) (at least, the first derivatives) must be taken at constant entropy.[22] This consideration has been ignored in the calculation of the pressure–volume isotherm Γ's which are given in Fig. 5, since the differences introduced would be in detail rather than in general behavior. Another rather interesting consideration arises since the major contribution in both of these expressions is due to $(\partial B/\partial P)$. The adiabatic bulk modulus (which is obtained from ultrasonic measurements) is related to the isothermal bulk

Vol. 18
1961

modulus by the relationship,

$$B_S = B_T(1+(TV\beta^2/k_T C_V)) = B_T(1+\beta\Gamma T), \tag{24}$$

where Γ is defined by the right-hand-side of equation (19b). The pressure derivative of B_S is given by,

$$\begin{aligned}(\partial B_S/\partial P)_T &= (\partial B_T/\partial P)_T(1+\beta\Gamma T)+B_T(\partial_\beta \Gamma T/\partial P)_T \\ &= (\partial B_T/\partial P)_T(1+\beta\Gamma T)- \\ &\quad VT(\partial\beta\Gamma/\partial V)_T. \end{aligned} \tag{25}$$

The variation of $\beta\Gamma$ with volume can be estimated from Fig. 5, equation (5) and the relationship that β/k_T is constant for a given temperature. Since both β and Γ decrease with decreasing volume, the effect of this second term is such as to decrease the difference between the pressure derivatives of the isothermal and adiabatic bulk moduli. In particular, at room temperature, B_S and B_T differ by about seven per cent, but the effect of the second term in equation (25) is to reduce the difference between their pressure derivatives to four per cent.

The data shown in Fig. 5 can be combined with zero pressure values of the entropy and equation (13) to ascertain qualitatively the validity of the Debye model as it applies to sodium. First, tables of the Debye functions[26] can be used to calculate the Debye θ at zero pressure by determining the values of θ/T to which the experimentally determined entropies correspond. The entropy at 20,000 atm can be calculated from equation (13), and a value for θ at 20,000 atm can be found similarly. Finally, the ratio $(\theta_{20,000}/\theta_0)$ can be obtained by integration of the left-hand-side of equation (19b) and from equation (21). The results of these calculations are given in Table 4 for 100°K, 200°K and 300°K. It again is not surprising that the results are in best agreement at room temperature where the small temperature dependence of Γ implies that a model containing a characteristic temperature is most likely to be correct.

Table 4. Comparison of the change in characteristic temperature in 20,000 atm as given by the Debye model expression for the entropy and the Mie-Grueneisen equation of state

T °K	θ_0 °K	$(\theta_{20,000}/\theta_0)_{\text{Debye}}$	$(\theta_{20,000}/\theta_0)_{\text{MG}}$
100	157	1·20	1·16
200	152	1·28	1·23
300	146	1·27	1·27

The failure of our simple assumption that the volume dependence of the thermodynamic functions depends only on a characteristic temperature is not surprising. This postulate requires that the lattice frequency distribution function first be independent of the temperature at constant volume, and, second, be unchanged in shape (although the magnitudes may be a function of volume) upon change in volume. Practically, this means that Poisson's ratio must not be a function of pressure or volume.[6] Recent ultrasonic measurements on the variation of single crystal elastic constants with pressure have furnished data which allow a direct test of this assumption.[13,27–30]

Two different Poisson's ratios can be defined for a cubic crystal,

$$\begin{aligned}\sigma_{100} &= (3B_S-2C')/(6B_S+2C') \\ \sigma_{111} &= (3B_S-2C_{44})/(6B_S+2C_{44}),\end{aligned} \tag{26}$$

where $C' = (C_{11}-C_{12})/2$ and $B_S = (C_{11}+2C_{12})_S/3$.[31] It can be seen by inspection that the logarithmic pressure derivatives of the elastic constants $[(\partial \ln B_S/\partial P)_T, (\partial \ln C_{44}/\partial P)_T, (\partial \ln C'/\partial P)_T]$ must be identical if the Γ's are to be unchanged by pressure. DANIELS' data give (in units of 10^{-11} $(\text{dyne}^{-1}\,\text{cm}^{-2})$), $(\partial \ln B_S/\partial P)_T = 5{\cdot}45$, $(\partial \ln C_{44}/\partial P)_T = 3{\cdot}89$, and $(\partial \ln C'/\partial P)_T = 3{\cdot}86$. Obviously, the condition that the Poisson's ratios are unchanged by pressure is not satisfied.

The variation of these ratios with volume can be calculated to give,

$$\begin{aligned}(\partial \ln \sigma_{100}/\partial \ln V)_T &= -0{\cdot}10, \\ (\partial \ln \sigma_{111}/\partial \ln V)_T &= -0{\cdot}94.\end{aligned}$$

SLATER draws an analogy between the effects of temperature and pressure on volume, and predicts that these derivatives should be positive.[6] His discussion does not take into account the fact that σ can have an explicit temperature dependence at constant volume which can be different from the above in sign. The necessary data are not available for sodium, but calculations which can be made from more complete data for Cu, Ag, Au[29] and

Al[30] show that σ increases with temperature at constant volume, as well as exhibiting qualitatively the same volume effect as sodium.

One major consideration which affects the calculations of the volume dependence of the thermodynamic functions is the range of their validity. First, the linear dependence of k_T on volume implies a minimum molar volume for sodium of 15·6 cm^3; BRIDGMAN's high pressure data show that appreciably smaller volumes can be obtained experimentally at 100,000 kg/cm^2.[8,10] No explicit conclusions can be drawn, however, since it is difficult to know which of BRIDGMAN's sets of data are to be preferred. Equation (5) and expressions derived from it should not be used for extrapolation to higher pressures.

The problem of calculating thermodynamic functions from our experimental pressure–volume data is complicated further by the following considerations. At sufficiently high pressures, the frequency spectrum of the lattice will be shifted to frequencies which are so high that the lattice behaves essentially as if it were at absolute zero. Hence, S and U^* will approach zero at both low temperatures and high pressures. Our assumption that k_T is independent of the temperature at the constant volume does not give this result, since for temperatures above 150°K equations (13) and (18) (which are dependent only on this assumption) give zero entropy and internal energy only for negative values of the molar volume.

The important missing factor is that even small deviations from this temperature independence of k_T (well within our experimental accuracy) can have significant effects on S and U^*. To see this, consider the bulk modulus to be given by the following,

$$B_T(T, V) = B_T(V)(1+\alpha(T))$$

or

$$(\partial P/\partial V)_T = dP/dV(1+\alpha(T)), \qquad (27)$$

where $\alpha(T)$ is a small number (of the order of a few per cent), and could not have been detected in our experiments. From this equation, one can write,

$$P = P_0(V)+\alpha(T)P_0(V)+A(T) \qquad (28)$$

$$(\partial S/\partial V)_T = (\partial P^*/\partial T)_V$$
$$= (d\alpha/dT)P_0(V)+(dA/dT) \qquad (29)$$

$$(\partial U^*/\partial V)_T = T(\partial P^*/\partial T)_V -$$
$$P^* = T(d\alpha/dT)P_0(V)+$$
$$T(dA/dT)-P^* = P_0(V)[(d\alpha/dT)-$$
$$\alpha(T)]+(TdA/dT-A). \qquad (30)$$

$A(T)$ may be identified to a first approximation with P^* as calculated previously (equation 15), with $(dA/dT) = \beta_0/k_{T0}$. One may also postulate that $\alpha(T)$ (which must be positive)† is of the form bT^2 (since by the third law of thermodynamics $d\alpha/dT$ must approach zero at absolute zero), and is (optimistically) of the order of 0·01 at 300°K. The net result is that at 20,000 atm P^* increases by about 7 per cent, $(\partial S/\partial V)_T$ increases by 15 per cent, and $(\partial U^*/\partial V)_T$ increases by 20 per cent, all with respect to their values with $\alpha = 0$. At very high pressures, the effect of terms such as these may be expected to dominate the volume independent terms, although at much higher pressures $\alpha(T)$ must disappear, since negative entropies and thermal energies are as abhorrent as non-zero positive values. Perhaps $\alpha(\theta(V)/T)$ would be a better approximation.

Thus, the changes in entropy and internal energy as calculated from our model are probably underestimated. Similarly, the thermal Γ's in Fig. 5 would be expected to increase at the highest pressures because the increase in P^* and the decrease in U^* are both more rapid than we have assumed. Accurate measurements of these quantities in the pressure range of interest would be very difficult.

5. CONCLUSIONS

The experimental pressure–volume isotherms which were obtained over a wide range of temperature (20–350°K) and pressure (0–20,000 atm) could be represented by an equation of state based on an isothermal compressibility which was temperature independent at constant volume and which varied linearly with the volume. This equation of state was used to calculate the volume (or pressure) variation of the various thermodynamic functions, and these calculations were used as a

† This is in agreement with ultrasonic measurements on copper, silver, and gold where the derivative $(\partial k_T/\partial T)_V$ was found to be negative.[27,28,29]

basis for discussion of the validity of the postulated equation of state. It was found that the results so derived could be valid at high pressures only if a slightly temperature-dependent contribution to the compressibility were allowed, such that $(\partial k_T/\partial T)_V < 0$. The magnitude of the effect which would be needed would be well within our estimated experimental error. The applicability of the Mie–Grueneisen equation of state to sodium also was investigated, as well as two other definitions of the Grueneisen constant, Γ, which are based on pressure–volume isotherms. The various definitions of Γ were found to be quite inconsistent, showing that below, roughly, 200°K, one cannot associate a characteristic temperature or a law of corresponding states with this metal. This conclusion could have been predicted, since ultrasonic measurements of the elastic constants can be interpreted to show that Poisson's ratio for sodium has a definite volume dependence, and, hence, the lattice frequency distribution function must change shape as the volume is varied.

Acknowledgements—The authors are indebted to Dr. N. BERNARDES for discussions on the general theory of temperature-dependent equations of state, and to Dr. J. F. SMITH for helping to clarify the role of Poisson's ratio.

They also gratefully acknowledge the patient assistance of Mr. W. E. SYLVESTER and Mr. T. NAIG, who were responsible for the construction and modification of the equipment which was used.

REFERENCES

1. HAM F. S., *Solid State Physics* (edited by SEITZ F. and TURNBULL D.) Vol. I, p. 127. Academic Press, New York (1955).
2. BERNARDES N., *Phys. Rev.* **112,** 1534 (1959).
3. SWENSON C. A., *Phys. Rev.* **99,** 423 (1955).
4. DUGDALE J. S. and SIMON F. E., *Proc. Roy. Soc.* **A218,** 291 (1953).
5. DOMB C. and DUGDALE J. S., *Progress in Low Temperature Physics* (edited by GORTER C. J.) Vol. II p. 388. Interscience, Amsterdam (1957).
6. SLATER J. C., *Introduction to Chemical Physics*, Chapters 13, 14. McGraw-Hill, New York (1939).
7. BRIDGMAN P. W., *Proc. Amer. Acad. Arts Sci.* **72,** 207 (1938).
8. BRIDGMAN P. W., *Proc. Amer. Acad. Arts Sci.* **74,** 425 (1942).
9. BRIDGMAN P. W., *Proc. Amer. Acad. Arts Sci.* **76,** 71 (1948).
10. BRIDGMAN P. W., *Proc. Amer. Acad. Arts Sci.* **76,** 55 (1948).
11. BRIDGMAN P. W., *Proc. Amer. Acad. Arts Sci.* **70,** 71 (1935).
12. SIEGAL S. and QUIMBY S. L., *Phys. Rev.* **54,** 76 (1938).
13. DANIELS W. B., *Pressure Variation of the Elastic Constants of Sodium*, ONR Tech. Report No. 3, Case Inst. of Tech. (June, 1958). To be published in *Phys. Rev.* We are indebted to Dr. DANIELS for making a copy of this report available to us.
14. BRIDGMAN P. W., *Proc. Amer. Acad. Arts Sci.* **76,** 1 (1945).
15. HULL D. and ROSENBERG H. M., *Phil. Mag.* **4,** 303 (1959).
16. SWENSON C. A. and STUHL R. H., *Rev. Sci. Instrum.* **25,** 608 (1954).
17. *Properties of Carboloy Cemented Carbides*, Engineering Bulletin HM–100A, Carboloy Department, General Electric Co., Detroit 32, Michigan (1951). Also unpublished thermal expansion data from our laboratory.
18. BEENAKKER J. J. M. and SWENSON C. A., *Rev. Sci. Instrum.* **26,** 1204 (1955); RICHARDS J. T. and BRICK R. M., *J. Metals, N.Y.* **6,** 574 (1954).
19. BIRCH F., *J. Geophys. Res.* **56,** 227 (1952).
20. BARRETT C. S., *Acta Cryst., Camb.* **9,** 671 (1956); BASINSKI Z. S. and VERDINI L., *Phil. Mag.* **4,** 1311 (1959).
21. MARTIN D. L., *The Specific Heat of Sodium from* 20°K *to* 300°K. *The Martensitic Transformation. Proc. Roy. Soc.* **A254,** 433 (1960). The authors are grateful to Dr. MARTIN for supplying us with a preprint of this paper prior to publication.
22. RICE M. H., MCQUEEN R. G. and WALSH J. M., *Solid State Physics* (edited by SEITZ F. and TURNBULL D.) Vol. VI, p. 1. Academic Press, New York (1958).
23. Ref. (6), Chapter 27.
24. Ref. (6), p. 239; GILVARRY J. J., *Phys. Rev.* **89,** 832 (1953).
25. DUGDALE J. S. and MACDONALD D. K. C., *Phys. Rev.* **89,** 832 (1953).
26. See, for instance, Landolt–Bornstein, *Physicalisch-Chemische Tabellen*, 5th Ed., first supplementary volume, p. 705. Verlag Julius Springer, Berlin (1923).
27. LAZARUS D., *Phys. Rev.* **76,** 545 (1949).
28. DANIELS W. B. and SMITH C. S., *Phys. Rev.* **111,** 713 (1958).
29. NEIGHBOURS J. R. and ALERS C. A., *Phys. Rev.* **111,** 707 (1958).
30. SCHMUNK R. E. and SMITH C. S., *J. Phys. Chem. Solids* **9,** 100 (1959).
31. ZENER C., *Elasticity and Anelasticity of Metals*. University of Chicago Press, Chicago (1948).

J. Phys. Chem. Solids Pergamon Press 1961. Vol. 18, No. 4, pp. 345–355. Printed in Great Britain.

THE DIFFUSION CONSTANTS OF THALLOUS (Tl^+) AND LEAD (Pb^{++}) IONS IN POTASSIUM CHLORIDE

A. GLASNER and R. REISFELD*

Department of Inorganic and Analytical Chemistry, The Hebrew University, Jerusalem, Israel.

(*Received* 4 *August* 1960)

Abstract—Diffusion constants of monovalent thallium and divalent lead into potassium chloride (in the low temperature range of the latter) were evaluated by a new spectral method. Results obtained are summarized in Table 5. Q, the activation energy of thallium ions, was found to be somewhat greater than that of the lead ions, the latter being about equal to the activation energy of the self-diffusion of the potassium ions. It is suggested that the comparatively small pre-exponential factor D_0 for lead is due to its complexation with cation vacancies.

The results obtained on heating the pressed disks differed widely from those with the mixed powders. The difference is accounted for by assuming a prevalence of "grain boundary diffusion" in the pressed disks, whilst "volume diffusion" is deactivated by the high pressure previously applied. The energy of activation with pressed disks is found to be about 10 per cent larger than the latent heat of fusion of the salts employed, namely thallium chloride and thallium sulphate.

Vol. 18
1961

1. INTRODUCTION

A KNOWLEDGE of the diffusion constants of ions in the ionic lattice is greatly desired, but the accumulation of data is slow because of the experimental difficulties[1] encountered with the currently accepted methods. In a previous paper[2] a new method for the evaluation of the diffusion constants in alkali halides was proposed, making use of the characteristic optical absorption of certain cations in the ultra-violet when substituting an alkali ion in the lattice. The characteristic spectra are developed on heating the mixed powders, and the absorption is measured in pressed disks prepared from samples taken at intervals.

In a preliminary study of this technique it was found that the spectra of certain cations, of comparatively volatile chlorides, are developed during the process of mixing the powders.[3]

In this article we report the diffusion constants obtained by this method for monovalent thallium and for divalent lead in potassium chloride.

2. THEORETICAL

It is assumed that the powder is made up of cubical grains of nearly equal size, with a mean edge length l. If each cube of the foreign salt is surrounded by cubes of the alkali halide, and there is a good contact between the grains, the boundary surface through which diffusion takes place is equal to $6\,l^2$. On integrating Fick's second equation:

$$\frac{dc}{dt} = D\left(\frac{d^2c}{dx^2} + \frac{d^2c}{dy^2} + \frac{d^2c}{dz^2}\right),$$

and introducing the limiting condition[4] $4\,Dt \ll 1$, one obtains:

$$D = \frac{M^2\pi}{(6l^2)^2C_0^2t} = \frac{(E_t/E_\infty)^2l^2\pi}{36t} \qquad (1)$$

where M is the total amount of foreign ions (expressed in gram mols) diffused through the boundary surface, C_0 is the molar concentration of the diffusing cation in its salt, t is the time of diffusion, E_t is the optical density measured at the peak of absorption after time t, and E_∞ is the maximum density obtained for complete diffusion at time infinity.

Thus, if E_∞ and l are known, D may be evaluated at any temperature simply by measuring E_t, or otherwise, a mean value may be obtained from the slope of a plot of E_t^2 versus t, from a number of measurements.

* This article is based on a Ph.D thesis submitted by R. R. to the Senate of the Hebrew University, Jerusalem.

3. EXPERIMENTAL

Materials

All salts used in this work were "Baker Analyzed" reagents.

Preparation of powders

The salts were finely ground in a mechanical mullite mortar, dried at 120°C, then accurately weighed, and mixed for 10 min in a Wig-L-Bug electric vibrator, in a plastic vial, to obtain mixtures containing one per cent by weight of the foreign salt. These mixtures were further diluted by the same procedure to give 0·02 per cent TlCl and 0·01 per cent $PbCl_2$. The total weight of each batch of powders was 2–3 g, from which ten or more disks could be prepared.

The time of grinding, as well as other factors which might influence the size of the grains in the powders, was always the same. Photographs taken under the microscope showed that most of the grains were of similar size, cubic form, about 20μ on the edge.

Heating at constant temperatures

In experiments up to 200°C a vapour bath (of the vacuum drying pistol type, widely used by organic chemists for desiccating under reduced pressure) with various constant boiling liquids, was employed. At higher temperatures, an oven wound with nichrome wire and regulated by a "Fielden electronic precision thermostat" was used. In both cases, the temperature was kept constant to $\pm$ 1°C. The Pyrex vial containing the mixed powder was transferred from the desiccator into the preheated oven, and kept there for fixed intervals. The portions taken for the preparation of a disk were measured out by volume with a funnel-shaped glass vessel, containing approximately 200 mg potassium chloride.

Pressing the disks

A Hilger potassium bromide press,[5] and a Loomis 20 ton hydraulic press served for this purpose. The die was evacuated and a total pressure of 25000 lb was applied for 20 min. The die was slightly heated during the same time to about 50°C, with the aid of a heating tape. The diameter of the circular die is 0·5 in., hence the force applied corresponds to a pressure of $\sim$ 9 tons per cm^2.

The disks thus obtained were clear and transparent, transmitting 70 per cent or more light in the near ultra-violet, and somewhat less at shorter wavelengths. When kept in the desiccator the disks did not tarnish for months.

Measurement of spectra and optical density

The spectra were taken with a Beckman DU spectrophotometer and photomultiplier. As a rule, points at intervals of 10 mμ were measured, against air, over the range of 200–400 mμ, and in the neighbourhood of the characteristic absorption peak at intervals of 1–2 mμ. The disks were placed in one of the circular holes of the filter holder soon after pressing, and an additional phosphorus pentoxide tube in the cell compartment ensured a dry atmosphere at the time of measurements. After taking the spectrum, the disks were weighed.

The peaks of the absorption bands were situated at 247 and at 272 mμ for the disks containing thallium and lead respectively. Disks showing a high absorbance, especially with thallium, exhibited a flat peak, supposedly because of the fluorescent nature of the materials.

In order to evaluate the diffusion constants, the optical density E_t was calculated as follows: The absorbance of a pure alkali halide disk, which had the same transparency in the spectral range 320–400 mμ as the disk containing the foreign metal cation, was subtracted from the measured value at the wavelength of maximum absorption. The result was then corrected for the weight of the disk to a standard of 200 mg, assuming direct proportionality between weight and absorbance. The actual maximum variance in the weight of the disks was $\pm$ 10 per cent.

Disks prepared from the powders, containing lead chloride, soon after mixing (but without heating) did not show any absorption bands, but those containing thallium chloride exhibited a characteristic absorption, corresponding to 4–5 per cent of the thallium in the mixture. Hence, diffusion of thallium took place to this extent during mixing and pressing.

The optical density E_∞ of a 200 mg disk after total diffusion was ascertained in two ways: (a) by heating the mixed powders for a sufficiently long period; (b) by wetting the powders, drying, and regrinding. The mean of a large number of

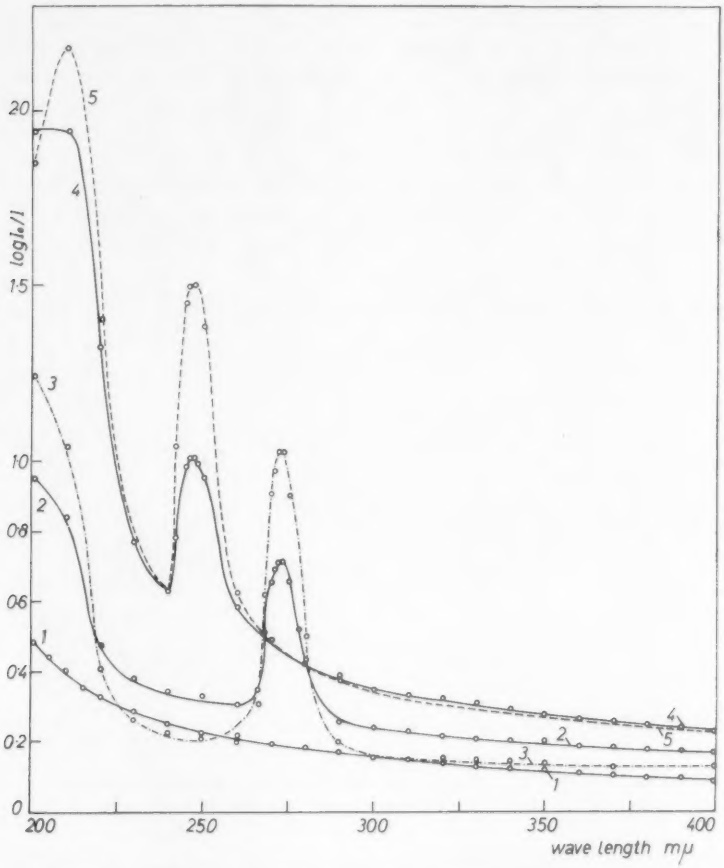

FIG. 1. A few typical spectra of doped potassium chloride disks pressed after heating the mixed powders.

1. Pure KCl
2. KCl:$PbCl_2$, 0·01 per cent, 350°C, 20 min.
3. KCl:$PbCl_2$, 0·01 per cent, 350°C, 60 min.
4. KCl:TlCl, 0·02 per cent, 187°C, 1 hr.
5. KCl:TlCl, 0·02 per cent, 187°C, 8 hr.

such measurements gave the values 1·50 and 1·20 for the 0·02 per cent KCl:TlCl and for the 0·01 per cent KCl:$PbCl_2$ mixtures respectively.

4. RESULTS

Diffusion measurements in powders of potassium chloride

Measurements on potassium chloride powders containing 0·02 per cent thallous chloride were made in the temperature range 150–200°C, and in potassium chloride powders containing 0·01 per cent lead chloride, in the temperature range 300–375°C. A few typical spectra of disks, compared to air, are shown in Fig. 1. Fig. 2 shows plots of E_t^2 vs. t in "thallous chloride" and in "lead chloride" powders at various temperatures. It may be seen that in all cases the experimental points lie on a straight line up to a high fraction of the total density, this being almost 70 per cent in the case of the thallium chloride disks and some-

what less in the case of the lead chloride disks. It should also be noted that the plot of the latter mixtures starts at the origin, whilst the extrapolated thallium chloride lines cut the abscissa at a value equal to minus $\frac{1}{3}$ hr. This is in accord with the observation that unheated "thallium chloride" disks exhibit a low absorption spectrum, i.e. some preliminary diffusion has taken place at the time of mixing.

One of the eight consecutive values given in the Table differs by almost 25 per cent from the rest. Rejecting this, the mean deviation is 4·6 per cent. Considering the various possible sources of error, such as incomplete mixing, fluctuations in temperature, and instability of the readings of the spectrophotometer, this small deviation from the mean appears very satisfactory.

In Fig. 4, log D was plotted vs. the inverse of

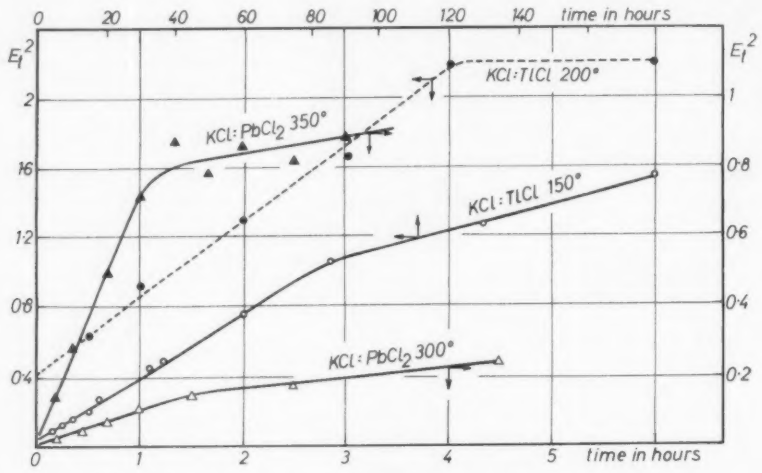

FIG. 2. Square of measured optical density vs. time of heating at temperatures indicated (E_t^2 vs. t). Arrows on curves indicate scales employed.

In Fig. 3, log E_t vs. log t was plotted. (For the thallous chloride series the time values were corrected by the addition of 20 min to the actual times.) In this plot also the points of each series of measurements lie on a straight line with a slope equal to 0·5, as required by equation (1). Hence after substituting the appropriate values for the constants in the last equation ($l = 20 \times 10^{-4}$ cm; $E_\infty^{Tl^+} = 1{\cdot}50$; $E_\infty^{Pb^{++}} = 1{\cdot}20$), D, the diffusion constant in cm^2 sec^{-1}, at several temperatures, was calculated from the slope of the straight lines exemplified in Fig. 2. The data thus obtained are summarized in Table 1.

As a matter of fact, D may be evaluated from each individual measurement, and it is of interest to compare these to the mean value obtained graphically. For this purpose a series of measurements with 0·02 per cent thallous chloride is given in Table 2 in detail.

the absolute temperature. The points for both thallous and lead chloride lie on straight lines, from the slopes of which the energies of activation Q were calculated. Substituting these in the Arrhenius equation $D = D_0 \exp(-Q/RT)$, one obtains the expressions:

$$D_{Tl^+} = 7{\cdot}14 \exp(-25{,}200/RT) \text{ cm}^2 \text{ sec}^{-1}$$

and

$$D_{Pb^{++}} = 4{\cdot}41 \times 10^{-3} \exp(-22{,}820/RT) \text{ cm}^2 \text{ sec}^{-1}$$

in the temperature ranges mentioned.

Diffusion in powders under reduced pressure

In order to find out the effect of atmospheric pressure on the calculated diffusion constants, a few series of experiments were carried out in partly evacuated vessels. The temperature in these experiments was hand-regulated by a "powerstat"

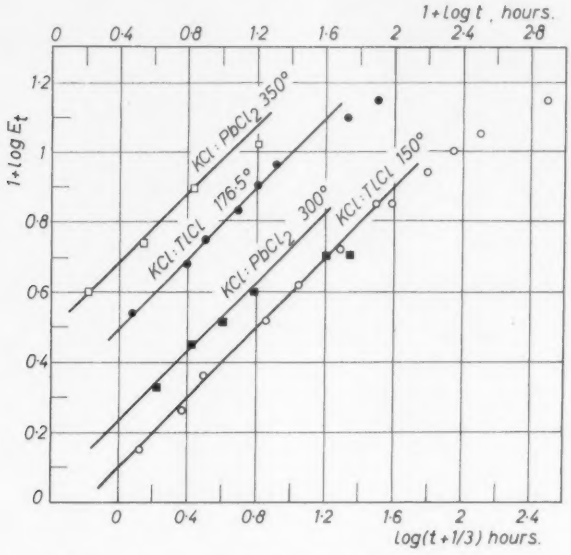

FIG. 3. Log E_t vs. log t plots for powders. For lead chloride mixtures use upper time scale.

Vol. 18
1961

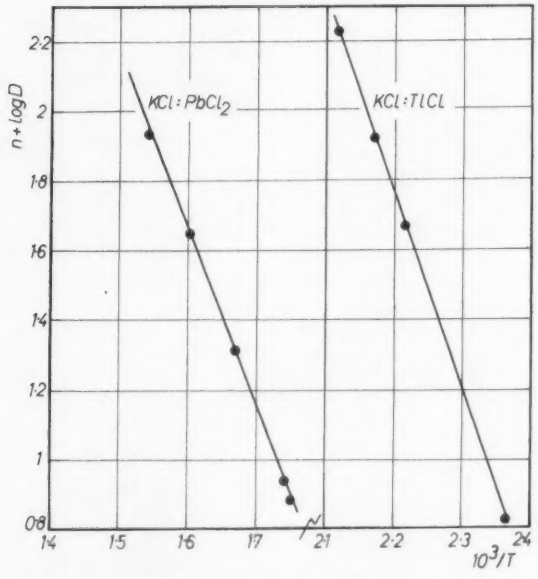

FIG. 4. Arrhenius plot of the diffusion constants D obtained with KCl:TlCl and KCl:$PbCl_2$ powders (n = 13, or 12 resp.).

Table 1. Diffusion constants of thallous chloride and lead chloride in potassium chloride

Thallous chloride		Lead chloride	
°C	$D\times10^{12}$	°C	$D\times10^{11}$
150	0·68	300	0·77
176·5	4·70	325	2·08
187	8·36	350	4·44
200	17·0	375	8·79

and measured by an ordinary mercury thermometer in outer contact with the tube holding the powders. The results obtained with three batches of KCl:TlCl powders, at about 150° (I and II) and at about 155°C (III) after heating for two hours, are given in Table 3.

Clearly, reduction of atmospheric pressure increases the absolute rate of diffusion, but this effect becomes smaller the higher the vacuum.

Experiments with thallous sulphate

Powdered mixtures of 0·021 per cent KCl:Tl_2SO_4 were prepared so as to contain an equivalent amount of thallium to the KCl:TlCl mixtures. The development of the spectra was slower with the thallous sulphate than with the chloride, and experiments were carried out at higher temperatures. The expected full optical density was attained only at 400°C; at lower temperatures the diffusion seemed to approach a lower limit even after prolonged heating. Fig. 5 shows the E_t^2 vs. time plots in the temperature range 190–400°C. Each of the curves obtained has an initial linear portion that cuts the ordinate at a relatively high point. From the slopes of these straight lines, the apparent diffusion constants were calculated in the same way as above. Also, on plotting the logarithms of the slopes $\Delta E_t^2/\Delta t$ vs. the inverse of absolute temperature (Fig. 6), the energy of activation was obtained. Thus, the results with thallous sulphate may be presented by the expression:

$$D_{Tl_2SO_4} = 5{\cdot}2\times10^{-8}\exp(-10{,}800/RT)\ \mathrm{cm^2sec^{-1}}$$

Table 2. D for 0·02 per cent KCl:TlCl, at 150°C calculated from single points

t^*, hr	E_t	$D\times10^{13}$	$\Delta D\times10^{13}$
1·33	0·143	6·63	−0·13
2·33	0·185	6·33	−0·43
3·33	0·236	7·21	+0·45
6·83	0·335	7·08	+0·32
10·83	0·420	7·02	+0·26
15·83	0·442	(5·32)	
18·83	0·533	6·50	−0·26
32·83	0·707	6·56	−0·20
		mean: 6·76 ± 0·31	

$$\sqrt{\left[\frac{\sum(\Delta D)^2}{n}\right]} = 0{\cdot}31\times10^{13}$$

* Corrected, to account for preliminary diffusion.

Table 3. Diffusion of thallium in potassium chloride under reduced pressure, at 150–155°C, heating time = 2 hr.

Pressure	I		II		III	
	$E_t\times10^3$	$D\times10^{12}$	$E_t\times10^3$	$D\times10^{12}$	$E_t\times10^3$	$D\times10^{12}$
O.D. prior to heating	83	—	87	—	88·5	—
*695 mm	139	0·27	149	0·32	243	1·10
60 mm	214	0·84	225	0·91	—	—
9 mm	—	—	—	—	386	3·04
0·5 mm	240	1·09	254	1·23	427	3·76
0·3 μ	297	1·75	—	—	450	4·19

* Normal barometric pressure in these laboratories.

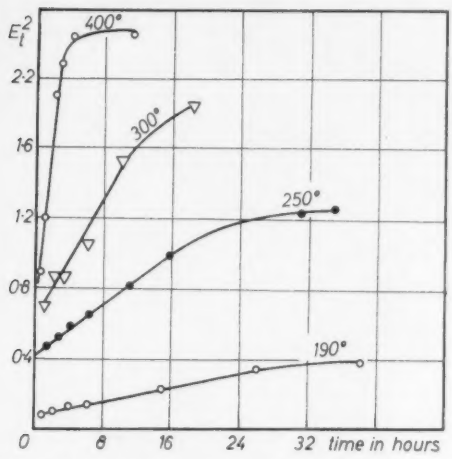

FIG. 5. Diffusion of thallium in KCl:Tl_2SO_4 powders.

Diffusion in potassium chloride disks

Several series of measurements were made with KCl:TlCl and KCl:Tl_2SO_4 disks prepared from the unheated powders (of the same concentration as above) in the temperature range 150–450°C. In these experiments the disks often lost their transparency after continued heating, especially at the higher temperatures, and had to be re-pressed before measuring their spectrum. This was accompanied by a small loss of weight, and an improvement in transmission. The E_t^2 vs. time curves (Fig. 7) resemble in many respects those obtained with thallous sulphate powders. The Arrhenius plot of the initial slope of these curves is shown in Fig. 6, and the expression for the apparent diffusion in the pre-pressed disks may be represented by:

$$D^a_{TlCl} = 4{\cdot}21 \times 10^{-10} \exp(-4670/RT) \text{ cm}^2 \text{ sec}^{-1}$$

$$D^a_{Tl_2SO_4} = 4{\cdot}91 \times 10^{-10} \exp(-6860/RT) \text{ cm}^2 \text{ sec}^{-1}$$

5. DISCUSSION

The straight lines obtained on plotting log E_t vs. log t, with a slope equal to 0·5 (Fig. 3), prove that the slowest step in a probable sequence of reactions, i.e. the reaction rate measured, is actually that of diffusion. Simultaneously, Figs. 2 and 3 prove the basic validity of equation (1), but

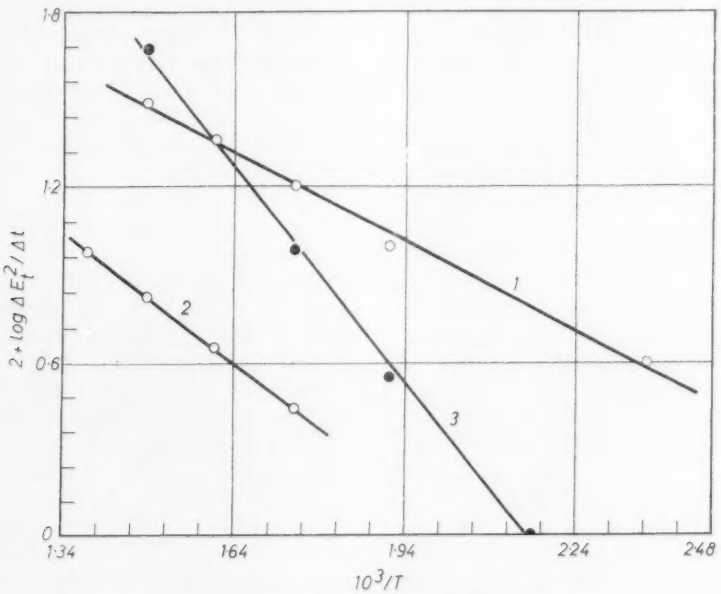

FIG. 6. Arrhenius plot of slope of diffusion curves:
1. KCl:TlCl, disk; 2. KCl:Tl_2SO_4, disk; 3. KCl:Tl_2SO_4, powder.

Vol. 18
1961

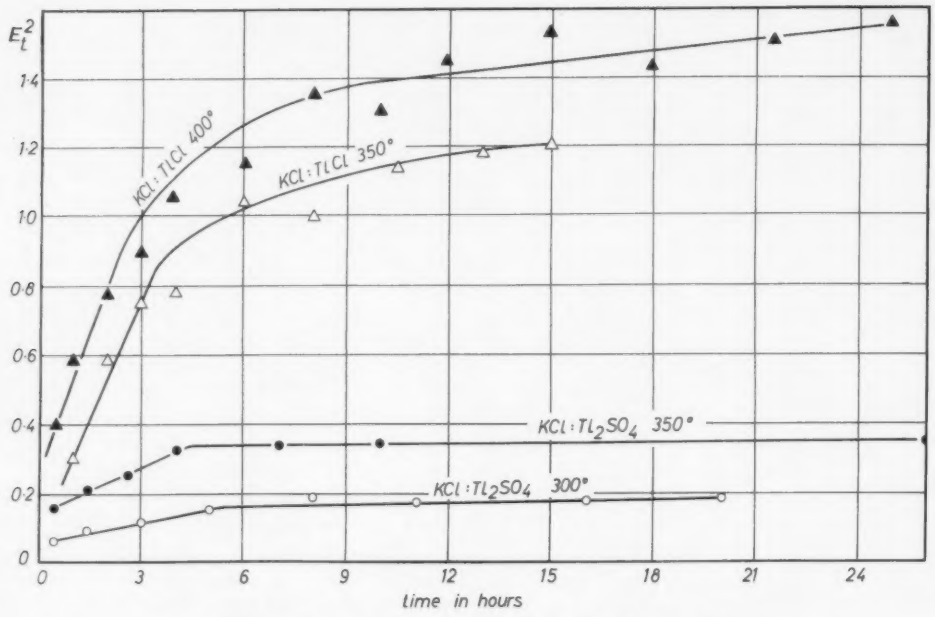

FIG. 7. Diffusion of thallium in KCl:TlCl and KCl:Tl_2SO_4 disks.

not the assumptions with respect to the area of the face-boundary through which diffusion progresses. Comparing the present values for the diffusion of cations in alkali halides with those available in the literature,[6] it appears that $6l^2$ (where l is the mean length of the edge of a powder grain) is not far wrong. Yet, for a critical evaluation of the diffusion constants, as well as other related parameters obtained in this work, a closer knowledge of the area of the face boundary is necessary.

Altogether in a heap of powders one would not expect a perfect contact between the grains. There are two possible mechanisms by which contact between grains at short distances may be improved: (*a*) surface diffusion (to be discussed later), and (*b*) sublimation. The experiments at reduced pressure (Table 3) are indicative of the mechanism occurring; E_t as well as D appears to increase when the pressure is reduced, and it may therefore be concluded that sublimation occurs. The latter is limited, at atmospheric pressure, by the "mean free path" in air, this being of the order of magnitude 10^{-5} cm.[7] Hence, the very small vapour pressure of thallous and lead chloride, at the temperature of the experiments, suffices to bridge small gaps between these salts and the potassium chloride grains. The mean free path is inversely proportional to pressure, but at high vacuum the effect of change of pressure on E_t becomes negligible, i.e. in spite of the very large mean free path, the foreign salt does not spread all over the surface of distant potassium chloride grains, being prevented from doing so by the wall of grains circumscribing the foreign particle.

To summarize, the surface of the potassium chloride cubes facing a foreign particle, at distances less than about 1 μ, are covered by the sublimate at atmospheric pressure. As pressure is reduced, the coverage increases two- or threefold, but not more, as evidently only a small fraction of the foreign salt is able to escape through the slits in the "enclosure". Hence, when working at atmospheric pressure the assumption that the "face boundary" is equal to $6l^2$ is a good first approximation, this being a reasonable fraction of the total area of the potassium chloride grains facing a foreign particle.

With respect to the effect of increasing temperature on the extent of sublimation, neither the increase of the mean free path nor that of the vapour pressure could have an influence comparable to that of a tenfold reduction of external pressure. This may be surmised from examination of Table 4 (which lists[8] melting points (M.P.), boiling points (B.P.) in degrees Centigrade, latent heats of fusion (L_f) and latent heats of vaporization (L_v), per gram mole, of a few relevant salts). The activation energies Q obtained in this work should therefore be very nearly correct, although the absolute values of D and D_0 may be in error by a small factor.

Table 4

Substance	M.P.	L_f	B.P.	L_v
TlCl	427	4260	807	24,420
TlBr	460	5990	819	23,800
Tl_2SO_4	632	5500	—	—
$PbCl_2$	498	5650	954	29,600
$BiCl_3$	224	2600	441	17,350
$HgCl_2$	277	4150	304	14,080

It must be pointed out that in a previous article[3] on the absorption spectra of mercury, bismuth and antimony halides in pressed alkali halide disks, it was observed that the spectra of these cations are fully developed without heating of the powders, owing to the volatility of their halides. This is so because the low melting points and low heats of fusion (Table 4) undoubtedly assist the surface diffusion of these salts, so that large surfaces of distant alkali halide particles are covered by them. The resulting great dispersion of these volatile salts makes them unsuitable for a diffusion study by the present spectral method.

The advantages of the method with less volatile salts are evident; results may be obtained on heating for short intervals, and the techniques and the mathematical equation for calculating D, the diffusion constant, are simple. Moisture must be excluded as it increases the surface boundary by dissolving the salts.

Diffusion constants may be obtained from a single measurement of the absorption peak, or a more reliable mean value results from a series of measurements (Table 2).

When a certain amount of the foreign cation has diffused, there is a change in the slope of the E_t^2 vs. time curves (Fig. 2); equation (1) is no longer valid when the limiting condition $4Dt \ll 1$ has been passed. In the case of thallium chloride, equation (1) seems to hold up to 70 per cent or more of the total amount of the foreign ion in the mixture. With lead chloride the bend in the curves occurs at a lower percentage. This may be due to the difference in the lattice of the two salts in the mixtures. The influence of the lattice is even more obvious in the case of thallium sulphate, where as a result of the process of diffusion an intervening layer of mixed potassium–thallium sulphate is formed between the original potassium chloride and thallium sulphate layers. This explains the very low apparent D_0 value obtained with the thallium sulphate mixtures, as well as the inequality of the activation energies, Q, with those of the thallium chloride mixtures. It is thought that Q in this case may stand for the energy of activation of the diffusion of thallium ions in the mixed potassium–thallium sulphate lattice.

Table 5 contains a summary of the constants of the Arrhenius equation obtained in this work, and a comparison with some of the scanty data available from previous publications. The constants for the diffusion of thallium and lead in powder mixtures are of the same order as those obtained by more conservative methods. The energy of activation for thallium is larger than that for lead, or for the self-diffusion of potassium. This may be due to the larger size of the thallium ion, as was to be expected with a mechanism of diffusion through vacancies.

The ratio of D_0 values for thallium and for lead is of the order of 10^3. Such, and even wider, variations had been observed with other cations. Hence,

Vol. 18
1961

Table 5

Diff. ion	Temp. range, °C	D_0 cm² sec⁻¹	Q kcal/mol	Ref.
in KCl				
Tl^+	150–200	7·14	25·2	This work
Pb^{++}	300–375	$4{\cdot}41\times10^{-3}$	22·8	This work
$Tl^+(Tl_2SO_4)$	190–400	$(5{\cdot}2\times10^{-8})$	10·8	This work
Tl^+ disk	150–400	$(4{\cdot}21\times10^{-10})$	4·67	This work
Tl^+ disk (Tl_2SO_4)	300–450	$(4{\cdot}91\times10^{-10})$	6·86	This work
K^+	$<460°$		19–23	9,10
in NaCl				
Na^+	$<550°$	$1{\cdot}6\times10^{-5}$	17·7	11
Cu^+		0·5	25·2	6
Ni^{++}		0·2	25·4	6

any conclusion with respect to the D_0 values is bound to be somewhat speculative. Yet, in the case of the small observed value for lead, it could be attributed to the retarding effect of a cation vacancy complexed with the divalent lead ion.[12] The latter may fluctuate between the two lattice points at its disposition, but its chances of advancing in any one direction are thereby reduced.

For the diffusion of a divalent impurity complex one has to assume either a previous dissociation of the complex or a sequence of jumps described by LIDIARD[13], in which (a) the impurity changes place with the vacancy (with probability w_2) and (b) the vacancy jumps around the impurity ion from one associated position to another (with probability w_1). By assuming the latter mechanism, LIDIARD explained the much larger absolute diffusion coefficient of zinc ions in sodium chloride than that of the sodium tracer, observed by Chemla in the *intrinsic range*. Even if LIDIARD's assumptions prove to be right in the *intrinsic* range, they may not be so at the lower temperatures of the *impurity* range. However, there are two conditions, *sine qua non*, for the above mechanism, as stated by LIDIARD (Ref. 13, p. 337): "Owing to the double charge on the impurity ion it is to be expected that the potential energy barrier opposing its movement will be increased and that the condition $w_2 \ll w_1$ will almost always be satisfied." But actually the activation energy for the diffusion of the zinc ion is found to be only 0·46 eV as against 0·77 eV for the self diffusion of the sodium ion. Hence it seems more probable that $w_2 \gg w_1$, and w_1 being "very small" "it is clear that the impurity ion merely jumps backwards and forwards without progressing very far on the average". The large diffusion coefficient of the zinc ion should therefore simply be attributed to its low activation energy.

The very low values for D_0 and for Q observed in the experiments with disks pressed before heating, is surprising. These results may only be due to the high pressure applied, i.e. a volume disactivation of the vacancy mechanism.[14,15] Further experiments under progress in this laboratory confirm the above conclusion. The measured activation energies Q are therefore thought to be due to a surface diffusion on the grain boundaries. The actual values 4·67 and 6·86 kcal/g mol for thallium chloride and thallium sulphate respectively are about 10 per cent higher than the molar heats of fusion of these salts (see Table 4), suggesting a straightforward relation between these two parameters.

The "apparent" D_0 values ($4{\cdot}2$–$4{\cdot}9\times10^{-10}$ cm² sec⁻¹), very nearly the same with both thallium salts, are a direct result of the very much smaller area of the available face boundary for surface diffusion, compared to that of volume diffusion. Hence, in the mixed powders, both

volume and surface diffusion occur, but owing to the large face boundary of the powdered salts, the part of the surface diffusion in the total diffusion of the foreign cation may be neglected, in spite of the much higher activation energy of the volume diffusion. On the other hand with pressed disks, while the volume diffusion is restricted, the spectral method affords means of measuring surface diffusion on the grain boundaries. The advance of surface diffusion in pressed pills of alkali-halides, in front of the volume diffusion, has been radiographically observed by BÉNARD and LAURENT[16].

Acknowledgement—The authors are most thankful to Professor A. HALPERIN, of the Department of Physics of the Hebrew University, for many fruitful discussions.

REFERENCES

1. MOORE W. J., *Ann. Rev. Phys. Chem.* **10,** 416–20 (1959).
2. GLASNER A. and REISFELD R., *J. Chem. Phys.* **25,** 381 (1956).
3. GLASNER A. and REISFELD R., *J. Chem. Phys.* **32,** 956 (1960).
4. JOST W., *Diffusion in Solids, Liquids, Gases*, p. 22. Academic Press, New York (1952).
5. FORD M. and WILKINSON G. R., *J. Sci. Instrum* **31,** 338 (1954).
6. See e.g. HAUFE K., *Reaktionen in und an festen Stoffen*, pp. 376–7, Table 17. Springer Verlag, Berlin (1955).
7. GLASSTONE S., *Textbook of Physical Chemistry* (2nd Ed.) pp. 274–81. Van Nostrand, New York (1950).
8. *Chemical Engineers' Handbook*, pp. 210–12 (edited by PERRY J. H.). McGraw Hill, New York (1950).
9. PHIPPS T. E. and PARTRIDGE E. G., *J. Amer. Chem. Soc.* **51,** 1331 (1929).
10. KELTING H. and WITT H., *Z. Phys.* **126,** 697 (1949).
11. MAPOTHER D., CROOKS H. N. and MAURER R., *J. Chem. Phys.* **18,** 1231 (1950).
12. WAGNER C., *J. Chem. Phys.* **18,** 1227 (1950).
13. LIDIARD A. B., *Encyclopedia of Physics*, Vol. XX, pp. 335–9 (edited by FLÜGGE S.) *Electrical conductivity* II. Springer Verlag, Berlin–Göttingen–Heidelberg (1957).
14. KURNICK S. W., *J. Chem. Phys.* **20,** 218 (1952).
15. TANNHAUSER D. S., *J. Phys. Chem. Solids* **5,** 224 (1958).
16. LAURENT J. F. and BÉNARD J., *J. Phys. Chem. Solids* **7,** 218 (1958).

BOOK REVIEWS

R. A. SMITH: **Semiconductors.** Cambridge University Press, London, 1959. xvii + 494 pp., 65s.

THE SUBJECT of semiconductor physics has expanded, and is expanding, so rapidly that few have dared write a book on this subject that might be out of date by the time of its publication. There have been, it is true, several accounts of transistor electronics and of the more elementary aspects of semiconductors. Where these texts have dealt with the physics of semiconductor behavior, they have been describing material generally regarded as established by those in the field. The main advances in understanding in the past decade have been included in a number of review articles that could cover only part of this wide field, and were occasionally only marginally committed to an attempt at pedagogical clarity.

Of the books available at an intermediate level, Dr. SMITH's effort must rank as one of the best. It is not, and does not pretend to be, a rigorous quantum-mechanical treatment of the subject; none of the recent books known to me are. It is, instead, a very readable account, from a physical point of view, of those topics that have been most investigated in the past few years. Dr. SMITH presents his material at a fairly constant level of difficulty, apparently choosing those proofs and demonstrations that will most easily persuade his reader. In so doing, he succeeds in avoiding to a large degree the pitfall into which many such texts fall: that of presenting the facile explanation that is really misleading, and requires correction at a later stage. After several years of teaching semiconductor physics at about this level to graduate students at an American university, I can say without reservation that this book is easily the closest to a good general text that we have tried.

The book opens with a discussion of some elementary properties of semiconductors, then passes on to present a review of the behavior of electrons moving in periodic potentials. The third chapter discusses the general imperfection in crystal lattices before particularizing to substitutional foreign atoms in Group IV and Group III–V semiconductors. The chapter closes with a brief discussion of excitons.

There follows a chapter on statistics, followed by a lengthy phenomenological treatment of transport phenomena, partly from the approach of the Boltzmann equation, and partly from consideration of the kinetics of the average particle. In the same chapter the major scattering mechanisms are discussed.

After a short chapter on thermal effects, we find a longer one—yet perhaps not long enough, in view of the great present interest in the subject—on the optical and magneto-optical properties of solids. This seems to be the place where it is evident that the writer must either survey the material and briefly report the quantum mechanically derived formulae, justifying those parameters in them that are easily explained, or settle down to a thorough-going explanation with no details omitted. The latter approach is not possible here, granted the original premises for the structure of the book. It is worth noting, however, in passing, that there is no one text at the moment that covers all of the material of this one at the higher level. Although such a well rounded, consistently-written account would be hard to write, it is one of the most needed books in semiconductor physics today.

To return to the details of the present work, the eighth chapter treats at length drift and diffusion theory, followed by a short discussion of recombination mechanisms and photoconductivity. One recalls that separate texts have recently been published on this last topic, so that the scant treatment of this book is rather summary dismissal. The mechanisms of recombination, as distinct from the phenomenology of recombination centers and capture cross-sections and the like, might also feel somewhat slighted by the briefness of their appearance.

After a general chapter on methods of determining semiconductor parameters, Dr. SMITH discusses in turn the present status of knowledge of germanium, silicon, diamond and gray tin; selenium, tellurium and boron; the Group III–V semiconductors, like InSb; Group I–V, II–IV, II–V semiconductors; the lead "salts"; the CdS series; and other more esoteric members of the species. The final chapter deals with the application

Vol. 19

of semiconductors in rectifiers, transistors, photodetectors, thermoelements, and the like, and runs to some fifty pages out of over four hundred.

Dr. SMITH remarks, in his preface, that some subjects had of necessity to be left out of his book. Thus it is easy to justify the absence of much reference to crystal purification techniques and transistor technology. The absence of an adequate discussion of the work on the surface properties of semiconductors and of the low mobility semiconductors extensively studied in the Soviet Union is however regrettable. The tunnel diode is, of course, not treated, simply because, although Esaki's work was published, its importance had not been recognized at the time the book was written: an example, surely, of the difficulties facing an author in a fast moving field. Another example is the omission of references to the identification of impurity centers using electron spin resonance.

The latter criticisms are not important for the immediate usefulness of this book, but will obviously affect its topicality in a few years time. The treatment of the first ten chapters is such that it may be expected to remain useful for some time to come; the relegation of discussion of the properties of specific semiconductors to the later chapters means that they alone will become out of date.

In summary, this reader feels that *Semiconductors* will prove a most useful text for senior (honour) year and first year graduate students in physics; for those physicists in industry or government who may never have had a formal course in semiconductor physics, or who require a comprehensive review of the subject; and for electronic engineers with some background in elementary quantum mechanics who desire to establish a foundation of knowledge of the physical processes underlying the operation of semiconductor devices.

WILLIAM PAUL

W. L. JOLLY: **Synthetic Inorganic Chemistry.** Prentice-Hall Inc., New Jersey, 1960. 196 pp., $8.00.

THIS SHORT book, comprising some sixteen chapters, represents an important contribution to the teaching of inorganic chemistry. The first five chapters, with their discussions of such subjects as searching the literature and the principles underlying various inorganic reactions, are intended as an introduction to the remainder of the book. Chapter 6 outlines a laboratory course taught to undergraduates at the University of California, while Chapters 7 through 15 describe a series of special experimental techniques, e.g. use of an electric discharge, use of high-pressure apparatus, vacuum manipulation, and the inert atmosphere box. Chapter 16 provides a detailed account of eighteen syntheses designed to emphasize the theoretical principles and laboratory techniques mentioned earlier.

In the opinion of this reviewer, Chapters 7 through 15 form the most valuable part of the book, representing the best single source of information on the techniques required for preparing inorganic compounds having some real significance. In a series of clear, concise chapters the author introduces the student to nine special techniques and the ancillary equipment necessary for their use. The value of each of these chapters is still further increased by the inclusion of a useful bibliography designed to lead the reader to more detailed sources of information. Experts will have little justification for advancing any wide criticism of this part of the book, although there are a few places where the text could be improved. Thus in Chapter 10, *The Vacuum Line*, the stopcocks described are rather more complicated and, therefore, more expensive than necessary, and there are better designs for mercury float valves than those suggested.

The publisher described *Synthetic Inorganic Chemistry* as being both a theoretical and operational text and not merely a cookbook or a book on techniques. These are certainly admirable objectives, but in this reviewer's opinion an adequate theoretical background is not provided, nor could it be provided in a book of this size. In Chapters 1 through 5 the author has covered too much material too rapidly, so that a student has to refer to other sources of information if he is to obtain anything like a reasonable knowledge of the formation and nature of the substances described later in the book. Chapter 2 in part contains a summary of the thermodynamic and the kinetic considerations involved in synthesis, but the treatment given is at the level of a freshman general chemistry course.

Vol. 18
1961

For example, the effect of temperature and pressure on the reversible reaction

$$N_{2(g)} + 3H_{2(g)} \rightleftharpoons 2NH_{3(g)}$$

is discussed. In Chapter 4 the chemistry of metal coordination compounds is reviewed in about nine pages, within which the reader is presented with a rather sophisticated explanation of the *trans*-effect, but in which the author omits any reference to the more generally important ligand field theory. It may be argued that wherever theoretical principles are discussed many references to both books and journals are given, so that a student can, if sufficiently stimulated, readily undertake supplementary reading. However, certain important references both to books and to journal articles are conspicuous by their absence. Thus the two review series, *Progress in Inorganic Chemistry, and Advances in Inorganic Chemistry and Radiochemistry* are not mentioned under the list of general reference books on page 11. One example of the omission of important journal references occurs under discussion of the use of $LiAlH_4$ to prepare metal hydrides (page 50). Preparation of GeH_4 from $GeCl_4$ using $LiAlH_4$ affords poor yields of the desired germane (see SUJISHI S. and KEITH J. N., *J. Amer. Chem. Soc.* **80,** 4138 (1958); and MACKLEN E. D., *J. Chem. Soc.* 1984 (1959)). A better example of the use of $LiAlH_4$ to prepare a hydride of a Group IV element would have been the synthesis of stannane from $SnCl_4$, which proceeds in high yield so long as a trace of oxygen is present (EMELÉUS H. J. and KETTLE S. F. A., *J. Chem. Soc.* 2444 (1958)).

More minor criticisms of the book include such matters as the omission of molecular weight determination under the list (page 55) of macroscopic measurements which establish structure type, and perhaps an over-emphasis on the question of nomenclature. While most practising chemists would agree that the substance of composition CuCl should be called copper (I) chloride, in view of common usage over a number of years it would appear best to call $LiAlH_4$ lithium aluminum hydride rather than lithium hydroaluminate. The problem of boron nomenclature, at present under review, is even more difficult, with the result that in the book we find such complex names as ammonium μ-amidohexahydrodiborate(1$^-$) for the substance $NH_4(H_3B{:}NH_2{:}BH_3)$. This would seem to be burdening the reader with excessive detail, in this case especially because of recent studies favoring a different structure for this substance. At present it may be best to refer to many boron compounds by formula, or by a trivial name, if such has developed by common usage.

The above remarks notwithstanding, this book will be extremely useful to all students of inorganic chemistry.

F. G. A. STONE

Photochemistry in the Liquid and Solid States. Edited by L. J. HEIDT, R. S. LIVINGSTON, E. RABINOWITCH and F. DANIELS. John Wiley, New York, 1960. 174 pp. $6.

THE remarkable manner in which nature is able to convert solar energy into chemical energy for the purpose of supporting life on this planet poses a constant challenge to man. Is it possible to devise other photochemical systems which, like photosynthesis, might store solar energy and release it upon demand at some later time to do useful work? In an attempt to answer this question, the National Academy of Sciences–National Research Council sponsored a symposium in 1957 at which ideas on this subject might be exchanged. This book consists of twenty-four papers presented at this symposium, covering such topics as the primary photophysical acts of excitation and energy transfer, the secondary photochemical processes of free radical production and the associated kinetics, and photoprocesses occurring in crystals and semiconductors. Gaseous systems were excluded from the discussions because of the large volumes required when energy storage is considered. Similarly, although photosynthesis is still the only example of the successful photochemical storage of energy, this topic was not specifically included as such because of its more than adequate coverage in other symposia.

A condensed listing of chapters follows: Chapter I, Introduction; Chapter II, Photochemical Reactions; Chapter III, Photosensitized Reactions; Chapter IV, Fluorescence; Chapter V, Kinetics; Chapter VI, Role of Triplet State; Chapter VII, Photochemical Reactions Involving Chlorophyll; Chapter VIII, Photoreactions in Solids; Chapter IX, Conclusions. Because there

are as many authors as there are papers, there is some unavoidable repetition and a certain unevenness in presentation, but this has been kept to a minimum by a judicious arrangement of the material. The presentation is considerably enhanced by a clearly written and succinct introduction by the editors in which the general subject is put in proper perspective and the major outlines of the field emphasized. This introductory chapter includes some criteria applicable to the selection of suitable photochemical reactions to utilize solar energy, a survey of known reactions, and a consideration of future possibilities. A concluding chapter by Professor DANIELS ably summarizes the results of the symposium. In his words, "... there is no easy solution just around the corner. However, there is no evidence that such storage of solar energy is impossible. Much more research is needed."

One of the more fascinating aspects of the field of photochemistry is the way in which it brings the different sciences together. Not so very long ago, physics, chemistry, and biology were entirely separate disciplines. Indeed, the field of chemistry itself was rather sharply sub-divided, and a professor of physical chemistry and a professor of biochemistry in the same university had little or no contact with one another except at an occasional faculty meeting. Today, what was once a rather sharp boundary between the physical sciences and the life sciences has become quite diffuse. Nowhere is this better illustrated than in the field of photochemistry. The enthusiastic application of solid state terminology and concepts to the problem of energy transfer mechanisms in biological systems is but one example of this trend. In reflecting this blending of ideas, this book illustrates the extent and usefulness of the combined physical–chemical–biological approach in modern photochemical studies.

It is regrettable that a report on Professor HEIDT's work on the photolysis of aqueous inorganic solutions was not included in what is otherwise a comprehensive look at current research in the field of photochemical utilization of solar energy. Only one error was noted: on page 23 the methyl free radical is shown as being formed by direct photochemical dissociation of ammonia. The book is attractively bound and clearly printed. It is recommended not only to those who are active workers in this field, but also to the non-specialist; the mental effort required to follow some of the detailed kinetic schemes and tables of experimental data will be amply repaid by the provocative and stimulating ideas presented.

V. J. LINNENBOM

C. L. ANDREWS: **Optics of the Electromagnetic Spectrum.** Prentice-Hall, New Jersey, 1960. 501 pp. $9.00.

THIS BOOK is a new text at the intermediate level in which the optics of electromagnetic radiation is presented in a relatively unified manner. Starting with an introductory chapter in which various forms of electromagnetic radiation are described and their measurement and production discussed, the usual sequence of topics is followed in successive chapters: wave propagation and superposition of waves, the velocity of light, various forms of interference of multiple sources, diffraction phenomena, electromagnetic theory of dispersion and absorption, and finally polarization phenomena including crystal optics and topics such as optical activity. Several innovations distinguish this book from similar texts in physical optics. For one thing, simple illustrations based upon microwaves are introduced to reinforce the classic demonstrations of multiple-slit interference and of diffraction of visible-light waves. Microwave applications are likewise discussed in the chapters on polarization phenomena. For the most part these microwave experiments are of such nature that they can be readily performed using relatively unsophisticated lecture demonstration equipment. This book is thus a convenient source of rather nice optics demonstrations based upon inexpensive commercially available 2450 megacycle oscillators and detectors.

As a second, rather interesting, change from the pattern of similar texts Dr. ANDREWS devotes a chapter to a detailed description of the over-all diffraction properties of apertures in plane screens. The development is based upon a theory ascribed to Thomas Young in which the total wave is the superposition of the geometrically shadowed incident beam and a diffracted wave reradiated from

Vol. 18
1961

points along the periphery of the aperture. To describe the dependence of the diffracted wave upon the incident wave a semi-empirical formula is used. This formula is based upon a series of microwave measurements made by the author. From it follow a number of approximate results for the field in the plane of various apertures, as well as the results normally obtained from the Huygens–Kirchhoff theory at large distances from this plane. Although this alternative approach to diffraction theory is as interesting as it is novel to the teaching of optics, I think it has received excessive emphasis for a general text at this level. Moreover it would perhaps have been desirable to mention somewhere, in an otherwise heavily footnoted chapter, the classic calculation of Sommerfeld for the diffraction by a conducting half plane.

The author's attempt to unify the discussion of the optics of the electromagnetic spectrum has not been entirely successful, and the reader occasionally finds himself with the impression that the various topics in microwave and visual optics have been merely interleaved rather than dissolved into a common solution, This difficulty is perhaps due to the fact that the difference in scale of the two forms of radiation lead to many very real differences in their experimental manifestations. For example the waveguide, which is a fundamental element for the student of microwaves, has had no analog for visual radiation until the very recent developments in fiber optics. On the other hand ten-thousand line diffraction gratings are at the moment impractical microwave devices. In spite of these intrinsic difficulties, however, I think the author could have achieved a smoother unification of his subject. In addition, somewhat greater discussion might have been devoted to the radiation process itself in which, after all, the common origin of various forms of electromagnetic radiation can be so well illustrated. A more extensive treatment of special relativity might also have been appropriate.

As a course text I think that this book would be suitable for students of applied physics who have already a fair competence in electromagnetic theory and who wish to survey physical optics in a relatively superficial manner.

On the other hand students of physics and engineering desiring to establish a firm foundation of knowledge relevant to the "Optics of the Electromagnetic Spectrum" are well advised to study a text having a more thorough and more profound treatment than that of the book under review.

R. H. MILBURN

Vol.
196

Vol. 18
1961